Acclimatation des récifs coralliens aux changements climatiques : écophysiologie et signatures géochimiques dans un contexte d'acidification des océans

Clément Tanvet

COLLEGE SCIENCES DOCTORAL DE LA MER BRETAGNE ET DU LITTORAL

UBO
Université de Bretagne Occidentale

THESE DE DOCTORAT DE

L'UNIVERSITE
DE BRETAGNE OCCIDENTALE

ECOLE DOCTORALE N° 598
Sciences de la Mer et du Littoral
Spécialité : *Écologie Marine*

Par

Clément TANVET

Acclimatation des récifs coralliens aux changements climatiques
Écophysiologie et signatures géochimiques dans un contexte d'acidification des océans

Thèse présentée et soutenue à Plouzané, le 24 Mai 2023

Unité de recherche : LEMAR (CNRS, IRD, UBO, Ifremer) **– ENTROPIE** (CNRS, IRD, UR, UNC, Ifremer)

Rapporteurs avant soutenance :

Paola FURLA	Professeure, UNS, France
Paolo MONTAGNA	Directeur de Recherche, ISP-CNR, Italie

Composition du Jury :

Président :	**Jean-Pierre GATTUSO**	Directeur de Recherche, LOV-CNRS, France
Rapporteurs :	**Paola FURLA**	Professeure, UNS, France
	Paolo MONTAGNA	Directeur de Recherche, ISP-CNR, Italie
Examinateurs :	**Francesca BENZONI**	Maitresse de Conférence, KAUST, Arabie-Saoudite
	Alexander VENN	Chargé de Recherche, CSM, Monaco
Directeur de thèse :	**Gérard THOUZEAU**	Directeur de Recherche, LEMAR-CNRS, France
Co-encadrants de thèse :	**Jill SUTTON**	Maitresse de Conférence, LEMAR-UBO, France
	Riccardo RODOLFO-METALPA	Chargé de Recherche, ENTROPIE-IRD, Nouvelle-Calédonie

Remerciements

Je souhaite remercier en premier lieu la région Bretagne et l'Université de Bretagne Occidentale pour le financement de ma thèse, ainsi que l'École Doctorale des Sciences de la Mer et du Littoral (EDSML). Je remercie également Géraldine Sarthou et Luis Tito de Morais, directrice/teur du LEMAR à l'IUEM de Plouzané, ainsi que Claude Payri, directrice d'ENTROPIE au centre IRD de Nouvelle-Calédonie, pour m'avoir accueilli dans leurs laboratoires respectifs.

Je tiens à remercier très sincèrement les membres de mon jury d'avoir accepté d'évaluer mon travail. Merci à Paola Furla et Paolo Montagna d'avoir accepté la lourde charge de rapporter sur cette thèse, et merci à Francesca Benzoni, Jean-Pierre Gattuso et Alexander Venn d'avoir accepté de l'examiner.

La suite de ces remerciements va bien évidemment tout droit à toi, Gérard, mon directeur de thèse, qui m'a encadré pendant ces (un peu plus de) trois années de thèse. Merci de m'avoir fait confiance et de m'avoir soutenu, dès mon poste d'ingénieur au PSO, dans la création de ce projet de thèse qui a demandé quelques années avant de trouver son financement et enfin débuter. Je n'oublie pas toutes les déconvenues et ton soutien sans faille avant même le début de cette thèse ! Tout en me laissant une très grande autonomie, tu as su rester disponible et attentif pour recadrer mon travail et je t'en remercie. Merci pour tes conseils avisés, ta bonne humeur, ton enthousiasme et ta rigueur. J'ai beaucoup appris à tes côtés sur le monde de la recherche, malgré les kilomètres qui nous ont parfois (souvent) séparés et je t'en suis extrêmement reconnaissant. Merci d'avoir été si présent à la fin de cette thèse, jusqu'à la dernière minute, à coups de relectures et de corrections nocturnes.

Un immense merci également à toi, Riccardo, mon co-encadrant de thèse, qui m'a dirigé et encadré en Nouvelle-Calédonie. Merci à toi de m'avoir fait confiance et d'avoir cru à ce projet de thèse. Merci de m'avoir aidé à Nouméa (alors même que la thèse n'était pas encore financée et n'avait pas débuté) pour développer et affiner ce projet à mes côtés. J'ai été très heureux de partager ces nombreuses missions à Bouraké avec toi. Bien que les semaines aient été rythmées par les nettoyages des coraux, les « buoyant weight » interminables, les moustiques, la chaleur et la fatigue, je n'en oublie pas moins les nems pâtes, les One et Gin-tonic, les « Pietro torna indietro », les repas chez Greg et Esmé et cette superbe mission « Supernatural » sur l'Alis. Je te remercie de m'avoir fait découvrir ce site d'exception et de

m’avoir transmis ta passion pour les coraux. Je n’oublie pas non plus notre expérience en aquariums à coups de bricolages, de nettoyages, de mesures, de prélèvements et d’astreintes quotidiennes pendant 4 mois, ni à nouveau les « buoyant weight », PAM ou autres interminables incubations P/R en pleine tachycardie… Merci d’avoir été si présent à coups de relectures et de nombreuses corrections et merci pour ton soutien, tes encouragements, ton honnêteté et ton franc-parler qui m’a souvent fait rire, parfois à mes dépens. Grazie !

Je tiens ensuite à exprimer toute ma gratitude à toi, Jill, ma co-encadrante de thèse, pour ta patience, tes encouragements et ta bienveillance, depuis si longtemps maintenant… (7 ans !) Je te remercie de m’avoir transmis ton savoir dès ces cours « Océan & Climat » en Master, qui sont à l’origine de mon appétence pour ce sujet de thèse. Merci pour tes conseils, ta gentillesse et nos discussions, qui m’ont rappelé qu’il y a aussi une vie en dehors de la thèse…

Un très grand merci à toi, Maxence, mon parrain à l’IUT de Lannion, au Master de Brest et enfin tout au long de cette thèse. Merci pour tout le temps que tu m’as accordé, tes précieux conseils et ton aide sur le Neptune, et merci aussi d’avoir ouvert la voie ! Après avoir été si longtemps dans ton sillage, je compte bien rester encore quelque temps dans tes pattes avec de nombreux futurs projets, car c’est un réel plaisir de travailler avec toi !

Merci à toi, Delphine, d’avoir fait partie de cette aventure. Merci pour ton aide, tes conseils et nos moments à Hawaii. Merci de m’avoir maintenu parfois les pieds sur terre et de me soutenir pour la suite. Et je l’espère, l’aventure continue !

Un grand merci également à ma première co-directrice de thèse, Anne Lorrain, merci pour ton aide, tes précieux conseils et ton suivi dès le montage de ce projet de thèse.

Merci à Claire Rollion-Bard, Sophie Martin et Alexander Venn, membres de mon comité de thèse, pour vos conseils et votre appui scientifique lors de ces réunions annuelles. Merci à Claire pour tes conseils et ton attention aux échéances, Sophie pour m’avoir accueilli à Roscoff pour mes analyses d’alcalinité, Alex pour tes conseils et nos discussions passionnantes, qui m’ont aidé à y voir plus clair sur la calcification et les transports ioniques.

Merci à mes collègues d’avant thèse, les ingénieurs de la plateforme PSO : Oanez, Marie-Laure, Céline, Bleuenn, Anne, Fabien, Philippe, Rudolph, merci à vous pour vos précieux conseils, votre aide sur chacun de vos spectros, ainsi que pour ces pauses de midi au LGO !

Merci aux chercheurs, ingénieurs, techniciens de Nouméa qui ont contribué au grand plaisir que furent mes séjours en Nouvelle-Calédonie. Fanny pour tes conseils, ta gentillesse et surtout ton aide sur ce fameux PAM ! Christine, Magali et Christophe pour votre aide sur le terrain, à l'aquarium, et en labo. Clarisse pour tes précieux conseils, ton aide et pour m'avoir transmis une partie de ton savoir en microbiologie. Merci à Miguel pour toutes tes histoires captivantes lorsque tu nous conduisais dans les mangroves de Bouraké avec l'Aldrick. Merci enfin à Richard Farman, directeur de l'Aquarium des Lagons pour m'avoir accueilli avec mes coraux, ainsi qu'aux équipes techniques pour leur aide lors de mes cultures.

Merci aux gestionnaires et ingénieurs de l'EDSML, de l'IUEM, d'ISblue et de l'IRD de Nouméa pour votre aide et votre bonne humeur. Je pense notamment à Véro, Nathalie, Sonia, Estelle, Elodie, Eric, Riwalenn, Quentin, Maxime, Lionel, Sophie, Nadine et bien d'autres…

Merci à tous les amis doctorants, ou déjà docteurs, aux stagiaires qui m'ont aidé lors de cette thèse, Charlotte et Raphaël. A ceux de l'IRD de Nouméa, Valou, Thibault, Fede, Andreas, Marie, Cinzia, Laure, Martin. Merci pour ces repas au faré, ces soirées à la CPS et au 3B, ces sorties kite et week-end îlots ! Et à ceux du bureau A107 de Brest, José, Maéva, Valentin, Laura, Manon. Merci pour tous ces moments ensembles !

Merci à mes amis de longue date, Anou, JB, Greg, Matou et tous les autres Nantais qui me manquent et que j'espère retrouver vite… Merci à ma super coloc Eva pour ta joie de vivre, ton soutient dans cette dernière ligne droite et nos fous-rires ensemble. Merci à vous tous pour ces précieux moments à profiter de la vie et à penser à autre chose.

Merci à mes amis de Nouméa, à qui je pense chaque jour et qui me manquent beaucoup, Ana, Marie, Manu et les Bétikuré, Marlène, Denis, Thomas, Petite-soeur, Pantoufle, Prz, Manu, Xavier, Cécile, Brioche, Ornella, Rémi, Claire et ma petite ma ma ma, ma ma Manon. Couti revient vite vous faire des endicrenas ! Et oui, il y a bien « deux types de boules » !

Enfin, un immense merci à ma famille. Merci de m'avoir encouragé et soutenu tout au long de ce chemin. Merci d'avoir partagé les moments de joie comme les moments de doutes et d'avoir toujours eu les bons mots pour me donner confiance et me remonter le moral dans les moments difficiles. Et pour tellement plus… Merci !

Allez, Dai !

Avant-Propos

Contexte de la thèse

Les résultats présentés dans ce manuscrit de thèse sont l'aboutissement d'un peu plus de 3 années de travail encadrées par Gérard Thouzeau, Riccardo Rodolfo-Metalpa et Jill Sutton. Cette thèse a été réalisée au sein de deux laboratoires : le laboratoire des sciences de l'environnement marin (LEMAR), à l'Institut Universitaire Européen de la Mer (IUEM) à Plouzané (France), et le laboratoire d'écologie marine tropicale des océans Pacifique et Indien (ENTROPIE) au centre IRD de Nouméa (Nouvelle-Calédonie). Ce travail de thèse, portant sur l'acclimatation des récifs coralliens aux changements climatiques, a débuté par l'échantillonnage des espèces de coraux étudiées en Nouvelle-Calédonie et la mise en place des cultures en aquariums. Les échantillons ont ensuite été préparés, analysés, et les résultats interprétés et discutés au cours de ces années avec l'appui de nombreuses personnes (techniciens, ingénieurs, post-doctorants, chercheurs) au sein de plusieurs équipes de recherches dont :

- L'**Aquarium des lagons** (Nouméa, Nouvelle-Calédonie), où la mise en place des cultures en aquariums et leur suivi ont été réalisés.

- L'équipe technique transversale du **laboratoire Entropie** (Nouméa, Nouvelle-Calédonie), pour les missions de prélèvements et d'échantillonnages en mer, les analyses physiologiques et génétiques des coraux, et les analyses physico-chimiques de l'eau des aquariums.

- L'équipe technique de la plateforme analytique du **Pôle Spectrométrie Océan** (PSO ; Plouzané, France) pour la formation, l'aide technique et les conseils avisés lors des analyses géochimiques sur les différents spectromètres utilisés (GB-IRMS, Kiel IV-MAT253, MC-ICP-MS, HR-ICP-MS et ICP-AES).

Tout au long de ce travail de thèse, de nombreux échanges et collaborations ont permis l'aboutissement de ce manuscrit, en particulier avec certains membres de l'**University of California Los Angeles** (UCLA, Los Angeles, USA), le Climate Change Cluster (C3) de l'**Université Technologique de Sydney** (UTS, Sydney, Australia), la **King Abdullah University of Science and Technology** (KAUST, Thuwal, Saudi Arabia), le **Laboratoire**

d'Océanographie et du Climat (LOCEAN, Paris, France), la **Station Biologique de Roscoff** (CNRS – Sorbonne Université), et le **Centre Scientifique de Monaco** (CSM).

Soutiens financiers

Ce travail de thèse a bénéficié d'une allocation de recherche doctorale cofinancée par la région Bretagne et le Ministère français de l'Enseignement Supérieur et de la Recherche, et attribuée dans le cadre de l'Ecole Doctorale des Sciences de la Mer et du Littoral (EDSML ; Bretagne-Loire).

Les échantillonnages, les cultures en aquariums et les analyses physiologiques ont été financés par le Ministère français des Affaires Etrangères et du Développement International (MAEDI), Fonds Pacifique (n°1976 ; projet SuperCoraux), porteur : Riccardo Rodolfo-Metalpa (IRD). Les échantillonnages et études physiologiques ont également été menés lors de la campagne océanographique « SuperNatural 2 » (https://doi.org/10.17600/18001102) à bord du R/V Alis (Flotte Océanographique Française), porteur : Riccardo Rodolfo-Metalpa.

Le séquençage Illumina de l'étude métagénomique a été mené à l'Australian Genome Research Facility (AGRF) et financé par le conseil australien de la recherche via l'ARC Discovery Early Career Research Award (DE190100142), porteur : Emma Camp (UTS).

Les analyses géochimiques et les différentes mobilités ont été financées par le Centre National de la Recherche Scientifique (CNRS) à travers la Mission pour les Initiatives Transverses et Interdisciplinaires (MITI ; AAP 2020 « Adaptation du vivant à son environnement » ; porteur : Gérard Thouzeau, CNRS) et ont été soutenues par le projet ISblue « Interdisciplinary graduate school for the blue planet » cofinancé par une aide de l'Etat gérée par l'Agence Nationale de la Recherche au titre du programme « Investissements d'Avenir » intégré à France 2030, portant la référence ANR-17-EURE-0015, porteur : Clément Tanvet.

Valorisation de la thèse

Les résultats obtenus dans chaque chapitre de ce manuscrit font l'objet de 4 publications scientifiques (deux publiées, une soumise en cours de révision, et une en préparation) :

Article n°1 **Tanvet C.**, Benzoni F., Peignon C., Thouzeau G. and Rodolfo-Metalpa R. (2022) High coral recruitment despite coralline algal loss under extreme environmental conditions. *Frontiers in Marine Sciences*. https://doi.org/10.3389/fmars.2022.837877 (**Chapitre 3**).

Article n°2 **Tanvet C.**, Camp F.E., Sutton J., Houlbreque F., Thouzeau G. and Rodolfo-Metalpa R. Corals adapted to extreme and fluctuating seawater pH increase calcification rates and modify symbiont communities. *Ecology and Evolution*. https://doi.org/10.1002/ece3.10099 (**Chapitre 4**).

Article n°3 **Tanvet C.**, Guillermic M., Thouzeau G., Rodolfo-Metalpa R. and Sutton J. Distinct physicochemical control of corals calcification to varying pCO_2 identified in geochemical proxies. *Geochimica et Cosmochimica Acta*. *Under review* (**Chapitre 5**).

Article n°4 **Tanvet C.**, Dissard D., Thouzeau G., Guillermic M., Sutton J. and Rodolfo-Metalpa R. First long-term (~30 years) coral acclimatization to ocean acidification recorded in geochemical signatures: A case study from New Caledonia. *In prep*, to be submitted to *Nature Communications* (**Chapitre 6**).

Les travaux réalisés lors de cette thèse font également l'objet de 2 publications annexes (une publiée et une en cours de révision) :

Article annexe n°1 Jacquemont J., Houlbrèque F., **Tanvet C.**, and Rodolfo-Metalpa R. (2022). Long-term exposure to an extreme environment induces species-specific responses in corals' photosynthesis and respiration rates. *Marine Biology*, 1–15. https://doi.org/10.1007/s00227-022-04063-6.

Article annexe n°2 Thibon F., Comeau S., Rodolfo-Metalpa R., Montanes M., Counillon L., McCulloch M., **Tanvet C.**, Poet M., Télouk P., and Vigier N. Internal pH regulation traced by Li isotopes in tropical corals exposed to high pCO_2. *Proceedings of the Royal Society B: Biological Sciences*. *Under review*.

En parallèle des publications scientifiques, les résultats de cette thèse ont été présentés lors de 4 conférences scientifiques (trois internationales et une nationale) :

- **Congrès ICRS 2021** (Brème, Allemagne) – **Tanvet C.**, Govan S. and Rodolfo-Metalpa R. Physiological plasticity of corals long-life acclimatized to naturally constant and extreme pH variability. (Présentation orale).

- **Congrès ICRS 2022** (Brème, Allemagne) – **Tanvet C.**, Dissard D., Guillermic M., Sutton J., Thouzeau G., Butscher J., Dubosc J. and Rodolfo-Metalpa R. First long-term (~30 years) coral acclimatization to ocean acidification recorded in geochemical signatures: A case study in New Caledonia. (Présentation orale).

- **Congrès Goldschmidt 2022** (Honolulu, Hawaii) – **Tanvet C.**, Guillermic M., Sutton J., Rodolfo-Metalpa R., Thouzeau G., Butscher J., Dubosc J. and Dissard D., First long-term (~30 years) coral acclimatization to ocean acidification recorded in geochemical signatures: A case study in New Caledonia. https://doi.org/10.46427/gold2022.10776 (Poster).

- **Colloque "ID en action" 2022 de la MITI-CNRS** au siège du CNRS (Paris, France) – **Tanvet C.**, Rodolfo-Metalpa R., Sutton J., Guillermic M., Dissard D., Benzoni F., Camp F.E. et Thouzeau G., Projet ACLICOST, Acclimatation des récifs coralliens aux changements globaux: Utilisation des signatures isotopiques pour évaluer l'impact de l'acidification des océans. (Présentation orale).

Table des matières

Remerciements 3
Avant-Propos 6
Table des matières 11
CHAPITRE 1 | INTRODUCTION GÉNÉRALE 15
1.1 Les récifs coralliens 17
1.1.1 Histoire et classification des coraux 17
1.1.2 Services écosystémiques des récifs coralliens 18
1.1.3 Les récifs coralliens inscrits au Patrimoine Mondial de l'UNESCO 18
1.2 Ecophysiologie des coraux 20
1.2.1 La biominéralisation du squelette calcaire 20
1.2.2 Les transports ioniques et la pompe à protons 23
1.2.3 L'association symbiotique des coraux 24
1.2.4 Le recrutement corallien et le stade juvénile 27
1.2.4.1 La reproduction des coraux 27
1.2.4.2 Interactions avec les algues coralliennes encroûtantes 29
1.3 Les coraux face aux changements climatiques 30
1.3.1 Impacts des changements climatiques sur les récifs coralliens 30
1.3.2 Acclimatation et adaptation des coraux aux changements climatiques 35
Encadré 1.A | Acclimatation versus adaptation 35
1.3.3 Les analogues naturels, modèles des prévisions climatiques 37
1.4 Les proxies géochimiques 39
1.4.1 Les isotopes du carbone et de l'oxygène 39
1.4.2 Les isotopes du bore 40
1.4.3 Les rapports élémentaires 42
OBJECTIFS DE LA THÈSE 43
CHAPTER 2 | MATERIALS AND METHODS 47

2.1 Study sites and species....49
2.1.1 The semi-enclosed lagoon of Bouraké....49
2.1.2 Biological materials: model species....50
2.2 Physiological measurements....51
2.2.1 Skeleton growth rate....51
2.2.2 Photosynthesis and respiration rates....52
2.2.3 Tissue parameters and surface measurements....53
2.2.4 Photosynthetic efficiency....54
2.3 Metagenomic analyses....56
2.3.1 DNA extraction....56
2.3.2 PCR amplification....57
2.3.3 Sequencing....57
2.4 Geochemical measurements....58
2.4.1 Laboratory facilities....58
2.4.2 Sample preparation....58
2.4.3 Stable carbon and oxygen isotopes....59
2.4.4 Boron purification....60
2.4.5 Stable boron isotope....61
2.4.6 Elemental ratio measurements....63
CHAPTER 3 | INFLUENCE OF CRUSTOSE CORALLINE ALGAE ON CORAL RECRUITMENT UNDER EXTREME AND VARIABLE ENVIRONMENT....65
3.1 Preamble....67
3.2 Article n°1: High coral recruitment despite coralline algal loss under extreme environmental conditions....68
CHAPTER 4 | PHYSIOLOGICAL RESPONSES OF CORALS TO VARYING pCO_2 CONDITION....89
4.1 Preamble....91
4.2 Article n°2: Corals adapted to extreme and fluctuating seawater pH increase calcification rates and have unique symbiont communities....92
CHAPTER 5 | PHYSIOCHEMICAL CONTROL OF CORAL CALCIFICATION....121

5.1 Preamble 123

5.1 Article n°3: Geochemical proxies reveal physiochemical control of calcification by corals exposed to naturally variable pCO_2 levels 124

CHAPTER 6 | RECORDS OF CORAL ACCLIMATIZATION IN GEOCHEMICAL SIGNATURES 147

6.1 Preamble 149

6.2 Article n°4: First long-term (~30 years) acclimatization of corals to ocean acidification recorded in geochemical signatures: A case study from New Caledonia 150

CHAPITRE 7 | SYNTHÈSE ET PERSPECTIVES 167

APPENDICES 182

Appendix Article n°1 - Chapter 3 184

Appendix Article n°2 - Chapter 4 191

Appendix Article n°3 - Chapter 5 206

Appendix Article n°4 - Chapter 6 216

Article annex n°1 218

Article annex n°2 233

INDEX OF FIGURES 258

INDEX OF TABLES 265

LEXICON 269

BIBLIOGRAPHY 271

CHAPITRE 1

INTRODUCTION GÉNÉRALE

Cette thèse porte sur la capacité des coraux tropicaux à faire face au changement climatique rapide. A travers une étude couplant écophysiologie, métagénomique et géochimie, l'objectif est d'étudier les mécanismes d'acclimatation, voire d'adaptation, de ces coraux aux changements climatiques. Des analogues naturels permettent d'évaluer l'impact potentiel de ces changements, caractérisés par une baisse du pH et de l'oxygène dissous, et une hausse de la température des océans. L'état de l'art des impacts des changements climatiques sur les récifs coralliens est présenté avant les objectifs détaillés de la thèse. Dans un premier temps, la classification des coraux, le rôle fondamental des récifs coralliens pour la biodiversité marine et leurs contributions bénéfiques pour la population humaine sont détaillés. La seconde partie traite de la complexité fonctionnelle et de l'écophysiologie des coraux. Les différents mécanismes d'acclimatation et d'adaptation des coraux face aux changements climatiques sont ensuite définis grâce à l'existence d'un analogue naturel en Nouvelle-Calédonie : la lagune semi-fermé de Bouraké. Enfin, les différents outils géochimiques utilisés pour permettre d'identifier ces mécanismes chez trois espèces de coraux branchus (*Acropora tenuis* et *Montipora digitata*) et massif (*Porites* sp.) sont présentés.

1.1 Les récifs coralliens

1.1.1 Histoire et classification des coraux

Souvent confondu avec une concrétion minérale, les coraux sont des invertébrés très anciens vivants dans l'océan. Au sein du règne animal, ils appartiennent au groupe des cnidaires (Verrill, 1865) qui seraient apparus dans les océans lors de la première ère géologique de l'histoire de la Terre, d'après des fossiles datés du Précambrien (~700 millions d'années). Les cnidaires existent sous deux formes différentes, les formes fixées (polypes : anémones de mer et coraux) et les formes libres (méduses). Quelle que soit leur forme, les cnidaires sont constitués d'un corps mou essentiellement composé d'eau. Les tissus mous hébergent une cavité gastrique ouverte sur l'extérieur par une bouche entourée de tentacules. Les anémones de mer et les coraux, qui présentent uniquement la phase polype fixé, sont regroupés au sein de la classe des Anthozoaires (Ehrenberg, 1834).

Les coraux bâtisseurs de récifs, ou scléractiniaires (anciennement appelés « madréporaires » ; Bourne, 1900), sont des coraux durs ; ils constituent, grâce à leur squelette fait de carbonate de calcium ($CaCO_3$), la formation naturelle bioconstruite la plus importante de notre planète : les récifs coralliens. Ces derniers sont réputés être la seule construction animale sur Terre visible depuis l'espace. Si les premiers fossiles de scléractiniaires connus remontent à environ 240 millions d'années, l'étude de l'ADN des

espèces vivantes a montré qu'ils sont plus anciens et qu'ils remonteraient au Paléozoïque, il y a 425 millions d'années. Leur diversité actuelle comprend plus de 800 espèces (Hoeksema and Cairns, 2022; Horton *et al.*, 2022). Les récifs coralliens se développent principalement dans les eaux chaudes des zones géographiques tropicales et équatoriales, dans les premières dizaines de mètres de la zone euphotique (couche supérieure de l'océan).

1.1.2 Services écosystémiques des récifs coralliens

Les récifs coralliens sont un réservoir de vie dans l'océan, abritant près de 30% de la biodiversité marine sur moins de 0,2% de la surface totale des océans. A titre d'exemple, 1km² de barrière corallienne équivaut à la biodiversité marine de l'ensemble des côtes de l'hexagone français. Les récifs coralliens tropicaux sont l'un des écosystèmes les plus diversifiés de la planète avec une richesse exceptionnelle d'environ 830 000 espèces estimées (Fisher *et al.*, 2015). La structure complexe (3D) des récifs fournit un abri important à une majorité d'espèces et génère des échanges trophiques diversifiés au sein de ces écosystèmes (Graham and Nash, 2013). Les produits de la pêche dans les environnements récifaux sont sources de subsistance et de revenus monétaires importants, particulièrement pour les populations proches du littoral (Golden *et al.*, 2016). Les zones récifales fourniraient 9 à 12% des poissons consommés dans le monde ; près de 6 millions de personnes en dépendent directement pour leur survie (Cinner, 2014). A titre d'exemple, entre 2009 et 2013, la pêche côtière à Hawaii a représenté plus de 7 millions de repas par an (Grafeld *et al.*, 2017). Le « tourisme récifal » est également une source notable de revenus, représentant 30% du tourisme mondial pour un apport global de 35,8 milliards de dollars américains par an (Spalding *et al.*, 2017). Les récifs coralliens contribuent aussi à la protection du littoral, en luttant contre l'érosion du trait de côte et en réduisant les impacts des évènements météorologiques, pour les populations et les infrastructures côtières (Beck *et al.*, 2018). En dissipant jusqu'à 97% de l'énergie des vagues, cette protection du littoral profite à 197 millions de personnes qui vivent à moins de 10 m d'altitude et dans un rayon de 50 km à partir des récifs (Ferrario *et al.*, 2014). Il est estimé que plus de 15% de la population mondiale dépend en partie ou en totalité des écosystèmes coralliens (Hoegh-Guldberg, 1999) ; ces derniers représenteraient dans leur globalité une valeur d'actifs de 9 900 milliards de dollars américains par an (Costanza *et al.*, 2014).

1.1.3 Les récifs coralliens inscrits au Patrimoine Mondial de l'UNESCO

L'Organisation des Nations Unies pour l'éducation, la science et la culture (UNESCO) a classé au patrimoine mondial les récifs coralliens les plus exceptionnels (en taille et en diversité). Dès

1981, la Grande Barrière de corail (GBR), qui s'étale le long des côtes du Nord-Est de l'Australie, fut reconnue comme la plus grande barrière récifale sur Terre. Le second plus grand récif se situe en Nouvelle-Calédonie, avec la plus longue barrière récifale continue, soit 1 600 km (**Figure I-1**).

Figure I-1 | *Photographies du lagon de Nouvelle-Calédonie (photo de gauche ; © M. Dosdane) et de sa barrière récifale (photo de droite ; © P.-A. Pantz)*

Cette barrière est inscrite au patrimoine mondial de l'UNESCO depuis 2008. L'archipel de Nouvelle-Calédonie, situé au cœur de l'Océan Pacifique sud et découvert en 1774 par James Cook, forme le lagon le plus grand du monde avec 24 000 km² (**Figure I-1**). Les récifs coralliens de Nouvelle-Calédonie présentent une diversité de formes récifales qui a été décrite pour la première fois par Charles Darwin lors de son voyage sur le Beagle (Darwin, 1842) :

- Les récifs frangeants (« *fringing reefs* ») : de faible profondeur, ils bordent le littoral et maintiennent une zone active de développement vers le large. L'accumulation de coraux morts côté littoral va former un platier avec le temps, qui deviendra un lagon de largeur variable.
- Les récifs barrières (« *barrier reefs* ») : ce sont d'anciens récifs frangeants qui se sont nettement éloignés du littoral vers le large (plusieurs kilomètres) en raison de l'enfoncement de l'île par un effet de subsidence (**Figure I-2**).
- Les atolls (« *atolls* ») : dernière évolution du récif, ce sont d'anciens récifs barrières ; ils se forment lorsque l'île a partiellement ou totalement disparu sous la mer, comme l'atoll d'Ouvéa en Nouvelle-Calédonie.

Figure I-2 | *Photographie de la pente externe d'un récif barrière sur la côte ouest de la Grande Terre en Nouvelle-Calédonie (© F. Benzoni).*

Les récifs coralliens de Nouvelle-Calédonie sont parmi les plus riches et les plus diversifiés au monde ; ils comptent 390 espèces de coraux durs, soit un tiers des espèces de coraux durs actuelles. Dans la région Indo-Pacifique, un hot spot de diversité des coraux durs (> 500 espèces), le « triangle de corail », concentre une des plus grandes biodiversités marines au monde (invertébrés, poissons, plantes) dans la zone englobant la Papouasie-Nouvelle-Guinée, les Philippines, les îles Salomon, et une partie de l'Indonésie et de la Malaisie. La proximité géographique de la Nouvelle-Calédonie, située à l'est de la mer de Corail et au sud du « triangle de corail », explique en partie la richesse de ses récifs coralliens. En 2014, le gouvernement néo-calédonien a créé une aire marine protégée afin de protéger et de valoriser ses écosystèmes marins uniques au monde : le Parc naturel de la mer de Corail. Cette aire marine protégée s'étend sur près de 1,3 million de kilomètres carrés et représente la deuxième plus grande zone économique exclusive (ZEE) de la France (derrière la Polynésie Française).

1.2 Ecophysiologie des coraux

1.2.1 La biominéralisation du squelette calcaire

La formation du squelette des coraux est l'étape principale de la croissance du corail. Ce squelette, formé de carbonate de calcium ($CaCO_3$), nécessite un apport suffisant en ions calcium (Ca^{2+}) et carbonate (CO_3^{2-}) pour sa formation. Le Ca^{2+} est naturellement présent dans le milieu extérieur ; en ce qui concerne le carbonate, plusieurs origines sont possibles en fonction de la forme chimique de ce carbone inorganique. Trois formes chimiques de carbone inorganique dissous (CID) existent dans l'eau selon le pH du milieu (**Figure I-3**).

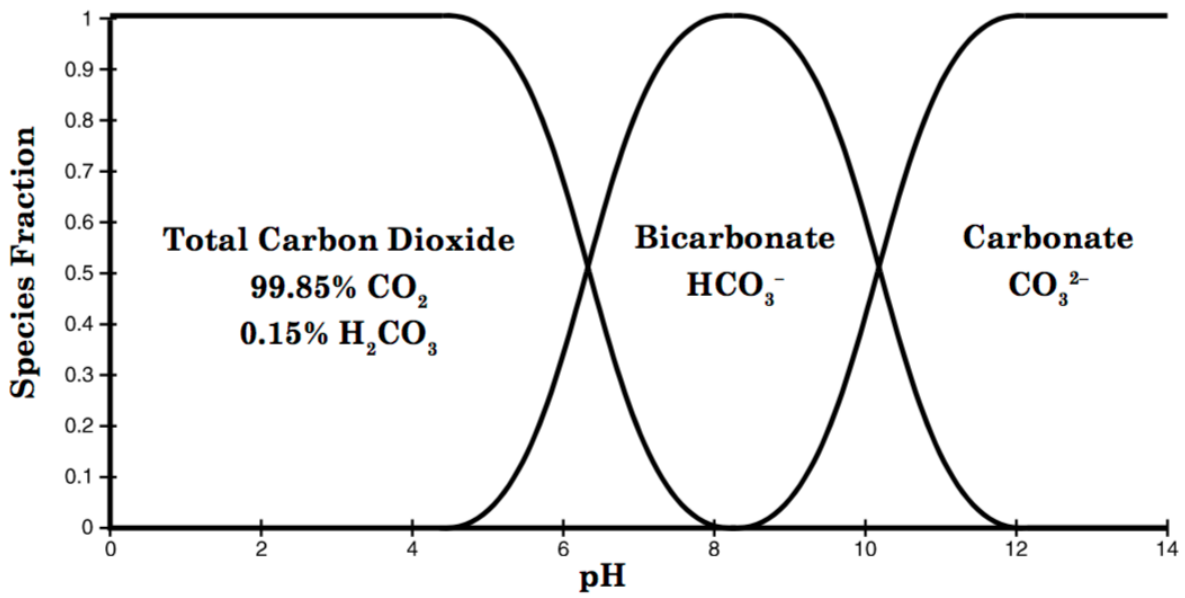

Figure I-3 | *Diagramme de prédominance des espèces de carbone inorganique dissous en fonction du pH (© J.A. Wojtowicz, 2001).*

La forme chimique de carbone inorganique dissous utilisée lors de la calcification implique des réactions de calcification qui diffèrent, de telle sorte que :

(I.1) $$Ca^{2+} + CO_2 + H_2O \leftrightarrow CaCO_3 + 2H^+$$

(I.2) $$Ca^{2+} + HCO_3{}^- \leftrightarrow CaCO_3 + H^+$$

(I.3) $$Ca^{2+} + CO_3{}^{2-} \leftrightarrow CaCO_3$$

Ces différentes réactions chimiques produisent plus ou moins de protons H^+ qui doivent être éliminés afin de maintenir des conditions de pH permettant d'augmenter l'état de saturation en aragonite (Ω_{Ar}) (une des formes cristallines du $CaCO_3$) et donc la précipitation du $CaCO_3$. Dans un milieu environnant tel que l'eau de mer (pH # 8,1), le carbone inorganique dissous est plutôt sous forme de bicarbonate. Le processus de calcification aussi appelé minéralisation biologiquement contrôlée ou biominéralisation des coraux, est donc plutôt traduit par l'équation de réaction I.2 (Furla *et al.*, 2000; Allemand *et al.*, 2004; Tambutté *et al.*, 2011). Toutefois, l'élimination de protons produit par l'équation I.2 est plus énergivore pour le corail (McCulloch *et al.*, 2012b). Dans le contexte des changements climatiques en cours, l'acidification des océans (cf. 1.3.2) réduit la concentration des carbonates tout en augmentant celle des bicarbonates, rendant la calcification plus complexe.

Le polype minéralise son squelette de carbonate de calcium à sa base. Les polypes constituent la partie vivante du corail, avec le cœnosarque entre eux (**Figure I-4**). Les tissus oraux font face au milieu environnant (eau de mer), tandis que les tissus aboraux font face au squelette.

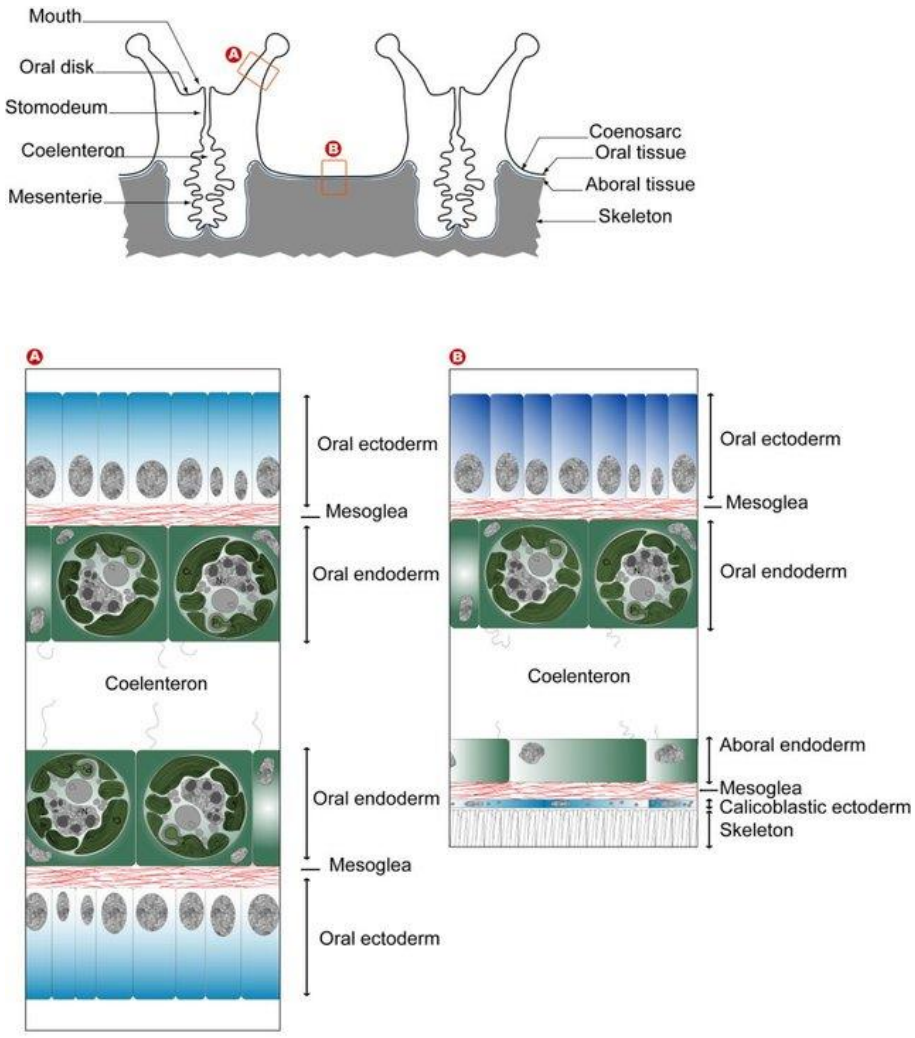

Figure I-4 | *Histologie d'un polype de corail (A) et du cœnosarque (B). D'après Vidal-Dupiol et al. (2009).*

Les coraux sont des organismes diploblastiques, à deux feuillets cellulaires, l'ectoderme et l'endoderme. Ces deux feuillets sont séparés par une substance extracellulaire de consistance gélatineuse : la mésoglée. La cavité délimitée par l'endoderme correspond à la cavité gastrique de l'animal, le cœlentéron. Le tissu hébergeant la calcification est l'épithélium calicoblastique (**Figure I-4**). Il existe un espace de largeur assez variable entre l'épithélium calicoblastique et le squelette que l'on nomme l'espace subcalicoblastique. La précipitation des cristaux d'aragonite ($CaCO_3$) se déroule dans cet espace au sein d'un milieu calcifiant extracellulaire (MCE) (Simkiss and Wilbur, 1989 ; Venn *et al.*, 2019). Le MCE, formant une sorte d'hydrogel composé de protéines et de polysaccharides accueillerait la première étape de la formation du cristal d'aragonite : la nucléation (Venn *et al.*, 2011). Il a été suggéré que les premières étapes de la calcification impliquent au préalable une phase transitoire de carbonate de calcium amorphe (CCA) dans les cellules calicoblastiques avant que ce CCA ne

soit finalement relâché dans le MCE où la cristallisation se produit (Mass *et al.*, 2017 ; Schmidt *et al.*, 2022).

1.2.2 Les transports ioniques et la pompe à protons

Le transport du matériel nécessaire à la calcification, (les ions Ca^{2+} et CO_3^{2-}), du milieu environnant vers les différentes couches de tissus jusqu'au MCE, est complexe et reste sujet à de nombreuses interrogations. Les cellules d'un tissu peuvent être liées les unes aux autres par deux types de jonctions, les jonctions septées (fermées) et les jonctions communicantes (ouvertes). Tandis que les jonctions septées impliquent un transport ionique préférentiellement par voie transcellulaire (via des enzymes spécialisées), les jonctions communicantes laissent passer de façon sélective certaines molécules en fonction de leur taille ou de leur charge. Il s'avère donc indispensable de déterminer la concentration ionique et le pH dans le fluide de calcification (pH_{MCE}) afin de comprendre les mécanismes de biominéralisation. Plusieurs études ont montré une élévation du pH_{MCE} amenant à une augmentation du $[CO_3^{2-}]_{MCE}$ et donc de l'état de saturation en aragonite $(\Omega_{Ar})_{MCE}$ chez les coraux (Jokiel, 2013 ; Allison *et al.*, 2014 ; McCulloch *et al.*, 2017). Le pH_{MCE} atteindrait des valeurs bien supérieures à celles de l'eau de mer environnante (Ries, 2011 ; McCulloch *et al.*, 2012a ; Venn *et al.*, 2019). Cette régulation du pH_{MCE} mobiliserait des transports ioniques actifs via l'activité enzymatique des ATPases dont la Ca-ATPase. Ces transports actifs permettraient l'échange de Ca^{2+} par des protons H^+, créant ainsi un « gradient de protons » à travers les couches calcifiantes des coraux (Al-Horani *et al.*, 2003 ; Venn *et al.*, 2022). Les coraux utilisent deux voies de transport ionique pour leur calcification, les voies paracellulaire (passive) et transcellulaire (active) (Barott *et al.*, 2015). Toutefois, le transport actif serait majoritaire dans le MCE par rapport au transport passif, en raison d'une plus forte imperméabilité paracellulaire, liée aux caractéristiques des jonctions septées de l'ectoderme calicoblastique (Venn *et al.*, 2022). Dans un contexte d'acidification des océans, une baisse de cette perméabilité a cependant été observée (Venn *et al.*, 2020). Le transport actif, basé sur l'activité enzymatique des ATPases et nommé mécanisme de « pompe à protons » (**Figure I-5**), consomme de l'énergie fournie par le métabolisme (McCulloch *et al.*, 2012b). La production d'ATPases dépend du taux de respiration des mitochondries, lui-même dépendant des produits de la photosynthèse des symbiontes (Al-Horani *et al.*, 2003 ; Wooldridge, 2009). Ces derniers ont ainsi un rôle fondamental dans la production d'énergie pour les transports ioniques transcellulaires des coraux (Al-Horani *et al.*, 2003).

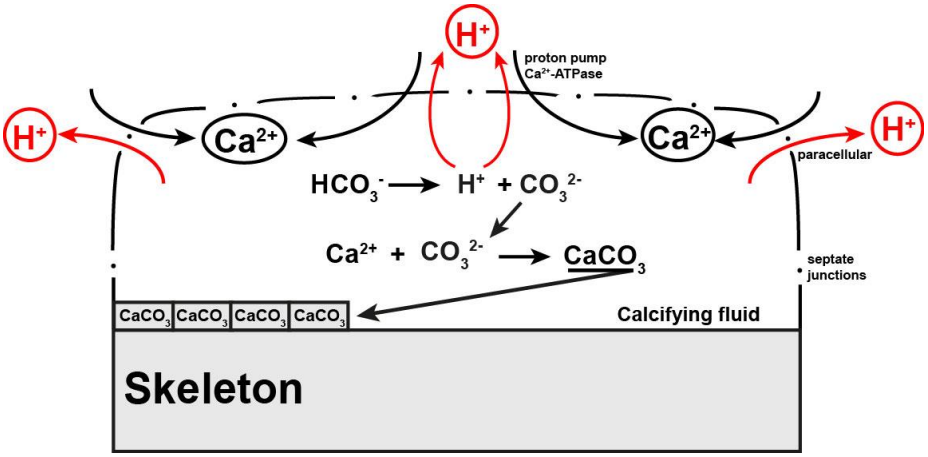

Figure I-5 | *Schéma de fonctionnement de la "pompe à protons" (modifié d'après Eagle R., comm. pers.)*

1.2.3 L'association symbiotique des coraux

La symbiose est une relation écologique durable entre deux ou plusieurs organismes d'espèces différentes, profitable à chacun d'eux. L'un des deux partenaires de la symbiose est appelé l'hôte (le plus gros des deux) et l'autre le symbionte (le plus petit des deux) ; ensemble, ils forment l'holobionte.

Cette association spécifique et durable entre deux espèces inclue plusieurs types de symbiose (Douglas, 1998; Paracer and Ahmadjian, 2000) :

- Le *mutualisme* : les deux symbiontes tirent profit de l'association (ex : le gobie et la crevette-pistolet) ;

- Le *commensalisme* : un des deux symbiontes tire un bénéfice de l'association sans nuire ni favoriser l'autre symbionte (ex : le rémora et le requin) ;

- Le *parasitisme* : un seul symbionte tire profit de l'association tandis que l'autre est pénalisé (ex : le poisson clown et l'isopode).

Les coraux scléractiniaires pratiquent la symbiose mutualiste avec des microalgues photosynthétiques unicellulaires, les dinoflagellés (Muscatine and Porter, 1977). Ces microalgues, de la famille des Symbiodiniaceae, mesurent entre 6 et 12 µm de diamètre ; elles sont communément appelées zooxanthelles (**Figure I-6**). Elles sont situées dans le cytoplasme des cellules de l'endoderme oral et aboral de l'hôte corallien.

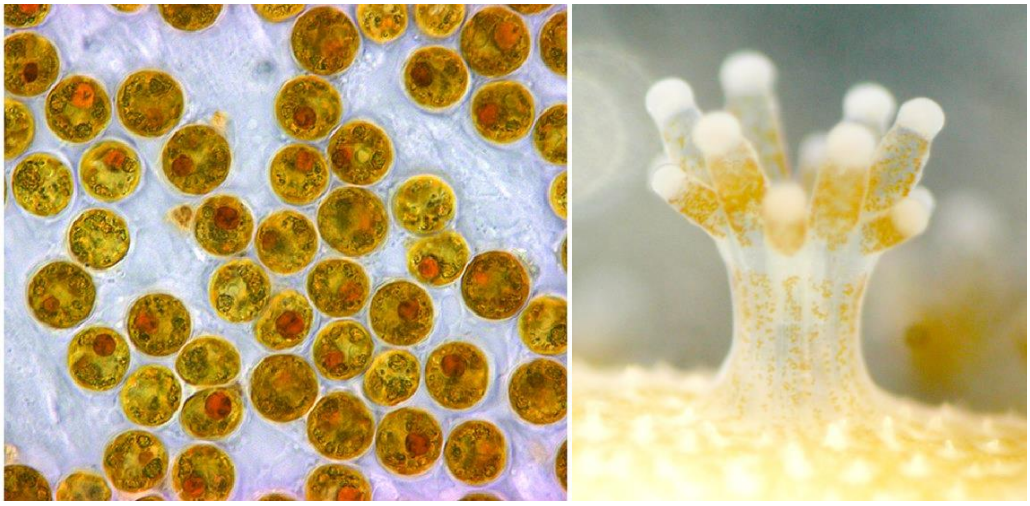

Figure I-6 | *Photographies de Symbiodiniaceae (à gauche ; © T.C. LaJeunesse) et d'un polype de corail en symbiose avec des Symbiodiniaceae (à droite ; © C. Shinzato)*

Les symbiontes coralliens ont initialement été classés en différents clades au sein du genre *Symbiodinium* (Blank and Trench, 1985), avant d'être récemment révisés en genres distincts au sein de la famille des Symbiodiniaceae nouvellement décrite par LaJeunesse *et al.* (2018). Cette nouvelle classification phylogénétique décrit six nouveaux genres en fonction de la composition génétique et de la diversité des espèces (**Figure I-7**).

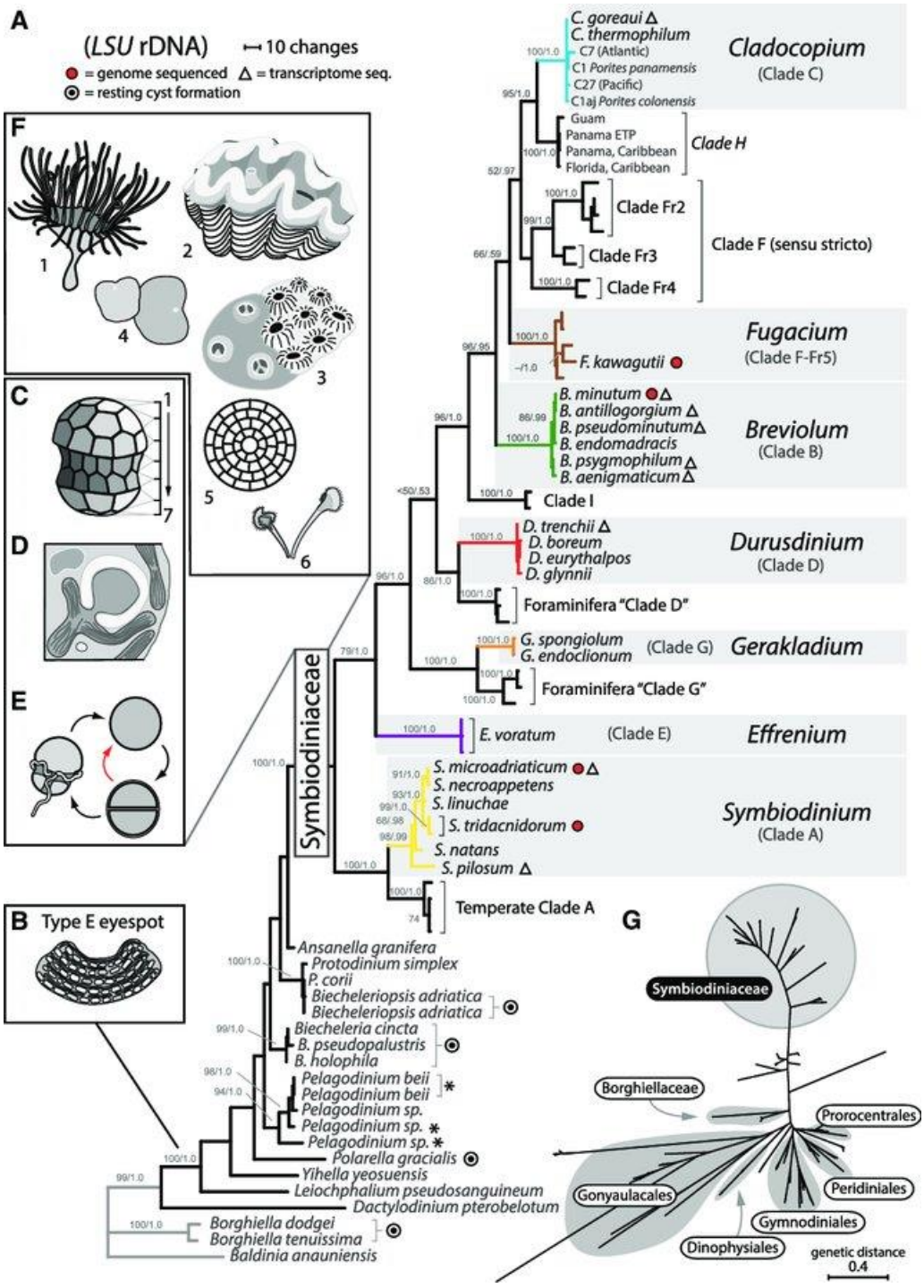

Figure I-7 | *Classification phylogénétique révisée des genres de Symbiodiniaceae. D'après LaJeunesse et al. (2018).*

L'hôte peut s'associer avec un ou plusieurs genres de symbiontes (Thornhill *et al.*, 2009 ; Silverstein *et al.*, 2012 ; Baums *et al.*, 2014). Ces associations sont flexibles et peuvent changer au cours de la vie de l'hôte corallien (Baker, 2003 ; Cunning *et al.*, 2017). Cette flexibilité s'opère selon deux modalités d'acquisition des symbiontes, plus ou moins privilégiées selon l'espèce corallienne : l'acquisition horizontale (transfert via l'environnement)

et l'acquisition verticale (transmission maternelle) (Stat *et al.*, 2008 ; Quigley *et al.*, 2017 ; Epstein *et al.*, 2019a).

Le genre *Cladocopium* (clade C) est le plus abondant et le plus largement représenté au sein des Symbiodiniaceae. De nombreuses espèces de coraux associées à ce genre ont été observées dans différents environnements (LaJeunesse *et al.*, 2003). Les coraux associés au genre *Cladocopium* démontrent des capacités d'adaptation et des performances physiologiques accrues parmi l'ensemble des genres (Cantin *et al.*, 2009 ; Howells *et al.*, 2012 ; Schoepf *et al.*, 2015 ; Morgans *et al.*, 2020). Le genre *Durusdinium* (Clade D) comprend, lui, des espèces thermo tolérantes permettant à l'hôte corallien de mieux résister aux épisodes de blanchissement (Silverstein *et al.*, 2017 ; Haydon *et al.*, 2021). En contrepartie, une diminution des performances physiologiques, en termes de croissance des individus hôtes, a été observée (Jones and Berkelmans, 2010).

Les environnements marginaux (mangroves, sources hydrothermales, zones intertidales), caractérisés par des conditions environnementales extrêmes et/ou fluctuantes, présentent des associations corail-symbiontes spécifiques (Schoepf *et al.*, 2015, 2020 ; Camp *et al.*, 2020 ; Haydon *et al.*, 2021). Alors que l'environnement local va, en fonction de l'espèce corallienne, influencer significativement une association symbiotique acquise de manière horizontale, l'acquisition « verticale » va transmettre cette association d'une génération à l'autre (Quigley *et al.*, 2019). La flexibilité de l'association symbiotique joue ainsi un rôle déterminant dans les capacités d'adaptation de l'hôte corallien (Putnam *et al.*, 2012 ; Grottoli *et al.*, 2018 ; Epstein *et al.*, 2019b ; Voolstra and Ziegler, 2020). Il est donc d'autant plus important d'étudier la mise en place de ces associations symbiotiques lorsque les individus adultes d'un même site présentent des capacités d'acclimatation, voire d'adaptation (cf. 1.3.2).

1.2.4 Le recrutement corallien et le stade juvénile

1.2.4.1 La reproduction des coraux

La reproduction des coraux est étudiée depuis plus de 200 ans, Cavolini (c. 1790, cité dans De Lacaze-Duthiers, 1873) ayant été le premier à la documenter en observant la planula (larve ciliée) du genre *Astroides* en Méditerranée (Harrison and Wallace, 1990). Depuis, le processus reproducteur a été très documenté et notamment depuis les années 80 lorsque les premières observations de pontes des coraux ont été faites sur la Grande Barrière de corail en Australie et sur la barrière de Nouvelle-Calédonie. Il existe quatre types de reproduction sexuée chez les coraux, liés à deux modes sexuels (hermaphrodisme et gonochorisme) et à deux types de fécondation (interne et externe). Parmi les coraux, on distingue ainsi :

- La fécondation externe et l'hermaphrodisme : les coraux hermaphrodites relâchent des gamètes mâles et femelles dans un œuf qui se dissout dans l'eau de mer lors d'une ponte massive et synchrone. Il s'agit du type de reproduction le plus courant (plus de 75% des coraux).

- La fécondation externe et le gonochorisme : les coraux possèdent un seul sexe, mâle ou femelle, et relâchent des gamètes correspondantes (spermatozoïdes ou ovules) dans l'eau de mer lors d'une ponte massive et synchrone.

- La fécondation interne et l'hermaphrodisme : les polypes des coraux hermaphrodites s'auto-fécondent et libèrent des larves (planula) dans l'eau.

- La fécondation interne et le gonochorisme : seuls les spermatozoïdes sont émis dans l'eau et viennent féconder l'ovule dans la cavité gastrique du polype femelle. Les larves (planula) sont ensuite libérées dans l'eau.

La ponte des coraux est un phénomène synchrone qui a lieu quelques nuits après la première pleine lune d'été ; elle ne dure que quelques heures. La libération synchrone des gamètes est corrélée avec le cycle lunaire et dépend également de nombreux autres facteurs environnementaux comme la température de l'eau, le cycle nycthéméral ou encore les vents et les courants (Harrison, 2011). Lorsque les conditions sont optimales, les coraux libèrent leurs œufs et des millions de gamètes qui vont remonter à la surface, donnant l'impression de « neige à l'envers », du fait de leur haute teneur en lipides moins denses que l'eau de mer (Arai *et al.*, 1993). Après la fécondation des gamètes, le développement des larves planula (**Figure I-8**) va durer de 4 à 7 jours avant leur fixation sur un substrat naturel (Babcock and Heyward, 1986). Une fois fixé, le premier calice du squelette calcaire se forme et permet la croissance du premier polype du juvénile corallien (**Figure I-8**). À la fixation, les algues corallines (de la famille des Corallinacées) constituent un substrat de colonisation préférentiel pour les larves de coraux (Morse *et al.*, 1988 ; Heyward and Negri, 1999 ; Harrington *et al.*, 2004 ; Nelson, 2009 ; Price, 2010).

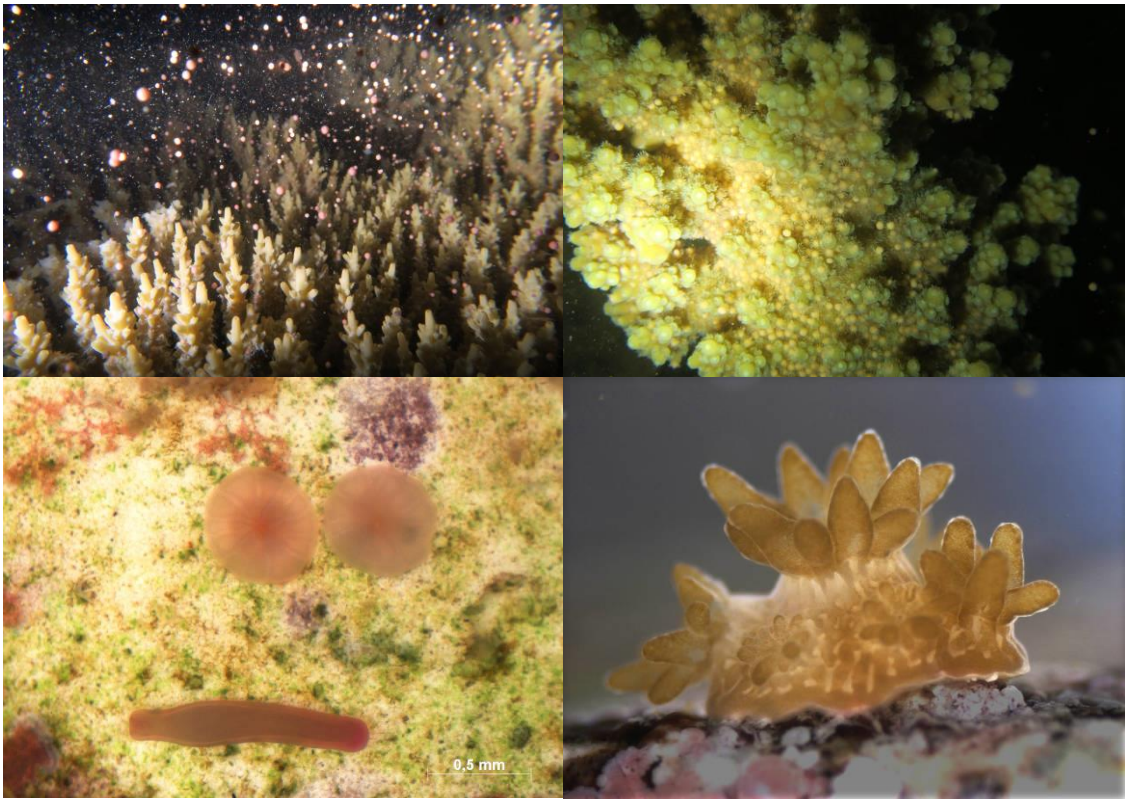

Figure I-8 | *Photographies de pontes de corail (photos du haut) : le corail relâche ses œufs roses composés de gamètes mâles et femelles (© C. Alessi). Photographies d'une larve planula et de deux premiers calices fixés sur un substrat naturel (en bas à gauche), et d'un individu juvénile (en bas à droite) (© D. Petersen).*

1.2.4.2 Interactions avec les algues coralliennes encroûtantes

Les algues coralliennes encroûtantes sont des algues rouges calcaires appartenant à l'ordre des Corallinales (Rhodophyta) (Heyward and Negri, 1999) (**Figure I-9**) qui inclut trois familles : les Corallinaceae (Lamouroux, 1812), les Lithophyllaceae (Athanasiadis, 2016), et les Porolithaceae (R.A. Townsend & Huisman, 2018). Ces algues ont notamment été observées comme étant d'excellents substrats naturels pour la fixation des larves planula des coraux grâce aux stimulants chimiques provenant des composés associés à leur paroi (glycoglycérolipides et polysaccharides) et, dans une moindre mesure, à leur biofilm bactérien (Morse *et al.*, 1988 ; Harrington *et al.*, 2004 ; Tebben *et al.*, 2015 ; Gómez-Lemos *et al.*, 2018). Ces interactions « fondamentales » à la métamorphose entre les algues coralliennes encroûtantes et les larves planula permettent le renouvellement des récifs coralliens (O'Leary *et al.*, 2012). Toutefois, cette fonctionnalité écologique est fragile en raison de facteurs abiotiques, tels que la lumière et la sédimentation (Fabricius and Wolanski, 2000 ; Bessell-Browne *et al.*, 2017), et biotiques via les interactions trophiques avec d'autres espèces d'algues, de poissons et de bryozoaires (Penin *et al.*, 2011 ; Fabricius *et al.*, 2015 ; Elmer *et*

al., 2018 ; Jorissen *et al.*, 2020). Cette niche écologique est d'autant plus menacée aujourd'hui par les changements climatiques, en particulier l'acidification des océans et l'augmentation de la température (Martin and Gattuso, 2009 ; Doropoulos *et al.*, 2012 ; Webster *et al.*, 2013 ; Mccoy and Kamenos, 2015 ; Cornwall *et al.*, 2021b).

Figure I-9 | *Photographies de Corallinales dans le lagon de Bouraké (© R. Rodolfo-Metalpa).*

1.3 Les coraux face aux changements climatiques

1.3.1 Impacts des changements climatiques sur les récifs coralliens

Depuis la troisième révolution industrielle dans les années 1970, les océans ont absorbé plus d'un quart des émissions de dioxyde de carbone (CO_2) provenant des activités humaines, et la quasi-totalité de la chaleur accumulée dans l'atmosphère par l'effet de serre (Gattuso *et al.*, 2015). Les océans recouvrent 71 % de la surface du globe, et absorbent près de 30 % des émissions de CO_2 anthropiques. Grâce à la photosynthèse, les forêts et les océans sont des puits de carbone essentiels pour la régulation du climat. De par leur taille, les océans sont plus performants que les forêts dans ce rôle de régulation en concentrant en leur sein plus de 50 fois la quantité de CO_2 présente dans l'atmosphère. La concentration de CO_2 atmosphérique est passée de 315 ppm en 1960 à 417 ppm en 2022, soit une augmentation de plus de 30 % en 62 ans, alors qu'elle a oscillée grossièrement entre 190 et 270 ppm pendant plus de 800 000 ans (The Keeling Curve, Scripps Institution of Oceanography at UC San Diego, USA ; keelingcurve.ucsd.edu). Cette teneur en CO_2 atmosphérique pourrait dépasser les 1000 ppm d'ici la fin du siècle d'après les prévisions du Groupe d'experts Intergouvernemental sur l'Evolution du Climat (GIEC) (IPCC Report, 2021) dans le scénario RCP (« Representative

Concentration Pathways ») le plus pessimiste. Les conséquences de cette augmentation sans précédent du CO_2 atmosphérique sur les écosystèmes coralliens sont dramatiques, rapides et imprévisibles via trois phénomènes climatiques principaux : l'acidification (Hoegh-Guldberg *et al.*, 2017), le réchauffement (Hughes *et al.*, 2018), et la désoxygénation (Hughes *et al.*, 2020) des océans.

- ***L'acidification des océans (AO)***

L'élévation des concentrations de CO_2 atmosphérique augmente le CO_2 dissous sous forme d'acide carbonique dans l'océan. La dissociation de l'acide carbonique en ions bicarbonate et carbonate va ensuite libérer des protons H^+ et entraîner une diminution du pH de l'eau de mer (**Figure I-10**). Comme mentionné précédemment (1.2.1), la prédominance des espèces carbonatées dépend du pH de l'eau de mer : l'acidification des océans induit une diminution des concentrations en ions carbonate CO_3^{2-} et de l'état de saturation en aragonite (Ω_{Ar}) de l'eau de mer. Or, la saturation de l'eau de mer en aragonite ($\Omega_{Ar} > 1$) permet sa précipitation tandis qu'une sous-saturation ($\Omega_{Ar} < 1$) engendre sa dissolution. La précipitation de $CaCO_3$ pour la calcification du squelette corallien devient donc plus limitée en conditions d'acidification des océans (AO) (Orr *et al.*, 2005). Cornwall *et al.* (2021a) ont estimé que la baisse du $CaCO_3$ produit par les coraux d'ici la fin du siècle atteindrait -76% pour le scénario du GIEC le plus optimiste (RCP 2.6), et -156% pour le scénario le plus pessimiste (RCP 8.5).

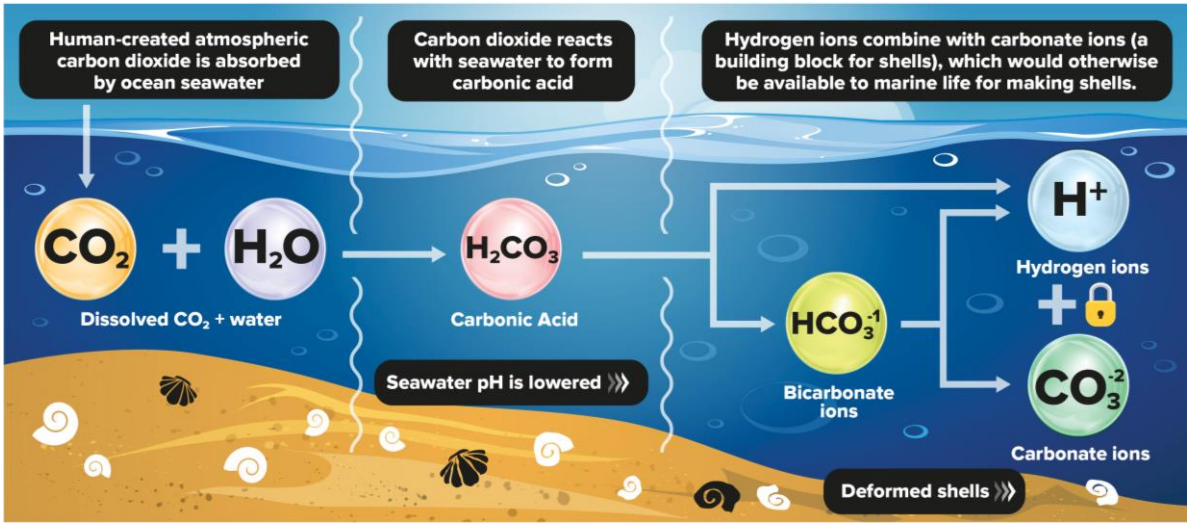

Figure I-10 | *Hydrolyse et dissociation du CO_2 dans l'océan (© UC Davis Biological Sciences, 2018).*

A titre d'exemple, et d'après les simulations de Cao *et al.* (2014), quand le CO_2 atmosphérique atteint 4 fois son niveau préindustriel (1120 ppm), la profondeur à partir de laquelle l'aragonite (Ω_{Ar}) de l'eau de mer est en sous-saturation (<1) chute de 1288 à 143 m. Depuis le début de l'ère industrielle, l'acidité des océans, mesurée par la baisse du pH de 8,2 à 8,1 (Howes *et al.*,

2015), a augmenté de 26% en raison de l'augmentation du CO_2 dissous dans l'eau de mer. Bien que plusieurs études aient montré l'effet négatif de l'AO sur la calcification des coraux (Gattuso *et al.*, 1998 ; Langdon *et al.*, 2000 ; Doney *et al.*, 2009 ; Kroeker *et al.*, 2010), d'autres travaux mentionnent des réponses plus variables et fonction des espèces de coraux considérées (Ries *et al.*, 2009 ; Fabricius *et al.*, 2011 ; Rodolfo-Metalpa *et al.*, 2011 ; Georgiou *et al.*, 2015 ; Comeau *et al.*, 2017, 2019a ; Schoepf *et al.*, 2017 ; Cornwall *et al.*, 2018). L'acidification des océans a récemment fait l'objet d'une revue nuançant son effet catastrophique sur la calcification et le devenir des coraux et soulignant l'importance d'étudier aussi bien la disparition de certaines espèces que la persistance d'autres en réponse à l'AO (Leung *et al.*, 2022).

- ***Le réchauffement des océans (RO)***

Le réchauffement de l'atmosphère implique une élévation de la température d'une grande partie de la zone euphotique des océans (~75 m). Cette augmentation de la température de surface de l'eau de mer peut entraîner la rupture de la symbiose entre le corail hôte et les zooxanthelles (Hoegh-Guldberg, 1999). Face au réchauffement, les zooxanthelles ne sont plus capable de transformer l'énergie lumineuse en composés organiques et il en résulte une surproduction de radicaux oxygénés (O_2^-, H_2O_2 et HO^-). Ces espèces réactives de l'oxygène (ROS = Reactive Oxygen Species) s'accumulent dans le corail au point de devenir toxique en endommageant l'ADN, les lipides et les protéines, ce qui conduit à la nécrose cellulaire (Fridovich, 1998 ; Halliwell and Gutteridge, 1999 ; Weis, 2008). Les coraux possèdent certaines défenses pour éliminer les ROS, telle que l'utilisation de métallo-enzymes antioxydantes (e.g., superoxyde dismutase) (Fridovich, 1998 ; Halliwell and Gutteridge, 1999). Lorsque les teneurs en ROS sont trop élevées par contre, ils rompent leurs associations avec les zooxanthelles par nécrose, apoptose ou exocytose des cellules symbiotiques (Steen and Muscatine, 1987 ; Brown *et al.*, 1995 ; Weis, 2008). L'expulsion des zooxanthelles laisse apparaitre des tissus translucides, au travers desquels le squelette blanc de carbonate de calcium devient visible par transparence (Fitt *et al.*, 2000) : on parle alors de blanchissement corallien. Le corail peut survivre sans symbiontes sur une courte période, mais un blanchissement prolongé conduit à la mort des individus, voire de la colonie (**Figure I-11** ; Grottoli *et al.*, 2004 ; Rodrigues and Grottoli, 2007 ; Anthony *et al.*, 2009 ; Ainsworth and Brown, 2021).

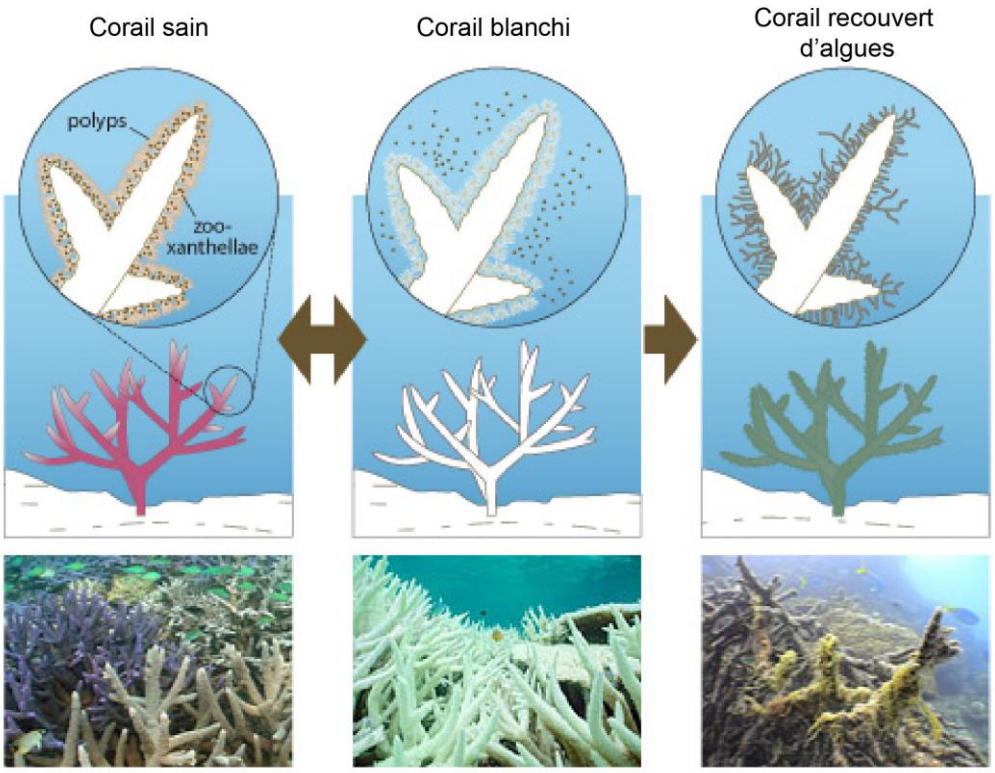

Figure I-11 | *Evolution temporelle du blanchissement corallien (© GBR Marine Park Authority)*

Une température plus élevée de 1 à 2°C de la surface des océans peut suffire à provoquer un épisode de blanchissement. De plus en plus d'épisodes de blanchissement massif des coraux sont signalés sur la GBR depuis les trente dernières années, avec une recrudescence d'épisodes très sévères (1998, 2002, 2016, 2017, 2020 et 2022) (Hoegh-Guldberg, 1999; Hughes *et al.*, 2018a; McClanahan *et al.*, 2019). C'est à la fois la fréquence et l'intensité de ces épisodes qui ne cessent d'augmenter (Ainsworth *et al.*, 2016; Hughes *et al.*, 2017, 2018b). En 1998, soit l'un des épisodes les plus sévères jamais enregistré, la mortalité des coraux a atteint 80 à 90% par endroits sur la GBR en Australie (Hoegh-Guldberg, 1999). Le dernier épisode de blanchissement (2022) fait partie des trois plus importants (avec 1998 et 2016), avec plus de 91% des récifs touchés dont près de la moitié de façon extrême (**Figure I-12**). Le GIEC prévoit une hausse de la température de surface de + 2°C d'ici 2050 dans le scénario de stabilisation des émissions de CO_2 dans l'atmosphère (RCP 4.5) (IPCC Report, 2022), ce qui pourrait faire disparaître la quasi-totalité des coraux dans le monde.

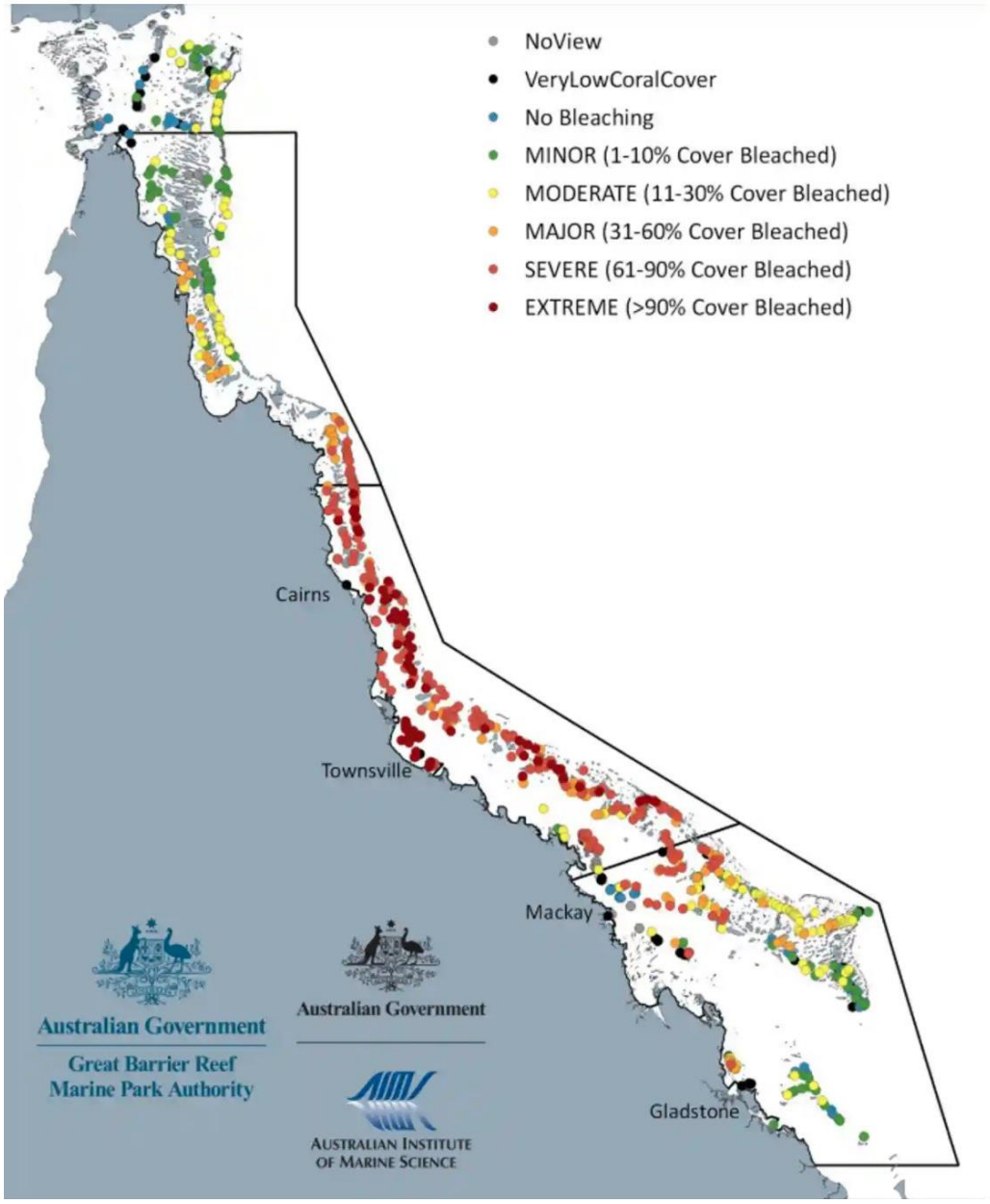

Figure I-12 | *Épisode de blanchissement des coraux sur la GBR en 2022, en pourcentage de la surface des récifs touchés (© GBR Marine Park Authority)*

- ***La désoxygénation des océans (DO)***

Le réchauffement des eaux de surface de l'océan augmente sa stratification et isole les eaux froides profondes. La diminution du mélange vertical de l'eau diminue sa ventilation et donc son oxygénation. Cette baisse de la pression partielle en oxygène (pO_2) conduit à une saturation en oxygène plus faible et à une augmentation des besoins microbiens en oxygène (Breitburg *et al.*, 2018) ; on parle alors de désoxygénation des océans. Cette dernière est

aggravée à une échelle plus locale, près des côtes, par la pollution des eaux résultant des activités humaines (agriculture, urbanisation et industrialisation). L'eutrophisation accrue des eaux de surface augmente les besoins en oxygène pour la reminéralisation de la matière organique par les bactéries aérobies. Dans les cas extrêmes, la respiration de ces bactéries diminue la pO_2, produit simultanément du CO_2, et aggrave l'acidité du milieu, générant des « zones mortes » anoxiques où les espèces animales tels que les coraux meurent (Altieri *et al.*, 2017). Les impacts de la désoxygénation des océans et les seuils de tolérance associés pour les récifs coralliens sont encore peu étudiés malgré le risque que cette désoxygénation peut engendrer sur la survie des coraux (Nelson and Altieri, 2019 ; Hughes *et al.*, 2020). Les quelques études portant sur les récifs coralliens ont montré des seuils de tolérance entre 3 et 4 mg O_2 L^{-1} (équivalent à 45-50% de saturation en oxygène à 27°C), seuils en dessous desquels le métabolisme du corail serait perturbé, pouvant entrainer une perte des tissus et la mort du corail (Haas *et al.*, 2014; Altieri *et al.*, 2017; Nelson and Altieri, 2019; Hughes *et al.*, 2020). Le GIEC prévoit une extension des OMZ (zones de minimum d'oxygène : < 2 mg O_2 L^{-1}) aux latitudes tropicales de près de 10% d'ici la fin du siècle (IPCC Report, 2021).

Les effets combinés des stress environnementaux (OA, RO et DO) sont annoncés dramatiques pour l'écosystème corallien (Bijma *et al.*, 2013 ; Breitburg *et al.*, 2018 ; Sampaio *et al.*, 2021). Face à ce « trio mortel », la grande majorité des récifs coralliens risque de se dégrader rapidement voire de disparaître d'ici 2050, avec les conséquences économiques qui en résulteront pour les plus de 500 millions de personnes qui en dépendent directement (Hoegh-Guldberg *et al.*, 2017 ; T. P. Hughes *et al.*, 2018b ; D. J. Hughes *et al.*, 2020).

1.3.2 Acclimatation et adaptation des coraux aux changements climatiques

Avant de discuter des mécanismes d'acclimatation voire d'adaptation des coraux face aux changements climatiques, la définition de ces termes est présentée dans l'encadré 1.A.

Encadré 1.A | Acclimatation versus adaptation

L'acclimatation est une modification phénotypique (anatomique, morphologique, moléculaire, physiologique, ou éthologique) rapide et réversible, présentée par un individu en réponse à un changement environnemental ; on parle également de **plasticité phénotypique**. Ce phénomène, apparaissant au cours de la vie d'un organisme, est sans base génétique et donc non transmissible sauf par des mécanismes **épigénétiques**. Les modifications épigénétiques concernent des changements dans l'activité des gènes, n'impliquant pas de

modifications de la séquence d'ADN et pouvant être transmis lors des divisions cellulaires. Contrairement aux mutations qui affectent la séquence d'ADN, les modifications épigénétiques sont réversibles. Par exemple, les jeunes saumons et esturgeons qui naissent en rivière connaissent des modifications physiologiques lors de leur migration vers la mer qui durent pendant plusieurs mois et leur permettent de supporter le changement de salinité. Ces modifications sont réversibles, puisque les individus reviendront se reproduire en eau douce à l'âge adulte : il s'agit bien d'une acclimatation ou plasticité phénotypique.

L'adaptation est un processus d'évolution qui produit un nouveau trait phénotypique d'un organisme, lui permettant de s'adapter à son environnement. Cette capacité d'évolution se produit à l'échelle d'une population ou d'une espèce, et non à celle d'un individu. L'adaptation est un phénomène irréversible transmissible à la descendance et modifiant le génome d'une population ou d'une espèce. L'évolution d'un nouveau trait phénotypique se produit par le biais de la sélection naturelle des individus résistants appartenant à une population exposée sur plusieurs générations.

Les mécanismes d'acclimatation et d'adaptation ne sont pas exclusifs, une plasticité transgénérationnelle sur de nombreuses générations pourrait faciliter l'adaptation chez les coraux. Le fait de distinguer la plasticité transgénérationnelle des autres formes de plasticité, et leur importance relative par rapport à l'adaptation génétique des coraux, requiert une large gamme d'espèces à tester avec des plans expérimentaux robustes (Torda *et al.*, 2017).

Comme mentionné précédemment, il est prévu que les facteurs de stress tels que l'OA, le RO et la DO impactent fortement les récifs coralliens qui devraient connaître un déclin dramatique d'ici 2050 (Hoegh-Guldberg *et al.*, 2017). De nombreuses études ont toutefois démontré des réponses spécifiques aux espèces et un potentiel d'acclimatation physiologique voire d'adaptation des coraux à l'un de ces stress et/ou à leur combinaison (Ries *et al.*, 2009 ; Rodolfo-Metalpa *et al.*, 2011 ; Cornwall *et al.*, 2018 ; Jury and Toonen, 2019 ; Altieri *et al.*, 2021 ; Carbonne *et al.*, 2021 ; Bove *et al.*, 2022 ; Comeau *et al.*, 2022).
Au regard de la calcification, la réponse aux stress hautement variable des espèces de coraux, notamment à l'AO réside dans le fait que certaines espèces seraient plus susceptibles que d'autres de réguler leur pH interne (pH_{ECM}) via la pompe à protons (cf. 1.2.2) (Ries, 2011 ; McCulloch *et al.*, 2012a ; Venn *et al.*, 2019 ; Guillermic *et al.*, 2021). Ainsi, certains coraux sont capables de maintenir, voire d'augmenter, leur taux de calcification malgré des valeurs élevées de pCO_2 (Ries *et al.*, 2009 ; Rodolfo-Metalpa *et al.*, 2010 ; Comeau *et al.*, 2013 ; Carbonne *et al.*, 2021 ; Cameron *et al.*, 2022). En parallèle du mécanisme de pompe à protons, les coraux

peuvent concentrer leurs apports en CID et en calcium dans les cellules calcifiantes (Furla *et al.*, 2000 ; Allison *et al.*, 2014 ; Decarlo *et al.*, 2018).

Parmi les hypothèses expliquant la résistance des coraux aux stress environnementaux tels que l'OA, le RO et la DO, figure le fait que les coraux exposés de manière chronique à une forte variabilité de ces stress seraient plus résistants aux changements futurs (Oliver and Palumbi, 2011a ; Enochs *et al.*, 2020 ; Schoepf *et al.*, 2020 ; Brown *et al.*, 2022 ; Comeau *et al.*, 2022). En revanche, ce postulat reste assez discuté car il est loin d'être systématique et il semble dépendre des espèces et de la durée d'exposition au(x) stress (Camp *et al.*, 2016 ; Rivest *et al.*, 2017 ; Cornwall *et al.*, 2018 ; Rathbone *et al.*, 2021).

Les mécanismes possibles d'acclimatation et/ou d'adaptation comprennent la plasticité physiologique mais aussi les modifications épigénétiques et/ou les modifications du microbiome des coraux (Putnam *et al.*, 2016 ; Camp *et al.*, 2017, 2020 ; Voolstra and Ziegler, 2020). Les réponses des coraux dépendent en grande partie de l'association entre l'hôte et ses algues symbiotiques (Berkelmans and Van Oppen, 2006 ; Jones *et al.*, 2008 ; Oliver and Palumbi, 2011). En effet, en s'associant avec certains genres de Symbiodiniaceae (Suggett *et al.*, 2017 ; LaJeunesse *et al.*, 2018), l'hôte corallien peut améliorer sa plasticité physiologique aux conditions environnementales (Jones *et al.*, 2008; Hume *et al.*, 2016; Grottoli *et al.*, 2018; Howells *et al.*, 2020). Ainsi, certains coraux vivant dans des environnements extrêmes sont associés à des symbiontes du genre *Durusdinium* (clade D), considéré comme un genre résistant au stress (Schoepf *et al.*, 2015 ; Haydon *et al.*, 2021 ; Ros *et al.*, 2021). Cependant, les apports bénéfiques des associations entre l'hôte et les Symbiodiniaceae restent en grande partie méconnus et difficiles à identifier.

1.3.3 Les analogues naturels, modèles des prévisions climatiques

Les changements climatiques sont si rapides qu'ils en deviennent perceptibles pour les générations humaines actuelles. Cependant, la prédiction, à l'échelle de la fin du siècle, des impacts de ces changements et des mécanismes d'acclimatation et/ou d'adaptation des écosystèmes, tels que les récifs coralliens, reste incertaine. En dehors de l'expérimentation en laboratoire, des réponses peuvent être apportées via l'étude de sites naturels particuliers présentant des conditions de température, de pH ou d'oxygène dissous extrêmes, proches des conditions futures : on parle alors d'analogues naturels. Ces systèmes naturels incluent les sources volcaniques hydrothermales (Hall-Spencer *et al.*, 2008 ; Fabricius *et al.*, 2011 ; Rodolfo-Metalpa *et al.*, 2011, 2015 ; Kamenos *et al.*, 2016 ; Agostini *et al.*, 2018 ; Pichler *et al.*, 2019 ; Enochs *et al.*, 2020 ; Teixidó *et al.*, 2020 ; Comeau *et al.*, 2022), les récifs

macrotidaux (Palumbi *et al.*, 2014 ; Schoepf *et al.*, 2015, 2020 ; Klepac and Barshis, 2020), les mangroves (Camp *et al.*, 2016b, 2019 ; Haydon *et al.*, 2021 ; Ros *et al.*, 2021), et les baies semi-fermées (Camp *et al.*, 2017; Kurihara *et al.*, 2021; Maggioni *et al.*, 2021; Jacquemont *et al.*, 2022 (Appendix Article n°1); Tanvet *et al.*, 2022). Ces environnements extrêmes (**Figure I-13**) présentent l'avantage de pouvoir offrir des stocks génétiques de coraux tolérants aux stress des conditions climatiques futures (Camp *et al.*, 2018).

Les expériences de laboratoire, limitées à de courtes durées, relèvent souvent d'un défi complexe pour combiner artificiellement tous les paramètres environnementaux, et se révèlent moins robustes que les systèmes naturels (Page *et al.*, 2022). Au contraire, les analogues naturels permettent d'étudier des processus d'acclimatation/adaptation qui se déroulent sur de longues échelles de temps et sur plusieurs générations.

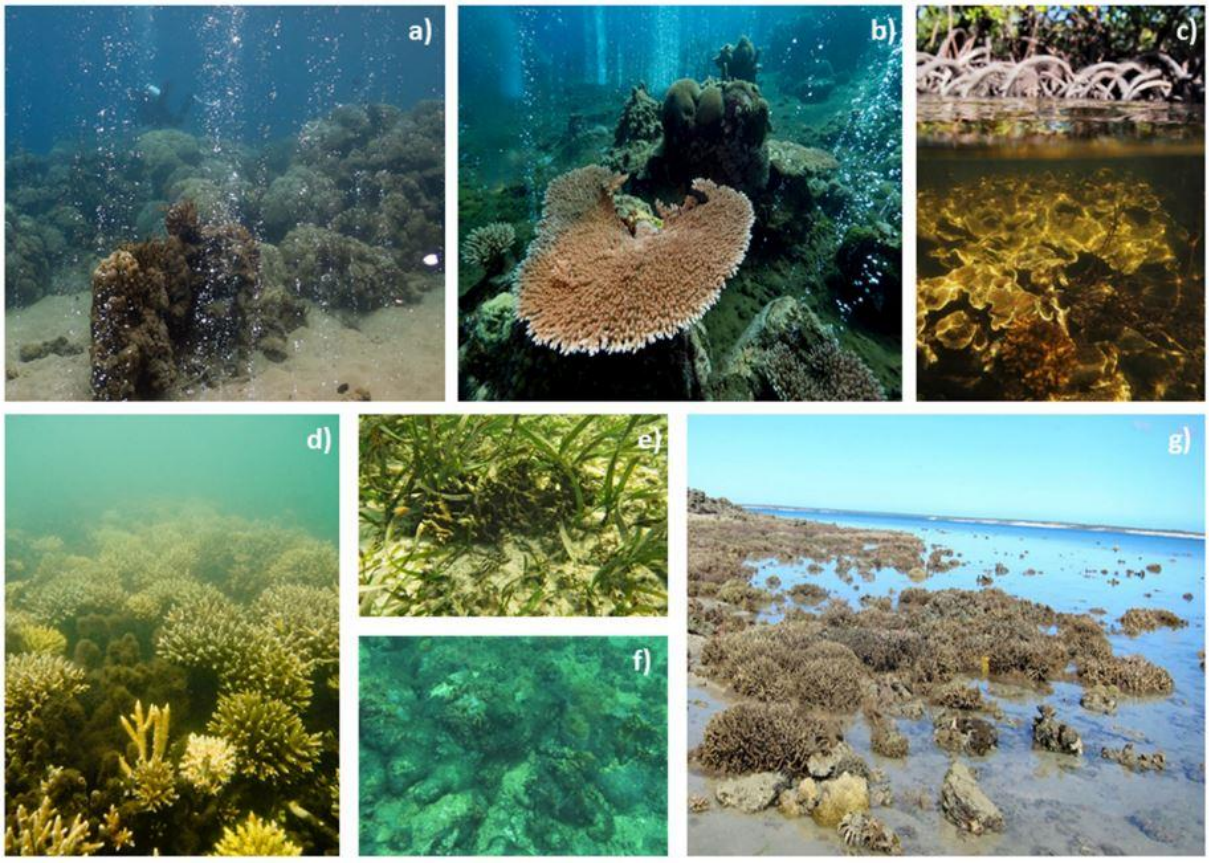

Figure I-13 | *Photographies de différents environnements coralliens extrêmes et marginaux. (a,b) Sites hydrothermaux en Papouasie-Nouvelle-Guinée (© R. Rodolfo-Metalpa et J.M. Boré), (c) système de mangrove de la GBR (© E. Camp), (d) système de Bouraké en Nouvelle-Calédonie (© E. Camp), (e) herbier marin des îles Caïmans (© E. Camp), (f) récif turbide de Salvador au Brésil (© E. Camp), (g) récif macrotidal de Kimberley (© V. Schoepf). D'après* Camp *et al.* (2018).

1.4 Les proxies géochimiques

1.4.1 Les isotopes du carbone et de l'oxygène

Les isotopes sont des éléments chimiques « X » ayant le même numéro atomique (nombre de protons) « Z » mais une masse atomique (nombre de nucléons) « A » différente ($^{A}_{Z}X$). Il existe deux isotopes stables du carbone dont l'un est très abondant et l'autre peu : ^{12}C (98.98%) et ^{13}C (1.11%). De la même manière, l'oxygène possède trois isotopes stables : ^{16}O (99.763%), ^{17}O (0.037%), et ^{18}O (0.199%). La composition isotopique d'un élément montre des variations liées à des mécanismes physico-chimiques et biologiques : on parle de fractionnement isotopique. Ces variations, souvent faibles, sont comparées à une valeur standard et exprimées par la notation conventionnelle delta (δ) en pour mille (‰), telle que :

(I.4) $$\delta^{13}C\ (‰) = 1000 \times \left(\frac{^{13}C/^{12}C_{Echantillon}}{^{13}C/^{12}C_{PDB}} - 1\right)$$

(I.5) $$\delta^{18}O\ (‰) = 1000 \times \left(\frac{^{18}O/^{16}O_{Echantillon}}{^{18}O/^{16}O_{PDB}} - 1\right)$$

Une valeur positive de δ représente un enrichissement en isotope lourd (^{13}C et ^{18}O), alors qu'une valeur négative représente un enrichissement en isotope léger (^{12}C et ^{16}O) par rapport au standard de référence. Le standard de référence utilisé pour le $\delta^{13}C$ et le $\delta^{18}O$ est un fossile de bélemnites (céphalopode) du Crétacé supérieur provenant de la formation de Pee Dee en Caroline du Sud (USA) ; il est nommé le Pee Dee Bélemnite (PDB). Aujourd'hui, d'autres références existent tels que le Vienna PDB (V-PDB) ou le SMOW (ou V-SMOW) pour 'Standard Mean Ocean Water', ce dernier servant de référence uniquement pour l'oxygène. Des standards de synthèse du PDB et du SMOW sont désormais élaborés par l'AIEA (Agence Internationale à l'Energie Atomique), basée à Vienne, d'où le « Vienna- » que l'on ajoute à leur nom.

Les différences de compositions isotopiques sont dues au fractionnement isotopique, lui-même dépendant de mécanismes physico-chimiques et biologiques. La mesure du $\delta^{13}C$ et du $\delta^{18}O$ dans le squelette calcaire ($CaCO_3$) du corail permet donc d'identifier les fractionnements isotopiques qui ont lieu lors de la biominéralisation. La mesure de ces fractionnements permet finalement de tracer des processus tels que les effets vitaux métaboliques, c'est-à-dire la photosynthèse et la respiration (assimilation préférentielle des isotopes légers par l'organisme), et les effets cinétiques (discrimination entre isotopes lourds et légers lors des réactions de dissociation du CO_2) (McConnaughey, 1989).

En plus de tracer les processus métaboliques des coraux, le $\delta^{18}O$ est utilisé en paléoclimatologie pour caractériser les températures du passé dans différentes matrices. Il est mesuré ainsi dans les carottes de glace polaire, dans les carottes de coraux, dans les foraminifères, dans certains mollusques, etc. Le $\delta^{18}O$ varie en fonction du fractionnement entre ^{18}O et ^{16}O qui dépend directement de la température ambiante (discrimination entre les isotopes lourds et légers lors de l'évaporation et de la condensation de H_2O). Toutefois, dans les modèles biologiques tels que les coraux, d'autres processus (notamment métaboliques) entrent en jeu et peuvent également modifier la composition isotopique du carbone et de l'oxygène et rendre leurs interprétations paléoclimatiques complexe : on parle alors « d'effets vitaux ».

1.4.2 Les isotopes du bore

Le bore est un élément conservatif dans l'océan avec un temps de résidence long (14 millions d'années) (Lemarchand *et al.*, 2000). Il existe sous deux formes dans l'océan : l'acide borique trigonal $B(OH)_3$ et l'ion borate tétraédrique $B(OH)_4^-$. La constante de dissociation de l'acide borique, égale à 8,6 (Dickson, 1990), est proche du pH de l'eau de mer (~8,1). Des changements légers du pH de l'eau de mer impliquent donc de fortes variations dans l'abondance des deux formes de bore (**Figure I-14**).

Il existe deux isotopes stables du bore avec des abondances différentes : ^{10}B (19.9%) et ^{11}B (80.1%). De la même manière que pour le carbone et l'oxygène, les variations isotopiques du bore sont exprimées par le $\delta^{11}B$:

(I.6) $$\delta^{11}B\ (‰) = 1000 \times \left(\frac{^{11}B/^{10}B_{Echantillon}}{^{11}B/^{10}B_{NIST\ 951a}} - 1\right)$$

Le matériel de référence utilisé pour le $\delta^{11}B$ est le standard NIST SRM 951a.

L'acide borique ($B(OH)_3$) est enrichi en ^{11}B comparé à l'ion borate ($B(OH)_4^-$), avec un écart constant entre les deux espèces chimiques donné par le facteur de fractionnement (α). Ce facteur a été déterminé empiriquement à 27.2 ± 0.6 ‰ dans l'eau de mer par Klochko *et al*. (2006). Comme les formes de bore sont directement dépendantes du pH, le $\delta^{11}B$ peut être utilisé comme un proxy fiable du pH et plus particulièrement du pH_{ECM} des coraux (**Figure I-14**). Il a ainsi été établi que le pH_{ECM} des coraux peut être calculé selon l'équation suivante (Eq I.7) (Hemming and Hanson, 1992; Zeebe and Wolf-Gladrow, 2001) :

(I.7) $$pH_{ECM} = pK_B - log\left(\frac{\delta^{11}B_{CS} - \delta^{11}B_{ECM}}{\delta^{11}B_{ECM} - (\alpha \times \delta^{11}B_{CS}) - 1000(\alpha - 1)}\right)$$

Le pK_B représente la constante de dissociation de l'acide borique ; il est calculé en fonction de la température et de la salinité (i.e., 8,5975 à une température de 25°C, une salinité de 35, et à pression atmosphérique) (Dickson, 1990). Le $\delta^{11}B_{CS}$ et le $\delta^{11}B_{ECM}$ représentent respectivement la composition isotopique du Bore dans le squelette corallien et dans le fluide calcifiant. α représente la constante d'équilibre des isotopes du Bore.

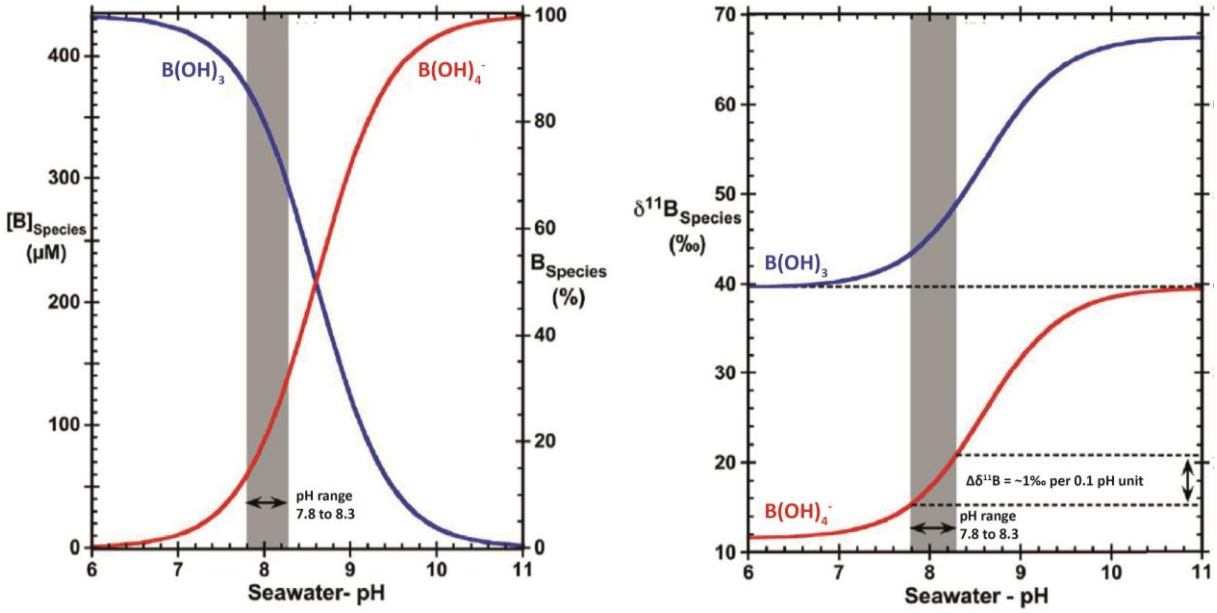

Figure I-14 | *Diagramme de spéciation des formes de bore dans l'eau de mer en fonction du pH (à gauche) ; $\delta^{11}B$ des formes de bore inorganique dissous en fonction du pH de l'eau de mer (à droite). Modifié d'après Guillermic et al. (2020).*

Il a été suggéré, que parmi les deux formes de bore, l'ion borate soit la seule forme incorporée dans le squelette aragonitique des coraux (Hemming and Hanson, 1992) pour être ensuite remplacé par les ions carbonates (CO_3^{2-}) dans le réseau d'aragonite (Mavromatis *et al.*, 2015; Noireaux *et al.*, 2015). Cependant, plusieurs équations de substitution ont été proposées pour maintenir l'équilibre des charges lors de la substitution de $B(OH)_4^-$ par CO_3^{2-} dans les cristaux d'aragonite, ce qui a donné lieu à des définitions divergentes du coefficient de partage B/Ca (K_D) (Eq I.8) (McCulloch *et al.*, 2017b; Decarlo *et al.*, 2018b).

(I.8) $$K_D = \frac{B/Ca_{CaCO3}}{[B(OH)_4^-]/[CO_3^{2-}]_{fluide}}$$

L'utilisation des isotopes du bore comme proxy du pH dépend donc uniquement de l'incorporation d'ions borate dans le réseau aragonitique. L'incorporation d'acide borique dans le squelette aragonitique du corail pourrait rendre l'interprétation du $\delta^{11}B$ plus difficile, mais $(B(OH)_3$ n'est qu'un composant mineur du bore incorporé. La quantification précise de ces deux formes reste cependant limitée par la sensibilité des instruments (RMN généralement).

Dans les coraux scléractiniaires, la gamme de $\delta^{11}B$ et l'utilisation d'approches indépendantes du $\delta^{11}B$, telles que les microélectrodes (Ries, 2011; Cai *et al.*, 2016; Sevilgen *et al.*, 2019; Guillermic *et al.*, 2021) et la microscopie confocale (Venn *et al.*, 2013, 2022; Holcomb *et al.*, 2014), ont permis de valider l'utilisation du $\delta^{11}B$ en tant que proxy du pH_{ECM}.

1.4.3 Les rapports élémentaires

De nombreuses espèces marine calcifiantes, telles que les coraux, foraminifères, coccolithophoridés ou bivalves, forment un squelette de carbonate de calcium ($CaCO_3$). Lors de la précipitation de ces minéraux sous forme d'aragonite et/ou de calcite, les coraux incorporent majoritairement du calcium, de l'ordre de 40%. Conjointement, d'autres éléments mineurs ou traces sont également incorporés dans la structure minérale du squelette carbonaté, tels que le lithium, le magnésium, le strontium ou l'uranium (Beck et al., 1992; Cuny-Guirriec, 2020). L'incorporation de ces éléments dans le squelette corallien est directement liée au coefficient de partage de chacun des éléments. Or, ce coefficient dépend en premier lieu de la température du milieu. Les processus d'incorporation d'éléments traces dans les carbonates biogéniques dépendent donc des paramètres physicochimiques lors de la formation des cristaux d'aragonite et/ou de calcite (Rollion-Bard et al., 2011, 2019 ; Füger et al., 2019 ; Holland et al., 2020). L'incorporation de certains éléments tels que le lithium, le magnésium ou encore le strontium dans le squelette d'espèces calcifiantes (e.g., coraux et foraminifères) dépend de la température et permet ainsi d'utiliser les rapports Li/Ca, Mg/Ca, Sr/Ca et Li/Mg en tant que proxies de la température (Alibert and McCulloch, 1997 ; Montagna et al., 2014 ; Cuny-Guirriec et al., 2019 ; Dissard et al., 2021). L'interprétation des proxies isotopiques tel que le $\delta^{18}O$ peut parfois être complexe due aux « effets vitaux » (cf. 1.4.1). Une alternative est de réaliser une approche multi-proxies en utilisant les rapports élémentaires. Ces rapports élémentaires permettent une mesure indépendante de la température qui, couplée avec le $\delta^{18}O$, conduisent à une meilleure estimation de la température (et de la salinité de l'eau de mer) (Schmidt et al., 2004; Corrège, 2006; Wu et al., 2014). De plus, contrairement au $\delta^{18}O$, certains éléments traces présentent l'avantage d'avoir un temps de résidence dans l'océan particulièrement long (quelques millions d'années), ce qui permet de retracer le climat sans que les reconstructions ne soient directement affectées par des changements de composition de l'eau de mer. Enfin, l'incorporation d'ions borates à la place des ions carbonates dans le réseau aragonitique des coraux dépend, lui, de la chimie des carbonates et permet donc, une fois couplé avec le $\delta^{11}B$, de calculer le système carbonaté complet du fluide de calcification (DIC_{ECM}, $[HCO_3^-]_{ECM}$, $[CO_3^{2-}]_{ECM}$) (Zeebe and Wolf-Gladrow, 2001; Decarlo et al., 2018b).

OBJECTIFS DE LA THÈSE

Cette thèse, ou projet ACLICOST « ACclimatation des récifs coralLIens aux Changements climatiques : ÉcOphysiologie et Signatures géochimiques dans un conTexte d'acidification des océans », vise à étudier les réponses de coraux probablement acclimatés voire adaptés à des conditions environnementales extrêmes, proches ou au-delà de celles prévues à l'avenir. Dans un contexte de changements climatiques rapides et sévères, les récifs coralliens sont menacés de disparition et leur survie demeure très incertaine. L'objectif principal de ce travail de thèse est donc de mettre en lumière les mécanismes d'acclimatation utilisés par des coraux scléractiniaires en réponse aux forçages environnementaux.

Des études récentes ont permis de découvrir un site naturel en Nouvelle-Calédonie (mangroves de Bouraké) présentant des conditions de pH/Température/Oxygène dissous de l'eau de mer proches voire dépassant les valeurs prédites par les scénarios d'évolution du GIEC à l'horizon 2100. Ce site présente des fluctuations environnementales quotidiennes, liées aux cycles de marée, atteignant des valeurs extrêmes de pH (7,23), de température (33,8°C) et d'oxygène (1,87 mg L^{-1} soit ~28% de saturation). Il héberge cependant des récifs coralliens diversifiés (> 66 espèces), en bonne santé apparente, qui semblent acclimatés voire adaptés à ces conditions extrêmes. Afin de distinguer les mécanismes mis en jeu par les coraux de Bouraké en réponse à ces conditions, et de mieux prédire leur devenir face aux changements climatiques, cette thèse comprend quatre objectifs spécifiques :

1. Déterminer l'efficacité du recrutement corallien à Bouraké, et identifier l'influence des algues coralliennes encroûtantes sur la fixation des coraux juvéniles dans ce système naturel « extrême ».

2. Déterminer expérimentalement (culture à différents niveaux de pH) les différences de performances physiologiques et de communauté symbiotique entre des coraux de Bouraké et des coraux provenant d'un récif contrôle adjacent.

3. Comparer la capacité de régulation de la chimie des carbonates dans le milieu calcifiant des coraux de Bouraké à celle des coraux provenant d'un récif contrôle adjacent via l'utilisation de proxies géochimiques dans leur squelette calcifié.

4. Tracer, à l'aide de proxies géochimiques, l'évolution temporelle sur plusieurs décennies du pH et de la température à Bouraké, afin de rechercher une éventuelle acclimatation à long terme des coraux de Bouraké.

Pour répondre à l'objectif **(1)**, nous avons mené une étude écologique sur deux ans du recrutement corallien et du taux de recouvrement d'algues coralliennes encroûtantes sur des plaques en terre cuite disposées *in situ* à Bouraké et dans deux sites de référence distincts. Question posée : *Quel est le succès du recrutement corallien à Bouraké au regard des conditions environnementales extrêmes ?* Les résultats obtenus sont présentés dans le **chapitre 3** et font l'objet d'une publication parue dans *Frontiers in Marine Science* (Tanvet *et al.*, 2022).

L'objectif **(2)** s'articule autour de la mise en place d'une expérience de 100 jours en aquarium, afin d'évaluer les réponses physiologiques, à quatre scénarios de pH différents, des espèces coralliennes *Acropora tenuis*, *Montipora digitata* et *Porites* sp. de Bouraké et d'un site de référence adjacent. Nous avons également identifié les communautés symbiotiques des individus mis en culture, grâce à une étude métagénomique à la fin de l'expérience. Question posée : *Les coraux de Bouraké ont-ils des performances physiologiques et/ou une communauté symbiotique distinctes de celles observées pour les individus issus du site de référence ?* L'ensemble des résultats sont présentés dans le **chapitre 4** et font l'objet d'une publication parue dans *Ecology and Evolution* (Tanvet *et al.*, 2023).

L'objectif **(3)** cible les différents mécanismes mis en place par les coraux de Bouraké (potentiellement acclimatés/adaptés) et du site de référence (non acclimatés/adaptés) pour maintenir, voire faciliter leur taux de calcification face aux différentes conditions de pH de l'expérience de culture du chapitre 4. Pour cela, nous avons mesuré et interprété les signatures isotopiques des proxies géochimiques ($\delta^{13}C$, $\delta^{11}B$, B/Ca) dans le squelette corallien. Question posée : *Les mécanismes d'acclimatation sont-ils plus efficaces et/ou actifs chez les coraux de Bouraké, comparativement aux coraux issus du site de référence ?* La synthèse des résultats est détaillée dans le **chapitre 5** et fait l'objet d'une publication en cours de révision dans *Geochimica et Cosmochimica Acta* (Tanvet *et al.*).

Afin de répondre à l'objectif **(4)**, nous avons prélevé deux carottes de *Porites* sp. d'environ 30 cm de long, l'une à Bouraké et l'autre au site de référence. Après avoir établi un modèle d'âge (rayons X) et sous-échantillonné ces carottes, nous avons mesuré les proxies géochimiques ad hoc ($\delta^{13}C$, $\delta^{18}O$, $\delta^{11}B$, Li/Mg, B/Ca) afin de retracer l'évolution du pH et de la température de l'eau de mer dans ces deux sites sur les trente dernières années. Questions posées : *Peut-*

on mettre en évidence une acclimatation voire une adaptation des coraux de Bouraké sur le long-terme ? Ces résultats sont-ils transposables aux coraux du site de référence confrontés aux changements climatiques en cours et à venir, ce qui signifierait une acclimatation potentielle de ces coraux aux conditions climatiques futures ? Les résultats obtenus sont présentés dans le **chapitre 6** et sont en cours de valorisation afin d'être soumis à *Nature Communications* (Tanvet *et al.*).

La dernière partie du manuscrit est consacrée à la synthèse des résultats de ce travail de thèse ainsi qu'aux perspectives qui en découlent. Ces éléments de discussion sont présentés dans le **chapitre 7**.

CHAPTER 2

MATERIALS AND METHODS

2.1 Study sites and species

2.1.1 The semi-enclosed lagoon of Bouraké

The coral species used in this study were sampled in a semi-enclosed lagoon named Bouraké and surrounded by mangroves in New Caledonia (**Figure II-1**). The lagoon ends with a narrow channel leading to the sea. This natural site has been discovered and described in the 1990s with regard to environmental conditions, fish abundance and food webs (Komornicki, 1988; Thollot, 1992; Thollot et al., 1999). Nevertheless, it is only recently that Bouraké has revealed itself as a new ecological site providing keys in the understanding of coral acclimatization to complex climatic scenarios (Camp et al., 2017). This study showed a rich coral community thriving in Bouraké despite extreme and variable environmental conditions in terms of pH, temperature and dissolved oxygen. Following these findings, a long-term environmental monitoring was undertaken between 2016 and 2020; it revealed that Bouraké exhibits strong diel fluctuations of seawater pH (range 7.23-8.06 pH_T units), temperature (range 17.5-33.8°C) and dissolved oxygen (range 1.87-7.24 mg L^{-1}) (Maggioni et al., 2021). These daily fluctuations are the result of water circulation and tidal direction due to the unique topographical and geomorphological characteristics of Bouraké. The lagoon connects to the ocean by an 80 m wide channel, which penetrates a mangrove forest and forms large 6-to-8-m-deep back pools bordered by a shallow coral reef. Water exchanges across the channel during tidal cycles result in large daily fluctuations in pH, temperature and dissolved oxygen, up to 0.69 pH_T, 6.50°C and 4.91 mg O_2 L^{-1}, respectively. Despite these environmental conditions, Maggioni et al. (2021) reported a diverse, high-coverage community of macroalgae, sponges, and corals representing 28, 11 and 66 species, respectively.

Figure II-1. | *The semi-enclosed lagoon of Bouraké, New Caledonia (aerial photo taken at 130m height; © R. Rodolfo-Metalpa).*

2.1.2 Biological materials: model species

In this thesis, we studied three different coral species belonging to the "complex" lineage of scleractinian corals widely present in the Indo-Pacific region and more specifically in New Caledonia. Species were selected based on their abundance within local coral reefs and their consistent presence in scientific studies on climate change. Two species were branching corals belonging to the Acroporidae family, which is the most represented in the world: ***Acropora tenuis*** (Dana, 1846) and ***Montipora digitata*** (Dana, 1846). One massive species belonging to the Poritidae family was also selected, since it is commonly used in geochemical record studies: ***Porites* sp.** (**Figure II-2**).

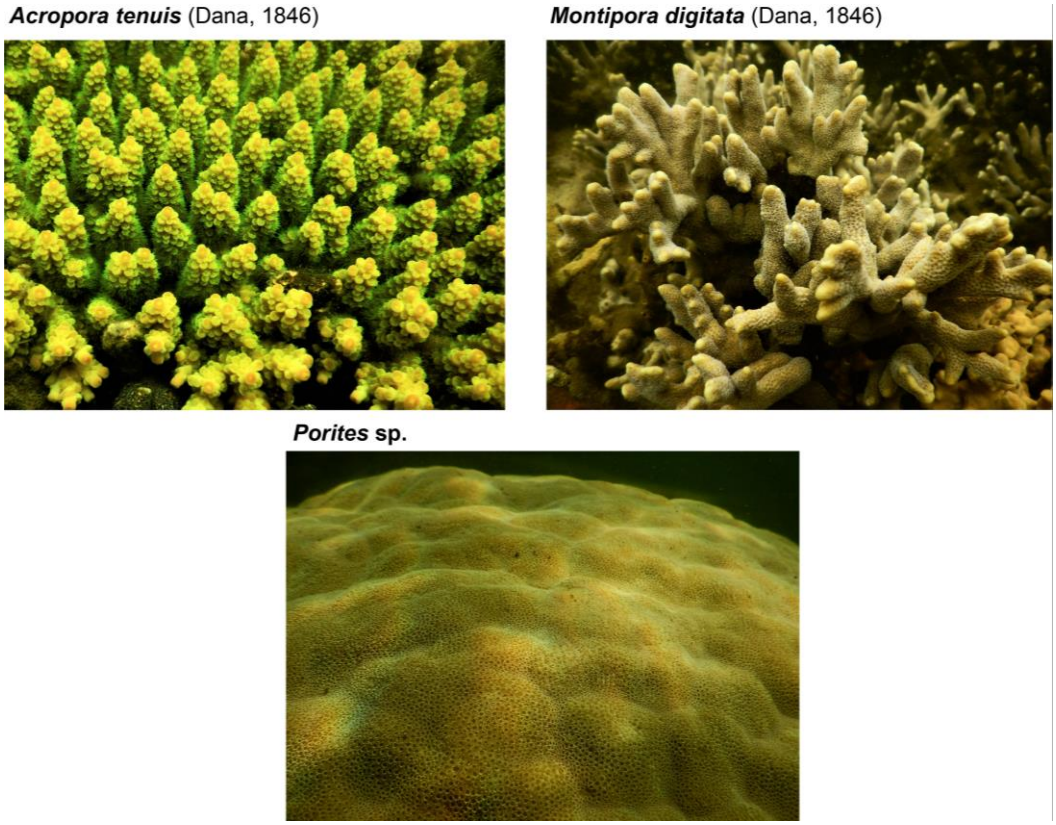

Figure II-2 | *Illustration of the three coral species studied in this thesis (© F. Maggioni).*

2.2 Physiological measurements

2.2.1 Skeleton growth rate

We determined the skeleton growth rate (in terms of calcification) using the buoyant weight technique (Davies, 1989). The coral was weighted in seawater to obtain its equivalent dry skeleton weight using the following equation:

$$D_{coral} = (W_{air} * D_{seawater})/(W_{air} - W_{seawater})$$

With D the density of the coral or seawater and W the weight of the coral in air or seawater. The samples were weighed suspended from a nylon thread in a beaker of seawater, using a Sartorius ENTRIS 224i-1S. We calculated the seawater density according to periodic measurements of temperature and salinity, using a YSI MPS 556 (YSI, USA). Then, we calculated the dry skeleton weight using the density of pure aragonite (2.94 g cm^{-3}). Growth rate (in terms of calcification rate) is the change in dry weight between the initial and the final

weight. According to the morphological differences between species (i.e., branching vs massive), we expressed the growth rate either in mg g^{-1} d^{-1} or in mg cm^{-2} d^{-1}.

2.2.2 Photosynthesis and respiration rates

Each coral individual was placed upright on a plastic grid in 100mL Pyrex beakers filled with seawater and sealed underwater with clear cellophane and a rubber band. Each beaker contained a stirring bar under the plastic grid, to avoid contact with the coral fragment and one pink O_2 sensor spot (PreSens) fixed on the glass (**Figure II-3**). The beakers were put on stirring plates (Telesystem 15, Thermo Scientific) settled at 350 rpm and semi-immersed in a water bath positioned above the stirring plates at a temperature of 26.0°C ± 0.5°C, using heaters and two submersible water pumps to homogenize water temperature.

Figure II-3 | *Coral individuals placed in beakers for light and dark incubations (© C. Tanvet).*

First, coral were incubated in light for 50 min under ca. 250 µmol photons m^{-2} s^{-1} and then in darkness for the same time (Biscéré et al., 2019; Jacquemont et al., 2022; Appendix Article n°1). Temperature (°C) and dissolved oxygen (DO; mg L^{-1}) were measured in each beaker after waiting 10 min under light or dark conditions (T_0) and at the end of each incubation (T_F) using a fiber optic (PreSens Fibox 4 trace). At the end of light incubation, beakers were opened to measure seawater volume and refilled with fresh seawater for the dark incubation. At the end of the two incubations, coral fragments were frozen at -20°C for further analysis of symbiont density, total chlorophyll, skeletal surface area, protein content and clades. Rates of net photosynthesis (P_n) in light and respiration in darkness (R_{dark}) were calculated according to DO concentration changes between T_F and T_0, after correction of the microbial activity measured in two empty beakers. Rates were standardized per incubation time (hours), seawater volume in each beaker (L), and skeletal surface area (cm^2). Gross photosynthesis (P_g) was calculated according to the following equation:

$$P_g = P_{net} + |R_{dark}|$$

Data were normalized per fragment area as described below in 2.2.3. Each rate was expressed in mg O_2 cm^{-2} h^{-1} and converted in µmol O_2 cm^{-2} h^{-1}. The ratio of photosynthesis to respiration (Pg:R) was calculated as follows:

$$P_g{:}R = \frac{P_g \times hours\ of\ daylight}{|R_{dark}| \times 24}$$

2.2.3 Tissue parameters and surface measurements

The coral fragments were first thawed and the tissues were extracted from the skeleton using a pressurized air jet using the air pick method (Rodolfo-Metalpa et al., 2010) in a known volume of seawater filtered at 0.45 µm. The tissue solutions were then homogenized with a Potter tissue grinder.

To determine symbiont density, 2 mL of the slurry was homogenized with a vortex and the number of Symbiodiniaceae was counted using a Neubauer cell under a stereomicroscope (n count = 8).

For total chlorophyll (*a* + c_2) measurement, 10 mL of the slurry was centrifuged at 5,000 g at 4°C for 10 min. The supernatant was discarded and the pellet containing the symbionts was re-suspended in 10 mL of pure acetone to extract pigments during 24h at 4°C in darkness. The solution was once again centrifuged at 10,000 g for 15 min and the supernatant was sampled to measure its absorbance at 630, 663 and 750 nm using a spectrophotometer (Evolution 201, Thermo Scientific). The absorbance measurement at 750 nm was performed to evaluate the solution turbidity to avoid a reading bias. Chlorophyll a and c_2 concentrations were calculated according to the equations from Jeffrey and Humphrey (1975):

$$[Chl\ a] = 11.43 \times (A_{663} - A_{750}) - 0.64 \times (A_{630} - A_{750})$$

$$[Chl\ c_2] = -3.63 \times (A_{663} - A_{750}) + 27.09 \times (A_{630} - A_{750})$$

With A the absorbance measured at 663, 630 or 750 nm. Chlorophyll concentrations in µg chl ml^{-1} were then normalized per total extracted tissue content and coral surface area and finally expressed in µg cm^{-2}.

Total protein were extracted by incubating coral fragments in a sodium hydroxide solution (1N) maintained in a water bath for 30 min at 90°C according to Hoogenboom et al. (2010). The protein content was estimated using a BCA assay kit (Uptima, Interchim). Bovine serum

albumin (BSA, Interchim) was used as a protein standard with concentrations of 0, 50, 100, 200, 350, 500, 750 and 1000 µg ml^{-1}. Samples were diluted in order to be in the range of the protein standard calibration line. Samples and standards were homogenized for 30 s on a microplate shaker within the spectrophotometer (Biotek ELx808). The absorbance was measured at 563 nm and the protein content was then calculated according to the standard calibration equation.

Photosynthesis and respiration rates, symbiont density, total chlorophyll concentrations and protein contents were normalized per coral surface area (cm^2). The skeletal surface area was estimated using the paraffin wax-dipping method (Stimson and Kinzie, 1991; Naumann et al., 2009) for the branching species (i.e., *Acropora tenuis* and *Montipora digitata*). For this method, skeletons were weighed dry and were then dipped twice in melted wax at 60°C with a short drying time between both dips to ensure an effective covering of the entire skeleton. The skeleton was weighed again after the dips and the surface area was determined according to the following calibration line obtained from previous measurements of wax weighted from several ceramic cylinders and parallelepipeds of distinct known surfaces:

$$Surface = 17.768 \times W_{wax} + 1.2061$$

With W_{wax} the wax weight of the sample and $R^2 = 0.9939$. Regarding the massive species *Porites* sp., we used the aluminum foil technique (Marsh, 1967) to determine the skeletal surface area. Following the same principle as the wax method, several ceramic cylinders and parallelepipeds of distinct known surface area were entirely covered with aluminum foil, which were then weighed to establish a calibration line and the following equation:

$$Surface = 343.53 \times W_{Al} - 0.0112$$

With W_{Al} the aluminum weight of the sample and $R^2 = 0.9996$.

2.2.4 Photosynthetic efficiency

Photosynthesis results from the enzymatic chain reaction within the two photosystems (PSI and PSII) of the symbiont in the chloroplast. The latter captures the photons of light to split water molecules (H_2O) in oxygen (O_2), protons (H^+) and electrons (e^-). This reaction occurs in the photosystem II (PSII), where chlorophyll pigments produce electrons after being excited by photons. These electrons after having crossed both photosystems produce an energetic molecule, the NADP (nicotinamide adenine dinucleotide phosphate). This energy is then used

to reduce CO_2 into energy in the form of glucose, the first form of organic carbon ($C_6H_{12}O_6$). Thus, the photosynthesis reaction is:

$$6\,CO_2 + 6\,H_2O\ + photons \rightarrow 6\,O_2 + C_6H_{12}O_6$$

The protons resulting in the splitting of H_2O are involved in the formation of ATP (adenosine triphosphate), the key molecule of cellular energy. Aerobic respiration produces the most important content of ATP in mitochondria using the oxygen and glucose produced during photosynthesis. Again, the first step of photosynthesis within the PSII is the emission of electrons from chlorophyll pigments after photons excitation. The chlorophyll de-excitation occurs by three different ways: (i) the emission of electron (used to produce NADP), (ii) energy in the form of heat production, and (iii) fluorescence (excited molecules emit light). These three mechanisms compete with each other. Increasing fluorescence intensity is therefore net losses for photosynthetic yield. Fluorescence intensity can thus be measured to inversely assess photosynthesis efficiency. Fluorescence intensity is measured on corals using a pulse amplitude modulation (PAM) fluorometer (DIVING-PAM, Walz, Germany, Schreiber *et al.*, 1986) Before measurements, corals are adapted to dark for 15 minutes to widely open the reaction centers of the PSII (Hoegh-Guldberg and Jones, 1999). Photosynthetic efficiency is measured in dark (no light source); the 8-mm optical fiber is maintained perpendicular to the coral's surface using a black-jacket at a fixed distance of 5 mm. The initial (F_o) and maximal (F_m) fluorescences of symbionts are measured by applying respectively a weak pulse of red light (LED 650 nm, 1 µmol photon m^{-2} s^{-1}, width 3 µs) and a saturating pulse of actinic light (max intensity reaching 8000 µmol photon m^{-2} s^{-1}, width 800 µs). The saturating pulse will result in the inhibition of the electron transport chain, after which the entire energy is emitted in fluorescence, the maximal fluorescence (F_m). Variable fluorescence is calculated as the result of F_m-F_0 while F_v/F_m values are used as the maximum quantum yield of PSII (Ralph and Gademann, 2005) giving the following equation:

$$\frac{F_v}{F_m} = \frac{(F_m - F_o)}{F_m}$$

The F_v/F_m values reflect the PSII efficiency to use light for photochemical conversion. For a healthy coral, the F_v/F_m value is around 0.75, but it diminishes under stress. Under 0.45, the coral has reduced photosynthetic performance, while its photosystems are damaged under 0.20. To measure the relative electron transport rate (rETR), rapid light curves (RLC) are made by nine steps of fluorescence measurements, as a function of increased photosynthetic active radiation (PAR). The RLC records the rETR at each step, which is equal to the effective

quantum yield of PSII (Φ_{PSII}) multiplied by the amount of light received (PAR) and the partition coefficient between the two photosystems (PSI and PSII) as follows (Ralph *et al.*, 1999):

$$rETR = \theta_{PSII} \times PAR \times 0.5$$

2.3 Metagenomic analyses

2.3.1 DNA extraction

Total coral holobiont DNA (i.e., Symbiodiniaceae, polyp and associated microorganisms DNAs) was extracted using a 2% CTAB-based protocol adapted from Mieog et al. (2009). The coral fragment was immersed into 600 µL of 2% CTAB/proteinase K (1000/1). The samples were then exposed to three successive thermal shocks consisting of 5 min in liquid nitrogen and 10 min thawing at room temperature. Cell lysis was obtained by incubation for 4 hours at 60°C. Once the 2% CTAB (containing the coral tissue) was incubated, proteins removal was done by several cleaning steps as follow:

1. Addition of 600µL of chloroform/isoamyl alcohol (24/1),
2. Homogenization by turning over for 2 min,
3. Centrifugation at 4°C for 15 min at 12,000 g to keep the aqueous phase,
4. Addition of 600 µL of isopropanol,
5. Homogenization by turning over and incubation at -20°C for 20 min,
6. Centrifugation at 4°C for 20 min at 12,000 g and discard of the supernatant,
7. Addition of 500 µL of fresh 75% ethanol,
8. Centrifugation at 4°C for 10 min at 12,000 g and discard of the supernatant,
9. Drying and recovery of the pellet from the tube containing the DNA,
10. Recovery of the pellet with 50 µL of Milli-Q water and storage at -20°C.

The quantity and quality of extracted DNA were checked twice using a Nanodrop 2000 spectrophotometer (Thermo Fisher Scientific, MA). We used 1.5 µL of sample per measurement and DNA concentrations were expressed in ng μL^{-1}. The 260/280 ratio should be close to or greater than 1.8; a lower value indicated the presence of phenol or protein contaminants absorbing at 280 nm. The extracted DNA was then diluted in the range of 30-70 ng μL^{-1} for PCR amplification.

2.3.2 PCR amplification

The Symbiodiniaceae nuclear DNA ribosomal internal transcribed spacer (ITS2) region was amplified with the forward primer ITS2-DINO [5'-TCGTCGGCAGCGTCAGATGTGTATAAGAGACAGGTGAATTGCAGAACTCCGTG-3'] (Pochon *et al.*, 2001) and reverse primer ITS2Rev2 [5'-GTCTCGTGGGCTCGGAGATGTGTATAAGAGACAGCCTCCGCTTACTTATATGCTT-3'] (Stat et al., 2009). The underlined segments represent the overhangs of the Illumina adapters (Illumina, San Diego, CA, USA). The PCRs were conducted in 25 µL mix reactions containing 12.5 µL of AmpliTaq 360 Master Mix, 1 µL of each 10 µM primer mix, 1 µL of 360 GC Enhancer, 2 µL of DNA template and DNAse-free water to adjust the reaction volume. The mix reactions were placed in 96-well plates without filling the side plates to avoid edge effects during the amplification cycle. The amplification was done by several cycles of denaturation, hybridization and elongation of the DNA using the Applied Biosystems™ Veriti™ Thermal Cycler (Thermo Fisher Scientific). The PCR incubation program was adjusted from Arif et al. (2014) as follows:

1. First denaturation	94°C	15 min	
2. Denaturation	95°C	30 sec	
3. Hybridization	49°C	1 min	x 35 cycles
4. Elongation	72°C	30 sec	
5. Final elongation	72°C	10 min	
6. Conservation	15°C	∞	

Table II-1 | *PCR program for DNA amplification cycle.*

To verify the success of the amplification and ensure that no contamination had occurred, DNA migration by electrophoresis was performed on a 1% agarose gel using 3 µL of each PCR product.

2.3.3 Sequencing

The resulting amplicons were sequenced using the Illumina MiSeq platform (2 x 300 bp) at the Australian Genome Research Facility (AGRF, Victoria, Australia). The returned demultiplexed FASTQ files were analyzed via the Symportal analytical framework (Hume et al., 2019), which predicts ITS2-type profiles from specific sets of defining intragenomic ITS2 sequence variants (DIVs) based on genetically differentiated Symbiodiniaceae taxa. Sequences were submitted directly to the SymPortal pipeline, where they were quality controlled and scanned against the

primers using bioinformatics software MOTHUR 1.39.5 (Schloss et al., 2009), BLAST+ (Camacho et al., 2009) and minimum entropy decomposition (MED; Eren et al., 2015).

2.4 Geochemical measurements

2.4.1 Laboratory facilities

For geochemical measurements, sample processing and chemical treatment procedures were performed at Ifremer (Plouzané, France), under ISO 5 (class 100) laminar flow hoods within an ISO 6 (class 1000) clean room. All geochemical analyses were carried at the oceanic spectrometry pole (PSO) shared between the European University Institute for Marine Studies (IUEM) and Ifremer at Plouzané, France. Ultra-pure reagents (i.e., HNO_3, HF, HCl, H_2O_2 and NH_4OH from Normatom® grade) were used for chemical procedures. All acids and further dilutions were made using double distilled 18.2 MΩ cm^{-1} Milli-Q water.

2.4.2 Sample preparation

Prior to geochemical measurements, newly formed skeletons from each coral sample were collected based on the apparent pink band of Alizarin Red S staining (Davies, 1989). Whilst the pink band of Alizarin Red S is evident for branching species (i.e., *Acropora tenuis* and *Montipora digitata*), it is less obvious for *Porites* sp., for which the new skeleton that calcified was collected on the Holdfast epoxy resin and/or plastic plate where the individuals attached. After air-drying, bulk powder of each coral fragments was collected using a micro drill (Dremel 3000) and homogenized using an agate mortar. The samples and standards were then cleaned using an oxidative cleaning method adapted from Grottoli et al. (2005), Wierzbowski (2007), and Sutton et al. (2018). A few milligrams of sample in 1.5 mL Eppendorf® tubes first underwent a cycle of three salt and clay washes with 1 mL of alkaline-buffered Milli-Q water (0.1 M NH_4OH). Samples were centrifuged at 10,000 rpm to remove the supernatant at the end of each wash. Next, the oxidation step was performed by adding 500 µL of 3% alkaline-buffered H_2O_2 to the sample placed in an ultrasonic bath for 40 min at 50°C, to accelerate the cleanup of organic matter. After the peroxide cleanup, a further cycle of three cleanups with alkaline-buffered Milli-Q water was performed on the samples until the pH of the supernatant matched that of the MQ water, which ensured that all of the oxidizing agent was removed. Finally, samples were dried in an oven at 60°C overnight.

2.4.3 Stable carbon and oxygen isotopes

Carbon and oxygen isotopes ratios of the carbonate-based skeleton of corals were measured on a Kiel IV Carbonate device coupled with a MAT 253 Isotope Ratio Mass Spectrometer (IRMS) (Thermo Fisher Scientific). After cleanup, 90 to 160 µg of skeleton powder were put in 10 mL glass vials using a XPR10 Metler Toledo microbalance (readability 1 µg). Then, vials were placed in a 48-position carousel in a chamber heated at 75°C in the Kiel IV Carbonate device (**Figure II-4**). A piston system places the vial on a Viton® O-ring to allow air to be evacuated by primary and secondary vacuum pumping. A few drops of H_3PO_4 (with a density higher than 1.92) were deposited on the sample to obtain CO_2 gas when H_3PO_4 reacts with calcium carbonate ($CaCO_3$). Along with the production of CO_2 and H_2O, this reaction produces O_2 and N_2, also called “uncondensables”, because of the presence of air residues. Whilst CO_2 and H_2O were cryogenically trapped by liquid nitrogen (-192°C), the “uncondensables” could not be trapped at -192°C and were removed by secondary vacuum pumping at the end of the reaction. The trap was then heated to -90°C, which allowed the CO_2 to become gaseous again while H_2O remained frozen. The CO_2 pressure obtained was perfectly proportional to the mass of carbonate in the sample. The CO_2 was then transferred into a micro-volume immersed in liquid nitrogen. This step allowed concentrating the CO_2 in a very small volume in order to obtain a sufficient pressure in the capillary that connects the Kiel IV Carbonate device to the mass spectrometer. The CO_2 was then ionized in the mass spectrometer source via a tungsten filament bombarding the CO_2 with electrons. The ionization was optimized with an ultra-vacuum and two magnets in opposition allowing a “spiral” trajectory. The ionized molecules were then accelerated, using a high voltage (10 kV), and separated using an electromagnet according to the m/z ratio (mass of the ion/charge of the ion). The different ion beams were collected in Faraday cages where the electrical signal was amplified and quantified, resulting in the ratios 46/44 and 45/44 (i.e., $^{12}C^{16}O^{16}O^{+}$ (44), $^{13}C^{16}O^{16}O^{+}$ (45) and $^{12}C^{18}O^{16}O^{+}$ (46)). By comparing these ratios with those of a reference gas and by analysis of carbonate standards, we obtained the carbon and oxygen isotopic composition reported as $\delta^{13}C$ and $\delta^{18}O$, respectively. The results were expressed in ‰ and calibrated against the Vienna Pee Dee Belemnite (VPDB) scale according to international standard NBS-19 and NBS-18. Analytical precision was determined on a home-made MNHN carbonate standard.

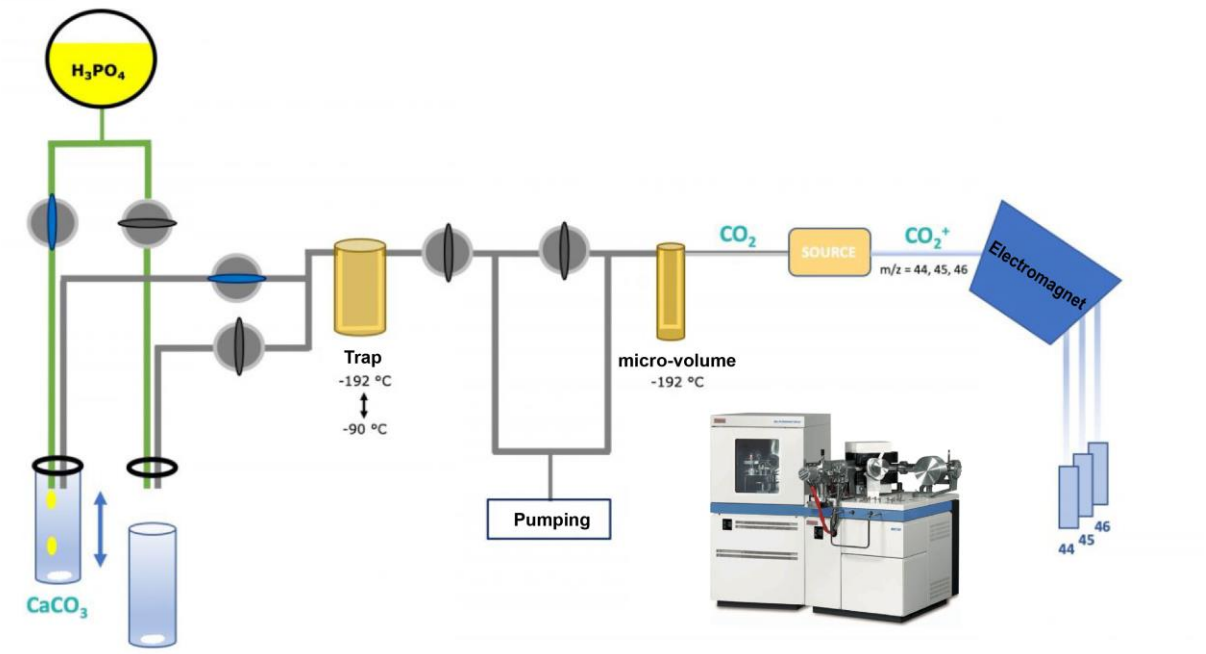

Figure II-4 | *Simplified schematic representation of the Kiel-IV Carbonate device coupled to a mass spectrometer MAT-253 IRMS (Thermo Fisher Scientific) (redrawn from F. Dewilde).*

2.4.4 Boron purification

Due to the high presence of boron in the environment, purification and measurements of boron require very careful work to avoid contaminations. The chemistry must be performed in clean rooms (e.g., ISO 6 (class 1000)) and the materials used must be plastic and preferentially Teflon®. The use of any glass-based materials should be strictly avoided throughout sample preparation, from sampling to measurement, because glass is made of borosilicate. Boron can be purified from coral skeleton using the microdistillation technique developed by Gaillardet et al. (2001) and adapted to Ca-rich matrices by Wang et al. (2010). According to the methodology of Misra et al. (2014) and Guillermic et al. (2021), 1.80 to 2.50 mg of skeleton powder samples and standards were weighed and put in 500 µL Eppendorf® tubes using a CP225D Sartorius balance (readability 0.01 mg). In the present work, the international standard used for boron measurements was the JCp-1 (*Porites* sp.; Gutjahr et al., 2021) from the Geological Survey of Japan, Tsukuba, Japan. The samples and standards were washed with 400 µL of 0.1M NH_4OH to remove potentially adsorbed boron. After a cycle of two washes with Milli-Q water, samples and standards were dissolved in 70 µL of 1M HCl. 60 µL of dissolved samples were loaded onto the inverted cap of a clean 5 mL conical beaker with fin (**Figure II-5 A**). The sealed beaker was placed on a hot plate in the digestion blocks (Analab®) at 95°C for 15h (**Figure II-5 B**). At the end of the microdistillation, the beakers were removed from the hot plate and cooled for 15 min. Then, the caps containing the microdistillation residue

were replaced by clean units and 0.3M HF was added to the distillate (**Figure II-5 C-D**). Residues were collected in 100 µL of 1M HCl and were set aside to evaluate the final microdistillation yield later on (see below 2.4.6).

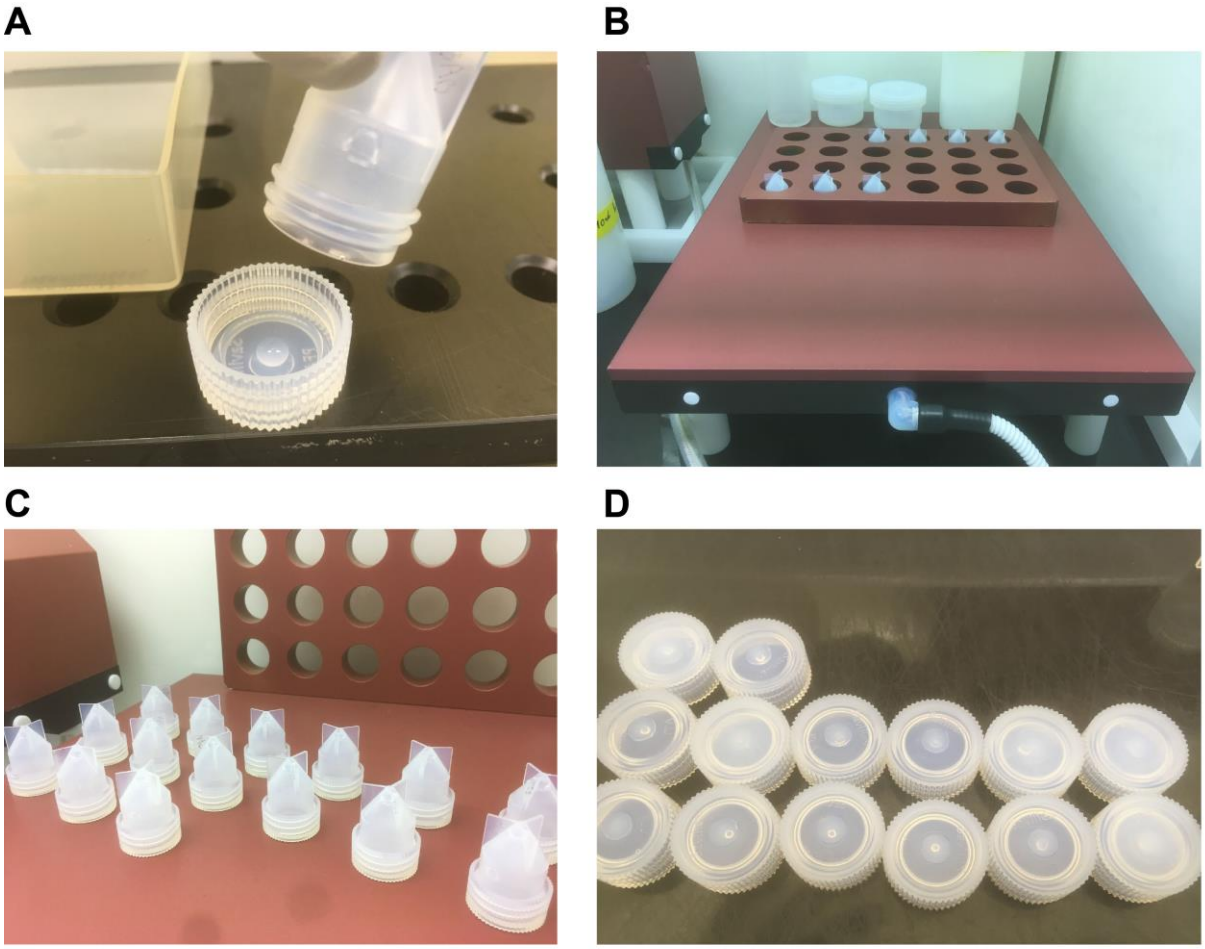

Figure II-5 | *Illustrations of boron purification process. Loading of the 60 µL dissolved sample on the beaker cap (A). Microdistillation at 95°C for 15 hours in the digestion block (B). Cooling of the beakers at the end of the microdistillation with the distillate drop (containing the purified boron) on the conical side of the beaker (C). Caps containing the tiny drop of microdistillation residues (collected for final yield assessment later on) (D) (© C. Tanvet).*

2.4.5 Stable boron isotope

Boron isotopes ratios, reported as delta values ($\delta^{11}B$) of the coral skeleton, were measured on a Multi Collector-Inductively Coupled Plasma-Mass Spectrometer (MC-ICP-MS) Neptune (Thermo Fisher Scientific) equipped with eight $10^{11}\Omega$ resistors. The Neptune mass spectrometer was dedicated to high-resolution isotope ratio measurements (analysis reproducibility ~0.002%). After chemical purification, samples were introduced in liquid phase by a pneumatic nebulizer via a peristaltic pump in a spray chamber. The resulting aerosol was injected into a plasma (~8000°C) made of argon (Ar) and generated by induction. The chemical

species in the aerosol were desolvated, atomized and ionized by the plasma. A portion of this plasma (~10%) was sampled through a first orifice of 1mm diameter at the top of a nickel or platinum cone ("the sampler"). It was then expanded under the effect of a moderate vacuum in a differential pumping chamber (which allowed the passage from atmospheric pressure to the high vacuum of the mass spectrometer) and then passed into a second orifice ("the skimmer"). The ions were accelerated via a differential vacuum system to the lens stack section and focused. In order to reduce energy dispersion, they were deflected by a double focusing system integrating an electrostatic sector, followed by an electromagnetic sector. The ion beams emerging from the two latter sectors were finally deflected according to their m/z ratio by an electromagnet and detected by a multicollection detection system with 9 Faraday cups (**Figure II-6**). The instrumental setup for boron measurement on the Neptune included Savillex® 100 µL min^{-1} C-flow self-aspirating nebulizer, a Teflon® spray chamber and a 2.0 mm alumina injector from ESI®. The Neptune was also equipped with a Thermo® Jet sample cone (Nickel) and 'X' type skimmer cones (Nickel).

After boron purification, the boron concentrations of the samples were first verified by rapid analysis on the Neptune. The samples were then analyzed in duplicate when boron concentration was high enough to reach the optimum intensity on ^{11}B. The standard solution (NIST SRM 951) was used as a bracketing standard to correct any bias shift during the analytical sessions.

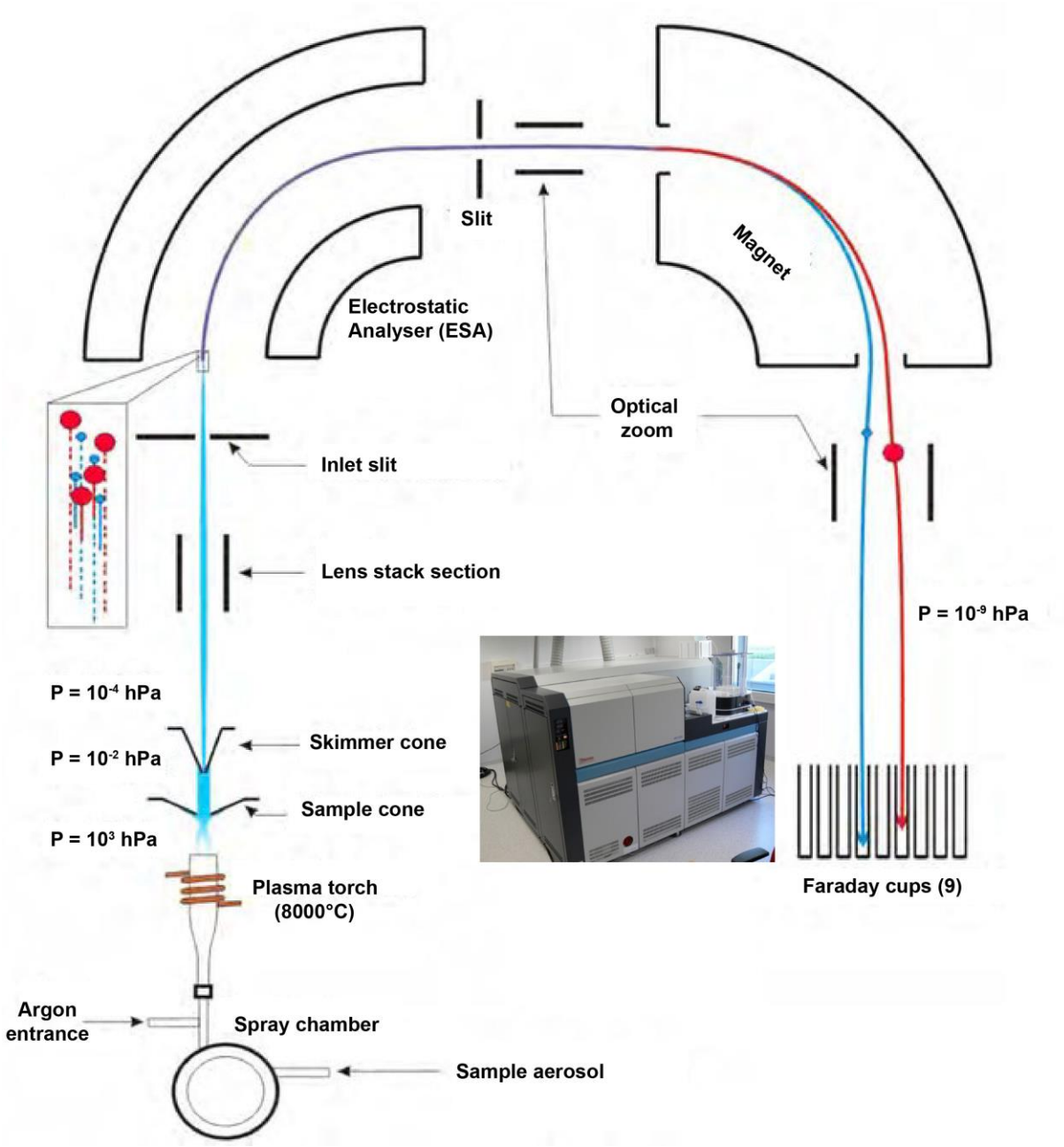

Figure II-6 | *Simplified schematic representation of the MC-ICP-MS Neptune (Thermo Fisher Scientific) functioning (redrawn from J. Milot)*

2.4.6 Elemental ratio measurements

Elemental ratios of the coral skeleton were measured on a High Resolution-Inductively Coupled Plasma-Mass Spectrometer (ICP-MS) Element XR (eXtended Range) (Thermo Fisher Scientific). The Element XR mass spectrometer is dedicated to trace and ultra-trace multi elements concentrations (the detection limit can be as low as 0.001 pg g^{-1} in JET mode). The operation of the Element XR is based on the same principle as an MC-ICP-MS (e.g., the

Neptune), but it differs in the detection process. The detection system allowed choosing between a Faraday cup and ion counter to estimate the element concentration. Prior to analysis with Element XR, we collected the remaining 10 µL of the same aliquot of the 70 µL of dissolved sample used for boron isotope measurements (see 2.4.4) with 200 µL 0.1M HNO_3. We also collected the microdistillation residue from boron purification with 100 µL HCl to assess the final yield of the microdistillation. Our carbonate-based samples had a Ca-rich matrix and were diluted to fixed calcium concentrations targeted at 30 ppm Ca, using 0.1M HNO_3 and 0.3M HF. To perform this dilution, we first measured calcium concentration in our samples using an Inductively Coupled Plasma Atomic Emission Spectroscopy (ICP-AES) Ultima 2 HORIBA (Thermo Fisher Scientific). To avoid the strong memory effect of boron and instrumental drift on the Element XR, a conditioning was performed prior to analyses using the lowest multi element standard concentration. The multi element standard concentration at the middle of the calibration range was used as a bracketing standard to correct any bias shift.

CHAPTER 3

INFLUENCE OF CRUSTOSE CORALLINE ALGAE ON CORAL RECRUITMENT UNDER EXTREME AND VARIABLE ENVIRONMENT

3.1 Preamble

The flourishing of well-diversified coral reefs relies first on the early-life stage of scleractinian corals, which is a harsh period for coral survival (Fabricius and Wolanski, 2000; Swierts and Vermeij, 2016; Elmer et al., 2018). Coral growth begins by a first life stage as pelagic larvae (planula) free in the water, seeking to metamorphose and fix itself to the reef before growing and establish as an adult (Harrison and Wallace, 1990). Coral recruitment depends on the success of larval settlement, which, in turn, depends on the abundance of their preferred settling substrates, such as crustose coralline algae (CCAs) (Heyward and Negri, 1999). CCAs play a fundamental role in inducing coral larval settlement and ensuring the replenishment of coral reefs. However, the complex interactions between CCAs and coral larvae could be compromised in the future considering the ongoing climate changes, in particular ocean acidification (OA) and rising temperatures (Cornwall et al., 2021b; Page et al., 2021). Extreme natural analogues are useful tools to study environmental parameters, such as sea surface pH and temperature, and test their integrated effect on coral recruitment and CCA abundance (Page et al., 2022). In this chapter, we explore the influence of environmental conditions in the semi-enclosed lagoon of Bouraké, hosting well-diversified coral assemblages despite fluctuating acidified, warm and deoxygenated environments, on CCA abundance and coral recruitment. Specifically the objectives of this **chapter 3** are: (**1**) to investigate, at Bouraké, the influence of extreme and fluctuating environmental conditions on CCA abundance and its interactions with algal turf and coral recruits, and (**2**) to determine the efficiency of coral recruitment. To address these objectives, we quantified the abundance of each taxa and identified the coral families recruited during two years on terracotta tiles deployed *in situ* in three different sites: Bouraké and two reference sites.

3.2 Article n°1: High coral recruitment despite coralline algal loss under extreme environmental conditions.

frontiers | Frontiers in Marine Science

ORIGINAL RESEARCH
published: 16 June 2022
doi: 10.3389/fmars.2022.837877

High Coral Recruitment Despite Coralline Algal Loss Under Extreme Environmental Conditions

Clément Tanvet[1,2,*], Francesca Benzoni[3], Christophe Peignon[1], Gérard Thouzeau[2] and Riccardo Rodolfo-Metalpa[1]

[1] ENTROPIE – UMR 9220 (CNRS, IRD, UR, UNC, IFREMER), Institut de Recherche pour le Développement, Nouméa, New Caledonia
[2] LEMAR – UMR 6539 (CNRS, IRD, UBO, IFREMER), Institut Universitaire Européen de la Mer, Plouzané, France
[3] Red Sea Research Center (RSRC), King Abdullah University of Science and Technology (KAUST), Thuwal, Saudi Arabia

[*] Corresponding author

Abstract (338 words)

The crucial role of crustose coralline algae (CCA) in inducing hard coral larval settlement and ensuring the replenishment of coral reefs is widely accepted, and so are the negative effects of anthropogenic CO2 emissions on both CCA abundance and coral development. However, diversified and well-developed coral reef communities have been recently discovered in natural conditions where CCA and corals would not be expected to thrive. Back-reef pools, volcanic CO2 vents, mangrove estuaries, and semi-enclosed lagoons systems can present seawater pH, temperature, and dissolved oxygen values reaching or even exceeding the conditions currently predicted by the Inter Panel on Climate Change (IPCC) for 2100. In the semi-enclosed lagoon of Bouraké (New Caledonia, southwest Pacific Ocean), seawater pHT, dissolved oxygen, and temperatures regularly fluctuate with the tide reaching respectively minimum values of 7.23 pHT units, 2.28 mg O2 L-1, and maximum of 33.85°C. This study reports the effect of such extreme environmental conditions on hard coral recruitment and CCA originally settled at a forereef on artificial substrates that were transplanted over two years in two fringing reefs and at the Bouraké lagoon. Our data emphasize the negative effects of the extreme conditions in our study sites on the CCA, which decreased in cover by ca. 80% and lost in the competition with turf algae, which, in turn, increased up to 162% at the end of the two years. Conversely, hard coral recruitment remained high at Bouraké throughout the study, three-fold higher than at two sites located outside Bouraké where environmental conditions were typical for coastal fringing reefs. Our findings show that while such extreme, climate change like-conditions have a direct and adverse effect on CCA abundance, and despite a certain persistence, coral larvae settlement was not affected. Based on previous findings from Bouraké, and the present observations, both coral recruits and adults seem to be unaffected despite the extreme environmental conditions. This study supports previous research illustrating how extreme natural and variable environments may reveal unexpected and positive insights into the processes underlying coral acclimatization and adaptation to global change.

Keywords: coral recruitment, crustose coralline algae (CCA), extreme environmental conditions, persistence, natural variability

Introduction

Scleractinian corals begin their life as pelagic larvae eventually settling to the reef, growing and establishing as adult, long- lasting colonies (Harrison and Wallace, 1990). Healthy and functional coral reef communities directly depend on coral recruitment success that, in turn, depends on the abundance of their preferred settling substrate i.e., crustose coralline algae (CCA, family Corallinaceae, Lithophyllaceae, and Porolithaceae) (Heyward and Negri, 1999). Indeed, CCA are known as framework binders and act as a preferential settlement substrate for coral larvae (Morse et al., 1988; Heyward and Negri, 1999; Harrington et al., 2004; Nelson, 2009; Price, 2010). Whilst, CCA thallus surface topography differences imply biotic interaction changes (Figueiredo et al., 1996), this preferred substrate is most likely induced by chemical cues from the CCA wall-associated compounds and to a lesser extent from their bacterial biofilm (Tebben et al., 2015; Gómez-Lemos et al., 2018). The early-life stage is a harsh period for coral survival since a multitude of biotic and environmental factors such as light (Bessell-Browne et al., 2017), smothering from sedimentation (Fabricius and Wolanski, 2000), and several complex trophic interactions (Fabricius et al., 2015) including competition with turf algae (Swierts and Vermeij, 2016; Jorissen et al., 2020), suspension-feeders (Elmer et al., 2018), grazers and predators (Penin et al., 2011; O'Leary et al., 2013), cause high mortality rates (67-99%) in coral recruits (Wilson and Harrison, 2005). In particular, competitive interactions play a significant role in the survival of both coral recruits and adult colonies (Penin et al., 2011; Swierts and Vermeij, 2016). In this context, the complex and only partially studied interactions between CCA and coral larvae and their consequences on larval settlement, have been shown to play a fundamental role in the replenishment of the reef (O'Leary et al., 2012). Likely, this complex ecological framework could be furthermore compromised in the future when considering climate changes, in particular rising temperatures and ocean acidification as it has been widely described across several studies (e.g., Cornwall et al., 2021; Mccoy & Kamenos, 2015; Page et al., 2021).

Ocean acidification (OA) is generally described as the rapid and global decline of pH and calcium carbonate saturation in surface seawater (Orr et al., 2005). Several lab-based experiments addressing the effects of OA on CCA have demonstrated reduced calcification and growth rates (Kuffner et al., 2008; Comeau et al., 2013), increased dissolution (Anthony et al., 2008; Diaz-Pulido et al., 2012) and reduced recruitment (Kuffner et al., 2008; Bradassi et al., 2013). Field studies have shown as well reduced recruitment (Fabricius et al., 2011, 2015) or impaired capacity to attract coral larval settlement (Doropoulos et al., 2012). However, it has been recently shown that lab-based versus field experiments tend to conclude that OA has a stronger impact on CCA (Page et al., 2022). Indeed, CCA and corals persist at CO2

seep sites (Kamenos et al., 2016; Enochs et al., 2020; but see also Fabricius et al., 2011 for an opposite finding) and at low pH environments in Palau (Barkley et al., 2015). For coral recruits, OA has been shown to cause skeletal malformations (Foster et al., 2016), and decrease in availability of settlement cues (Albright et al., 2010; Albright and Langdon, 2011). Thus, in general, OA could affect coral recruitment by dissolving CCA or changing their microbial biofilms compounds, hence decreasing the availability of a supposedly ideal substrate for coral recruits (Webster et al., 2013) and finally affecting the recruit survival (Doropoulos et al., 2012; Doropoulos and Diaz-Pulido, 2013). However, OA is only one of the ongoing threats to coral reefs, and its combination with both ocean warming (OW) and deoxygenation (OD) will likely cause CCA bleaching and mortality (Diaz-Pulido et al., 2012; Cornwall et al., 2019; Hughes et al., 2020), and impairment of coral larvae settlement (Jorissen and Nugues, 2021). Combining all those environmental parameters and testing their effects using short-term lab-based experiments is challenging. Natural systems that are exposed to natural in-situ gradients can be used to study their integrated effect (Page et al., 2022). Despite several limitations, few study sites have been recognized as natural laboratories to study the response of species and ecosystem levels to future extreme environmental conditions (e.g., Hall-Spencer et al., 2008; Fabricius et al., 2011; Kroeker et al., 2013; Barkley et al., 2015; Agostini et al., 2018). The semi- enclosed lagoon of Bouraké in New Caledonia is one of these natural laboratories; it hosts well-diversified and complex coral assemblages despite fluctuating acidified, warm, and deoxygenated environments (Camp et al., 2017; Maggioni et al., 2021). In this study, the Bouraké site provided the opportunity to test the long-term responses of CCA and coral recruitment to multiple stressors in a natural setting, which would be hard to reproduce in tank experiments artificially mimicking future climatic conditions.

Here, we assessed the effects of extreme and fluctuating environmental conditions (i.e., low pH, O2, and high temperature) on the abundance of CCA, algal turf, and coral recruits. To address this objective, we obtained CCA-covered tiles from a forereef and moved them to three fringing coastal reef sites with distinct environmental conditions. We investigated the effect of the environmental conditions typical of coastal fringing reefs on the CCA cover twice during the two years experiment and we quantified and identified the coral family recruited on the tiles at the end. Based on the reported effect of OA on CCA cover and coral recruitment rates, we hypothesized that in Bouraké both will be heavily affected by the extreme conditions.

Materials and Methods

Study sites, coral community characterization, and environmental assessment

This study was conducted from September 2017 to October 2019 at a semi-enclosed lagoon within a mangrove ecosystem in Bouraké, New Caledonia (St B3, **Figure III-1B**), and at two fringing reefs, one adjacent to Bouraké (St R2 in **Figure III-1C**, 4 km away) and another one (St M1) located 80 km south in the Maa's Bay (**Figure III-1D**). Station R2 is a large bay-sheltered reef that is enclosed between two islets and has an abundant and scattered reef. Station M1 is a typical fringing reef that is open to the lagoon. In Bouraké extreme conditions are recorded in seawater temperature (range 17.5 - 33.8°C), dissolved oxygen (range 1.87 - 7.24 mg L^{-1}), and pH (range 7.23 - 7.92 pH_T units) (Maggioni et al., 2021). Those environmental parameters fluctuate regularly according to the tide (ca. 1m high) and only return close to coastal values during the high tide of spring tides when seawater of the semi-enclosed lagoon is partially renewed with seawater entering from the external lagoon. As a result, daily fluctuations of dissolved oxygen (DO), temperature, and pH fluctuate can reach 4.91 mg O2 L^{-1}, 6.50°C, and 0.69 pH_T units, respectively. Despite these harsh conditions, at least 66 coral species form compact and wealthy reefs all along the lagoon (Maggioni et al., 2021). In the first assessment of the Bouraké lagoon (Camp et al., 2017), the authors found that these coral species spent 44% of the time at pH_T 7.7–7.8, thus reaching the worst scenarios RCP7.0 and RCP8.5 predicted in global ocean by the Inter Panel on Climate Change for the end of the century (IPCC Report, 2021). During particularly warm years, such as the El Niño event in 2016 (Camp et al., 2017), they experienced temperatures predicted for the end of this century 71% of the time, while facing now the best case scenarios RCP2.6 and RCP1.9 (IPCC Report, 2021).

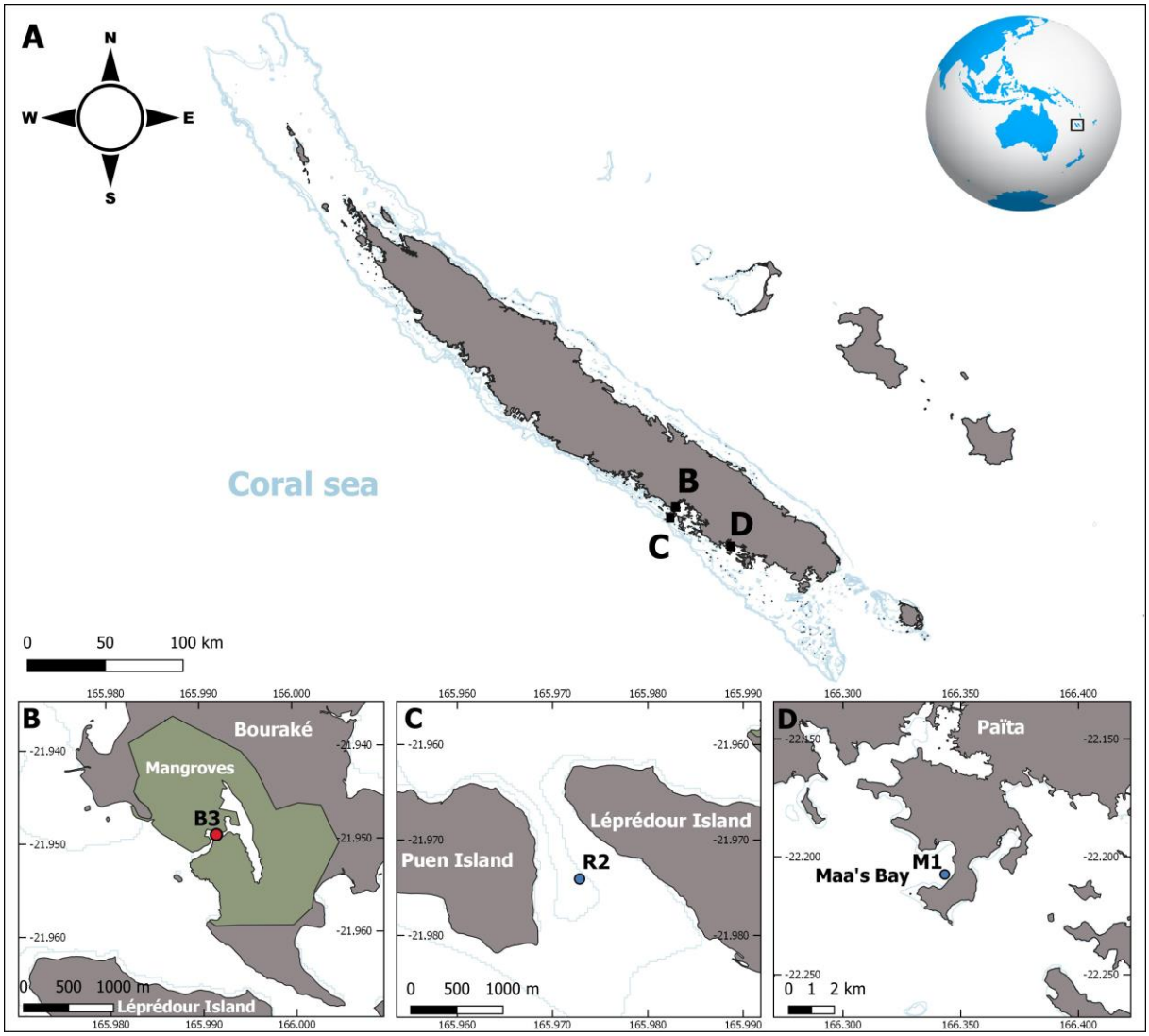

Figure III-1 | *Map showing the location of the study sites in New Caledonia **(A)** and the position of the stations where the 2-year experiment took place **(B-D)**. Station B3 was located in the semi-enclosed lagoon of Bouraké **(B)**, while two other stations were located either near Bouraké (St R2) **(C)** or in Maa's Bay (St M1) **(D)**.*

The composition of the reef communities was assessed at each station visually, by taking photographs of the corals found along three 30-m line transects, and when necessary by collecting fragments of corals and further observing their skeletal structure under a stereomicroscope for final identification. Most of the corals, which are common fringing reef species, were recognized at the genus and species level, with reference to a species list previously established for B3 and R2 (Maggioni et al., 2021). Because the reef community composition might affect coral recruitment rates and the comparison between sites, we verified that the reef diversity was similar among the three stations using the Shannon's diversity index (H) on identified species trough the stations (**Appendix Tables VIII-1, VIII-4**). The three stations were chosen because in addition to have similar reef composition, they allow to

compare the effect of a gradient of seawater carbonate chemistry on the larvae and CCA settlement. In fact, as previously found (Maggioni et al., 2021) and also during our measurements (see results section), R2 could be considered as an intermediate station between B3 and M1, regarding pH absolute value. Therefore, this continuum in the pH experienced by the organisms allows us to evaluate the impact of three different pH scenarios: the end of the century, future 30 years, and the actual conditions (i.e., B3, R2 and M1, respectively).

For stations, B3 and R2, total scale seawater pH_T, dissolved oxygen, and temperature were periodically undertaken since 2016 (Maggioni et al., 2021) using Seabird SeaFET pH loggers, YSI 600 OMS-M, and Hobo water temperature Pro V2, all settled at 10-min logging intervals. For station M1, seawater pH_T and dissolved oxygen content (DO, mg L^{-1}) were measured during three 7-14 day periods (August 2017, June 2018, and January 2019). Unfortunately, the temperature probe was lost twice, therefore the temperature variations could not be assessed for this site.

Terracotta tiles set-up and settlement analyses

A total of 60 red terracotta tiles (11 x 11 x 1 cm) were deployed after being soaked for 7 months at a forereef (22°17.152'S, 166° 10.992'E) at 12 meters depth. In September 2017, they were transferred and randomly deployed at the three stations B3, R2, and M1. This experimental approach was necessary to obtain 60 tiles having both the same CCA community and a similar percentage cover that could be difficult to obtain if the tiles were pre-soaked directly at the stations. This same basis cover allowed us to consider in particular the effects of environmental changes. At each station, 20 tiles were secured to the reef with metal rods at 1.5-2 m depth. Tiles were arranged with a 30- degree inclination at approximately 10 cm from the substrate. They were positioned ca. 3 m distant along a transect of ca. 60 m. The tiles were therefore photographed underwater before moving them to the three stations (T_0), two months after their deployment (T_2), and two years after deployment ($T_{24/26}$). The top sides of 39 (off 60) randomly chosen tiles were photographed in situ at T_0, using an underwater Canon G16 camera. The top sides of all the tiles were imaged at T_2. Tiles from B3 and R2 were retrieved in September 2019 (T_{24}). Tiles from M1 were collected in October 2019 (T_{26}). Of the 20 tiles initially installed at St B3 and M1, only 15 and 19 were found, respectively. All the deployed tiles were recovered at R2. In the laboratory, both top and bottom sides were photographed under a dissecting stereomicroscope (tiles were immersed in seawater). All photographs were analyzed using the photoQuad software (version 1.4) as in Trygonis and Sini, (2012), and the percent cover of sessile organisms was assessed. Each photograph was calibrated for size and pixels-

segmented to the highest level possible (segments ignored < 10 pixels). PhotoQuad's image segmentation is based on the SRM algorithm developed by Nock and Nielsen, (2004). The photograph's size was usually comprised between 3x106 pixels to 9x106 pixels for a surface area typically around 125 cm^2. For top sides, three main categories describing the settled organisms were identified: (i) Algal turf, (ii) CCA, and (iii) empty (i.e., tile surface devoid of any recognizable benthic organisms). For bottom tile sides, one more category was assessed, namely: (iv) suspension-feeders (i.e., ascidians, sponges, serpulid worms, and bryozoans). At the end of the experiment, tiles were cleaned for 24 h in a 10% NaOH solution to remove all organic material, rinsed, and dried. The coral recruits settled on the top, bottom, and the four lateral sides (all sides pooled) of the tiles were counted under a stereomicroscope and identified to the lowest possible taxonomic level. We were able to categorize the coral recruits into three families: Acroporidae, Poritidae, and Pocilloporidae.

Statistical analyses and data presentation

The database for the map (**Figure III-1**) was collected from map tiles at www.georep.nc (©Georep contributors) and customized in QGIS (version 3.4.14). Statistical analyses were conducted and figures were produced using RStudio (R Development Core Team, version 4.1.0, 2021), including the packages: "ggplot2", "stats", "dunn.test", "FSA". Homogeneity of variance was tested using the Levene test and the normality of variance distribution was tested using the Shapiro-Wilk test and checked graphically with a Q-Q plot. When data did not conform to normality or homogeneity of variance, we used the non-parametric Wilcoxon test or the Kruskal-Wallis followed by the Dunn's multiple comparisons test (Bonferroni-adjusted). First, for each site separately we used two factors Wilcoxon test (two groups) for each of the three categories of organisms (CCA, Turf, and Empty) settled on the top sides of tiles to test for statistical differences first after two months of incubation (i.e., T_0 vs T_2), and then after two years (i.e., T_2 vs $T_{24/26}$). To compare significant differences between stations (i.e., B3, R2, and M1) at the start of the study (T_2), we used the non-parametric Kruskal-Wallis followed by the Dunn's multiple comparisons test (Bonferroni-adjusted). The latter was also used for each of the four categories identified on the bottom sides of tiles (i.e., Turf, CCA, Suspension-feeders, and Empty) and the three categories identified on the top sides of tiles (i.e., Turf, CCA and Empty) at the end of the experiment ($T_{24/26}$) to test for statistical differences between stations (B3, R2, M1). The same tests were also used for statistical differences in coral recruits between stations (B3, R2, and M1) from all tiles sides pooled at $T_{24/26}$. Data were graphically reported as median values ± 25^{th} and 75^{th} percentiles (box), minimum and maximum values (whiskers), otherwise specified.

Results

Environmental parameters

Our results showed differences in the main environmental parameters between stations with lower values at B3, intermediates at R2, and normal at M1 (**Table III-1**). At B3, pH was strongly correlated with the tidal cycle decreasing and increasing with the ebb and rising tide, respectively (**Figure III-2**). Within a tidal cycle, the pH reached a minimum of 7.23 and a maximum of 8.06 pH_T units at B3 (**Table III-1**) and it changed on average by about 0.15 units per hour. At stations R2 and M1, pH fluctuated between 7.69 and 8.12 pH_T units for R2, and from 7.93 to 8.18 pH_T units for M1. Similar to pH values, the mean dissolved oxygen concentration (DO) was lower in the Bouraké lagoon than at the other stations. DO concentrations were lower in the early morning at R2 and M1 and higher at mid-day, while they were tidally driven at B3 with low and high values coincident with low and high tide, respectively. Over a 48-hour cycle, DO fluctuates up to 4.25 mg L^{-1} at station R2 and 3.75 mg L^{-1} at stations M1 and B3.

Study site		**B3**	**R2**	**M1**
Temperature (°C)	Mean	26.13	26.08	-
	(SD)	(2.67)	(2.28)	-
	Min	17.49	19.22	-
	Max	33.85	31.74	-
pH_T (total scale)	Mean	7.67	7.89	8.07
	(SD)	(0.23)	(0.08)	(0.05)
	Min	7.23	7.69	7.93
	Max	8.06	8.12	8.18
DO (mg L^{-1})	Mean	5.23	6.48	6.10
	(SD)	(0.89)	(1.05)	(1.31)
	Min	2.28	3.24	3.24
	Max	7.10	10.06	9.18

Table III-1 | *Main environmental parameters measured at Bouraké (B3) and the stations M1 and R2. Study site B3 R2. Mean (SD), minimum (min) and maximum (max) values of temperature, pHT (total scale), and dissolved oxygen (DO). Values were calculated from data collected during August 2017, June 2018 and January 2019 at station M1, and during 3-year long-term monitoring at B3 and R2 considering both diel and seasonal fluctuations, and compiling several thousands of measurements (Camp et al., 2017; Maggioni et al., 2021). The temperature at station M1 was only occasionally recorded during the 2-year study period, therefore not presented.*

Changes in Crustose Coralline Algae and Turf Covers

After 7 months of conditioning at a forereef, i.e., just before they were moved and randomly shared between the three study stations (T_0), the top sides of the tiles were predominantly covered in CCA (median percent cover of 69.21%, all tiles pooled), while algal turf was rare

(median percent cover of 11.95%). Two main CCA genera were recognized on the tiles on a simple visual check regarding the conceptacles size and disposal: *Porolithon* and *Neogoniolithon*. After two months (T_2) at the three stations, the CCA median percent cover was significantly different among stations and significantly decreased at B3 from 69.21% to 41.4% (**Figure III-3; Table III-2**). CCA cover significantly increased at the two stations R2 and M1, respectively 64.4% and 81.3%. In contrast, turf cover was significantly different between stations, reaching the highest values in B3 (20.4%), and only 6.4% and 9.7% at R2 and M1, respectively. After two years of deployment ($T_{24/26}$), CCA median percent cover on the top sides of the tiles was lower than the one at T_2 at all stations: this decrease was dramatic at B3 (from 41.4% to 8.4%) and M1 (from 81.3% to 1.5%), but to a much lower extent at R2 (from 64.4% to 49.3%).

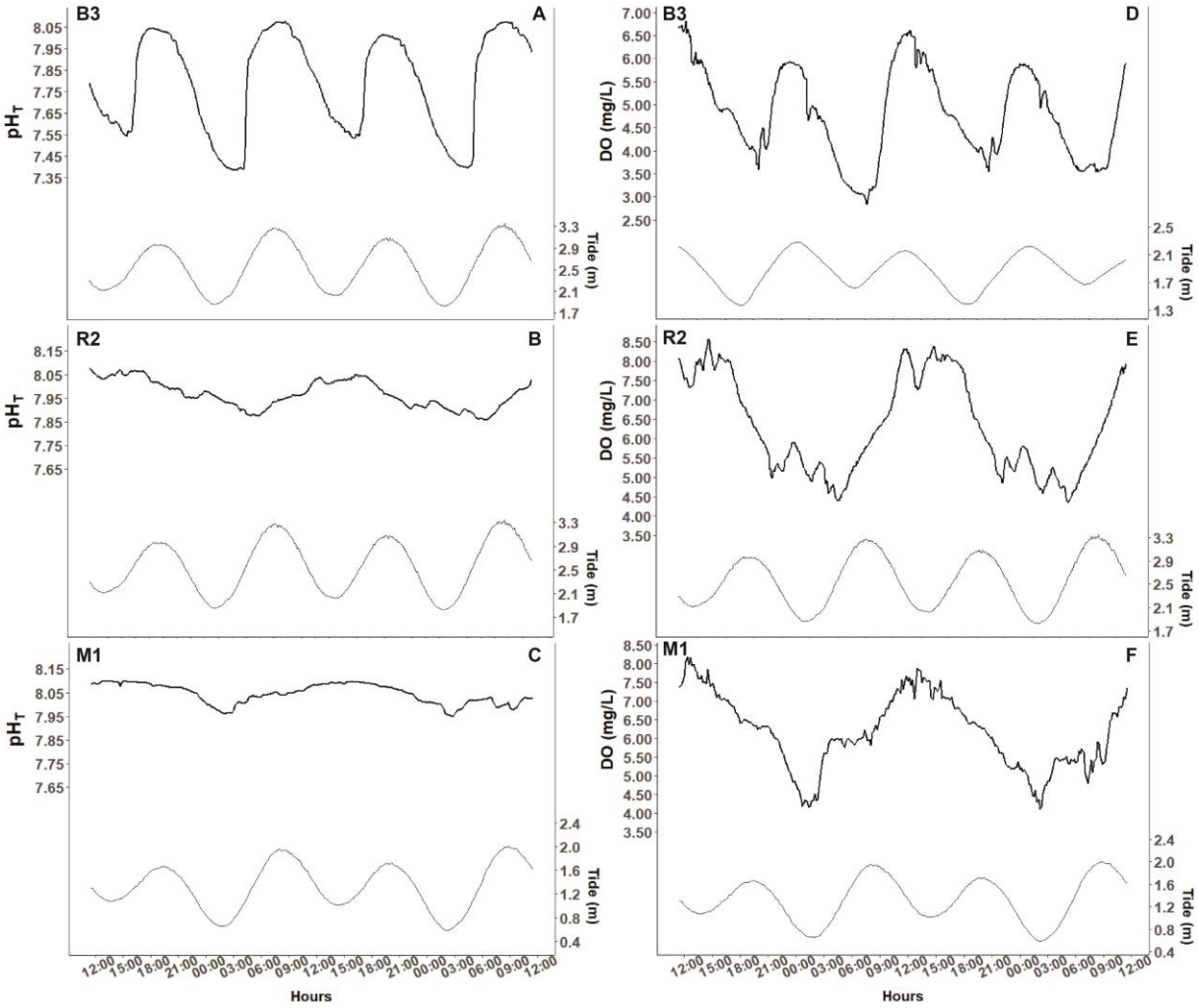

Figure III-2 | *Seawater pH_T* ***(A–C)*** *and dissolved oxygen (DO)* ***(D–F)*** *variations (black lines) recorded during 48 hours at Bouraké (St B3) and stations R2 and M1. Data were collected at the end of March 2019 at St R2 for pH* ***(B)*** *and DO* ***(E)*** *and at St B3 for pH* ***(A)****. DO was measured at St B3 at the beginning of April 2019* ***(D)****. At St M1, data were collected at the end of January 2019* ***(C, F)****. Tidal variations (grey lines) are on the right y-axis.*

Turf cover on the top significantly increased at all stations, dramatically at both B3 and M1 (from 20.4% to 53.5%, and from 9.7% to 91.2%, respectively), to a much lower extent at R2 (from 6.4% to 18.7%). Similarly, Turf cover on the bottom was significantly different between stations (**Appendix Table VIII-3; Figure VIII-3**), low at B3 (31.89%) and high at R2 and M1 (71.79% and 71.56%, respectively). Crustose coralline algae median percent cover on the bottom was similar at B3 (16.12%) and R2 (21.21%), and significantly lower at M1 (3.42%) after two years of immersion Suspension-feeder percent covers on the bottom of tiles in B3 and R2 were as low as 2.74% and 9.57% for B3 and M1, respectively, and rare for R2 (**Appendix Table VIII-3**). Tile surface areas devoid of settlers significantly differed between stations. They were similar at M1 and R2 (6.78% and 6.26%, respectively) and higher at B3 (39.47%).

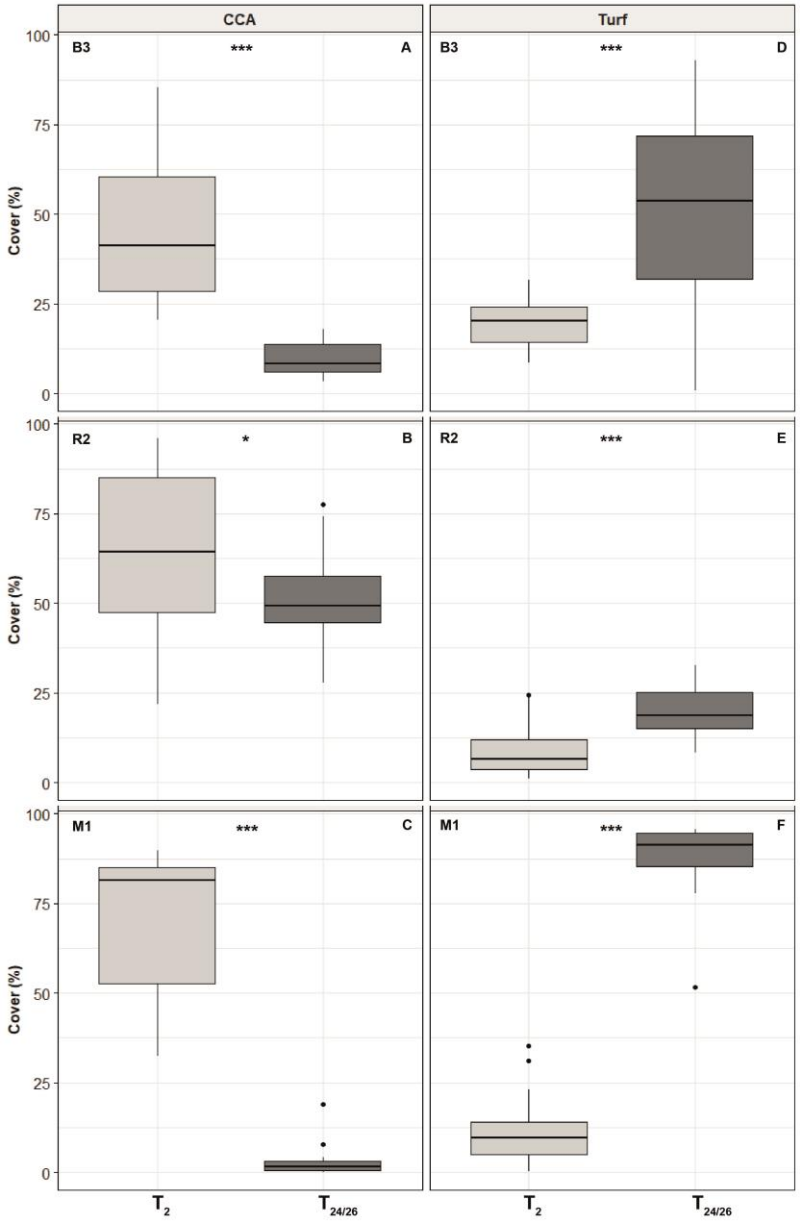

Figure III-3 | *Change in crustose coralline algae (CCA)* ***(A–C)*** *and Turf percent cover* ***(D–F)*** *on top sides of the tiles between the beginning (two months after the time of deployment, T_2) and the end (after ca two years of deployment, $T_{24/26}$) of collector deployment at study stations B3, R2 and M1 (number of tiles n = 15, 20 and 19, respectively). Data are median values ± 25th and 75th percentiles (box), minimum and maximum values (whiskers), and outliers (dots). Stars represent statistical significance (see* ***Table III-2****).*

A)

Station	*Category*	*df*	*W*	*p*
Top sides, T_0 vs T_2				
B3	CCA	(1, 54)	445	**0.002**
	Turf	(1, 54)	66	**<0.001**
	Empty	(1, 54)	173	**0.021**
R2	CCA	(1, 59)	373	0.798
	Turf	(1, 59)	480	0.149
	Empty	(1, 59)	379	0.866
M1	CCA	(1, 58)	257	0.061
	Turf	(1, 58)	395	0.691
	Empty	(1, 58)	506	**0.024**

B)

Top sides, T_2 vs $T_{24/26}$				
B3	CCA	(1, 30)	0	**<0.001**
	Turf	(1, 30)	195	**<0.001**
	Empty	(1, 30)	129	0.507
R2	CCA	(1, 40)	123	**0.037**
	Turf	(1, 40)	348	**<0.001**
	Empty	(1, 40)	222	0.561
M1	CCA	(1, 38)	0	**<0.001**
	Turf	(1, 38)	361	**<0.001**
	Empty	(1, 38)	131	0.154

C)

Top sides, T_2 between stations	*df*	*K-W*	*p*	*Dunn's multiple comparison*
CCA	(2, 54)	9.084	**0.010**	B3 < M1 = R2 (***p* < 0.025**)
Turf	(2, 54)	13.770	**<0.001**	B3 > M1 = R2 (***p* < 0.001**)
Empty	(2, 54)	5.326	0.070	
Top sides, $T_{24/26}$ between stations	*df*	*K-W*	*p*	*Dunn's multiple comparison*
CCA	(2, 54)	43.876	**<0.001**	R2 > B3 > M1 (***p* < 0.014**)
Turf	(2, 54)	38.877	**<0.001**	M1 > B3 > R2 (***p* < 0.014**)
Empty	(2, 54)	25.311	**<0.001**	M1 < B3 = R2 (***p* < 0.001**)

Table III-2 | *Statistical data on CCA, turf and empty cover on the top sides of tiles.* ***(A and B)*** *Non-parametric Wilcoxon tests between the beginning (T_0) and after two-month incubation (T_2); and between the T_2 and 2-year ($T_{24/26}$) at the three stations.* ***C)*** *Non-parametric Kruskal-Wallis test, followed by the Dunn's multiple comparisons, between stations for CCA, Turf and Empty measured at the beginning (T_2) and the end ($T_{24/26}$). Significant values are in bold ($p<0.05$).*

Spatial variability in coral recruitment

Coral recruitment significantly differed among stations and sides after two years of tile immersion (**Appendix Table VIII-3**). It was found to be ca. 3-fold higher at B3 than at R2 and M1 with 18.4, 4.6, and 5.5 recruits per tile (all tiles pooled per station), respectively. Regarding where the larvae preferentially settled on the tile, the number of recruits was always higher on the bottom than on the top, and scarce on the lateral sides (**Figure III-4**).

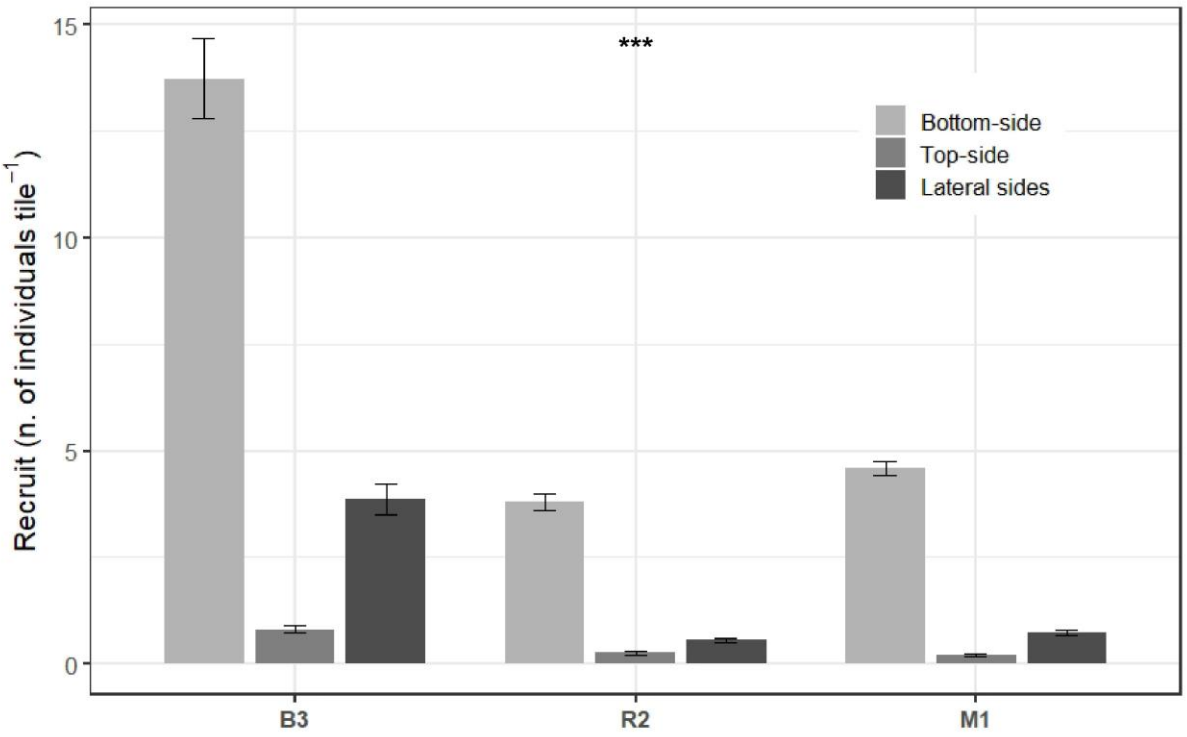

Figure III-4 | *Number of coral recruits (per tile) found on the different sides of the tiles immersed during ca. two years at Bouraké (B3) and stations R2 and M1. Data are means ± SD (number of tiles n = 15, 20, and 19, for B3, R2, and M1, respectively). Data from the lateral sides were pooled. Stars represent statistical significance (see* ***Appendix Table VIII-3****).*

Acroporidae was the dominant family of coral recruits settled in our experiment (**Appendix Figure VIII-4**), with similar relative abundances between stations (65.58%, 73.91%, and 67.33%, at B3, R2, and M1, respectively). Pocilloporidae was the second most abundant family, with recruits who equally settled at all three stations in terms of relative abundance (14.85%, 17.39%, and 16.83% at B3, R2, and M1, respectively). Only a few Poritidae were found at B3 and M1 (17.39%, and 6.52%), and none at M1 which exhibit more unknown genera.

Discussion

Coral larvae are tied to preferred settlement substrates such as CCA (Harrington et al., 2004; Price, 2010), which in turn can be severely affected by environmental conditions, such as OA. In fact, reducing both the availability of preferred substrate for coral settlement, such as CCA and biofilms and increasing turf algae cover, may negatively reduce recruitment rates and coral population replenishment and/or recovery (Doropoulos et al., 2012; O'Leary et al., 2012; Fabricius et al., 2017). Although the CCA we transplanted at study sites suffered from moderate bleaching, partially confounding the effect of environmental conditions on their survival, the present study corroborates previous findings reporting a decline in CCA cover and

a shift towards an increase in turf algae under extreme conditions (Kuffner et al., 2008; Martin et al., 2008; Barott et al., 2012; Kroeker et al., 2013; Porzio et al., 2013; Enochs et al., 2015). While the CCA abundance decline was expected, surprisingly, coral recruitment rates in Bouraké were higher than outside, at both the two fringing reefs. Our study sites differed in several ways, one is tidally driven and exhibits variable and extreme pH, temperature and hypoxia while the two others are far less variable and close to ambient values. While our findings appear to contradict results from several OA laboratory-based experiments (e.g., Doropoulos et al., 2012; Webster et al., 2013; Jorissen et al., 2020), they are in accordance with some field experiments (Kamenos et al., 2016; Enochs et al., 2020) showing in general, a lesser impact of OA (Page et al., 2022). All these observations together reinforce the idea that coral recruitment is possible even under extreme conditions and that, particularly for the Bouraké site, corals may have adapted to such variable and extreme environmental conditions.

Shift between CCA and turf algae

CCA cover on the top sides of the tiles remarkably declined at Bouraké after only 2 months of immersion, while remaining stable or slightly higher at the two other reef stations. This suggests that ca. 40% of CCA settled during the tiles pre- deployment, dissolved during a short-term exposure, therefore further indicating a strong negative effect of the Bouraké natural environmental conditions on CCA. At the same time, turf algae cover was significantly higher at Bouraké than at other reef stations. It could be argued that our findings were mostly due to the effect of an abrupt change of environmental conditions, including light exposure, from those characterizing the forereef where the tiles were soaked before deployment to the three study sites. The abrupt deployment could have impacted the benthic organisms present on tiles and indeed, moderate bleaching was evident after the first two months at the study sites (see **Figure III-5 (A–C)**), potentially accelerating a decline in the CCA abundance. However, such deployment effect, should be common across the three stations, and this has not been observed. Indeed, while CCA cover decreased in Bouraké, it was stable or slightly increased at the two stations R2 and M1, after two months (**Table III-2**), which we believe to be a long enough time for any consequence of an abrupt displacement to occur. Furthermore, the initial phase-shift between CCA and turf seen after the first two months at Bouraké, was still confirmed after our two-year in situ experiment: a significant loss in CCA cover (ca. 80%) and a significant increase of turf algae (up to 162%) were measured (**Figure III-5 (D–F)**). While we cannot fully dismiss the hypothesis that the initial deployment has affected the tiles, our 2-years observation did not show a substantial recovery in the color of the settled CCA and we are unable to discern the effect of bleaching from that environmental conditions. A potential

caveat of our experimental design is that forereef where the CCA community (mostly *Porolithon* and *Neogoniolithon*) had settled on the tiles was characterized by different environmental condition compared to the three study sites where the tiles were kept during the 2-year incubation. Although both CCA families are also commonly found on coastal fringing reefs (Claude Payri, personal communication), and the same families were also found at our study sites, we are unable to verify whether the CCAs we transplanted were the same as those that would be found naturally at the study sites.

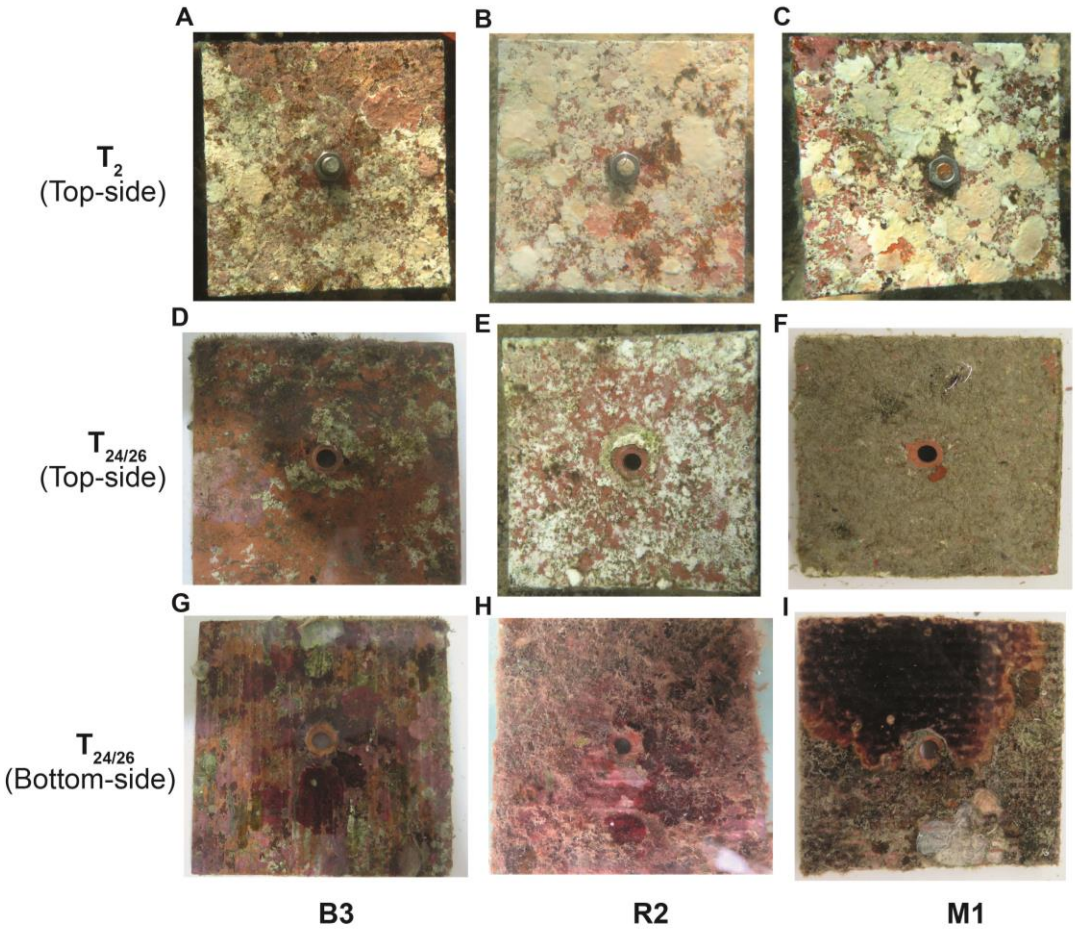

Figure III-5 | *Photos of the tiles (randomly selected) deployed at Bouraké B3 (left), station R2 (middle), and station M1 (right). Pictures of the top sides were taken after two months of deployment (T2)* ***(A–C)****, and after 24* ***(D, E)*** *and 26 months of deployment* ***(F)****. Pictures of bottom sides of tiles after 24 months* ***(G, H)*** *and ca. 26 months of deployment* ***(I)****.*

Inter-species interactions, in combination with a direct effect of acidification and the extreme environmental conditions in the Bouraké system on CCA skeletons, could partially explain this cover drop-off despite a certain persistence obtained by altering skeletal mineralogy, although it remains difficult to assess with certainty (Goffredo et al., 2014; Kamenos et al., 2016). In Bouraké, seawater pH decreased down to 7.23 and exhibited a mean value of 7.67, thus reducing carbonate ion concentrations ($[CO_3^{2-}]$) available and the saturation

state of seawater with respect to aragonite and calcite (Ω_{arag}). Low values of seawater pH have been experimentally shown to cause a decrease in CCA growth and an increase in skeletal dissolution (Kuffner et al., 2008; Comeau et al., 2013; Fabricius et al., 2015; Foster et al., 2016), and are known to reduce their skeletal density (Chan et al., 2019; Williams et al., 2021). Our findings are in agreement with several reports of overall CCA cover reduction ranging from 43% to 92% under low pH (Jokiel et al., 2008; Kuffner et al., 2008; Doropoulos et al., 2012; Fabricius et al., 2015), and from 60% to 100% in combination with high temperature (Martin and Gattuso, 2009; Diaz-Pulido et al., 2012; Vogel et al., 2016). Dissolved oxygen concentration in Bouraké exhibits a mean value of 5.23 mg L^{-1} with a minimum of 2.28 mg L^{-1} (**Table III-1**) which is equivalent to depletion by ca. 30% compared to both stations R2 and M1. Despite the lack of research on hypoxia effects, we could hypothesize an additional negative effect from low dissolved oxygen on CCA growth as it has been previously reported (Altieri et al., 2017; Nelson and Altieri, 2019). The decline of CCA cover could also be due to the combined effect of decreased light exposure and high sedimentation. Indeed, under OA conditions, CCA growth significantly decreases under the combination of low light and low flow conditions (Comeau et al., 2019b), and faces dissolution in shade environments (Martin et al., 2013; Bessell-Browne et al., 2017; McNicholl and Koch, 2021). Although light irradiance was not measured and sedimentation rates in the Bouraké lagoon have yet to be comprehensively measured, it has been suggested that high turbidity in Bouraké could attenuate solar radiation (Jacquemont et al., 2022 (Appendix Article n°1)). Indeed, the Bouraké lagoon is inside a mangrove forest, and when the sediment interstitial water is sucked by the current that empties the mangrove and arrives in the lagoon during ebb tide (spring ebb tide in particular), turbidity temporally increases because of the organic compounds released from the mangrove. This, in turn, and either alone or combined with the high pCO_2 and the warm temperatures in Bouraké may enhance turf algae productivity by alleviating carbon limitation (Johnson et al., 2017). Although such potential negative mechanisms, in Bouraké more than 66 species of corals, and also some CCA on coral rubbles were found (Maggioni et al., 2021). Further measurements of light availability to CCA along diel and seasonal cycles, as well as specific experiments will be necessary to disentangle the contribution of turbidity in combination with high pCO_2 on the CCA growth and dissolution. However, CCA and turf algae cover on the bottom sides of the tiles i.e., the CCA cover median was low in B3 than in R2, and quasi absent in M1, partially confirmed data found on the top sides (**Figure III-5 (G–I)**). While the quasi absence of CCA at M1 could be due to both the high turf algae cover (ca. 75%) and the presence of suspension feeders such as bryozoans, known to be efficient competitors for space (Glassom et al., 2004; Elmer et al., 2018), the presence of CCA at both B3 and R2 at bottom side support the

hypothesis that the decline of CCA found at the top side is due to the combination of the high pCO_2 and other factors such as light and sedimentation.

Our results emphasized the extent to which CCA growth is limited at Bouraké when compared to the station R2 where CCA cover decreased by 24% during the two years of deployment. This result was a bit unexpected because although previous measurements suggested that R2 could show averaged pH values lower than for a typical reef (Maggioni et al., 2021), the study stations were selected having in mind that R2 and M1 were two reef stations having the main environmental parameters (e.g., seawater pH) close to ambient values typical for a coastal fringing reef. However, in terms of seawater pH, R2 turned out to be intermediate between Bouraké and M1 according to recent data on the same site (Maggioni et al., 2021). With regard to R2, the low seawater pH (mean of 7.89 and a minimum of 7.69 pH_T units) might explain why we measured some decrease in CCA cover, since similar pH values have led experimentally to a significant loss in CCA cover (Kuffner et al., 2008; Doropoulos et al., 2012; Comeau et al., 2013; Fabricius et al., 2015). In fact, this presupposed reference station actually exhibited a pH close to values expected in global ocean from the RCP7.0 scenario in 30-40 years (IPCC Report, 2021). These unexpected environmental conditions widened our opportunities to study the effect of OA on CCA and coral recruitment. The low pH was likely due to the site topography. Indeed, R2 is located in a “cul-de-sac” between two islets with sparse but abundant reefs. It is characterized by a fine sediment bottom, and a low seawater renewal rate, likely such as for the Rock Islands in Palau (Micronesia) (Barkley et al., 2015; Shamberger et al., 2018; Kurihara et al., 2021). The combined effect of biological activities and carbonate disequilibrium likely caused such low pH values which are frequent and typical for many coastal fringing reefs with limited seawater exchanges with the lagoon. In contrast to Bouraké, turbid waters were never observed at R2 that benefits from greater light intensity; despite low pH, environmental conditions would still allow CCA persistence.

At station M1, CCA was completely dissolved after two years and tiles were recovered by turf algae. While the effect of pH, in this case, can be discarded (ambient pH of ca. 8.07 pH_T units), the combined effect of lower grazing pressure and well- established wave exposure may partially explain this evolution. It has been shown that grazer presence depends directly on factors such as overfishing, tidal height and wave exposure (Doropoulos et al., 2017). In particular, turf algae seems more abundant where wave action is greater and grazers are less present. Conversely, turf algae are less abundant in sheltered areas where grazers are more active (Underwood and Jernakoff, 1984; Doropoulos et al., 2017). While Bouraké and R2 are sheltered from wave action and quite isolated sites, M1 is an open bay much more subject to wave action and a more intense fishing pressure due to its proximity to Nouméa. Our findings

are in agreement with previous studies reporting both limited CCA growing on the top of the tiles (O'Leary et al., 2012, 2013) and an increase in the turf algal cover (Penin et al., 2011). In addition, we observed a high sedimentation rate in M1 with fine particles being trapped by the dense algal cover. This accumulation of sediment certainly contributed to smothering the underlying CCA.

Coral recruitment seems to be maintained in Bouraké

Ocean acidification, warming and deoxygenation have been shown to negatively affect coral larvae settlement by reducing the growth of favorite substrate (e.g., Diaz-Pulido et al., 2012; Doropoulos et al., 2012) and altering chemical biofilm and microbiological cues for settlement onto CCA (Albright et al., 2010; Albright and Langdon, 2011; Webster et al., 2013; Fabricius et al., 2017; Jorissen et al., 2021). Our findings seem to provide an alternative scenario using a natural extreme environment where coral recruits survived. In fact, although the extreme conditions reduced the CCA cover in Bouraké, after two years of exposure we observed a 3-fold increase in coral recruits when compared with the stations R2 and M1. Recruitment rates recorded in this study are difficult to compare with the literature because values are quite variable. For instance, in French Polynesia, it varies from 0 to 10.8 recruits $tile^{-1}$ (Gleason, 1996; Adjeroud et al., 2007; Bramanti and Edmunds, 2016), and it was less in the Virgin Islands (average of 3 recruits $tile^{-1}$; Edmunds, 2021) and in Palau (0.3 to 3.9 recruits $tile^{-1}$; Victor, 2008), while no data is available for New Caledonia. There might be several explanations for our uncommon and counterintuitive findings. Firstly, because the whole set of tiles was maintained in situ for two years, potentially acted as substrates during two consecutive spawning events. The latter follows the full moon in November, coincident with the mass spawning period on the Great Barrier Reef in Australia (Baird et al., 2010). During the first spawning event, which happened 1-2 months after deployment, the CCA cover was still quite high (41.4%) and still may have allowed tiles to attract coral larvae. If coral recruitment intensity on tiles was the result of a single spawning event, it was quite massive and unusual. According to the disruptive effect of OA on the coral skeleton, especially during early life stages (Cohen et al., 2009; Foster et al., 2016), coral recruits would have been dissolved after two years or at least would have shown important malformation which was not the case (see below some considerations about the site M1). Most likely, our tiles received recruits also during the second spawning event, in spite of the low CCA cover. The role of biofilm acting as an ideal chemical cue for coral larvae settlement (Tebben et al., 2015) could be crucial in this case. Alternatively, coral spawning was either low during two consecutive years at R2 and M1 or recruits did not survive and were covered by competitors, such as bryozoans. The unexpected higher recruitment in B3 could

also be due to high concentrations of organic carbon and high levels of nutrients such as $[Si(OH)_4]$, $[NO_x]$and $[PO_4]^{3-}$ which were 8.88, 0.54 and 0.19 µmol L^{-1}, respectively, in Bouraké (Maggioni et al., 2021) and were, in general, more concentrated (up to 5 times) than at station R2. These concentrations coupled together would have increased coral heterotrophic rates and helped recruits to cope with the extreme conditions (Anthony, 2006; Houlbrèque and Ferrier-Pagès, 2009; Ragazzola et al., 2013; Goldberg, 2018). Increasing the energy budget through heterotrophic nutrition could enhance juvenile growth and facilitate coral recruitment under high temperatures (Huffmyer et al., 2021). This energy budget enhancement could also benefit coral larvae under deoxygenation which has recently been shown to increase the coral larvae energy needs at a dissolved oxygen concentration of around 2 mg L^{-1} (Alderdice et al., 2021). The role of water circulation in the semi-enclosed lagoon of Bouraké has also to be considered since a close water circulation could enhance coral larvae settlement via a decrease in larval dispersal (O'Connor et al., 2007). The particular morphology and hydrodynamics of Bouraké could make this lagoon a real recruitment hotspot as recently observed in St. John, US Virgin Islands (Edmunds, 2021). Recruitment was especially noticeable on the bottom sides of the tiles for each station, likely because tiles act as a shelter against grazing and predation and enhance coral recruitment compared with the top or lateral sides (Penin et al., 2011). Indeed, the top and lateral sides are prone to a more intense grazing activity. In addition, recruits face high levels of sedimentation on top sides which induces smothering (Fabricius and Wolanski, 2000), settlement limitation (Ricardo et al., 2017) and decreases in fertilization, embryogenesis and larval development (Jones et al., 2015). This response was similar among the three stations despite the different environmental conditions.

Our recruit identification revealed the same proportions of corals taxa settled between stations with the Acroporidae as the dominant family (70% of all recruits) followed by the Pocilloporidae (ca. 16%) and only a few Poritidae. This is in agreement with previous studies showing that Acroporidae and other broadcasting corals have high recruitment rates, especially in low water-circulation systems like Bouraké (Oprandi et al., 2019). The dominance of branching morphologies (Acroporidae and Pocilloporidae) may be due to their ability to compete with vertical CCA growth for space in light-limited environments (Jorissen et al., 2020). On the contrary, recruits from massive species such Poritidae, which mainly have a planar growth form, were rare, likely because they are unable to face competitive interactions with other coral species, CCA or suspension feeders. In agreement with this hypothesis, we found only a few recruits of Poritidae at R2 (6.52%) and zero at M1, the latter exhibiting a high density of bryozoans. At site M1 some recruit malformations were found and most of the recruits were classified as unknown genera. Such skeleton malformations are likely to be due

to the competition with other organisms recovering the recruits, than to the effect of dissolving seawater carbonate values.

In this study, we used one of the few natural sites exhibiting extreme and highly variable environmental conditions including high temperature, low DO and low pH. Therefore, our experimental setting benefits from the natural conditions, but in a unique setting where CCA, adult corals and their recruits have been exposed to extreme conditions for several generations over likely hundreds of years. In particular, high pCO_2 and low dissolved oxygen in Bouraké were even worse than what is expected for 2100. Surprisingly, healthy and diversified coral populations still persist as likely because of unexpected high coral recruitment (this study) that gives a glimpse of hope for the future of coral reefs facing climate change. However, our findings need to be used with caution as the Bouraké system is not a typical reef ecosystem. In fact, although our results showed that recruitment is possible even under extreme conditions, it does not mean that it might be the case for other reefs in the future. For instance, it has been shown that OA can cause morphological changes to the coral skeleton and thus, reduce their bulk density and wave resistance (Fantazzini et al., 2015; Tambutté et al., 2015). Further measurements on the skeleton of coral recruits and adults (i.e., SEM observations) from Bouraké are underway to shed light on this possibility.

Importantly, habitats displaying natural variability like Bouraké have been hypothesized to be populated by resilient coral reef organisms (Padilla-Gamiño et al., 2016; Vargas et al., 2017; Kapsenberg and Cyronak, 2019; Enochs et al., 2020). Coral recruits could as well benefit from such high natural variability (Jiang et al., 2017, 2020), although some studies described small influences from variability on some corals and CCA (Cornwall et al., 2018), increased negative effect of OA on CCA calcification (Johnson et al., 2019), or no systematic coral tolerance to warming (Klepac and Barshis, 2020). Defining how variability in multiple co-varying parameters could influence tolerance in biological responses of coral reef organisms remains a significant challenge for the scientific community (Kapsenberg et al., 2015; Boyd et al., 2016; Rivest et al., 2017). Even though the effect of environmental parameters has not been fully deciphered yet, we could assume that Bouraké's corals could have acquired specific mechanisms providing recruits with the ability to face extreme environmental conditions (Putnam et al., 2016, 2017). Which mechanism is used and to what extent acclimation vs adaptation is involved was not the objective of this study and would need further experiments using genomic approaches and reciprocal transplantations between Bouraké and reference stations. However, the present study provided evidence that survival and specific high coral recruitment are possible in natural and extreme habitats such as Bouraké leading to lifelong adapted coral reefs.

CHAPTER 4

PHYSIOLOGICAL RESPONSES OF CORALS TO VARYING pCO_2 CONDITION

4.1 Preamble

High coral recruitment and persistence observed from early life stage at Bouraké in **chapter 3** highlight the potential acclimatization of Bouraké corals to extreme environmental conditions. The specific adaptive mechanisms developed by these corals to persist in such environment may include a certain physiological plasticity compared to corals from reference sites. It is fundamental to determine how such a plasticity set up and how it evolves as a function of pCO_2 levels. In fact, this plasticity may be accompanied with trade-offs in the main physiological traits, such as reduced calcification rate and photosynthesis or changes in the autotrophic nutrition capacities (Bay and Palumbi, 2016; Camp et al., 2020; Wall et al., 2020). The determination of physiological performances in corals potentially acclimated to OA is of major interest to understand coral acclimatization mechanisms. Coral associations with distinct dominant Symbiodiniaceae taxa under extreme environments have shown that coral resilience is particularly influenced by the coral symbiotic community (Camp et al., 2020; Voolstra and Ziegler, 2020; Haydon et al., 2021; Ros et al., 2021). The fact that corals chronically exposed to fluctuating environmental conditions would be more resilient (Enochs et al., 2020; Schoepf et al., 2020; Comeau et al., 2022) is one of the most likely hypotheses to explain coral resilience to high pCO_2 levels. Hence, in **chapter 4**, we determined the differences in physiological performances and symbiotic communities between adult corals of our three model species (*Acropora tenuis*, *Montipora digitata* and *Porites* sp.) at Bouraké and at a reference site. To do so, we set up a 100-day culture experiment under four distinct pH levels, including a fluctuating condition, and we performed a complete physiological and metagenomic study on cultured corals. Specifically, the objectives of this chapter were (**1**) to determine if Bouraké corals exhibit higher physiological performances under OA than corals from the reference site, and (**2**) if they host distinct symbiont communities compared to individuals from the reference site.

4.2 Article n°2: Corals adapted to extreme and fluctuating seawater pH increase calcification rates and have unique symbiont communities

Received: 3 January 2023 | Revised: 18 April 2023 | Accepted: 3 May 2023

DOI: 10.1002/ece3.10099 Ecology and Evolution Open Access WILEY

RESEARCH ARTICLE

Corals adapted to extreme and fluctuating seawater pH increase calcification rates and have unique symbiont communities

Clément Tanvet[1,2,3,*], Emma F. Camp[4], Jill Sutton[2], Fanny Houlbrèque[1,3], Gérard Thouzeau[2] and Riccardo Rodolfo-Metalpa[1,3]

[1] Centre IRD Nouméa, UMR ENTROPIE (CNRS, IRD, UR, UNC, IFREMER), Institut de Recherche pour le Développement, Nouméa, New Caledonia
[2] Univ Brest, CNRS, IRD, Ifremer, LEMAR, F-29280 Plouzané, France
[3] Labex ICONA, International CO_2 Natural Analogues Network, Shimoda, Japan
[4] Climate Change Cluster, University of Technology Sydney, Ultimo, NSW 2007, Australia

* Corresponding author

Abstract

Ocean acidification (OA) is a severe threat to coral reefs mainly by reducing their calcification rate. Identifying the resilience factors of corals to decreasing seawater pH is of paramount importance to predict the survivability of coral reefs in the future. This study compared corals adapted to variable pH_T (i.e., 7.23-8.06) from the semi-enclosed lagoon of Bouraké, New Caledonia, to corals adapted to more stable seawater pH_T (i.e., 7.90-8.18). In a 100-day aquarium experiment, we examined the physiological response and genetic diversity of Symbiodiniaceae from three coral species *(Acropora tenuis*, *Montipora digitata* and *Porites* sp.) from both sites under three stable pH_{NBS} conditions (i.e., 8.11, 7.76, 7.54) and fluctuating pH_{NBS} conditions (i.e., between 7.56 and 8.07). Bouraké corals consistently exhibited higher growth rates than corals from the stable pH environment. Interestingly, *A. tenuis* from Bouraké showed the highest growth rate under the 7.76 pH_{NBS} condition, whereas for *M. digitata*, and *Porites* sp. from Bouraké, growth was highest under the fluctuating regime and the 8.11 pHNBS conditions, respectively. While OA generally decreased coral calcification by ca. 16%, Bouraké corals showed higher growth rates than corals from the stable pH environment (21% increase for *A. tenuis* to 93% for *M. digitata*, with all pH conditions pooled). This superior performance coincided with divergent symbiont communities that were more homogenous for Bouraké corals. Corals adapted to variable pH conditions appear to have a better capacity to calcify under reduced pH compared to corals native to more stable conditions. This response was not gained by corals from the more stable environment exposed to variable pH during the 100-day experiment, suggesting that long-term exposure to pH fluctuations and/or differences in symbiont communities benefit calcification under OA.

Key words: Adaptation; Bouraké; Calcification; Coral; Natural analogue; New Caledonia; Ocean acidification; Physiology; Symbiodiniaceae

1. Introduction

Coral reefs have been suggested to be at risk of disappearance in the coming decades due to their sensitivity to the deadly trio of stressors including ocean warming (OW), acidification (OA), and deoxygenation (OD) (e.g., Hoegh-Guldberg et al., 2017; D. J. Hughes et al., 2020; T. P. Hughes et al., 2018). These stressors are expected to increase over the coming decades, leading to a dramatic decline of coral reefs by as early as 2050 (Hoegh-Guldberg et al., 2017; IPCC Report, 2021). However, species-specific responses to abiotic stressors (Rodolfo-Metalpa et al., 2011; Jury and Toonen, 2019; Altieri et al., 2021; Comeau et al., 2022), and *in vitro* experiments (Cornwall et al., 2018; Comeau et al., 2019a) have shown that some corals

can be resilient to one stressor or to the combination of more stressors (e.g., OA, OW, OD). Among the most likely hypotheses to explain coral resilience to OA is the phenomenon that corals chronically exposed to major environmental changes are more resilient to future changes of pH and/or temperature (Enochs et al., 2020; Schoepf et al., 2020; Comeau et al., 2022). Possible mechanisms that could support resilience include physiological plasticity, epigenetics, and host more tolerant microbiome and Symbiodiniaceae (Putnam et al., 2016; Camp et al., 2017, 2020; Voolstra and Ziegler, 2020; Ros et al., 2021).

Corals thriving under variable seawater pH and temperature conditions in mangrove lagoons have showed a shift in dominant host-associated Symbiodiniaceae taxa (Ros et al., 2021), likely contributing to the persistence of corals in such extreme environments (Howells et al., 2012; Camp et al., 2018, 2020; Voolstra and Ziegler, 2020; Haydon et al., 2021). Interestingly, some corals from stressful and/or variable environments have associated with *Durusdinium* (formerly clade D) (Stat and Gates, 2011; Lesser et al., 2013; Stat et al., 2013; Schoepf et al., 2015; Wall et al., 2021) that is considered a 'stress-tolerant' taxa, although this is not always the case (Camp et al., 2019, 2020). Whilst corals with a stable host-Symbiodiniaceae association have been suggested to be physiologically more resilient under stressful conditions (Grottoli et al., 2018; Howells et al., 2020), it remains relevant to explore how stability (i.e., fidelity) and flexibility in the Symbiodiniaceae diversity benefit host fitness under stress conditions (Putnam et al., 2012; Fabina et al., 2013; Ziegler et al., 2015; Smith et al., 2017; McIlroy et al., 2020).

More generally, coral resilience to extreme conditions includes trade-offs in the main physiological traits, such as reduced calcification rate (Cunning et al., 2015; Bay and Palumbi, 2016; Camp et al., 2020) and photosynthesis (Camp et al., 2020), increased photodamage (Silverstein et al., 2017), and change in the autotrophic nutrition capacities (Wall et al., 2020). For instance, corals with thermotolerant symbionts have been reported to resist bleaching but grow more slowly (Jones and Berkelmans, 2010). Most of these trade-offs remain poorly tested on corals already adapted to conditions close to or even worse than the ones predicted for the end of this century. Yet, extreme environments, such as mangrove lagoons have been identified to be faithful natural laboratories for studying species living under the combination of future extreme conditions in OA, OD, and OW (Camp et al., 2018).

The semi-enclosed lagoon of Bouraké in New Caledonia is one of these extreme environments which has been recently environmentally and ecologically characterized (Camp et al., 2017; Maggioni et al., 2021; Tanvet et al., 2022). Bouraké has fluctuating acidified, warm and deoxygenated conditions, although a highly-diversified coral reef develops. The environmental variability in the dissolved oxygen, temperature and pH in Bouraké is directly related to the tidal cycle with changes on a single day by up to 4.91 mg O_2 L^{-1}, 6.50°C and 0.69

pH_T units (Maggioni et al., 2021), respectively. Such environmental conditions likely enhanced the coral respiration rates and total chlorophyll contents, while reducing photosynthesis and calcification rates (Camp et al., 2017; Jacquemont et al., 2022 (Appendix Article n°1)). In addition to the particular physiological response of some corals from Bouraké, Camp et al. (2020) also found differences in host-microorganisms associations between Bouraké and an adjacent reef. Although species-specific, the differences in the Symbiodiniaceae found in three coral species (Camp et al., 2020) highlight the potential role that Symbiodiniaceae play in influencing coral holobiont resilience to environmental stress (Sampayo et al., 2008). Corals in Bouraké have likely either adapted to, or sustain key trade-offs to achieve resilience in an environment somewhat reproducing future climate conditions.

In the present study, we conducted a 100-day OA experiment in aquaria using three coral species (*Acropora tenuis*, *Montipora digitata* and *Porites* sp.) from the highly variable Bouraké and a less variable adjacent reference reef to assess: i) whether corals adapted to ambient or fluctuating pH conditions alter their metabolic rates and calcification under different levels of OA (i.e., 7.54, 7.76, 8.11 and 7.56-8.07), and ii) whether Symbiodiniaceae communities are distinct between habitats and treatments at the end of the experiment. In addition, we considered both static pH_{NBS} (7.54 ± 0.08; 7.76 ± 0.07; 8.11 ± 0.05) and variable (ranging from 7.56 ± 0.07 to 8.07 ± 0.07) pH_{NBS} conditions to assess the role that fluctuating pH may play in the success of Bouraké corals, and whether corals adapted to stable pH can acclimate when exposed during 100 days to variable pH. We hypothesize that corals from Bouraké exhibit enhanced physiological rates and a distinct Symbiodiniaceae community, compared with corals from the less variable reef, and that the natural diel fluctuations in seawater pH promote their resilience to OA.

2. Materials and Methods

2.1 Study sites, coral collection and acclimation

All corals were collected at the end of January 2020 in the semi-enclosed lagoon of Bouraké, New Caledonia (21°57'3.971"S 165°59'24.233"E) (**Appendix Figure VIII-5**), and at one reference reef adjacent to Bouraké (21°58'6.966"S 165°56'43.907"E) (St R1, 4 km away). Both sites were environmentally characterized during multiple monitoring since 2016 (Camp et al., 2017; Maggioni et al., 2021). In Bouraké, dissolved oxygen (DO) and pH regularly fluctuated according to the tide (ca. 1 m tidal range), from 1.87 to 7.24 mg O_2 L^{-1} (mean diel of 5.23 ± 0.89 mg O_2 L^{-1}) and from 7.23 to 8.06 pH_T (mean diel of 7.67 ± 0.23 pH_T), respectively. Seawater temperature varied from 17.50°C in winter to 33.80°C during summer, when

temperature might change by up to 6.50°C in a single day (mean diel of 25.63 ± 2.85°C). In comparison, DO, pH and temperature were more stable at the reference site (hereafter reference) and yearly averaged 6.45 ± 0.95 mg O_2 L^{-1}, 8.02 ± 0.04 pH_T, and 25.25 ± 1.89°C (Camp et al., 2017; Maggioni et al., 2021). For example, from February to March 2016, these reefs spent 44% of the time at pH_T of 7.7-7.8, and 71% of the time at temperatures predicted for the end of the century under scenario RCP7.0 (Camp et al., 2017). Notwithstanding such extreme and chronic conditions, 66 coral species form reefs all along the Bouraké lagoon (Maggioni et al., 2021).

Fifteen mature colonies (30 - 60 cm diameter) of the branching *Acropora tenuis* (Dana, 1846) and *Montipora digitata* (Dana, 1846), and the massive *Porites* sp. were sampled at each site at ca. 2 meter depth. Only colonies at a distance of at least 5 m from each other were collected to limit the risks of clonality in our sampling. From each branching colony, four terminal portions of branches (ca. 3 - 5 cm long) were collected using pliers. For *Porites* sp., four samples (mean of ca. 8 cm^2) were collected from each colony using a 3-cm-diameter steel tube and a hammer. Coral fragments were transported in a cooler to the "Aquarium des Lagons" (Nouméa), which is 2 h distant from Bouraké, in individual hermetic zip bags (one for each colony of each species) containing seawater from the collection site. At the laboratory, fragments of *A. tenuis* and *M. digitata* were attached on nylon wires and suspended in two 200 L tanks, one for each site of collection (see below). Fragments of *Porites* sp. were mounted on labeled 2x2 cm PVC plates using epoxy resin (Holdfast, Aquarium Systems) and placed at the bottom of the tanks. Exposed skeleton was covered with the resin to avoid turf algae proliferation and potential skeletal dissolution. All 360 fragments (2 sites, 3 species, 15 colonies per species, 4 samples per colony, resulting in a base replication of n = 15 per treatment) were allowed to recover for three weeks in the two flow-through aquaria (see below for more details) settled at the same temperature (26.0 ± 0.5°C) recorded *in situ* at the time of collection. Seawater pH and carbonate chemistry replicated mean values of Bouraké and reference sites (ca. 7.7 and 8.1 pH_{NBS} units, respectively). Temperature and pH were kept constant using heaters and bubbling pure CO_2 in each tank. All tanks were connected to an IKS logger system (IKS, AquaStar, Germany, accuracy ± 0.05 pH unit and 0.1 °C). During the recovery period, coral fragments received the same lighting intensity (ca. 250 µmol photons m^2 s^{-1}) using four Aquablue Plus neon bulbs (15.000K, Giesemann, Germany), and they were fed once a week with freshly hatched *Artemia salina* nauplii (regular equivalent quantities tossed in the tanks; Houlbrèque et al., 2015). At the end of the three weeks recovery period, the naked skeleton of branching corals were already covered by the tissue, while new tissue was visible on the resin embedding *Porites* sp.

2.2 Aquarium setup and physiological measurements

2.2.1 Aquarium conditions and experimental set-up

At the end of the recovery period, corals from each site of collection (called origin hereafter) were assigned to one of the 12 experimental tanks as follows. Three replicate 10 L tanks were set up for each of the four conditions of pH (monitored with an IKS logger system and pH Metrohm in NBS scale) (Table 1): i) stable pH (Control; pH_{NBS} 8.11 ± 0.05; pCO_2 474 µatm); ii) future reef pH based on the RCP7.0 IPCC scenario (IPCC Report, 2021) (Future; pH_{NBS} 7.76 ± 0.07; pCO_2 1192 µatm); iii) extreme stable pH (Extreme; pH_{NBS} 7.54 ± 0.08; pCO_2 2115 µatm); and iv) variable pH reproducing the semidiurnal tide phase variation of pH in Bouraké with four peaks of pH on a 24-h basis, two at low and two at high pH (Variable; mean pH_{NBS} ranging from 7.56 ± 0.07 to 8.07 ± 0.07; pCO_2 ranging from 1968 to 533 µatm). While extreme stable pH were arbitrarily chosen, control and variable pH were settled based on the mean and variance data collected respectively at reference and Bouraké reef between 2016 and 2020 (see Maggioni et al., 2021). Five fragments per coral species (n = 3) and per origin (n = 2) were randomly positioned in each tank. *Porites* samples were positioned on the bottom of the tanks while the branching corals were suspended.

Seawater in the tanks was renewed at a rate of 16.5 L h^{-1} (renewal rate of ca. 165% h^{-1}) and mixed using a submersible pump (micro-jet MC 320, Aquarium system, USA). Each tank was supplied with seawater pumped from one to three 60 L sump tanks settled at different pH (7.4, 7.7, and 8.1). In addition, three more sump tanks were set up respectively at pH 7.6, 7.8 and 7.9 and were used to better simulate the pH variation in the variable treatment (see below). Each sump tank was continuously supplied with 50 µm-filtered seawater pumped at 5 m depth in front of the Aquarium des Lagons (Baie des Citrons, Nouméa). Each sump contained a submersible pump (23 W Eheim), a heater and an external refrigerating system, both connected to an IKS logger system (IKS, AquaStar, Germany), and temperature and pH probes. Seawater pH_{NBS} and temperature values were continuously monitored by an IKS pH logger and daily verified using a portable pH-meter (Metrohm 826 coupled with a LL Aquatrode Plus SC, sensitivity of 0.001 pH units), both calibrated using NBS solutions (pH 4.0 and 7.0 from the Seawater National Bureau of Standards). Sumps were all maintained at 26.3 ± 0.7°C, and at one of the 6 pH conditions, automated by IKS (AquaStar, Germany). Seawater pH was set to the desired value by bubbling pure CO_2 gas. Each experimental tank received seawater at the assigned temperature and pH from the respective sump tank. In contrast, for the variable pH treatment, the time function of the IKS system was used to simulate the pH changes measured at Bouraké, according to a semidiurnal tide cycle with high pH in the middle of the

day/night and a low pH in the beginning of the day/night. Briefly, tanks received seawater either from one or simultaneously from different sumps according to a predetermined timetable (**Appendix Table VIII-5**; **Figure VIII-6**). Irradiance in all tanks increased from 0 to ca. 250-300 µmol photons m^{-2} s^{-1} on a 12:12 h light:dark cycle (06:00-18:00 h lighting vs 18:00-06:00 h darkness; ramp until 10:00 h and decline from 14:00 h) using LED lights (Mitras LX6100, GHL Germany; see **Appendix Table VIII-6** for led brightness wave simulation) according to Biscéré et al., (2019), Houlbrèque et al., (2015) and Jacquemont et al. (2022) (Appendix Article n°1). Irradiance was monitored during 48-h cycles using a NKE PAR with LI-193 spherical quantum sensor and showed maximum values ranging from ca. 270 to 320 µmol photons m^{-2} s^{-1} (**Appendix Figure VIII-7**). Tanks' positions were repeatedly changed during the duration of the experiment to minimize any potential spatial variability in the light intensity received by corals. A Seabird SeaFET pH logger and YSI 600 OMS-M probes were periodically used to measure over a 48-h cycle seawater temperature, pH_T, salinity and dissolved oxygen (DO) in the experimental tanks with the intention to document the variation in such a parameter over repeated diel cycles. Colonies were fed with freshly hatched *Artemia salina nauplii* once a week (regular equivalent quantities tossed in the tanks) and were maintained under these experimental conditions for 100 days. Tanks, resins and wires were regularly cleaned for turf algae proliferation.

Total alkalinity (A_T) was measured twice a month at various daytime to have the average total alkalinity reflecting the different pH values on each of the 12 tanks over the experiment. For that, water samples were filtered at 0.45µm (GF/F Whitman), preserved with saturated $HgCl_2$ and stored in the dark at 4°C to avoid biological alteration. Two 20-mL replicates were analyzed using an auto titrator (Eco Titrator, Metrohm), and A_T was calculated from the Gran function. Results were corrected against A_T standards (Andrew G. Dickson, batch no. 155, Scripps, USA). Dissolved inorganic carbon (DIC), pCO_2 and saturation states of aragonite (Ω_{arag}) were calculated with the software CO2SYS, using pH (NBS scale), A_T, temperature, values for the K1 and K2 carbonic acid constants from Lueker et al. (2000), for $KHSO_4$ from Dickson, (1990), for KHF from (Perez and Fraga, 1987), for $[B]_l$ from (Lee et al., 2010), and an averaged atmospheric pressure of 1.015 atm (Météo France).

Nutrient content was measured twice a month on each of the 12 tanks. The sampling of nutrients (orthosilicic acid $[Si(OH)_4]$, nitrogen oxide $[NO_x]$ (i.e., the sum of NO_2^- and NO_3^-), and phosphate $[PO_4]^{3-}$) was done using 20 mL polypropylene vials, rinsed three times using filtered seawater (Whatman™ Puradisc CA syringe filters 0.45 µm), filled with the sample, and immediately poisoned with 20 µL saturated $HgCl_2$. Measurements of PO_4^{3-}, NO_x and $Si(OH)_4$ were performed by colorimetry (Seal Analytical).

2.2.2 Growth rate

After the recovery period and at the end of the experiment, each coral fragment was weighed using the buoyant weight technique (Davies, 1989). Samples were weighed using a Sartorius ENTRIS 224i-1S electronic balance (readability 0.1 mg) in seawater of known density (calculated from temperature and salinity, both measured each ten samples). Dry skeleton weight was calculated using the density of pure aragonite (2.94 g cm^{-3}); growth rates (in term of calcification rates) were calculated as the change in dry weight between the initial (T_0) and the final weight (T_F) during the experiment and expressed either in mg g^{-1} d^{-1} (normalized per weight of $CaCO_3$) or mg cm^{-2} d^{-1} (normalized per surface area of the coral, see below) depending on the species.

2.2.3 Photosynthetic efficiency

During the last week of the 100 day experiment, maximum photochemical efficiency (F_v/F_m) and the relative electron transport rate (rETR) of the photosystem II (PSII) of symbionts *in hospite* were measured on all corals using a pulse amplitude modulation (PAM) fluorometer (DIVING-PAM, Walz, Germany, Schreiber et al., 1986). Before measurements, coral fragments were dark adapted during 15 minutes (Hoegh-Guldberg and Jones, 1999). Measurements were performed at dark (no light source apart from the use of red headlamp); the 8 mm optical fiber was maintained perpendicular to the fragment's surface using a black-jacket at a fixed distance of 5 mm. Rapid-light curves used a measure of ETR, determined as follow (rETR = $\Delta F/F'_m$ x 0.5 x PAR) with nine steps of fluorescence measurements (4, 120, 191, 278, 376, 546, 729, 1078, 1544 µmol photon m^{-2} s^{-1}) according to Ralph et al. (1999). Because corals were dark adapted we considered the first point the maximal quantum yield F_v/F_m. RLC uses a very short illumination period and it is incorrect as it does not measure the real ETR (see Enríquez & Borowitzka 2010). Because we could not perform long RLC on the 135 corals, we limited our analysis on the maximum $rETR_{max}$, assuming this limitation for all corals and conditions. Comparisons between treatments and origin were done on the maximum quantum yield F_v/F_m and the maximum $rETR_{max}$.

2.2.4 Photosynthesis and respiration rates

At the end of the experiment, seven corals for each pH condition (n= 4), each origin (n= 2) and each species (n= 3) were randomly selected (n= 168 total) and their oxygen production and consumption rates were measured daily in the light and dark during four consecutive days. Corals were individually placed in 100 mL Pyrex glass beakers which were filled with seawater from their respective tank treatment and hermetically sealed underwater with transparent

cellophane and a rubber band Jacquemont et al. (2022) (Appendix Article n°1). Two control beakers without coral fragments were used to measure any metabolic activity of microbes in the water. We were able to process 28 samples simultaneously (plus two empty beakers) using two 15-place magnetic stirring plates (Telesystem 15, Thermo Scientific). The 30 beakers were semi-immersed in a water bath positioned above the stirring plates and settled at a temperature of 26.0°C ± 0.5°C using one heater and two submersible water pumps to homogenize water temperature. Each beaker had one O_2 sensor spot (PreSens) fixed on the glass, and contained a stirring bar and a bridge made of plastic mesh to separate the coral fragment from the bar. Corals were first incubated in the light for 50 min under ca. 250 µmol photons m^2 s^{-1} and then in the dark for the same time (Biscéré et al., 2019; Jacquemont et al., 2022 (Appendix Article n°1)). Incubation time was preliminary defined to avoid both hyperoxic and hypoxic conditions in the beakers. Temperature and dissolved oxygen (DO) in mg L^{-1} were measured at the beginning and at the end of each incubation in each beaker using an optical fiber (PreSens Fibox 4 trace). Before measurement, corals were left for 10 min under either light or dark conditions and then DO was measured. At the end of the light incubation, each beaker was opened and seawater volume was measured using a graduated cylinder to normalize the DO concentration to the seawater volume of each incubation. Fresh seawater from the corresponding experimental tank was then added, before the beakers were resealed and placed on the stirring plates under dark conditions. At the end of each incubation pair (dark and light) for all pH conditions, coral fragments were frozen at -20°C for further analysis of the chlorophyll, symbiont density, symbiont community analysis and protein contents, and to determine their skeletal surface area.

Rates of net photosynthesis (P_{net}) and respiration in the dark (R_{dark}) were calculated using the change in DO concentrations in each beaker corrected by the mean of the microbial activity measured in the two empty beakers, and normalized by the incubation duration (hours), the volume of seawater in each beaker (L), and the coral's surface (cm²). Rates of gross photosynthesis (P_g) were calculated as:

$$P_g = P_{net} + |R_{dark}| \quad (1)$$

Data were normalized per surface area of the fragment as described below. P_{net}, P_g and R_{dark} are expressed in mg O_2 cm^{-2} h^{-1} then converted in µmol O_2 cm^{-2} h^{-1}. Photosynthesis to respiration ratio (P_g:R) was calculated using the value of daylight hours equal to 12 to calculate an integrated P_g:R ratio for a 24h day as follows:

$$P_g{:}R = \frac{P_g \times hours\ of\ daylight}{|R_{dark}| \times 24} \quad (2)$$

2.2.5 Tissue and surface measurements

All fragments used to assess the coral photosynthesis and respiration rates were prepared and analyzed for their Symbiodiniaceae and chlorophyll contents. Protein measurements were performed on the same individual used during photosynthesis and respiration incubations for *Acropora tenuis* and *Montipora digitata* and from a new individual for *Porites* sp. Then, their skeleton's surface areas were measured. Coral tissue was extracted from the skeleton using an air pick in 20 mL filtered seawater and homogenized with a Potter tissue grinder. For symbiont density measurement, 2 mL of the slurry was sampled to count the number of Symbiodiniaceae (n count = 8) using a Neubauer's cell under a stereomicroscope. Ten mL subsamples were centrifuged at 5,000 g for 10 min, the supernatant was discarded, and the pellet containing the symbiont was re-suspended in 10 mL of pure acetone to extract during 24 h at 4°C in darkness the chlorophyll *a* and c_2. The solution was then centrifuged at 10,000 g for 15 min and the supernatant was sampled to measure its absorbance at 630, 663 and 750 nm using a spectrophotometer (Evolution 201, Thermo Scientific). Chlorophyll *a* and c_2 concentrations were calculated using the spectrophotometric equations for dinoflagellates of Jeffrey & Humphrey, (1975). Chlorophyll *a* and c_2 are given as total chlorophyll expressed in µg cm^{-2}.

Protein content was quantified using a BCA assay kit (Uptima, Interchim). Total protein was extracted according to (Hoogenboom et al., 2010) by incubating each fragment in a sodium hydroxide solution (1 N) maintained in a water bath for 30 min at 90°C. Samples were then diluted by a factor of 15 before being transferred into 96-well microplates and incubated with a dye reagent (Uptima Reagents, Interchim) for 30 min at 60°C. Bovine serum albumin (BSA, Interchim) was used as a protein standard with concentrations of 0, 50, 100, 200, 350, 500, 750 and 1000 µg ml^{-1}. Samples and standards were homogenized for 30 s on a microplate shaker within the spectrophotometer (Biotek ELx808); absorbances were measured at 563 nm, and the protein contents were calculated according to the standard equation and expressed in mg cm^{-2}.

The skeletal surface areas of samples were estimated using the paraffin wax-dipping method with two wax dips (Stimson and Kinzie, 1991; Naumann et al., 2009) for branching species

(i.e., *Acropora tenuis* and *Montipora digitata*) and the aluminum foil technique (Marsh, 1967) for the massive species *Porites* sp.

2.3 Symbiodiniaceae community analysis

2.3.1 DNA extraction, PCR amplification and sequencing

Fragments of corals (n= 2-6 per species, depending on origin and pH treatment) were collected and stored at -20°C. Total coral holobiont DNA (i.e., Symbiodiniaceae, polyp and associated microorganisms DNAs) was extracted using a 2% CTAB-based protocol adapted from (Mieog et al., 2009). The quantity and quality of extracted DNA were checked using a NanoDrop 2000 spectrophotometer (Thermo Fisher Scientific, MA). Extracted DNA was then diluted to a range of 30-70 ng μL^{-1} for PCR amplification. The Symbiodiniaceae nuclear DNA ribosomal internal transcribed spacer (ITS2) region was amplified with the forward primer ITS2-DINO [5'-TCGTCGGCAGCGTCAGATGTGTATAAGAGACAGGTGAATTGCAGAACTCCGTG-3'] (Pochon et al., 2001) and reverse primer ITS2Rev2 [5'-GTCTCGTGGGCTCGGAGATGTGTATAAGAGACAGCCTCCGCTTACTTATATGCTT-3'] (Stat et al., 2009). The underlined segments represent Illumina adapter overhangs (Illumina, San Diego, CA, USA). The PCRs were conducted in 25 µL reactions using 12.5 µL of AmpliTaq 360 Master Mix, 1 µL of each 10 µM primer mix, 1 µL of 360 GC Enhancer, 2 µL of DNA template and DNAse-free water to adjust the reaction volume. The amplification cycle was set and adjusted from (Arif et al., 2014) as follows: 94°C for 15 min; 35 cycles each at 95°C for 30 s, 49°C for 1 min, and 72 °C for 30 s; and a final extension at 72°C for 10 min. To check amplification success, 3 µL of each PCR product was run on a 1% agarose gel. The resulting amplicons were sequenced using the Illumina MiSeq platform (2 x 300 bp) (Australian Genome Research Facility, Victoria, Australia). Returned demultiplexed FASTQ files were analyzed via the SymPortal analytical framework (Hume et al., 2019). The SymPortal framework predicts from raw sequences, ITS2 type profiles from specific sets of defining intragenomic ITS2 sequence variants (DIVs) based on genetically differentiated Symbiodiniaceae taxa. Quality control was assessed using MOTHUR 1.39.5 (Schloss et al., 2009), BLAST+ suite of executables (Camacho et al., 2009) and minimum entropy decomposition (MED; Eren et al., 2015) to predict Symbiodiniaceae taxa from the ITS2 marker.

2.4 Statistical analyses and data presentation

Statistical analyses were conducted, and figures were produced using RStudio (R Development Core Team, version 4.1.0, 2021), including the packages *ggplot2*, *ggpubr*, *car*,

and *vegan*. Homogeneity and the normality of variance distributions were tested using respectively the Levene test and the Shapiro-Wilkinson test, and graphically verified with Q-Q plots. Statistical analyses were performed separately for each species as the three species we used are morphologically different. Each response variable was evaluated with a separate linear mixed-effects models using the package *lme4* (Bates et al., 2015). To evaluate differences in the main environmental parameters in the tanks during the experiment, i.e., pH, temperature and nutrients measurements, the full model included pH as a fixed factor and tank as a random factor. To evaluate coral physiological responses, the full model included coral's origin (two levels: Bouraké and reference) and pH conditions (4 levels: control, future, extreme and variable) as fixed factors and tank as a random factor. The significance of fixed factors was evaluated with two-way ANOVAs (type III) using Satterthwaite's method. Significant differences between fixed factors were determined with Tukey's *post hoc* pairwise comparisons using the package *emmeans*. In contrast, F_v/F_m data did not meet the assumption of normality and they were compared using the non-parametric two-way Aligned Rank Transformed (ART) ANOVA (Type III) followed by a Bonferroni p-levels adjusted post hoc using the package *ARTool*. Data were described as box plots using median values ± 25th and 75th percentiles (box), minimum and maximum values (whiskers) and dots as outliers, otherwise specified. Differences in Symbiodiniaceae ITS2 profiles were analyzed on square-root transformed data using three-factorial permutational multivariate analysis of variance (PERMANOVA) with 999 permutations of residuals and based on Bray-Curtis distances to test for differences between sites (two levels), pH conditions (four levels) and species (three levels).

3. Results

3.1 Seawater parameters

Seawater pH, temperature and carbonate chemistry were maintained at the target experimental values during the 100-day experiment (**Table IV-1; Appendix Table VIII-7; Table VIII-8**).

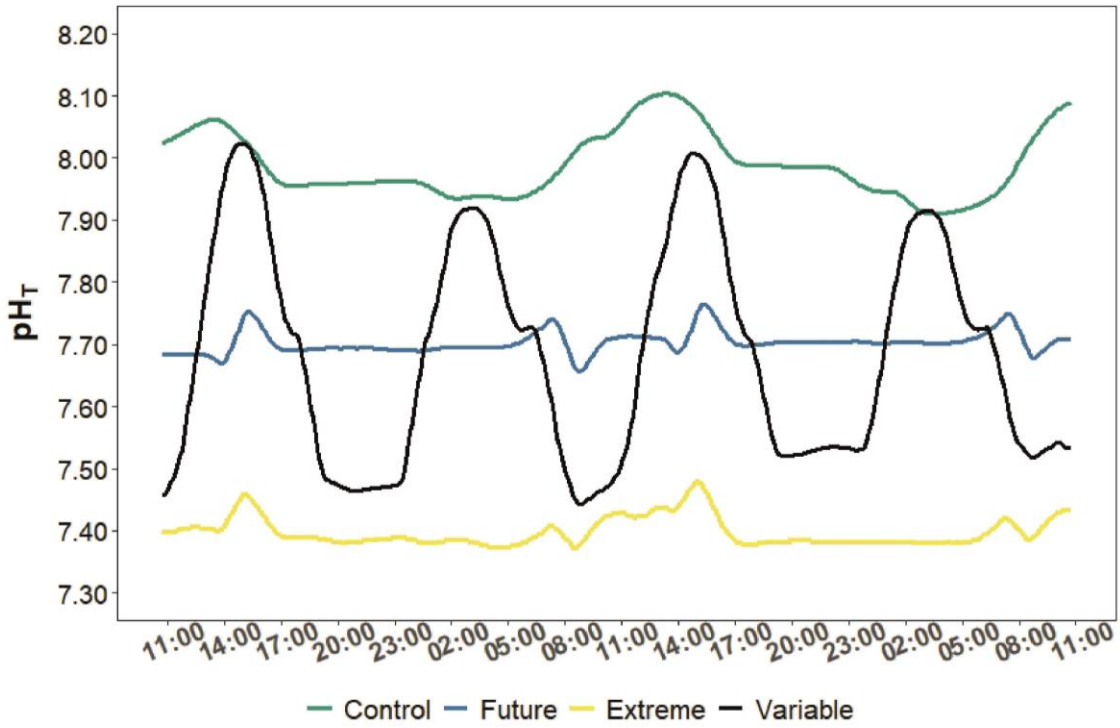

Figure IV-1 | *Seawater pH_T variations recorded with a SeaFet during a 48-h cycle in four experimental pH conditions (Control, pH_{NBS} 8.11; Future, pH_{NBS} 7.76; Extreme, pH_{NBS} 7.54; and Variable, pH_{NBS} 7.56-8.07). See Table IV-1 and Appendix Table VIII-7 for all data.*

There is a significant difference between conditions regarding temperatures (**Appendix Table VIII-9**). However, the average temperatures were rather similar between conditions (ranging from 26.18°C to 26.41°C). Minimum and maximum values were recorded in the extreme (23.90°C) and variable treatment tanks (28.30°C), respectively, due to an occasional 24-h malfunction of the temperature control system for this treatment that occurred during the first week of the experiment. The pH was significantly different between the four pH conditions with minimum and maximum values recorded in the extreme (7.31) and the control condition (8.27), respectively (**Appendix Table VIII-7; Table VIII-9**). According to the SeaFet measurements, seawater pH values varied by ca. 0.60-0.65 pH_T units in the variable condition, and by only 0.05-0.1 pH_T units in the other conditions (**Figure IV-1**).

Nutrients concentrations were similar between conditions (**Appendix Table VIII-9; Table VIII-10**). Averaged values (± SD) of NO_x varied from 0.59 (± 0.21) to 0.67 (± 0.25) µmol L^{-1} for control and future conditions, respectively. PO_4^{3-} concentrations were equal to 0.30-0.31 µmol L^{-1} for all treatments, while $Si(OH)_4$ varied from 2.79 (± 1.06) to 2.89 (± 1.18) µmol L^{-1} for variable and future conditions, respectively.

		Measured		Calculated				
Condition		**Temp** (°C)	**pH** (NBS)	pCO_2 (µatm)	**DIC** (µmol kg^{-1})	HCO_3^- (µmol kg^{-1})	CO_3^{2-} (µmol kg^{-1})	Ω_{arag}
Control	Mean	26.23	8.11	479	1926	1731	182	2.89
	SD	0.49	0.05	72	30	47	19	0.30
	Min	24.20	7.96	300	1834	1587	136	2.16
	Max	27.50	8.27	717	2002	1847	239	3.79
Future	Mean	26.18	7.76	1207	2097	1970	94	1.49
	SD	0.52	0.07	198	26	34	14	0.22
	Min	24.20	7.63	622	1993	1823	69	1.10
	Max	27.50	8.01	1679	2148	2032	152	2.43
Extreme	Mean	26.33	7.54	2141	2173	2056	58	0.93
	SD	0.50	0.08	381	26	27	11	0.17
	Min	23.90	7.31	683	2009	1849	35	0.55
	Max	28.30	7.98	3610	2249	2115	141	2.24
Variable	Mean	26.39	7.75	1427	2090	1951	101	1.60
	SD	0.58	0.23	710	93	124	50	0.79
	Min	24.20	7.37	370	1893	1671	40	0.63
	Max	28.30	8.20	3181	2230	2103	212	3.36

Table IV-1 | *Seawater parameters measured during the 100-day experiment, and carbonate chemistry calculated for each pH condition (the 3 replicated tanks were pooled). Seawater carbonate chemistry was calculated using mean values for A_T (2187, 2204, 2202, and 2202 µmol kg^{-1} for Control, pH_{NBS} 8.11; Future, pH_{NBS} 7.76; Extreme, pH_{NBS} 7.54; and Variable, pH_{NBS} 7.56-8.07, respectively), and mean salinity value of 35.61.*

3.2 Growth rate

Growth rates of the three coral species (**Figure IV-2**) were significantly different according to corals' origin and pH conditions, but not their interactions, with the exception of *M. digitata* showing a *p*-value = 0.086 for pH (2-way ANOVA, **Table IV-2** and **Appendix Table VIII-11** for all data analyses). The mean growth rates of the three corals originated from the reference and maintained at control pH, generally decreased when maintained at future, extreme and also variable pH. This decrease was more evident in the two branching corals than on *Porites* sp. For instance, the calcification rates of *A. tenuis*, *M. digitata*, and *Porites* sp. originating from the reference site decreased by 9.3%, 19.0% and 17.6%, respectively, in the future pH (pH_{NBS}

7.76) condition and by 15.4%, 53.5%, and 20.7% in the extreme pH (pH_{NBS} 7.54), compared to the control pH (pH_{NBS} 8.11).

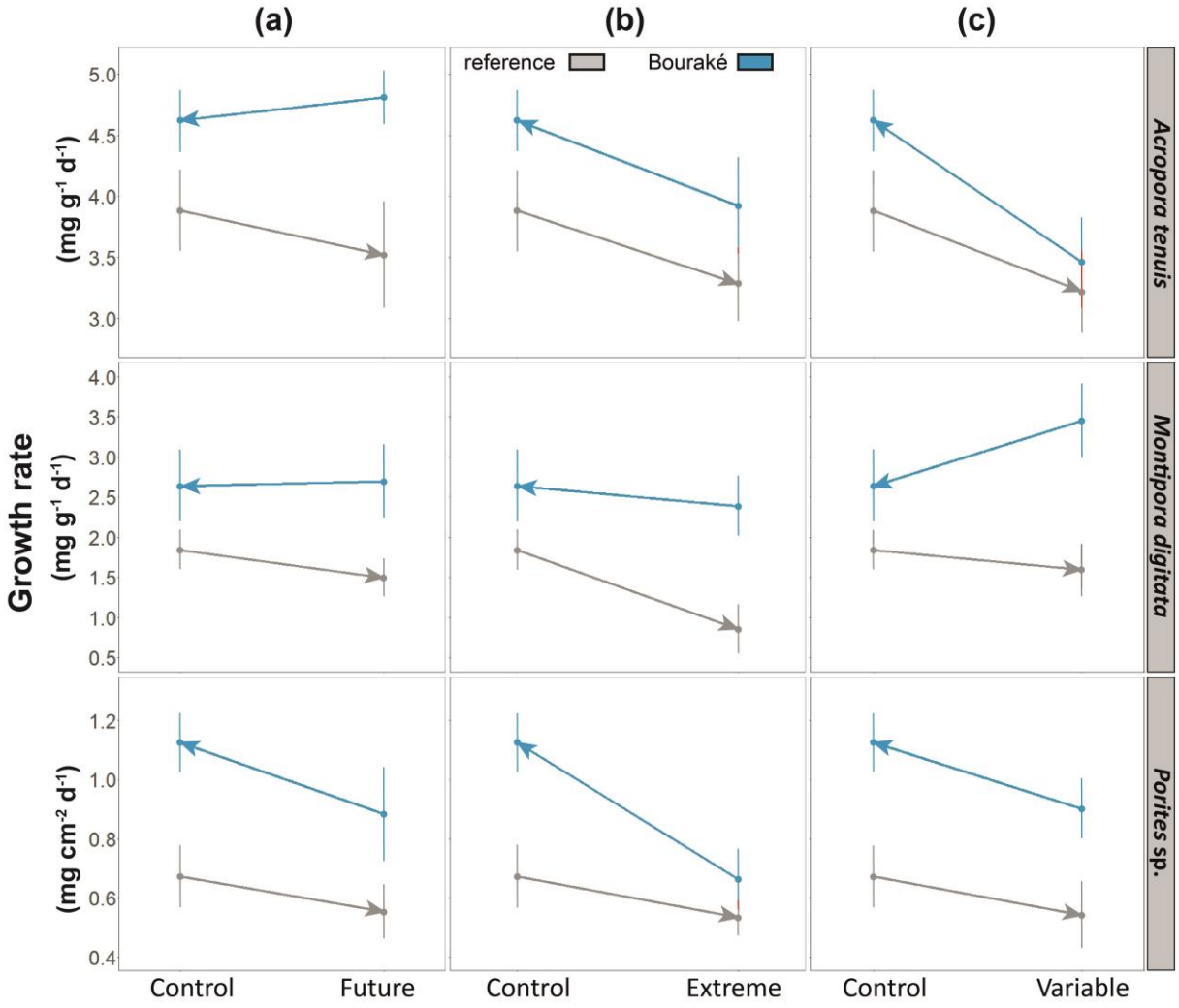

Figure IV-2 | *Reaction norm of the growth rates of corals from Bouraké (blue) and reference (grey) site maintained during 100 days at four pH conditions (Control, pH_{NBS} 8.11; Future, pH_{NBS} 7.76; Extreme, pH_{NBS} 7.54; and Variable, pH_{NBS} 7.56-8.07). The arrow indicates the direction of the change from the condition of origin, assuming that corals from Bouraké might originate from seawater at either pH 7.7 (Future pH) or 7.4 (Extreme pH), to the experimental pH condition. Data represented as dots are means of the three replicate tanks ± SE (overlapping SEs are in red) (n = 13-16, depending on species and pH condition; see Appendix Table VIII-11 for all post hoc comparisons).*

Parameter	Fixed factor	*A. tenuis*	*M. digitata*	*Porites* sp.
Growth	Origin	**0.003**	**<0.001**	**<0.001**
	pH	**0.020**	0.092	**0.044**
	O x pH	0.491	0.519	0.473
F_v/F_m	Origin	**0.001**	0.717	0.274
	pH	**0.018**	0.606	0.559
	O x pH	0.803	0.180	0.881
$rETR_{max}$	Origin	**<0.001**	0.858	0.822
	pH	0.379	0.445	0.586
	O x pH	0.939	0.457	0.615
P_g	Origin	0.063	0.543	**0.010**
	pH	**0.008**	0.126	**<0.001**
	O x pH	0.297	0.096	0.052
R_{dark}	Origin	**0.022**	0.717	**0.009**
	pH	**0.002**	0.163	**0.018**
	O x pH	0.316	0.468	0.372
P_g **: R**	Origin	0.355	0.706	0.913
	pH	0.188	0.632	0.054
	O x pH	0.092	0.291	0.346
Symbiont	Origin	**0.015**	0.946	0.100
	pH	**0.044**	0.113	0.294
	O x pH	**0.035**	0.261	**0.049**
Total chl	Origin	**0.002**	0.802	0.576
	pH	0.058	0.770	0.210
	O x pH	0.278	0.462	**0.032**
Proteins	Origin	0.311	0.336	0.423
	pH	**0.029**	0.138	**0.002**
	O x pH	0.669	0.726	0.436

Table IV-2 | *Two-way ANOVAs (type III) summary with Satterthwaite's method of linear mixed effect model (LMER) on the effects of colony origin (O), pH conditions and their interactions on the physiological responses of three coral species after 100 days of incubation. Non-parametric two-way Aligned Rank Transformed (ART) ANOVAs (Type III) followed by a Bonferroni p-levels adjusted post hoc test was used for F_v/F_m. Significant values are in bold ($p < 0.05$). All statistical analyses with the post hoc and random effects are in the Appendix Table VIII-11.*

In contrast, the mean growth rates of the three corals originated from Bouraké and maintained at future, extreme and variable pH i) were always higher than their counterpart originated from the reference and maintained at the same pH condition; ii) were almost always (with one exception, *A. tenuis* at variable pH) higher than their counterpart originated from the reference and maintained at the control pH condition; iii) were almost always higher or did not change (with one exception, M. digitata at variable pH) when maintained at the control pH condition (**Figure IV-2**). For instance, the calcification rate of *A. tenuis*, *Porites* sp., *M. digitata* originating from Bouraké and maintained at the variable pH, which is what they normally experience at

their site of origin, increased by 33.4% and 25.0% and decreased by 23.5%, respectively in the control pH (pH_{NBS} 8.11).

3.3 Photosynthetic efficiency and electron transport rate

The maximum photochemical efficiency (F_v/F_m) and the maximum relative electron transport rates ($rETR_{max}$) were significantly different for *A. tenuis* only (**Table IV-2**; **Appendix Table VIII-11**). The F_v/F_m of *A. tenuis* differed according to both corals' origin (*p*-value = 0.001) and pH conditions (*p*-value = 0.018), whereas only corals' origin had an influence on $rETR_{max}$ (p-value < 0.001). Both $rETR_{max}$ (**Figure IV-3**) and F_v/F_m (**Appendix Figure VIII-8**) were higher for *A. tenuis* individuals from Bouraké, as compared to individuals from the reference site, regardless the pH treatment. The F_v/F_m for *A. tenuis* also showed higher values for future and extreme pH conditions than for control and variable pH conditions.

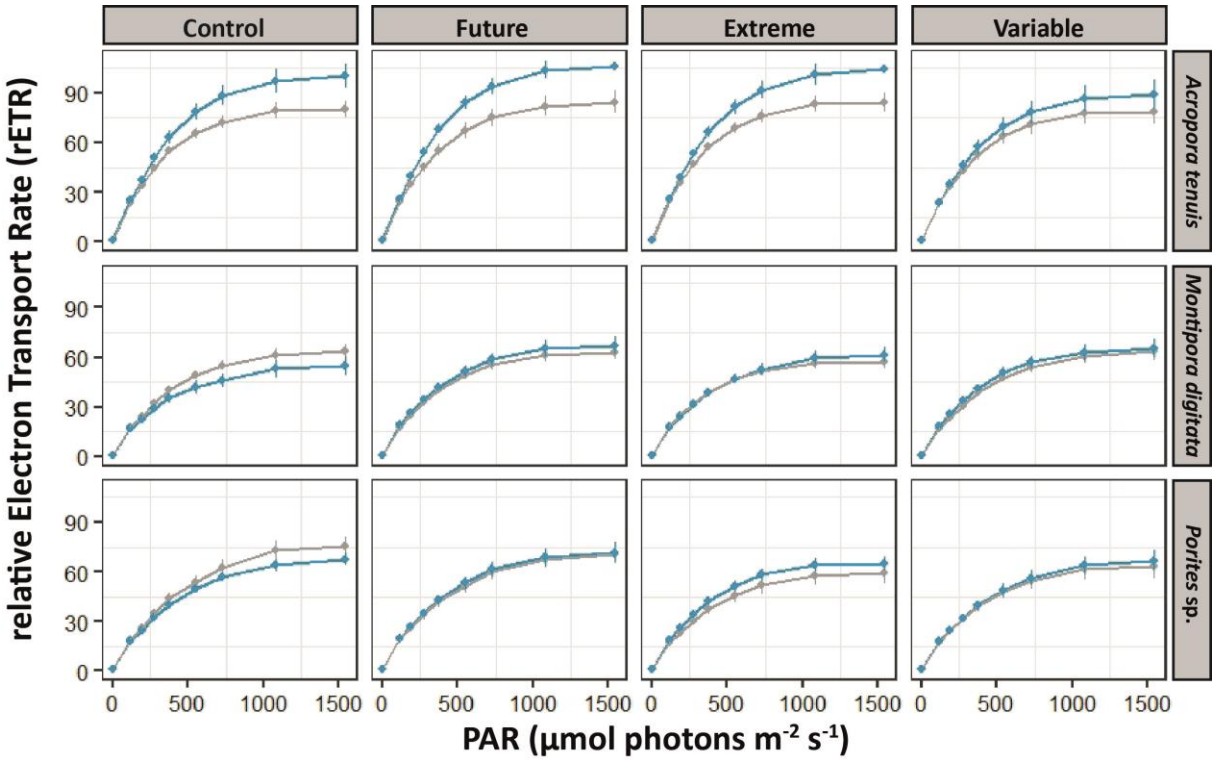

Figure IV-3 | *Relative electron transport rate (rETR) measured during RLC curves of corals after 100 days of incubation at four pH conditions (Control, pH_{NBS} 8.11; Future, pH_{NBS} 7.76; Extreme, pH_{NBS} 7.54; and Variable, pH_{NBS} 7.56-8.07). Bouraké corals are in blue, while reference corals are in grey. Data are mean ± SE; n=12-16, depending on species and pH condition; see Appendix Table VIII-11 for all post hoc comparisons).*

3.4 Photosynthesis and respiration rates

Metabolic rates (i.e., P_g, R_{dark}, P_g:R) of the three coral species significantly varied between origins and pH conditions without a clear pattern of response. ANOVAs showed significant

differences between origins in the P_g (only *Porites* sp.), R_{dark} (both *A. tenuis* and *Porites* sp.), but not for their ratio (**Table IV-2**; **Appendix Figure VIII-9**; **Table VIII-11**), and between pH conditions in the P_g and R_{dark} for *A. tenuis* and *Porites* sp. Overall, P_g and R_{dark} values were higher for future and extreme pH conditions for *A. tenuis* and *Porites* sp. (**Figure IV-4**; **Appendix Table VIII-11**).

3.5 Symbiodiniaceae, chlorophyll and protein content

A significant effect of pH was only found for Symbiodiniaceae density of the coral *A. tenuis* (**Table IV-2**; **Appendix Table VIII-11**). Site of origin significantly affected the Symbiodiniaceae density and total chlorophyll content of *A. tenuis* (**Table IV-2**; **Figure IV-5**; **Appendix Figure VIII-10**). Some interaction between pH and origin were also significant. Most of these differences were driven by the higher data variability in the extreme condition, especially for corals originating from the reference site (**Figure IV-5**; **Appendix Figure VIII-10**; **Table VIII-11**). For protein, both *A. tenuis* and *Porites* sp. significantly differed between pH conditions (**Table IV-2**; **Appendix Table VIII-11)**, and although values were very similar (**Figure IV-5**) post hoc comparisons showed higher protein contents for corals kept at the control pH condition compared to the variable (*A. tenuis*) and future (*Porites* sp.) pH conditions.

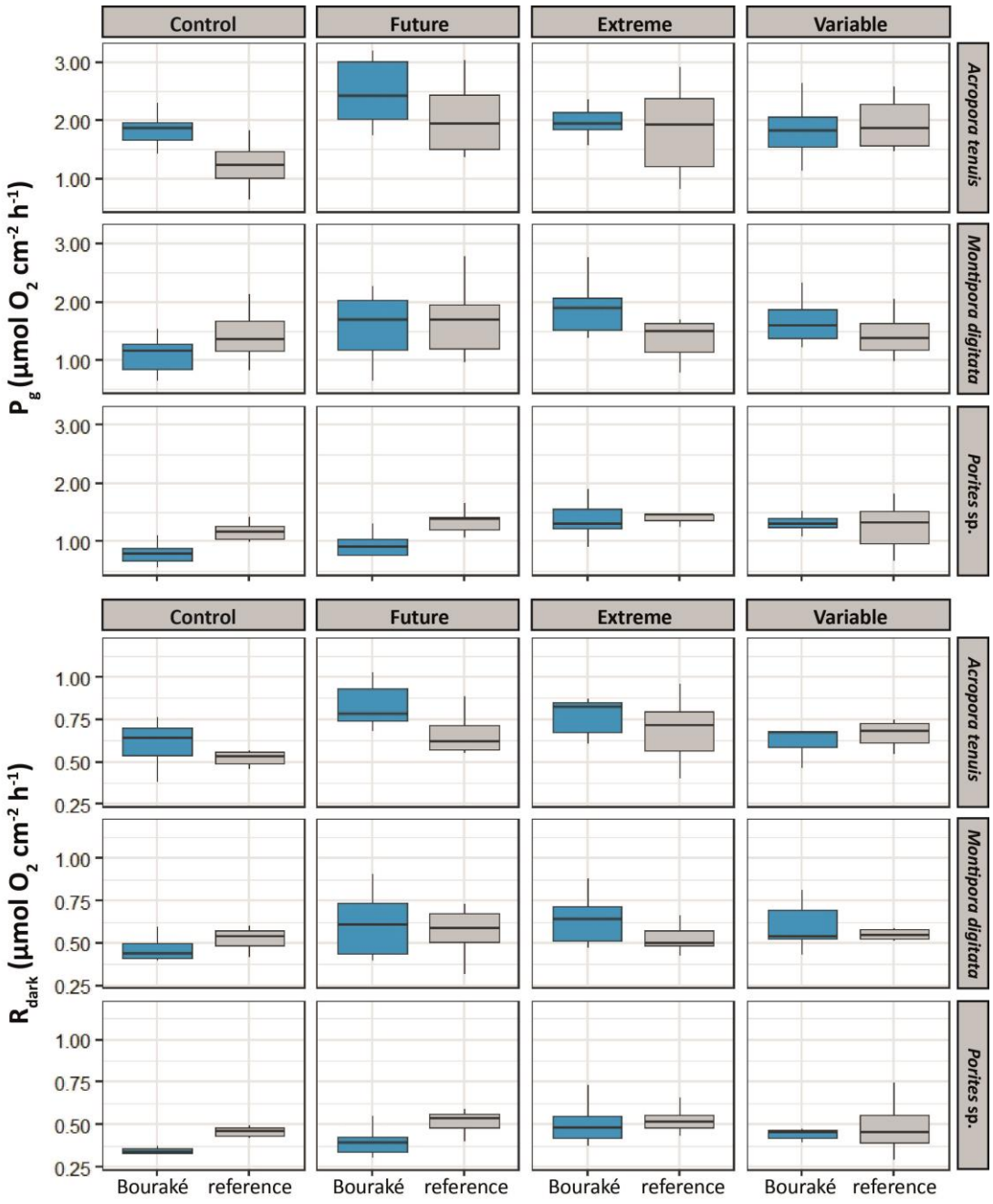

Figure IV-4 | *Gross photosynthesis (P_g) and respiration (R_{dark}) rates of corals from Bouraké (in blue) and the reference (in grey) site at four pH conditions (Control, pH_{NBS} 8.11; Future, pH_{NBS} 7.76; Extreme, pH_{NBS} 7.54; and Variable, pH_{NBS} 7.56-8.07). Data are median ± 25th and 75th percentiles (n = 7); see Appendix Table VIII-11 for all post hoc comparisons).*

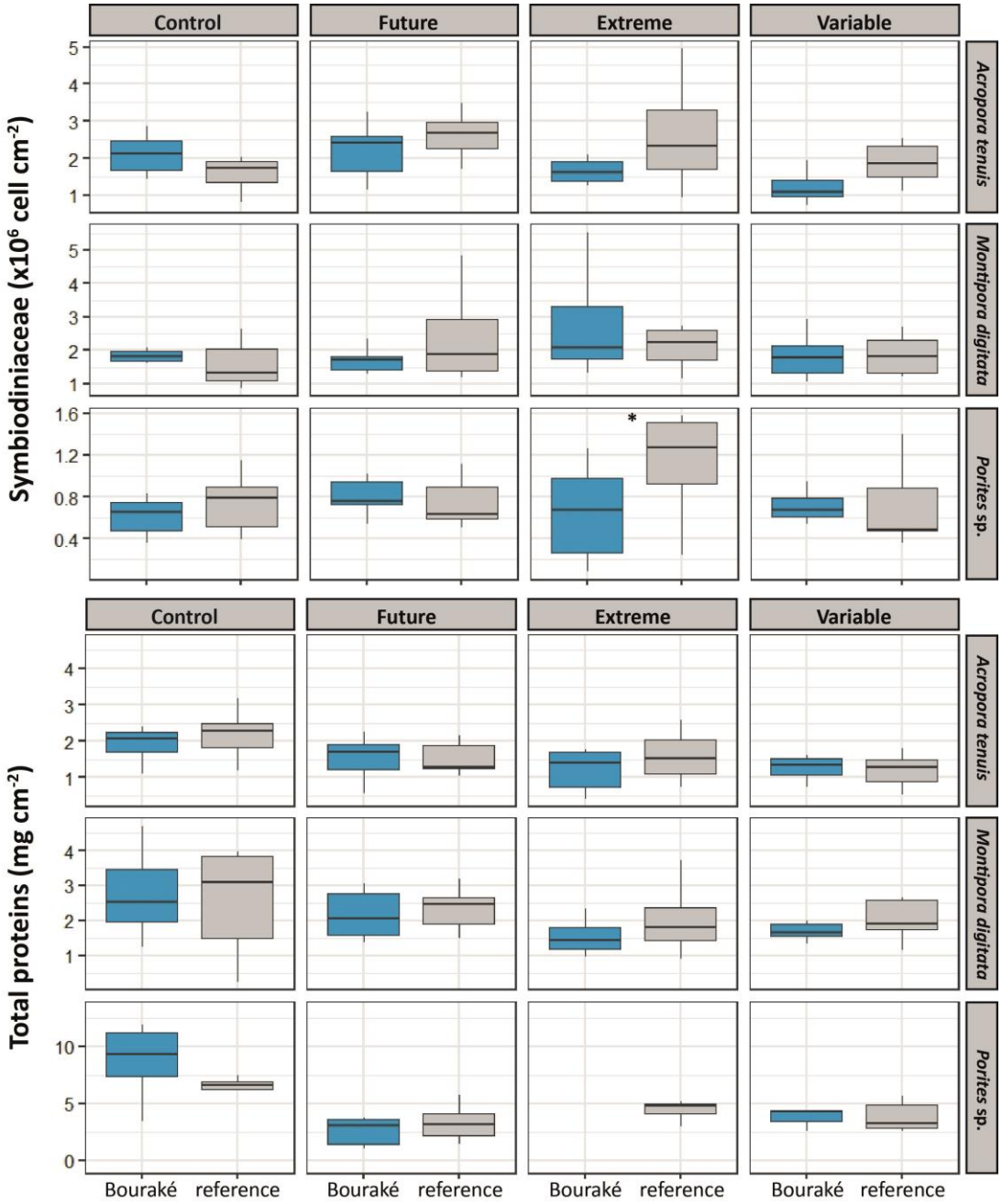

Figure IV-5 | *Symbiodiniaceae density and total protein content of corals from Bouraké (in blue) and the reference (in grey) site after 100 days of incubation at four pH conditions (Control, pH_{NBS} 8.11; Future, pH_{NBS} 7.76; Extreme, pH_{NBS} 7.54; and Variable, pH_{NBS} 7.56-8.07). Data are median ± 25th and 75th percentiles (n = 6-8, depending on species and pH condition). No data are available for the protein content of Porites sp. from Bouraké incubated at the Extreme pH condition. Asterisks indicate statistical significance at p < 0.05; see Appendix Table VIII-11 for all post hoc comparisons.*

3.6 Symbiodiniaceae communities

The three coral species were consistently associated with Symbiodiniaceae of the genus *Cladocopium* but were dominated by distinct ITS2 type profiles. The latter were significantly different between species, coral origin, and their interaction (**Table IV-3**; **Figure IV-6**).

Parameter	*df*	*F-value*	*p-value*
Origin	1	5.109	<**0.001**
pH	3	1.141	0.275
Species	2	18.736	<**0.001**
O x pH	3	0.882	0.649
O x Species	2	5.526	<**0.001**
pH x Species	6	0.894	0.688
Origin x Species	6	0.733	0.937
Residuals	88		

Table IV-3 | *Three-factorial PERMANOVA analysis testing the effects of colony origin (O), pH conditions, coral species and their interactions on the Symbiodiniaceae ITS2 type profiles. Significant values are in bold (p < 0.05).*

The major ITS2 type profiles (most abundant) of corals from the reference site comprised 58.1-91.1%, 42.6-87.5% and 76.4-96.2% of the total sequences in each sample for *Acropora tenuis, Montipora digitata and Porites* sp*.,* respectively. Under control condition, *A. tenuis* had 4 major ITS2 DIV type profiles, with C3k-C3bo-C50a-C3ba-C50q most common (3 of 5 samples), while *Porites* sp. had 3 major type profiles, with C15-C15ce-C15cc-C15n-C15cf-C15l-C15qh most common (3 of 5 samples). Two major type profiles were found in *Montipora digitata* (C15/C15vi-C15vj-C15f-C15he and C73-C73a-C21). For corals from Bouraké, the major ITS2 type profiles comprised 72.6-92.5%, 64.5-95.7% and 82.2-93.3% of the total sequences in each sample for *A. tenuis, M. digitata and Porites* sp*.,* respectively. For *A. tenuis*, the major type profile was C1-C1b-C42.2-C1c-C1bh-C1br-C1cb (one sample was also C3/C15), while *Porites* sp. was predominantly C15-C15bq-C15iq (one replicate was C15-C15ce-C15cc-C15n-C15cf-C15l-C15qh). *M. digitata* had 9 major type profiles, with C15/C15vi-C15vj-C15f-C15he the most common (found in 50% of the samples).

The pH treatments did not result in a significant change in the Symbiodiniaceae major type profiles for any coral species (**Table IV-3**). However, an interesting observation was that in general corals from Bouraké had more consistent major ITS2 type profiles between replicate colonies, than corals from the reference site (**Figure IV-6**). Individuals of the three coral species originating from the reference site had 3 times more type profiles when maintained at future or variable pH conditions than individuals under the control pH.

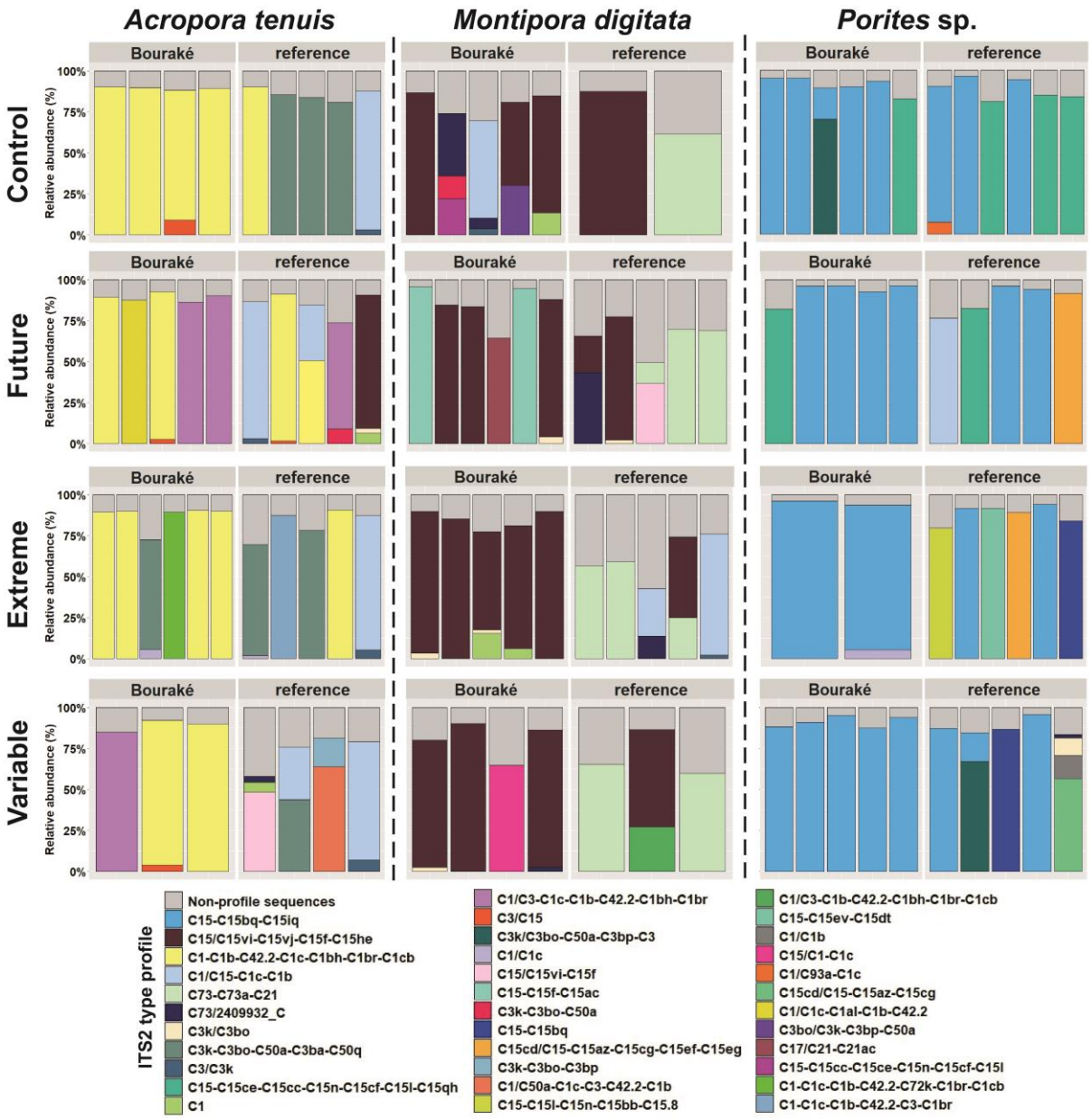

Figure IV-6 | *Predicted major ITS2 type profiles of corals from Bouraké and the reference site after 100 days of incubation at four pH conditions (Control, pH_{NBS} 8.11; Future, pH_{NBS} 7.76; Extreme, pH_{NBS} 7.54; and Variable, pH_{NBS} 7.56-8.07). Within each cell of this 3-by-4 matrix, samples are plotted as stacked bar charts with a single column representing a sample from a specific origin: Bouraké (left) and reference (right). The number of individuals per condition varies from 2 to 6 depending on the number of samples available.*

4. Discussion

Corals from the Bouraké lagoon have evolved over generational time scales in an environmental condition (pH, temperature, dissolved oxygen) chronically exceeding those predicted by the IPCC scenarios for the end of this century (IPCC Report, 2021). The Bouraké geomorphology, coupled with an intense oxidative activity in the mangrove sediments, have

been shown to cause seawater acidification, deoxygenation, and warming in the lagoon (Maggioni et al., 2021). Despite the extreme levels of acidification measured, which have been suggested to hinder coral calcification (Kleypas et al., 1999a), an abundant, and well-diversified coral reef has developed in the lagoon. By assessing the holobiont physiological responses and the Symbiodiniaceae profiles of three coral species from both Bouraké and a reference reef to a large range in pH, we found that corals from Bouraké always exhibited higher growth rates and had a specific and more consistent ITS2 majority sequence than corals from the reference reef both under low and variable pH conditions. It seems likely that such patterns were linked to the strong life-long environmental fluctuations, which might have promoted coral resilience as previously suggested for other corals (e.g., Brown et al., 2022; Comeau et al., 2022; Enochs et al., 2020; Rivest et al., 2017; Schoepf et al., 2020). We are aware that this study explored only a few of the compensatory mechanisms that might be at the origin of the resilience observed for corals from Bouraké. We also admit that these coral populations may have developed such mechanisms in a much longer time scale than corals that will have to cope with rapid climate change. However, results from this study would suggest that adaptation to future OA conditions could be possible in the wild.

Coral potential resilience to ocean acidification: what do we learn from lifetime adapted corals?

In agreement with the consensus on the effect of OA on coral calcification (Gattuso et al., 1999), recently revised by Leung et al., (2022), we found that calcification rates of the both *A. tenuis* and *Porites* sp. reference corals were significantly decreased when exposed to future and extreme pH levels. These results are consistent with coral species-specific responses to OA with respect to calcification. We observed species-specific responses to OA on corals from Bouraké although almost always (with one exception, *A. tenuis* at variable pH) showed higher calcification rates than their counterpart originated from the reference and maintained at the control pH condition. The marginal effect of OA observed in corals from Bouraké has been observed on some others coral species (e.g., *Pocillopora damicornis*; *Porites cylindrica; Siderastrea siderea*) in previous aquaria experiments (Comeau et al., 2013, 2019a; Aichelman et al., 2021; Bell et al., 2022; Brown et al., 2022) and recently revised (Bove et al., 2020; Leung et al., 2022).

Our data showed that all three coral species from Bouraké calcified from 19.0% (*A. tenuis*) to 67.3% (*Porites* sp.) more than their counterpart from the reference site, when maintained at control pH (**Figure IV-2a,b**). This unexpected finding suggests that Bouraké corals have adapted to OA because they have been exposed to extreme conditions throughout their lives,

regain even higher rates of calcification than the same coral counterparts adapted to actual pH conditions, once at actual pH.

The innovative aspect of our study is that we compared corals adapted to ambient seawater pH with corals likely adapted, or at least fully acclimated, to an extreme and fluctuating environment overlaying future climate scenarios. This study demonstrated that Bouraké corals have become more resilient to OA, likely using plastic and/or assimilated mechanisms such as changes in coral-associated microorganisms(Camp et al., 2020). Brown et al. (2022) incubated in aquaria with stable (218 ± 9 µatm) and variable daily pCO_2 amplitude (911 ± 31 µatm) conditions the coral *Pocillopora damicornis* from both a flat and a sloping reef, where mean daily pCO_2 amplitude differed (797 ± 20 and 399 ± 8 µatm d^{-1}, respectively). As in our study, they found higher rates of calcification for corals from the more variable environment. The authors measured lower secondary calcification (i.e., $CaCO_3$ density) on corals from the variable environment with less intracellular pH acidosis, as previously found for other corals (Gibbin and Davy, 2014; Cornwall et al., 2018; Comeau et al., 2022). Clearly, this compensatory mechanism might have a cost. Among the potential hypotheses explaining how corals can cope with the additional energy required to maintain high calcification rates using for instance the proton pumping (McCulloch et al., 2012a; Guillermic et al., 2021), it is known that corals: (i) might boost their endosymbiotic algal production (Schoepf et al., 2013; Castillo et al., 2014; Barott et al., 2015), (ii) use their energy reserves, such as proteins and lipids (Edmunds and Wall, 2014; Towle et al., 2015), and (iii) increase heterotrophy (Edmunds, 2011; Houlbrèque et al., 2015).

Our data do not consistently suggest that Bouraké corals have acquired a particular mechanism that accounts for better physiological plasticity to cope with low pH conditions, thereby maintaining higher calcification rates. Indeed, we did not find a clear effect of coral origin with systematic increase in photosynthetic rates, higher contents of Symbiodiniaceae, chlorophylls, and protein in Bouraké corals. However, our study confirms previous findings on the positive effect of high pCO_2 on photosynthetic rates, which might boost endosymbiotic photosynthates production for coral proton pumping mechanism. It is well known that under acidified conditions, the photosynthetic activity of algal symbionts in coral increases up to exceeds the maximum level of CO_2 consumed by the algae (e.g., Barott et al., 2015; Gattuso et al., 1999; Gibbin & Davy, 2014). Although CO_2-induced photosynthetic fertilization of symbionts may be less effective for *M. digitata*, *A. tenuis* and *Porites* sp. showed higher photosynthesis under OA scenarios compared to the control condition. This was accompanied by higher ETR_{max}, F_v/F_m values, and a better exploitation of lower light intensities for *A. tenuis*. This species also had the highest growth rates, which highlights the symbionts involvement in coral growth. Higher productivity was supported by an increased concentration in the

Symbiodiniaceae density and/or chlorophylls, but not consistently among species as previously reported (Anthony et al., 2008; Wall et al., 2014). Moreover, the respiration rates were higher under acidified conditions for *A. tenuis* and *Porites* sp. The high photosynthetic rates are consistent with the beneficial effect of elevated pCO_2 on the productivity of corals living in CO_2 vents in Papua New Guinea (Biscéré et al., 2019). These trends of increasing photosynthetic and respiration rates under OA do not match with the observations made by Jacquemont et al. (2022) (Appendix Article n°1), for whom OA had no effect on photosynthetic and respiration rates of Bouraké corals, although, unlike our study, they found significantly different rates between Bouraké and the reference site. Differences between the two studies could be due to the different setup of the two experiments as Jacquemont et al. (2022) (Appendix Article n°1) measured coral metabolic rates under conditions mimicking the Bouraké environment, at high and low tide, and using seawater collected directly during both tidal periods. We measured the effect of medium-term incubation at different seawater pH on corals from Bouraké and the reference site, while Jacquemont et al. (2022) (Appendix Article n°1) tested the effect of a combination of factors, including pH, oxygen and organic matter.

This study also found significant depletion of protein levels in all pH treatments, although this loss remained equivalent between the two corals origins, suggesting an alternative energy source used by Bouraké corals to maintain higher growth rates. Interestingly, *A. tenuis* and *Porites* sp. had lower protein levels under variable pH, suggesting that corals must bear an additional cost to cope with the large change in pH measured at Bouraké. The negative effect of OA on coral protein metabolism could be the result of accelerated proteins catabolism at elevated pCO_2 (Edmunds and Wall, 2014), which can be exacerbated when pH fluctuates over time. The loss of proteins under acidified conditions could also be explained by the species-specific ability of corals to preferentially allocate energy either toward inorganic growth (calcification) or somatic growth (tissues) when facing elevated pCO_2 (Agostini et al., 2021). We recognize that protein content can only partially describe the change in the coral energy reserves, since lipids and carbohydrates were not measured. Corals exposed to higher pCO_2 might catabolize energy reserves to increase or maintain calcification, although this response is species-specific (Schoepf et al., 2013; Wall et al., 2017; Grottoli et al., 2018) . In our study corals were fed once a week with *Artemia salina* nauplii and such heterotrophic inputs might have helped them (Cohen and Holcomb, 2009; Edmunds, 2011; Drenkard et al., 2013; Houlbrèque et al., 2015). Indeed, it has been observed that the artificial diet we used, although limited compared to previous studies, helps corals maintain appropriate energy expenditure and calcify under acidified conditions (Houlbrèque and Ferrier-Pagès, 2009; Houlbrèque et al., 2015). This is one of the potential limitations of most existing experiments in aquaria. Indeed, it is difficult to imitate the natural contribution of zooplankton to the diet of corals in an aquarium.

However, all individuals were fed in the same manner and the nutrient levels (i.e., NO_x, PO_4^{3-} and $Si(OH)_4$) measured in the aquaria were quite similar between tanks and throughout the experiment. Thus, the diet could perhaps explain some of the apparent resistance of corals to OA, but not the different responses with regards to calcification between Bouraké and the reference site.

To what extent do pH fluctuations improve the physiological performances of corals?

One of our hypotheses to explain the success of Bouraké corals was the potential positive effect that diurnal pH fluctuations could have on coral metabolism, as previously found for corals in GBR mangrove lagoons (Camp et al., 2019), St Vincent and the Grenadines CO_2 vents (Enochs et al., 2020), and for others incubated in mesocosms (Dufault et al., 2012; Brown et al., 2022). Our results show that short-term exposure (i.e. acclimation of reference corals during our experiment) to fluctuating pH has a negative effect on coral calcification as all coral species from the reference decreased their growth when incubated at variable pH (**Figure IV-2c**). In contrast, Bouraké corals, which are acclimatized and/or adapted to local conditions, when exposed to variable pH calcified from 7.6% (*A. tenuis*) to 116.2% (*M. digitata*) more than their counterpart from the reference site. Furthermore, Bouraké corals incubated at future and extreme pH maintained these higher growth rates and even increased them when grown under control conditions, confirming their resistance to OA. Although the duration of our experiment was longer than most OA experiments (i.e., 77% lasted 1-11 weeks; Brown et al., 2022; Ziegler et al., 2021), we acknowledge that the duration of variable pH exposure experienced by corals from the reference site during the course of the experiment was too short to compare with that experienced by corals at Bouraké. Corals exposed to a variable environment throughout their life are physiologically more plastic than corals adapted to stable environments (Kenkel and Matz, 2017); such plasticity is probably time-dependent. Future experiments should take into account the length of exposure to variable pH (as well as other environmental parameters) that the corals experienced before the collection.

Does their Symbiodiniaceae community raise the physiology of Bouraké corals?

It is thought that species-specific metabolic responses to environmental stress could be due to different symbiont communities hosted by corals (Barott et al., 2015; Ziegler et al., 2015). Our data suggest that seawater pH level, whether stable or variable, at future or extreme levels, does not affect the Symbiodiniaceae major ITS2 type profiles of corals (at least over a 100-

day period), since at the end of the experiment we found no significant effect among treatments. Interestingly however, Bouraké corals exhibited more consistent major ITS2 type profiles between replicate colonies at low and variable pH than corals from the reference site. Microbiome stability (both for symbionts and/or bacteria) was linked to greater physiological resilience to OA (Quigley et al., 2017, 2019; Grottoli et al., 2018; Ge et al., 2021; Ros et al., 2021), suggesting that consistent major ITS2 type profiles for Bouraké corals under pH treatments could facilitate their success; however, further work will be needed to verify this hypothesis.

We observed distinct major ITS2 type profiles between coral species and native habitat (e.g. Bouraké versus reference site). All coral species in this study were associated with the genus *Cladocopium* (LaJeunesse et al., 2018). We could have expected to find the Symbiodiniaceae genus *Durusdinium* as it is often found in stress-tolerant corals (Lajeunesse et al., 2014; Hoadley et al., 2019; Haydon et al., 2021). However, some species of *Cladocopium* seem to be competitively dominant against *Durusdinium* in a multi stressors environment such as Bouraké (Barshis et al., 2010; Hume et al., 2016). For example, *Cladocopium* was found to be the dominant genus on corals species such as *Porites lutea* from the mangrove lagoon of Woody Isles (Australia, Camp et al., 2019), and both *Acropora pulchra* and *A. muricata* in Bouraké (Camp et al., 2020). In Bouraké, distinct symbiont type profiles for each coral host species, across environments, support previous hypotheses of species-specific strategies of environmental adaptation (Camp et al., 2020):

(i) *A. tenuis* in Bouraké had a major type profile of C1-C1b-C42.2-C1c-C1bh-C1br-C1cb. Corals associated with C1 as a major ITS2 sequence have been found across many environments (LaJeunesse et al., 2003), and exhibit apparent capabilities to adapt to locally stressful and/or fluctuating environments (Howells et al., 2012; Schoepf et al., 2015; Ng and Ang, 2016). Corals from Bouraké exhibited lower Symbiodiniaceae density than the reference corals, but had higher photosynthetic efficiency. Corals associated with *Cladocopium goreaui* (C1) have previously shown elevated photosynthetic efficiency with regards to other Symbiodiniaceae species (Stat et al., 2008b; Cantin et al., 2009; Morgans et al., 2020; Wall et al., 2020). It is therefore possible that elevated photosynthesis is a common trait within some taxa from the C1 radiation and may explain the higher photosynthetic efficiency mechanism of C1 to face OA as observed by Ge et al. (2021) in *Acropora valida*. The elevated photosynthetic capacity of *A. tenuis* in Bouraké, coupled with the dominance of major ITS2 sequence C1, could explain their significantly higher growth rates, as previously observed in *A. tenuis* juveniles (Little et al., 2004; Cantin et al., 2009). The C1 ITS2 sequence was still dominant for some colonies of *A. tenuis* from the reference site (albeit different ITS2 type profiles that suggest different species), but in most instances, ITS2 sequences from the C3 radiation (i.e.,

C3k and C3bo) were most abundant; these are not among the most efficient in photosynthetic capabilities (Hoadley et al., 2016). We note the uncommon prevalence of C15 in *A. tenuis* (**Appendix Figure VIII-11**). We are confident from our negative control gels that this is real (**Appendix Figure VIII-12**), and could perhaps result from expelled symbionts from the other coral taxa during the stress experiment. Further work would need to validate this hypothesis.

(ii) *Porites* sp. from both Bouraké and the reference site maintained an association with *Cladocopium* of the C15 radiation, but there were more numerous C15 major ITS2 type profiles at the reference site. Interestingly, discrete C15 genotypes (distinct ITS2 type profiles) were observed across habitats (i.e., extreme vs reference) in *Porites lutea* from Bouraké (Camp et al., 2020) and from a mangrove lagoon on the Great Barrier Reef (Camp et al., 2019). This is in agreement with the recent finding of Hoadley et al. (2021) demonstrating that within C15, diverged lineages exist for *Porites* sp. living in different reef habitats and that it brings physiological differences.

(iii) M. digitata from Bouraké had nine major ITS2 type profiles, with C15/C15vi-C15vj-C15f-C15he the most common. *Cladocopium* of the C15 radiation are considered physiologically resistant (Fitt et al., 2009; Fisher et al., 2012; Nitschke et al., 2018). The same C15 major type profile was also found for the reference corals, alongside C73-C73a-C21. Coral association with C73 is rarely found and appears to be present according to relative light levels (Stat et al., 2008a). With this in mind and according to the equivalent light irradiance measured between tanks in our experiments, we could assume that light regimes of the native environment of corals modified their Symbiodiniaceae community associations. For instance, turbid environments such as Bouraké have been observed to limit the diversity of the associated symbiont community and could lead to predominant local adaptive genotypes (Smith et al., 2020). While it is beyond the intent of this study to determine which environmental drivers shape symbiotic communities, our data supports the growing body of evidence (Howells et al., 2016; Ziegler et al., 2017; Camp et al., 2020) that corals from distinct environments often have unique symbiotic partners that could be crucial to support their survival.

While we cannot define the role of each Symbiodiniaceae ITS2-profile in the coral stress response, the difference in symbiotic partners' genotypes between sites highlights how important local environmental conditions are and how symbiotic stability (fidelity) versus flexibility ultimately enhances holobiont resilience (Putnam et al., 2012; Grottoli et al., 2018; Epstein et al., 2019b).

In conclusion, we show that under the OA scenarios tested here, corals adapted to an extreme and variable environment have systematically higher calcification rates than reef corals living at a more stable environment. Although not all physiological measurements revealed significant differences between coral's origin, Bouraké corals showed that their calcification

rates have been somewhat boosted, regardless of pH level and variability. Concomitantly, they maintain divergent symbionts with more consistent Symbiodiniaceae communities than corals from a more stable environment. The comparison between corals that have been exposed during their life to variable pH with corals exposed only during the 100-day incubation suggests that this is not rapid mechanism. Upcoming studies should explore the effects of the exposure duration (i.e., short vs long-term) to variable pH on coral biomineralization mechanisms, which already appear to differ between more stable and fluctuating environmental conditions of pH (Comeau et al., 2022). The different dynamics of symbiotic partners might greatly influence calcification processes via distinct translocation of photosynthates ultimately influencing mechanisms of internal pH regulation (Cameron et al., 2022; Venn et al., 2022; Allen-Waller and Barott, 2023). The use of isotopic tools such as the boron pH proxy in the coral skeleton would help that way, via tracing and defining the inputs of specific symbiotic partners into biomineralization mechanisms.

CHAPTER 5

PHYSIOCHEMICAL CONTROL OF CORAL CALCIFICATION

5.1 Preamble

Although they live in an extreme and fluctuating environment, Bouraké corals exhibited significantly higher calcification rate than corals from the reference site in the culture experiment presented in **chapter 4**. Depending on species, the higher calcification was not always accompanied by superior performances regarding the physiological parameters measured. Nevertheless, Bouraké corals maintained divergent symbionts within Symbiodiniaceae communities with greater consistency than corals from the reference site. This result indicates that Bouraké corals can acquire specific contributions from their Symbiodiniaceae communities, which ultimately influence their calcification. Coral calcification is a complex process depending on the surrounding environmental conditions (Gattuso et al., 1998). In the last decades, studies have shown that corals can control and regulate their internal carbonate chemistry to enhance calcification (e.g., Furla et al., 2000; Ries, 2011; McCulloch et al., 2012a; Venn et al., 2019). It is thought that symbiont-coral associations play a role in the physiochemical control of coral calcification via distinct photosynthetic performances and related carbon translocation (e.g., Guillermic et al., 2021; Cameron et al., 2022; Eagle et al., 2022; Venn et al., 2022; Allen-Waller and Barott, 2023). In **chapter 5**, we sought to highlight the links between calcification, symbiont-coral associations, physiological performances, and the regulation of internal carbonate chemistry. We tested the hypothesis that corals from Bouraké have better physico-chemical control of their calcification than corals from the reference site, thanks to their specific communities of Symbiodiniaceae, in order to survive in an extreme and fluctuating environment. To explore this hypothesis, we used different geochemical proxies ($\delta^{11}B$, $\delta^{13}C$, B/Ca) that we measured in the skeletal material produced by corals during the previous 100-day aquarium experiment. Geochemical data were coupled with the physiological and metagenomics results of **chapter 4** to improve our understanding of the acclimatization strategies used by Bouraké corals.

5.1 Article n°3: Geochemical proxies reveal physiochemical control of calcification by corals exposed to naturally variable pCO_2 levels

Geochimica et Cosmochimica Acta

ELSEVIER

Received: 17 March 2023; ***Under review***

Geochemical proxies reveal physiochemical control of calcification by corals exposed to naturally variable pCO_2 levels

Clément Tanvet[1,2,3,*], Maxence Guillermic[4], Gérard Thouzeau[1], Riccardo Rodolfo-Metalpa[2,3] and Jill Sutton[1]

[1] Univ Brest, CNRS, IRD, Ifremer, LEMAR, F-29280 Plouzané, France
[2] Centre IRD Nouméa, UMR ENTROPIE (CNRS, IRD, UR, UNC, IFREMER), Institut de Recherche pour le Développement, Nouméa, New Caledonia
[3] Labex ICONA, International CO2 Natural Analogues Network, Shimoda, Japan
[4] Department of Earth, Planetary, and Space Sciences, Department of Atmospheric and Oceanic Science, Institute of the Environment and Sustainability, UCLA, University of California Los Angeles, CA 90095, USA

* Corresponding author

Abstract

The influence of on-going rapid ocean acidification (OA) on the physiochemical control of calcification by corals is poorly understood. Here, we used geochemical proxies (e.g. $\delta^{11}B$, $\delta^{13}C$, and B/Ca) to measure the extracellular calcifying medium pH (pH_{ECM}) and carbonate chemistry of three corals (i.e. *Acropora tenuis*, *Montipora digitata* and *Porites* sp.) grown in aquaria under stable and fluctuating OA conditions. Coral specimens originated from the semi-enclosed lagoon of Bouraké, characterized by diurnal extreme and variable seawater pH (7.23 to 8.06 pH_T units), and an adjacent reference site with more stable pH values (7.90 to 8.18 pH_T units). All corals consistently raised their pH_{ECM} above seawater pH and continued to calcify during the 100-day aquarium experiments, however the corals from the different sites responded differently to OA. The corals from the Bouraké site had higher calcification rates despite a lower pH_{ECM} relative to Reference and lacking pH_{ECM} homeostasis. This suggests that corals adapted to variable pH conditions have different strategies in energy allocation and/or ionic transports to promote calcification. By combining geochemical proxies with physiological and metagenomic data, we observed different physiochemical control of the coral ECM under OA accompanied with distinct symbiont communities. We show that corals adapted from Bouraké have implemented strategies other than pH_{ECM} homeostasis after a long-term exposure to extreme and fluctuating OA.

Key words: Ocean acidification; Coral reefs; Adaptation; Calcification; Geochemical proxies; Symbiont; Calcifying fluid; pH variability

1. Introduction

Corals are widely recognized as keystone species forming one of the most productive and diverse ecosystems on Earth. Coral reefs provide shelter for nearly 30% of marine organisms and sustain almost 10% of the world's human populations through fisheries, tourism, and shoreline protection (Costanza et al., 2014). Increased anthropogenic atmospheric CO_2 is leading to global warming and ocean acidification (Hoegh-Guldberg et al., 2017; Hughes et al., 2018b). Ocean acidification (OA) is described by the decrease in seawater pH and calcium carbonate saturation state, which can adversely affect calcifying organisms including corals (Gattuso et al., 1998; Kleypas and Yates, 2009). Although coral calcification is known to be affected by OA (e.g., Ries et al., 2009; Comeau et al., 2013, 2019; Cornwall et al., 2021), the large species-specific responses measured during the last decade of experimentations in both natural settings (Rodolfo-Metalpa et al., 2011; Jury and Toonen,

2019; Comeau et al., 2022) and aquariums (Cornwall et al., 2018; Comeau et al., 2019a; Cameron et al., 2022) suggest that some corals are more resilient than others. Coral resilience (referring to the capacity to resist climate change disturbances and to recover the initial status following disturbances; Mumby et al., 2014) has been partly attributed to their ability to control chemistry of their internal calcifying medium, therefore promoting calcification (Ries, 2011; McCulloch et al., 2012a; Schoepf et al., 2017).

Calcification, or the construction of aragonite-based skeletal structures in corals, is a complex process that greatly depends on the surrounding environmental conditions (Gattuso et al., 1998). It begins with the precipitation of $CaCO_3$ crystals in the subcalicoblastic space (between the skeleton and the connective tissue) from an extracellular calcifying medium (ECM) (Mass et al., 2017; Venn et al., 2019; Schmidt et al., 2022). The biological upregulation of the pH_{ECM}, $[CO_3^{2-}]_{ECM}$ and ultimately the aragonite saturation state $(\Omega_{Ar})_{ECM}$ are key processes in coral skeleton building (Allison et al., 2014; McCulloch et al., 2017a); these parameters can be influenced by various stressors such as OA (Holcomb et al., 2014; Comeau et al., 2017; Eagle et al., 2022) and/or temperature (Guillermic et al., 2021; Cameron et al., 2022). For example, some corals can raise the pH of their calcifying fluid (pH_{ECM}), under both normal and acidified conditions, to values up to 0.3-1.0 pH units above the pH of the seawater in which they reside (Ries, 2011; McCulloch et al., 2012a; Venn et al., 2019; Guillermic et al., 2021). It has been suggested that this pH_{ECM} upregulation occurs via the active removal of protons driven by enzyme activity exchanging Ca^{2+} for H^+ (i.e., Ca^{2+}-ATPase) (Al-Horani et al., 2003; Ries, 2011; Venn et al., 2011; Comeau et al., 2017). The Ca^{2+}-ATPase requires ATP production, which depends on the symbiont photosynthates (e.g., sugar) degradation by mitochondria (Wooldridge, 2013). The supply of sufficient ATP by photosymbionts is then crucial for the coral host to regulate its pH_{ECM} and cope with OA (Bove et al., 2022; Cameron et al., 2022). The success of coral reefs also relies on their ability to use sufficient $[CO_3^{2-}]$ sourced from the seawater DIC to build their calcium carbonate skeleton (McCulloch et al., 2017b). Simultaneously with ATP production, corals concentrate their metabolic supply of DIC in calcifying cells (via increased respiration of photosynthates) as a source for calcification (Furla et al., 2000; Allison et al., 2014). These DIC concentrating mechanisms induce an increase of the ECM saturation state of aragonite $(\Omega_{Ar})_{ECM}$. In addition, they depend on the host energy reserve and respiration rate (Eagle et al., 2022).

Disentangling the links between calcification, symbionts-coral associations, photosynthesis/respiration rates, and ECM carbonate chemistry of corals is challenging. Coupling the physiological responses of corals and their associated symbiotic algae, the Symbiodiniaceae, to their geochemical signatures would permit a better understanding of these biogeochemical interactions. In this respect, the boron isotope composition ($\delta^{11}B$) of the

coral carbonate skeleton has been developed as a biogeochemical tool to detect changes in OA but many questions remain regarding its use as a proxy of changes in ECM pH (McCulloch et al., 2012b; D'Olivo et al., 2015; Comeau et al., 2017). Briefly, the use of $\delta^{11}B$ as a pH proxy is based on the assumption that between the two major dissolved forms of boron, boric acid (i.e. $B(OH)_3$) and borate ion (i.e. $B(OH)_4^-$), $B(OH)_4^-$ is the only form incorporated into the aragonite-based skeleton of corals (Hemming and Hanson, 1992) and that it is substituted for CO_3^{2-} in the aragonite lattice (Mavromatis et al., 2015; Noireaux et al., 2015). The relative abundances of $B(OH)_4^-$ and boric acid, preferentially enriched in ^{10}B and in ^{11}B, respectively, depend on pH (dissociation constant, K_B; Dickson, 1990). Considering the isotope equilibrium fractionation between the two dissolved forms of boron (fractionation of 27.2‰; Klochko et al., 2006), the isotopic composition of $B(OH)_4^-$ and $B(OH)_3$ also depends on pH. Assuming that the skeletal isotopic composition reflects the isotopic composition of $B(OH)_4^-$, the skeletal $\delta^{11}B$ can be used as coral biomineralization proxy of pH_{ECM}. Accordingly, independent approaches to measure pH_{ECM}, such as confocal microscopy (Venn et al., 2013, 2022; Holcomb et al., 2014) or microelectrodes (Ries, 2011; Cai et al., 2016; Sevilgen et al., 2019; Guillermic et al., 2021), have reinforced the viability of $\delta^{11}B$ as a proxy for pH_{ECM}. When applied to biogenic samples, boron isotope measurements show an offset from theoretical calculations due to the biological control of the calcification process (e.g., photosynthesis/respiration), the so-called vital effects. As a result, the enriched coral skeletal $\delta^{11}B$ can be used to reflect pH_{ECM} regulation by individual corals (Rollion-Bard et al., 2011; Comeau et al., 2017; McCulloch et al., 2017a). A controversial, but emerging proxy couples $\delta^{11}B$ and B/Ca ratios of corals allowing an improved estimation of carbonate ion availability ($[CO_3^{2-}]_{ECM}$). The $[CO_3^{2-}]_{ECM}$ calculation requires to know the relevant partition coefficient in aragonite (K_D) relating the molar ratio of $(B/Ca)_{CaCO3}$ to the concentration of the carbonate $[CO_3^{2}-]_{ECM}$ and borate $[B(OH)_4^-]$. However, several substitution equations have been proposed when substituting $B(OH)_4^-$ for CO_3^{2-} in aragonite, resulting in different K_D formulations (Holcomb et al., 2016; McCulloch et al., 2017b; Decarlo et al., 2018b). Still, recent measurements using pH microelectrodes (Cai et al., 2016; Sevilgen et al., 2019) supported calculating $[CO_3^{2-}]_{ECM}$ from the combined boron proxies $\delta^{11}B$ and B/Ca in coral skeleton. In this study, we used the coupled $\delta^{11}B$ and B/Ca as a proxy of the DIC_{ECM} and $[CO_3^{2-}]_{ECM}$.

It is thought that corals chronically exposed to pH variability would better cope with future pH conditions (Rivest et al., 2017; Enochs et al., 2020; Schoepf et al., 2020; Jacquemont et al., 2022 (Appendix Article n°1); chapter 4). In a previous study (chapter 4), we studied both physiology and symbiont metagenomics on three coral species sampled on a reference reef (named Reference hereafter) and at Bouraké, an extreme environment (Schoepf et al., 2023) where 66 coral species appear to be adapted to a trio of stressors, namely warming,

acidification and deoxygenation (Camp et al., 2017; Maggioni et al., 2021; Tanvet et al., 2022). According to the tidal-cycle, the semi-enclosed lagoon of Bouraké exhibits diurnal variable and extreme environmental conditions characterized by temperature ranging from 17.5 to 33.8°C, dissolved oxygen (DO) ranging from 1.87 to 7.24 mg O_2 L^{-1}, and pH ranging from 7.23 to 8.06 (total scale). Corals were exposed in aquaria for 100 days to four pH_{NBS} conditions i.e., Control (8.11), Future (7.76), Extreme (7.53) and Variable (7.56 - 8.07). Individuals from Bouraké consistently exhibited higher growth rates, regardless of their exposure to different pH conditions, and had distinct symbiont communities. While higher growth was attributed to the species-specific Symbiodiniaceae, host adaptation to OA and specifically to the variable environment of Bouraké remained unknown, especially with regard to the coral calcification mechanisms. Long-term exposure to pH variability was suggested to enhance the coral physiological control on its ECM carbonate chemistry (Georgiou et al., 2015; Comeau et al., 2022). However, to our knowledge, only one laboratory experiment investigated the effect of diel pH variability on the regulation of ECM chemistry (Cornwall et al., 2018). In the present study, we assessed the regulation of ECM chemistry in corals exposed to variable and stable pH environments. To do this, the geochemical composition (i.e., $\delta^{11}B$, $\delta^{13}C$, B/Ca) of the skeletal material produced by corals during the 100-day experiment in chapter 4 was compared between individuals sampled in Bouraké and Reference to determine if a long-term exposition to variable seawater pH triggers a certain degree of acclimation to these species. Data were coupled with physiological and metagenomics results from chapter 4 to distinguish the potential adaptive mechanisms to OA, and improve our understanding on the coping strategies used by the Bouraké corals, which are supposed to be adapted to future environmental conditions (RCP7.0).

2. Materials and Methods

2.1 Coral cultures

Three coral species, *Acropora tenuis*, *Montipora digitata* and *Porites* sp., were subsampled from a prior study (chapter 4). Half of the individuals originated from the semi-enclosed lagoon of Bouraké (New Caledonia), which is characterized by the extreme and variable environmental conditions mentioned above (The environmental conditions were measured over several periods from February 2016 to April 2020 with an average temperature of 25.63 ± 2.85°C, dissolved oxygen (DO) of 5.23 ± 0.89 mg O_2 L^{-1}, and pH (total scale) of 7.67 ± 0.23 pH_T). The other half of the individuals originated from a nearby reference reef (Reference), which is characterized by stable and ambient pH conditions (average of

temperature of 25.25 ± 1.89°C, dissolved oxygen (DO) of 6.45 ± 0.95 mg O_2 L^{-1}, and pH (total scale) of 8.02 ± 0.04 pH_T). A detailed description of the environmental conditions of both sites are available in Maggioni et al., (2021). All individuals (n=360; 120 per species) were reared in seawater at constant temperature (26°C) during 100 days under four pH set up: i) reference reef pH (Control; pH_{NBS} 8.11 ± 0.05; mean pCO_2 474 µatm); ii) future reef pH based on the RCP7.0 IPCC scenario (IPCC Report, 2021) (Future; pH_{NBS} 7.76 ± 0.06; mean pCO_2 1192 µatm); iii) extreme mean pH (Extreme; pH_{NBS} 7.53 ± 0.07; mean pCO_2 2115 µatm); and iv) variable pH reproducing the daily variation of pH in Bouraké (Variable; mean pH_{NBS} from 7.56 ± 0.07 to 8.07 ± 0.07; mean pCO_2 from 1968 to 533 µatm; total mean pH_{NBS} of 7.75 ± 0,23). A detailed description of the conditions and experimental design are available in chapter 4.

At the beginning and at the end of the culture experiment, each fragment (n=360) was weighed using the buoyant weight technique (Davies, 1989). Dry skeleton weight was calculated using the density of pure aragonite (2.94 g cm^{-3}), and the net calcification was calculated as the change in dry weight between the initial and the final time, and expressed in total weight % per 100 days.

2.2 Geochemical analyses

2.2.1 Sample preparation and laboratory facilities

We performed the geochemical analyses on the new skeleton that was deposited during the experiment under the different conditions defined above. For that, at the beginning of the experiment, we marked all corals with alizarin Red S (10 mg L^{-1}) during a 24-hour incubation (Davies, 1989). At the end of the experiment, overt the 360 coral fragment we randomly selected and prepared for the analyses 7 to 11 samples per condition and per origin, according to species (depending on material available). We air-dried the coral fragments for 36h before wrapping them in aluminum foil, and stored them in labeled Ziploc bags within a box until chemical purification and analysis.

A clear pink band (i.e. Alizarin Red S) was evident for *Acropora tenuis* and *Montipora digitata*, allowing us to easily collect at least 0.5 to 1 cm of newly calcified skeleton well above the red alizarin band. In contrast, the Alizarin band was less obvious to detect in *Porites* sp, making it difficult to collect newly calcified skeletons. As a result, we preferentially collected the new skeleton that calcified on the Holdfast epoxy resin and plastic plates where individuals were fixed. From each sample, bulk powder was collected using a micro drill (Dremel 3000), then homogenized using an agate mortar, and stored in 1.5 mL Eppendorf tubes placed in a Ziplock bag until geochemical analyses. Sample processing and chemical treatment procedures were performed under ISO 5 (class 100) laminar flow hoods within an ISO 6 (class

1000) clean room at Ifremer (Plouzané, France). All geochemical analyses were performed within the Ocean Spectrometry Pole (PSO). Analyses of $^{13}C/^{12}C$ and $^{18}O/^{16}O$ ratios were carried out using a Thermo Fisher Scientific MAT 253 IRMS (Isotope Ratio Mass Spectrometer) coupled to Kiel IV Carbonates device, while $^{11}B/^{10}B$ ratios were estimated using a Thermo Fisher Scientific Neptune MC-ICPMS (Multi-Collector Inductively Coupled Plasma Mass Spectrometer). Elemental ratios were measured on a Thermo Fisher Scientific Element XR HR-ICP-MS (High-Resolution Inductively Coupled Plasma Mass Spectrometer). Ultra-pure reagents (i.e., HNO_3, HF, HCl, H_2O_2, NH_4OH from Normatom® grade) were used for all chemical procedures. All acids and further dilutions were made using double distilled 18.2 MΩ cm^{-1} MQ water. Standards for isotopic ratio and trace element measurements were freshly diluted during each analytical session with the same acids used for sample preparation to avoid any matrix effects. International standard JCP-1 (Gutjahr et al., 2021) was used through all analytical sessions.

Samples were cleaned with an oxidative cleaning method adapted from previous studies (Grottoli et al., 2005; Wierzbowski, 2007; Sutton et al., 2018). First, a cycle of three cleaning steps with 1 mL of alkaline-buffered (0.1M NH_4OH) MQ water was performed to remove salts and clay. Samples were vortexed and centrifuged at 10,000 rpm to remove the supernatant at the end of each cleaning. Next, the oxidative step was done by adding 500 µL of 3% alkaline-buffered H_2O_2 to remove organic matter. Samples were placed in an ultrasonic bath for 40 min at 50°C to expedite cleaning. After peroxide cleaning, multiple washes (typically three) with alkaline-buffered MQ water were performed on samples until the pH of the supernatant matched that of the MQ water, which ensured removal of all of the oxidizing agent. Samples were then dried in an oven at 60°C overnight.

2.2.2 Stable carbon isotope measurements

Carbonate $\delta^{13}C$ was measured on a Kiel IV Carbonate device coupled to a MAT 253 IRMS. Between 90 and 160 µg of the skeleton powder samples were weighed using a XPR10 Mettler Toledo microbalance (readability 1 µg) and then digested in H_3PO_4. The CO_2 resulting from the dissolution of $CaCO_3$ was analyzed for isotope abundance in the mass spectrometer. Results were calibrated versus the Vienna Pee Dee Belemnite (VPDB) scale by international standard NBS-19 and NBS-18. Analytical precision on the home-made carbonate standard MNHN was better than 0.01‰ for $\delta^{13}C$ (SD, n = 50). The $\delta^{13}C$ of CO_2 gas bottles used during the aquaria experiment for setting the pH were measured on a Thermo Fisher Scientific GasBench II coupled to an IRMS. Several gas samplings were performed throughout the

aquaria experiment using 12mL Exetenairs® vials (Labco 736W) that were sealed with parafilm until analysis.

2.2.3 Boron purification and stable boron isotope measurement

Boron was purified using the microdistillation technique developed by Gaillardet et al. (2001) and adapted for Ca-rich matrices by Wang et al. (2010). The methodology used in this study can be found in Misra et al. (2014) and Guillermic et al. (2021). Samples and the international standards JCp-1 (coral *Porites* sp.; Gutjahr et al. (2021)) from the Geological Survey of Japan, Tsukuba, Japan were weighted (1.80 to 2.50 mg) and cleaned as described in section 2.2.1. Samples and standards were dissolved with 70 µL of 1M HCl and 60 µL of the dissolved samples were loaded on an upside down cap of a clean fin legged 5 mL conical beaker. The tightly closed beaker was put on a hot plate in digestion blocks (Analab®) at 95°C for 15 h. The beakers were removed from the hot plate and allowed to cool for 15 min. Caps containing the microdistillation residue were replaced by clean units and 0.3M HF was added to the distillate. The residues were collected with 100 µL of 1 M HCl and were set aside to assess the final yield of the microdistillation determined by Element XR-ICP-MS (93.21 ± 1.35% ; 95% confidence interval, n = 226).

Boron isotope ratios, reported as delta values ($\delta^{11}B$) in permil (‰), were measured with a Thermo Fisher Scientific Neptune MC-ICP-MS equipped with $10^{11}\Omega$ resistors. The instrumental setup included Savillex® 100 µL min^{-1} C-flow self-aspirating nebulizer, a Teflon® spray chamber, a 2.0 mm alumina injector from ESI©, a Thermo™ Jet sample cone (Nickel), and 'X' type skimmer cones (Nickel). Each analysis consisted of a 2-min simultaneous collection of masses 11 and 10 on Faraday cups H3 and L3. Boron concentrations in the samples ranged typically from 300 ppb (~50 ng B) to 1ppm (~160 ng B). Instrumental sensitivity for ^{11}B on the standard solution (NIST SRM 951) was typically 10.6 $mV.ppb^{-1}$ on ^{11}B with a flow rate of 100 $\mu L.min^{-1}$. Procedural boron blanks reached a maximum of 1.4 ng B contributing to less than 1% of the sample signal. The acid blanks (i.e., 0.3M HF) used during analyses were measured at ≤ 2mV on ^{11}B, meaning a contribution of less than 1% of the sample intensity. Samples were all analyzed in duplicate except when the boron concentration was not high enough to reach the optimal intensity on ^{11}B. The standard solution (NIST SRM 951) was used as a bracketing standard to correct any shift during the analytical sessions. A certified $B(OH)_3$ standard, the ERM© AE120 ($\delta^{11}B$ = -20.2 ± 0.6‰) and a seawater standard, the Nass6-1, were also added in some analytical sessions to ensure reproducibility. The isotopic composition of the ERM© AE120 was $\delta^{11}B_{AE120}$ = -20.22 ± 0.53‰ (2SD, n = 6), versus $\delta^{11}B_{Nass6\text{-}1}$ = 39.86 ± 0.35‰ (SE, n = 4) for the Nass6-1. Regarding the inter-laboratory coral standard

JCp-1 (*Porites* sp.), $\delta^{11}B_{JCp-1}$ was 24.69 ± 0.43‰ (2SD, n = 33) over 18 analytical sessions. Our results for $\delta^{11}B_{JCp-1}$ are within the error of published values (Gutjahr et al., 2021).

2.2.4 Elemental ratio measurements

Microdistillation residues from boron purification were collected with 100 µL 1 N HCl to quantify the yield. Elemental ratios were measured using an aliquot of the dissolved sample and measured on an HR-ICP-MS (Element XR). Prior to analyses, the Ca concentration of the samples was measured on all samples with an inductively coupled plasma atomic emission spectroscopy (ICP-AES) Ultima 2 HORIBA. Samples were diluted to target fixed concentration of calcium at 30 ppm using 0.1 M HNO_3 and 0.3 M HF. Data quality and external reproducibility were determined with the international standard JCp-1. Typical measured concentrations of procedural blanks for the trace element analyses at 30 ppm Ca were ^{7}Li < 5.6%, ^{11}B < 1.01%, ^{25}Mg < 0.2% and ^{43}Ca < 0.05 %. The analytical uncertainties, calculated from the reproducibility of JCp-1 (SE, n=29) measured during sessions, were determined for Li/Ca (± 0.4 µmol mol^{-1}), B/Ca (± 12.8 µmol mol^{-1}) and Mg/Ca (± 90.9 µmol mol^{-1}).

2.2.5 Calculations of $pH_{total\ scale}$, pH_{ECM}, DIC_{ECM} and $[CO_3^{2-}]_{ECM}$

The $pH_{total\ scale}$ relative to pH_{NBS} measured in aquariums was calculated using the definition of $pH_{seawater\ scale}$ derived from pH_{NBS} and according to a mean temperature of 26.2 °C and a mean salinity of 35.6 psu. Finally, we obtained a delta of 0.13 between the $pH_{total\ scale}$ and the pH_{NBS}, such that:

$$pH_{total\ scale} = pH_{NBS} - 0.13 \quad (1)$$

The pH_{ECM} was calculated from measurements of coral skeletal $\delta^{11}B$ (Hemming and Hanson, 1992; Zeebe and Wolf-Gladrow, 2001):

$$pH_{ECM} = pK_B - log\left(\frac{\delta^{11}B_{CS} - \delta^{11}B_{ECM}}{\delta^{11}B_{ECM} - (\alpha \times \delta^{11}B_{CS}) - 1000(\alpha - 1)}\right) \quad (2)$$

With pK_B representing the dissociation constant of $B(OH)_3$ and calculated according to temperature and salinity measured in aquaria (Dickson, 1990), $\delta^{11}B_{CS}$ representing the boron isotopic composition of the coral skeleton, $\delta^{11}B_{ECM}$ representing the boron isotopic composition of the calcifying fluid (acquired from the $\delta^{11}B$ of seawater, which was measured both in our aquaria experiments and at the natural sites of Bouraké and Reference; **Appendix Table VIII-13**), and α representing the boron isotope equilibrium constant equal to 1.0272 (Klochko et al., 2006).

The $[CO_3^{2-}]_{ECM}$ and DIC_{ECM} were calculated using the R code *Boronsystem* provided by Decarlo et al. (2018). We used combined coral skeleton B/Ca ratios and $\delta^{11}B_{CS}$ (‰) to calculate $[CO_3^{2-}]_{ECM}$, following the rationale:

$$\left[CO_3{}^{2-}\right]_{ECM} = K_D \times \frac{[B(OH)_4{}^-]}{B/Ca} \quad (3)$$

With the partition coefficient (K_D) derived from McCulloch et al. (2017b), based on inorganic precipitation experiments from Holcomb et al. (2016):

$$K_D = 0.00297 \times \exp\left(-0.0202 \times [H^+]\right) \quad (4)$$

Given pH_{ECM} and $[CO_3^{2-}]_{ECM}$, DIC_{ECM} can be calculated using the known dissociation constants for carbonate speciation at known temperature and depth.

2.3 Statistical analyses and data presentation

Statistical analyses were conducted and figures were produced using RStudio (R Development Core Team, version 4.1.0, 2021), including the packages “ggplot2”, “stats” and “car”. Homogeneity of variance of the data was tested using Levene test and the normality of the variance distribution using Shapiro-Wilkinson test, and also checked graphically using a Q-Q plot. Statistical tests were performed separately for each species as they were morphologically different. Geochemical parameters which verified normality and homoscedasticity conditions were tested using a two-way ANOVA to characterize the effect of pH (4 conditions: Control, Future, Extreme and Variable), coral’s origin (two conditions: Bouraké and Reference), and their interactions. Post hoc Tukey HSD (honestly significant difference) tests were run to assess significant interactions. The ECM carbonate chemistry parameters were tested between the Variable and Future pH conditions for each species using a Welch T-test.

3. Results

3.1 Net calcification

Net calcification exhibited a broad individual response, ranging from -8% to 212% of total weight. Data significantly differed between coral origins (**Figure V-1**; **Table V-1**; **Appendix Table VIII-12**; **Table VIII-16**) with higher growth rates recorded in corals from Bouraké, and consistently for the three species. In contrast, pH conditions had a significant effect on *M. digitata* and *Porites* sp., with lower calcification rates recorded under the extreme

pH condition for individuals from Reference and Bouraké, respectively. Generally, the lowest net calcification values of all the corals samples were observed for *M. digitata* and *Porites* sp. from the reference reef maintained under extreme pH while the highest net calcification was reported for *A. tenuis* maintained under the future condition for individuals from Bouraké. Calcification rates of *A. tenuis, M. digitata* and *Porites* sp. from Bouraké were 35%, 153% and 78% higher than those from Reference, respectively.

Corals from Bouraké and Reference showed a decrease in mean net calcification rates with a decrease in pH from 8.11 to 7.53 pH_{NBS} units. These decreases in mean net calcification under OA conditions were species-specific and differed between sites. At Reference, the massive coral *Porites* sp. and the branching *A. tenuis* showed the lowest changes (-22 and -25%, respectively), whilst a -52% decrease was measured for the branching *M. digitata*. In contrast, at Bouraké, *A. tenuis* and *M. digitata* showed the lowest changes (-18 and -15%, respectively), whilst a -45% decrease was measured for *Porites* sp.

3.2 Geochemical results

3.2.1 Measured $\delta^{13}C$, $\delta^{11}B$, and B/Ca

Both $\delta^{13}C$ and $\delta^{11}B$ signatures exhibited remarkably similar trends and appear significantly dependent on the seawater pH conditions, with a systematic decrease with seawater acidification (**Figure V-1**; **Table V-1**; **Appendix Table VIII-12**; **Table VIII-16**). Most of the $\delta^{13}C$ values ranged from -8‰ to -4‰ and were significantly different between Bouraké and the reference site for *M. digitata* and *Porites* sp. *M. digitata* demonstrated a greater variability, especially for individuals from the reference site maintained under the most acidified condition. The $\delta^{11}B$ values of all species ranged roughly from 22‰ to 26‰ and showed significantly different values between Bouraké and the reference site for *A. tenuis* and *M. digitata*. A similar spread in the $\delta^{11}B$ data was observed for *M. digitata* originating from the reference site. *A. tenuis* exhibited $\delta^{11}B$ values much less scattered, while *Porites sp*. showed even less dispersed $\delta^{11}B$ values. Interestingly, the $\delta^{13}C$ and $\delta^{11}B$ signatures of *M. digitata* from Reference showed not significant trends with OA. The B/Ca ratio for all species at all sites ranged between 303 to 799 µmol mol^{-1}. These values differed significantly between pH_{sw} conditions for *Porites* sp., with lower B/Ca ratio in corals at the lower pH conditions (Future and Extreme). The B/Ca ratio also differed between origins regarding *M. digitata*, with increased ratios in corals from the reference site.

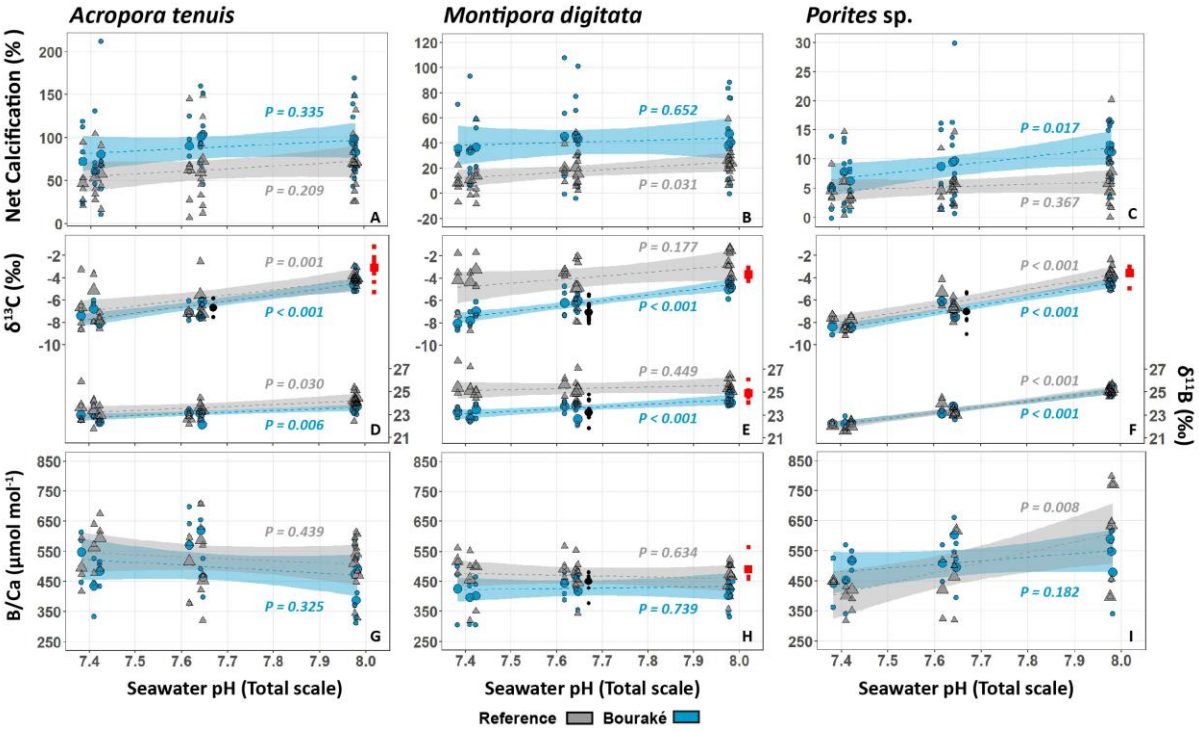

Figure V-1 | *Net calcification (**A-C**), $\delta^{13}C$ and $\delta^{11}B$ (**D-F**), and B/Ca ratio (**G-I**) of Acropora tenuis, Montipora digitata and Porites sp. measured at the experimental stable pH_{sw} conditions (Extreme, pH_{NBS} 7.54; Future, pH_{NBS} 7.76; Control, pH_{NBS} 8.11). Blue circles and grey triangles correspond to Bouraké and Reference colonies, respectively. Largest symbols represent averaged values, while the smallest symbols represent data for each individual colony. Dashed lines represent linear model regressions fitted using linear model function in RStudio with 95% confidence interval represented by the envelopes. (n=7-17 per pH conditions, depending on parameters, site of origin and species). The black dots for Bouraké and the red squares for the reference site represent the respective geochemical parameters measured on samples collected in situ and not incubated in aquaria (n=3-22, depending on parameters, site of origin and species). $\delta^{11}B$ and B/Ca of the in situ samples were only measured for M. digitata (n=5 for Reference and n=10 for Bouraké). Please, note that the scales for net calcification are different between species and that for clarity we do not present the Variable pH_{sw} condition (see Appendix Figure VIII-14 and Figure VIII-15).*

In order to enhance clarity in the results, data from the variable pH condition were excluded independently of the stable pH conditions as the former condition represents a fluctuating range of seawater pH values. However, the $\delta^{13}C$, $\delta^{11}B$ and B/Ca values of the variable pH condition were in the same range as those of stable seawater pH conditions (**Appendix Figure VIII-14**; **Figure VIII-15**). Only for *A. tenuis* $\delta^{13}C$ was significantly different between origins in both the variable and stable pH condition (**Appendix Table VIII-15**).

Parameters	Factors	*A. tenuis*	*M. digitata*	*Porites* sp.
Net calcification	Origin	**0.003**	**<0.001**	**<0.001**
	pH	0.118	0.160	**0.012**
	O x pH	0.902	0.583	0.138
$\delta^{13}C$	Origin	0.142	**<0.001**	**0.014**
	pH	**<0.001**	**<0.001**	**<0.001**
	O x pH	0.648	0.186	0.736
$\delta^{11}B$	Origin	**0.010**	**<0.001**	0.764
	pH	**<0.001**	**0.011**	**<0.001**
	O x pH	0.719	0.202	0.313
pH_{ECM}	Origin	**0.014**	**<0.001**	0.717
	pH	**<0.001**	**0.006**	**<0.001**
	O x pH	0.734	0.209	0.298
B/Ca	Origin	0.317	**0.027**	0.438
	pH	0.210	0.907	**<0.003**
	O x pH	0.856	0.564	0.128
$[CO_3^{2-}]_{ECM}$	Origin	0.877	0.224	0.658
	pH	**0.027**	0.227	0.697
	O x pH	0.777	0.843	0.313
DIC_{ECM}	Origin	0.261	**0.012**	0.462
	pH	0.197	0.593	**0.002**
	O x pH	0.767	0.541	0.147

Table V-1 | *Probability values from two-way ANOVAs testing the effects of colony origins (Bouraké and Reference sites), pH conditions (Extreme, pH_{NBS} 7.54; Future, pH_{NBS} 7.76; Control, pH_{NBS} 8.11), and their interaction for the three coral species. Significant values are in bold ($p < 0.05$). All statistical analyses, including the post-hoc comparisons, are in the Appendix Table VIII-12.*

3.2.2 Calculated pH_{ECM}, DIC_{ECM} and $[CO_3^{2-}]_{ECM}$

Using $\delta^{11}B$ and B/Ca values, we calculated the carbonate chemistry of the calcifying fluid (**Figure V-2**). The pH_{ECM} was significantly different between origins and pH conditions for all corals species, with the exception of *Porites* sp. (**Figure V-2**; **Table V-1**; **Appendix Table VIII-12**; **Table VIII-16**). The pH_{ECM} in *Porites* sp. from both origins decreased from 8.55 for the control condition to 8.35 for the extreme condition, while it decreased from ca 8.47 to 8.41 for *A. tenuis* from both origins, as well as for *M. digitata* from Bouraké. In contrast, and in agreement with $\delta^{13}C$ and $\delta^{11}B$ data, the pH_{ECM} of *M. digitata* from Reference was more variable, which resulted in a not significant trend of pH_{ECM} with OA (**Figure V-2**).

The DIC_{ECM} and $[CO_3^{2-}]_{ECM}$ concentrations barely show clear responses to pH changes and origin conditions. For *A. tenuis*, $[CO_3^{2-}]_{ECM}$ significantly differed between pH conditions and

decreased at lower seawater pH. DIC_{ECM} was significantly different between origins for *M. digitata*, with lower values for Reference compared to Bouraké, and between pH conditions for *Porites* sp., with lower values at higher seawater pH. As for the measured geochemical signatures, the corresponding ECM carbonate chemistry calculations of the variable pH condition showed a similar range as those of stable seawater pH conditions (**Appendix Figure VIII-14**; **Figure VIII-15**). Moreover, pH_{ECM}, $[CO_3^{2-}]_{ECM}$ and DIC_{ECM} were statistically equivalent between the variable pH condition and the stable Future pH condition (i.e., pH_{NBS} = 7.76), the latter closely represents the mean seawater pH value of the variable pH condition (i.e., pH_{NBS} = 7.75) (**Table V-2**).

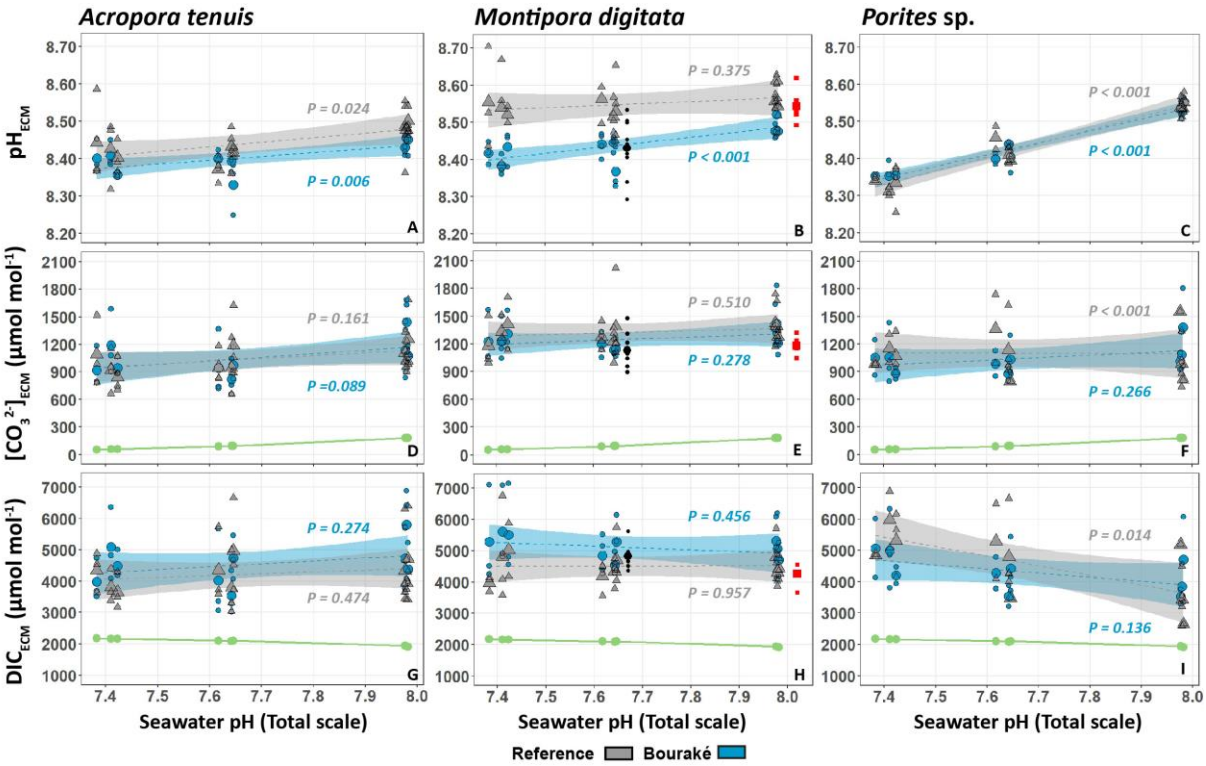

Figure V-2 | *pH_{ECM} (**A-C**), $[CO_3^{2-}]_{ECM}$ (**D-F**), and DIC_{ECM} (**G-I**) of Acropora tenuis, Montipora digitata and Porites sp. calculated on boron proxies at the experimental stable pH_{SW} conditions (Extreme, pH_{NBS} 7.54; Future, pH_{NBS} 7.76; Control, pH_{NBS} 8.11). Blue circles and grey triangles correspond to Bouraké and Reference colonies, respectively. Largest symbols represent averaged values, while the smallest symbols represent data for each individual colony. Dashed lines represent linear model regressions fitted using linear model function in RStudio with 95% confidence interval represented by the envelopes. (n=6-11 per pH conditions, depending on parameters, site of origin and species). Continuous green lines represent DIC_{SW} or $[CO_3^{2-}]_{SW}$. Calcifying fluid parameters were also calculated for M. digitata individuals sampled in situ and represented by black dots for Bouraké (n=10) and red squares for Reference (n=5). ECM: Extracellular Calcifying Medium; SW: Seawater. Please, note that for clarity we do not present the Variable pH_{SW} condition (see Appendix Figure VIII-14 and Figure VIII-15).*

Species	*df*	*T*	*p*
pH_{ECM}			
A. tenuis	36	-1.099	0.278
M. digitata	39	1.653	0.106
Porites sp.	18	1.488	0.154
$[CO_3]^{2-}_{ECM}$			
A. tenuis	35	-1.365	0.181
M. digitata	38	-0.075	0.941
Porites sp.	25	-0.647	0.523
DIC_{ECM}			
A. tenuis	34	-0.755	0.456
M. digitata	38	-1.427	0.162
Porites sp.	25	-1.197	0.242

Table V-2 | *Results of a Welch T-test testing the differences between the two pH conditions Future, pH_{NBS} 7.76 and Variable pH_{NBS} 7.56 - 8.07 on the ECM carbonate chemistry (pH_{ECM}, $[CO_3]^{2-}_{ECM}$ and DIC_{ECM}) for each coral species. Significant values are in bold ($p < 0.05$).*

4. Discussion

Recent characterizations of the Bouraké site highlighted a particular environment with highly variable and extreme pH, temperature, and dissolved oxygen conditions (Camp et al., 2017; Maggioni et al., 2021). Therefore, it is reasonable to assume that Bouraké is a hostile environment for coral reef development (Kleypas et al., 1999b). Despite this harsh environment, net calcification was higher for all three coral species at Bouraké compared to the Reference site (chapter 4). The coral mean net calcification for individuals from both sites are consistent with the general consensus of reduced coral calcification under OA (Gattuso et al., 1999; Comeau et al., 2013; Leung et al., 2022). The species-specific differences measured in net calcification between sites indicate some variability in the efficiency of the physiochemical mechanisms used by corals to maintain calcifying processes under OA. Moreover, the consistent higher net calcification of Bouraké corals suggests that they have adapted physiochemical mechanisms that promote bio-calcification.

The study of the influence of ocean acidification on coral calcification and resilience must consider carbonate chemistry of the ECM as it drives the crystallization of aragonite (Venn et al., 2011; Allison et al., 2014; McCulloch et al., 2017a; Sevilgen et al., 2019). However, parameters affecting coral ECM chemistry are not well understood. By studying carbon and boron isotope signatures in the coral skeleton, differences in ECM regulation mechanisms were observed between Bouraké corals and corals from the more stable Reference environment. Building on the physiological and metagenomic data of the chapter 4

and geochemical proxies from this study, we highlighted the unique influence of the symbiont community on the host coral in managing the physiochemical control of its ECM, ultimately promoting calcification under OA.

4.1. Geochemical signatures of coral bio-calcification under OA

The physiochemical mechanisms regulating coral calcification are most likely in direct relation with the ECM carbonate chemistry (e.g., pH_{ECM} and DIC_{ECM}). Based on their $\delta^{11}B$ signatures, all scleractinian corals exhibited high pH_{ECM} relative to seawater pH in this study. The $\delta^{11}B$ composition of all corals showed decreasing isotopic signature with decreasing seawater pH. Accordingly, all three coral species showed a decrease in pH_{ECM} in response to experimental seawater acidification, regardless of coral origin, which is consistent with other studies (McCulloch et al., 2012a; Comeau et al., 2019a; Cameron et al., 2022; Eagle et al., 2022). The three coral species showed different degrees of pH_{ECM} regulation under OA, with values ranging from 8.20 to 8.70 for all experimental conditions and *Porites* sp. showing a pH_{ECM} decrease more than twice that of the other two species (ca 0.2 pH units). Our results demonstrate species-specific regulation of the pH_{ECM} relative to seawater pH (up to 1.15 pH units). This finding is consistent with previous studies on corals grown experimentally in OA conditions (Ries, 2011; McCulloch et al., 2012a; Venn et al., 2019; Guillermic et al., 2021; Eagle et al., 2022) and corals living in extreme environments (Schoepf et al., 2017; Cornwall et al., 2018; Comeau et al., 2022).

A. tenuis and *M. digitata* individuals from Bouraké exhibited $\delta^{11}B$ composition and corresponding pH_{ECM} significantly lower than their counterparts from Reference. In contrast, there was no significant difference between sites of origin for *Porites* sp. The latter and *A. tenuis* showed similar decreases in pH_{ECM} with OA, regardless of coral origin. On the contrary, *M. digitata* individuals from Reference showed high inter individual variability in pH_{ECM} values, with average values higher than Bouraké ($p<0.001$) and higher than the two other species regardless of origins ($p<0.001$). In contrast to other individuals, *M. digitata* from Reference do not present a pH_{ECM} decrease with OA. This results in a pH_{ECM} homeostasis trend (i.e., no change of inter individual pH_{ECM} average regardless of seawater pH conditions; Georgiou et al., 2015), while individuals from Bouraké exhibited a decrease of 0.1 pH unit under OA. Corals capable of maintaining a constant pH_{ECM} would be more resistant to OA (Georgiou et al., 2015; McCulloch et al., 2017a; Comeau et al., 2019a). Interestingly, *M. digitata* individuals from Bouraké did not show pH homeostasis while maintaining pH_{ECM} higher than seawater pH. Whilst it is generally believed that a higher pH_{ECM} promotes calcification (McCulloch et al., 2012a; Cornwall et al., 2018; Guillermic et al., 2021; Cameron et al., 2022; Eagle et al., 2022),

the distinct pH_{ECM} levels measured according to the site of origin in this study were inversely correlated with the net calcification trends. Net calcification is a combination of calcification and dissolution processes influenced by physicochemical controls concealing a clear relationship with the pH_{ECM}. Consequently, pH_{ECM} and net calcification are not necessarily coupled (Comeau et al., 2017; Liu et al., 2020). This discrepancy was observed for Bouraké corals, which exhibited higher calcification rates than Reference corals despite the absence of pH_{ECM} homeostasis and/or lower pH_{ECM} values.

It has been shown that pH_{ECM} is not the only parameter influencing calcification: DIC_{ECM} concentration can also counteract the drop in pH_{ECM} and ultimately influence the saturation state of aragonite (Ω_{Ar}) to promote calcification (Furla et al., 2000; Schoepf et al., 2017; Sevilgen et al., 2019; Wall et al., 2019a; Comeau et al., 2022). Consequently, the significant increase of DIC_{ECM} with OA (+35% on average) in *Porites* sp. may sustain coral calcification. In addition, the statistically higher DIC_{ECM} in *M. digitata* individuals from Bouraké compared to Reference, could promote bio-calcification of Bouraké corals. Although this mechanism of DIC_{ECM} concentration may help corals maintain calcification in low pH environments, it probably plays a minor role in regulating calcification compared to pH_{ECM} regulation (Comeau et al., 2022). The DIC_{ECM} pool is to some extent regulated by physiological processes that can be further studied using $\delta^{13}C$ from the coral skeleton (Swart et al., 1996; Grottoli, 2002; Grottoli et al., 2017).

In corals, skeletal $\delta^{13}C$ reflects the host-symbiont relationship, with photosynthesis preferentially consuming ^{12}C, which increases coral skeletal $\delta^{13}C$ and enriches the DIC pool (McConnaughey, 1989; Swart et al., 1996; Grottoli, 2002). The decrease in coral skeletal $\delta^{13}C$ signatures under OA was relatively consistent between species and origins in this study (ranging from -8‰ to -4‰; **Figure V-1**); it was also consistent with values previously reported in OA experiments (Krief et al., 2010; Eagle et al., 2022). In chapter 4, we showed that *A. tenuis* and *Porites* sp. had higher rates of photosynthesis under OA treatments, due to their symbiont activities, compared to control conditions. In contrast, *M. digitata* did not show increased photosynthetic rates under OA and appeared to be less efficient during CO_2-induced fertilization of photosynthesis by symbionts. We might expect an increase in $\delta^{13}C$ related to an increase in photosynthetic rate under OA conditions, but the DIC isotopic composition of seawater (derived from depleted fossil carbon sources) is more likely to alter the $\delta^{13}C$ signature of the coral skeleton (Swart et al., 1996; Grottoli, 2002). Therefore, the sources of carbon incorporated into the coral skeleton must be identified. The systematic decrease in $\delta^{13}C$ with pH in this study may be due to the ^{13}C-depleted CO_2 used in the culture experiments (-17.23‰ to -22.01‰; **Appendix Table VIII-13**) relative to the atmospheric $\delta^{13}C$ signature (ca. -7‰; Affek and Yakir, 2014). However, this potential bias should be identical for all coral populations.

Therefore, by comparing the single pH conditions between Bouraké and Reference, we should be able to identify any physiological response.

We can explore differences between sites by comparing the $\delta^{13}C$ measured in each species for each origin (i.e., $\delta^{13}C_{Reference}$ - $\delta^{13}C_{Bouraké}$). For *Porites* sp. and *A. tenuis*, the difference between sites (0.5‰ and 0.9‰, respectively) is smaller than for *M. digitata* individuals (3.7‰) in the Extreme OA condition (**Appendix Figure VIII-12**). This difference is relatively important for *M. digitata* because Reference individuals show high variability in $\delta^{13}C$ values under OA (as observed for $\delta^{11}B$) resulting in a less pronounced decrease in $\delta^{13}C$ compared to the other species and origin. This result may indicate lower respiration and/or higher photosynthetic activities under OA for *M. digitata* individuals from Reference. However, in chapter 4 we reported no significant differences for P_g:R ratios (gross photosynthesis versus dark respiration rate ratio) between sites (see **Appendix Figure VIII-12** and **Table VIII-15**). Therefore, photosynthesis and respiration are not the only factors controlling $\delta^{13}C$ values in the coral skeleton (e.g. heterotrophy). In addition, geochemical proxies such as $\delta^{13}C$ record time-integrated physiochemical signatures, which limits their comparison to the short-term physiological measurements such as photosynthesis and respiration made *in vitro* but might better reflect the overall physiological performance of the organism.

To summarize, the $\delta^{11}B$ and $\delta^{13}C$ geochemical signatures measured in the skeleton of the three coral species at Bouraké present distinct differences when compared to Reference. The physiochemical mechanisms controlling these differences remain to be determined.

4.2. Physiochemical control of calcification under OA

Bouraké corals showed higher calcification rate than Reference corals, but lower $\delta^{11}B$ values, which corresponded to lower pH_{ECM}. This is contrary to what was expected, i.e., positive relationship between pH_{ECM} and calcification rate (Ries, 2011; Allison et al., 2014; McCulloch et al., 2017a). Indeed, all coral specimens from Bouraké showed higher calcification rates and lower, or similar, $\delta^{11}B$ values, compared to Reference corals. As discussed above, the DIC_{ECM} increase could counteract a drop in pH_{ECM} and explain increased calcification in *M. digitata* individuals from Bouraké. However, DIC_{ECM} increase cannot explain higher calcification rates of Bouraké corals for the other two species, since DIC_{ECM} values remained similar between sites. Several mechanisms related to host-microorganism associations, energy budget/allocation and/or ionic transports could explain higher calcification rates in Bouraké corals. Specific associations of symbionts have been proposed to promote the physiological performances of the host corals (Howells et al., 2012; Ziegler et al., 2015; Ros et al., 2021). For example, corals associated with “stress-tolerant” symbiont taxa, such as

Durusdinium (clade D), would be heat tolerant by maintaining symbiont density (Silverstein et al., 2017), elevating metabolism through energy generation (Haydon et al., 2023), and/or sustaining translocation of organic compounds from symbionts (Ros et al., 2021). In parallel, coral hosts may benefit from greater energy storage thanks to larger heterotrophic inputs (Edmunds, 2011; Drenkard et al., 2013; Houlbrèque et al., 2015). Finally, ECM carbonate chemistry can be impacted by the relative contribution of the two ionic pathways, the active transport through epithelial cells (i.e. the transcellular pathway) and the passive transport by diffusion through intercellular spaces (i.e. the paracellular pathway) (Hohn and Merico, 2015; Ohno et al., 2017; Venn et al., 2020; Capasso et al., 2021).

Physiological data from chapter 4 reported species-specific physiological differences between sites and/or pH conditions, such as changes in symbiont density and association. Symbiont density increased significantly between Reference and Bouraké for *A. tenuis* and *Porites* sp. under the Extreme OA condition, Reference presenting higher symbiont density. Although the influence of symbionts on the regulation of ECM carbonate chemistry has not been fully elucidated, some recent studies suggest that symbionts can physiologically control ECM through translocated photosynthates (Sevilgen et al., 2019; Cameron et al., 2022; Eagle et al., 2022; Venn et al., 2022; Allen-Waller and Barott, 2023). A change in symbiont density could result in a change in energy allocation to corals and ultimately in regulation of ECM carbonate chemistry (Hoogenboom et al., 2010; Gibbin et al., 2014). The fact that *A. tenuis* and *Porites* sp. individuals from Bouraké had lower pH_{ECM} and DIC_{ECM}, respectively than Reference could also result from lower symbiont density under the Extreme OA condition. Sevilgen et al. (2019) showed in an *in vivo* experiment using pH microelectrodes that frequent contractions and retractions of the polyps induce compressed tissue and greater density of symbionts. Photosynthesis by symbionts generates a higher pH gradient that ultimately modulates pH_{ECM} (Venn et al., 2009, 2022; Jokiel, 2011). In addition, photosynthesis by symbionts also modulates pH of the mesoglea, which acts as a buffering space between seawater and ECM (Venn et al., 2022). In summary, the decreased symbiont density under the Extreme pH condition of *A. tenuis* and *Porites* sp. from Bouraké could influence their physiochemical control of the ECM under OA. In contrast, *M. digitata* had a similar density of symbionts despite significant change in pH_{ECM} between sites. This could indicate species-specific physiochemical control of ECM depending on coral symbiont species.

In chapter 4, we reported with a metagenomic study that *Cladocopium* (i.e. clade C; LaJeunesse et al., 2018) was the only genus found in the studied corals. They also found different symbionts associated with corals depending on the species and origins. Bouraké corals, in which more stable symbiotic associations were present, were mainly associated with symbiont species C15 (*M. digitata* and *Porites* sp.) and C1 (*A. tenuis*). *M. digitata* individuals

from Reference are predominantly associated with species C73. *M. digitata* showed the same symbiont density whatever the individual origin, but different symbiont communities. The latter could explain the significantly different pH_{ECM} measured at Bouraké and Reference. It is widely recognized that symbiotic associations play a key role in the physiological resilience of corals under stressful conditions (Howells et al., 2012; Schoepf et al., 2015; Camp et al., 2018, 2020; Grottoli et al., 2018; Hoadley et al., 2019, 2021; Voolstra and Ziegler, 2020); they could, to some extent, benefit the corals of Bouraké. However, the specificities of each symbiont species and their contributions to host physiology remain poorly understood.

The reallocation of energy leads to the synthesis and secretion of macromolecules called “organic matrix” towards the mineralizing site, initiating the nucleation of aragonite (Allemand et al., 2004). This organic matrix may reduce the energy required for aragonite nucleation by hosting amorphous calcium carbonate (ACC) nanoparticles, which could promote coral calcification beneath OA (Von Euw et al., 2017). For example, the attachment of ACC particles could induce aragonite growth more than 100 times faster than ion-by-ion growth (Mass et al., 2017). Although further characterization of these biomineralization patterns is needed, it suggests that corals, which allocate more energy toward these organic molecules, may not require very high Ω_{Ar} in the ECM to calcify (Sevilgen et al., 2019). It would be interesting to look at the energy available for the species studied here, but only the protein content has been quantified (chapter 4), which does not complete the energy budget. Protein content decreased significantly with OA for *A. tenuis* and *Porites* sp. suggesting a depleted energy budget under OA. These two species could adapt their energy allocation to continue calcifying, while *M. digitata* would benefit from distinct symbiont associations.

Variations in energy allocation, such as the amount of photosynthate (carbohydrates) translocated from the symbiont to the host coral, influence the regulation of ECM carbonate chemistry and ultimately benefit calcification (Al-Horani et al., 2003; Aichelman et al., 2021; Cameron et al., 2022). The energetic costs associated with calcification remain to be accurately quantified (McCulloch et al., 2012a; Hohn and Merico, 2015; Galli and Solidoro, 2018). Galli and Solidoro (2018) reported higher energetic costs for calcification under OA by ATP supply than previous constraints. Since regulation of pH_{ECM} can be energetically expensive, altering the energy budget could lead to a reallocation of energy to mechanisms others than ECM regulation, and then reducing the ECM chemistry parameters is a potential trade-off for the organism (i.e. pH_{ECM} is still elevated compared to seawater) to sustain growth under OA conditions (Wall et al., 2019b). Variations in energy availability/allocation by symbionts can increase or decrease active ion transport to the ECM, via a greater or lesser supply of ATP, ultimately affecting calcification (Cameron et al., 2022; Venn et al., 2022; Allen-Waller and Barott, 2023).

The ion transport activity may also depend on the surrounding environment. The influence of paracellular transport over transcellular pathways is thought to be due to species-specific permeability (Capasso et al., 2021). The latter varies with environmental conditions (Ganot et al., 2015; Hohn and Merico, 2015; Venn et al., 2020, 2022). Increased OA exacerbates paracellular permeability, resulting in leakage of calcium and carbonate ions from the ECM, thereby reducing calcification rates (Hohn and Merico, 2015; Venn et al., 2020). However, it is unclear how the permeability of the coral host cell membrane might change between species and/or origins. Giorgia et al. (2022) reported metagenomic changes in a scleractinian coral living along a natural CO_2 gradient. They would be expected to enhance protective cell structures, e.g. ensuring the maintenance of membrane and cell wall integrity. The present results once again highlight the significant role of micro-organism associations in the physiochemical control of the coral host to promote calcification under OA.

4.3. Are pH fluctuations beneficial to the physiochemical control of the ECM?

Environmental pH variability can have either a positive effect (Camp et al., 2019; Enochs et al., 2020; Brown et al., 2022; Comeau et al., 2022) or no measurable impact (Camp et al., 2016a; Cornwall et al., 2018) on coral responses to OA. The benefits of variable pH in the environment remain equivocal (Rivest et al., 2017), due to the length of exposure required experimentally to induce eventual acclimation of corals to OA (Comeau et al., 2019a; Aichelman et al., 2021; chapter 4). Although a growing number of studies are investigating the influence of pH variability on coral acclimation to OA, only two studies (one *in vitro* and one *in vivo*) have so far examined the influence of pH variability on the regulation of ECM chemistry (Cornwall et al., 2018; Comeau et al., 2022). In the present study, the potential benefits of pH variability on the regulation of ECM chemistry were tested using two different exposure durations: the long-term, represented by Bouraké coral individuals, and the short-term, with the variable pH condition assessed in aquaria for 100 days.

The short-term variable pH condition did not alter the coral ECM chemistry range of values (i.e., pH and DIC) relative to the other pCO_2 conditions (**Appendix Figure VIII-14**). In addition, pH_{ECM} and DIC_{ECM} of corals exposed to the variable pH condition were not significantly different from those exposed to the stable pH of 7.7 (Future), the average pH value of the Variable condition (**Table V-2**). This result is consistent with the observations of Cornwall et al. (2018) that average pH_{ECM} was determined by average seawater pH rather than pH variability. The carbonate chemistry of the ECM, calculated using both $\delta^{11}B$ and B/Ca, recorded a time-integrated signature and not a diurnal variability. Future work should use real-time pH_{ECM} measurements (e.g., with pH microelectrodes) to determine high-frequency changes in ECM

carbonate chemistry under fluctuating pH conditions. In this study, the similarity of seawater pH averages under constant and variable pH conditions masked the effect of diurnal seawater pH fluctuations on ECM carbonate chemistry. The duration of exposure modulates the response of corals to stressors such as warming and acidification (Aichelman et al., 2021), as this response could take more than a year or even several generations (Comeau et al., 2019a). Therefore, a 100-day aquaria experiment may not be long enough to characterize the physiochemical control of coral ECM. On the other hand, on the scale of a long-term exposure to a variable pH (case of Bouraké corals), corals could have developed adaptive mechanisms during several generations in order to maintain the calcification of the skeleton under extreme conditions.

5. Conclusion

The physiochemical control of coral ECM was shown using geochemical tools (e.g. $\delta^{11}B$, $\delta^{13}C$ and B/Ca). Notably, the physiochemical control of coral ECM permits calcification to continue under OA, though its degree of influence is dependent on an organism's site of origin. Our results support the existence of species-specific responses in the regulation of ECM carbonate chemistry under OA conditions. Bouraké corals, adapted to extreme conditions, were able to raise their pH_{ECM} compared to the pH of seawater but presented lower pH_{ECM} than their counterpart from Reference despite better calcification. It is interesting to note that these corals did not maintain a stable pH_{ECM} under OA, on the contrary of *M. digitata* from Reference, which presented a pH_{ECM} homeostasis trend. The present study shows that pH_{ECM} is not the only parameter reflecting the calcification capabilities, with the reduced pH_{ECM} in corals from Bouraké potentially being a trade-off for these organisms. The enhanced calcification of corals from Bouraké implies additional physiochemical strategies to promote calcification.

This study links the role of symbionts in the physiochemical regulation of coral ECM under OA. Symbiont density and/or associations appear to mitigate the negative effects of OA on coral calcification. Specifically, symbionts provide energetic resources that promote regulation of ECM carbonate chemistry, while associating with specific symbiont communities seem to influence the physiochemical control of the coral host to promote calcification under OA. However, the specific contributions of symbiotic partners in the physiochemical control of coral ECM remain poorly known and remain to be identified. Future field and laboratory work should aim to use methods to characterize the benefits of the microbiome for the physiochemical control of coral ECM under extreme conditions. Although fluctuating seawater pH did not affect the regulation of ECM carbonate chemistry in the short-term, we believe that long-term exposure of corals to varying pH conditions could help corals to adapt, as observed in Bouraké

corals. By combining geochemical, physiological and metagenomic approaches, our study demonstrates that corals can employ strategies other than pH_{ECM} homeostasis to cope with ongoing rapid OA, but that the duration of exposure to extreme conditions can affect the implementation of these strategies.

CHAPTER 6

RECORDS OF CORAL ACCLIMATIZATION IN GEOCHEMICAL SIGNATURES

6.1 Preamble

In the previous chapters of this thesis, we highlighted the specific abilities of Bouraké corals to acclimatize to extreme and fluctuating environmental conditions. These abilities could occur early in the life of corals as suggested in **chapter 3**, supporting the hypothesis that these corals are potentially acclimatized over several generations. This hypothesis would imply that Bouraké corals inherit a transgenerational acclimatization likely related to epigenetic processes and/or micro-organisms associations, which ultimately enable rapid adaptive responses to climate changes (Torda et al., 2017). One way to prove potential transgenerational acclimatization of corals at Bouraké is to reconstruct past environmental conditions, such as seawater pH and temperature, in long-lived specimens from Bouraké. The use of geochemical proxies in coral cores provides a unique and detailed archive of past environmental conditions on a high-resolution timescale (e.g., D'Olivo et al., 2018, 2019; Wu et al., 2018; Tarique et al., 2021). It is interesting to note that these coral-based paleoclimatic reconstructions have been little explored for corals long established in an extreme and fluctuating environment. This is why, in **Chapter 6**, we sought to reconstruct the pH and temperature of the seawater at Bouraké over the last few decades (around 30 years) in order to identify any long-term acclimatization of Bouraké corals. To achieve this objective, we measured at annual resolution the geochemical proxies δ13C, δ11B, δ18O and Li/Mg in two *Porites* sp. cores, one from Bouraké (covering the period 1992-2018 CE) and the other from Puen, an adjacent reference site (covering the period 1988-2018 CE). The reconstitution of seawater pH and temperature at the adjacent reference site will help determine whether the potential long-term acclimatization at Bouraké is transferable to corals facing current and future climate changes.

6.2 Article n°4: First long-term (~30 years) acclimatization of corals to ocean acidification recorded in geochemical signatures: A case study from New Caledonia

In prep, ***to be submitted***

First long-term (~30 years) acclimatization of corals to ocean acidification recorded in geochemical signatures: A case study from New Caledonia

Clément Tanvet[1,2,*], Delphine Dissard[3], Gérard Thouzeau[1], Maxence Guillermic[4], Jill Sutton[1] and Riccardo Rodolfo-Metalpa[2]

[1]Univ Brest, CNRS, IRD, Ifremer, LEMAR, F-29280 Plouzané, France
[2]UMR ENTROPIE (CNRS, IRD, UR, UNC, IFREMER), Centre IRD de Nouméa, New Caledonia
[3]UMR LOCEAN (CNRS, IRD, MNHN, Sorbonne Université), Centre IRD de Nouméa, New Caledonia
[4]Department of Earth, Planetary, and Space Sciences, Department of Atmospheric and Oceanic Science, Institute of the Environment and Sustainability, UCLA, University of California Los Angeles, CA 90095, USA

* Corresponding author

Abstract

The rapid and ongoing decline in surface ocean pH (pH_{sw}) resulting from increased anthropogenic CO_2, termed Ocean Acidification (OA), poses a serious threat to calcifying marine organisms. Recent modern OA records remain limited and require additional reconstructions of pH_{sw} variability over the last decades. Here, we performed paleoclimate reconstructions by measuring geochemical proxies on coral skeletons from two *Porites* sp. cores from the extreme and fluctuating environment of Bouraké and the adjacent and more stable shallow reef of Puen. Results from our control core at Puen showed an increase in anthropogenic CO_2 uptake by seawater between 1988 and 2018 CE, coinciding with a decrease in pH_{sw} of ~0.13 pH units. A strong influence of the El Niño Southern Oscillation on pH_{sw} and sea surface temperature variabilities has also been observed. In contrast, pH_{sw} did not vary in the extreme Bouraké environment, with a mean value of ~7.56 pH units, stable from 1992 to 2018 CE. This provides the first long-term record of coral acclimatization to OA.

Key words: Ocean acidification; Coral cores; Paleoclimate reconstructions; Acclimatization; Geochemical proxies

Introduction

Atmospheric carbon dioxide (CO_2) has increased by 51% since the industrial era (from 278 to 420 ppm) leading to major environmental changes (Keeling et al., 2001). The uptake of approximately 30% of the anthropogenic CO_2 emissions by oceans induces a rapid global decline in ocean surface pH, commonly referred to as "ocean acidification (OA)" (e.g., Caldeira and Wickett, 2003; Orr et al., 2005; Gattuso et al., 2015). The end-of-the-century projections of the Intergovernmental Panel on Climate Change (IPCC) predict a decrease in global seawater pH by up to 0.4 pH units (IPCC Report, 2021). One of the major consequences of OA on biological marine ecosystems is the alteration of seawater carbonate chemistry, resulting in a decrease in the saturation state of calcium carbonate (Doney et al., 2009). OA is therefore a major threat to calcifying organisms, including scleractinian corals, one of the keystones of global marine biodiversity (Gattuso et al., 1998; Kleypas and Yates, 2009). The Great Barrier Reef (GBR) has already lost half of its initial coverage since 1985 (De'Ath et al., 2012). Future projections indicate that the majority of coral reefs will be severely and rapidly degraded over the next few decades, with up to 94% erosion by 2050 (Hoegh-Guldberg et al., 2017; Cornwall et al., 2021a).

Most of the current measurements of pH in the global ocean come from ship and mooring track records, and from global observing networks with increasing but still limited spatio-temporal data (Bates et al., 2014; Newton et al., 2014; Takahashi et al., 2014; Lauvset et al., 2015; Wanninkhof et al., 2019). Accurate measurements of seawater pH (pH_{sw}) over the past few decades are essential to quantify the evolution of OA and its impact on reef ecosystems. Coral cores are unique and detailed archives of past environmental conditions: using proxy data, it is possible to study pH and temperature changes on a high-resolution time scale (e.g., Corrège, 2006; D'Olivo et al., 2018, 2019; Wu et al., 2018; Tarique et al., 2021). Boron isotopic composition ($\delta^{11}B$) of biogenic carbonate is a robust proxy of pH generally used in paleo-pH reconstructions in scleractinian coral skeletons. pH_{sw} reconstructions based on $\delta^{11}B$ from coral cores have recorded significant recent OA since the industrial era (Wei et al., 2009; D'Olivo et al., 2015; Wu et al., 2018; Chen et al., 2021). These records also highlighted the influence of seasonal fluctuations, modulated by physical oceanographic processes such as the El Niño-Southern Oscillation (ENSO) phenomena, on pH_{sw} variability (Tarique and Rahaman, 2022). Given future warming scenarios and the resulting increase in the amplitude of ENSO events, pH_{sw} variability will be more frequent and larger (Tarique et al., 2021).

Over the past decade, a growing number of studies have shown that corals chronically exposed to daily and seasonally fluctuating environmental conditions are more resilient to future changes (Rivest et al., 2017; Enochs et al., 2020; Schoepf et al., 2020). For instance, when facing fluctuating and extreme pCO_2 conditions, corals can control the pH of their extracellular calcifying medium (pH_{ECM}) (Georgiou et al., 2015; Comeau et al., 2022). A growing but limited number of studies using $\delta^{11}B$ as a tool to record pH_{sw} and/or pH_{ECM} have been published over the past decade (see Thompson, 2022 for review). Current pH_{sw} reconstructions from corals focus mainly on corals from typical reefs in the South China Sea (Liu et al., 2014; Chen et al., 2021), Arabian Sea (Tarique et al., 2021), Caribbean Sea (Fowell et al., 2018) and the Coral Sea (Wei et al., 2009; D'Olivo et al., 2015; Wu et al., 2018). However, long-term reconstructions of pH_{sw} in corals potentially adapted to marginal and/or extreme environments remain poorly explored. Long-term recording of coral adaptation or acclimatization (process by which coral organisms adapt to a new environment through a reversible phenotypic change; Putnam, 2021) to an extreme environment is critically important for understanding the resilience mechanisms of corals to future climate projections. Thompson et al. (2022) and Chen et al. (2019) recorded the long-term evolution of $pH_{sw,}$ pH_{ECM} and seawater temperature in *Porites* sp. cores from the Galapagos marginal environment and the thermally extreme Kimberley coastline, respectively. However, to date, none have used paleo-proxy in coral cores collected in an extreme environment combining highly variable pH and seawater temperature.

In the South West Pacific Ocean, the semi-enclosed lagoon of Bouraké in New Caledonia is home to more than 66 species of corals in an environment subject to combined stressors such as warming, acidification and deoxygenation (Camp et al., 2017). This semi-enclosed lagoon was recently environmentally monitored and described as an extreme and variable environment with temperatures ranging from 17.5 to 33.8°C, pH ranging from 7.23 to 8.06 (total scale), and dissolved oxygen ranging from 1.87 to 7.24 mg O_2 L^{-1} (Maggioni et al., 2021; Schoepf et al., 2023). Recent studies have highlighted the unique characteristics of Bouraké corals compared to those of an adjacent control reef (Puen) with respect to physiological performances (Camp et al., 2017; Jacquemont et al., 2022 (Appendix Article n°1); chapter 4), coral recruitment (Tanvet et al., 2022), Symbiodiniaceae community (Camp et al., 2020; chapter 4), and calcifying fluid regulation (chapter 5). However, we still lack knowledge on the evolution of sea surface temperature and pH undergone by Bouraké corals during the last decades. Adaptive responses of corals to environmental change, although assumed to be faster when derived from transgenerational plasticity (Munday et al., 2013; Torda et al., 2017), still require several generations. This leads to the following questions, which we attempt to answer here. Can we demonstrate the long-term acclimatization of corals in the semi-enclosed lagoon of Bouraké using geochemical proxies? Can we show ongoing OA in an adjacent open water reef (Puen)?

To address these questions, we present here ca. 30 years of annually resolved $\delta^{13}C$, $\delta^{18}O$, $\delta^{11}B$, Li/Mg results from a massive slow-growing scleractinian coral, *Porites* sp. A core of this species was collected in Bouraké and in the adjacent control reef of Puen. In this study, we provide evidence of a stable OA for the past 30 years in the semi-enclosed lagoon of Bouraké, with pH values equivalent to those predicted by the most severe IPCC scenario (RCP 8.5) for the end of this century. We also show an unbroken trend of OA and decreasing pH (ca. -0.13 pH_T units) in corals from the Puen control reef since the third Industrial Revolution. Furthermore, the reconstructed pH_{sw} at Puen shows high variations modulated by ENSO events. We suggest that high environmental variability at Bouraké, independent of anthropogenic CO_2 forcing and ENSO events, would be the primary factor responsible for the long-term acclimatization of Bouraké corals to future OA.

Materials and Methods

Coral core sampling

Cores covering the last 30 years or so were drilled in two *Porites* sp. in June 2020 at 2-3 m depth, one sampled in the semi-enclosed lagoon of Bouraké (B2) and the other in an

adjacent reference reef near Puen Island (R1) in New Caledonia (**Appendix Figure VIII-16**). Back at the Institut de Recherche pour le Développement (IRD) in Nouméa, New Caledonia, the cores were cut in half along the central vertical growth axis and an intermediate slice about 8 mm thick was extracted from each core (**Appendix Figure VIII-17**). Each slice was radiographed to establish an age model, then we performed a density analysis by CT scan in a medical facility, the Kuindo-Magnin clinic in Nouméa.

We counted growth bands and predicted an age of 29 years for B2 (1992-2020 CE) and 33 years for R1 (1988-2020 CE) (**Appendix Figure VIII-18**) based on the positive X-radiographs of the coral slices with well-defined annual skeletal density bands. Next, we were able to take subsamples along the length of the core each year using a micro-drill, for a total of 29 samples for B2 and 33 for R1. Due to the presence of organic tissue layers in the first few millimeters of the cores, we did not sample in the last two years of growth (i.e., 2019 and 2020) for geochemical analysis to eliminate possible biases, resulting in data sets of 31 years for Puen (1988-2018 CE) and 27 years for Bouraké (1992-2018 CE).

Geochemical analyses

Samples preparation and laboratory facilities

Geochemical analyses were performed on core subsamples powder collected at annual resolution with a micro-drill. Each sample, representing one year of growth, was individually homogenized using a mortar. Sample preparation and laboratory facilities used in this study follow the same procedures as described in chapter 5. Samples were cleaned using an oxidative cleaning method adapted from previous studies (Grottoli et al., 2005; Wierzbowski, 2007; Sutton et al., 2018). Briefly, samples were first cycled through three cleanings with 1 mL alkaline buffered MQ water (0.1M NH_4OH) to remove salts and clay. An oxidation step was then performed by adding 500 µL of 3% alkaline buffered H_2O_2 to remove organic matter. Samples were placed in an ultrasonic bath at 50°C for 40 min to accelerate the cleaning. After the peroxide cleanup, the samples were washed several times (usually three) with alkaline buffered MQ water until the pH of the supernatant matched that of the MQ water to ensure that all oxidants were removed. The samples were then dried in an oven at 60°C overnight.

Sample processing and chemical treatment procedures were performed in ISO 5 (class 100) laminar flow hoods in an ISO 6 (class 1000) clean room at Ifremer (Plouzané, France). Ultra-pure reagents (i.e., HNO_3, HF, HCl, H_2O_2, NH_4OH from Normatom© grade) were used for all chemical procedures. All acids and subsequent dilutions were prepared using double-distilled 18.2 $M\Omega cm^{-1}$ MQ water. Standards for isotope ratio and trace element measurements

were freshly diluted during each analytical session with the same acids used for sample preparation, to avoid any matrix effect.

Stable isotope measurements in coral cores ($\delta^{13}C$ and $\delta^{18}O$)

90-160 µg of core powder samples were weighed using a Mettler Toledo XPR10 microbalance (1 µg reading accuracy) and then digested in H_3PO_4. The CO_2 resulting from the dissolution of $CaCO_3$ was then measured isotopically in a mass spectrometer. The analyses of $\delta^{13}C$ and $\delta^{18}O$ were performed with a Thermo Fisher Scientific MAT 253 IRMS (Isotope Ratio Mass Spectrometer) connected to a Kiel IV Carbonates instrument at the analytical facilities of the Pôle Spectrométrie Océan (PSO) at the European Institute for Marine Studies (IUEM, Plouzané, France). The results were calibrated against the Vienna Pee Dee Belemnite (VPDB) according to the international standards NBS-19 and NBS-18; the analytical precision of the MNHN homemade carbonate standard was better than 0.01‰ for $\delta^{13}C$ (SD, n = 50).

Boron purification and chemical preparation of elemental ratios

Boron was purified by microdistillation using the method developed by Gaillardet et al. (2001) and adapted to Ca-rich matrices by Wang et al. (2010). International standard JCp-1 (coral *Porites* sp., Gutjahr et al., 2021) from the Geological Survey of Japan was used in all analytical sessions (see chapter 5 for complete methodology). Samples and JCp-1 were weighted (1.80 to 2.50 mg) and washed with 400 µL of 0.1M NH_4OH to remove potentially adsorbed boron. After a cycle of two washes with MQ water, they were dissolved with 70 µL of 1N HCl. 60 µL of the dissolved samples were loaded onto an inverted cap of a clean 5 mL fin-legged conical beaker. The sealed beaker was placed on a hot plate in digestion blocks (Analab©) at 95°C for 15 h. The beakers were removed from the hot plate and allowed to cool for 15 minutes. The cap containing the microdistillation residue was replaced with a clean cap and 0.3M HF was added to the distillate. The residues were taken up with 100 µL of 1N HCl and set aside to evaluate the final microdistillation yield as determined by Element XR-ICP-MS. The remaining 10 µL from the same 70 µL aliquot of dissolved sample for Boron isotope measurement was collected with 200 µL 0.1M HNO_3. Prior to elemental ratio measurements on the Element XR HR-ICP-MS, a Ca^{2+} concentration check was performed on all samples using a HORIBA Ultima 2 inductively coupled plasma atomic emission spectrometer (ICP-AES). Our carbonate samples have a Ca-rich matrix and are diluted with 0.1M HNO_3 and 0.3M HF to set calcium concentrations targeting 30 ppm Ca.

Boron isotope and elemental ratio measurements

Stable boron isotope ratios were measured using a Thermo Fisher Scientific Neptune MC-ICPMS (Multi-Collector Inductively Coupled Plasma Mass Spectrometer) at the PSO, Ifremer (Plouzané, France). Elemental ratios were measured on a Thermo Fisher Scientific Element XR HR-ICP-MS (High-Resolution Inductively Coupled Plasma Mass Spectrometer) at the PSO, IUEM (Plouzané, France). The standard solution (NIST SRM 951) was used as a bracketing standard to correct for any bias during the analytical sessions for $\delta^{11}B$ measurements. Data quality and external reproducibility were determined on the international standard JCp-1. Full details of the instrumental set-up, sensitivity, procedural blanks, boron yields, and results for the inter-laboratory coral standard JCp-1 can be found in chapter 5.

Seawater pH calculations from corals

It has been shown that $\delta^{11}B$ from coral skeletons can be used as a proxy of the internal pH of the extracellular calcifying medium (pH_{ECM}) (McCulloch et al., 2017a). The pH_{ECM} was calculated from $\delta^{11}B$ measurements in coral skeleton (Hemming and Hanson, 1992; Zeebe and Wolf-Gladrow, 2001) as:

$$pH_{ECM} = pK_B - log\left(\frac{\delta^{11}B_{CS} - \delta^{11}B_{ECM}}{\delta^{11}B_{ECM} - (\alpha \times \delta^{11}B_{CS}) - 1000(\alpha - 1)}\right) \quad (1)$$

With pK_B representing the dissociation constant of boric acid and calculated according to temperature and salinity (pK_B = 8.5975 at 25°C and 35 PSU; Dickson, 1990), $\delta^{11}B_{CS}$ representing the boron isotopic composition of the coral skeleton, $\delta^{11}B_{ECM}$ representing the boron isotopic composition of the extracellular calcifying medium (acquired from the $\delta^{11}B$ of seawater, which was measured in natural sites of Bouraké and Reference (values reported in chapter 5)), and α representing the boron isotope equilibrium constant equal to 1.0272 (Klochko et al., 2006).

The estimated seawater pH (pH_{sw}) was calculated from the pH_{ECM} using the following equation, Eq. (2) from McCulloch et al. (2012) based on *Porites* spp.:

$$pH_{sw} = (pH_{ECM} - 5.954)/0.32 \quad (2)$$

Seawater temperature calculations from corals

The $\delta^{18}O$ signature of coral aragonite is thought to depend on the $\delta^{18}O$ signature of ambient seawater ($\delta^{18}O_{sw}$) and temperature (Epstein and Mayeda, 1953; Quinn et al., 1998).

Therefore, we estimated past seawater temperature from $\delta^{18}O$ measurements in the skeleton of *Porites* sp. in New Caledonia according to Quinn et al. (1996) and the equation, Eq. (3):

$$SST = -5.28 * \delta^{18}O_{coral} + 0.02 \quad (3)$$

With SST representing sea surface temperature. However, Eq. (3) does not take into account sea surface salinity (SSS), while $\delta^{18}O_{sw}$ depends on the $^{18}O/^{16}O$ ratio which varies during evaporation and precipitation via different fractionation processes depending on the ocean basins considered (Corrège, 2006). Therefore, we used Eq. (4) considering SSS and SST in $\delta^{18}O$ of *Porites* sp. in the tropical Pacific Ocean according to Cahyarini (2006):

$$\delta^{18}O_{coral} = -0.16 * SST + 0.46 * SSS - 16.738 \quad (4)$$

The Li/Mg ratios in coral skeleton were found to be highly correlated with SST and, as with the $\delta^{18}O$ signature, allowed reconstruction of SST from the coral skeleton (Montagna et al., 2014). We used this additional SST proxy to corroborate our data following Montagna et al. (2014) and the equation, Eq (5):

$$Li/Mg = 5.41exp\,(-0.049 * SST) \quad (5)$$

Statistical analyses and data presentation

Statistical analyses were performed, and figures were generated using RStudio (R Development Core Team, version 4.1.0, 2021), including packages “ggplot2”, “stats”, and “car”. The homogeneity of variance of the data was tested with Levene’s test and the normality of the variance distribution with the Shapiro-Wilk test, and checked graphically with a Q-Q plot. To assess the significance of trends in geochemical signatures over time, we used one-way ANOVAs testing the effect of time for each site (Bouraké and Puen).

Results

$\delta^{11}B$, $\delta^{13}C$ & pH reconstructions

The $\delta^{11}B$ values in the Puen core ranged from 23.18‰ to 26.20‰ and showed significantly decreasing values over 31 years. This decrease equates to a loss of ca. 0.13 pH

units with a mean pH of ca. 8.03 in the most recent sample years (between 2014 to 2018 CE). In contrast, we did not observe such a loss at Bouraké, which shows a stable $\delta^{11}B$ with a mean pH of ca. 7.54 since 1992 CE (**Figure VI-1**; **Table VI-1**). We find that the mean pH value calculated at Bouraké since 1992 CE and at Puen in the most recent years is within the range of pH values measured *in situ* for both sites with a mean pH of 7.67 ± 0.23 at Bouraké and of 8.02 ± 0.04 at Puen. *In situ* monitoring was conducted with Seabird SeaFet pH loggers over several periods from February 2016 to April 2019 at Bouraké, and for two weeks in March 2019 at Puen (Maggioni et al., 2021) (**Figure VI-1**). The $\delta^{13}C$ signatures, measured independently using different analytical techniques and machines, showed remarkably similar trends for both sites. The $\delta^{13}C$ values at Puen decreased significantly over 31 years, in the range from -2.55‰ to -1.47‰ (**Table VI-1**). Bouraké showed a stable trend in $\delta^{13}C$ signatures over 27 years, ranging from -7.31‰ to -5.83‰. We observed a strong depletion of $\delta^{11}B$ and $\delta^{13}C$ signatures from Puen to Bouraké with, based on the average values of the periods considered, -2.86‰ and -4.48‰, respectively.

We identified strong relationships between severe and moderate La Niña - El Niño climate events and boron isotope signatures at Puen, while they are less evident in the semi-enclosed Lagoon of Bouraké. ENSO events were characterized using the Ocean Niño Index (ONI) calculated from the 3-month running mean of ERSST.v5 SST anomalies in the Niño 3.4 region (Huang et al., 2017).

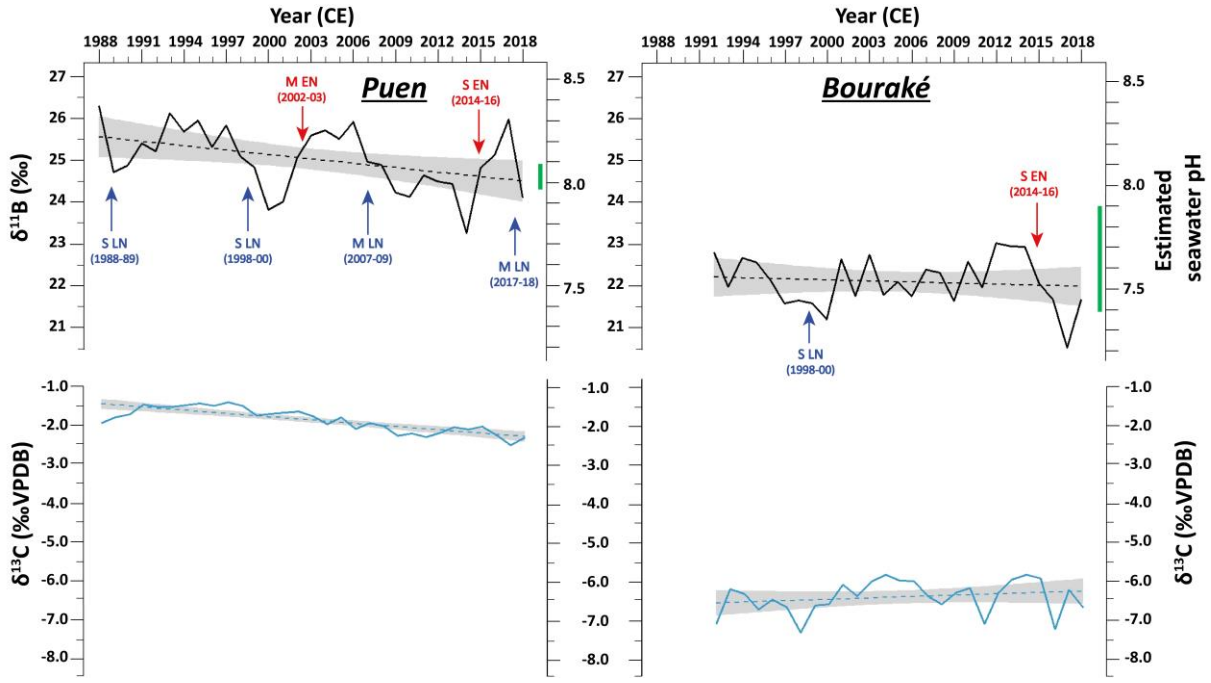

Figure VI-1 | *Temporal evolution of $\delta^{11}B$ (black) and $\delta^{13}C$ (blue) signatures in* Porites *sp. cores collected at Puen (left) and Bouraké (right), over 31 and 27 years, respectively. The estimated seawater pH corresponding to the $\delta^{11}B$ signatures is plotted on the second y-axis (right side of the graphs). The range*

*of variation in seawater pH_T values measured in situ using SeaFet over several time intervals between February 2016 and April 2019 at Bouraké, and for two weeks in March 2019 at Puen (Maggioni et al., 2021), is represented by the green bars. To highlight the significance of trends, we applied linear models (dashed line with 95% confidence interval in grey). Historical, Severe (**S**; ± 0.5-1.5°C) or Moderate (**M**; ± 1.6-2.6°C) El Niño (**EN**; red) and La Niña (**LN**; blue) events are identified by the Oceanic Niño Index (ONI) from the 3-month running mean of ERSST.v5 SST anomalies in the Niño 3.4 region (Huang et al., 2017). ENSO events are represented by arrows and their periods of occurrence are indicated in parentheses.*

$\delta^{18}O$, Li/Mg & SST reconstructions

The $\delta^{18}O$ values ranged from -4.20‰ to -5.41‰ and showed an increasing, yet not significant, trend at Puen over 31 years. In contrast, $\delta^{18}O$ values since 1992 CE were more stable at Bouraké, although lower, around ~0.50‰ (**Figure VI-2**; **Table VI-1**). Equivalent SST values were calculated using Eq. (4) for $\delta^{18}O$ and Eq. (5) for Li/Mg at Bouraké, while the average SST was higher at Puen using Li/Mg compared to $\delta^{18}O$ (increase of about 1.66°C). Regarding the evolution during the different periods, we observed exactly the same trend for $\delta^{18}O$ and Li/Mg values, which means a higher SST at Puen and a stable and slightly cooler SST at Bouraké. The higher salinity at Bouraké than at Puen (means values of 36.02 and 35.18 PSU, respectively, measured *in situ* using YSI 600 OMS-M loggers over several periods representative of seasonal variability within the annual cycle between July 2019 and March 2021; Maggioni et al., 2021), is consistent with the greater calculated difference between salinity-corrected SST (using Eq. (4)) and uncorrected SST (using Eq. (3)) at Bouraké (+3.11°C) compared to Puen (+1.17°C). Based on the estimated salinity-corrected SST (i.e., the orange curve in **Figure VI-2**), Puen had a 31-year average SST of about 26.64 degrees.

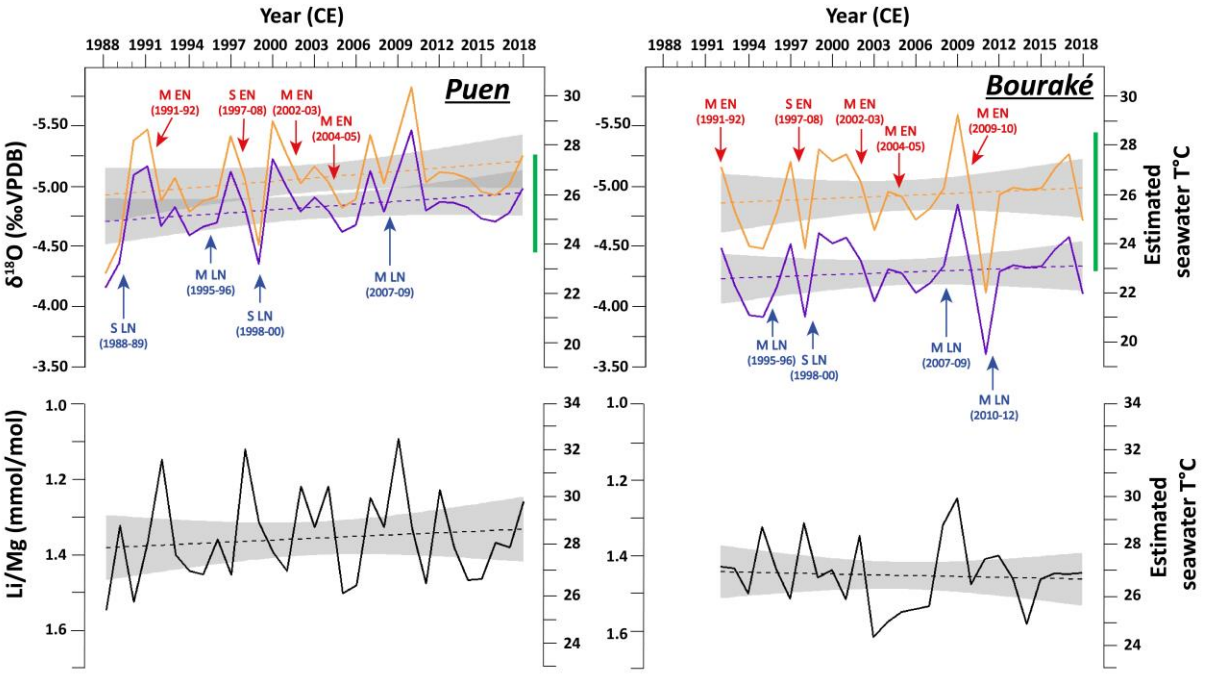

Figure VI-2 | *Temporal evolution of $\delta^{18}O$ (purple) and Li/Mg (black) signatures in* Porites *sp. cores collected at Puen (left) and Bouraké (right), over 31 and 27 years, respectively. The estimated sea surface temperature (SST) corresponding to $\delta^{18}O$ and Li/Mg signatures is plotted on the second y-axis (right side of the graphs). Temperature recalculated from $\delta^{18}O$ signatures, and corrected with in-situ measured sea surface salinity (SSS), is represented by the orange curves. The range of SST values measured in-situ using SeaFet over a continuous period from January 2019 to April 2020 for Bouraké and Puen (Maggioni et al., 2021), is represented by the green bars. To highlight the significance of trends, we applied linear models (dashed line with 95% confidence interval in grey). Historical, Severe (**S**; ± 0.5-1.5°C) or Moderate (**M**; ± 1.6-2.6°C) El Niño (**EN**; red) and La Niña (**LN**; blue) events are identified by the Oceanic Niño Index (ONI) from the 3-month running mean of ERSST.v5 SST anomalies in the Niño 3.4 region (Huang et al., 2017). ENSO events are represented by arrows and their periods of occurrence are indicated in parentheses.*

In comparison, Bouraké showed a slightly cooler average of about 25.93 degrees from 1992 to 2018 CE. Mean SST values calculated from both equations are in the range of SST monitoring values measured *in situ* at Puen (mean of 25.25 ± 1.89°C) with Hobo Water Temperature Pro V2 loggers between January 2019 and April 2020 (Maggioni et al., 2021). In contrast, only the salinity-corrected SST values are in the range of the values measured *in situ* at Bouraké between January 2019 and April 2020 (mean of 25.63 ± 2.83 °C). We identify strong relationships between severe and moderate La Niña - El Niño events and variations in SST estimated at both sites with increasing and decreasing SST linked to La Niña and El Niño events, respectively (**Figure VI-2**).

The Li/Mg ratios are in good agreement with the oxygen isotope data at Bouraké, showing the same slightly cooler trend in SST compared to Puen (**Figure VI-2**). The mean SST calculated from Li/Mg ratios at Bouraké is about 26.77°C, which is close to the mean SST of 25.93°C obtained with oxygen isotope data (using salinity correction). In contrast, at Puen,

the mean SST calculated from Li/Mg ratios (28.30°C) is higher than the mean SST obtained with oxygen isotope data (26.64°C).

Parameter		Puen	Bouraké
$\delta^{11}B$ & pH_{sw}	*p*-value	**0.016**	0.589
	F-value	6.516	0.299
	df	29	25
$\delta^{13}C$	*p*-value	**<0.001**	0.280
	F-value	57.740	1.219
	df	29	25
$\delta^{18}O$ & T°C	*p*-value	0.148	0.547
	F-value	2.209	0.373
	df	29	25
Li/Mg & T°C	*p*-value	0.504	0.744
	F-value	0.457	0.109
	df	29	25

Table VI-1 | *Probability values from one-way ANOVAs testing the effects of time on each geochemical parameter over the study period for each site (Puen and Bouraké). Significant values are in bold ($p < 0.05$).*

Discussion

Reconstructions of seawater pH (pH_{sw}) using coral skeletal $\delta^{11}B$ performed in the Atlantic and Pacific Oceans have reported a steadily declining trend in pH_{sw} over the past decades (Tarique et al., 2021). These data highlight the significant uptake of anthropogenic CO_2 emission by the oceans since the industrial era. Because anthropogenic CO_2 is derived from fossil fuel combustion and is enriched in isotopically light carbon (^{12}C), its uptake by the ocean results in a decrease in the $\delta^{13}C$ value of coral skeletons in modern times (Swart et al., 2010). This phenomenon, known as the Suess effect, changes the $\delta^{13}C$ signatures of coral skeletons at an average rate of -0.01‰ to -0.03‰ per year (Swart et al., 2010). The pronounced decrease in $\delta^{13}C$ observed in the Puen Reef over 31 years, of about -0.02‰ per year, demonstrates the significant uptake of anthropogenic CO_2 emissions in this region. The $\delta^{13}C$ depletion observed at Puen in this study is consistent with similar long-term $\delta^{13}C$ depletion of -0.02‰ per year found previously in a *Porites* sp. core near Puen (Wu et al., 2018). Along with these consistent trends confirming increased modern uptake of anthropogenic CO_2 by the tropical oceans, we expect an associated decrease in pH_{sw}. From 1988 to 2018 CE, our reconstruction of pHsw from $\delta^{11}B$ values at Puen shows a decreasing trend. This decrease of about 0.13 pH units is consistent with previously reported evidence of OA in coral-based pH reconstructions (e.g., Wei et al., 2009; Liu et al., 2014; Wu et al., 2018; D'Olivo et al., 2019;

Tarique et al., 2021). Interestingly, this pH trend of -0.0041 yr^{-1} is twice as high as that observed by Sutton et al. (2014) in the equatorial Pacific between 1997 and 2011. This increasing pH depletion recorded in the southwestern Pacific may be a result of accelerating anthropogenic CO_2 accumulation in the atmosphere and its increasing storage in the Pacific in the early 21st century (Carter et al., 2019).

On an interannual timescale, the annually resolved $\delta^{11}B$ at Puen shows pronounced oscillations that contrast with the stable downward trend in $\delta^{13}C$ (**Figure VI-1**). These fluctuations indicate large interannual changes in $\delta^{11}B$ that mimic the variability of pH_{sw}. Ocean climate oscillations such as ENSO and the Pacific decadal oscillation (PDO) may account for ca. 17% of the pH_{sw} variability in the Pacific Ocean (Tarique and Rahaman, 2022) and are known to vary $\delta^{11}B$ signatures in coral-based reconstructions (Liu et al., 2014; Wu et al., 2018; Tarique and Rahaman, 2022). ENSO events occur at a higher frequency (interannual scale) than PDO events (decadal scale) (Mantua and Hare, 2001). Because our reconstruction of pH at Puen covers the period from 1988 to 2018 CE, it is easier to observe the influence of interannual climate events such as ENSO during this period. Sutton et al. (2017) suggest that ENSO events are the primary mechanisms influencing seawater pCO_2 and resulting pH_{sw} variation in the Pacific Ocean on interannual to decadal time scales. Our study highlights the existence of strong relationships between ENSO climate events (i.e., La Niña and El Niño) and the annually resolved $\delta^{11}B$ at Puen (**Figure VI-1**). ENSO events correspond to major changes in $\delta^{11}B$, sometimes exceeding 1‰ for a single event under the most severe conditions. In addition, the relationships found for La Niña (LN) and El Niño (EN) events are equivalent to a decrease and increase in $\delta^{11}B$, respectively. Regardless of the intensity of the LN and EN events, they do not result in a similar magnitude change in $\delta^{11}B$, which questions the capacity of corals to regulate pH_{ECM}. The fluctuations found in our pH reconstruction based on coral $\delta^{11}B$ reflect the influence of recurrent climate patterns (ENSO) on CO_2 uptake in the ocean (Wu et al., 2018). In summary, we can attribute the major interannual variations in $\delta^{11}B$ at Puen from 1988 to 2018 to ENSO events, while the overall decrease in $\delta^{11}B$ equivalent to a loss of ca. -0.13 pH units is the result of rapid ongoing OA from increasing anthropogenic CO_2.

Over the period 1992-2018 CE, our unique $\delta^{11}B$ record from the extreme and variable environment of Bouraké (**Appendix Figure VIII-16**) shows a stable evolution of pH_{sw} with a mean of ca. 7.54 pH units. We observe the same stable trend for $\delta^{13}C$ over the period. However, the $\delta^{11}B$ and $\delta^{13}C$ values at Bouraké are highly depleted compared with those found in the Puen reference reef. While the mean depletion is 2.86‰ for $\delta^{11}B$ (equivalent to 0.57 pH units), it is 4.48‰ for $\delta^{13}C$. This result suggests that, unlike Puen, the extreme environment of Bouraké is more influenced by local disturbances than by anthropogenic CO_2 uptake. Bouraké is a semi-enclosed lagoon surrounded by mangroves where temperature and pH fluctuations

are mainly driven by the tide and organic inputs from the mangrove forest and associated sediments (Maggioni et al., 2021). The levels of terrigenous organic matter are significantly higher at Bouraké than at Puen (Maggioni et al., 2021). High bottom-water and sediment organic matter contents at Bouraké increase microbial remineralization, which result in higher dissolved inorganic carbon (DIC) concentration in seawater as observed in mangroves near Bouraké (Leopold et al., 2013). Therefore, terrigenous organic matter would be primarily responsible for the low and stable pH_{sw} at Bouraké. During degradation of organic matter, light isotopic carbon is released, lowering its $\delta^{13}C$ signatures (Zeebe and Wolf-Gladrow, 2001). Organic matter in New Caledonian mangroves has highly depleted $\delta^{13}C$ signatures of about -30.17‰ (Briand et al., 2015). The high organic matter content decreases the $\delta^{13}C$-DIC in seawater used in photosynthesis by the coral symbiont. In summary, Bouraké corals exhibit depleted but stable $\delta^{11}B$ and $\delta^{13}C$ trends due to the specificity of local disturbances compared to the Puen open water reef. Although anthropogenic CO_2 uptake may play a role in the pH_{sw} values at Bouraké, it should be minor compared to the influence of local features. A major result of this study is that we demonstrate that Bouraké corals survived a low mean pH_{sw} of 7.54 pH units from 1992 to 2018 CE, providing the first long-term record of coral acclimatization to OA.

Our annually resolved $\delta^{11}B$ reconstruction does not record the highly variable pH_{sw} of the Bouraké environment (Camp et al., 2017; Maggioni et al., 2021). In addition, the $\delta^{11}B$ records a time-integrated signal, which limits the recording of daily pH variations. However, on an interannual scale, ENSO events, when strong, can influence the $\delta^{11}B$ signatures of Bouraké corals. Indeed, major La Niña (1998-2000) and El Niño (2014-2016) events resulted in strong $\delta^{11}B$ and pH_{sw} depletions at Bouraké (**Figure VI-1**). However, the relationships between $\delta^{11}B$ fluctuations and ENSO events remain less evident at Bouraké than at Puen. Although we assumed this minor influence of ENSO events at Bouraké, we emphasized the role of strong ENSO events on the dynamics of natural pH_{sw} variability at Bouraké. The $\delta^{13}C$ trend at Bouraké, although stable over the period 1992-2018, shows larger interannual fluctuations compared to Puen. Unlike $\delta^{11}B$, it is quite difficult to attribute these fluctuations to ENSO events (no clear relationships). Fluctuations in $\delta^{13}C$ at Bouraké may reflect the variable nature of organic inputs and their degradation in the mangrove. Overall, this study once again highlights the strong influence of Bouraké's natural dynamics on $\delta^{13}C$ and $\delta^{11}B$ reconstructions.

Another striking result from our coral reconstructions is the observed long-term differences in $\delta^{18}O$ signatures between Bouraké and Puen. The mean $\delta^{18}O$ depletion of ca. -0.50‰ observed at Bouraké relative to Puen results in a reconstructed mean sea surface temperature (SST) that is about 2.65°C cooler. The lower SST at Bouraké was estimated using an equation established by Quinn et al. (1996) on *Porites* sp. in New Caledonia. Although the

SSTs estimated from the $\delta^{18}O$ of coral skeleton are in the range of the SSTs measured at Puen, this is not the case at Bouraké (**Figure VI-2**, trends in purple). The estimated mean SST of ~22.81°C at Bouraké seems unlikely in such a shallow (maximum depth of ~8 m) semi-enclosed lagoon in the tropical Pacific Ocean. Applying the sea surface salinity (SSS) correction of Cahyarini (2006), the reconstructed mean SST at both sites falls within their respective ranges of measured in situ SSTs (**Figure VI-2**, trends in orange). The higher SST delta observed at Bouraké (+3.12°C) compared to Puen (+1.18°C), between the equations with and without SSS correction, results from a higher SSS in the measurements made at Bouraké between July 2019 and March 2021 (Maggioni et al., 2021). However, a bias in the SST reconstruction cannot be ruled out, in that the SSS values used for the $\delta^{18}O$ equation correction are averaged over a more recent period than those covered by the *Porites* cores.

In the western tropical Pacific Ocean, SSS can be influenced by seasonal, interannual, ENSO and/or PDO variations (Delcroix and Hénin, 1991; Gouriou and Delcroix, 2002; Ramos et al., 2019). This highlights the limitations of SST reconstructions based on coral $\delta^{18}O$, with shifts in $\delta^{18}O$ in coral resulting from distinct variations in seawater $\delta^{18}O$, SST and SSS (e.g., Cahyarini, 2006; Corrège, 2006; Stevenson et al., 2013, 2015; Conroy et al., 2017; Thompson, 2022). Because coral $\delta^{18}O$ is a mixture of SST and SSS signals associated with spatio-temporal variabilities, its interpretation and translation into estimated SST is difficult. However, coral $\delta^{18}O$ can capture the influences of climate events such as ENSO on interannual fluctuations in SST (e.g., Cobb et al., 2003; Thompson et al., 2011; Stevenson et al., 2013, 2015). We observed strong relationships between $\delta^{18}O$ and ENSO events in the Bouraké and Puen cores with $\delta^{18}O$ increasing with El Niño events and decreasing with La Niña events. Interestingly, these relationships are strong in Bouraké regardless of ENSO strength (i.e., moderate or severe) and corroborate the typical increase in SST due to La Niña and decrease in SST due to El Niño. This suggests that unlike pH_{sw}, ENSO events overcome the influence of the local environment at Bouraké with respect to SST. This greater influence of ENSO events on the local environment is a result of the strong local perturbations caused by ENSO events such as heavy rainfall (significant variation in local SSS) and/or severe drought (significant variation in local SST).

Comparison of SST reconstructions from coral $\delta^{18}O$ and Li/Mg ratios provides a more robust estimate of SST, overcoming potential limitations of using $\delta^{18}O$, such as SSS. The reconstruction of SST at Puen from Li/Mg ratio shows a higher estimated mean SST than that obtained from $\delta^{18}O$ (ca. + 1.66°C). In contrast, the difference between these two proxies is less pronounced at Bouraké (+ 0.84°C). Given their respective uncertainties of ± 1.55°C and ± 1.56°C, the two proxies $\delta^{18}O$ and Li/Mg based on corals give the same range of SST at Bouraké and Puen. The use of Li/Mg ratio as a proxy for SST in corals is accompanied by

biases, such as the mechanisms of Li and Mg incorporation into the skeleton during coral calcification (Montagna et al., 2014; Rollion-Bard and Blamart, 2015). The reliability of the Li/Mg ratio as a proxy for SST reconstructions is also dependent on organic matter and/or calcite contamination in the coral skeleton, but tropical *Porites* spp. remain a suitable candidate for SST reconstructions (Cuny-Guirriec et al., 2019). Although coral-based $\delta^{18}O$ and Li/Mg proxies are robust tools to record SST fluctuations, their accuracy is limited by SSS and/or coral calcification mechanisms (Stevenson et al., 2013; Montagna et al., 2014). The use of a Li/Mg and Sr/Ca multi-regression approach could improve the accuracy obtained in SST reconstructions at Bouraké and Puen (Cuny-Guirriec et al., 2019).

In summary, our $\delta^{11}B$ and $\delta^{13}C$ records in *Porites* sp. cores highlight a steady increase in anthropogenic CO_2 uptake since 1988 in the southwestern Pacific Ocean. We observed a resulting significant downward trend in pH of ca. -0.13 pH units in the Puen control reef, confirming a fast, continuous OA. Our reconstruction of a low mean pH_{sw} of 7.54 pH units between 1992 and 2018 at Bouraké provides the first long-term record of coral acclimatization to OA. The temporal consistency of $\delta^{11}B$ with ENSO events highlights their strong influence on pH_{sw} variability in a typical open water reef, whereas a semi-enclosed environment such as Bouraké appears to be more impacted by local perturbations. The $\delta^{18}O$ is highly related to ENSO events for both sites and highlights the influence of these climatic events on the temporal evolution of SST. Our results provide new perspectives on the use of coral-based proxies to reconstruct past pH_{sw} and SST, and show the increasing uptake of anthropogenic CO_2 in the South Pacific. They provide the first description of long-term coral acclimatization to OA.

CHAPITRE 7

SYNTHÈSE ET PERSPECTIVES

Ce dernier chapitre synthétise les résultats obtenus lors de ce travail de thèse ayant pour objectif principal d'étudier l'acclimatation des récifs coralliens aux changements climatiques en utilisant une approche écophysiologique combinée à une approche géochimique. Au-delà d'apporter des éléments de réponses aux objectifs énoncés au début de ce manuscrit, ce chapitre met en perspective les implications et les nouveaux questionnements soulevés par les résultats obtenus, lors du raisonnement scientifique mené au cours de cette thèse. Les mécanismes d'acclimatation demeurent essentiels pour la persistance et le devenir des coraux face aux changements climatiques rapides en cours, dont l'acidification des océans. Ces mécanismes incluent la plasticité physiologique, l'épigénétique, les associations avec des micro-organismes ou encore le contrôle physio-chimique de la calcification ; ils peuvent être influencés par la variabilité environnementale. Il subsiste encore de nombreuses incertitudes quant au fonctionnement de ces mécanismes et à leur intensité, selon les espèces considérées. Ce travail de thèse s'est donc articulé autour de ces problématiques ; la combinaison de techniques innovantes associant écophysiologie, métagénomique, et isotopie, a permis une approche intégrée multidisciplinaire et l'étude combiné des différents processus impliqués dans les mécanismes d'acclimatation des coraux. De plus, l'utilisation d'un analogue naturel, la lagune semi-fermée de Bouraké en Nouvelle-Calédonie, a permis d'étudier : (**i**) le recrutement corallien (**chapitre 3** ; **7.1**), (**ii**) la plasticité physiologique des coraux et les communautés symbiotiques associées (**chapitre 4** ; **7.2**), (**iii**) le contrôle physio-chimique de la calcification des coraux (**chapitre 5** ; **7.3**), et (**iv**) une reconstruction paléoenvironnementale, sur 3 décennies, de la température de surface de la mer (SST) et du pH de l'eau de mer (pH_{SW}) (**chapitre 6** ; **7.4**). En fournissant des éléments de réponses essentiels sur les mécanismes d'acclimatation des coraux aux stress environnementaux, les résultats présentés dans cette thèse ont également soulevé de nouvelles interrogations scientifiques et de nouvelles perspectives de recherche, exposées dans ce chapitre.

7.1 Les CCAs et le recrutement corallien face aux conditions extrêmes de Bouraké

7.1.1 Évolution de l'abondance des CCAs et interactions inter-espèces à Bouraké

L'abondance de CCAs (Crustose Coralline Algae) a été mesurée sur des plaques en terre cuite, positionnées à 10 cm du substrat dans trois sites présentant des conditions environnementales différentes entre leur date d'immersion (T_0), deux mois après (T_2), et au

bout de deux ans (T_{24}). Les taux de recouvrement en CCAs observés sur les plaques à la fin de l'expérience (T_{24}) ont montré une baisse significative de la présence en CCAs à Bouraké (ca. ~80%). Bien que ce résultat soit peu étonnant étant donné les conditions extrêmes de pH dans la lagune, la baisse significative (près de 40%) enregistrée sur un temps très court, dès le début de l'expérience, entre le placement *in situ* (T_0) et les deux mois suivants (T_2), souligne le fort impact négatif sur les CCAs des conditions environnementales naturelles à Bouraké. En effet, le pH moyen dans cette lagune semi-fermée (7.67) et ses valeurs extrêmes (7.23) correspondent à des eaux acidifiées qui présentent une baisse importante de la quantité disponible d'ions carbonates, et donc de l'état de saturation en aragonite, limitant ainsi la calcification et la croissance des CCAs. A la fin de l'expérience (T_{24}), nous observons toutefois une communauté de CCAs toujours présente et identique, en termes d'espèces, à celle recensée naturellement à Bouraké (essentiellement *Porolithon* et *Neogoniolithon*). Cette persistance des CCAs à Bouraké indique que certaines communautés/espèces de CCAs peuvent maintenir une croissance positive en conditions de pH faible, sans doute au prix d'un coût supérieur pour l'organisme, comme par exemple l'altération de la minéralogie de leur squelette (Goffredo *et al.*, 2014 ; Kamenos *et al.*, 2016). La validation de cette hypothèse à Bouraké requiert une étude de la minéralogie et de la porosité du squelette des CCAs présentes dans la lagune, notamment en utilisant des techniques de densitométrie (CT-Scan) et de spectroscopie Raman et/ou de diffraction X (XRD). Les résultats du **chapitre 3** confirment néanmoins l'impact de l'AO sur la diminution du pourcentage de recouvrement des plaques en CCAs et sur l'augmentation de la dissolution de leur squelette carbonaté (Kuffner *et al.*, 2008; Comeau *et al.*, 2013; Fabricius *et al.*, 2015). Les communautés de CCAs sont d'autant plus impactées à Bouraké qu'il y a une combinaison des effets de l'AO avec ceux de la température de l'eau de mer, particulièrement élevée (pouvant atteindre 33.80°C), et ceux de la concentration en oxygène dissous, particulièrement faible (pouvant descendre à 28% de saturation). En revanche, les conditions environnementales des deux sites de référence étudiés sont plus favorables à la croissance des CCAs, ce que confirme une baisse moindre de l'abondance des CCAs (ca. ~23%) à la fin de l'expérience (T_{24}) dans l'un des deux sites (R2). Par contre, et malgré des conditions de pH, de température et d'oxygène dissous apparemment propices au développement des CCAs, nous observons une diminution quasi totale de l'abondance des CCAs (ca. ~98%) dans le deuxième site de référence (M1), au cours de l'expérience. Cette diminution, proche de celle de Bouraké en valeur absolue, s'accompagne d'une augmentation conséquente de la présence de turf (ca. ~91%) sur le dessus des plaques, et de bryozoaires sur le dessous des plaques (ca. ~10%). Ce résultat traduit *pro parte* l'importance de la compétition inter-espèces dans la régulation du développement des CCAs, que ce soit dans un site extrême (au regard de ses conditions

environnementales) ou pas. De plus, le recouvrement de CCAs, de turf et de bryozoaires diffère selon les faces considérées des plaques (dessus/dessous). Cette étude écologique souligne ainsi l'influence de facteurs abiotiques spécifiques aux sites, tels que la quantité de lumière disponible (liée à la turbidité), le taux de sédimentation des particules en suspension dans l'eau, la disponibilité en nutriments… dans ces « shifts » d'espèces dominantes au cours de l'expérimentation. Des expériences complémentaires pourraient être menées en laboratoire afin de préciser l'impact respectif de ces différents facteurs de l'environnement sur le devenir des CCAs. *In fine*, les interactions biotiques, couplées avec les effets directs de l'AO et des autres conditions environnementales extrêmes, expliqueraient la baisse drastique de CCAs enregistrée à Bouraké. La conséquence en est une limitation de la disponibilité en substrat préférentiel pour le recrutement corallien dans la lagune semi-fermée.

7.1.2 Un recrutement corallien élevé à Bouraké

Un recrutement corallien particulièrement élevé a été enregistré sur les collecteurs artificiels à Bouraké, en comptant les recrues de coraux et en identifiant, au niveau taxonomique le plus bas possible, les familles de coraux présentes sur les plaques à la fin de l'expérience (T_{24}). Dans ce site naturel extrême, le recrutement corallien est près de trois fois supérieur à ceux des deux sites de référence étudiés. Bien que ce résultat du **chapitre 3** soit particulièrement inattendu, si l'on considère les conditions environnementales de Bouraké et le faible recouvrement en CCAs, plusieurs raisons peuvent expliquer ce paradoxe apparent. Cette étude écologique s'étant déroulée sur deux années, il est possible que les plaques aient servi de substrat de fixation à deux pontes consécutives de coraux. La première ayant eu lieu seulement 1 à 2 mois après le déploiement des plaques *in situ*, le recouvrement en CCAs aurait été, à ce stade, encore suffisamment important pour induire une fixation des larves (planula) de coraux sur les supports. Cependant, il est peu probable que le fort recrutement observé après 2 ans d'immersion des plaques à Bouraké soit le résultat de la seule ponte de la deuxième année, au regard de l'abondance des recrues. Cette dernière souligne l'efficacité de la reproduction et une survie des larves et des recrues de coraux à Bouraké qui ne sont pas observées dans les deux sites de référence. Alors que nous pouvions nous attendre à un effet délétère de l'AO sur ces recrues au bout des deux années de suivi, aucun signe de malformation et/ou de dissolution du squelette n'a été observé. L'existence d'interactions biotiques (compétition inter-espèces et/ou prédation) plus importantes dans les sites de référence, si elle permettrait d'expliquer une survie moindre des recrues par rapport à Bouraké, reste à démontrer. L'abondance du recrutement corallien à Bouraké peut être liée aux apports de matière organique provenant de la mangrove, induisant des concentrations en carbone

organique et en nutriments ($[Si(OH)_4]$, $[NO_x]$ et $[PO_4]^{3-}$) pouvant être près de cinq fois supérieures à celles des sites de référence (Maggioni *et al.*, 2021). Il est en effet admis que les apports hétérotrophiques peuvent aider à la fixation des larves coralliennes et à la croissance des juvéniles dans des conditions extrêmes de pH, de température et/ou d'oxygène dissous (e.g., Anthony *et al.*, 2006 ; Houlbrèque et Ferrier-Pagès, 2009 ; Alderdice *et al.*, 2021 ; Huffmyer *et al.*, 2021). La topographie particulière (lagune semi-fermée) et l'hydrodynamisme peuvent également favoriser le recrutement corallien à Bouraké. La circulation de l'eau de mer dans cette lagune est plus limitée que dans les sites de référence ; elle pourrait favoriser l'accumulation des larves au sein de zones de rétention, conférant ainsi à Bouraké le statut de « hotspot » du recrutement corallien. Le rôle de la circulation tidale dans le devenir des larves de coraux est corroboré par les résultats taxonomiques pour lesquels les coraux dominants à Bouraké appartiennent à la famille des Acroporidae (70% des recrues). Cette famille compte en majorité des espèces à reproduction externe, favorisées dans les sites présentant une circulation d'eau limitée (Oprandi *et al.*, 2019). La persistance des recrues coralliennes dans les conditions extrêmes de Bouraké suggère néanmoins que ces coraux auraient acquis des mécanismes d'acclimatation voire d'adaptation. Afin d'identifier les mécanismes à l'origine de cette persistance des coraux à Bouraké, une approche épigénétique et des expériences de transplantations d'individus entre Bouraké et les sites de référence pourraient permettre d'obtenir des éléments de réponse sur la capacité des coraux de Bouraké à se développer dans des conditions environnementales extrêmes.

7.2 La plasticité physiologique des coraux face à l'AO

7.2.1 Une calcification accrue à Bouraké

La persistance des coraux à Bouraké, et le succès du recrutement benthique malgré des valeurs de pCO_2 élevées, soulignent leur potentiel adaptatif à l'AO. Cette plasticité physiologique supposée a été testée expérimentalement sur trois espèces majeures, *Acropora tenuis*, *Montipora digitata* et *Porites* sp. (**Chapitre 4**), avec la mise en place d'une étude comparative en aquarium pendant 100 jours à différents niveaux de pCO_2 (dont une condition fluctuante représentative des variations naturelles quotidiennes du pH à Bouraké). Les coraux de Bouraké ont présenté une calcification systématiquement supérieure à leurs homologues du site de référence, et ce, quel que soit la condition de pH testée. Nous avons également observé un effet négatif de l'AO sur la calcification du squelette, en accord avec le consensus général (e.g., Gattuso et al., 1999 ; Doney et al., 2009, Comeau et al., 2019). Nos résultats ont également confirmé l'effet parfois marginal de l'AO rapporté par Leung et al. (2022), suivant l'espèce et le site d'origine des coraux en culture. Bien que les coraux de Bouraké présentent

une calcification accrue, nos données ne montrent pas systématiquement une plasticité physiologique particulière liée à l'origine des coraux et leur permettant des ajustements de leurs performances photosynthétiques ou de leurs teneurs en symbiontes, en pigments chlorophylliens, ou en protéines au niveau cellulaire. Cependant, notre étude confirme globalement une augmentation de la photosynthèse et de la respiration, liée à la baisse du pH environnant, pour les individus issus de Bouraké. Cela met en évidence que des coraux soumis depuis des décennies à des conditions acidifiées peuvent maintenir une calcification sous condition d'AO, grâce à l'activité photosynthétique de leurs symbiontes et à l'augmentation de la production de photosynthates. Afin de maintenir leur calcification, les coraux peuvent modifier leur allocation d'énergie, ce qui peut nécessiter/engendrer des compromis, notamment dans la minéralogie du squelette précipité. Il existe des coraux acclimatés à des conditions fluctuantes de pCO_2, comme ceux de Bouraké, qui peuvent maintenir leur calcification nette, mais avoir une densité en carbonate de calcium ($CaCO_3$) plus faible (Brown *et al.*, 2022). Afin de confirmer ou d'infirmer cette hypothèse d'un compromis énergétique mis en place par les coraux adultes et juvéniles en réponse à l'acidification, des expériences comparant des mesures de calcification nette, d'extension linéaire et de densité en $CaCO_3$ pourraient être menées sur les coraux de Bouraké. L'hypothèse qu'un pH fluctuant pourrait avoir un effet bénéfique sur la plasticité physiologique des coraux n'a pas été concluante sur un court terme, lors de notre étude expérimentale de 100 jours en aquarium (**chapitre 4**). En revanche, nos travaux montrent qu'une exposition à long terme à un pH variable à l'échelle du jour (cas des coraux de Bouraké) permet une certaine acclimatation à des conditions extrêmes. Cette dernière nécessiterait un temps relativement long (restant à définir) pour se manifester. Il serait donc judicieux d'explorer l'effet de la durée d'exposition (court, moyen, et long terme) à un pH variable sur les mécanismes de biominéralisation des coraux, et sur l'existence éventuelle de variations inter-spécifiques liées à la taxonomie des espèces considérées (e.g., clades complexes versus robustes), à la position (distance) des individus par rapport au fond (coraux branchus/massifs), à la longévité des espèces, etc.

7.2.2 Des communautés symbiotiques distinctes

Les différences de communautés symbiotiques observées entre les coraux de Bouraké et ceux du site de référence (Puen) soulignent l'influence de l'environnement sur l'holobionte corallien dans son ensemble. *Cladocopium* est l'unique genre de Symbiodiniacées trouvé dans les coraux de Bouraké lors de l'expérience de culture en aquariums, alors que nous nous attendions à trouver des genres connus pour être présents dans les coraux tolérants au stress, tel que le genre *Durusdinium* (Lajeunesse *et al.*, 2014 ; Haydon *et al.*, 2021). En fait, *Cladocopium* s'avère être un genre dominant face à *Durusdinium* dans des espèces

coralliennes provenant d'environnements à facteurs de stress multiples, tels que les lagunes de mangroves comme celle de Bouraké (Camp *et al.*, 2019, 2020). En plus de posséder des communautés symbiotiques distinctes, les coraux de Bouraké hébergent une communauté symbiotique plus stable et plus homogène que celle des coraux du site de référence. Il a été démontré que la stabilité du microbiome corallien était liée à une meilleure plasticité physiologique des coraux face à l'AO (e.g., Quigley *et al.*, 2017, 2019 ; Grottoli *et al.*, 2018 ; Ge *et al.*, 2021). Il serait donc intéressant d'étudier également les communautés bactériennes des coraux de Bouraké pour savoir si, au-delà d'une stabilité du microbiome dans son ensemble, ces coraux hébergent des bactéries particulières, comme il a déjà été observé notamment chez *Acropora muricata* et *Acropora pulchra* (Camp *et al.*, 2020). Bien qu'il soit difficile d'identifier les bénéfices spécifiques à chaque espèce de symbionte pour le corail hôte, nous faisons l'hypothèse que les différentes associations symbiotiques observées chez les coraux de Bouraké ont une influence directe sur la physiologie et la calcification de ces coraux, modulant finalement leur capacité d'acclimatation.

7.3 Le contrôle physio-chimique de la calcification face à l'AO

7.3.1 La régulation du milieu calcifiant extracellulaire

Après avoir montré dans le **chapitre 4** que les coraux de Bouraké avaient une calcification accrue sous AO, en lien avec des communautés symbiotiques distinctes, il apparaissait essentiel de comprendre la régulation de leur(s) mécanisme(s) de calcification. Pour ce faire, l'utilisation de proxies géochimiques, tels que le $\delta^{11}B$, le $\delta^{13}C$ et le rapport B/Ca, nous a permis de détecter une régulation positive forte sous AO de la chimie des carbonates du milieu calcifiant extracellulaire (MCE) dans des coraux mis en cultures sous différentes conditions de pCO_2. En effet, l'estimation du pH_{MCE} et du CID_{MCE} des coraux via l'utilisation des proxies isotopiques a montré des niveaux très supérieurs à ceux de l'eau de mer environnante, comme il a déjà été observé dans plusieurs études (e.g., Furla *et al.*, 2000 ; Ries *et al.*, 2011 ; McCulloch *et al.*, 2012a ; Venn *et al.*, 2019). Le MCE a toutefois présenté des différences entre les coraux de Bouraké et ceux de Puen, suggérant une variabilité des mécanismes de régulation du MCE liée aux caractéristiques physiologiques des coraux et aux conditions environnementales locales. Les paramètres physio-chimiques influençant les mécanismes de régulation du MCE sont notamment liés aux types de transports ioniques impliqués dans la calcification, à la perméabilité paracellulaire, ou encore à l'allocation d'énergie (énergie disponible pour la calcification). Afin de déterminer précisément de quelle manière les coraux de Bouraké régulent leur MCE, et ainsi leur calcification, des mesures

directes du pH interne du corail (incluant le MCE, l'ectoderme calicoblastique et la mésoglée) pourraient être menées à l'aide de microélectrodes et/ou de la microscopie confocale. En parallèle, la détermination du budget énergétique complet (protéines, lipides, carbohydrates) des coraux de Bouraké et de Puen permettrait d'identifier d'éventuelles variations dans la stratégie d'allocation de l'énergie entre les deux sites, en lien avec l'intensité du processus de calcification sous AO.

7.3.2 L'influence des communautés symbiotiques

Les différences de communautés symbiotiques observées entre les coraux de Bouraké et ceux du site de référence (Puen) semblent être en accord avec les différences de régulation physio-chimique du MCE identifiées avec les proxies géochimiques. Nos résultats sont originaux car nous avons montré pour la première fois que l'espèce *Montipora digitata* venant du site de référence présente une tendance apparente (sur les valeurs moyennées) à l'homéostasie de son pH_{MCE} en condition d'acidification, et que cela s'accompagne d'associations symbiotiques dominées par les espèces C73 et C73a. Ces résultats, obtenus dans le **chapitre 5,** résultent des approches géochimiques et métagénomiques ; ils mettent en avant l'influence notable des espèces de Symbiodinacées sur la chimie des carbonates du MCE et donc sur la calcification. On pourrait penser que certaines espèces de Symbiodiniacées auraient une productivité de photosynthates, et donc d'énergie pour la calcification du corail, plus importante que d'autres. Bien que cette hypothèse ait été montrée très récemment chez l'espèce *Montipora capitata* (Allen-Waller et Barott, 2023), les apports respectifs de chaque espèce de Symbiodiniacées restent à déterminer. Des éléments de réponses pourraient être apportés via des expériences d'inoculation de coraux juvéniles avec des monocultures d'espèces de Symbiodiniacées, afin d'évaluer leur influence sur le contrôle physio-chimique de la calcification sous AO. Même si une telle expérimentation est techniquement ambitieuse, au regard de la fragilité des coraux juvéniles et du choix de la technique à utiliser pour estimer le pH du MCE (e.g., proxies géochimiques, microélectrode, microscopie confocale), elle n'en demeure pas moins essentielle pour notre compréhension du rôle des Symbiodiniacées dans la régulation de la calcification des coraux soumis à des conditions acidifiées.

7.4 Reconstructions paléoenvironnementales

7.4.1 Enregistrement d'une acidification des océans causée par une absorption croissante de CO_2 anthropique

Les reconstructions paléoenvironnementales menées dans le **chapitre 6** sur des carottes de *Porites* ont mis en évidence une absorption croissante de CO_2 anthropique dans le site de référence entre 1988 et 2018. Ce résultat corrobore le tout dernier rapport d'évaluation du GIEC montrant une hausse de 54% des émissions de CO_2 entre 1990 et 2019 (IPCC Report, 2023). Cette absorption croissante de CO_2 dans le sud-ouest de l'océan Pacifique coïncide avec une baisse du pH de l'eau de mer de près de 0.13 unités de pH. Ces résultats confirment l'existence d'une acidification des océans depuis les dernières décennies, comme des études récentes de reconstitution du pH de l'eau de mer basées sur des carottes de *Porites* sp. l'ont montré (e.g., Wu *et al.*, 2018 ; D'Olivo *et al.*, 2019 ; Wei *et al.*, 2019 ; Tarique *et al.*, 2021). Nous avons également montré l'impact majeur des fluctuations climatiques interannuelles liées aux évènements (anomalies climatiques) du type El Niño (EN) et La Niña (LN) sur les reconstitutions du pH et de la température de l'eau de mer dans la carotte de *Porites* du site de référence entre 1988 et 2018. Ces évènements climatiques influencent directement la température et l'hygrométrie dans la région de l'océan Pacifique sud-ouest ; ils sont reconnus pour entraîner une variabilité du pH et de la température de l'eau de mer (Delcroix et Hénin, 1991 ; Gouriou et Delcroix, 2002 ; Tarique *et al.*, 2022 ; Thompson *et al.*, 2022). Toutefois, l'influence des évènements EN et LN semble être moins marquée à Bouraké en ce qui concerne le pH de l'eau de mer, car seuls deux évènements climatiques sévères peuvent être couplés avec une variation du pH à Bouraké entre 1992 et 2018. Cette plus grande stabilité du pH de l'eau de mer à Bouraké sur la période étudiée, également observée pour la signature en $\delta^{13}C$ du squelette des coraux, indique que l'influence des perturbations locales à Bouraké l'emporte sur l'impact de l'absorption de CO_2 anthropique. Ce résultat du **chapitre 6** démontre la forte influence des caractéristiques environnementales locales sur les paramètres hydrologiques de la lagune semi-fermée de Bouraké.

7.4.2 Les coraux de Bouraké acclimatés depuis plus de 30 ans à l'AO ?

Au cours du dernier chapitre de cette thèse (**chapitre 6**), nous avons montré pour la première fois une acclimatation corallienne sur le long-terme à des conditions de pH extrêmes et variables. En effet, l'enregistrement d'un pH moyen de 7,54 entre 1992 et 2018, obtenu dans une carotte de *Porites* collectée à Bouraké, nous indique que la population de coraux de

cette lagune, diversifiée (plus de 66 espèces recensées) et installée depuis plusieurs générations, persiste depuis plus de 30 ans dans ces conditions acidifiées. Ce résultat soulève de nombreuses interrogations sur les processus d'acclimatation de ces coraux, interrogations pour lesquelles cette thèse a apporté des éléments de réponses, notamment au niveau de la plasticité physiologique, des communautés symbiotiques associées, du contrôle physio-chimique de la calcification, des compromis potentiels au niveau énergétique (trade-off), ou encore d'une exposition longue à une fluctuation environnementale. Cet enregistrement d'une acclimatation sur le long-terme à l'AO pose également la question du rôle de l'épigénétique (rôle des facteurs environnementaux sur l'expression génétique) dans la plasticité transgénérationnelle supposée des coraux de Bouraké. Il est admis que les processus épigénétiques et les micro-organismes associés aux coraux ont un rôle déterminant dans les réponses adaptatives rapides (Torda *et al.*, 2017). Bien que nous ayons observé des communautés symbiotiques plus homogènes et distinctes dans les coraux de Bouraké que dans ceux du site de référence (**chapitre 4**), de futures études sont nécessaires pour estimer le degré de plasticité adaptative à Bouraké. Le couplage d'une étude épigénomique des coraux de Bouraké avec une étude métagénomique des micro-organismes associés (incluant symbiontes et bactéries) aiderait à déterminer le potentiel adaptatif des coraux de Bouraké aux changements climatiques.

7.5 Les micro-organismes associés aux coraux, un rôle clé dans leur acclimatation ?

Les principales conclusions des **chapitres 4** et **5** soulignent le rôle majeur joué par les associations symbiotiques dans l'acclimatation des coraux. Les différences observées dans la composition des communautés symbiotiques entre les coraux de Bouraké et ceux de Puen nous conduisent à émettre l'hypothèse de l'influence de l'environnement sur l'holobionte corallien dans son ensemble. Les résultats du **chapitre 3** mettent en évidence la "prédisposition environnementale" du site de Bouraké à induire une forte résistance des coraux aux conditions stressantes, dès le stade juvénile. Il serait donc intéressant de déterminer à partir de quel moment l'acquisition d'associations symbiotiques tolérantes aux stress environnementaux s'effectue, et comment la communauté de symbiontes évolue entre les générations de coraux. L'acquisition des symbiontes peut s'effectuer par le milieu extérieur (transmission horizontale) et/ou par héritage parental (transmission verticale). Bien que certaines espèces telle que *Montipora digitata* utilisent préférentiellement une transmission verticale, il est admis que la plupart des espèces de coraux ont un mode de transmission combiné, verticale et horizontale (Quigley et al., 2017, 2019; Epstein et al., 2019). Cela

suggère que les coraux de Bouraké pourraient bénéficier d'une exposition transgénérationnelle aux stress environnementaux afin d'avoir des associations symbiotiques optimales. En considérant les différents types d'acquisitions, les conditions environnementales ont une influence déterminante dans les différentes associations de micro-organismes avec les coraux. Comme évoqué précédemment (**7.2.2** et **7.4.2**), ces associations peuvent s'accompagner chez les coraux d'une certaine plasticité physiologique et de réponses adaptatives à un environnement stressant. Bien que le bénéfice de certaines associations symbiotiques dans la résilience des coraux aux changements climatiques ait été démontré (e.g., Schoepf *et al.*, 2015 ; Grottoli *et al.*, 2018 ; Camp *et al.*, 2020 ; Haydon *et al.*, 2021), les contributions spécifiques de chaque espèce de Symbiodiniacées sont encore méconnues et sont désormais un centre d'intérêt majeur des études actuelles (Allen-Waller et Barott, 2023), comme celle du **chapitre 5**. De la même façon, le microbiome des coraux joue un rôle facilitateur dans la propension des coraux à présenter des réponses adaptatives rapides aux changements environnementaux (Torda *et al.*, 2017; Voolstra and Ziegler, 2020; Barreto *et al.*, 2021; Ge *et al.*, 2021). Par exemple, les communautés bactériennes telles que les diazotrophes symbiotiques contribuent aux besoins accrus en azote des coraux exposés à des niveaux élevés de pCO_2 (Meunier *et al.*, 2021). Comme pour les associations symbiotiques, on peut penser que le microbiome des coraux de Bouraké soit lui aussi « ajusté », via une exposition transgénérationnelle aux stress environnementaux, pour permettre une acclimatation des coraux. Cette dernière hypothèse a été récemment montrée chez *Pocillopora damicornis*, espèce pour laquelle, après une exposition transgénérationnelle à des niveaux élevés de pCO_2, les larves avaient une capacité adaptative renforcée alors que la communauté du microbiome ne changeait pas chez les colonies adultes (Zhou *et al.*, 2021). En termes de perspectives, il serait intéressant de retracer l'évolution dans le temps des communautés de micro-organismes associés aux coraux exposés à des niveaux élevés de pCO_2, en réalisant par exemple une étude paléogénomique d'une carotte de *Porites* comme celle étudiée à Bouraké dans le **chapitre 6**. En plus d'être particulièrement innovante d'un point de vue technique au regard de l'obtention d'ADN ancien de symbiontes, une telle étude fournirait des informations cruciales sur l'évolution de la communauté des micro-organismes associés aux coraux faisant face aux changements climatiques en cours. L'évolution de la tolérance des symbiontes aux stress climatiques, couplée à un changement des associations symbiotiques au sein des coraux, permettrait, en fonction des scénarios du GIEC, d'augmenter la future production nette de carbonate de calcium par les coraux (Cornwall *et al.*, 2023).

7.6 Vers une meilleure compréhension de la régulation de la calcification des coraux

Le maintien de la calcification des coraux fait partie intégrante de leur persistance dans des environnements stressants. Le **chapitre 5** a mis en évidence l'importance de la régulation physio-chimique de la calcification des coraux et l'influence des communautés symbiotiques sur ce contrôle. Toutefois, la compréhension du mécanisme de régulation de la chimie des carbonates du MCE reste partielle et certaines interrogations demeurent. Tout d'abord il faut rappeler que plusieurs types de transports ioniques sont impliqués dans le contrôle physio-chimique de la calcification, incluant des transports transcellulaire (actif) et paracellulaire (passif), et/ou des transporteurs spécifiques acheminant des équivalents d'acides ou de bases tels que H^+ et HCO_3^- (Boron, 2004; Casey *et al.*, 2010). Ces transporteurs véhiculent les protons H^+ à l'intérieur et à l'extérieur des cellules par le biais d'une polarité acide-base fonctionnelle, comme cela a été décrit précédemment dans l'épithélium oral de deux cnidaires, les anémones (Furla *et al.*, 1998) et les coraux (Venn *et al.*, 2022). La respiration cellulaire des produits de la photosynthèse des symbiontes (photosynthates) par les mitochondries est une source majeure de production d'Adénosine-Triphosphate (ATP). Cet ATP permet de faire fonctionner les transporteurs transmembranaires tels que la Ca^{2+}-ATPase qui transporte les protons en dehors du MCE et à travers les tissus, optimisant la chimie des carbonates du MCE pour la calcification. Bien qu'il y ait de nombreuses mitochondries dans les cellules calicoblastiques, l'apport de photosynthates jusqu'à ces cellules demeure inexpliqué étant donné que les symbiontes se situent dans l'endoderme oral, i.e., particulièrement loin des cellules calicoblastiques. La localisation des symbiontes et une production suffisante de photosynthates pouvant atteindre les cellules calicoblastiques sont essentielles. Comme précédemment suggéré (**chapitre 5** et **7.3.2**) et démontré dans la récente étude de Allen-Waller et Barott (2023), certaines espèces de symbiontes (e.g., C73 et C31) produiraient plus de photosynthates que d'autres. Les symbiontes peuvent également influencer les transports paracellulaires, notamment par une production supérieure de photosynthates dans l'endoderme oral et aboral, ce qui augmente le pH dans le cœlenteron. Ce phénomène peut générer un gradient favorable de diffusion entre la mésoglée et le cœlenteron, ce qui souligne le rôle tampon de la mésoglée entre l'eau de mer et le MCE (Venn *et al.*, 2022). Nous avons également suggéré dans le **chapitre 5** que des changements des micro-organismes associés aux coraux pourraient renforcer les structures cellulaires protectrices de ces derniers et maintenir une certaine perméabilité membranaire sous AO. Cela limiterait la fuite des ions calcium et carbonate du MCE et permettrait une meilleure persistance de la calcification sous AO. Nous soulignons une nouvelle fois l'importance d'examiner et de considérer les espèces

de micro-organismes associés aux coraux dans les futures études sur le contrôle physio-chimique de la calcification. Nous conseillons également de poursuivre les recherches sur l'allocation d'énergie au sein du processus de calcification, ainsi que sur les transports de protons autres que les ATPases. En effet, il a été montré que l'export de protons du MCE pouvait aussi être régulé par les différentes familles de canaux à protons (H_vCN) et par les échangeurs Na^+-H^+ (NHEs) (Capasso *et al*., 2021). L'activation par certaines espèces de coraux des échangeurs NHEs exportant les protons H^+ pour des ions Na^+ et Li^+ afin d'élever le pH de leur MCE est discutée et démontrée via l'utilisation des isotopes du Lithium dans l'**Article Annexe n°2**. Bien que le mécanisme de calcification des coraux soit particulièrement complexe au vu des nombreux facteurs biotiques et abiotiques qui l'influence, sa compréhension demeure fondamentale afin de prédire l'adaptation des coraux face à l'acidification des océans et aux changements climatiques rapides en cours.

7.7 Nouvelles hypothèses et perspectives expérimentales

Parmi les nouvelles hypothèses qui émergent de ce travail de thèse, nous identifions trois hypothèses principales (H_0) :

1. L'acclimatation à long terme des coraux de Bouraké est associée à des communautés de micro-organismes spécifiques et stables dans le temps.
2. Le contrôle physio-chimique de la calcification est régulé par des apports spécifiques aux communautés symbiotiques associées.
3. Les communautés de micro-organismes associées aux coraux de Bouraké conditionnent leur plasticité physiologique.

En termes de perspectives expérimentales pour tester ces hypothèses, une première étude consisterait à reconstruire sur le long terme l'évolution des communautés symbiotiques et bactériennes associées aux coraux de Bouraké (étude paléogénomique) afin de répondre à l'hypothèse n°1.

L'hypothèse n°2, quant à elle, peut être vérifiée par une expérience de marquage isotopique au carbone 13 (^{13}C) en aquariums. Après une étude physiologique de *Montipora digitata* provenant de Bouraké (symbionte C15) et du site Référence (symbionte C73) en aquariums à différents pH (par exemple, 7,4, 7,7 et 8,1), comprenant une estimation du budget énergétique complet (protéines, lipides et glucides), les coraux seraient marqués au ^{13}C puis incubés à la lumière avant de mesurer le $\delta^{13}C$ de l'hôte corallien et de ses symbiontes. Cette expérience permettrait de tracer et de quantifier la proportion de carbone provenant de la

photosynthèse utilisée par l'holobionte, et ainsi de déterminer l'influence de chaque espèce de symbiontes (C73 et C15) dans la production de photosynthates et leur utilisation par l'hôte.

Enfin, l'hypothèse n°3 pourrait être testée par une expérience d'inoculation de coraux juvéniles (par exemple, des individus d'*Acropora tenuis* provenant de Bouraké et du site Référence) avec différentes espèces symbiotiques. Ces coraux seraient ensuite mis en culture à différents pH (par exemple, 8,1 et 7,4) afin de déterminer leurs capacités physiologiques.

À travers le test de ces hypothèses, nous devrions être en mesure d'apporter des réponses plus ciblées/spécifiques sur les mécanismes d'acclimatation des coraux aux changements climatiques.

APPENDICES

Appendix Article n°1 - Chapter 3

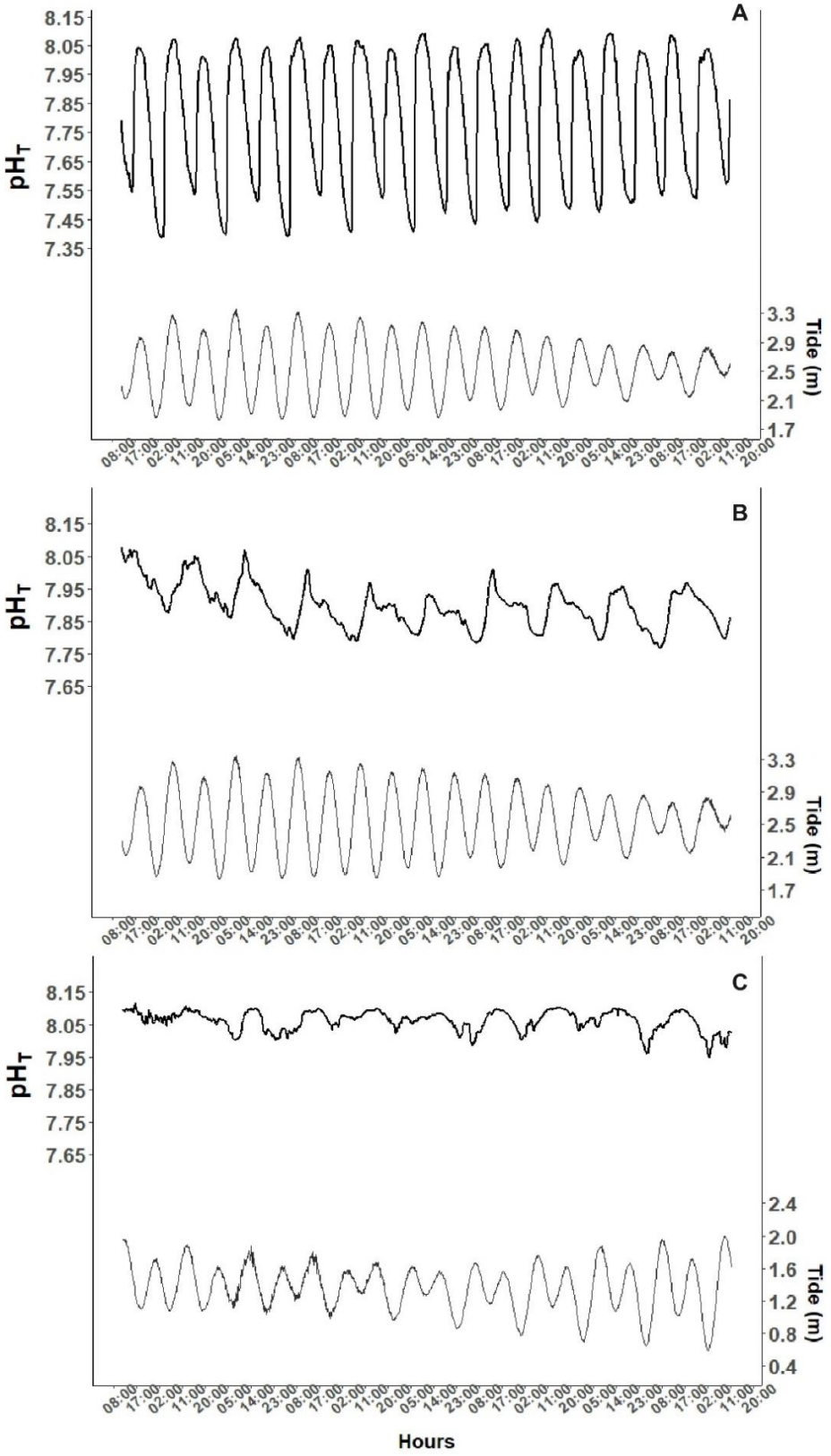

Figure VIII-1 | *An example of the seawater pH_T coupled with the tidal variations, measured during 11 days at the end of March 2019 at St B3 and St R2 (A and B), and 11 days in January 2019 at St M1 (C).*

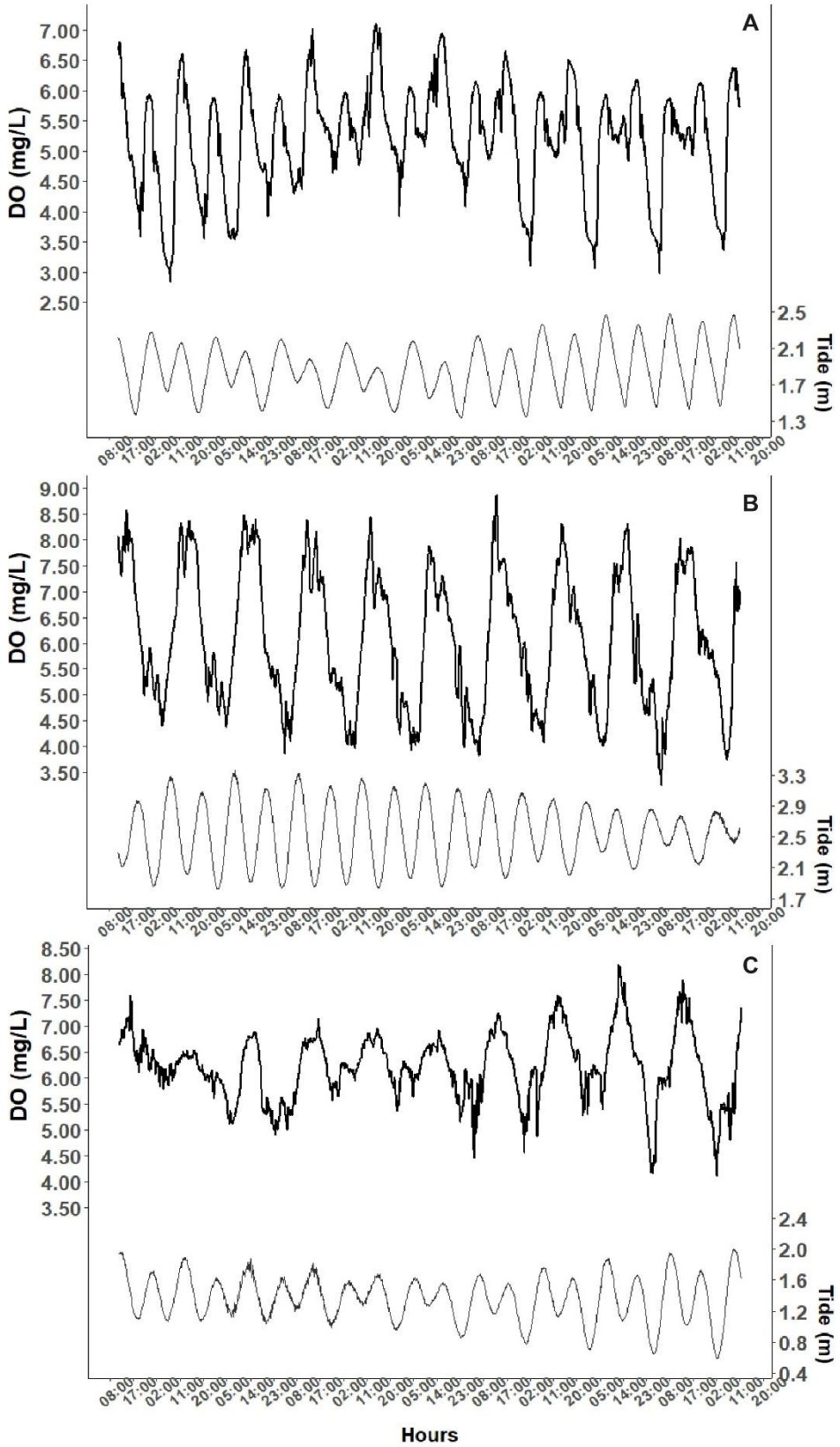

Figure VIII-2 | *An example of the seawater dissolved oxygen concentrations, coupled with the tidal variations, measured during 11 days at the beginning of April 2019 at St B3 (A), at the end of March 2019 at St R2 (B), and at the end of January 2019 at St M1 (C).*

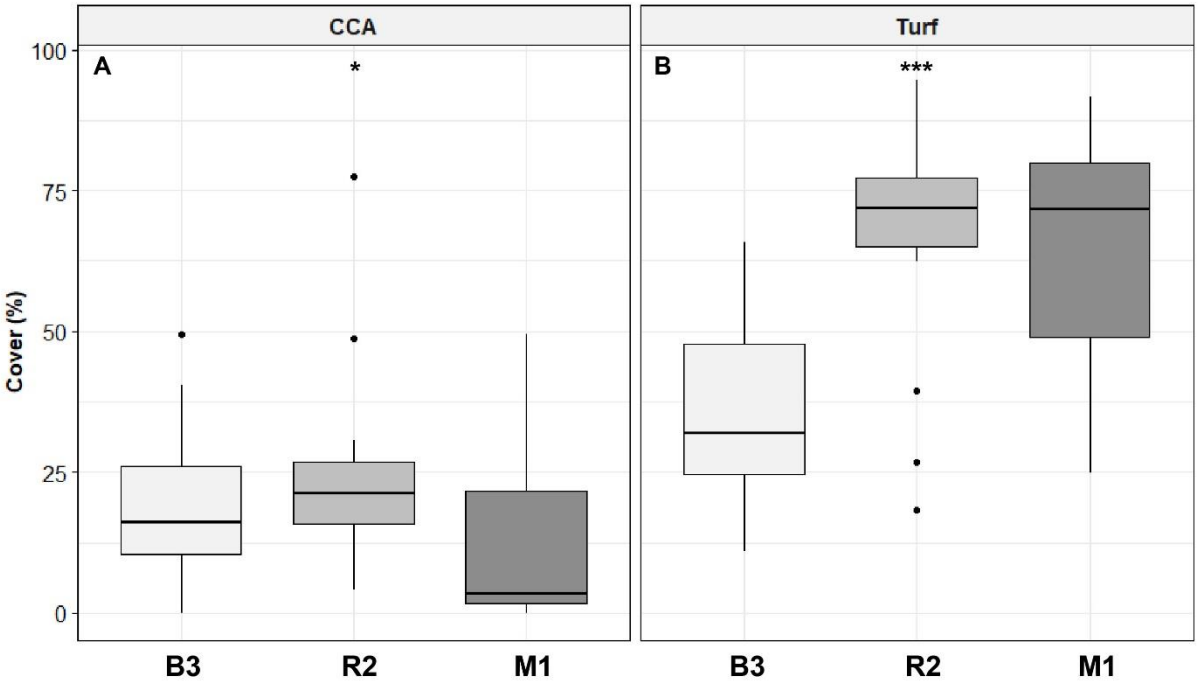

Figure VIII-3 | *CCA (A) and Turf percent cover (B) measured on the bottom sides of the tiles after ca. two years of tile immersion at stations B3, R2, and M1 (number of tiles n = 15, 20, and 19, respectively). Data are median values ± 25th and 75th percentiles (box), minimum and maximum values (whiskers), and outliers (dots). Stars represent statistical significance (see Appendix Table VIII-3).*

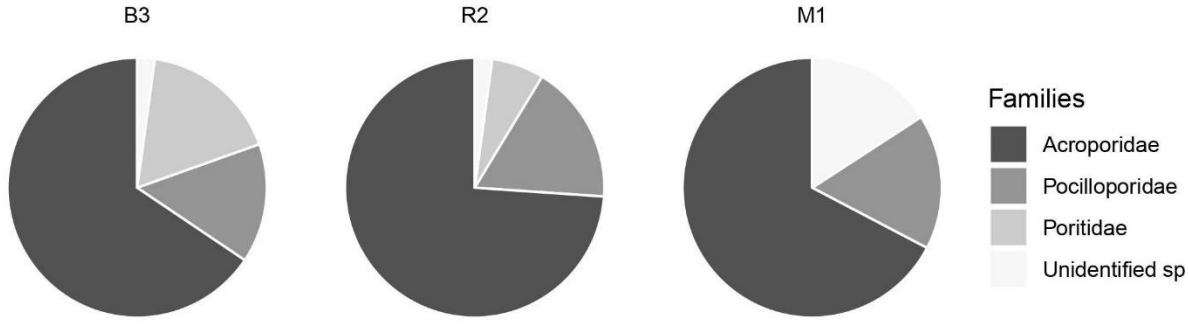

Figure VIII-4 | *Mean relative abundances (%) of the coral families which settled on the tiles (all sides pooled) during the two years of tile immersion in Bouraké (B3) and stations R2 and M1.*

Table VIII-1 | *List of coral species identified in the Bouraké lagoon (B3) and at sites R2 and M1.*

CORALS (Scleractinians)

Clade Complex

Family	Genus	Species	Site
Acroporidae	*Acropora*	*aculeus* (Dana, 1846)	B3-M1
Acroporidae	*Acropora*	*cf. acuminata* (Verrill, 1864)	R2
Acroporidae	*Acropora*	*aspera* (Dana, 1846)	B3-R2-M1
Acroporidae	*Acropora*	*austera* (Dana, 1846)	R2
Acroporidae	*Acropora*	*carduus* (Dana, 1846)	B3
Acroporidae	*Acropora*	*cerealis* (Dana, 1846)	B3-M1
Acroporidae	*Acropora*	*divaricata* (Dana, 1846)	B3-M1
Acroporidae	*Acropora*	*echinata* (Dana, 1846)	B3
Acroporidae	*Acropora*	*florida* (Dana, 1846)	R2-M1
Acroporidae	*Acropora*	*gemmifera* (Brook, 1892)	R2
Acroporidae	*Acropora*	*grandis* (Brook, 1892)	R2-M1
Acroporidae	*Acropora*	*horrida* (Dana, 1846)	B3-R2-M1
Acroporidae	*Acropora*	*humilis* (Dana, 1846)	B3-R2-M1
Acroporidae	*Acropora*	*kirstyae* Veron & Wallace, 1984	B3-R2-M1
Acroporidae	*Acropora*	*latistella* (Brook, 1892)	R2
Acroporidae	*Acropora*	*cf. longycyathus* (Milne Edwards, 1860)	R2
Acroporidae	*Acropora*	*microphthalma* (Verrill, 1869)	B3-R2-M1
Acroporidae	*Acropora*	*millepora* (Ehrenberg, 1834)	R2-M1
Acroporidae	*Acropora*	*muricata* (Linnaeus, 1758)	B3-R2-M1
Acroporidae	*Acropora*	*nana* (Studer, 1879)	B3
Acroporidae	*Acropora*	*polystoma* (Brook, 1891)	R2
Acroporidae	*Acropora*	*pulchra* (Brook, 1891)	B3-R2-M1
Acroporidae	*Acropora*	*robusta* (Dana, 1846)	R2
Acroporidae	*Acropora*	*retusa* (Dana, 1846)	R2
Acroporidae	*Acropora*	*samoensis* (Brook, 1891)	B3-R2-M1
Acroporidae	*Acropora*	*cf. secale* (Studer, 1878)	R2-M1
Acroporidae	*Acropora*	*tenuis* (Dana, 1846)	B3-R2-M1
Acroporidae	*Acropora*	*tortuosa* (Dana, 1846)	M1
Acroporidae	*Acropora*	*valida* (Dana, 1846)	B3-R2-M1
Acroporidae	*Acropora*	*vaughani* Wells, 1954	B3-R2-M1
Acroporidae	*Anacropora*	*forbesi* Ridley, 1884	B3
Acroporidae	*Anacropora*	*matthai* Pillai, 1973	B3-R2
Acroporidae	*Anacropora*	*puertogalerae* Nemenzo, 1964	R2
Acroporidae	*Isopora*	*palifera* (Lamarck, 1816)	R2-M1
Acroporidae	*Montipora*	*aequituberculata* Bernard, 1897	R2
Acroporidae	*Montipora*	*angulata* (Lamarck, 1816)	M1
Acroporidae	*Montipora*	*cactus* Bernard, 1897	B3-M1
Acroporidae	*Montipora*	*digitata* (Dana, 1846)	B3-R2-M1
Acroporidae	*Montipora*	*efflorescens* Bernard, 1897	R2
Acroporidae	*Montipora*	*hispida* (Dana, 1846)	B3-R2-M1
Acroporidae	*Montipora*	*mollis* Bernard, 1897	R2
Acroporidae	*Montipora*	*cf. nodosa* (Dana, 1846)	R2
Acroporidae	*Montipora*	*stellata* Bernard, 1897	B3-R2-M1

CORALS (Scleractinians) *(continue Table VIII-1)*

Clade Complex

Family	Genus	Species	Site
Agariciidae	*Pavona*	*cactus* (Forskål, 1775)	B3-R2-M1
Agariciidae	*Pavona*	*clavus* Dana, 1846	R2
Agariciidae	*Pavona*	*decussata* (Dana, 1846)	B3-R2-M1
Caryophylliidae	*Polycyathus*	*fulvus* Wijsman-Best, 1970	B3
Dendrophylliidae	*Turbinaria*	*mesenterina* (Lamarck, 1816)	B3
Dendrophylliidae	*Turbinaria*	*stellulata* (Lamarck, 1816)	R2
Dendrophylliidae	Turbinaria	reniformis (Bernard, 1896)	M1
Dendrophylliidae	*Tubastraea*	*coccinea* Lesson, 1830	B3
Dendrophylliidae	*Tubastraea*	*micranthus* (Ehrenberg, 1834)	B3
Euphylliidae	*Galaxea*	*fascicularis* (Linnaeus, 1767)	B3-R2-M1
Incertae sedis	*Pachyseris*	*rugosa* Lamarck, 1801	B3-R2-M1
Incertae sedis	*Pachyseris*	*speciosa* Dana, 1846	B3-R2-M1
Poritidae	*Goniopora*	*cf. minor* Crossland, 1952	B3
Poritidae	*Porites*	sp.	B3-M1
Poritidae	*Porites*	*cf. annae* Crossland, 1952	B3-M1
Poritidae	*Porites*	*lutea* Edwards & Haime, 1851	B3-R2-M1
Poritidae	*Porites*	*lobata* Dana, 1846	B3-R2-M1
Poritidae	*Porites*	*cylindrica* Dana, 1846	B3-R2-M1
Poritidae	*Porites*	*rus* (Forskål, 1775)	R2
Siderastreidae	*Pseudosiderastrea*	*tayamai* Yabe & Sugiyama, 1935	B3

Clade Robust

Family	Genus	Species	Site
Fungiidae	*Heliofungia*	*actiniformis* (Quoy & Gaimard, 1833)	B3
Fungiidae	*Halomitra*	*pileus* (Linnaeus, 1758)	B3
Fungiidae	*Fungia*	*fungites* (Linnaeus, 1758)	B3
Fungiidae	*Ctenactis*	*echinata* (Pallas, 1766)	B3-M1
Fungiidae	*Cantharellus*	*noumeae* Hoeksema & Best, 1984	B3
Fungiidae	*Sandalolitha*	*dentata* Quelch, 1884	B3
Leptastreidae	*Leptastrea*	*purpurea* (Dana, 1846)	B3-M1
Lobophylliidae	*Echinophyllia*	*aspera* (Ellis & Solander, 1786)	B3
Lobophylliidae	*Lobophyllia*	*cf. hemprichi* (Ehrenberg, 1834)	B3-M1
Lobophylliidae	*Lobophyllia*	*corymbosa* (Forskål, 1775)	R2
Merulinidae	*Coelastrea*	*aspera* (Verrill, 1866)	B3-R2
Merulinidae	*Cyphastrea*	*serailia* (Forskål, 1775)	R2-M1
Merulinidae	*Cyphastrea*	sp.	B3-M1
Merulinidae	*Dipsastrea*	*pallida* (Dana, 1846)	B3-M1
Merulinidae	*Dipsastrea*	*cf. lizardensis* (Veron, Pichon, & Wijsman-Best, 1977)	B3
Merulinidae	*Echinopora*	*lamellosa* (Esper, 1795)	B3-R2-M1
Merulinidae	*Echinopora*	*horrida* Dana, 1846	R2
Merulinidae	*Favites*	*abdita* (Ellis & Solander, 1786)	B3-M1
Merulinidae	*Favites*	*melicerum* (Ehrenberg, 1834)	B3-M1
Merulinidae	*Goniastrea*	*favulus* (Dana, 1846)	B3-R2
Merulinidae	*Goniastrea*	*pectinata* (Ehrenberg, 1834)	R2
Merulinidae	*Hydnophora*	*rigida* (Dana, 1846)	B3
Merulinidae	*Merulina*	*scabricula* Dana, 1846	B3-M1

CORALS (Scleractinians) *(continue Table VIII-1)*

Clade Robust

Family	Genus	Species	Site
Merulinidae	*Merulina*	*ampliata* (Ellis & Solander, 1786)	B3-M1
Merulinidae	*Pectinia*	*lactuca* (Pallas, 1766)	R2-M1
Merulinidae	*Pectinia*	*paeonia* (Dana, 1846)	B3-R2
Merulinidae	*Platygyra*	*sinensis* (Milne Edwards & Haime, 1849)	B3-M1
Merulinidae	*Platygyra*	*daedalea* (Ellis & Solander, 1786)	B3-M1
Merulinidae	*Trachyphyllia*	*geoffroyi* (Audouin, 1826)	B3
Pocilloporidae	*Pocillopora*	*damicornis* (Linnaeus, 1758)	B3-R2-M1
Pocilloporidae	*Pocillopora*	*verrucosa* (Ellis & Solander, 1786)	R2
Pocilloporidae	*Stylophora*	*pistillata* (Esper, 1797)	R2
Psammocoridae	*Psammocora*	*contigua* (Esper, 1794)	B3-R2-M1

CORALS (non-scleractinians)

Family	Genus	Species	Site
Alcyioniidae	*Sinularia*	sp.	B3

Table VIII-2 **|** *Summary of cover percentages for each category (CCA, Turf and suspension feeders) per site (B3, R2 and M1), for top (**A**) and bottom sides (**B**) of tiles. Data are mean ± SE (n=15, 20 and 19 for B3, R2 and M1, respectively). Minimum and maximum values are also reported.*

A)

Top sides, T_2		B3	R2	M1
CCA	Mean	46.94 ± 5.71	65.80 ± 5.30	70.89 ± 4.16
	Max	85.33	95.99	89.67
	Min	20.55	21.89	32.32
Turf	Mean	19.64 ± 1.80	8.84 ± 1.57	10.11 ± 1.97
	Max	31.57	24.52	35.31
	Min	8.50	1.03	0.20
Top sides, $T_{24/26}$				
CCA	Mean	9.73 ± 1.27	50.23 ± 2.95	2.88 ± 1.00
	Max	17.85	77.53	18.97
	Min	3.49	27.74	0.00
Turf	Mean	49.49 ± 6.97	20.37 ± 1.66	88.39 ± 2.40
	Max	92.80	32.73	97.17
	Min	0.82	8.42	51.56

B)

Bottom sides, $T_{24/26}$				
CCA	Mean	19.81 ± 3.45	23.99 ± 3.52	12.41 ± 3.25
	Max	49.54	77.46	49.39
	Min	0.00	4.06	0.00
Turf	Mean	35.44 ± 4.48	67.00 ± 4.21	64.75 ± 4.65
	Max	65.82	94.42	91.69
	Min	10.95	18.18	24.78

B) *(continue Table VIII-2)*

Bottom sides, $T_{24/26}$				
Suspension feeders	Mean	4.17 ± 1.05	0.45 ± 0.37	15.35 ± 4.77
	Max	12.09	7.32	70.75
	Min	0.51	0.00	0.00

Table VIII-3 | *Statistical data for each category of organisms settled on the bottom sides of tiles after two years of deployment (TF). Non-parametric Kruskal-Wallis tests, followed by Dunn's multiple comparisons, were run between stations for each category of organisms.*

A)

Bottom sides, $T_{24/26}$ between stations	*df*	*K-W*	*p*	*Dunn's multiple comparison*
CCA	(2, 54)	7.530	**0.020**	M1 < R2 = B3 (***p* < 0.010**)
Turf	(2, 54)	18.135	**<0.001**	B3 < M1 = R2 (***p* < 0.001**)
Susp. feeders	(2, 54)	21.066	**<0.001**	B3 = M1 > R2 (***p* < 0.001**)
Empty	(2, 54)	27.090	**<0.001**	B3 > M1 = R2 (***p* < 0.001**)

B)

Recruits, $T_{24/26}$ between stations				
Recruits	2	17.521	**<0.001**	B3 > R2 = M1 (***p* < 0.001**)

C)

Recruits, $T_{24/26}$ between sides				
B3	2	23.676	**<0.001**	B > L > T (***p* < 0.020**)
R2	2	30.161	**<0.001**	B > L = T (***p* < 0.001**)
M1	2	26.729	**<0.001**	B > L = T (***p* < 0.001**)

Table VIII-4 | *Non-parametric Kruskal-Wallis test run on Shannon Index Diversity (H) between the three stations (i.e., H= 4.17, 4.02, and 3.97 for stations B3, R2 and M1, respectively.*

Species diversity between stations	*df*	*K-W*	*p*
Shannon Index Diversity	2	2	0.368

Appendix Article n°2 - Chapter 4

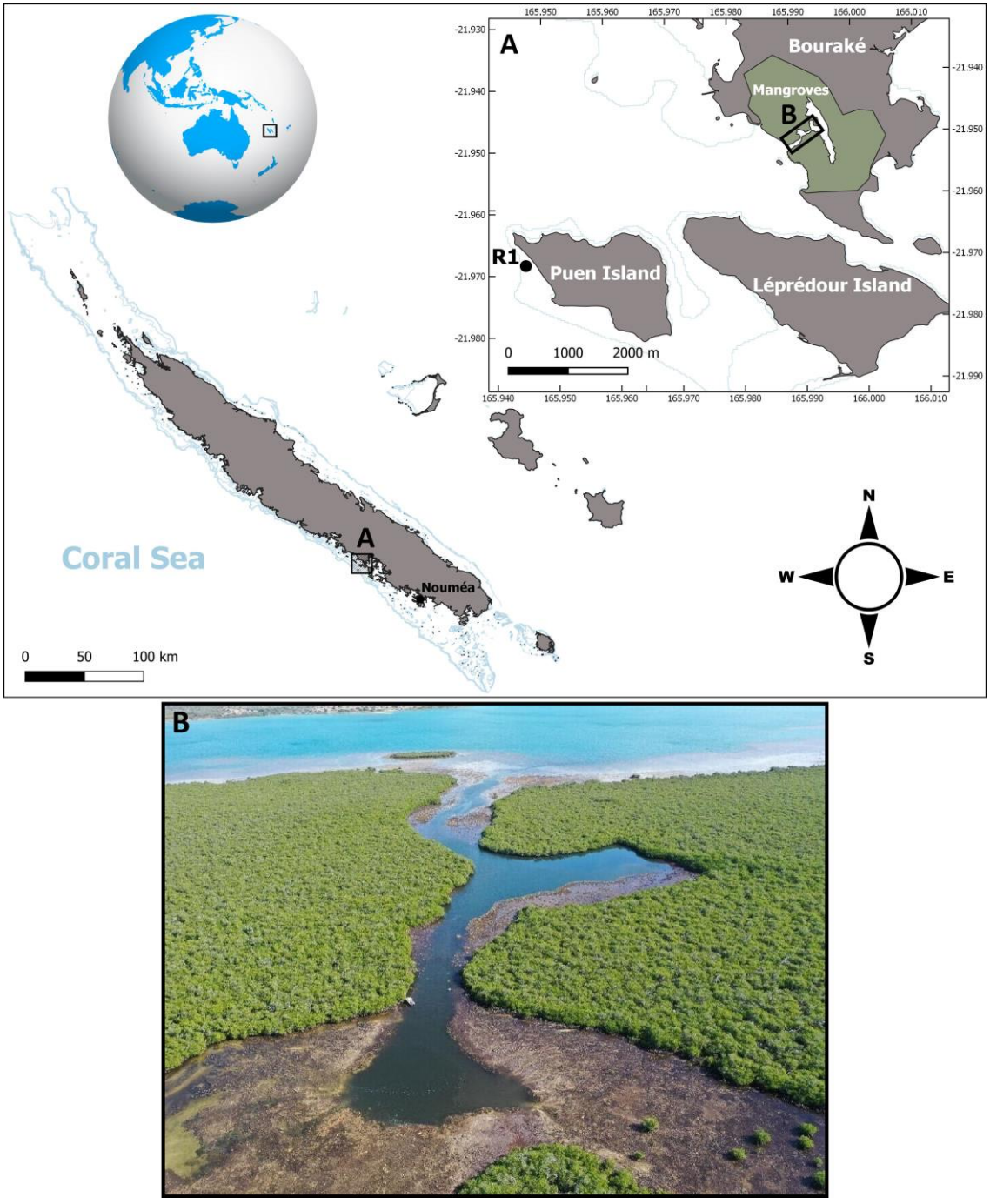

Figure VIII-5 | *Map of the study sites (B and R1) in New Caledonia where corals were collected. Photo (B) is an aerial pic of the Bouraké lagoon (taken at 130 m height).*

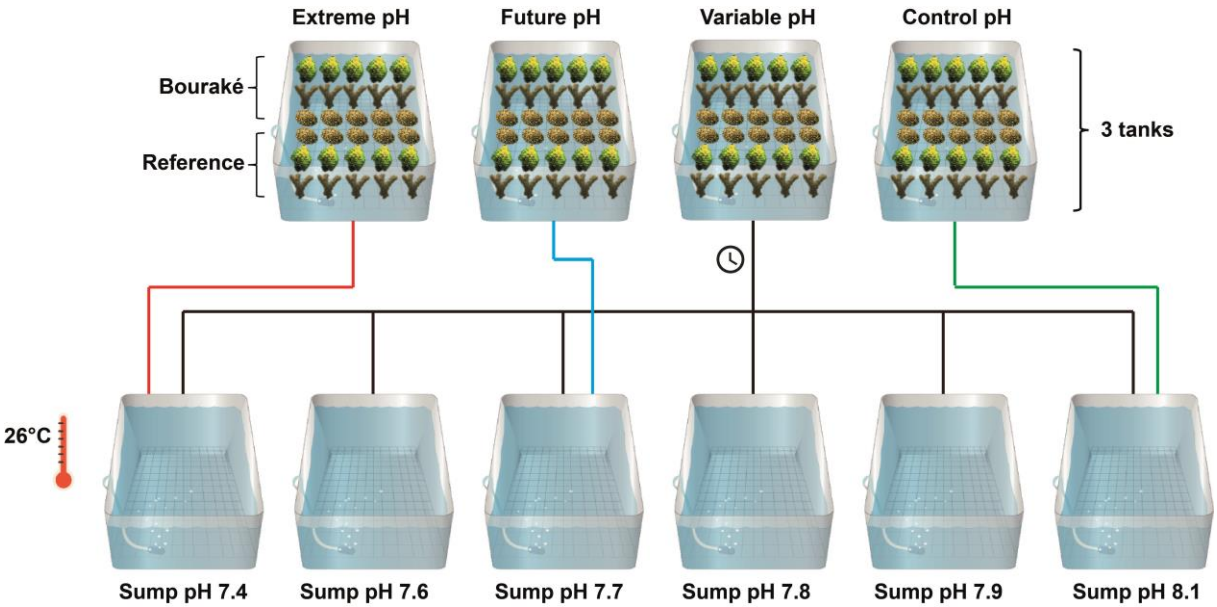

Figure VIII-6 | *Schematic representation of the experimental set up with four pH conditions (Control, pH_{NBS} 8.11; Future, pH_{NBS} 7.76; Extreme, pH_{NBS} 7.54; and Variable, pH_{NBS} 7.56-8.07), each replicated in three experimental tanks, and 6 tank sumps that alimented the experimental tanks. In each experimental tank, 30 coral fragments were positioned, half from Bouraké and half from the reference site. The 'Variable' condition was supplied by one or more sumps simultaneously according to a time table mimicking pH variation in Bouraké (see Appendix Table VIII-6). Sump temperature was maintained at ca. ~26°C.*

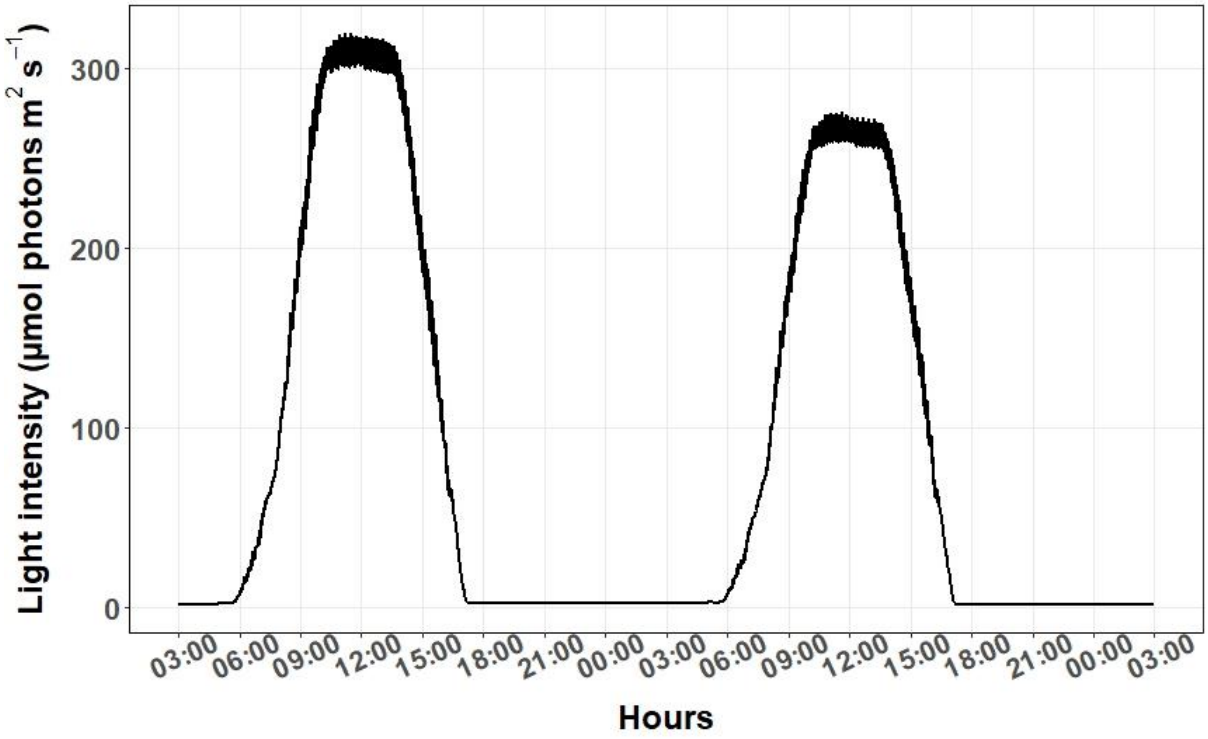

Figure VIII-7 | *Example of the light intensity received by the corals during the 100-day incubation, and measured in two tanks having a different position below the LED lights (see Appendices Tables VIII-5 and VIII-6 for setting).*

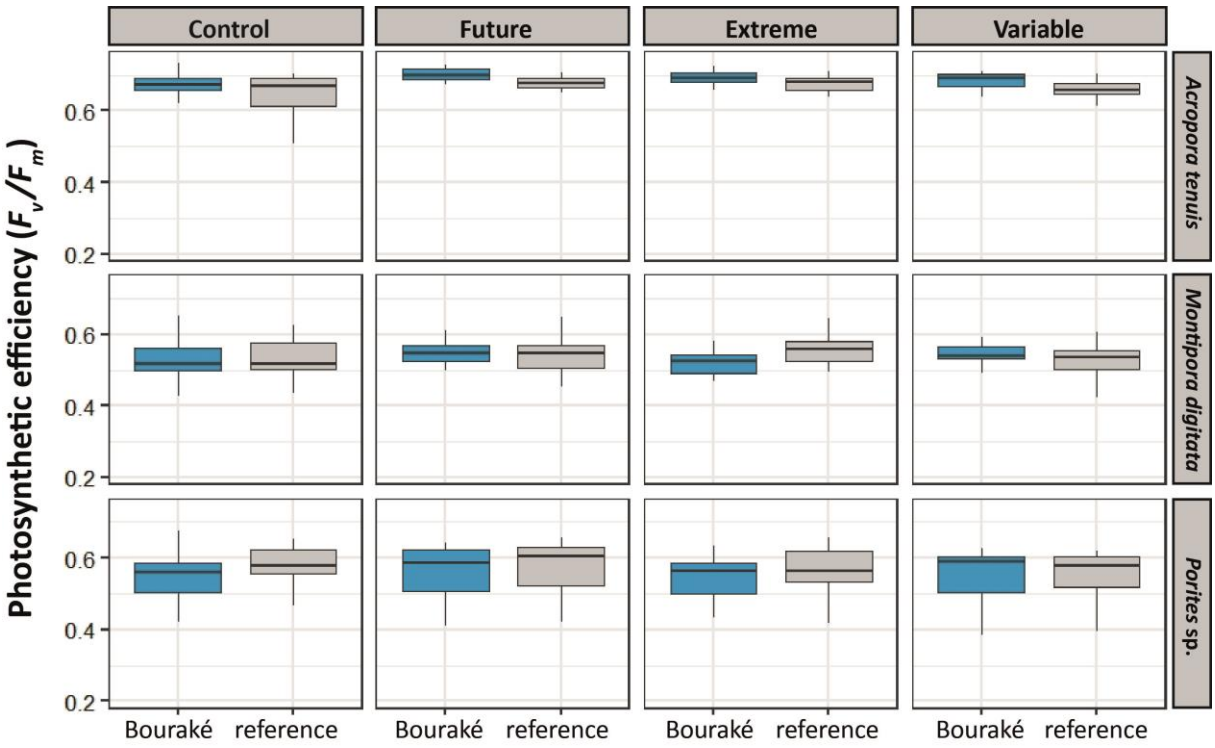

Figure VIII-8 | *Photosynthetic efficiency (F_v/F_m) of corals from Bouraké (in blue) and reference (in grey) sites measured after 100 days of incubation at four pH conditions (Control, pH_{NBS} 8.11; Future, pH_{NBS} 7.76; Extreme, pH_{NBS} 7.54; and Variable, pH_{NBS} 7.56-8.07). Data are median ± 25th and 75th percentiles (n=12-16, depending on species and pH condition ; see Appendix Table VIII-11 for all post hoc comparisons).*

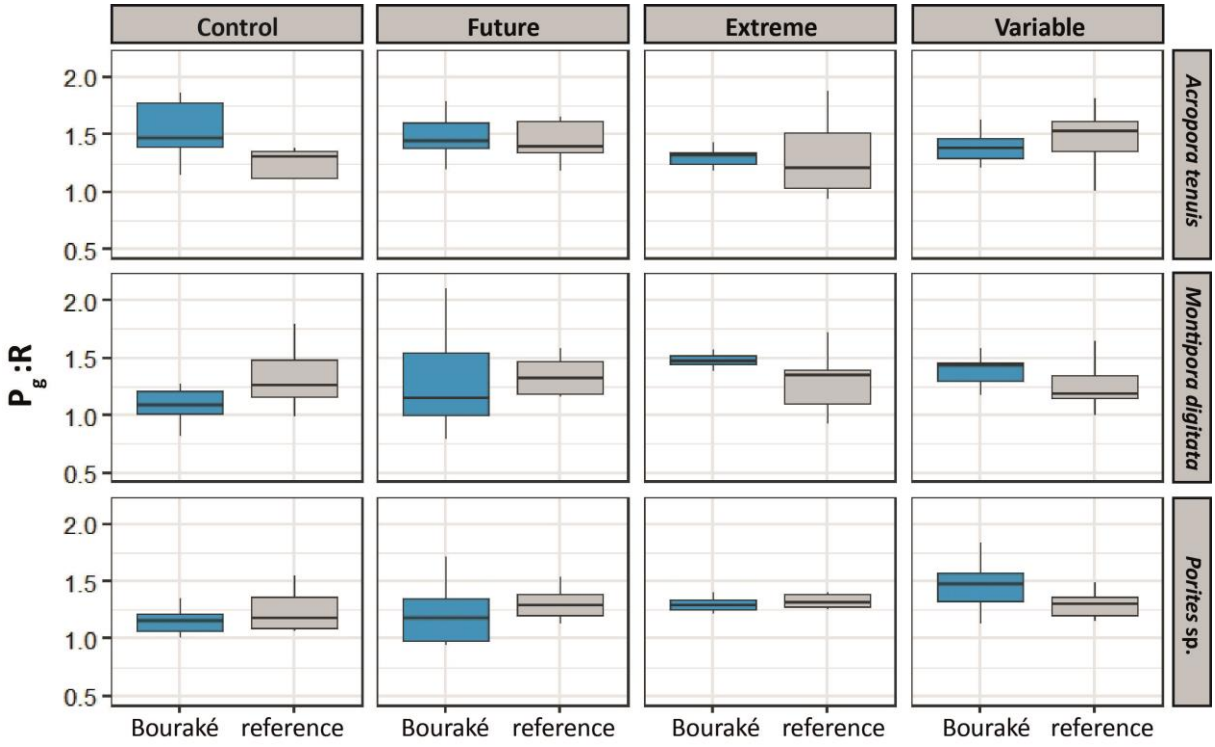

Figure VIII-9 | *Gross photosynthesis to respiration ratio (P_g:R) of corals from Bouraké (in blue) and the reference site (in grey) incubated at four pH conditions (Control, pH_{NBS} 8.11; Future, pH_{NBS} 7.76;*

Extreme, pH_{NBS} 7.54; and Variable, pH_{NBS} 7.56-8.07). Data are median ± 25th and 75th percentiles (n = 7; see Appendix Table VIII-11 for all post hoc comparisons).

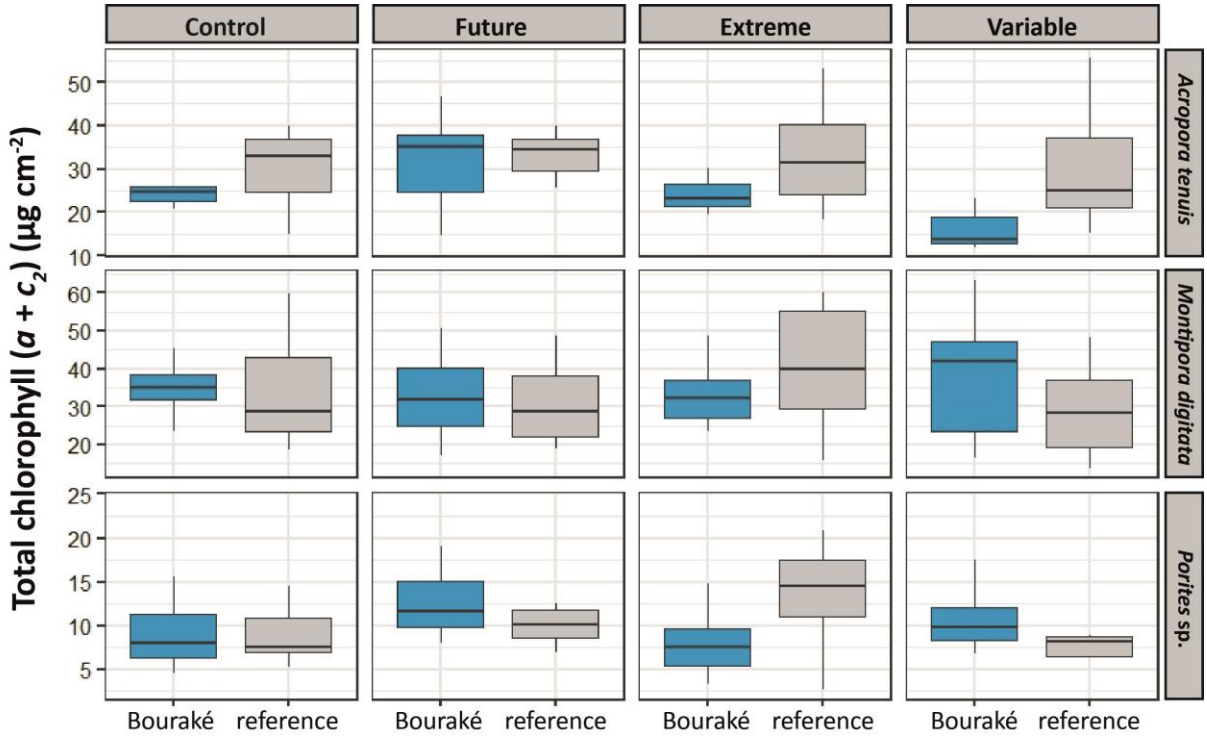

Figure VIII-10 | *Total chlorophyll (a + c_2) content of corals from Bouraké (in blue) and reference (in grey) sites after 100 days of incubation at four pH conditions (Control, pH_{NBS} 8.11; Future, pH_{NBS} 7.76; Extreme, pH_{NBS} 7.54; and Variable, pH_{NBS} 7.56-8.07). Data are median ± 25th and 75th percentiles (n = 7; see Appendix Table VIII-11 for all post hoc comparisons).*

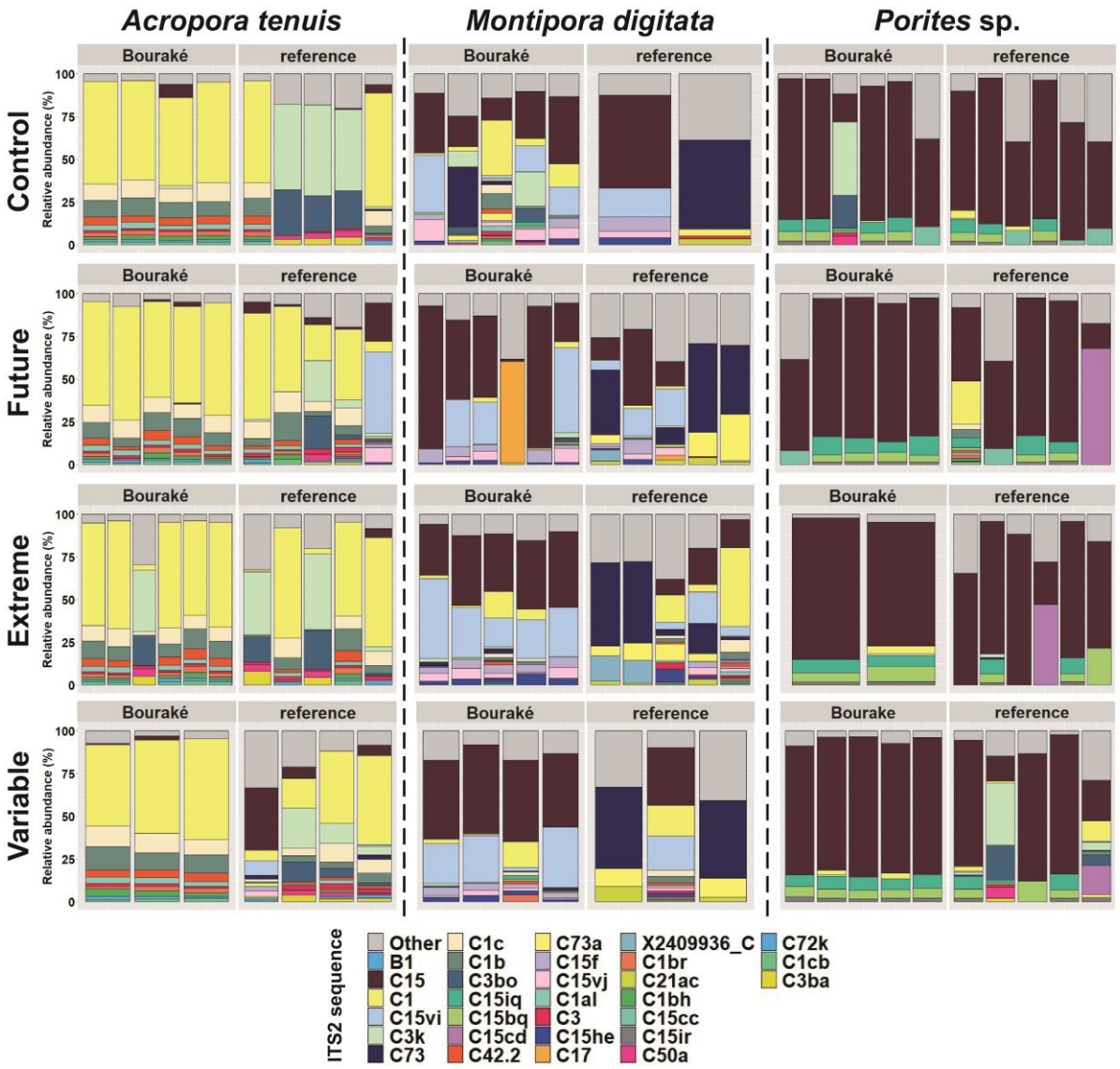

Figure VIII-11 | *Relative abundance (%) of ITS2 sequence of corals from Bouraké and the reference site after 100 days of incubation at four pH conditions (Control, pH_{NBS} 8.11; Future, pH_{NBS} 7.76; Extreme, pH_{NBS} 7.54; and Variable, pH_{NBS} 7.56-8.07). Within each cell of this 3-by-4 matrix, samples are plotted as stacked bar charts with a single column representing a sample from a specific origin: Bouraké (left) and reference (right). Only the 30 most abundant ITS2 sequences have been assigned colors. Low-abundance sequences are in grey. Sequences with designated names (e.g., B1, C15, or C1) refer to sequences previously characterized in the literature or that have been run through the SymPortal analytical framework. Less common sequences and those that have not been used to characterize ITS2-type profiles are designated using a unique database ID and their associated clade/genera (e.g., X2409936_C; the latter letter refers to* Cladocopium *genera (Clade C)).*

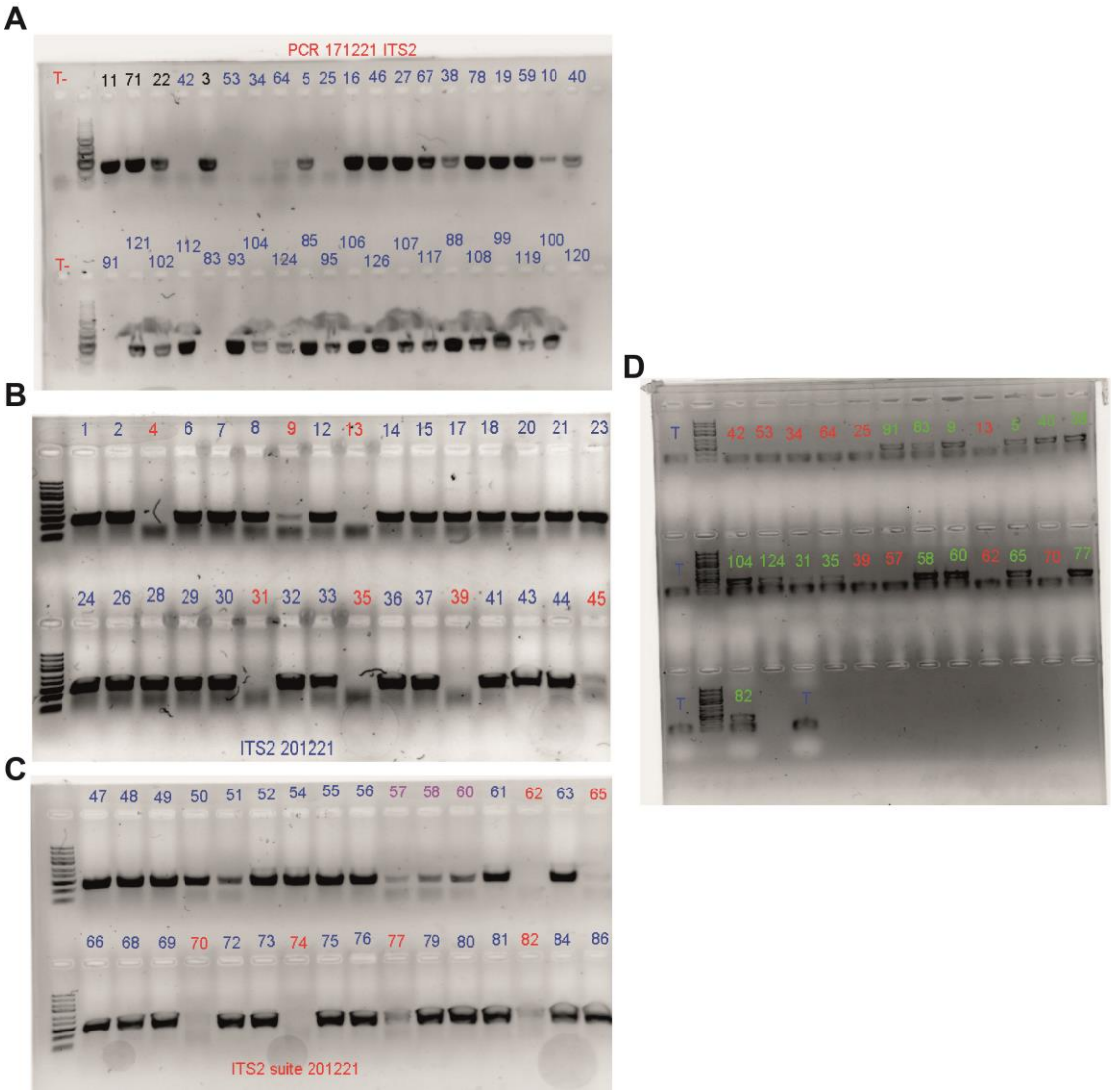

Figure VIII-12 | *Control gels of the PCR. Negative controls are represented with a T. First, we ran random PCR samples on gels (A); after noticing some unsuccessful PCR, we checked all PCR samples from the same session on gels (B & C). The unsuccessful PCR were run again during a new session with adjustments of the hybridation time, and were checked again on gels (D). The remaining unsuccessful PCR (n=10), and those that did not pass the AGRF quality control were removed from the study (n=4), leading to a total of 112 samples for ITS2 sequencing.*

Table VIII-5 | *Time table used by the IKS logger (Timer function) in the Variable condition to mimic the natural pH variation measured at Bouraké. For each time step, IKS activated the pump that supplied seawater from the sump to the experimental tanks at the desired value.*

Step	Time start	Time end	pH sump
1	00:00:00	00:30:00	7.6
2	00:30:00	01:00:00	7.7
3	01:00:00	01:30:00	7.8
4	01:30:00	02:30:00	7.9
5	02:00:00	05:00:00	8.1
6	04:30:00	05:30:00	7.9
7	05:30:00	06:30:00	7.8
8	06:30:00	07:30:00	7.7
9	07:30:00	08:30:00	7.6
10	08:30:00	12:00:00	7.4
11	12:00:00	12:30:00	7.6
12	12:30:00	13:00:00	7.7
13	13:00:00	13:30:00	7.8
14	13:30:00	14:30:00	7.9
15	14:00:00	17:00:00	8.1
16	16:30:00	17:30:00	7.9
17	17:30:00	18:30:00	7.8
18	18:30:00	19:00:00	7.7
19	19:00:00	21:30:00	7.6
20	21:00:00	00:00:00	7.4

Table VIII-6 | *Percentage of irradiance intensity for each of the LED light spectra during a diel cycle (from 6 am to 5 pm).*

Hour	Blue	Royal blue	Cool white	Red	True green	Hyper red	Yellow	Neutral white
05:00:00	0	0	0	0	0	0	0	0
06:00:00	10	10	20	20	0	0	0	20
07:00:00	20	20	40	30	0	0	0	25
08:00:00	30	30	60	45	10	0	10	30
10:00:00	40	40	80	60	10	10	15	40
11:00:00	80	80	90	60	15	25	15	60
12:00:00	100	100	100	60	20	40	20	80
14:30:00	100	100	100	60	20	40	20	80
16:00:00	80	80	40	20	10	20	10	40
16:30:00	60	40	20	10	0	0	0	0
17:00:00	0	0	0	0	0	0	0	0

Table VIII-7 | *Daily measurements of seawater carbonate chemistry during the 100 days of incubation at four pH conditions (Control, pH_{NBS} 8.11; Future, pH_{NBS} 7.76; Extreme, pH_{NBS} 7.54; and Variable, pH_{NBS} 7.56-8.07), for each replicate tank (A, B and C). Seawater carbonate chemistry was calculated using mean values for A_T (2187, 2204, 2202, and 2202 µmol kg^{-1} for Control, Future, Extreme, and Variable conditions, respectively) and the mean salinity value of 35.61.*

		Measured		Calculated				
		Temp (°C)	**pH** (NBS)	***p*CO$_2$** (µatm)	**DIC** (µmol kg^{-1})	**HCO$_3^-$** (µmol kg^{-1})	**CO$_3^{2-}$** (µmol kg^{-1})	**Ω_{arag}**
Control								
Tank A	Mean	26.29	8.11	484	1932	1737	182	2.89
	SD	0.48	0.05	72	29	45	18	0.29
	Min	24.20	7.96	348	1870	1640	136	2.17
	Max	27.30	8.22	719	2007	1851	220	3.49
Tank B	Mean	26.15	8.11	472	1916	1721	182	2.89
	SD	0.49	0.05	67	30	46	18	0.29
	Min	24.20	8.00	299	1825	1579	148	2.34
	Max	27.30	8.27	629	1972	1806	238	3.78
Tank C	Mean	26.26	8.11	481	1930	1734	183	2.90
	SD	0.49	0.06	77	32	50	20	0.31
	Min	24.20	7.97	326	1850	1609	141	2.24
	Max	27.50	8.24	693	1999	1839	232	3.69
Future								
Tank A	Mean	26.15	7.75	1252	2096	1971	90	1.43
	SD	0.54	0.06	172	21	27	11	0.17
	Min	24.20	7.63	797	2027	1878	69	1.09
	Max	27.50	7.92	1673	2139	2024	127	2.02
Tank B	Mean	26.15	7.78	1184	2104	1974	97	1.54
	SD	0.53	0.08	220	21	40	16	0.25
	Min	24.20	7.65	625	2003	1832	73	1.16
	Max	27.20	8.01	1609	2151	2033	154	2.44
Tank C	Mean	26.24	7.77	1186	2091	1964	95	1.51
	SD	0.49	0.07	192	25	33	13	0.21
	Min	24.20	7.66	732	2018	1862	75	1.19
	Max	27.20	7.95	1540	2132	2015	136	2.16
Extreme								
Tank A	Mean	26.31	7.51	2262	2183	2066	55	0.88
	SD	0.48	0.06	354	21	19	8	0.12
	Min	24.30	7.31	1377	2120	2001	35	0.55
	Max	28.00	7.71	3626	2252	2117	81	1.29
Tank B	Mean	26.30	7.55	2070	2169	2051	61	0.97
	SD	0.53	0.09	430	32	35	14	0.22
	Min	23.90	7.38	686	2011	1851	41	0.66
	Max	27.80	7.98	3051	2225	2100	141	2.24
Tank C	Mean	26.38	7.54	2115	2168	2052	59	0.93
	SD	0.49	0.07	335	22	22	9	0.14
	Min	24.30	7.38	1168	2091	1966	41	0.64
	Max	28.30	7.77	3113	2222	2097	93	1.47

Table VIII-7 continued

		Measured		Calculated				
		Temp (°C)	**pH** (NBS)	**pCO_2** (µatm)	**DIC** (µmol kg^{-1})	**HCO_3^-** (µmol kg^{-1})	**CO_3^{2-}** (µmol kg^{-1})	**Ω_{arag}**
Variable								
Tank A	Mean	26.32	7.74	1456	2093	1954	99	1.57
	SD	0.60	0.23	730	94	124	50	0.79
	Min	24.30	7.39	371	1893	1671	42	0.66
	Max	28.30	8.20	2979	2222	2098	212	3.36
Tank B	Mean	26.39	7.76	1379	2088	1949	102	1.62
	SD	0.60	0.22	670	91	121	48	0.77
	Min	24.20	7.40	404	1910	1696	42	0.67
	Max	28.00	8.17	2948	2222	2098	203	3.22
Tank C	Mean	26.46	7.75	1446	2089	1948	101	1.61
	SD	0.52	0.24	733	96	128	51	0.82
	Min	24.40	7.37	412	1912	1701	40	0.63
	Max	28.10	8.16	3179	2229	2102	200	3.17

Table VIII-8 | *Seawater daily measurements of temperature and pH_{NBS} during 100 days in the 6 tank sumps (i.e., pH_T of 7.4, 7.6, 7.7, 7.8, 7.9 and 8.1) that alimented the experimental tanks.*

Sump tank		**Temp (°C)**	**pH_{NBS}**
7.4	Mean	26.26	7.43
	SD	0.47	0.07
7.6	Mean	26.50	7.57
	SD	0.90	0.06
7.7	Mean	26.10	7.68
	SD	0.60	0.08
7.8	Mean	26.51	7.82
	SD	0.88	0.03
7.9	Mean	26.40	7.90
	SD	0.87	0.03
8.1	Mean	26.05	8.06
	SD	0.53	0.04

Table VIII-9 | *Aligned Rank Transformed (ART) ANOVAs (Type III) summary with Kenward-Roger method of linear mixed effects model (LMER) on the effects of temperature, pH and nutrients between pH conditions (Control, pH_{NBS} 8.11; Future, pH_{NBS} 7.76; Extreme, pH_{NBS} 7.54; and Variable, pH_{NBS} 7.56-8.07). Significant values are in bold ($p < 0.05$).*

Fixed factors	*df*	*F*	*p*	**Random factors**	Variance	SD
Temperature	(3, 1206)	9.855	**<0.001**	Tank	0.001	0.039
pH	(3, 1206)	889.130	**<0.001**	Tank	<0.001	0.010
NO_x	(3, 90)	0.588	0.624	Tank	0.000	0.000
PO_4^{3-}	(3, 90)	0.038	0.990	Tank	0.000	0.000
$Si(OH)_4$	(3, 90)	0.040	0.989	Tank	0.000	0.000

Table VIII-10 | *Seawater nutrient contents measured two times a month during the 100 days of incubation at four pH conditions (Control, pH_{NBS} 8.11; Future, pH_{NBS} 7.76; Extreme, pH_{NBS} 7.54; and Variable, pH_{NBS} 7.56-8.07) for each replicated tank (A, B and C).*

pH condition			**NO_x** (µmol L^{-1})	**PO_4^{3-}** (µmol L^{-1})	**$Si(OH)_4$** (µmol L^{-1})
Control	Tank A	Mean	0.56	0.30	2.86
		SD	0.20	0.04	1.07
		Min	0.31	0.26	1.86
		Max	0.84	0.35	4.92
	Tank B	Mean	0.52	0.30	2.71
		SD	0.17	0.06	1.20
		Min	0.28	0.19	1.49
		Max	0.79	0.36	5.12
	Tank C	Mean	0.68	0.30	2.92
		SD	0.26	0.04	1.39
		Min	0.35	0.25	1.18
		Max	1.08	0.37	5.65
Future	Tank A	Mean	0.71	0.31	3.00
		SD	0.31	0.07	1.44
		Min	0.33	0.22	1.07
		Max	1.21	0.41	5.63
	Tank B	Mean	0.64	0.30	2.83
		SD	0.19	0.05	1.01
		Min	0.36	0.22	1.68
		Max	0.87	0.38	4.54
	Tank C	Mean	0.65	0.31	2.84
		SD	0.26	0.05	1.22
		Min	0.40	0.21	1.01
		Max	1.14	0.39	4.70
Extreme	Tank A	Mean	0.63	0.30	2.85
		SD	0.21	0.03	1.27
		Min	0.39	0.25	1.01
		Max	0.93	0.33	5.31
	Tank B	Mean	0.68	0.30	2.97
		SD	0.23	0.05	1.37
		Min	0.37	0.24	0.85
		Max	1.06	0.41	5.58
	Tank C	Mean	0.57	0.31	2.56
		SD	0.18	0.04	1.11
		Min	0.21	0.25	1.03
		Max	0.76	0.38	4.66
Variable	Tank A	Mean	0.60	0.30	2.79
		SD	0.15	0.03	0.89
		Min	0.40	0.24	1.81
		Max	0.90	0.34	4.27
	Tank B	Mean	0.67	0.30	2.80
		SD	0.17	0.04	1.25
		Min	0.48	0.26	1.63
		Max	0.93	0.39	5.13
	Tank C	Mean	0.68	0.31	2.78
		SD	0.29	0.04	1.17
		Min	0.32	0.27	1.76
		Max	1.23	0.39	5.12

Table VIII-11 | *Two-way ANOVAs (type III) summary with Satterthwaite's method of linear mixed effect model (LMER) on the effects of colony origin (Bouraké and reference), pH conditions (Control, pH_{NBS} 8.11; Future, pH_{NBS} 7.76; Extreme, pH_{NBS} 7.54; and Variable, pH_{NBS} 7.56-8.07), and their interactions for each coral species and for each physiological measurement. When a significant effect was found on pH (4 levels: Control, Future, Extreme and Variable), we used a post-hoc Tukey HSD. Non-parametric two-way Aligned Rank Transformed (ART) ANOVA (Type III) with Kenward-Roger method followed by a Bonferroni p-levels adjusted post hoc was used for F_v/F_m. For simplicity, Control = 8.1; Future = 7.8; Extreme = 7.5; Variable = Var; R = reference; B = Bouraké. Significant values are in bold (p < 0.05).*

Species	*Fixed factors*	*df*	*F*	*p*	*Post hoc*
A) Growth rate					
A. tenuis	Origin	1	9.334	**0.003**	
	pH	3	3.429	**0.020**	8.1 > Var ($p < 0.05$)
	Origin x pH	3	0.809	0.491	
	Residuals	111			
	Random factor		*Variance*	*SD*	
	Tank		0.000	0.000	
	Fixed factors	*df*	*F*	*p*	*Post hoc*
M. digitata	Origin	1	27.563	<**0.001**	
	pH	3	2.203	0.092	
	Origin x pH	3	0.760	0.519	
	Residuals	107			
	Random factor		*Variance*	*SD*	
	Tank		0.000	0.000	
	Fixed factors	*df*	*F*	*p*	*Post hoc*
Porites sp.	Origin	1	18.407	<**0.001**	
	pH	3	2.787	**0.044**	8.1 > 7.5 ($p < 0.05$)
	Origin x pH	3	0.843	0.473	
	Residuals	110			
	Random factor		*Variance*	*SD*	
	Tank		0.000	0.000	
B) F_v/F_m	*Fixed factors*	*df*	*F*	*p*	*Post hoc*
A. tenuis	Origin	1	11.213	**0.001**	
	pH	3	3.517	**0.018**	7.8 = 7.5 > 8.1 ($p < 0.05$)
	Origin X pH	3	0.330	0.803	
	Residuals	108			
	Random factor		*Variance*	*SD*	
	Tank		<0.001	0.007	
	Fixed factors	*df*	*F*	*p*	*Post hoc*
M. digitata	Origin	1	0.132	0.717	
	pH	3	0.615	0.606	
	Origin X pH	3	1.660	0.180	
	Residuals	107			
	Random factor		*Variance*	*SD*	
	Tank		0.000	0.000	

Table VIII-11 continued

Species	*Fixed factor*	*df*	*F*	*p*	*Post hoc*
Porites sp.	Origin	1	1.207	0.274	
	pH	3	0.691	0.559	
	Origin X pH	3	0.222	0.881	
	Residuals	107			
	Random factor		*Variance*	*SD*	
	Tank		<0.001	0.012	
C) ETR_{max}	*Fixed factors*	*df*	*F*	*p*	*Post hoc*
A. tenuis	Origin	1	16.449	<**0.001**	
	pH	3	1.038	0.379	
	Origin x pH	3	0.134	0.939	
	Residuals	108			
	Random factor		*Variance*	*SD*	
	Tank		0.000	0.000	
	Fixed factors	*df*	*F*	*p*	*Post hoc*
M. digitata	Origin	1	0.032	0.858	
	pH	3	0.890	0.445	
	Origin x pH	3	0.874	0.457	
	Residuals	107			
	Random factor		*Variance*	*SD*	
	Tank		1.422	1.192	
	Fixed factors	*df*	*F*	*p*	*Post hoc*
Porites sp.	Origin	1	0.051	0.822	
	pH	3	0.647	0.586	
	Origin x pH	3	0.602	0.615	
	Residuals	107			
	Random factor		*Variance*	*SD*	
	Tank		0.000	0.000	
D) P_g	*Fixed factors*	*df*	*F*	*p*	*Post hoc*
A. tenuis	Origin	1	3.609	0.063	
	pH	3	4.375	**0.008**	8.1 < 7.8 ($p < 0.01$)
	Origin x pH	3	1.265	0.297	
	Residuals	48			
	Random factor		*Variance*	*SD*	
	Tank		0.000	0.000	
	Fixed factors	*df*	*F*	*p*	*Post hoc*
M. digitata	Origin	1	0.376	0.543	
	pH	3	2.001	0.126	
	Origin x pH	3	2.240	0.096	
	Residuals	48			

Table VIII-11 continued

	Random factor		*Variance*	*SD*	
	Tank		0.000	0.000	
	Fixed factors	*df*	*F*	*p*	*Post hoc*
Porites sp.	Origin	1	7.277	**0.010**	
	pH	3	8.503	**<0.001**	8.1 = 7.8 < Var = 7.5 ($p < 0.04$)
	Origin x pH	3	2.771	0.052	
	Residuals	48			
	Random factor		*Variance*	*SD*	
	Tank		0.000	0.000	
E) R_{dark}	*Fixed factors*	*df*	*F*	*p*	*Post hoc*
A. tenuis	Origin	1	5.585	**0.022**	
	pH	3	5.538	**0.002**	Var = 8.1 < 7.8 = 7.5 ($p < 0.03$)
	Origin x pH	3	1.211	0.316	
	Residuals	48			
	Random factor		*Variance*	*SD*	
	Tank		0.000	0.000	
	Fixed factors	*df*	*F*	*p*	*Post hoc*
M. digitata	Origin	1	0.133	0.717	
	pH	3	1.786	0.163	
	Origin x pH	3	0.862	0.468	
	Residuals	48			
	Random factor		*Variance*	*SD*	
	Tank		<0.001	0.013	
	Fixed factors	*df*	*F*	*p*	*Post hoc*
Porites sp.	Origin	1	7.436	**0.009**	
	pH	3	3.676	**0.018**	8.1 < 7.5 (p < 0.02)
	Origin x pH	3	1.067	0.372	
	Residuals	48			
	Random factor		*Variance*	*SD*	
	Tank		0.000	0.000	
F) P_g : R	*Fixed factors*	*df*	*F*	*p*	*Post hoc*
A. tenuis	Origin	1	0.874	0.355	
	pH	3	1.658	0.188	
	Origin x pH	3	2.274	0.092	
	Residuals	48			
	Random factor		*Variance*	*SD*	
	Tank		0.000	0.000	
	Fixed factors	*df*	*F*	*p*	*Post hoc*
M. digitata	Origin	1	0.143	0.706	
	pH	3	0.579	0.632	
	Origin x pH	3	1.285	0.291	

Table VIII-11 continued

Species	*Fixed factor*	*df*	*F*	*p*	*Post hoc*
	Residuals	48			
	Random factor		*Variance*	*SD*	
	Tank		<0.001	0.023	
Porites sp.	Origin	1	0.012	0.912	
	pH	3	2.728	0.054	
	Origin x pH	3	1.132	0.346	
	Residuals	48			
	Random factor		*Variance*	*SD*	
	Tank		0.000	0.000	
G) Symbiont	*Fixed factors*	*df*	*F*	*p*	*Post hoc*
A. tenuis	Origin	1	5.870	**0.015**	
	pH	3	2.700	**0.044**	
	Origin x pH	3	2.860	**0.035**	R 7.5 > B Var ($p < 0.05$)
	Residuals	54			
	Random factor		*Variance*	*SD*	
	Tank		0.000	0.000	
	Fixed factors	*df*	*F*	*p*	*Post hoc*
M. digitata	Origin	1	0.005	0.946	
	pH	3	1.987	0.113	
	Origin x pH	3	1.335	0.261	
	Residuals	48			
	Random factor		*Variance*	*SD*	
	Tank		0.000	0.000	
	Fixed factors	*df*	*F*	*p*	*Post hoc*
Porites sp.	Origin	1	2.707	0.100	
	pH	3	1.237	0.294	
	Origin x pH	3	2.622	**0.049**	R 7.5 > B 7.5 ($p < 0.05$)
	Residuals	54			
	Random factor		*Variance*	*SD*	
	Tank		>9.999	>9.999	
H) Total chl	*Fixed factors*	*df*	*F*	*p*	*Post hoc*
A. tenuis	Origin	1	10.695	**0.002**	
	pH	3	2.652	0.058	
	Origin x pH	3	1.319	0.278	
	Residuals	54			
	Random factor		*Variance*	*SD*	
	Tank		0.000	0.000	
	Fixed factors	*df*	*F*	*p*	*Post hoc*

Table VIII-11 continued

Species	*Fixed factor*	*df*	*F*	*p*	*Post hoc*
M. digitata	Origin	1	0.064	0.802	
	pH	3	0.378	0.770	
	Origin:pH	3	0.872	0.462	
	Residuals	48			
	Random factor		*Variance*	*SD*	
	Tank		0.000	0.000	
Porites sp.	Origin	1	0.316	0.576	
	pH	3	1.560	0.210	
	Origin:pH	3	3.155	**0.032**	
	Residuals	54			
	Random factor		*Variance*	*SD*	
	Tank		0.000	0.000	
I) Proteins	*Fixed factors*	*df*	*F*	*p*	*Post hoc*
A. tenuis	Origin	1	1.047	0.311	
	pH	3	3.263	**0.029**	8.1 > Var ($p < 0.04$)
	Origin:pH	3	0.522	0.669	
	Residuals	48			
	Random factor		*Variance*	*SD*	
	Tank		0.000	0.000	
	Fixed factors	*df*	*F*	*p*	*Post hoc*
M. digitata	Origin	1	0.945	0.336	
	pH	3	1.928	0.138	
	Origin:pH	3	0.439	0.726	
	Residuals	48			
	Random factor		*Variance*	*SD*	
	Tank		0.049	0.221	
	Fixed factors	*df*	*F*	*p*	*Post hoc*
Porites sp.	Origin	1	0.654	0.423	
	pH	3	5.782	**0.002**	8.1 > Var = 7.7 ($p < 0.01$)
	Origin:pH	2	0.848	0.436	
	Residuals	40			
	Random factor		*Variance*	*SD*	
	Tank		0.000	0.000	

Appendix Article n°3 - Chapter 5

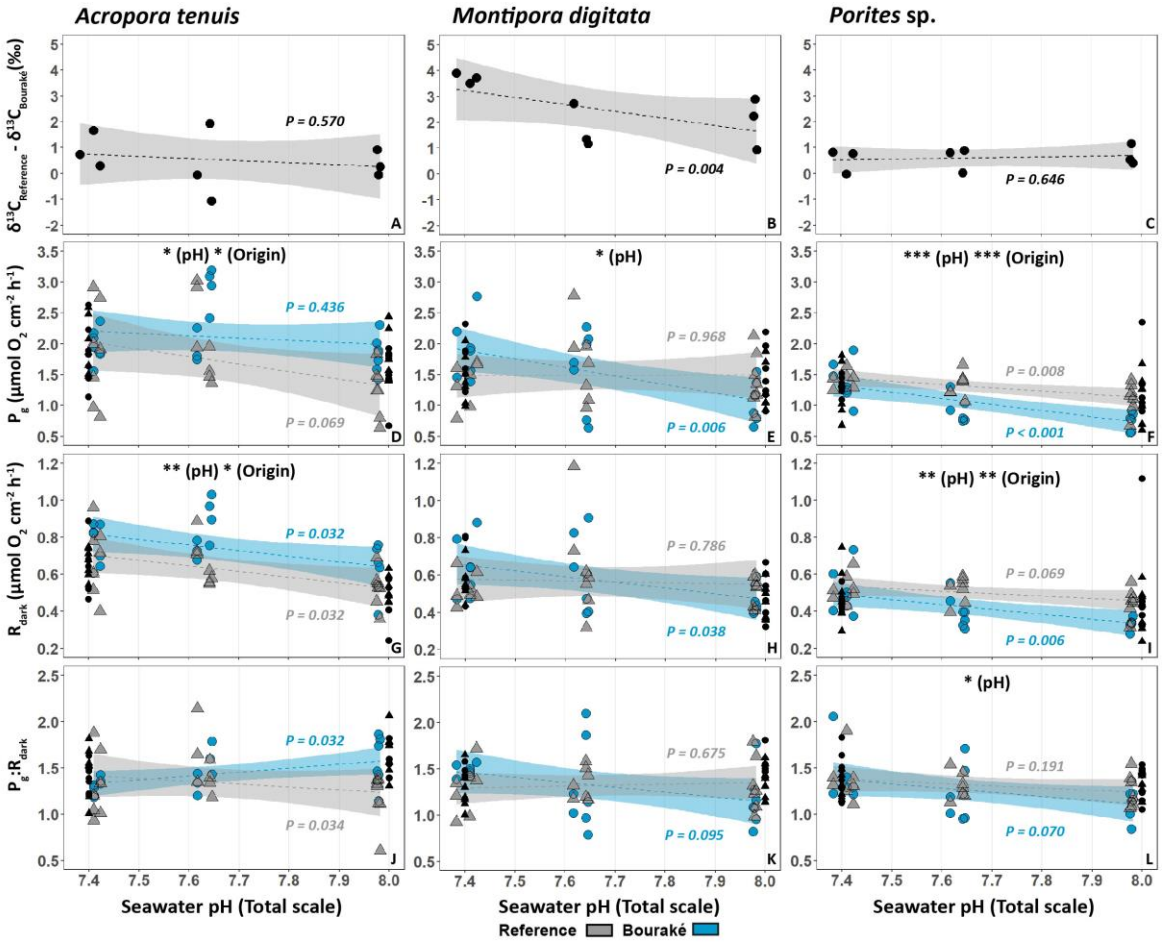

Figure VIII-13 | *$\delta^{13}C_{Reference}$ - $\delta^{13}C_{Bouraké}$ (**A-C**), Gross photosynthesis (P_g) (**D-F**), dark respiration (R_{dark}) (**G-I**), and P_g:R_{dark} ratios (**J-L**) of Acropora tenuis, Montipora digitata and Porites sp. measured at the experimental pH_{sw} conditions. Black dots represent the difference between $\delta^{13}C_{Reference}$ and $\delta^{13}C_{Bouraké}$. Blue circles and grey triangles correspond to Bouraké and Reference colonies, respectively. Largest symbols represent averaged values, while the smallest symbols represent data for each individual colony. Dashed lines represent linear model regressions fitted using linear model function in RStudio with 95% confidence intervals represented by the envelopes. (n=7 per pH conditions, parameters, site of origin and species). The black symbols (dots for Bouraké and triangle for Reference) represent data for the Variable pH condition (incubated for photosynthesis and respiration rates measurements at both Extreme (7.53) and Control (8.11) pH) and are not included in the regressions. Stars represent statistical significance (Appendix Table VIII-14). Please, note that data in panels **D-L** comes from the study of chapter 4.*

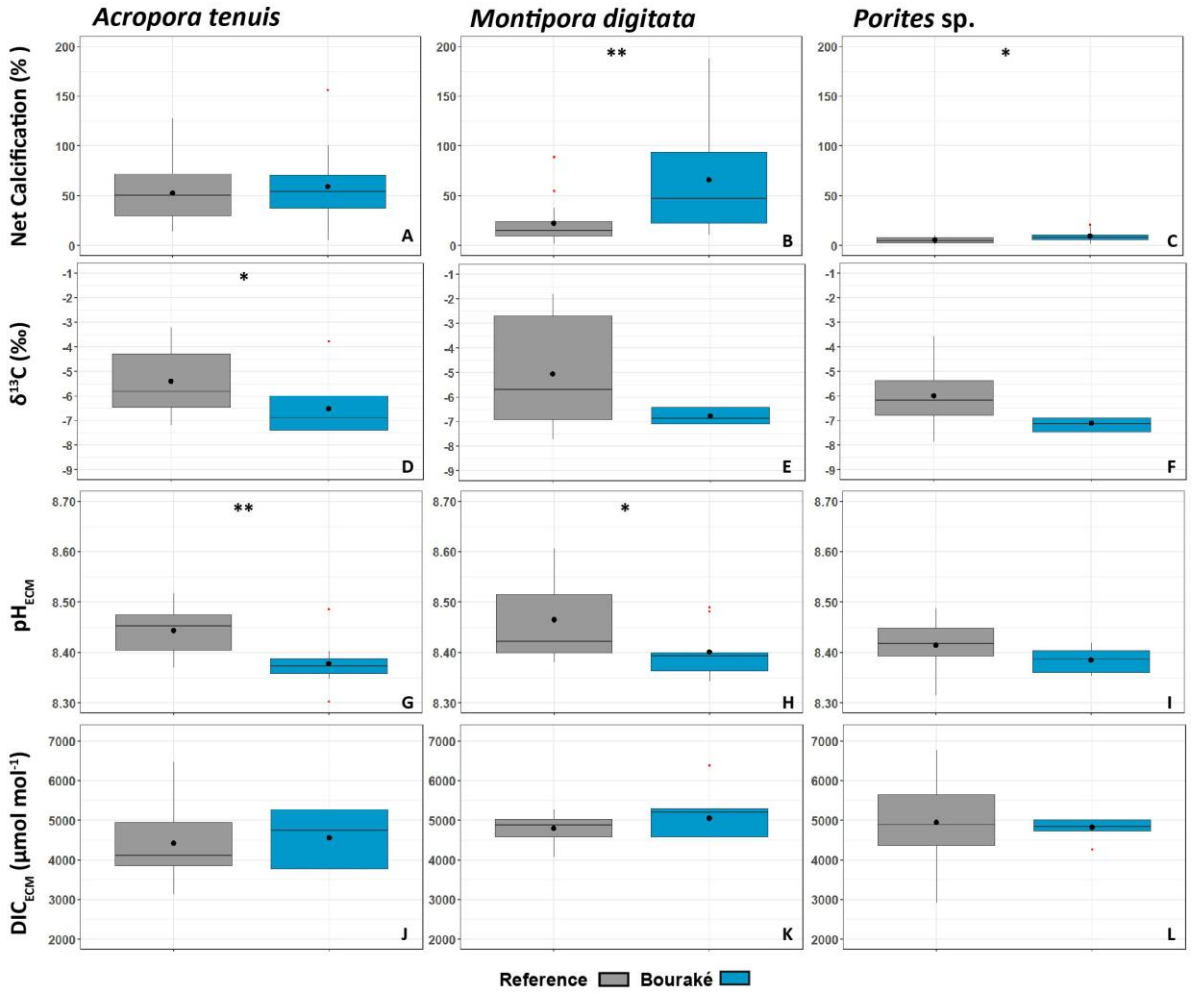

Figure VIII-14 | *Comparisons according to colony origin (Bouraké and Reference) for the Variable pH condition. Net calcification (**A-C**), $\delta^{13}C$ (**D-F**), pH_{ECM} (**G-I**), and DIC_{ECM} (**J-L**) of Acropora tenuis, Montipora digitata and Porites sp. (n=7-16 depending on parameters, site of origin and species). Data are median values ± 25th and 75th percentiles (box), minimum and maximum values (whiskers), mean values (black dots) and outliers (red dots). Stars represent statistical significance at p < 0.05 (*) and p < 0.01 (**); see Appendix Table VIII-15.*

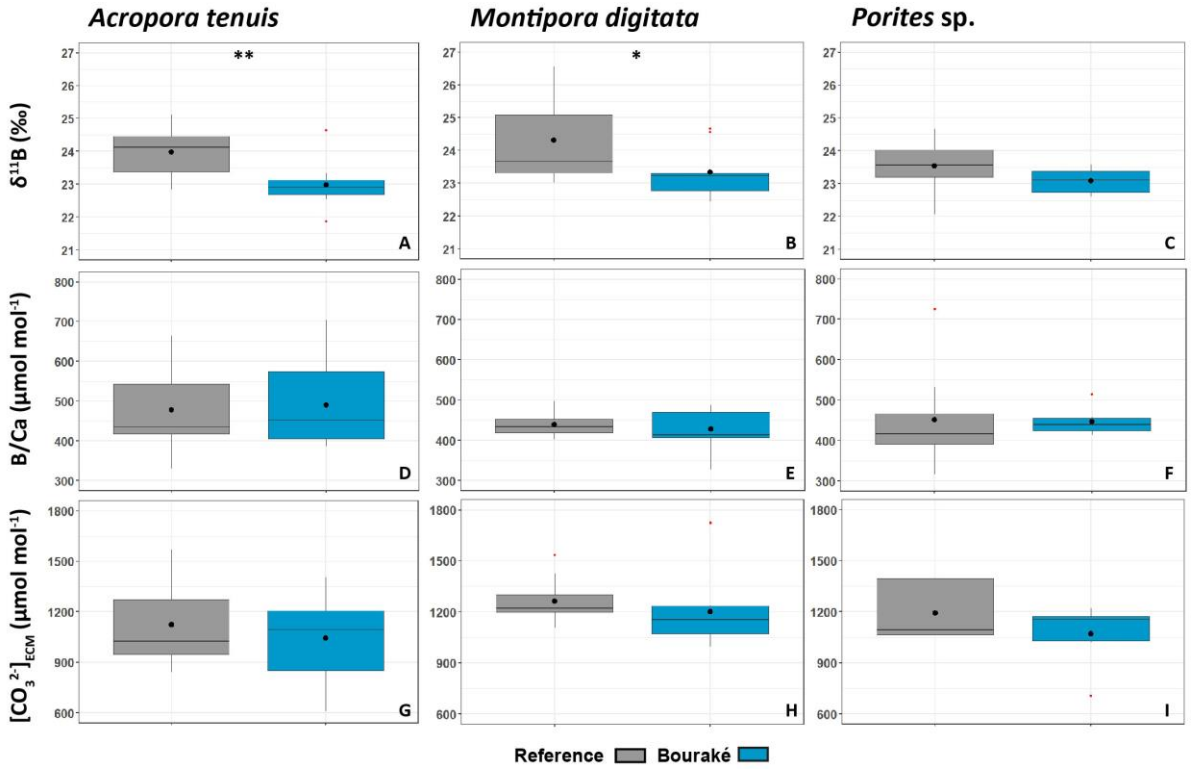

Figure VIII-15 | *Comparisons according to colony origin (Bouraké and Reference) for the Variable pH condition. $\delta^{11}B$ (**A-C**), B/Ca (**D-F**), $[CO_3^{2-}]_{ECM}$ (**G-I**) of Acropora tenuis, Montipora digitata and Porites sp. (n=7-13 depending on parameters, site of origin and species). Data are median values ± 25th and 75th percentiles (box), minimum and maximum values (whiskers), mean values (black dots) and outliers (red dots). Stars represent statistical significance at p < 0.05 (*) and p < 0.01 (**); see Appendix Table VIII-15.*

Table VIII-12 | *Results of Two-way ANOVAs testing the effects of colony origins (Bouraké and Reference sites), pH treatments (Extreme, pH_{NBS} 7.54; Future, pH_{NBS} 7.76; Control, pH_{NBS} 8.11), and their interactions for the three coral species. Significant values are in bold (p < 0.05). Post hoc comparisons were performed on significant interactions (Tukey HSD) between pH and origin.*

Species	*Factor*	*df*	*F*	*p*	*Post hoc (Tukey HSD)*
Net Calcification					
A. tenuis	Origin	1	9.548	**0.003**	
	pH	1	2.493	0.118	
	O x pH	1	0.015	0.902	
	Residuals	85			
M. digitata	Origin	1	19.711	<**0.001**	
	pH	1	2.008	0.160	
	O x pH	1	0.303	0.583	
	Residuals	81			
Porites sp.	Origin	1	12.399	<**0.001**	
	pH	1	6.534	**0.012**	
	O x pH	1	2.245	0.138	
	Residuals	85			

Table VIII-12 continued

Species	*Factor*	*df*	*F*	*p*	*Post hoc (Tukey HSD)*
$\delta^{13}C$					
A. tenuis	Origin	1	2.225	0.142	
	pH	1	46.556	<**0.001**	
	O x pH	1	0.211	0.648	
	Residuals	52			
M. digitata	Origin	1	31.495	<**0.001**	
	pH	1	16.504	<**0.001**	
	O x pH	1	1.792	0.186	
	Residuals	52			
Porites sp.	Origin	1	6.596	**0.014**	
	pH	1	180.919	<**0.001**	
	O x pH	1	0.115	0.736	
	Residuals	38			
$\delta^{11}B$					
A. tenuis	Origin	1	7.016	**0.010**	
	pH	1	12.444	<**0.001**	
	O x pH	1	0.130	0.719	
	Residuals	52			
M. digitata	Origin	1	45.623	<**0.001**	
	pH	1	6.861	**0.011**	
	O x pH	1	1.669	0.202	
	Residuals	51			
Porites sp.	Origin	1	0.091	0.764	
	pH	1	274.779	<**0.001**	
	O x pH	1	1.044	0.313	
	Residuals	38			
pH_{ECM}					
A. tenuis	origin	1	6.457	**0.014**	
	pH	1	13.283	<**0.001**	
	O x pH	1	0.116	0.734	
	Residuals	52			
M. digitata	Origin	1	44.803	<**0.001**	
	pH	1	7.931	**0.006**	
	O x pH	1	1.617	0.209	
	Residuals	51			
Porites sp.	Origin	1	0.134	0.717	
	pH	1	277.028	<**0.001**	
	O x pH	1	1.114	0.298	
	Residuals	38			

Table VIII-12 continued

Species	*Factor*	*df*	*F*	*p*	*Post hoc (Tukey HSD)*
B/Ca					
A. tenuis	Origin	1	1.019	0.317	
	pH	1	1.612	0.210	
	O x pH	1	0.033	0.856	
	Residuals	52			
M. digitata	Origin	1	5.177	**0.027**	
	pH	1	0.014	0.907	
	O x pH	1	0.337	0.564	
	Residuals	51			
Porites sp.	Origin	1	0.614	0.438	
	pH	1	9.881	**0.003**	
	O x pH	1	2.421	0.128	
	Residuals	37			
$[CO_3]^{2-}_{ECM}$					
A. tenuis	Origin	1	0.024	0.877	
	pH	1	5.165	**0.027**	
	O x pH	1	0.081	0.777	
	Residuals	52			
M. digitata	Origin	1	1.515	0.224	
	pH	1	1.493	0.227	
	O x pH	1	0.039	0.843	
	Residuals	51			
Porites sp.	Origin	1	0.199	0.658	
	pH	1	0.154	0.697	
	O x pH	1	1.045	0.313	
	Residuals	37			
DIC_{ECM}					
A. tenuis	Origin	1	1.299	0.261	
	pH	1	1.708	0.197	
	O x pH	1	0.089	0.767	
	Residuals	52			
M. digitata	Origin	1	6.747	**0.012**	
	pH	1	0.289	0.593	
	O x pH	1	0.379	0.541	
	Residuals	51			
Porites sp.	Origin	1	0.551	0.462	
	pH	1	11.003	**0.002**	
	O x pH	1	2.196	0.147	
	Residuals	37			

Table VIII-13 | *$\delta^{11}B$ of the seawater measured in-situ at Bouraké and Reference (A) and during the aquaria experiment in each tank condition (B). Mean pH values measured are presented as mean ± SD for B. $\delta^{13}C$ of the two CO_2 gas bottles used during the aquaria experiments (C) with each replicate equivalent to n=3-5 sampling made through the length of the experiment.*

A)

Site	pH_{NBS}	$\delta^{11}Bsw$ (‰)	2SD (‰)
B2	8.01	39.87	0.23
B2	7.43	39.31	0.19
B2	7.60	39.57	0.17
R1	8.04	39.65	0.13

B)

Tank			
Ambient	8.11 ± 0.05	39.71	0.29
Extreme	7.54 ± 0.08	39.72	0.28
Future	7.76 ± 0.07	39.93	0.27
Variable	7.75 ± 0.23	40.04	0.26

C)

CO_2 bottle	Replicate	$\delta^{13}C$ (‰)	SE (‰)
N°1	A	-22.22	0.49
	B	-21.81	0.84
N°2	A	-17.37	0.03
	B	-17.10	0.34

Table VIII-14 | *Results of a Wilcoxon test testing the effect of pH on $\delta^{13}C_{Reference}$ - $\delta^{13}C_{Bouraké}$ (A). Results of Two-way ANOVAs testing the effects of colony origin (Bouraké and Reference); pH treatments (Extreme, pH_{NBS} 7.54; Future, pH_{NBS} 7.76; Control, pH_{NBS} 8.11), and their interactions for the three coral species (B). Significant values are in bold (p < 0.05). Post hoc comparisons were performed on significant interactions (Tukey HSD) between pH and origin.*

Species	*Factor*	*df*	*W*	*p*
A)				
$\delta^{13}C_{Reference}$ - $\delta^{13}C_{Bouraké}$				
A. tenuis	pH	8	35.000	0.164
M. digitata	pH	8	25.649	**0.004**
Porites sp.	pH	8	44.000	**0.008**

Species	*Factor*	*df*	*F*	*p*	*Post hoc (Tukey HSD)*
B)					
P_g					

Table VIII-14 continued

Species	*Factor*	*df*	*F*	*p*	*Post hoc (Tukey HSD)*
P_g					
A. tenuis	Origin	1	4.853	**0.034**	
	pH	1	4.109	**0.049**	
	O x pH	1	1.176	0.285	
	Residuals	38			
M.digitata	Origin	1	0.031	0.861	
	pH	1	4.497	**0.040**	
	O x pH	1	4.777	**0.035**	
	Residuals	38			
Porites sp.	Origin	1	13.506	<**0.001**	
	pH	1	26.319	<**0.001**	
	O x pH	1	2.431	0.127	
	Residuals	38			
R_{dark}					
A. tenuis	Origin	1	6.867	**0.012**	
	pH	1	10.754	**0.002**	
	O x pH	1	0.000	0.996	
	Residuals	38			
M.digitata	Origin	1	0.013	0.912	
	pH	1	2.773	0.104	
	O x pH	1	1.572	0.218	
	Residuals	38			
Porites sp.	Origin	1	9.973	**0.003**	
	pH	1	13.080	**<0.001**	
	O x pH	1	1.507	0.227	
	Residuals	38			
P_g:R_{dark}					
A. tenuis	Origin	1	1.714	0.198	
	pH	1	0.090	0.765	
	O x pH	1	4.028	0.052	
	Residuals	38			
M.digitata	Origin	1	0.002	0.969	
	pH	1	1.334	0.255	
	O x pH	1	2.783	0.104	
	Residuals	38			
Porites sp.	Origin	1	0.821	0.371	
	pH	1	5.526	**0.024**	
	O x pH	1	0.493	0.487	
	Residuals	38			

Table VIII-15 | *Probability values of non-parametric Wilcoxon tests testing the effects of colony origin (Bouraké and Reference) on geochemical data obtained in the Variable pH treatment, for the three coral species. Significant values are in bold (p < 0.05).*

Site	*Category*	*df*	*W*	*p*
Bouraké vs Reference				
A. tenuis	Net Calcification	(1, 28)	126	0.595
	$\delta^{13}C$	(1, 18)	21	**0.031**
	$\delta^{11}B$	(1, 18)	85	**0.007**
	B/Ca	(1, 21)	65	1.000
	pH_{ECM}	(1, 18)	15	**0.007**
	$[CO_3^{2-}]_{ECM}$	(1, 18)	57	0.630
	DIC_{ECM}	(1, 18)	58	0.579
M. digitata	Net Calcification	(1, 28)	184	**0.002**
	$\delta^{13}C$	(1, 18)	31	0.175
	$\delta^{11}B$	(1, 18)	76	**0.046**
	B/Ca	(1, 18)	57	0.602
	pH_{ECM}	(1, 18)	23	**0.048**
	$[CO_3^{2-}]_{ECM}$	(1, 18)	69	0.152
	DIC_{ECM}	(1, 18)	62	0.370
***Porites* sp.**	Net Calcification	(1, 29)	174	**0.033**
	$\delta^{13}C$	(1, 12)	12	0.128
	$\delta^{11}B$	(1, 12)	38	0.097
	B/Ca	(1, 13)	20	0.397
	pH_{ECM}	(1, 12)	11	0.097
	$[CO_3^{2-}]_{ECM}$	(1, 12)	31	0.456
	DIC_{ECM}	(1, 12)	20	0.620

Table VIII-16 | *Measured values of $\delta^{13}C$, $\delta^{11}B$ and elemental ratios (B/Ca) within the skeletons of A. tenuis, M. digitata and Porites sp. and corresponding reconstructed parameters of the extracellular calcifying medium (pH_{ECM} (total scale) and DIC_{ECM}).*

pH_{NBS}	Tank	Specie	Site	NetCal (%)	n	$\delta^{13}C$ (‰)	SD	$\delta^{11}B$ (‰)	SD	pH_{ECM}	SD	n	B/Ca_{carb} (µmol mol^{-1})	SD	DIC_{ECM} (µmol mol^{-1})	SD	n
7.513	**A**	*A. tenuis*	BOURAKE	72.33	5	-7.37	1.12	23.00	0.70	8.40	0.05	3	548	89	3975	661	3
		M. digitata	BOURAKE	35.80	4	-8.05	0.86	23.25	0.47	8.42	0.03	3	425	105	5290	1573	3
		Porites sp.	BOURAKE	5.07	5	-8.36	1.01	22.28	0.05	8.35	0.00	2	443	115	5068	1337	2
		A. tenuis	REFERENCE	47.33	5	-6.64	2.95	23.66	1.93	8.44	0.12	3	496	91	4356	646	3
		M. digitata	REFERENCE	8.46	5	-4.15	2.82	25.40	2.14	8.55	0.14	3	519	42	3974	238	3
		Porites sp.	REFERENCE	4.63	6	-7.54	0.42	22.10	0.00	8.34	0.00	2	450	4	4843	49	2
7.553	**B**	*A. tenuis*	BOURAKE	80.55	5	-8.08	0.42	22.34	0.10	8.36	0.01	3	485	45	4488	444	3
		M. digitata	BOURAKE	36.85	4	-6.91	0.71	23.51	0.71	8.43	0.05	3	403	87	5502	1426	3
		Porites sp.	BOURAKE	6.25	5	-8.46	0.41	22.31	0.12	8.35	0.01	2	517	46	4201	371	2
		A. tenuis	REFERENCE	58.17	5	-7.78	0.74	23.04	0.67	8.40	0.04	3	595	94	3657	583	3
		M. digitata	REFERENCE	14.29	6	-3.20	2.16	24.86	0.50	8.52	0.03	2	500	105	5033	1203	2
		Porites sp.	REFERENCE	3.30	5	-7.69	0.47	22.03	0.99	8.33	0.07	3	421	89	5320	1045	3
7.540	**C**	*A. tenuis*	BOURAKE	60.96	5	-6.77	0.99	23.13	0.55	8.41	0.04	3	435	97	5091	1161	3
		M. digitata	BOURAKE	33.87	5	-7.79	0.69	22.72	0.43	8.38	0.03	3	396	78	5603	1282	3

		Specie	Site	NetCal (%)	n	$\delta^{13}C$ (‰)	SD	$\delta^{11}B$ (‰)	SD	pH_{ECM}	SD	n	B/Ca_{carb} ($\mu mol\ mol^{-1}$)	SD	DIC_{ECM} ($\mu mol\ mol^{-1}$)	SD	n
7.540	**C**	*Porites* sp.	BOURAKE	7.84	5	-8.54	0.26	22.29	0.65	8.35	0.04	3	453	115	4995	1263	3
		A. tenuis	REFERENCE	53.63	5	-5.11	2.48	23.42	1.42	8.43	0.09	3	564	82	3820	527	3
		M. digitata	REFERENCE	11.05	5	-4.29	4.01	25.18	2.19	8.54	0.08	3	457	123	4813	1707	3
		Porites sp.	REFERENCE	6.21	5	-8.56	0.81	21.70	0.23	8.31	0.02	2	399	72	5983	1272	2
7.747	**A**	*A. tenuis*	BOURAKE	90.37	4	-7.10	0.91	23.18	0.39	8.40	0.03	3	572	172	4033	1430	3
		M. digitata	BOURAKE	45.47	5	-6.18	1.35	23.80	0.47	8.44	0.03	4	444	53	4834	601	4
		Porites sp.	BOURAKE	8.74	5	-6.08	0.34	23.14	0.30	8.40	0.02	2	509	86	4274	713	2
		A. tenuis	REFERENCE	62.89	5	-7.15	0.10	22.73	0.50	8.37	0.03	3	517	121	4357	1206	3
		M. digitata	REFERENCE	20.20	5	-3.45	0.31	25.69	0.90	8.56	0.06	3	493	65	4193	545	3
		Porites sp.	REFERENCE	4.63	4	-5.27	1.66	24.02	0.69	8.46	0.04	2	422	138	5294	1684	2
7.776	**B**	*A. tenuis*	BOURAKE	103.67	5	-6.12	0.26	22.14	1.03	8.33	0.07	3	465	65	4740	691	3
		M. digitata	BOURAKE	43.48	5	-5.99	0.92	22.69	0.87	8.37	0.06	3	416	66	5278	881	3
		Porites sp.	BOURAKE	9.70	5	-7.50	0.20	23.23	0.58	8.40	0.04	3	496	93	4429	890	3
		A. tenuis	REFERENCE	73.56	5	-7.17	0.61	23.42	0.22	8.42	0.01	3	455	126	4978	1518	3
		M. digitata	REFERENCE	15.65	5	-4.82	2.97	25.17	1.46	8.53	0.09	4	447	71	4711	737	4
		Porites sp.	REFERENCE	5.88	5	-6.61	ND	23.09	ND	8.39	ND	1	617	ND	3474	ND	1
7.772	**C**	*A. tenuis*	BOURAKE	100.93	5	-7.45	0.26	23.09	0.42	8.39	0.02	3	619	114	3543	696	3
		M. digitata	BOURAKE	45.70	5	-6.21	0.49	23.85	0.28	8.44	0.02	4	469	31	4532	321	4
		Porites sp.	BOURAKE	9.49	5	-6.75	0.83	23.76	0.15	8.44	0.01	2	603	81	3543	475	2
		A. tenuis	REFERENCE	59.37	5	-5.51	2.61	23.68	0.99	8.43	0.04	3	587	147	3786	1056	3
		M. digitata	REFERENCE	21.12	5	-4.86	2.83	24.96	0.76	8.51	0.05	3	483	62	4333	502	3
		Porites sp.	REFERENCE	4.89	5	-6.72	0.96	23.32	0.34	8.41	0.02	4	464	98	4802	1248	4
8.106	**A**	*A. tenuis*	BOURAKE	94.66	5	-4.66	0.61	23.42	0.35	8.43	0.02	4	474	119	4717	1165	4
		M. digitata	BOURAKE	37.99	5	-4.97	0.80	24.12	0.30	8.47	0.02	3	402	52	5312	691	3
		Porites sp.	BOURAKE	11.42	5	-4.44	0.42	25.07	0.40	8.54	0.02	2	590	54	3525	306	2
		A. tenuis	REFERENCE	70.74	5	-3.73	0.54	24.30	1.35	8.49	0.09	4	512	115	4333	1334	4
		M. digitata	REFERENCE	26.46	5	-2.73	0.24	25.39	0.30	8.56	0.02	3	437	74	4813	822	3
		Porites sp.	REFERENCE	5.89	4	-3.91	0.54	25.10	0.67	8.54	0.04	2	397	ND	5187	ND	1
8.112	**B**	*A. tenuis*	BOURAKE	83.43	5	-4.28	0.88	23.72	0.60	8.45	0.04	3	492	69	4388	722	3
		M. digitata	BOURAKE	40.66	4	-4.79	0.28	24.10	0.14	8.48	0.01	3	404	73	4714	772	3
		Porites sp.	BOURAKE	11.24	5	-4.09	0.58	25.50	0.26	8.55	0.02	2	479	196	4708	1918	2
		A. tenuis	REFERENCE	71.63	5	-4.02	0.85	24.50	0.55	8.50	0.03	3	473	139	4722	1531	3
		M. digitata	REFERENCE	24.65	3	-3.86	0.28	25.15	0.36	8.54	0.02	3	468	36	4444	386	3
		Porites sp.	REFERENCE	7.81	5	-3.68	1.19	25.30	0.62	8.55	0.04	2	772	ND	2647	ND	1
8.109	**C**	*A. tenuis*	BOURAKE	99.01	5	-4.13	1.04	23.80	0.17	8.45	0.01	3	388	115	5796	1501	3
		M. digitata	BOURAKE	47.64	4	-4.34	0.29	24.83	0.80	8.52	0.05	3	424	86	5061	1063	3
		Porites sp.	BOURAKE	12.42	5	-4.72	0.52	24.90	0.32	8.52	0.02	3	549	85	3845	626	3
		A. tenuis	REFERENCE	69.45	5	-4.17	0.09	24.16	0.21	8.48	0.01	3	542	85	3954	663	3
		M. digitata	REFERENCE	21.07	5	-1.45	0.27	26.28	0.21	8.61	0.01	3	475	67	4316	637	3
		Porites sp.	REFERENCE	4.47	5	-3.56	1.37	25.07	0.42	8.54	0.03	3	635	172	3437	973	3
Variable (7.5-8.1)	**A**	*A. tenuis*	BOURAKE	52.08	5	-5.63	1.80	22.74	0.78	8.36	0.05	3	536	149	4201	1026	3
		M. digitata	BOURAKE	63.61	5	-6.35	0.27	23.42	1.14	8.37	0.07	3	448	36	4971	486	3
		Porites sp.	BOURAKE	11.02	5	-7.05	ND	23.58	ND	8.42	ND	1	435	ND	4877	ND	1

		Specie	Site	NetCal (%)	n	$\delta^{13}C$ (‰)	SD	$\delta^{11}B$ (‰)	SD	pH_{ECM}	SD	n	B/Ca_{carb} ($\mu mol\ mol^{-1}$)	SD	DIC_{ECM} ($\mu mol\ mol^{-1}$)	SD	n
Variable (7.5-8.1)	**A**	*A. tenuis*	REFERENCE	48.08	5	-6.50	0.17	23.60	0.80	8.42	0.05	3	496	167	4651	1684	3
		M. digitata	REFERENCE	24.48	5	-2.45	0.78	25.26	0.78	8.53	0.05	3	479	17	4310	225	3
		Porites sp.	REFERENCE	4.35	4	-4.87	1.83	23.63	0.08	8.42	0.01	2	542	260	4436	2154	2
Variable (7.5-8.1)	**B**	*A. tenuis*	BOURAKE	55.23	5	-7.30	0.37	22.85	0.22	8.37	0.01	4	469	102	4745	949	4
		M. digitata	BOURAKE	68.65	5	-6.90	0.49	23.71	0.73	8.42	0.05	3	408	80	5334	1015	3
		Porites sp.	BOURAKE	7.26	6	-6.83	0.53	22.32	1.27	8.33	0.09	4	450	47	4826	429	4
		A. tenuis	REFERENCE	58.07	5	-4.63	2.20	24.30	0.90	8.46	0.06	3	461	92	4594	970	3
		M. digitata	REFERENCE	20.61	5	-6.53	0.98	23.80	0.85	8.43	0.05	4	427	9	4963	77	4
		Porites sp.	REFERENCE	5.26	6	-7.47	0.55	23.21	0.35	8.39	0.02	2	388	66	5787	1383	2
Variable (7.5-8.1)	**C**	*A. tenuis*	BOURAKE	70.99	5	-6.36	0.89	23.40	1.10	8.40	0.07	3	426	113	4670	975	3
		M. digitata	BOURAKE	66.00	5	-7.07	0.16	22.86	0.33	8.37	0.02	3	429	36	5028	390	3
		Porites sp.	BOURAKE	9.98	5	-7.67	0.16	23.04	0.49	8.38	0.03	2	447	10	4787	75	2
		A. tenuis	REFERENCE	51.18	5	-5.14	0.95	24.01	0.66	8.44	0.04	4	481	74	4115	507	4
		M. digitata	REFERENCE	21.20	5	-5.57	2.65	24.12	1.64	8.45	0.0	4	422	19	4996	311	4
		Porites sp.	REFERENCE	4.59	5	-5.73	0.64	23.70	1.43	8.42	0.09	3	455	67	4721	715	3

Appendix Article n°4 - Chapter 6

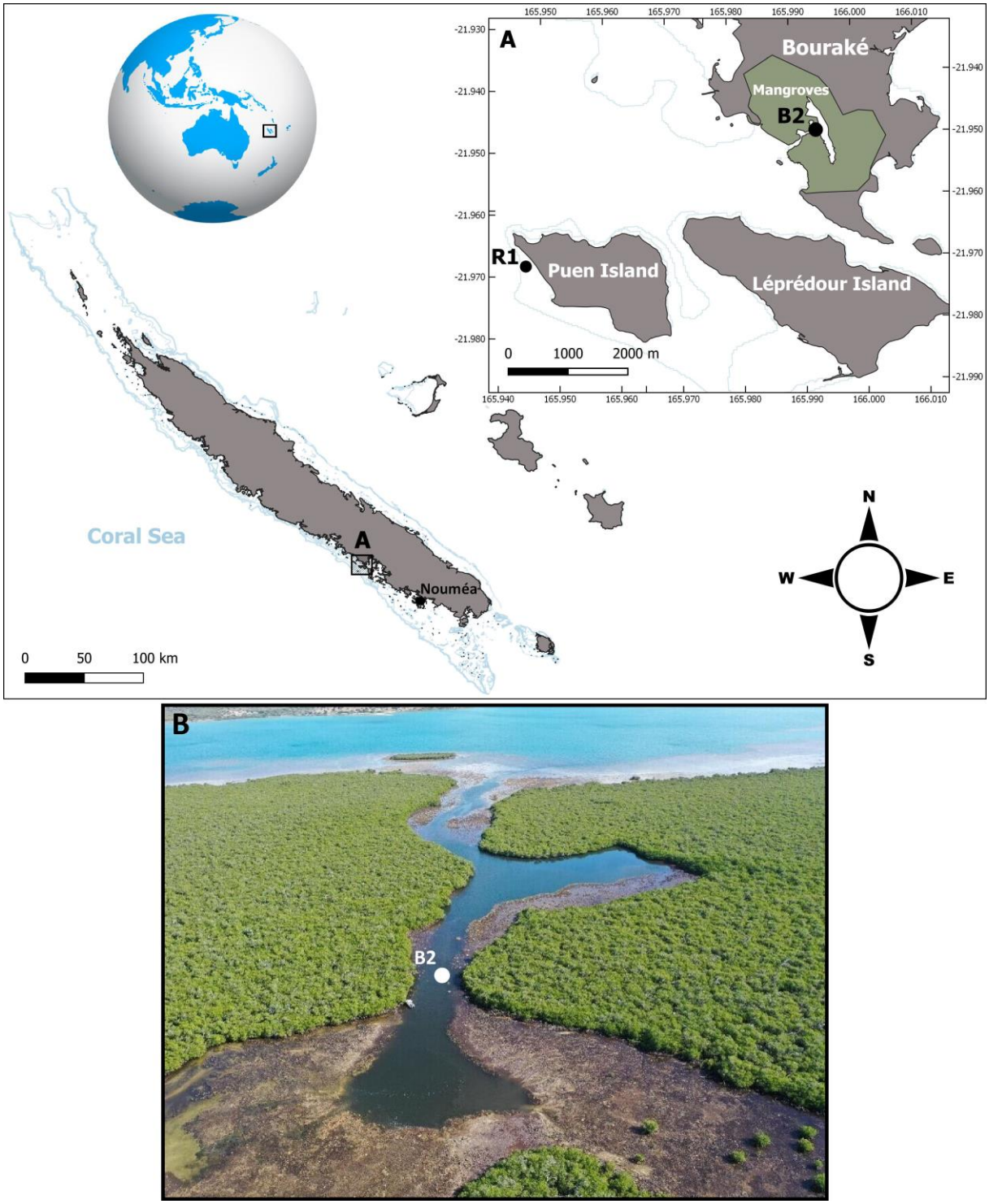

Figure VIII-16 | ***(A)*** *Location of coral core sampling sites, Bouraké (B2) and Puen (R1), in New-Caledonia.* ***(B)*** *Aerial photo of Bouraké lagoon (taken at 130 m altitude) with the coral core sampling site (B2).*

Figure VIII-17 | *Drilling and cutting of the two* Porites *sp. cores from Bouraké and Puen (core length: ~35 cm; core diameter: ~7 cm).*

Figure VIII-18 | *Positive X-radiographs of the two coral cores (Bouraké B2 and Puen R1) in New Caledonia. The model-age follows the density bands of the skeleton (red lines).*

Article annex n°1

Marine Biology (2022) 169:82
https://doi.org/10.1007/s00227-022-04063-6

ORIGINAL PAPER

Long-term exposure to an extreme environment induces species-specific responses in corals' photosynthesis and respiration rates

Juliette Jacquemont[1] · Fanny Houlbrèque[1] · Clément Tanvet[1,2] · Riccardo Rodolfo-Metalpa[1]

Received: 22 March 2021 / Accepted: 20 April 2022

Abstract
Extreme reef environments have become useful natural laboratories to investigate physiological specificities of species chronically exposed to future-like climatic conditions. The lagoon of Bouraké in New Caledonia (21°56′56.16″ S; 125°59′36.82″ E) is one of the only reef environments studied where the three main climatic stressors predicted to most severely impact corals occur. In this lagoon, temperatures, seawater pH_T and dissolved oxygen chronically fluctuate between extreme and close-to-normal values (17.5–33.85 °C, 7.23–7.92 pH_T units and 1.87–7.24 mg O_2 L^{-1}, respectively). In March 2020, the endosymbiont functions (chl *a*, cell density and photosynthesis) and respiration rates were investigated in seven coral species from this lagoon and compared with those of corals from an adjacent reference site using hour-long incubations mimicking present-day and future conditions. Corals originating from Bouraké displayed significant differences in these variables compared to reference corals, but these differences were species-specific. Photosynthetic rates of Bouraké corals were all significantly lower than those of reference corals but were partially compensated by higher chlorophyll contents. Respiration rates of the Bouraké corals were either lower or comparable to those of reference corals. Conversely, photosynthesis and respiration rates of most studied species were similar regardless of the incubation conditions, which mimicked either present-day or future conditions. This study supports previous work indicating that no unique response can explain corals' tolerance to sub-optimal conditions and that a variety of mechanisms will be at play for corals in a changing world.

Keywords Coral reefs · Extreme environments · Ocean acidification · Photosynthesis · Respiration · Climate change

Abbreviations

Chl	Chlorophyll
Day R	Day respiration
DO	Dissolved oxygen
P	Photosynthesis
P_{chl}	Photosynthesis per chlorophyll *a*
P_g	Gross photosynthesis
P_S	Photosynthesis per surface area
R/V	Research vessel
T	Temperature

Responsible Editor: S. Harii.

✉ Juliette Jacquemont
juliette.jacquemont.fr@gmail.com

[1] ENTROPIE – IRD – Université de la Réunion – CNRS – IFREMER, Université de Nouvelle-Calédonie, Nouméa 98848, New Caledonia

[2] LEMAR (UMR 6539 CNRS/IRD/UBO), Institut Universitaire Européen de La Mer, rue Dumont d'Urville, 29280 Plouzané, France

Introduction

Coral-dominated ecosystems are predicted to decline by 99% under a temperature increase of 2 °C (Hoegh-Guldberg et al. 2019), which remains an optimistic scenario for 2100 given our current pathway (IPCC 2019). As a result, it seems likely that most reef ecosystems will disappear or significantly degrade in the coming decades. However, outlying coral populations are being identified in extreme environments, which are characterized by one or more abiotic conditions outside of corals' usual range of tolerance (Kleypas et al. 1999). The identification of these resistant corals (Grottoli et al. 2017; Camp et al. 2018a) provides new insights into how coral populations could persist in a warm, acidified and deoxygenated ocean, which is the trio of climate-induced

Published online: 26 May 2022

stressors predicted to most impact corals in the future (IPCC 2019).

Ocean acidification is driven by the dissolution of atmospheric CO_2 in the ocean, which is increasing due to elevated anthropogenic CO_2 emissions. As a result, sea surface pH_T has been declining by a range of 0.01–0.03 units per decade since the late 1980s (Hoegh-Guldberg et al. 2017), and is predicted to decrease another 0.28–0.29 units by 2100 (RCP8.5 scenario; IPCC 2019). Ocean acidification leads to a decline in the saturation state of calcium carbonate, as well as a concomitant decrease in $[CO_3^{2-}]$ and increase in $[HCO_3^-]$, which is thought to decrease corals' calcification rates (Hoegh-Guldberg et al. 2008). Ocean deoxygenation, i.e. the decrease in partial pressure of oxygen (pO_2), is due to global warming and local eutrophication, which lead to lower O_2 saturation and increased microbial O_2 demands (Breitburg et al. 2018). The impacts of deoxygenation on coral reefs have received little attention, and hypoxia thresholds of main scleractinian groups remain unknown (Hughes et al. 2020). However, the proximity of tropical dead zones to reef ecosystems suggests that it could constitute an important threat (Altieri et al. 2017).

Some marginal and extreme environments expose corals to climate conditions comparable to or exceeding those predicted for the end of the century. Such environments provide natural laboratories where corals have developed in ecologically realistic and complex systems, which cannot be fully reproduced in tank experiments. Additionally, they allow one to investigate long-term mechanisms involved in corals' tolerance to climatic stressors, which do not have time to occur in most tank experiments that rarely exceed a year. Long-term acclimatory or adaptive mechanisms could play an important role in corals' ability to cope with future climatic conditions as climate change likely occurs at a speed allowing for acclimation and rapid adaptation processes to take place in coral populations (Kenkel et al. 2018; Logan et al. 2014; Palumbi et al. 2014; Torda et al. 2017). To characterize these long-term processes, an increasing number of studies are using marginal and extreme reef sites as natural laboratories to study corals' responses to future conditions (reviewed by Camp et al. 2018b). Currently, most studies have focused on sites displaying high and highly variable temperatures, such as back-reef pools (Oliver and Palumbi 2011; Schoepf et al. 2015) or the Red Sea (Howells et al. 2016; Grottoli et al. 2017), and sites displaying low pCO_2, such as CO_2 vents (Fabricius et al. 2011; Inoue et al. 2013; Rodolfo-Metalpa et al. 2011; Strahl et al. 2015). However, a significant limit to most sites is that they display a single stressor and consequently fail to inform on the combined effects of low pH, low dissolved oxygen (DO), and high temperature (T) that will simultaneously affect corals in the future. While no natural site described can serve as a realistic analogue to all upcoming climatic and environmental conditions, the recently identified site of Bouraké in New Caledonia is unique because it combines these three main stressors (Camp et al. 2017). The site of Bouraké is a semi-enclosed lagoon surrounded by mangroves and characterized by low pH, low DO and high T, all fluctuating according to tidal and diel cycles. To date, it is among the only sites in the world where healthy and diverse coral populations have been identified despite values of pH and DO exceeding those forecasted for the open ocean by 2100 (Bopp et al. 2013; IPCC 2019), and temperatures of 1–3 °C higher than surrounding local values (Camp et al. 2017).

One of the most sensitive aspects of corals' physiology under climate change is their energy budget. Prolonged heat stress can cause corals to bleach, a process in which Symbiodiniaceae are expelled from their host, depriving them of the transfer of photosynthates, their main energy source when healthy (Muscatine 1990; Grottoli et al. 2006). Additionally, ocean acidification is expected to marginally increase the energy costs required to maintain calcification rates and growth (McCulloch et al. 2012). It has been suggested that corals developing in acidified environments could display increased respiration rates to compensate for their additional energy requirements, but this remains inconclusive. So far, studies have shown equivocal results, as the effects of high pCO_2 on corals' photosynthesis and respiration rates have appeared to be species-specific and dependant on experimental designs (e.g., Crawley et al. 2010; Rodolfo-Metalpa et al. 2011; Edmunds 2012; Comeau et al. 2017; McLachlan et al. 2020) and feeding levels (Schoepf et al. 2013). Concerning photosynthesis, a meta-analysis showed that the latter was not affected by short-term exposure to acidified conditions during lab experiments (Kroeker et al. 2010, 2013), but the few studies using low pH environments showed that photosynthesis rates were increased in acclimatized coral populations (Inoue et al. 2013; Strahl et al. 2015; Biscéré et al. 2019). The combined effects of acidification and warming on corals' photosynthesis and respiration rates have only been investigated during short-term experiments, which cannot account for realistic and adaptive processes (Anthony et al. 2008; Schoepf et al. 2013; Hoadley et al. 2015; Brown et al. 2019). Consequently, an important knowledge gap remains in the understanding of how corals' photosynthesis and respiration rates will be affected by climate change, and whether corals could rely on their metabolic plasticity under extreme environmental conditions.

This study investigated the photosynthesis, respiration rates and symbiotic parameters of corals originating from a natural environment combining elevated T, decreased pH and decreased DO. To do so, we carried out incubations of corals originating from Bouraké in present-day or end-of-the-century conditions and compared their photosynthesis and respiration rates with those of corals from an adjacent reference site incubated in similar conditions. This

experiment was conducted at the end of the austral summer season, i.e., when corals were exposed to the most extreme environmental conditions. We hypothesized that long-term adaptive processes would prevail on the short-term plasticity of the corals' photosynthesis and respiration rates, meaning that (1) endosymbiotic functions, photosynthesis and respiration rates of corals from Bouraké would differ from those of corals from the reference reef; (2) incubating corals from either site in contrasting conditions (present-day or future conditions) would not modify their photosynthesis and respiration rates.

Material and methods

Study site

Corals were sampled from shallow reefs (1–2 m depth) in the lagoon of Bouraké (site B2, 21°56′56.16″ S; 125°59′36.82″ E) and in an adjacent fringing reef (site R1, 21°58′13.12″ S; 165°56′45.66″ E), located on the west coast of New Caledonia in the Southwest Pacific Ocean (Fig. 1) on the 12th and 13th of March 2020. The Bouraké lagoon (described in Camp et al. 2017) is connected to the ocean by a channel approximately 4–5 m wide which enters a mangrove forest and forms large back pools 5–7 m deep. It displays a diverse and abundant coral population (66 coral species, up to 96% coral cover; Maggioni et al. 2021) that develops despite acidified (pH_T down to 7.23), warm (up to 33.85 °C) and deoxygenated (down to 2.28 mg O_2 L^{-1}) conditions. Water parameters in the Bouraké lagoon also undergo large fluctuations following tidal and diel cycles, during which they regularly exceed forecasted values for 2100 (Camp et al. 2018b). The lowest values for pH, DO and the highest for T are reached at low tide, while high tides display values close to present-day conditions. In contrast, R1 displays present-day and relatively stable conditions for pH, T and DO, and is outside of the area influenced by the mangrove ecosystem (Table 1). As such, it is used in this study as a reference site.

A fine-scale abiotic and biotic characterization of both sites has been conducted since 2016 (Camp et al. 2017; Maggioni et al. 2021). Here, we used data collected from Maggioni et al. (2021) to characterize the two study sites. Data were collected during a four-year-long monitoring campaign (from 03/2016 to 04/2020) and accounted for both diel and seasonal fluctuations, compiling several thousands of measurements (Table 1). Seawater temperature (°C), dissolved oxygen content (DO, mg L^{-1}), and seawater pH_T

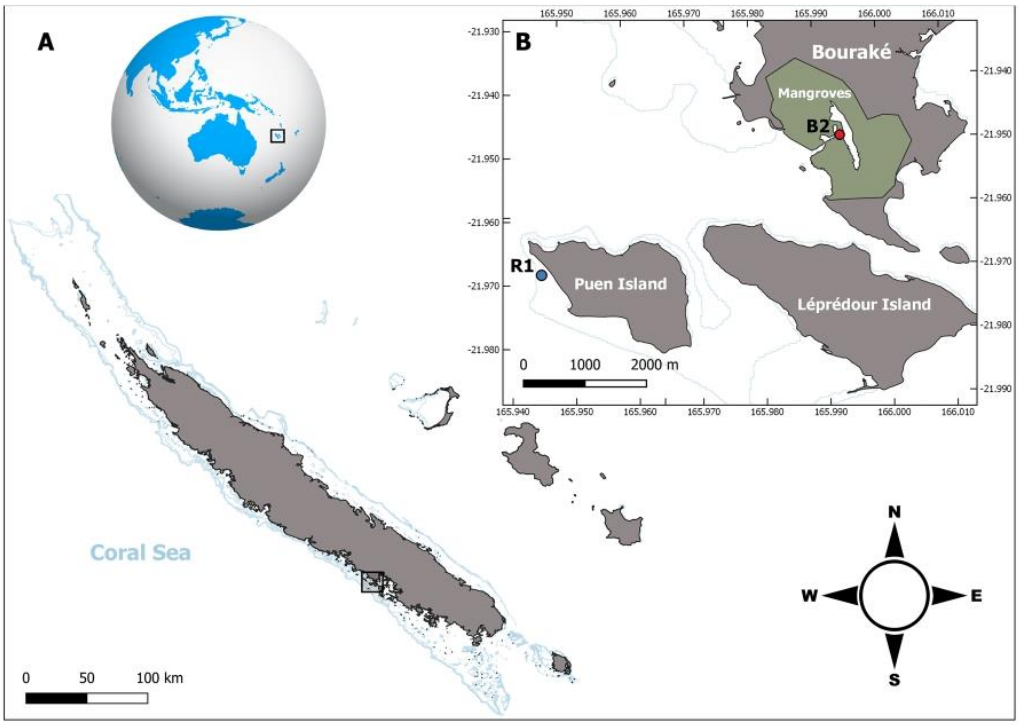

Fig. 1 **A** Location of New Caledonia within the Pacific South-West and **B** location of the two study sites: the Bouraké lagoon (B2) and the reference site (R1). Map tiles were collected from www.georep.nc (© Georep contributors)

Table 1 Main environmental parameters measured at the reference (R1) and at the Bouraké site (B2)

		R1	B2
Temperature (°C)	Mean ± SD	25.25 ± 1.89	26.13 ± 2.67
	Min	19.98	17.49
	Max	30.54	33.85
pH_T (total scale)	Mean ± SD	8.01 ± 0.04	7.67 ± 0.23
	Min	7.91	7.23
	Max	8.18	8.06
pCO_2 (µatm)	Mean ± SD	353.4 ± 7.24	1318.9 ± 819.8
	Min	343.3	464.7
	Max	361.5	2860.7
DO (mg L^{-1})	Mean ± SD	6.45 ± 0.95	5.23 ± 0.89
	Min	3.06	2.28
	Max	10.65	7.10
Salinity	Mean ± SD	35.44 ± 0.049	36.97 ± 1.18
	Min	35.24	35.59
	Max	36.65	39.37

Mean (± SD), minimum (min) and maximum (max) values of temperature, pH_T (in total scale), dissolved oxygen (DO), salinity, and calculated pCO_2. Values for temperature, pH, pCO_2 and DO were obtained through a four-year long monitoring (from 03/2016 to 04/2020) considering both diel and seasonal fluctuations, and compiling several thousands of measurements (Maggioni et al. 2021). Salinity was averaged between two sets of continuous measurements: during the winter of 2019 (from 15/07/2019 to 18/07/2019), and the summer of 2020 (from 29/11/2020 to 04/12/2020)

(total scale), were periodically recorded using 600 OMS-M (YSI, USA), SeaFET pH loggers (Sea-Bird, USA), and Hobo water temperature Pro V2 (Onset, USA), all settled at a 10-min logging interval. Salinity was measured only during the winter of 2019 (from the 15th to the 18th of July), and the summer of 2020 (from the 29th of November to the 4th of December, see Maggioni et al. (2021) for further details on the probe deployments).

Coral sampling

Six coral fragments (3–5 cm long) of *Acropora tenuis* (Dana, 1846), *Pocillopora damicornis* (Linnaeus, 1758) and *Montipora digitata* (Dana, 1846) were collected at B2 and R1 on the 8th of March 2020. Coral fragments were collected from distinct mother colonies ($n = 6$ at both sites) at least 10 m apart from each other, using a plier. In B2, corals were collected along a reef of ca 150 × 20 m, while in R1 they were collected in a larger area of about 250 × 20 m. Additionally, $n = 5$–7 coral fragments of *Acropora samoensis* (Brook, 1891), *Acropora tenuis* (Dana, 1846), *Echinopora* spp. (Lamark, 1816), *Montipora stellata* (Bernard, 1897), and *Porites cylindrica* (Dana, 1846) were collected using the same sampling methodology on the 12th and 13th of March 2020. Only one fragment was sampled from each mother colony. Fragments collected on the 8th of March were immediately frozen at − 20 °C and fragments collected on the 12th and 13th were frozen after being incubated for photosynthesis and respiration measurements on that same day.

Symbiont density, chlorophyll concentration and surface measurements

All fragments collected were unfrozen and measured for symbiont density and chlorophyll concentrations throughout March and April 2020. This resulted in the analysis of $n = 12$ fragments of *A. tenuis*, $n = 5$–7 fragments of the 4 other species used in the incubations, and $n = 6$ fragments of *M. digitata* and *P. damicornis*.

Coral tissue was extracted in 20 mL of filtered seawater (GF/F 47 mm filters) using an air pick, and the slurry obtained was homogenised with a potter tissue grinder. For symbiont density measurement, 2 mL of the slurry was sampled to count the number of Symbiodiniaceae using a Neubauer's cell under a stereomicroscope. Four to six replicates were measured for each sample. For chl content measurement, 10 mL of the slurry was centrifuged at 5,000 g for 10 min, after which the supernatant was discarded. The remaining algal pellet was re-suspended in 10 mL of pure acetone, and pigments were extracted over 24 h at 4 °C in darkness. The extract was then centrifuged at 10,000 g for 15 min, and the supernatant was sampled to measure its absorbance at 630, 663 and 750 nm using a spectrophotometer (Evolution 201, Thermo Scientific). Chlorophyll *a* and c_2 concentrations were calculated using the spectrophotometric equations by Jeffrey and Humphrey (1975). Surface area of coral fragments was measured using the single wax method (Veal et al. 2010).

Experimental design of the incubations

The incubations were performed on board the research vessel (R/V) Alis, which was moored in front of the study sites. The incubations were designed to test the effects of short- and long-term exposure to present-day and future-like conditions on corals' photosynthesis, day respiration and symbiont content. Effects of long-term exposure were tested by comparing these variables between corals originating from two contrasting environmental conditions: i) the site of Bouraké (B2), where corals have been chronically exposed to fluctuating and extreme conditions; ii) the reference site (R1), where conditions are those of a typical fringing reef. Effects of short-term exposure were tested by comparing the photosynthesis and respiration rates of corals during hour-long incubations carried out under both present-day and future-like conditions. The incubation reproducing future-like conditions displayed temperatures higher by 2 ±

0.2 °C, pH lower by 0.3 ± 0.03 units and DO lower by 1.3 ± 0.02 mg L^{-1} than the incubation in present-day conditions (Table 2). Incubations under present-day conditions were achieved by collecting seawater in the lagoon of Bouraké during high tide, while incubations under future-like conditions were achieved by collecting seawater in the lagoon of Bouraké during falling tide when values of T, pH and DO reach their extremes. Consequently, both coral groups were incubated in seawater collected from the lagoon of Bouraké, which was an opportunity to carry out our experiment using ecologically realistic conditions rather than artificially reproduced ones. The experimental design thus encompassed four types of incubations, to account for the two groups of corals both incubated under two seawater conditions. Corals from the Bouraké and the reference site were collected and incubated following the same methodology on two different days (respectively the 12th and 13th of March 2020) because of logistic constraints. Characteristics of seawater collected at Bouraké were found to be in very close ranges on both incubation days (Table 2), ensuring comparable incubation conditions for both coral groups.

Experimental set up of incubations

The coral fragments ($n = 5$–7) of *Acropora samoensis* (Brook, 1891), *Acropora tenuis* (Dana, 1846), *Echinopora* spp. (Lamark, 1816), *Montipora stellata* (Bernard, 1897), and *Porites cylindrica* (Dana, 1846) collected from the Bouraké site on the 12th of March 2020, and from the reference site on the 13th of March 2020 were used for the photosynthesis and respiration measurements. Fragments were collected during the morning, one hour before the high tide (11:19 am and 11:53 am local time on the 12th and 13th of March, respectively) to avoid any bias due to diurnal variations (Edmunds and Davies, 1988). Fragments were transported onboard the R/V in individual hermetic plastic bags containing seawater and immersed in a cooler. Fragments were then transferred in a 100 L tank in the indoor laboratory of the vessel where the temperature was maintained close to the one that was measured with a dive computer in situ during collection. The tank was equipped with a submersible pump and an air stone for water circulation, and filled with seawater freshly collected in Bouraké. A low light level (ca. 70 µmol m^{-2} s^{-1}) was provided by the same source of light used for the incubations (see below) to allow corals to recover for an hour.

Fragments were first incubated twice for 50 ± 10 min in the morning under high tide conditions. The first incubation was carried out in the dark to measure day respiration (day R) rates and the second in the light to measure net photosynthesis (P_n) rates. P_n rates were measured using saturating light intensity (250 ± 10 µmol m^{-2} s^{-1}) provided by one bank of four T5 bulbs (10,000°K, Giesemann, Germany). Seawater in beakers was renewed between the dark and the light incubations using the same sample of seawater collected in Bouraké during sampling. After the first two incubations (i.e., dark and light), corals were let to recover for two hours under a low light level in fresh seawater collected in Bouraké at intermediate conditions between high and low tide. During the afternoon falling tide, when the seawater in the lagoon reached values close to projected future conditions, fresh seawater was collected again and the corals were gently transferred and let to recover in the collected seawater for about one hour. Two incubations were then carried out in the afternoon to measure the P_n and R rates of corals under low tide conditions, using the same methodology as the incubations carried out in the morning. Because pO_2 levels are low at the falling tide, P_n was conducted first in the afternoon so that R would not be constrained by low pO_2. This resulted in a total of four sets of incubations of the same 30 coral fragments collected in the morning (see also Supplementary Figure S1 for a summarized representation of the incubation chronology). This exact sampling procedure and incubation protocol were carried out on the 12th of March with corals from Bouraké, and on the 13th of March with corals from the reference site.

Photosynthesis and day respiration rates

The experimental set-up used (i.e., incubation duration and volume of beakers) was as in Biscéré et al. (2019), which allows to measure clear DO variations without variations exceeding 15–20% during the incubation. For each incubation, coral fragments ($n = 5$–7) of the five species were placed in individual 100 mL Pyrex glass beakers ($n = 30$) filled with seawater and hermetically sealed underwater with transparent cellophane and a rubber band after all air bubbles were removed, to avoid any bias from O_2 exchanges

Table 2 Values of pH_T (in total scale), temperature (T) and dissolved oxygen (DO) used during the four incubations of corals from the reference (R1) and Bouraké (B2) sites under present-day, and future conditions

Seawater	Incubation R1 corals			Incubation B2 corals		
Conditions	pH_T	T (°C)	DO (mg L^{-1})	pH_T	T (°C)	DO (mg L^{-1})
Present-day	8.03	29.8	6.0	7.98	29.4	5.9
Future	7.73	32.0	4.6	7.65	31.3	4.8

with air (Biscéré et al. 2019). Three control beakers, in which no coral fragment was placed, were used to measure the metabolic microbial activity of the water. Control beakers were emptied and filled again with fresh seawater for each new incubation. Beakers were placed on two submersible multi-stirring plates with $n = 18$ individual stirring positions each (Fig. S1), which continuously stirred the seawater in each beaker, and were semi-submersed in a thermostatic water bath settled at ± 0.5 °C from the temperature of the collected seawater (Table 2). After five minutes of incubation, and at the end of each incubation, concentrations of DO were measured in each beaker, where O_2 sensor spots were fixed, using an optical fiber (PreSens Fibox 4 trace). Rates of P_n and day R were calculated using the change of DO concentrations in each beaker, corrected by the mean of the microbial activity measured in three empty beakers, and normalized by the incubation duration, the volume of seawater in each beaker, and either the coral's surface or its content in chl *a* (Edmunds and Gates 2002).

Rates of gross photosynthesis P_g were calculated as the sum of $|P_n|$ and |R|. Photosynthesis to respiration ratio (P_g: day R) was calculated as:

$$P_g : \text{day R} = \frac{P_g \times \text{hours of daylight}}{\text{day R} \times 24}$$

with P_g and day R in µmol O_2 cm^{-2} h^{-1}. The value of hours of daylight equalled 12.2 on March 13th in New Caledonia. At the end of each incubation pair (dark and light), coral fragments were frozen at −20 °C for subsequent measurements of chlorophyll (chl) concentration and symbiont density and surface area. Values of P_g are presented hereafter as normalized by the chl content (P_{chl}) or by the surface area (P_S) of each coral fragment.

Statistical analyses and data presentation

Statistical analyses were carried out and figures were produced using RStudio v.4.1.0 (2021), including the packages {ggplot2}, {stats}, {ARTool} and {car}. Data were first visually inspected and abnormal values were deleted. Homogeneity of variance was tested using the Bartlett test and the distribution of variances within groups was checked graphically on a normal P-P plot (i.e., expected vs observed). Chlorophyll and Symbiodiniaceae contents did not meet the assumptions of normality so values from both sites were compared using the non-parametrical Kruskal–Wallis test. Day R, P_{chl}, P_s and P_g: day R rates verified normality and homoscedasticity conditions, so a 2 × 2-way ANOVA was run to test for the effect of long-term exposure (i.e. site of origin: reference and Bouraké) and the effect of short-term exposure (i.e. incubation conditions: present-day and future), and their interaction on corals' *P* and R rates. As no interaction term was significant, post hoc Tukey HSD tests were not performed. *P*-levels were not adjusted. Data were presented using boxplots displaying median values (line) ± 25th and 75th percentiles (box), minimum and maximum values (whiskers), and mean values (dots).

Results

Environmental parameters at the study sites

Environmental data collected from 2016 to 2020 (see Maggioni et al. (2021) for full data set) clearly demonstrated the large differences between the reference site R1 and the Bouraké site (Table 1). While the environmental parameters for seawater measured at the reference site R1 were all within the normal range known for New Caledonia, seawater temperature was on average 1 °C higher in Bouraké, and up to 3 °C higher during the hot season. Measured pH was ca. 0.2 pH_T units lower, reaching the extreme value of 7.23 pH_T and pCO_2 was three times higher in Bouraké than at R1. Measured DO was on average 1 mg L^{-1} lower than at R1 and salinity was on average 1 point higher, reaching extreme values during the summer (+ 3 points). Dissolved oxygen, temperature, pH and salinity fluctuated in relation to the tide, respectively up to 4.91 mg O_2 L^{-1}, 6.50 °C, 0.69 pH_T units, and 3.42 points within a day.

Chlorophyll and Symbiodiniaceae content

Chlorophyll and symbiont contents in coral fragments significantly differed between the Bouraké and the reference site (Fig. 2; Table 3). Bouraké fragments displayed significantly higher content of chl *a* for 4 out of 7 species; higher content of chl c_2 for *A. tenuis* and *M. stellata,* higher symbiont density for *A. samoensis, A. tenuis* and *P. cylindrica* and higher chl *a* per symbiont for *A. tenuis* and *M. stellata*.

Photosynthesis and day respiration rates

ANOVA showed no significant effect of incubation conditions (present day vs. future) on the photosynthesis and respiration rates of corals (Fig. 3 for the corals from the Bouraké site, Fig. S2 for corals from the reference site and Table 4 for statistical values).

In contrast, significant differences between corals from different sites were observed for the P_{chl} of all coral species, the P_s of three coral species, the P_g: day R of two species and the day R rates of *Echinopora* spp. (Table 4). Figure 4 presents the values of the four measured variables for fragments from both sites, after having pooled together both incubation conditions. Mean photosynthesis rates per chl *a* (P_{chl}) were lower for all corals originating from Bouraké compared

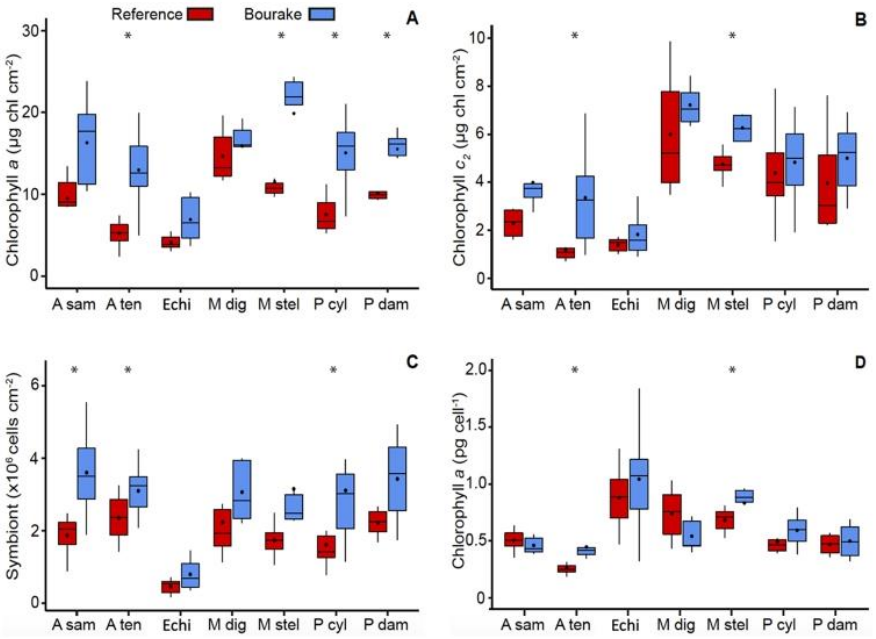

Fig. 2 **A** Chl *a* and **B** chl c_2 content per unit surface area of the skeleton (µg cm^{-2}); **C** symbiont density per unit surface area ($\times 10^6$ cells cm^{-2}), and **D** chl *a* content per symbiont (pg $cell^{-1}$) measured on corals collected at the reference site and Bouraké site ($n=12$ for *A. tenuis* and $n=5$–7 for other species). Data are represented as median value (line) ± 25th and 75th percentiles (box), minimum and maximum values (whiskers) and mean value (dot). Asterisks indicate statistical differences between sites of origin (see Table 3)

to the reference fragments (Fig. 4A). When normalizing P rates per surface area (P_S), contrasting trends were observed depending on the species. While colonies of *P. cylindrica* from Bouraké increased P_S, *A. tenuis* and *Echinopora* spp. displayed decreased P_S, and the two other species had similar P_S compared to colonies from the reference site (Fig. 4B). Mean respiration (day R) rates were lower for *Echinopora* spp. from Bouraké compared to the reference site, and comparable for the other species between both sites (Fig. 4C). The mean P_g: day R ratios of Bouraké fragments were higher for *M. stellata, Echinopora* spp. and *P. cylindrica* but similar for *A. samoensis* and *A. tenuis* compared to fragments from the reference site (Fig. 4D).

Discussion

Zooxanthellae and chlorophyll contents of corals from the Bouraké lagoon were in similar ranges or higher than those of usual tropical corals in New Caledonia and in the GBR: 1–6 $\times 10^6$ cells cm^{-2} of symbionts, 5–25 µg cm^{-2} of chl *a* and chl c_2, 2–15 $\times 10^{-6}$ pg $cell^{-1}$ of chl *a* (e.g., Connolly et al. 2012; Schoepf et al. 2015; Camp et al. 2020). These results demonstrate that despite developing in a site with extreme conditions, corals from the Bouraké lagoon display healthy levels of symbionts and chlorophyll, even during the hottest period of the year (February to March), when fragments were collected for this study. This is coherent with the field observations made during sampling for this study, during which no sign of bleaching of corals in either site was observed. For a majority of species (five out of seven), chl *a* concentrations per surface area were even found to be higher at the Bouraké site than at the reference site. This resulted from increased symbiont densities and/or increased chl per symbiont in Bouraké corals compared to the reference site. The ability of Bouraké corals to maintain "normal" symbiont and chlorophyll contents under combined stressors could result from genetic adaptations, but several additional mechanisms could explain this ability. A first explanation could be related to the high levels of turbidity in the lagoon, especially at the end of the falling tide when the system empties and receives water rich in organic matter from the surrounding mangrove forest. Although light irradiance in the lagoon has yet to be extensively measured, the attenuation of solar radiations by turbidity has been shown to mitigate the stress exerted on corals from elevated temperatures and UV radiations by reducing photoinhibition and thus bleaching (Lesser and Farrell 2004; Sully and Woesik 2020). Many studies have reported lower bleaching rates at sites displaying higher turbidity levels in comparison to adjacent clear-water reefs (e.g., van Woesik et al. 2012; Morgan et al. 2017), and a similar mechanism could be at play in the Bouraké lagoon. A second mechanism involved could originate from the high nutrient concentrations (Rees and Smith 1991) which are likely to occur in the lagoon in relation to the surrounding mangrove ecosystem (Kristensen et al. 2008). Increased heterotrophy has previously been evidenced in turbid coastal environments (Anthony 2000) and has been shown to strengthen corals' symbiosis and help to maintain chlorophyll contents and high symbiont

Table 3 Results from non-parametric Kruskal–Wallis test on the corals' chlorophyll (chl) and symbiont contents

Species	Parameters	*df*	H	*p*-value
A. samoensis	chl *a*	1,13	3.50	0.063
	chl c_2	1,13	2.94	0.086
	Symbionts	1,13	5.90	**0.015**
	chl *a* cell^{-1}	1,13	0.51	0.475
A. tenuis	chl *a*	1,24	13.53	**0.000**
	chl c_2	1,24	11.49	**0.000**
	Symbionts	1,24	6.06	**0.014**
	chl *a* cell^{-1}	1,24	15.30	**0.000**
Echinopora spp.	chl *a*	1,13	2.47	0.116
	chl c_2	1,13	0.18	0.668
	Symbionts	1,13	2.04	0.153
	chl *a* cell^{-1}	1,13	0.31	0.574
M. digitata	chl *a*	1,11	0.13	0.715
	chl c_2	1,11	1.63	0.201
	Symbionts	1,11	2.13	0.144
	chl *a* cell^{-1}	1,11	2.70	0.100
M. stellata	chl *a*	1,13	4.60	**0.032**
	chl c_2	1,13	4.00	**0.045**
	Symbionts	1,13	2.94	0.086
	chl *a* cell^{-1}	1,13	4.00	**0.045**
P. cylindrica	chl *a*	1,15	8.37	**0.004**
	chl c_2	1,15	0.12	0.728
	Symbionts	1,15	4.34	**0.037**
	chl *a* cell^{-1}	1,15	1.77	0.183
P. damicornis	chl *a*	1,12	7.41	**0.006**
	chl c_2	1,12	1.25	0.262
	Symbionts	1,12	3.10	0.078
	chl *a* cell^{-1}	1,12	0	1

Statistically significant values are in bold

densities under warm and acidified conditions (Edmunds 2011; Ferrier-Pagès et al. 2010; Houlbrèque et al. 2015). The combination of attenuated solar radiations and increased heterotrophy could be an explanation for how corals can maintain unchanged densities of symbionts despite developing in extreme environmental conditions. Isotopic analyses in both Symbiodiniaceae and tissues as well as measurements of nutrients, dissolved and particulate organic carbon, and different plankton populations are currently being carried out in the Bouraké lagoon to confirm whether increased heterotrophy could indeed support both hosts and symbionts in this extreme environment. A last specificity of the Bouraké lagoon that could influence the chlorophyll and symbiont content of corals is its high salinity, with daily fluctuations in the summer ranging from normal values to 40 in relation to the tide (Maggioni et al. 2021). Indeed, higher thermotolerance and reduced sensitivity to bleaching were found on Aiptasia from the hypersaline Red Sea, partially explaining the strong heat tolerance of corals from the northern Red Sea, and the Gulf of Aqaba (Gegner et al. 2017). Although corals from the Bouraké lagoon are not constantly exposed to high salinity as in the above-mentioned seas, they experience extreme levels which are comparable, therefore the same unknown mechanisms might have improved the persistence of symbionts in the corals from Bouraké, an interesting hypothesis that should be experimentally tested. Lastly, previous studies showed no effect of acidification on chlorophyll and symbiont contents in both short-time tank experiments (Godinot et al. 2011; Schoepf et al. 2013) and experiments using corals from volcanic CO_2 seeps (Noonan et al. 2013; Biscéré et al. 2019), which suggests that acidity is not a key factor in their determination.

Although this study mostly focused on the symbionts' responses to an extreme environment, the holobiont response as a whole was also investigated by characterizing the photosynthesis and day respiration of corals. By incubating corals from an extreme and a reference site under both future and present-day conditions, we obtained information on (1) the respiration and photosynthesis responses of corals to a short-term exposure to future conditions; (2) the endosymbiont specificities of corals originating from two contrasting environments. Photosynthesis and respiration rates measured during the incubations were in the same ranges as those measured in previous studies carried out in the Bouraké lagoon (Camp et al. 2017, 2020) and in other sites in New Caledonia (Biscéré et al. 2017, 2018). As hypothesized, a short-term exposure to future conditions (i.e. increased temperatures of 2 ± 0.2 °C, decreased pH_T of 0.3 ± 0.03 and decreased DO of 1.3 ± 0.02 mg L^{-1}) did not significantly modify corals' photosynthesis and respiration in comparison to present-day conditions. To the best of our knowledge, this is the first time that the effects of a short-term exposure to this trio of stressors is investigated. Previous studies that examined the effects of a short-term exposure to combined low pH and high temperature on corals' P and R rates have shown conflicting and non-linear results (e.g., Brown et al. 2019; Godinot et al. 2011; Hoadley et al. 2015). Overall, past results showed that temperature was the most impacting factor on corals' P and R rates, while the little effect of short-term exposure to acidified conditions was observed (e.g., Rodolfo-Metalpa et al. 2011; Comeau et al. 2017). The absence of detected effects on corals' *P* and R rates in this study could come from the length of the incubations used in this study, which was shorter than in the aforementioned studies (hour long vs. 10 days to a month in previous studies) and might not allow for plasticity or inhibition processes to occur. The unchanged P and R rates could also result from offsetting effects between increased T and decreased pH and DO. Longer exposure of adapted and non-adapted corals to low pH, DO and high T would allow to assess whether the absence of changes observed in this study is due to the

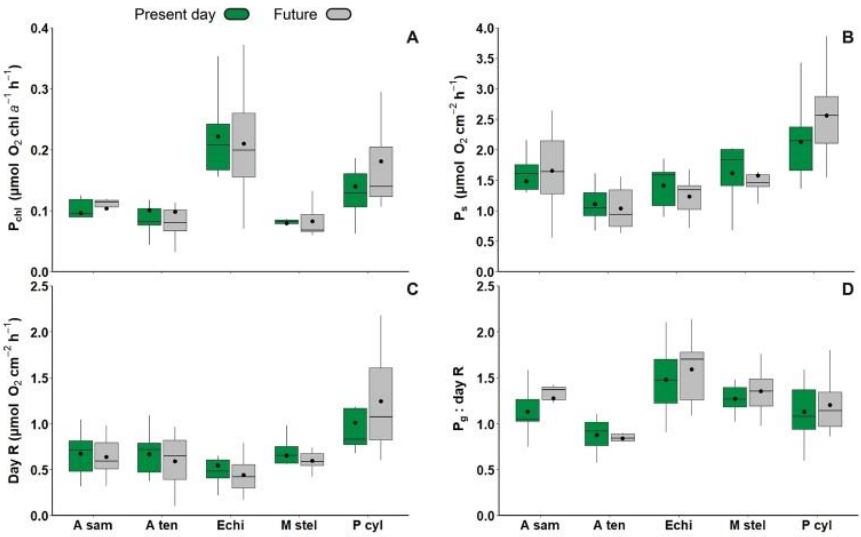

Fig. 3 Photosynthesis and respiration rates of fragments from Bouraké ($n=5$–7 depending on species) incubated either under present-day (green) or future conditions (grey). See Table 2 for seawater conditions. **A** Gross photosynthesis rates normalized by chl *a* content (P_{chl}, µmol O_2 chl a^{-1} h^{-1}); **B** gross photosynthesis rates normalized by surface (P_S, µmol O_2 cm^{-2} h^{-1}); **C** day respiration rates normalized by surface (Day R, µmol O_2 cm^{-2} h^{-1}), and **D** their P_g: day R ratios. Data are represented as median values (lines) ± 25th and 75th percentiles (box), minimum and maximum values (whiskers) and mean values (dots). No significant differences between incubation conditions were found (see Table 4)

Table 4 Results of a two x two-way ANOVA testing the effect of colonies' origin (Bouraké and reference); seawater condition during incubations (HT: present-day and LT: future), and their interaction on the gross photosynthesis rates per chlorophylent (P_{chl}), and per surface area (P_S), day respiration (day R), and photosynthesis to day respiration ratio (P_g: day R) of colonies from five coral species

Species	Factor	Pchl				Ps				day R				Ps: day R			
		df	SS	F	P	df	SS	F	P	df	SS	F	P	df	SS	F	P
A. samoensis	Origin	1	0.035	26.38	**0.000**	1	0.005	0.02	0.898	1	0.109	1.52	0.230	1	0.035	0.257	0.617
	Condition	1	0	0.33	0.568	1	0.126	0.40	0.535	1	0.001	0.02	0.887	1	0.201	1.49	0.235
	Origin × cond	1	0	0	0.983	1	0.006	0.02	0.889	1	0.002	0.03	0.853	1	0.005	0.03	0.856
	Error	22	0.029			22	6.979			22	1.584			19	2.966		
A. tenuis	Origin	1	0.471	14.70	**0.001**	1	1.107	6.90	**0.017**	1	0.013	0.24	0.631	1	0.229	0.38	0.544
	Condition	1	0.011	0.35	0.563	1	0.007	0.04	0.838	1	0.184	3.26	0.088	1	1.982	3.31	0.085
	Origin × cond	1	0.021	0.66	0.426	1	0.107	0.66	0.425	1	0.105	1.87	0.188	1	0.319	0.53	0.475
	Error	18	0.577			18	2.892			18	1.014			18	10.768		
Echinopora spp.	Origin	1	0.439	13.33	**0.001**	1	1.892	5.70	**0.026**	1	0.760	8.71	**0.007**	1	0.622	3.04	0.095
	Condition	1	0.006	0.18	0.674	1	0.186	0.56	0.462	1	0.091	1.04	0.318	1	0.161	0.78	0.385
	Origin × cond	1	0.002	0.06	0.808	1	0.001	0.002	0.965	1	0.002	0.02	0.886	1	0.012	0.06	0.809
	Error	22	0.724			22	7.298			22	1.919			22	4.502		
M. stellata	Origin	1	0.012	10.39	**0.004**	1	0.378	1.97	0.175	1	0.092	2.53	0.126	1	0.714	9.45	**0.006**
	Condition	1	0	0.35	0.557	1	0.077	0.40	0.532	1	0.001	0.03	0.853	1	0.003	0.04	0.843
	Origin × cond	1	0.001	0.58	0.455	1	0.025	0.13	0.723	1	0.010	0.26	0.612	1	0.020	0.27	0.610
	Error	22	0.025			22	4.223			22	0.805			22	1.663		
P. cylindrica	Origin	1	0.030	6.36	**0.018**	1	4.399	9.25	**0.005**	1	0.123	0.88	0.357	1	0.796	10.02	**0.004**
	Condition	1	0	0.10	0.759	1	0.413	0.87	0.359	1	0.057	0.40	0.531	1	0.001	0.02	0.880
	Origin × cond	1	0.010	2.08	0.161	1	1.249	2.63	0.117	1	0.195	1.39	0.250	1	0.025	0.31	0.583
	Error	26	0.121			26	12.358			26	3.651			26	2.066		

Significant values are in bold

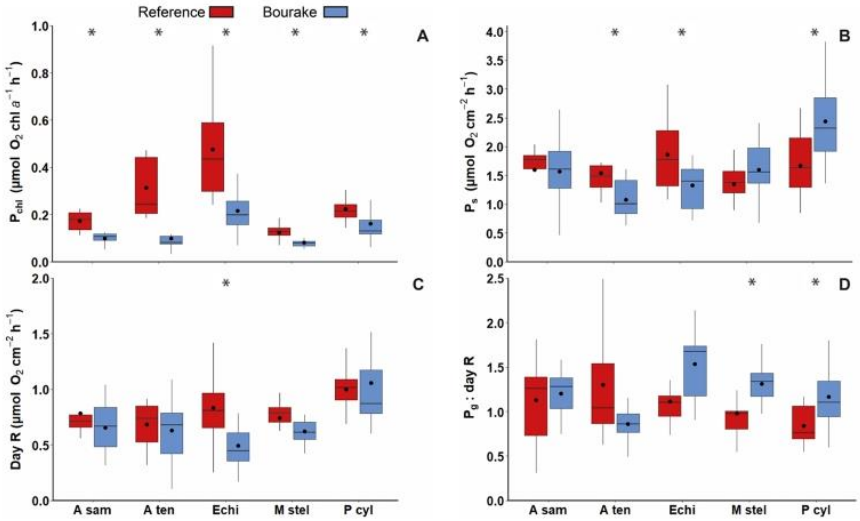

Fig. 4 Photosynthesis and respiration rates of fragments from the reference and the Bouraké site pooled between incubation conditions ($n = 5$–7 depending on species). **A** Gross photosynthesis rates normalized by chl *a* content (P_{chl}, µmol O_2 chl a^{-1} h^{-1}); **B** gross photosynthesis rates normalized by surface (P_S, µmol O_2 cm^{-2} h^{-1}); **C** day respiration rates normalized by surface (Day R, µmol O_2 cm^{-2} h^{-1}), and **D** P_g: day R ratios. Data are represented as median values (lines) ± 25th and 75th percentiles (box), minimum and maximum values (whiskers) and mean values (dots). Asterisks indicate statistical differences between sites of origin (see Table 4)

incubation length used or to compensating effects between the three stressors.

Conversely, corals' origin had a significant and species-specific effect on respiration and photosynthetic rates. While the incubation conditions were identical for both groups of corals, the rate of P_{chl} was significantly lower for all species from the Bouraké site. This could result from the higher density of chl *a* in Bouraké corals, which can lead to self-shading and lower the absorption efficiency of pigments (Enríquez et al. 2005). Symbionts from Bouraké could also have adapted to the lower light intensity in the lagoon by displaying lower light intensity saturation points, leading to lower productivity compared to reference symbionts. The differences in the measured P_{chl} rates could also be caused by a change in symbiont types between Bouraké and the reference site, which has been shown to be a common adaptive feature in extreme environments (Howells et al. 2016). Camp et al. (2020) found differences in symbiont types between Bouraké corals and nearby reference corals. These changes were species-specific, which is consistent with the species-specific results found for P_{chl} rates. Adaptation of symbionts to acidified environments could for example take the form of the ability to enhance *P* rates by taking advantage of increased pCO_2. This adaptation has been shown to occur for some, but not all, host + symbiont assemblages (Biscéré et al. 2019; Inoue et al. 2013; Langdon and Atkinson 2005). However, the decrease in photosynthetic rates per chl *a* of Bouraké corals was counterbalanced by the increase in the chl *a* content of these corals per surface area. These two compensating factors resulted in *P* rates per surface area (P_S) lower for *A. tenuis* and *Echinopora* spp., higher for *P. cylindrica* and comparable for the two other species at the Bouraké site. Furthermore, the differences observed between sites in the P_s rates were less pronounced than those observed for P_{chl}. In previous studies conducted at the Bouraké site, Camp et al. (2017) found no changes in P_S rates for fragments of *A. pulchra*, *A. muricata* and *P. lutea*. Collectively, these results suggest that P_S rates of the Bouraké corals are either comparable or slightly lower than those of corals from adjacent reference reefs.

Corals' origin also had a significant effect on respiration rates, which were lower for two out of five species from the Bouraké site. It is established that water acidification increases energy demands to maintain calcification rates, although marginally (McCulloch et al. 2012). In an acidified environment like the Bouraké lagoon, unchanged or lower R rates of corals as observed in this study suggest either lower growth rates or reallocation of the energy budget. The former outcome seems likely, as Camp et al. (2017) reported lower calcification rates of Bouraké corals compared to reference corals. A study conducted at another mangrove site in Sulawesi, Indonesia also found that corals did not increase their R rates compared to control fragments (Camp et al. 2016). Low pO_2 characteristic of mangrove habitats (Kristensen et al. 2008) could be a limiting factor in the ability of corals to increase their day R rates, especially at night when O_2 is not being produced by symbionts. It is to be noted that previous studies carried out in Bouraké found that day R

rates of Bouraké corals were higher than those of reference corals (Camp et al. 2017, 2020). The discrepancy in results could come from the differences in experimental design, as well as differences in the species studied. Indeed, these previous studies incubated Bouraké and reference corals using seawater from their respective sites, while we compared P and R rates of both groups using seawater collected only in Bouraké.

Altogether, our results show that corals that have been chronically exposed to extreme conditions display different P and R rates than corals from an adjacent reference site. These differences persisted even when corals were exposed during short-term periods to contrasting incubation conditions, suggesting that they originate from intrinsic traits rather than differing environmental conditions. This study does not allow to discriminate the role played by acclimatization (resulting from corals' plasticity) and adaptation (resulting from genetic modifications) in the differences observed between both sites. As acclimation occurs at a faster rate than adaptation, knowing which process is prevalent is important to assess if corals' have the potential to keep up with climate change (Palumbi et al. 2014). Transplantation experiments and metatranscriptomic approaches would be necessary to assess the respective roles of adaptation and acclimation, which have never been carried out yet in an environment combining this trio of stressors.

The Bouraké site is the first site displaying multiple and fluctuating stressors where corals' endosymbiont functions, photosynthesis and respiration have been investigated. This study consolidates previous results from single-stressor sites, such as CO_2 seeps, showing that corals' responses to extreme conditions are largely species-specific. Indeed, variations of P and day R rates between Bouraké and reference corals were heterogeneous among species, and both increases and decreases in these values were observed. This is consistent with findings from coral communities developing around volcanic CO_2 seeps in Papua New Guinea (Biscéré et al. 2019; Strahl et al. 2015), which showed species-specific rather than stereotyped responses of *P* and R rates to their acidified environment. While Strahl et al. (2015) found no effect of pCO_2 on R rates and heterogeneous effects on P_g rates, Biscéré et al. (2019) found increased P_g, day R and P_g: day R under elevated pCO_2. This suggests that corals' adjustments to extreme environments can take diverse forms and that responses are species- and site-dependent rather than stereotyped (Hoadley et al. 2015). This study also highlights that some coral species might have more limited abilities to adjust to unfavorable conditions. For example, we found that the two Acroporidae species (*A. tenuis* and *A. samoensis*) displayed the lowest P_g: day R rates and were the only species for which this value was not higher than that of the reference colonies. Increased *P* rates and P_g: day R ratios have been linked to higher productivity, which is thought to play an important role in corals' tolerance to acidified conditions (Fabricius et al. 2011). This suggests that Acroporidae species are undergoing higher energetic stress, and could thus be more vulnerable to any additional stressor occurring in the Bouraké lagoon. Past studies have also evidenced a lower resistance of Acroporidae to extreme conditions, suggesting they could be potential losers in our world's future oceans (Loya et al. 2001; Schoepf et al. 2013). The vulnerability of Acroporidae could be further exacerbated by their typically low heterotrophic intakes and low heterotrophic plasticity compared to other genera such as Montiporidae or Pocilloporidae (Palardy et al. 2008; Conti-Jerpe et al. 2020; Sangmanee et al. 2020). However, comparison of results between species is limited because tissue extraction and wax surface measurement is known to vary depending on each species' structure and geometry (Edmunds and Gates 2002), leading to a species bias for chlorophyll contents, symbiont contents and surface area. As our results for photosynthesis and respiration rates were normalized by chlorophyll and area values, species comparison for any of our studied variables is to be considered cautiously, which is why it was not further developed in this study.

The persistence of knowledge gaps on how single environmental stressors affect corals' metabolism obscures the interpretation of how these stressors could affect photosynthesis and respiration when combined. While the effects of acidification and warming have been largely investigated, at least separately and on non-adapted corals, the effects of low DO on corals' physiology are poorly understood. Deoxygenation is predicted to increasingly affect marine ecosystems as a result of global warming and eutrophication (Hughes et al. 2020). The few studies conducted on coral reefs (Altieri et al. 2017; Haas et al. 2014; Hughes et al. 2020) reported hypoxic thresholds around 3–4.0 mg L^{-1}, although this value is likely to vary according to species and site. As DO reach a minimum of 2.28 mg L^{-1} in the Bouraké lagoon, it likely acts as a stressor on corals' metabolism. Additionally, as low DO limits aerobic metabolism, it is thought to be even more harmful when combined with other stressors such as high temperatures or acidification, which tend to increase the energy requirements of marine organisms (Breitburg et al. 2018). While hyposalinity has been shown to be detrimental to corals' metabolism (Moberg et al. 1997; Ferrier-Pages et al. 1999; Alutoin et al. 2001; Gardner et al. 2016), the effects of high salinity have received little attention, although some evidence suggests it could convey thermotolerance to coral species (Gegner et al., 2017). The numerous and concomitant stressors occurring in the Bouraké lagoon are thus both what make it a unique and valuable natural laboratory and what limit the interpretation of our results.

We recognise that our experimental approach has limitations and that several caveats might interfere with our results

reporting low metabolic "stress" in corals that have developed in the extreme conditions of the lagoon of Bouraké. First of all, we compared only two sites: one within the Bouraké lagoon and one adjacent reference fringing reef, which does not allow us to investigate whether spatial variations occur in our studied system. Although environmental conditions are quite homogeneous within the Bouraké lagoon, which is why we based our experiment on a single site, we would recommend future studies to sample corals from several sites both within the lagoon of Bouraké and in adjacent fringing reefs. Furthermore, this experiment measured the photosynthesis and respiration of corals during the morning low tide and during the afternoon high tide. This could introduce a bias in the comparison of photosynthesis and respiration under low tide and high tide conditions because metabolism is known to change in relation to the time of the day. Ideally, our experiment should also be repeated during the night to test both low and high tide conditions on corals fully dark adapted, although such an experiment would come with logistic and security constraints on a research vessel.

Although some limitations exist, corals from naturally extreme environments are an invaluable tool to understand the mechanisms supporting higher tolerance to future climatic conditions. This study showed that corals that have been exposed their whole life, and possibly across generations, to extreme and fluctuating T, pH and DO, are able to maintain unaltered levels of symbionts and chlorophylls, as well as sustained photosynthesis and respiration rates. As such, the lagoon of Bouraké provides evidence that corals are able to maintain their autotrophic source of energy even under the combined effects of warming, acidification and deoxygenation, which have been feared to impair the physiological mechanisms necessary for corals' survival (Breitburg et al. 2018; Hughes et al. 2020). The variability of T, pH and DO occurring in the Bouraké lagoon could play a significant role in the ability of corals to cope with extreme conditions. Although research on the role of environmental variability is in its prime, it has been suggested to enhance corals' plasticity and possibly their tolerance to future projected conditions (Oliver and Palumbi 2011; Rivest et al. 2017; Schoepf et al. 2015). Undergoing chronic varying conditions could have helped the Bouraké corals to survive the 2016 bleaching episode that impacted most reefs of New Caledonia (Benzoni et al. 2017; Camp et al. 2017). Other specificities of the Bouraké lagoon, such as higher turbidity levels and potentially higher nutrient concentrations, could also play a role in the survival of the documented coral species by counterbalancing the negative effects of local stressors. The combination of these specificities could explain why the lagoon of Bouraké is one of the only sites where corals developing under warm, acidified and deoxygenated conditions have been observed. While providing evidence for the ability of corals to develop under such stressors, it does not ensure that this ability could be generalized to other sites displaying a different set of unique environmental conditions and that this ability will be maintained in a warmer future (Grottoli et al. 2014; Schoepf et al. 2015; Nohaïc et al. 2017).

Supplementary Information The online version contains supplementary material available at https://doi.org/10.1007/s00227-022-04063-6.

Acknowledgements We thank the whole crew on board of the Alis vessel to have enabled us to conduct this fieldwork. We thank the IRD of Nouméa for having provided facilities and the equipment necessary to conduct this study. We are grateful to Federica Maggioni for her help during fieldwork and for data sharing. We thank Saki Harii for his help throughout the reviewing and editing process of this article, and Kaleb Trunnell for English proofreading. The base data to drawn Figure 1 were collected from map tiles at www.georep.nc (©Georep contributors).

Author contributions The study conception and design were performed by RRM. Material preparation and data collection were performed by JJ and CT, under the supervision of RRM and FH. Data analysis and writing of the first draft were performed by JJt. All authors read and approved the final manuscript.

Funding This work was partially funded by the LabEx-Corail (project SURF to F.H.), and the Ministère des Affaires étrangères et du développement international (MAEDI) Fonds Pacifique (project Super Coraux to R.R.-M.). Data were collected during the cruise SuperNatural 2 (https://doi.org/10.17600/18001102) onboard the R/V Alis (Flotte Océanographique Francaise).

Availability of data The datasets generated and analysed during the current study are available from the corresponding author on reasonable request

Code availability Not applicable.

Declarations

Conflict of interest The authors declare that they have no competing interests.

Ethics approval All corals were collected under permits issued by the Province Sud of New Caledonia (# 3413–2019)).

References

Altieri AH, Harrison SB, Seemann J, Collin R, Diaz RJ, Knowlton N (2017) Tropical dead zones and mass mortalities on coral reefs. Proc Natl Acad Sci USA 114:3660–3665. https://doi.org/10.1073/pnas.1621517114

Alutoin S, Boberg J, Nyström M, Tedengren M (2001) Effects of the multiple stressors copper and reduced salinity on the metabolism of the hermatypic coral *Porites lutea*. Mar Env Res 52:289–299. https://doi.org/10.1016/S0141-1136(01)00105-2

Anthony KRN (2000) Enhanced particle-feeding capacity of corals on turbid reefs (Great Barrier Reef, Australia). Coral Reefs 19:59–67. https://doi.org/10.1007/s003380050227

Anthony K, Kline D, Diaz-Pulido G, Dove S, Hoegh-Guldberg O (2008) Ocean acidification causes bleaching and productivity loss in coral reef builders. Proc Natl Acad Sci USA 105:17442–6. https://doi.org/10.1073/pnas.0804478105

Benzoni F, Houlbreque F, Andre L, Payri C (2017) Plan d'action rapide et adaptatif, en cas de blanchissement corallien : le cas de la Nouvelle-Calédonie, épisode 2016: synthèse

Biscéré T, Lorrain A, Rodolfo-Metalpa R, Gilbert A, Wright A, Devissi C, Peignon C, Farman R, Duvieilbourg E, Payri C, Houlbrèque F (2017) Nickel and ocean warming affect scleractinian coral growth. Mar Pollut Bull 120:250–258. https://doi.org/10.1016/j.marpolbul.2017.05.025

Biscéré T, Zampighi M, Lorrain A, Jurriaans S, Foggo A, Houlbrèque F, Rodolfo-Metalpa R (2019) High pCO_2 promotes coral primary production. Biol Lett 15:20180777. https://doi.org/10.1098/rsbl.2018.0777

Biscéré T, Ferrier-Pagès C, Gilbert A, Pichler T, Houlbrèque F (2018) Evidence for mitigation of coral bleaching by manganese. Sci Rep 8:16789. https://doi.org/10.1038/s41598-018-34994-4

Bopp L, Resplandy L, Orr JC, Doney SC, Dunne JP, Gehlen M, Halloran P, Heinze C, Ilyina T, Seferian R, Tjiputra J (2013) Multiple stressors of ocean ecosystems in the 21st century: projections with CMIP5 models. Biogeosciences 10:6225–6245. https://doi.org/10.5194/bg-10-6225-2013

Breitburg D, Levin LA, Oschlies A, Grégoire M, Chavez FP, Conley DJ, Garçon V, Gilbert D, Gutiérrez D, Isensee K, Jacinto GS, Limburg KE, Montes I, Naqvi SWA, Pitcher GC, Rabalais NN, Roman MR, Rose KA, Seibel BA, Telszewski M, Yasuhara M, Zhang J (2018) Declining oxygen in the global ocean and coastal waters. Science. https://doi.org/10.1126/science.aam7240

Brown KT, Bender-Champ D, Kenyon TM, Rémond C, Hoegh-Guldberg O, Dove S (2019) Temporal effects of ocean warming and acidification on coral–algal competition. Coral Reefs 38:297–309. https://doi.org/10.1007/s00338-019-01775-y

Camp EF, Suggett DJ, Gendron G, Jompa J, Manfrino C, Smith DJ (2016) Mangrove and seagrass beds provide different biogeochemical services for corals threatened by climate change. Front Mar Sci 3:52. https://doi.org/10.3389/fmars.2016.00052

Camp EF, Nitschke MR, Rodolfo-Metalpa R, Houlbreque F, Gardner SG, Smith DJ, Zampighi M, Suggett DJ (2017) Reef-building corals thrive within hot-acidified and deoxygenated waters. Sci Rep 7:2434. https://doi.org/10.1038/s41598-017-02383-y

Camp EF, Schoepf V, Mumby PJ, Hardtke LA, Rodolfo-Metalpa R, Smith DJ, Suggett DJ (2018) The future of coral reefs subject to rapid climate change: Lessons from natural extreme environments. Front Mar Sci 5:4. https://doi.org/10.3389/fmars.2018a.00004

Camp EF, Schoepf V, Suggett DJ (2018b) How can "Super Corals" facilitate global coral reef survival under rapid environmental and climatic change? Glob Change Biol 24:2755–2757. https://doi.org/10.1111/gcb.14153

Camp EF, Suggett DJ, Pogoreutz C, Nitschke MR, Houlbreque F, Hume BCC, Gardner SG, Zampighi M, Rodolfo-Metalpa R, Voolstra CR (2020) Corals exhibit distinct patterns of microbial reorganisation to thrive in an extreme inshore environment. Coral Reefs 39:701–716. https://doi.org/10.1007/s00338-019-01889-3

Comeau S, Carpenter RC, Edmunds PJ (2017) Effects of pCO_2 on photosynthesis and respiration of tropical scleractinian corals and calcified algae. ICES J Mar Sci 74:1092–1102. https://doi.org/10.1093/icesjms/fsv267

Connolly SR, Lopez-Yglesias MA, Anthony KRN (2012) Food availability promotes rapid recovery from thermal stress in a scleractinian coral. Coral Reefs 31:951–960. https://doi.org/10.1007/s00338-012-0925-9

Conti-Jerpe IE, Thompson PD, Wong CWM, Oliveira NL, Duprey NN, Moynihan MA, Baker DM (2020) Trophic strategy and bleaching resistance in reef-building corals. Sci Adv. https://doi.org/10.1126/sciadv.aaz5443

Crawley A, Kline D, Dunn S, Anthony K, Dove S (2010) The effect of ocean acidification on symbiont photorespiration and productivity in *Acropora formosa*. Glob Change Biol 16:851–863. https://doi.org/10.1111/j.1365-2486.2009.01943.x

Edmunds PJ (2011) Zooplanktivory ameliorates the effects of ocean acidification on the reef coral *Porites* spp. Limnol Oceanogr 56:2402–2410. https://doi.org/10.4319/lo.2011.56.6.2402

Edmunds P (2012) Effect of pCO_2 on the growth, respiration, and photophysiology of massive *Porites* spp. in Moorea. French Polynesia Mar Biol 159:2149–2160. https://doi.org/10.1007/s00227-012-2001-y

Edmunds PJ, Davies PS (1988) Post-illumination stimulation of respiration rate in the coral *Porites porites*. Coral Reefs 7:7–9. https://doi.org/10.1007/BF00301975

Edmunds P, Gates R (2002) Normalizing physiological data for scleractinian corals. Coral Reefs 21:193–197. https://doi.org/10.1007/s00338-002-0214-0

Enríquez S, Méndez ER, Iglesias-Prieto R (2005) Multiple scattering on coral skeletons enhances light absorption by symbiotic algae. Limnol Oceanogr 50:1025–1032. https://doi.org/10.4319/lo.2005.50.4.1025

Fabricius KE, Langdon C, Uthicke S, Humphrey C, Noonan S, De'ath G, Okazaki R, Muehllehner N, Glas MS, Lough JM (2011) Losers and winners in coral reefs acclimatized to elevated carbon dioxide concentrations. Nat Clim Change 1:165–169. https://doi.org/10.1038/nclimate1122

Ferrier-Pages C, Gattuso J, Jaubert J (1999) Effect of small variations in salinity on the rates of photosynthesis and respiration of the zooxanthellate coral *Stylophora pistillata*. Mar Ecol Prog Ser 181:309–314. https://doi.org/10.3354/meps181309

Ferrier-Pagès C, Rottier C, Beraud E, Levy O (2010) Experimental assessment of the feeding effort of three scleractinian coral species during a thermal stress: Effect on the rates of photosynthesis. J Exp Mar Biol Ecol 390:118–124. https://doi.org/10.1016/j.jembe.2010.05.007

Gardner SG, Nielsen DA, Laczka O, Shimmon R, Beltran VH, Ralph PJ, Petrou K (2016) Dimethylsulfoniopropionate, superoxide dismutase and glutathione as stress response indicators in three corals under short-term hyposalinity stress. Proc R Soc B-Biol Sci 283:20152418. https://doi.org/10.1098/rspb.2015.2418

Gegner HM, Ziegler M, Rädecker N, Buitrago-López C, Aranda M, Voolstra CR (2017) High salinity conveys thermotolerance in the coral model *Aiptasia*. Biology Open 6:1943–1948. https://doi.org/10.1242/bio.028878

Godinot C, Houlbrèque F, Grover R, Ferrier-Pagès C (2011) Coral uptake of inorganic phosphorus and nitrogen negatively affected by simultaneous changes in temperature and pH. PLoS ONE 6:e25024. https://doi.org/10.1371/journal.pone.0025024

Grottoli AG, Rodrigues LJ, Palardy JE (2006) Heterotrophic plasticity and resilience in bleached corals. Nature 440:1186–1189. https://doi.org/10.1038/nature04565

Grottoli AG, Warner ME, Levas SJ, Aschaffenburg MD, Schoepf V, McGinley M, Baumann J, Matsui Y (2014) The cumulative impact of annual coral bleaching can turn some coral species winners into losers. Glob Change Biol 20:3823–3833. https://doi.org/10.1111/gcb.12658

Grottoli A, Tchernov D, Winters G (2017) Physiological and biogeochemical responses of super-corals to thermal stress from the Northern Gulf of aqaba. Red Sea Front Mar Sci 4:215. https://doi.org/10.1038/srep18371

Haas A, Smith J, Thompson M, Deheyn D (2014) Effects of reduced dissolved oxygen concentrations on physiology and fluorescence of hermatypic corals and benthic algae. PeerJ 2:235. https://doi.org/10.7717/peerj.235

Hoadley KD, Pettay DT, Grottoli AG, Cai WJ, Melman TF, Schoepf V, Hu X, Li Q, Xu H, Wang Y, Matsui Y, Baumann JH, Warner ME (2015) Physiological response to elevated temperature and pCO_2 varies across four Pacific coral species: Understanding the unique host+symbiont response. Sci Rep 5:18371. https://doi.org/10.1038/srep18371

Hoegh-Guldberg O, Mumby P, Hooten AJ, Steneck RS, Greenfield P, Gomez E, Harvell C, Sale P, Edwards A, Caldeira K, Knowlton N, Eakin CM, Iglesias-Prieto R, Muthiga N, Bradbury R, Dubi A, Hatziolos M (2008) Coral reefs under rapid climate change and ocean acidification. Science 318:1737–1742. https://doi.org/10.1126/science.1152509

Hoegh-Guldberg O, Poloczanska E, Skirving W, Dove S (2017) Coral reef ecosystems under climate change and ocean acidification. Front Mar Sci 4:158. https://doi.org/10.3389/fmars.2017.00158

Hoegh-Guldberg O, Jacob DM, Taylor M, Bindi S, Brown I, Camilloni A, Diedhiou R, Djalante KL, Ebi F, Engelbrecht J, Guiot Y, Hijioka S, Mehrotra A, Payne SI, Seneviratne A, Thomas R, Zhou G (2018) Impacts of 1.5ºC Global Warming on Natural and Human Systems. In: Global Warming of 1.5°C. An IPCC Special Report on the impacts of global warming of 1.5°C above pre-industrial levels and related global greenhouse gas emission pathways, in the context of strengthening the global response to the threat of climate change, sustainable development, and efforts to eradicate poverty (In Press)

Houlbrèque F, Tambutté E, Ferrier-Pagès C (2003) Effect of zooplankton availability on the rates of photosynthesis, and tissue and skeletal growth in the scleractinian coral *Stylophora pistillata*. J Exp Mar Biol Ecol 296:145–166. https://doi.org/10.1016/S0022-0981(03)00259-4

Houlbrèque F, Reynaud S, Godinot C, Oberhänsli F, Rodolfo-Metalpa R, Ferrier-Pagès C (2015) Ocean acidification reduces feeding rates in the scleractinian coral *Stylophora pistillata*. Limnol Oceanogr 60:89–99. https://doi.org/10.1002/lno.10003

Howells EJ, Abrego D, Meyer E, Kirk NL, Burt JA (2016) Host adaptation and unexpected symbiont partners enable reef-building corals to tolerate extreme temperatures. Glob Change Biol 22:2702–2714. https://doi.org/10.1111/gcb.13250

Hughes DJ, Alderdice R, Cooney C, Kühl M, Pernice M, Voolstra CR, Suggett DJ (2020) Coral reef survival under accelerating ocean deoxygenation. Nat Clim Change 10:296–307. https://doi.org/10.1038/s41558-020-0737-9

Inoue S, Kayanne H, Yamamoto S, Kurihara H (2013) Spatial community shift from hard to soft corals in acidified water. Nat Clim Change 3:683–687. https://doi.org/10.1038/nclimate1855

IPCC (2019) Summary for policymakers. In: Pörtner HO, Roberts DC, Masson-Delmotte V, Zhai P, Tignor M, Poloczanska E, Mintenbeck K, Alegría A, Nicolai M, Okem A, Petzold J, Rama B, Weyer NM (eds) IPCC Special Report on the Ocean and Cryosphere in a Changing Climate (In press)

Jeffrey SW, Humphrey GF (1975) New spectrophotometric equations for determining chlorophylls a, b, c_1 and c_2 in higher plants, algae and natural phytoplankton. Biochem Physiol Pflanz 167:191–194. https://doi.org/10.1016/S0015-3796(17)30778-3

Kenkel CD, Moya A, Strahl J, Humphrey C, Bay LK (2018) Functional genomic analysis of corals from natural CO_2 -seeps reveals core molecular responses involved in acclimatization to ocean acidification. Glob Change Biol 24:158–171. https://doi.org/10.1111/gcb.13833

Kleypas JA, McManus JW, Menez LA (1999) Environmental limits to coral reef development: where do we draw the line? Am Zool 39:146–159. https://doi.org/10.1093/icb/39.1.146

Kristensen E, Bouillon S, Dittmar T, Marchand C (2008) Organic carbon dynamics in mangrove ecosystems: A review. Aquatic Botany Mangrove Ecol Applic Forestry Coastal Zone Manag 89:201–219. https://doi.org/10.1016/j.aquabot.2007.12.005

Kroeker KJ, Kordas RL, Crim RN, Singh GG (2010) Meta-analysis reveals negative yet variable effects of ocean acidification on marine organisms. Ecol Lett 13:1419–1434. https://doi.org/10.1111/j.1461-0248.2010.01518.x

Kroeker KJ, Kordas RL, Crim R, Hendriks IE, Ramajo L, Singh GS, Duarte CM, Gattuso JP (2013) Impacts of ocean acidification on marine organisms: quantifying sensitivities and interaction with warming. Glob Change Biol 19:1884–1896. https://doi.org/10.1111/gcb.12179

Langdon C, Atkinson M (2005) Effect of elevated pCO_2 on photosynthesis and calcification of corals and interactions with seasonal change in temperature/irradiance and nutrient enrichment. J Geophysical Res. https://doi.org/10.1029/2004JC002576

Le Nohaïc M, Ross CL, Cornwall CE, Comeau S, Lowe R, McCulloch MT, Schoepf V (2017) Marine heatwave causes unprecedented regional mass bleaching of thermally resistant corals in northwestern Australia. Sci Rep 7:111. https://doi.org/10.1038/s41598-017-14794-y

Lesser MP, Farrell JH (2004) Exposure to solar radiation increases damage to both host tissues and algal symbionts of corals during thermal stress. Coral Reefs 23:367–377. https://doi.org/10.1007/s00338-004-0392-z

Logan CA, Dunne JP, Eakin CM, Donner SD (2014) Incorporating adaptive responses into future projections of coral bleaching. Glob Change Biol 20:125–139. https://doi.org/10.1111/gcb.12390

Loya Y, Sakai K, Yamazato K, Nakano Y, Sambali H, van Woesik R (2001) Coral bleaching: the winners and the losers. Ecol Lett 4:122–131. https://doi.org/10.1046/j.1461-0248.2001.00203.x

Maggioni F, Pujo-Pay M, Aucan J, Cerrano C, Calcinai B, Payri C, Benzoni F, Letourneur Y, Rodolfo-Metalpa R (2021) The Bouraké semi-enclosed lagoon (New Caledonia)–a natural laboratory to study the lifelong adaptation of a coral reef ecosystem to extreme environmental conditions. Biogeosciences 18:5117–5514. https://doi.org/10.5194/bg-18-5117-2021

McCulloch M, Falter J, Trotter J, Montagna P (2012) Coral resilience to ocean acidification and global warming through pH up-regulation. Nat Clim Change 2:623–627. https://doi.org/10.1038/nclimate1473

McLachlan RH, Price JT, Solomon SL, Grottoli AG (2020) Thirty years of coral heat-stress experiments: a review of methods. Coral Reefs 39(4):885–902. https://doi.org/10.1007/s00338-020-01931-9

Moberg F, Nyström M, Kautsky N, Tedengren M, Jarayabhand P (1997) Effects of reduced salinity on the rates of photosynthesis and respiration in the hermatypic corals *Porites lutea* and *Pocillopora damicornis*. Mar Ecol Prog Ser 157:53–59. https://doi.org/10.3354/meps157053

Morgan KM, Perry CT, Johnson JA, Smithers SG (2017) Nearshore turbid-zone corals exhibit high bleaching tolerance on the Great barrier reef following the 2016 ocean warming event. Front Mar Sci 4:224. https://doi.org/10.3389/fmars.2017.00224

Muscatine L (1990) The role of symbiotic algae in carbon and energy flux in reef corals. Ecosyst World 25:75–87

Noonan SHC, Fabricius KE, Humphrey C (2013) Symbiodinium community composition in scleractinian corals is not affected by lifelong exposure to elevated carbon dioxide. PLoS ONE 8:e63985. https://doi.org/10.1371/journal.pone.0063985

Oliver TA, Palumbi SR (2011) Do fluctuating temperature environments elevate coral thermal tolerance? Coral Reefs 30:429–440. https://doi.org/10.1007/s00338-011-0721-y

Palardy JE, Rodrigues LJ, Grottoli AG (2008) The importance of zooplankton to the daily metabolic carbon requirements of healthy and bleached corals at two depths. J Exp Mar Biol Ecol 367:180–188. https://doi.org/10.1016/j.jembe.2008.09.015

Palumbi S, Barshis D, Traylor-Knowles N, Bay R (2014) Mechanisms of reef coral resistance to future climate change. Science 344:895–898. https://doi.org/10.1126/science.1251336

Rees TV, Smith D (1991) Are symbiotic algae nutrient deficient? Proc R Soc B-Biol Sci 243:227–233. https://doi.org/10.1098/rspb.1991.0036

Rivest EB, Comea S, Cornwall CE (2017) The role of natural variability in shaping the response of coral reef organisms to climate change. Curr Clim Change Rep 3:271–281. https://doi.org/10.1007/s40641-017-0082-x

Rodolfo-Metalpa R, Houlbrèque F, Tambutté É, Boisson F, Baggini C, Patti FP, Jeffree R, Fine M, Foggo A, Gattuso JP, Hall-Spencer JM (2011) Coral and mollusc resistance to ocean acidification adversely affected by warming. Nat Clim Change 1:308–312. https://doi.org/10.1038/nclimate1200

RStudio Team (2019) RStudio: Integrated Development for R. RStudio Inc., Boston. https://www.rstudio.com

Sangmanee K, Casareto BE, Nguyen TD, Sangsawang L, Toyoda K, Suzuki T, Suzuki Y (2020) Influence of thermal stress and bleaching on heterotrophic feeding of two scleractinian corals on picononanoplankton. Mar Pollut Bull 158:111405. https://doi.org/10.1016/j.marpolbul.2020.111405

Schoepf V, Grottoli A, Warner M, Cai WJ, Melman T, Hoadley K, Pettay D, Hu X, Li Q, Xu H, Wang Y, Matsui Y, Baumann J (2013) Coral energy reserves and calcification in a high-CO_2 world at two temperatures. PLoS One 8:e75049. https://doi.org/10.1371/journal.pone.0075049

Schoepf V, Sta M, Falter JL, McCulloch MT (2015) Limits to the thermal tolerance of corals adapted to a highly fluctuating, naturally extreme temperature environment. Sci Rep 5:17639. https://doi.org/10.1038/srep17639

Strahl J, Stolz I, Uthicke S, Vogel N, Noonan SHC, Fabricius KE (2015) Physiological and ecological performance differs in four coral taxa at a volcanic carbon dioxide seep. Comp Biochem Phys A 184:179–186. https://doi.org/10.1016/j.cbpa.2015.02.018

Sully S, van Woesik R (2020) Turbid reefs moderate coral bleaching under climate-related temperature stress. Glob Change Biol 26:1367–1373. https://doi.org/10.1111/gcb.14948

Titlyanov EA, Titlyanova TV, Yamazato K, van Woesik R (2001) Photo-acclimation dynamics of the coral *Stylophora pistillata* to low and extremely low light. J Exp Mar Biol Ecol 263:211–225. https://doi.org/10.1016/S0022-0981(01)00309-4

Torda G, Donelson JM, Aranda M, Barshis DJ, Bay L, Berumen ML, Bourne DG, Cantin N, Foret S, Matz M, Miller DJ, Moya A, Putnam HM, Ravasi T, van Oppen MJH, Thurber RV, Vidal-Dupiol J, Voolstra CR, Watson SA, Whitelaw E, Willis BL, Munday PL (2017) Rapid adaptive responses to climate change in corals. Nat Clim Change 7:627–636. https://doi.org/10.1038/nclimate3374

Van Woesik R, Houk P, Isechal AL, Idechong JW, Victor S, Golbuu Y (2012) Climate-change refugia in the sheltered bays of Palau: analogs of future reefs. Ecol Evol 2:2474–2484. https://doi.org/10.1002/ece3.363

Veal CJ, Carmi M, Fine M, Hoegh-Guldberg O (2010) Increasing the accuracy of surface area estimation using single wax dipping of coral fragments. Coral Reefs 29:893–897. https://doi.org/10.1007/s00338-010-0647-9

Article annex n°2

PROCEEDINGS OF THE ROYAL SOCIETY B
THE ROYAL SOCIETY PUBLISHING
BIOLOGICAL SCIENCES
Received: 10 February 2023; ***Under review***

Internal pH regulation traced by Li isotopes in tropical corals exposed to high pCO_2

Fanny Thibon[a,f], Steeve Comeau[a,d], Riccardo Rodolfo Metalpa[b], Maryline Montanes[a], Laurent Counillon[c], Malcolm McCulloch[d], Clément Tanvet[b,e], Mallorie Poet[c], Philippe Télouk[f], Nathalie Vigier[a]

[a] Laboratoire d'Océanographie de Villefranche (LOV), CNRS, Sorbonne université, 06230 Villefranche-sur-Mer, France

[b] Centre IRD Nouméa, UMR ENTROPIE (IRD, Université de la Réunion, Université de la Nouvelle-Calédonie, Ifremer), Nouméa 98848, New Caledonia

[c] Université Côte d'Azur, CNRS, Laboratoire de Physiologie Cellulaire et Moléculaire (LP2M), 06107 Nice, France

[d] Oceans Graduate School, The University of Western Australia, Crawley 6009, Western Australia, Australia

[e] Univ Brest, CNRS, IRD, Ifremer, LEMAR, F-29280 Plouzané, France

[f] Laboratoire de Géologie de Lyon – Terre Planètes Environnement (LGL-TPE), CNRS, ENS-UCBL-UJM, 69007 Lyon, France

Abstract

Combined lithium (δ^7Li) and boron (δ^{11}B) isotopic and Li/Mg, B/Ca elemental ratios are investigated in coral aragonite as palaeoceanographic proxies for the carbonate chemistry of the calcifying-fluid. Unlike for fossil biogenic calcite, Li isotope data are limited for biogenic aragonite archives, particularly for scleractinian corals. Here we use δ^7Li and δ^{11}B isotopic systematics together with Li/Mg and B/Ca to understand how changes in seawater pH influence calcification mechanisms and the carbonate chemistry of the calcifying fluid from which coral skeleton is precipitated. We report the Li and B isotopic systematics of eight tropical coral species living under two pH conditions in Papua New Guinea: (1) low seawater pH (mean pH_T = 7.66) in a shallow water volcanic CO_2 seeps site, and (2) ambient seawater pH (pH_T = 8.01) in a control site. The $\delta^{11}B_{carb}$ skeletal composition ranges from 20.7 ‰ to 25.4 ‰, corresponding to an internal calcifying fluid pH_{cf} from 8.2 to 8.5, with significant species-specific effect but no detectable differences between sites. In contrast, δ^7Li_{carb} ranges from 18.1 ‰ to 20.4 ‰ with small but significant differences among species and between sites. An anti-correlation between Δ^7Li and pH_{cf} indicates that the skeleton enrichment in ^{6}Li is linked to the organism's ability to maintain elevated pH_{cf}. We propose that this trend is due to the active involvement of Na^+-H^+ transporters (NHE) in the internal pH regulation and their role in enhancing Li transport at the cellular level. We show that the combination of B and Li isotopes provides unique insights into the influence of pH and hence ocean acidification on coral calcification mechanisms, and also offers a new quantitative approach to assess the biological impacts of ocean acidification on coral calcification.

Keywords: Scleractinian corals, Li isotopes, B isotopes, Ocean acidification, CO_2 seeps.

Introduction

Ocean uptake of atmospheric CO_2 produced by human activities leads to profound modification of the seawater carbonate chemistry, which includes an increase in dissolved inorganic carbon and a decrease in pH in a process known as ocean acidification (1). Ocean acidification can have major effects on marine organisms, particularly on calcifying species such as scleractinian – aragonitic – corals. They rely on the precipitation of calcium carbonate ($CaCO_3$) to build their skeleton, with coral reefs representing 7 to 15 % of marine $CaCO_3$ production (2). Coral colonies consist of individual polyps linked together by a coenosarc covering an aragonitic skeleton. Calcification takes place in the

extracellular calcifying medium (or Calcifying Fluid, CF) that separates the skeleton from the overlying calcifying cell layer.

Scleractinian corals appeared during the mid-Triassic period (~237Ma) and are valuable taxa for reconstructing paleoenvironments of the Mesozoic and Cenozoic eras. Most of the research on past oceans environmental conditions relies on geochemical analyses (*e.g.*, Mg/Ca, Li/Mg), boron (B) isotopes, and B/Ca ratios) performed in fossil skeletons (3-7). For instance, corals skeleton Li/Mg has been recognized as a proxy of past seawater temperature (8-11). Li/Mg ratios from cold-water-corals have been used to reconstruct Holocene bottom water temperature (12,13). Nevertheless, some caveats have been raised. For example, the reliability of this proxy depends on the absence of contamination by organic matter and diagenetic calcite (9), and possibly on the reef location (backreef-based or forereef-based (14)). Additionally, boron (B) chemistry ($\delta^{11}B$ and B/Ca) has recently been used in physiological studies to estimate the pH and dissolved inorganic carbon concentration of coral calcifying fluids under a variety of environmental conditions (15-18). However the combined effects of climate change and ocean acidification on coral calcification mechanisms remain to be fully investigated (15,17-19). It is, therefore, crucial to better understand how environmental parameters (such as ocean pH) may affect coral biogeochemistry, with the aim to use them as tracers of ancient environmental conditions and as tools to understand the effects of present climate change.

Lithium isotopes in marine biogenic carbonate have been used as a proxy of Li isotope composition of the ocean and hence to trace continental erosion and the CO_2 cycle over the long-term. Li isotopes are significantly fractionated during chemical weathering of silicate rocks, which impacts the Li isotopic composition of river waters, a major source of Li to the ocean (20-25). Silicate rock weathering is a major sink of atmospheric CO_2 and is thus related to the ocean carbonate chemistry. Due to its long oceanic residence time (~1.2 million years; (21)), Li is homogeneously distributed throughout the water column (26). Although intensively investigated in foraminifera and biogenic calcite (13,22,23,27,28), Li isotope data remain scarce in biogenic aragonite, with only a few studies in corals. As a consequence, the inter-species effects and the impact of biological and calcifying processes under various environmental conditions still need to be unraveled (22,29-31).

This study reports a detailed geochemical study of eight species of tropical shallow-water scleractinian corals collected in Tutum Bay (Ambitle Island, Papua New Guinea) where natural CO_2 seeps have been evidenced (32,33). Li and B isotopes ratios together with major elements concentrations ratios are measured in the skeleton of corals collected from two sites that display different pH conditions: (1) a site with low seawater pH (pH_T = 7.66) located close to CO_2 seeps, and (2) a control site, where seawater is at ambient pH (pH_T = 8.01). This study aims firstly at evaluating how seawater pH may impact coral skeletal Li and Li/Mg geochemistry in combination with B geochemistry

and their utility for paleoenvironmental reconstructions; secondly, we want to determine if these isotopic proxies exhibit vital (biological) and species effects; and thirdly, we propose transcellular pathways and physiological mechanisms that explain the results presented here.

1. Material and Methods

1.1. Environmental characterisation and sampling

The biochemistry of seawater and gases released over Tutum Bay at Ambitle Island (New Ireland, Papua New Guinea) have been extensively characterized (33). The whole bay has a mean pH ranging from 7.6 to 7.7 and an approximately constant 30º C temperature year-round. Reduced seawater pH -and consequent changes in the seawater carbonate chemistry- is due to the continued and massive release of CO_2 gases from four main volcanic vents and seeps dispersed throughout the large bay. From 2016 to 2018 the site was visited four times using the R/V Alis (e.g., (34)) and seawater pH_T (in total scale) was measured during daily to weekly-cycles using SeaFET logger (Sea-Bird Scientific, Bellevue, WA, USA) set to measure at 5-min interval. Here, we report the environmental data collected during the fieldwork from 2016 and 2017 both at stations 1, 3-6 (Fig. S1; see also (33) for a whole bay data assessment) and at a control site located 1.8 km south of the main seep site, where the corals were collected in May 2017. Seawater temperature at seeps and at the control site were measured from September 21, 2016 to May 23, 2017 by Pendant Hobo (Onset, Bourne, MA, USA), logging at 5-min intervals and fixed at 3 m depth. Seawater samples were collected to measure total alkalinity (see (33)). Gas composition of the seeps in Tutum Bay was determined as: 93 to 98% CO_2, with minor amounts of nitrogen (N_2, 2 to 5%), methane (CH_4, < 2%), oxygen, (<1%), a trace of helium and, most importantly, no traces of toxic sulfur compounds, such as H_2S (33).

We sampled three fragments from three spatially separated (>10 m distance) corals for each of the selected shallow-water scleractinian corals skeletons, both at CO_2 seep site and a control site. The investigated species are either branching (*Acropora* sp1., *Acropora* sp2., *Pocillopora* c.f. *damicornis*), massive (*Galaxea fascicularis*, *Porites* sp.), foliated (*Montipora* sp., *Echinopora lamellosa*), or encrusting (*Psammocora* sp.) (Figs. 1 & S2). Also, as shown in figure 1, the surface/volume ratio (specific area) is different among species, from massive almost flat surface *Porites* sp. to the fine lace built by *G. Fascicularis*. Coral tissues were carefully removed on board using an air-pick in a seawater medium and dry at 40°C overnight. Corals were analyzed at the University of Western Australia for $\delta^{11}B$, B/Ca, and Li/Mg. Extraction and purification for Li isotope analyses were undertaken on the same specimens at the Laboratoire d'Océanographie de Villefranche (LOV, France).

1.2. Methods

All following procedures were performed in a pressurized clean laboratory to minimize procedural blanks, under fume-hood, using distilled reagents and pre-cleaned Teflon vessels.

1.2.1. Elemental ratios and B isotopes measurements

As described in details in Comeau et al. (32), samples were cleaned with mQ water, bleached for 24 h in 6.25 % NaClO and dried for 48 h in a drying oven at 50°C. For Acroporidae and Pocilloporidae genera, $\delta^{11}B$ and B/Ca were determined on a ~ 1 cm long piece of skeleton from the tip of three branches for each of the three colonies analysed that were pooled together to smooth potential spatial differences. For massive corals (e.g., *Favites*, *Galaxea*), a fragment of 0.5 cm^3 located ~ 0.5 cm below the surface was sampled. For *Montipora* sp. and *Echinopora lamellosa*, a section of the skeleton close to the tip was sampled using cutting pliers. The selected portions of skeletons were bleached for an additional 24 hrs in 6.25 % NaClO and then rinsed three times with mQ water before drying for 48h at 50°C. The samples were then crushed in a mortar with a pestle to powder.

In the clean laboratory of the Advanced Geochemical Facility for Indian Ocean Research (AGFIOR, University of Western Australia), 10 mg of each coral aragonitic powder were cleaned and then dissolved in 0.5 N HNO_3, from which a 10-ppm Ca aliquot was prepared for trace element determinations. Boron was quantitatively separated on ion exchange columns with B/Ca ratios determined on the same sub-aliquot of the solution used for trace-elements. Boron isotope compositions are expressed in conventional delta notation relative to the boric international standard (NBS951): $\delta^{11}B$ (‰) = ($^{11}B/^{10}B_{sample}$ / $^{11}B/^{10}B_{standard}$ -1)*1000. $\delta^{11}B$ was measured on a NU II Multicollector Inductively Coupled Plasma Mass Spectrometer (MC-ICP-MS). Measurements of the international carbonate standard JCP-1 (nominal value of 24.33 ± 0.11 ‰ (SE)) yielded a mean value of 24.43 ± 0.08 ‰ (mean ± SE, n = 10). pH_{cf} was estimated from $\delta^{11}B$ using the calculations described by Trotter et al. (35), as:

$$pH_{cf} = pK_B - \log\left[\frac{(\delta^{11}B_{SW} - \delta^{11}B_{carb})}{\left(\alpha_{(B3-B4)}\delta^{11}B_{carb} - \delta^{11}B_{SW} + 1000\left(\alpha_{(B3-B4)} - 1\right)\right)}\right] \quad (1)$$

where pK_B is the dissociation constant dependent on temperature and salinity, $\delta^{11}B_{sw}$ = 39.61 (36), and $\alpha_{(B3\text{-}B4)}$ is the boron isotopic fractionation factor for the pH dependent equilibrium of the borate ($B(OH)_4^-$) relative to the boric acid ($B(OH)_3$) species in the calcifying fluid, with a value of 1.0272 (37).

Furthermore, $[CO_3^{2-}]_{cf}$ can also be reconstructed using the equilibrium reaction of borate ion incorporation into carbonates ($0.5\ CaCO_3 + B(OH)_4^- \leftrightarrow Ca_{0.5}B(OH)_4 + 0.5\ CO_3^{2-}$) (15,17,18). Assuming $B(OH)_4^-/(CaCO_3)^{0.5} \sim (B/Ca)_{carb}$, we can write:

$$[CO_3^{2-}]_{cf} = K_D \frac{[B(OH)_4^-]}{\left(\frac{[B]}{[Ca]}\right)_{CaCO_3}} \quad (2)$$

with K_D, the distribution coefficient of borate incorporation into carbonate (18). Knowing pH_{cf} and $[CO_3^{2-}]_{cf}$, dissolved inorganic carbon concentration of calcifying fluid (DIC_{cf}) can be calculated using carbonate equilibrium equations:

$$DIC_{cf} = [CO_3^{2-}]_{cf} \times \left(1 + \frac{[H^+]}{K_2} + \frac{[H^+]^2}{K_1 + K_2}\right) \quad (3)$$

where K_1 and K_2 are equilibrium constants (first and second dissociation constants of carbonic acid, respectively).

1.2.2. Li isotopes measurements

Following the same strategy as for boron, coral samples were weighted and transferred into 5 mL clean centrifuge tubes. To remove external contamination, corals were leached for two days with a mixture of H_2O:H_2O_2 in proportion 2:1 at ambient temperature. Afterwards, samples were rinsed with distilled water, dried at 60°C, and ground into a fine powder with an agate mill. Aliquots of 15 mg were transferred to 1.5mL centrifuge tubes. A second leaching procedure was performed with HNO_3 0.05N + H_2O_2 10% for one day at ambient temperature to ensure the removal of residual organic matter. After a rinse with distilled water, samples were dissolved with 0.5 mL of 1N HCl at ambient temperature.

Seawater samples were collected in the control site and ca. 50 m upstream the vents between the stations 1 to 6 (Figure S1). The sampling was done using 20 mL polypropylene vials, previously rinsed three times using filtered seawater (Whatman™ Puradisc CA syringe filters 0.45 µm). Samples were immediately poisoned with 20 µL saturated $HgCl_2$, and then sub-sampled in 1.5 mL tubes. Aliquots were dried up and taken up in 0.5 mL of 1N HCl before Li separation.

Lithium extraction and purification were operated according to Vigier et al. (38). The samples dissolved in 0.5 mL of 1N HCl were loaded on AG 50-X12 (200-400 mesh) cationic resin in 8.5 cm high Teflon columns. Li was eluted and purified with 1N HCl. This fraction was then dried down and re-dissolved in 0.05N HNO_3 before measurements. The delta notation, expressed in per-mill (‰), is classically used

for reporting the $^{7}Li/^{6}Li$ isotope ratio: $\delta^{7}Li_{sample}$ (‰) = $\left(\frac{\left(\frac{7Li}{6Li}\right)_{sample}}{\left(\frac{7Li}{6Li}\right)_{standard}} - 1\right) * 1000$. Measurements of Li isotopic ratio were performed in the CNRS-INSU Facilities at Ecole Normale Supérieure de Lyon, using MC-ICP-MS (Thermo-Fisher Neptune *Plus*) (29,39,40). The instrument was set in dry plasma conditions and low-resolution mode. The sample-standard bracketing method (using LSVEC reference material) was applied for instrumental mass bias correction. Analytical blanks, as well as total procedural blanks, were found to be negligible. The internal reproducibility was, on average, ± 0.04‰ (2σ). The precision (external reproducibility) was estimated by 2 to 5 replicated measurements of 12 different samples, and was ~0.3‰ (2SD, ranging from 0.07‰ to 0.76‰). The whole procedure accuracy was checked by the analyses of a biogenic calcium carbonate reference material (JCp-1, *Porites sp.* coral), with a mean $\delta^{7}Li$ value of 18.8 ± 0.6 ‰ (2 SE, n = 9) (29).

1.3. Statistical treatment

For each species, we calculated its average value for $\delta^{11}B_{carb}$, $\delta^{7}Li_{carb}$, Li_{carb}, Li/Mg_{carb}, Mg/Ca_{carb}, B/Mg_{carb}, B/Ca_{carb}, Li/Ca_{carb}, pH_{cf} and DIC_{cf}, based on n = 2 to 5 individual measurements, except for *Acropora* sp.1 and *Montipora* sp., for which n = 1. Since normality and homoscedasticity of the Li compositional and isotopic data were not validated (using Q-Q plots and Residuals vs. Fitted plots), we used non-parametric statistical tests. The Mann-Whitney-Wilcoxon test was thus used to compare median values between two observational series between seeps and control corals. Tests were performed using R software (41) using the functions *wilcox.test*. The level of significance for statistical analyses was set at $p < 0.05$. The relationship between quantitative variables (pH_{cf}, DIC_{cf}, $\delta^{7}Li_{carb}$, Li/Ca_{carb}, B/Mg_{carb}, B/Ca_{carb}, and Li_{carb}) was also investigated using principal component analysis (PCA, see section 3.1), using R software (41).

2. Results

2.1. Seawater chemistry

As previously reported in the literature for this area (15,33,42-45) and in open access database (https://doi.pangaea.de/10.1594/PANGAEA.939651), mean seawater pH is lower at the seep site when compared to the control (Fig. S1). In the seep area, where we collected the corals, pH fluctuates between 7.47 and 7.80 pH_T units (5th and 95th percentile), corresponding to Ω_{arag} 2.03 - 3. (5th and 95th percentile), pCO_2 of 793-1863 μatm (5th and 95th percentile), and DIC values of 2135 – 2276 $\mu mol.kg^{-1}$ (5th and 95th percentile). Seawater pH was between 7.6–7.8 (pCO_2 = 799 -1349 μatm) for 60% of the

time, below 7.6 (pCO_2 < 1349 μatm) for 24% of the time, and above 7.8 (pCO_2 > 799 μatm) for 16% of the time. In contrast, at the control site, pH was higher, more stable (pH_T ~ 7.94 -8.06; pCO_2 ~ 376 – 530 μatm; 5th and 95th percentile), close to the ambient value of 8.00 pH_T units, while DIC was 1955 – 2029 μmol.kg^{-1} (5th and 95th percentile). Mean ± SD seawater temperature measured from September 2016 to May 2017 were 30.61 ± 0.23 °C, and 30.76 ± 0.25 °C at the control and seeps site, respectively. Several seawater samples collected at the control site give δ^7Li value and Li concentration typical of the open ocean, within uncertainties (31.5 ± 1.1‰ and 0.18 ± 0.01 μg.mL^{-1}, respectively). At the seep site, the Li concentrations are found to be more variable and slightly higher than the open ocean, although not statistically significantly different (236 ± 42 ng.mL^{-1}). The corresponding average δ^7Li value of the seawater at the seep site is 29.2 ± 0.7‰, slightly but significantly lower than at the control site. This observation is consistent with a slight contribution from the hydrothermal input at the seep site, as hydrothermal fluids are enriched in Li compared to the open ocean by 2-3 orders of magnitude (46). Assuming that this fluid has a δ^7Li typical of most marine hydrothermal fluids (8‰), and a Li content of 100 μg.mL^{-1} (47), a 0.015 % of contribution of this fluid may explain the observed difference between the seep and the control Li isotopic signature. Due to its contrasted concentration and isotopic signature, Li sensitivity to hydrothermal input is unique and our Li data from the seeps site demonstrate that the contribution from hydrothermal fluid is small since Ambitle seeps are overall mostly composed of CO_2 gas.

2.2. Coral chemistry

Aragonite B isotope ratio ($\delta^{11}B_{carb}$), Li isotope ratio (δ^7Li_{carb}), Li concentrations ($Li_{\mathbf{carb}}$), elemental molar ratios ($Li/Mg_{\mathbf{carb}}$, $Mg/Ca_{\mathbf{carb}}$, $B/Mg_{\mathbf{carb}}$, $B/Ca_{\mathbf{carb}}$, $Li/Ca_{\mathbf{carb}}$), and calcifying fluid pH and DIC (pH_{cf} and DIC_{cf}) are reported for each sample in Table S1.

2.2.1. Boron chemistry

As described in Comeau et al. (32) for the same samples, B/Ca_{carb} range between 445 μmol.mol^{-1} (*E. lamellosa* from the seep site) and 592 μmol.mol^{-1} (*G. fascicularis* from the seep site, see figure S3). $\delta^{11}B_{\mathbf{carb}}$ varied from 20.7 ‰ (in *E. lamellosa* from the seep site) to 25.4 ‰ (in *Acropora* sp2. from the control site, see figure S3), indicating that all corals are significantly enriched in ^{10}B, the light boron isotope, compared to the seawater ($\delta^{11}B_{\mathbf{SW}}$ = 39.6 ‰, (36)). δ^{11}B range from 21.9 to 25.7 ‰ in the control site and from 20.7 to 24.5 ‰ in seeps site, with a variability of 3.4‰ and 3.8‰, respectively (Fig. S3). The difference in Δ^{11}B between the seep and control site ranges between -2.8 (for *E. lamellosa*) and -0.3 ‰ (for *Montipora sp*.) (except for *G. fascicularis* showing a positive difference of

2.4‰), indicating that the impact of seawater pH on the skeleton $\delta^{11}B$ composition is specie-specific (Fig. S3).

From equations 1 and 2, Comeau et al. (32) calculated that calcifying fluid pH_{cf} range from 8.2 to 8.5 and DIC_{cf} range from 3468 to 4859 µmol.kg^{-1}, which is within the range for tropical corals (Table S1) (15,18,48,49). Although the average differences between sites for pH_{cf} and DIC_{cf} are not significant, some species show larger pH_{cf} and DIC_{cf} difference than others ($pH_{cf\text{-}VENT}$ - $pH_{cf\text{-}CTRL}$ = -0.19 for *E. lamellosa.*, and -0.02 for *Montipora* sp.).

2.2.2. Lithium chemistry

Coral skeleton Li concentrations are low but within the range published for marine biogenic tissues (29,50,51). Lithium contents vary from 0.36 ± 0.08 µg.g^{-1} in *Porites* sp. from the control site (2 SE, n = 5) to 0.67 µg.g^{-1} in *Montipora* sp. from the control site (n = 1). Coral $\delta^7Li_{\mathbf{carb}}$ values range from 18.3 ± 0.3 ‰ in *G. fascicularis* from the seep site (2 SE, n = 2) to 20.4 ± 0.9 ‰ in *G. fascicularis* from the control site (2 SE, n = 3), and are systematically highly enriched in the light ^6Li isotope compared to the seawater value. Although the number of published isotopic data is scarce for corals, these values match the published range (from 17.1 ± 0.9 ‰ to 23.8 ± 0.9 ‰, Table S1) (22,29,31).

δ^7Li values of corals grown at the control site display a narrow range of 1.45 ‰, highlighting a small species effect. This range is, however, twice that given by seven species living in an aquarium fed by Mediterranean seawater from Monaco Bay (range of 0.7 ‰, see (29)). Moreover, the average δ^7Li_{carb} value displayed by the cultured corals (17.3 ± 0.2 ‰, 2 SE, n = 28, (29)) is different from the one found here on corals living in natural conditions (19.5 ± 0.4 ‰, 2 SE, n = 24), despite identical seawater Li isotope composition. This strongly suggests an "aquarium effect"- perhaps related to their feeding with Artemia - even though experimental conditions mimicked at best natural environmental parameters, such as pH, salinity, DIC, temperature, and light intensity (although light was artificial) (29). Studying corals sampled from their natural environment appears therefore particularly important for Li isotopes.

For Li concentrations (and Li/Ca ratio), there is no statistical difference between corals living under low pH conditions and those living in control pH ($p > 0.05$). At the control site, the mean Li_{carb} is 0.50 ± 0.06 µg.g^{-1}, ($2\sigma_n$, n = 8) and at the seeps site, Li_{carb} is 0.48 ± 0.06 µg.g^{-1} ($2\sigma_n$, n = 8) (Figs. 2A & 3A).

In contrast, the mean δ^7Li_{carb} values of corals from the seep site is 18.8 ± 0.2 ‰ (n = 8), statistically lower than the mean δ^7Li_{carb} displayed by corals from the control site (δ^7Li_{carb} = 19.5 ± 0.4 ‰, n = 8) (Wilcox. test, $p < 0.001$, Figs. 2B and 3C). The relative difference between seeps and control can be

represented as $\Delta^7Li_{seep\text{-}CTRL} = \delta^7Li_{carb\text{-}seep} - \delta^7Li_{carb\text{-}CTRL}$, and varies from -0.2 ‰ for *E. lamellosa* to -2.1 ‰ for *G. fascicularis*.

Since the δ^7Li value of the seawater at the seeps site is found to be lower than at the control site (by -2.3 ‰), it is not possible to directly compare coral isotopic composition between both sites in order to study the pH impact. Therefore, we calculate an isotope fractionation, which corresponds, at each site, to the difference in Li isotopic composition between the two phases (seawater and coral skeleton). The average seawater–coral Li isotope fractionation ($\Delta^7Li_{CTRL\text{-}sw} = \delta^7Li_{carb} - \delta^7Li_{sw}$) at the control site is -12.0 ± 0.4 ‰. At the seep site, $\Delta^7Li_{seep\text{-}sw}$ is slightly but significantly lower (-10.4 ± 0.2 ‰). Thus, in agreement with the literature, all coral skeletons are enriched in ^6Li compared to seawater, resulting in strongly negative isotopic fractionation (22,29,31). However, their isotopic fractionation is distinct between the two sites (Wilcox. test, $p < 0.001$).

Another difference can be highlighted between the seeps and the control sites. At the control site, when reported as a function of the Li coefficient partition D_{Li} ($=[Li/Ca]_{\mathbf{carb}}/[Li/Ca]_{SW}$), $\delta^7Li_{\mathbf{carb}}$ averaged for each species follows a slight decrease (Fig. 5). In contrast, at the seep site, species $\delta^7Li_{\mathbf{carb}}$ correlates positively with D_{Li} (see Fig. 5). Low Li level coral species therefore appear more sensitive to the environment in which they grow, since corals with high Li/Ca ratio exhibit smaller differences in their $\delta^7Li_{\mathbf{carb}}$ between the two sites. Although more data would be needed to confirm this observation, the trends shown in figure 5 further support that a lower seawater pH impacts the Li isotope signatures of coral skeletons, in particular species incorporating smaller amounts of Li from their environment.

3. Discussion

3.1. No impact of pH and high pCO_2 on the Li/Mg_{coral} temperature proxy

Molar Mg/Ca_{carb} ratio (from 4.1 to 5.9 10^{-3}) and Li/Mg_{carb} (from 1.0 to 1.5 10^{-3}) ratios measured in coral skeletons are close to what other studies reported for other species (Table S1) (11,15,29,31,52,53). With our dataset, it is possible to test whether the seawater pH can affect Li/Mg ratios of coral skeletons. Coral Li/Mg ratios follow a well-defined anti-correlation with seawater temperature. The different corals species studied here fall within the exponential curve defined by Montagna et al. (11) and Stewart et al. (13) when considering the average temperature monitored *in situ* (Fig. 6). The Li/Mg_{carb} variability observed at a given temperature (~± 0.1, 2 SE) is fully consistent with that of Montagna et al. (11). Thus, at first sight, we can assume that a seawater pH decrease of 0.4 pH unit, as projected by the end of the century (54), does not influence the SST-Li/Mg_{carb} proxy. Indeed, corals Li/Mg_{carb} in the seeps and control sites (1.32 ± 0.07 and 1.26 ± 0.08 $mmol.mol^{-1}$, respectively, 2 SE, n = 8) translate to temperatures of 29.8 ± 1.4 °C and 28.6 ± 1.0 °C (2 SE, n = 8), respectively, using the

Montagna's empirical relationship (Fig. 6). These values are in agreement with the 30.6 and 30.7°C measured *in situ*. Nevertheless, considering corals under seep condition only, Li/Mg_{carb} is positively correlated with pH_{cf}, whereas is it not the case for corals from the control site (r=0.58 vs. 0.003, respectively, see Table S2). Further investigations will therefore be needed to constrain the effect of a larger seawater pH decrease on this proxy as other metabolic activities (i.e. control of the calcifying fluid chemistry) may affect it.

3.2. Significant influence of high pCO_2 on coral δ^7Li

Here we assess whether 1) the pH may change the Li isotope fractionation during the skeleton growth and 2) different coral species may display distinct Li isotope signatures and respond differently to environmental variations. Vital – biological - effects can be evidenced when comparing the geochemical and isotopic composition of coral skeleton to the one measured in inorganic aragonite formed in similar conditions (e.g. 55-57). Among the eight collected coral species, the estimated Li partition coefficients D_{Li} (= $(Li/Ca)_{carb}/(Li/Ca)_{SW}$) display a small variation, with $LogD_{Li}$ ranging from -3.38 to -3.26 (Table S1 and Fig. 5). It is striking that this range is one order of magnitude lower than the one determined for inorganic aragonite formed in the laboratory in similar conditions ($LogD_{Li}$ value between -2.37 and -2.52 at pH = 8.1-8.3, (30)). This suggests that corals are able to extract a significant amount of lithium from their soft tissues before precipitating aragonite, and might indicates a significant vital effect during their growth.

We can consider that at pH=8.1, the $\delta^7Li_{inorganic\text{-}aragonite}$ value is 19.2 ‰ ± 1.5 ‰ (± 2 SE, n = 3) (average obtained based on experimental inorganic aragonite precipitation (30,58,59)). Consequently, by comparison, a vital effect of -1.9 ± 1.2 ‰ (2 SE) is determined for scleractinian corals species grown at the CSM (Monaco Scientific Center) aquarium (29). A smaller vital effect of -0.4 ± 1.5 ‰ (2 SE) is observed for corals from Jarvis Island (22). Here, the corals from Papua New Guinea at the control site exhibit a vital effect consistent with the Jarvis Island of -0.37 ± 1.5 ‰ (n = 16, 2 SE). It is not possible to make this estimation at the seeps site as there is no experimental data published for inorganic aragonite grown at low pH. Nevertheless, the biological vital effect appears to be greater for corals grown in an aquarium, than those collected from their natural environment. It is difficult at this stage to determine what causes this difference. Perhaps, the peculiar chemistry of the Mediterranean seawater alimenting the aquarium (higher salinity and total alkalinity) played a role. We can also hypothesize that the different conditions in aquariums compared to the natural environment (food supply, species interactions, daily and seasonal variability in environmental parameters) affect the physiology of corals and therefore Li isotopes. This vital effect is species-dependent with *G. fascicularis.*

and *Montipora* sp. displaying the largest vital effect in the control site (Figure 2b). Overall, these observations indicate that large ocean pH variations may significantly impact scleractinian skeleton Li isotopic compositions and that specific species calibrations are therefore required for a reliable use of δ^7Li as a palaeoceanographic proxy.

3.3. Implications at a cellular level for the relationship between DIC, pH and Li transport

Despite the δ^7Li value of seawater samples from the seeps site being lower by 2 ‰ compared to the open ocean and to the control site, the δ^7Li value of each coral species collected in the seeps site exhibits on average only a slight difference with corals of the same species living at the control site (Fig. 3b). Similarly, the average Li concentration of all coral species is similar in the seeps and control site. This strongly suggests that biological processes internally regulate the internal Li as in other marine calcifying species (60). We performed a principal component analysis (PCA) in order to study more closely the relationships between seven quantitative variables measured in the Papua New Guinea coral skeletons (pH_{cf}, DIC_{cf}, $\delta^7Li_{\mathbf{carb}}$, $Li/Ca_{\mathbf{carb}}$, $B/Mg_{\mathbf{carb}}$, $B/Ca_{\mathbf{carb}}$, $Li_{\mathbf{carb}}$). pH_{cf} and $\delta^7Li_{\mathbf{carb}}$ are not prominent in the composition of PC1 and PC2 (Fig. 7) but are the two main variables that participate in the principal components 3 and 4 (PC3 and PC4, Fig. 7). The calcifying fluid pH_{cf} and $\delta^7Li_{\mathbf{carb}}$, when combined, allow to clearly distinguish both sites, which indicates that a decrease in seawater pH can induce – for several coral species – a physiological effect on both the calcifying fluid pH and the skeleton Li isotope signature.

As shown in figure 8, for each species, the difference in coral $\delta^7Li_{\mathbf{carb}}$ between the control site and the vent site ($\Delta^7Li_{seep\text{-}CTRL}$) exhibits strong correlations with DIC_{cf} and pH_{cf} measured in corals from the seep site. Note that the use of $\Delta^7Li_{seep\text{-}CTRL}$ (= $\delta^7Li_{carb\text{-}seep} - \delta^7Li_{carb\text{-}CTRL}$) is done to correct the δ^7Li values from the natural variability observed at the control site. The correlations shown in figure 8 strongly support a close link between the biological regulation of pH_{cf}, seawater pH, and the Li isotope composition of the coral skeleton.

This link can be explained by considering the current knowledge of both coral biology and Li transport. Indeed, coral B chemistry shows that pH_{cf} is kept at high levels even under low seawater pH, which permits to maintain elevated aragonite saturation state in the extracellular calcifying medium (31,32,48,49). It can thus be hypothesized that the cellular pH or/and DIC regulation process is responsible for the ^6Li excesses observed in corals being able to maintain an elevated pH_{cf}.

Intracellular pH is biologically regulated by several factors: (1) intra-cell chemical reactions and (2) transmembrane transport of proton (H^+) or bicarbonate ions (HCO_3^-). In cells, CO_2 (H_2CO_3) is produced by mitochondrial respiration. Under cellular equilibrium at pH 7, this CO_2 engenders proton liberation through carbonic acid production (H_2CO_3), which acidifies the cytoplasm. Several transmembrane

transporters of bicarbonate ions (HCO_3^-) or proton (H^+) participate in the cell pH balance: (i) Cl^-/ HCO_3^- exchangers (ii) Na^+/ HCO_3^- symporters (iii) Na^+/H^+ antiporters (NHE) that balance the cell pH by mediating H^+ efflux in exchange for Na^+ uptake, and (iv) different ATP_{ase} that can transport protons in or out of the cell or intracellular compartments. All these transporters have been identified in corals (61-65) (see schematic representation in figure 9). Among them, it has been shown by numerous experiments - based on genetically modified cells - that NHE transporters operate a very efficient Li^+ transport from the external medium to the intracellular cytoplasm (66).

$CaCO_3$ precipitation releases H^+ and consumes Ca^{2+} and HCO_3^- ions. Maintaining elevated aragonite saturation in the calcifying fluid under unfavorable conditions can be obtained by a greater excretion of Ca^{2+} and HCO_3^- from the calicoblastic cells. Ca^{2+} can be transported to the calcifying fluid by (i) Ca^{2+} channels (67), (ii) H^+/Ca^{2+} ATP_{ase} (68), and (iii) Na^+/Ca^{2+} exchangers (69) (Fig. 9). Similarly as for NHE's, several experiments have shown that Na^+/Ca^{2+} exchangers are able to transport Li^+ efficiently (70). The H^+ in excess produced by the precipitation reaction are exported back to the calicoblastic cells through Ca^{2+}-ATP_{ase}, and this acidification process of the cell cytoplasm is compensated by the transporters described above, including the NHE's, which use Li^+ and Na^+ as counter ions.

Overall, to preserve an optimal calcification rate while the external pH is low, the activity of several transporters involving H^+, HCO_3^-, Ca^{2+}, Na^+, and Li^+ must be enhanced. As these transporters result in kinetic transport in favor of the lighter isotope, ^6Li (71), their enhanced activity can explain the larger ^6Li enrichment (lower Δ^7Li , Fig. 2B), for corals which maintained high pH_{cf} under low seawater pH (*G. fascicularis*., *Acropora* sp.1 and *Acropora* sp.2, Fig. 8B). These observations support an intensification of basal NHE activation in corals able to preserve a high $pH_{cf,}$ and DIC_{cf} under a low pH external environment.

4 Conclusion

Overall, ours results show a negligible species and pH effect on Li concentrations but a significant effect of these parameters on Li isotopes. The calcifying fluid of some coral species regulates its pH and its Li level, and both processes result in significant Li isotopic variations. The B isotope geochemistry shows that corals living at control and seeps sites maintain an elevated pH and DIC in their calcifying fluid. This similitude could *a priori* be interpreted as a weak effect of ocean acidification on tropical corals. However, Li isotopes provide a different point of view. Indeed, coral species with the highest pH_{cf} at the seeps site (*G. fascicularis.* and *Acropora* sp.2) display the largest decrease in δ^7Li. Correlations between coral skeleton δ^7Li and pH_{cf} or DIC_{cf} show that Li isotopes are directly related to the organism ability to optimize the carbonate chemistry in its calcifying fluid to sustain aragonite precipitation.

Using constraints from ion transport through cellular membranes and transporters identified in corals, our results confirm the role of active – energy-demanding – Li^+ and H^+ transporters such as NHEs. Thus, the coral skeleton Li isotopic composition indicates a change of the internal Li homeostasis that is caused by a metabolic response to a decrease of seawater pH. This upregulation is performed through the intensification of specific cellular transporters such as NHE and Ca-Na exchangers, which transports and isotopically fractionate Li unlike B. Thus, the combination of B and Li isotopes illustrates for the first time how some coral species are able to adapt their physiology when living in a low pH environment. The energetic cost of this effort remains to be fully evaluated.

5 Acknowledgements

We are grateful for access to facilities provided by the Oceanographic laboratory of Villefranche-sur-Mer (LOV) and the Ecole Normale Supérieure de Lyon (ENSL, Philippe Télouk). This work benefited from the support of ANR ISO2MET (Project-ANR-18-CE34-0002). We are grateful to the population of Tutum Bay in Ambitle for allowing us to conduct the study on their reefs, and to the National Research Institute, the Milne Bay Provincial Research Committee, the New Ireland Provincial Administration, and the Conservation and Environment Protection Authority of Papua New Guinea for permits. We are indebted with Prof. Ralph Mana (University of UPNG) and to Prof. Katharina Fabricius (AIMS) for their invaluable help during the CARIOCA project. Thanks to the crew of the R/V Alis for their support during the cruise.

6 Fundings

This work was supported by the ANR [ISO2MET project, ANR-18-CE34-0002]; MTM was supported by an ARC Laureate Fellowship (LF120100049); SC was supported by an ARC DECRA (DE160100668). Sampling at the PNG study site was partially funded by the French National Research Agency (ANR; project CARIOCA, ANR-15-CE02-0006-01, to RR-M), and by the Flotte Océanographique Française for using the research vessel Alis.

7 Data

The datasets supporting this article have been uploaded as part of the supplementary material.

8 Competing interests

The authors declare no competing interests.

9 CRediT

FT: Methodology, Validation, Investigation, Formal analysis, Visualization, Writing - original draft, Writing - review & editing. **SC**: Conceptualization, Project administration, Writing - review & editing. **RRM**: Resources, Supervision, Writing - review & editing. **MM, PT**: Methodology, Validation. **LC, MP**: Writing - review & editing. **MMc**: Resources, Writing - review & editing. **CT**: Methodology, Validation, Formal analysis, Writing - review & editing. **NV**: Conceptualization, Supervision, Funding acquisition, Project administration, Writing - review & editing.

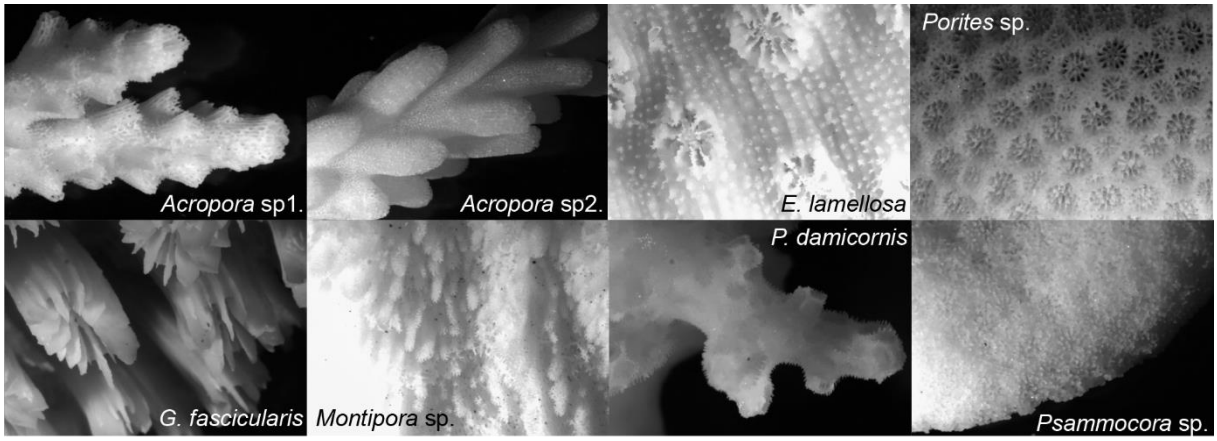

Figure 1: Pictures of the sampled coral skeletons, using a 10x binocular magnifier. The various structures and shapes highlight strong differences in biomineralisation mode and rate.

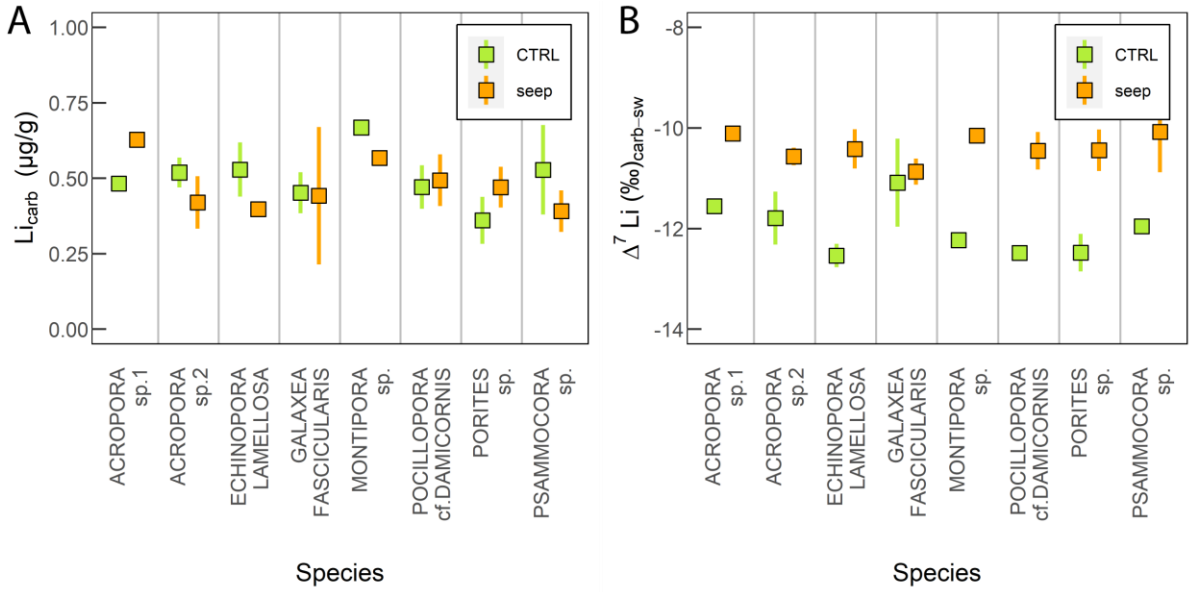

Figure 2: (A) Coral Li concentration (µg/g) and **(B)** Li isotope composition δ^7Li_{carb} (‰) for each species collected at the control (CTRL, green) and seep sites (seep, orange). The squares are the means, and the error bars show the standard error ($2\sigma_n$). The species effect on both Li concentration and δ^7Li_{carb} is generally observed to be small despite different skeleton morphologies (see Figs. 1 and S2).

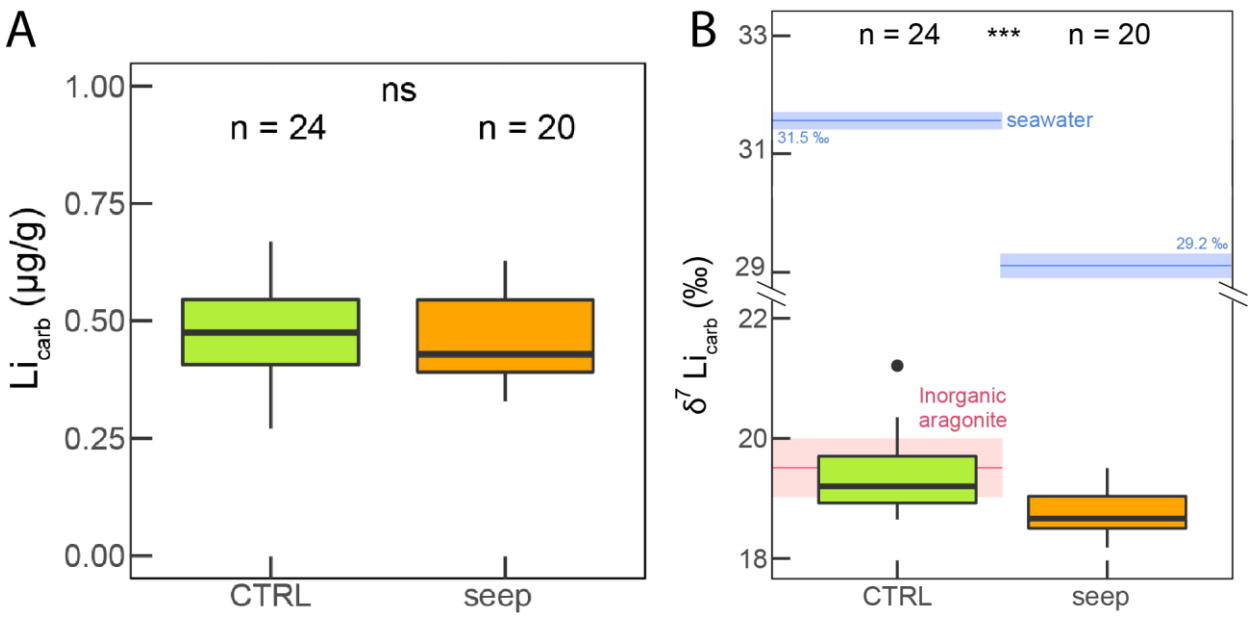

Figure 3: Box plots showing (A) the Li concentration (µg/g), (B) the Li isotope composition δ^7Li_{carb} (‰) of corals living under high pCO_2 seawater (seep) and ambient seawater at the (CTRL) site. Inorganic aragonite (IA) and seawater (SW) δ^7Li are added for comparison at the control site (30,58,59). There is no published inorganic aragonite data for low pH condition. The numbers at the top of each box indicate the number of replicates. Asterisks show the significance of the Mann-Whitney-Wilcoxon tests used to observe differences between pairs of groups: ns (not significant) for $p > 0.05$, * for $p < 0.05$, ** for $p < 0.01$, *** for $p < 0.001$, **** for $p < 0.0001$ (highly significant difference). Outliers (> 1.5 Interquartile range) are plotted as black circles.

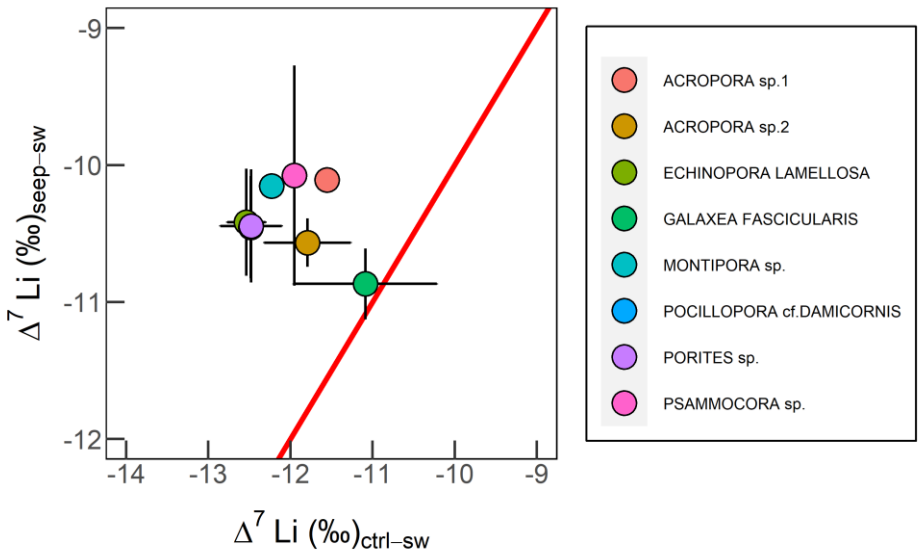

Figure 4: Coral Li isotope composition δ^7Li_{carb} (‰) at seep site versus CTRL site. Each purple dot represents the mean value for one coral species. Error bars in 2 SE ($2\sigma_n$), the red line represents the identity line.

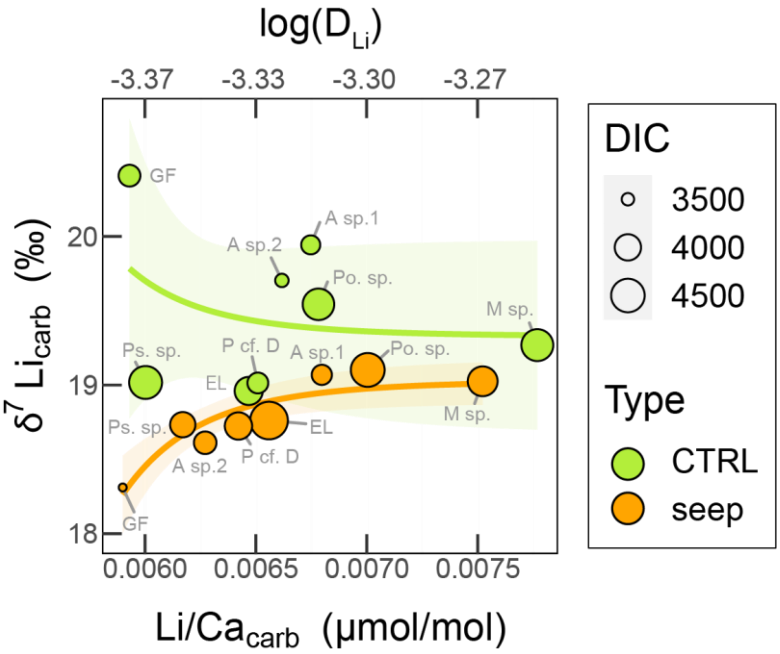

Figure 5: Coral Li isotope composition δ^7Li_{carb} (‰) versus coral Li/Ca_{carb} concentration ratio (bottom x-axis) and partition coefficient D_{Li} (top x-axis). Orange circles are for corals living at the seep site, while green circles are for corals living at the CTRL site. Circle sizes are proportional to DIC_{cf} (µmol/kg). Solid lines are the exponential fits, and the shadow zones, the confidence intervals. Grey text refers to the initials of the corals species (see Table S1).

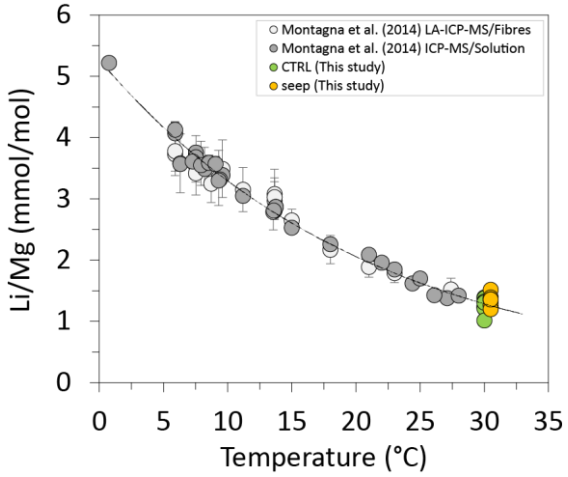

Figure 6: Corals Li/Mg_{carb} ratios versus seawater temperature. Each circle corresponds to one coral individual. Data from Montagna et al. (11) consist of *C. caespitosa, Acropora sp., Porites sp., L. pertusa, M. oculata,* and *F. impensum*, from various geographic origins (Mediterranean Sea, Atlantic, Pacific, and Southern Oceans), and cultured corals species *C. caespitosa*, and *Acropora sp*. Yellow and green circles code from this study corals (CTRL and seep), *i.e., Acropora* sp1*., Acropora* sp2*., G. fascicularis, Porites* sp*., Montipora* sp*., E. lamellosa, Pasammocora* sp*.,* and *P.* cf. *damicornis*. Shadow areas underline the temperature range evaluated from Li/Mg_{carb} under each condition (CTRL in green and seep in orange).

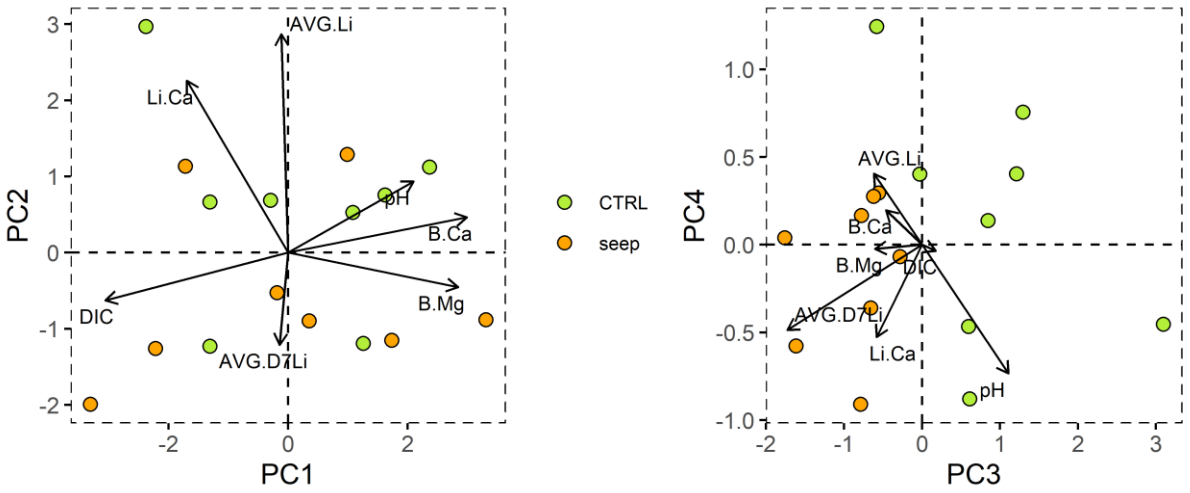

Figure 7: Results obtained with a PCA applied to coral skeleton parameters. PC3 and PC4 are for principal components 3 and 4 and represent 23 % of the variability of the dataset. Points are for individuals. Variable row length is proportional to their contribution to the principal components. Thus, pH_{cf} and δ^7Li are the main variables that contribute to PC3 and PC4. Furthermore, PC3 and PC4 can discriminate seep and CTRL groups (*i.e.,* seep data plot mainly in the bottom left panel, and CTRL data plot mainly in the top right panel). Therefore, both groups can clearly be distinguished based on pH_{cf} and δ^7Li.

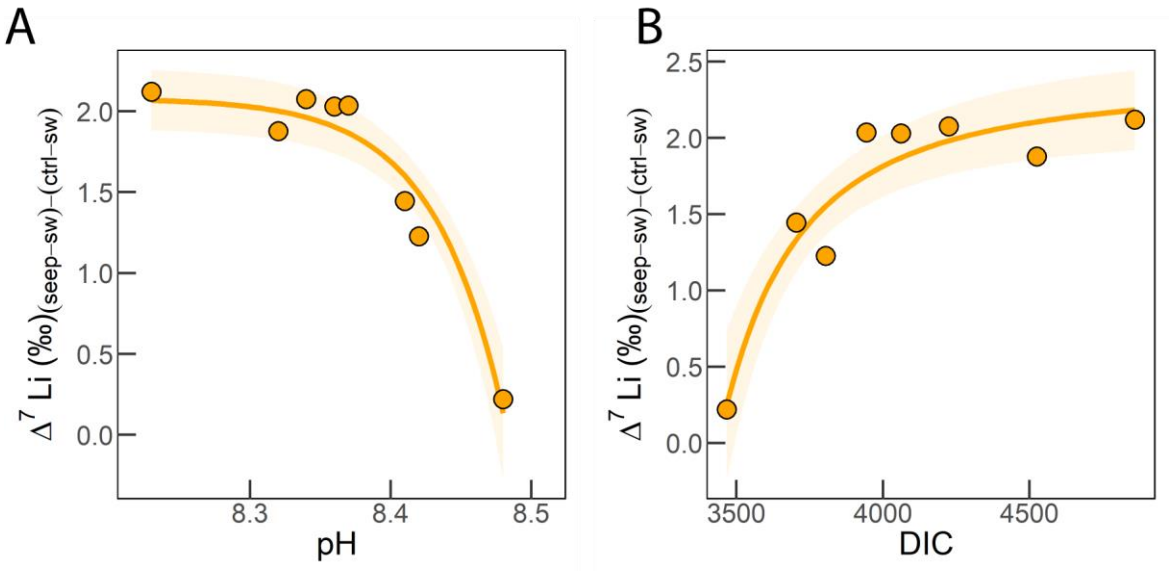

Figure 8: $\Delta^7Li_{seep\text{-}CTRL}$ as a function of pH_{cf} (**A**) and DIC_{cf} (**B**) of corals living under high pCO_2 seawater (seep). Orange lines represent the exponential fits, and the shadow orange zones, the confidence intervals.

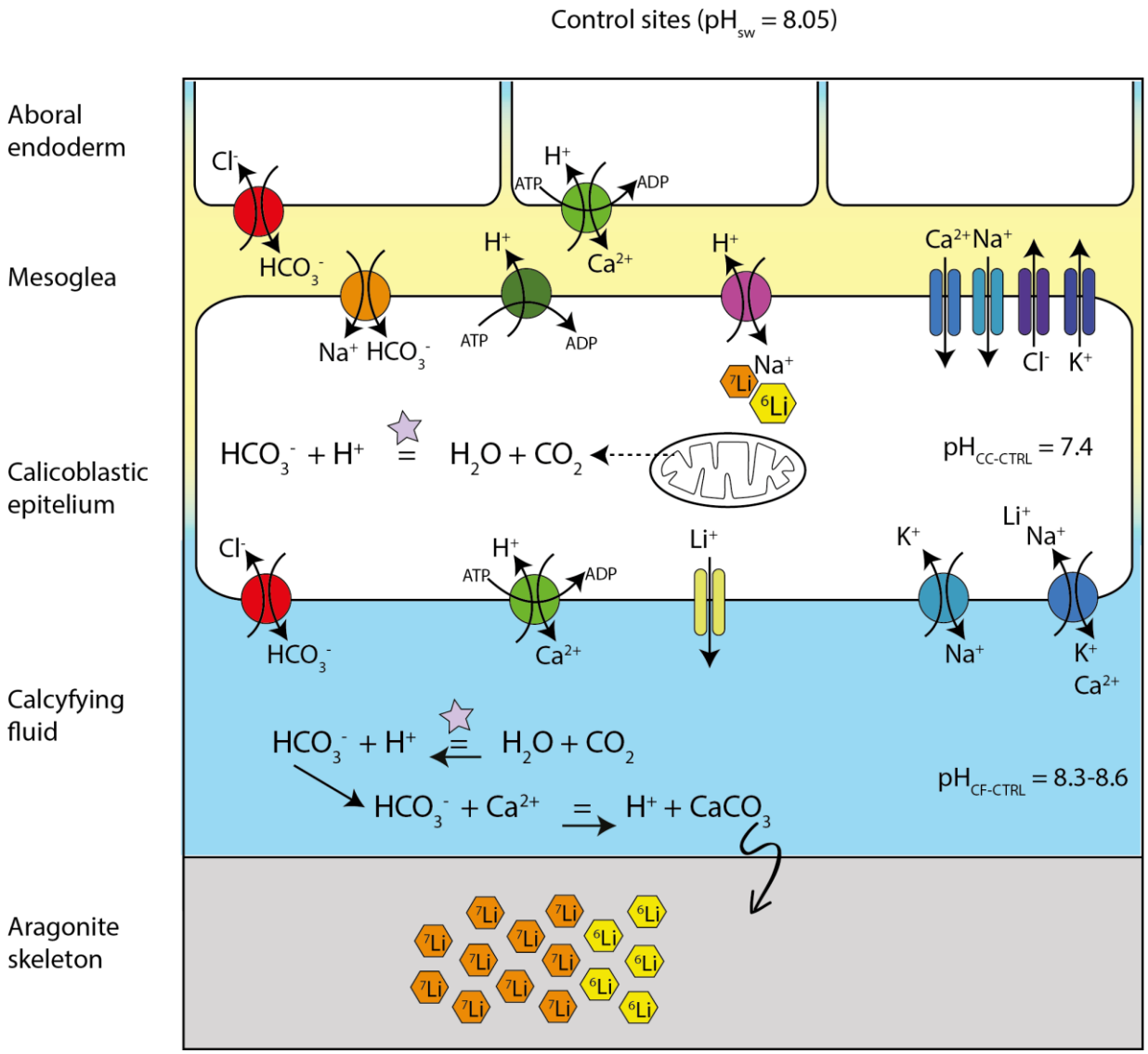

Figure 9: Schematic diagram of coral tissue cross-sections from aboral endoderm (top) to aragonite skeleton (bottom), and associated ion transport processes controlling calcifying fluid composition (for full cross-section, see figure S6). Individual cells are represented by white rectangles. Ion transporters (symporters, antiporters, or pumps) are in colored circles, while passive ion channels are in colored rectangles. The stars represent the action of carbonic anhydrase. Heavy Li isotopes are in orange hexagons, and light Li isotopes, in yellow hexagons. Kinetic transport by NHE's favor the light ^{6}Li isotope. Some coral species are able to elevate the pH of their calcifying fluid by activating NHEs, exporting H^+ in exchange of Na^+ and Li^+.

REFERENCES

1. Orr JC, Fabry VJ, Aumont O, Bopp L, Doney SC, Feely RA, et al. Anthropogenic ocean acidification over the twenty-first century and its impact on calcifying organisms. Nature. sept 2005;437(7059):681-6.

2. Suzuki A, Kawahata H. Reef Water CO 2 System and Carbon Production of Coral Reefs: Topographic Control of System-Level Performance [Internet]. undefined. 2004 [cité 5 mars 2021]. Disponible sur: /paper/Reef-Water-CO-2-System-and-Carbon-Production-of-of-Suzuki-Kawahata/7f110fa4b5a028c2ce8a2b1aa6999eafcfe8ceb0
3. Clarke H, D'Olivo JP, Falter J, Zinke J, Lowe R, McCulloch M. Differential response of corals to regional mass-warming events as evident from skeletal Sr/Ca and Mg/Ca ratios. Geochemistry, Geophysics, Geosystems. 2017;18(5):1794-809.
4. Fallon SJ, McCulloch MT, Alibert C. Examining water temperature proxies in Porites corals from the Great Barrier Reef: a cross-shelf comparison. Coral Reefs. 1 déc 2003;22(4):389-404.
5. Mitsuguchi T, Matsumoto E, Abe O, Uchida T, Isdale PJ. Mg/Ca Thermometry in Coral Skeletons. Science. 8 nov 1996;274(5289):961-3.
6. Quinn TM, Sampson DE. A multiproxy approach to reconstructing sea surface conditions using coral skeleton geochemistry. Paleoceanography. 2002;17(4):14-1-14-11.
7. Zeebe RE, Wolf-Gladrow D. CO2 in Seawater: Equilibrium, Kinetics, Isotopes. Gulf Professional Publishing; 2001. 382 p.
8. Case DH, Robinson LF, Auro ME, Gagnon AC. Environmental and biological controls on Mg and Li in deep-sea scleractinian corals. Earth and Planetary Science Letters. 1 déc 2010;300(3):215-25.
9. Cuny-Guirriec K, Douville E, Reynaud S, Allemand D, Bordier L, Canesi M, et al. Coral Li/Mg thermometry: Caveats and constraints. Chemical Geology. 30 sept 2019;523:162-78.
10. D'Olivo JP, Sinclair DJ, Rankenburg K, McCulloch MT. A universal multi-trace element calibration for reconstructing sea surface temperatures from long-lived Porites corals: Removing 'vital-effects'. Geochimica et Cosmochimica Acta. 15 oct 2018;239:109-35.
11. Montagna P, McCulloch M, Douville E, López Correa M, Trotter J, Rodolfo-Metalpa R, et al. Li/Mg systematics in scleractinian corals: Calibration of the thermometer. Geochimica et Cosmochimica Acta. 1 mai 2014;132:288-310.
12. Bonneau L, Colin C, Pons-Branchu E, Mienis F, Tisnérat-Laborde N, Blamart D, et al. Imprint of Holocene Climate Variability on Cold-Water Coral Reef Growth at the SW Rockall Trough Margin, NE Atlantic. Geochemistry, Geophysics, Geosystems. 2018;19(8):2437-52.
13. Stewart JA, Robinson LF, Day RD, Strawson I, Burke A, Rae JWB, et al. Refining trace metal temperature proxies in cold-water scleractinian and stylasterid corals. Earth and Planetary Science Letters. 1 sept 2020;545:116412.
14. Fowell SE, Sandford K, Stewart JA, Castillo KD, Ries JB, Foster GL. Intrareef variations in Li/Mg and Sr/Ca sea surface temperature proxies in the Caribbean reef-building coral Siderastrea siderea. Paleoceanography. 2016;31(10):1315-29.
15. Comeau S, Cornwall CE, McCulloch MT. Decoupling between the response of coral calcifying fluid pH and calcification to ocean acidification. Scientific Reports. 8 août 2017;7(1):7573.
16. Foster GL, Rae JWB. Reconstructing Ocean pH with Boron Isotopes in Foraminifera. Annual Review of Earth and Planetary Sciences. 2016;44(1):207-37.
17. Holcomb M, Venn AA, Tambutté E, Tambutté S, Allemand D, Trotter J, et al. Coral calcifying fluid pH dictates response to ocean acidification. Scientific Reports. 6 juin 2014;4(1):5207.
18. McCulloch MT, D'Olivo JP, Falter J, Holcomb M, Trotter JA. Coral calcification in a changing World and the interactive dynamics of pH and DIC upregulation. Nature Communications. 30 mai 2017;8(1):15686.

19. Venn AA, Tambutté E, Comeau S, Tambutté S. Proton gradients across the coral calcifying cell layer: Effects of light, ocean acidification and carbonate chemistry. Frontiers in Marine Science [Internet]. 2022 [cité 7 déc 2022];9. Disponible sur: https://www.frontiersin.org/articles/10.3389/fmars.2022.973908
20. Hathorne EC, James RH. Temporal record of lithium in seawater: A tracer for silicate weathering? Earth and Planetary Science Letters. 2006;246(3-4):393-406.
21. Huh Y, Chan LH, Zhang L, Edmond JM. Lithium and its isotopes in major world rivers: implications for weathering and the oceanic budget. Geochimica et Cosmochimica Acta. 1 juin 1998;62:2039-51.
22. Marriott CS, Henderson GM, Belshaw NS, Tudhope AW. Temperature dependence of δ7Li, δ44Ca and Li/Ca during growth of calcium carbonate. Earth and Planetary Science Letters [Internet]. 2004 [cité 2 oct 2020];222(2). Disponible sur: https://ora.ox.ac.uk/objects/uuid:da911db7-6061-4c8d-9959-241667f59bbf
23. Misra KC. Introduction to geochemistry: principles and applications. John Wiley & Sons; 2012.
24. Pogge von Strandmann PAE, Burton KW, James RH, van Calsteren P, Gíslason SR, Mokadem F. Riverine behaviour of uranium and lithium isotopes in an actively glaciated basaltic terrain. Earth and Planetary Science Letters. 15 nov 2006;251(1):134-47.
25. Vigier N, Gislason SR, Burton KW, Millot R, Mokadem F. The relationship between riverine lithium isotope composition and silicate weathering rates in Iceland. Earth and Planetary Science Letters. 15 oct 2009;287(3):434-41.
26. Misra S, Froelich PN. Lithium Isotope History of Cenozoic Seawater: Changes in Silicate Weathering and Reverse Weathering. Science. 2012;335(6070):818-23.
27. Dellinger M, West AJ, Paris G, Adkins JF, Pogge von Strandmann PAE, Ullmann CV, et al. The Li isotope composition of marine biogenic carbonates: Patterns and mechanisms. Geochimica et Cosmochimica Acta. 2018;236:315-35.
28. Vigier N, Rollion-Bard C, Levenson Y, Erez J. Lithium isotopes in foraminifera shells as a novel proxy for the ocean dissolved inorganic carbon (DIC). Comptes Rendus Geoscience. 2015;347(1):43-51.
29. Bastian L, Vigier N, Reynaud S, Kerros ME, Revel M, Bayon G. Lithium Isotope Composition of Marine Biogenic Carbonates and Related Reference Materials. Geostandards and Geoanalytical Research. 2018;42(3):403-15.
30. Marriott CS, Henderson GM, Crompton R, Staubwasser M, Shaw S. Effect of mineralogy, salinity, and temperature on Li/Ca and Li isotope composition of calcium carbonate. Chemical Geology. 26 nov 2004;212(1):5-15.
31. Rollion-Bard C, Vigier N, Meibom A, Blamart D, Reynaud S, Rodolfo-Metalpa R, et al. Effect of environmental conditions and skeletal ultrastructure on the Li isotopic composition of scleractinian corals. Earth and Planetary Science Letters. 2009;286(1-2):63-70.
32. Comeau S, Cornwall CE, Shlesinger T, Hoogenboom M, Mana R, McCulloch MT, et al. pH variability at volcanic CO2 seeps regulates coral calcifying fluid chemistry. Global Change Biology. 2022;28(8):2751-63.
33. Pichler T, Biscéré T, Kinch J, Zampighi M, Houlbrèque F, Rodolfo-Metalpa R. Suitability of the shallow water hydrothermal system at Ambitle Island (Papua New Guinea) to study the effect of high pCO2 on coral reefs. Marine Pollution Bulletin. 1 janv 2019;138:148-58.
34. Rodolfo-Metalpa R. CARIOCA 3 cruise, Alis R/V. 2018 [cité 18 mai 2021]; Disponible sur: https://campagnes.flotteoceanographique.fr/campagnes/18000522/

35. Trotter J, Montagna P, McCulloch M, Silenzi S, Reynaud S, Mortimer G, et al. Quantifying the pH 'vital effect' in the temperate zooxanthellate coral Cladocora caespitosa: Validation of the boron seawater pH proxy. Earth and Planetary Science Letters. 1 mars 2011;303(3):163-73.
36. Foster GL, von Strandmann PAEP, Rae JWB. Boron and magnesium isotopic composition of seawater. Geochemistry, Geophysics, Geosystems [Internet]. 2010 [cité 2 oct 2020];11(8). Disponible sur:
https://www.academia.edu/10769546/Boron_and_magnesium_isotopic_composition_of_seawater
37. Klochko K, Kaufman AJ, Yao W, Byrne RH, Tossell JA. Experimental measurement of boron isotope fractionation in seawater. Earth and Planetary Science Letters. 15 août 2006;248(1):276-85.
38. Vigier N, Decarreau A, Millot R, Carignan J, Petit S, France-Lanord C. Quantifying Li isotope fractionation during smectite formation and implications for the Li cycle. Geochimica et Cosmochimica Acta. 2008;72(3):780-92.
39. Balter V, Vigier N. Natural variations of lithium isotopes in a mammalian model. Metallomics. 2014;6(3):582-6.
40. Thibon F, Weppe L, Montanes M, Telouk P, Vigier N. Lithium isotopic composition of reference materials of biological origin TORT-2, DORM-2, TORT-3, DORM-4, SRM-1400 and ERM-CE278k. J Anal At Spectrom. 7 juill 2021;36(7):1381-8.
41. R Core Team. R: A language and environment for statistical computing. R Foundation for Statistical Computing, Vienna, Austria [Internet]. 2017; Disponible sur: https://www. R-project. org
42. Bell JJ, Shaffer M, Luter HM, Mana R, Rodolfo-Metalpa R. Phototrophic sponge productivity may not be enhanced in a high CO2 world. Global Change Biology. 2022;28(16):4900-11.
43. Biscéré T, Zampighi M, Lorrain A, Jurriaans S, Foggo A, Houlbrèque F, et al. High pCO2 promotes coral primary production. Biology Letters. 26 juill 2019;15(7):20180777.
44. Geissler L, Meunier V, Rädecker N, Perna G, Rodolfo-Metalpa R, Houlbrèque F, et al. Highly Variable and Non-complex Diazotroph Communities in Corals From Ambient and High CO2 Environments. Frontiers in Marine Science [Internet]. 2021 [cité 5 déc 2022];8. Disponible sur: https://www.frontiersin.org/articles/10.3389/fmars.2021.754682
45. Meunier V, Geissler L, Bonnet S, Rädecker N, Perna G, Grosso O, et al. Microbes support enhanced nitrogen requirements of coral holobionts in a high CO2 environment. Molecular Ecology. 2021;30(22):5888-99.
46. Verney-Carron A, Vigier N, Millot R. Experimental determination of the role of diffusion on Li isotope fractionation during basaltic glass weathering. Geochimica et Cosmochimica Acta. 15 juin 2011;75(12):3452-68.
47. Pichler T, Veizer J, Hall GEM. The chemical composition of shallow-water hydrothermal fluids in Tutum Bay, Ambitle Island, Papua New Guinea and their effect on ambient seawater. Marine Chemistry. 1 mars 1999;64(3):229-52.
48. Guillermic M, Cameron LP, De Corte I, Misra S, Bijma J, de Beer D, et al. Thermal stress reduces pocilloporid coral resilience to ocean acidification by impairing control over calcifying fluid chemistry. Science Advances. 8 janv 2021;7(2):eaba9958.
49. Venn AA, Tambutté E, Holcomb M, Laurent J, Allemand D, Tambutté S. Impact of seawater acidification on pH at the tissue–skeleton interface and calcification in reef corals. Proc Natl Acad Sci U S A. 29 janv 2013;110(5):1634-9.

50. Thibon F, Goedert J, Séon N, Weppe L, Martin JE, Amiot R, et al. The ecology of modern and fossil vertebrates revisited by lithium isotopes. Earth and Planetary Science Letters. 1 déc 2022;599:117840.
51. Thibon F, Weppe L, Vigier N, Churlaud C, Lacoue-Labarthe T, Metian M, et al. Large-scale survey of lithium concentrations in marine organisms. Science of The Total Environment. 2020;751:1453.
52. Dissard D, Douville E, Reynaud S, Juillet-Leclerc A, Montagna P, Louvat P, et al. Light and temperature effects on δ11B and B / Ca ratios of the zooxanthellate coral Acropora sp.: results from culturing experiments. Biogeosciences. 20 nov 2012;9(11):4589-605.
53. Douville E, Paterne M, Cabioch G, Louvat P, Gaillardet J, Juillet-Leclerc A, et al. Abrupt sea surface pH change at the end of the Younger Dryas in the central sub-equatorial Pacific inferred from boron isotope abundance in corals (Porites). Biogeosciences. 16 août 2010;7(8):2445-59.
54. Hoegh-Guldberg O, Cai R, Poloczanska ES, Bewer PG, Sundby S, Hilmi K, et al. The Ocean. In: Climate Change 2014: Impacts, Adaptation, and Vulnerability Part B: Regional Aspects Contribution of Working Group II to the Fifth Assessment Report of the Intergovernmental Panel on Climate Change. Cambridge University Press. Cambridge, United Kingdom and New York; 2014.
55. Grossman EL. Stable isotopes in modern benthic foraminifera; a study of vital effect. Journal of Foraminiferal Research. 1 janv 1987;17(1):48-61.
56. Juillet-Leclerc A, Reynaud S, Rollion-Bard C, Cuif JP, Dauphin Y, Blamart D, et al. Oxygen isotopic signature of the skeletal microstructures in cultured corals: Identification of vital effects. Geochimica et Cosmochimica Acta. 15 sept 2009;73(18):5320-32.
57. Saulnier S, Rollion-Bard C, Vigier N, Chaussidon M. Mg isotope fractionation during calcite precipitation: An experimental study. Geochimica et Cosmochimica Acta. 15 août 2012;91:75-91.
58. Day CC, Pogge von Strandmann PAE, Mason AJ. Lithium isotopes and partition coefficients in inorganic carbonates: proxy calibration for weathering reconstruction. Geochimica et Cosmochimica Acta [Internet]. 13 mars 2021 [cité 24 mars 2021]; Disponible sur: https://www.sciencedirect.com/science/article/pii/S0016703721001435
59. Gabitov RI, Schmitt AK, Rosner M, McKeegan KD, Gaetani GA, Cohen AL, et al. In situ δ7Li, Li/Ca, and Mg/Ca analyses of synthetic aragonites. Geochemistry, Geophysics, Geosystems [Internet]. 2011 [cité 19 nov 2020];12(3). Disponible sur: https://agupubs.onlinelibrary.wiley.com/doi/abs/10.1029/2010GC003322
60. Thibon F, Metian M, Oberhansli F, Montanes M, Vassileva E, Orani AM, et al. Bioaccumulation of lithium isotopes in mussel soft tissues and implications for coastal environments. ACS Earth and Space Chemistry. 2021;5(6):1407-17.
61. Al-Moghrabi S, Goiran C, Allemand D, Speziale N, Jaubert J. Inorganic carbon uptake for photosynthesis by the symbiotic coral-dinoflagellate association II. Mechanisms for bicarbonate uptake. Journal of Experimental Marine Biology and Ecology. 1 août 1996;199(2):227-48.
62. Bhattacharya D, Agrawal S, Aranda M, Baumgarten S, Belcaid M, Drake JL, et al. Comparative genomics explains the evolutionary success of reef-forming corals. Bohlmann J, éditeur. eLife. 24 mai 2016;5:e13288.
63. Capasso L, Ganot P, Planas-Bielsa V, Tambutté S, Zoccola D. Intracellular pH regulation: characterization and functional investigation of H+ transporters in Stylophora pistillata. BMC Molecular and Cell Biology. 8 mars 2021;22(1):18.

64. Ortega MJ. Identification and Characterization of a Sodium/Hydrogen Exchanger in the Coral Species Acropora yongei: a potential role in biomineralization. [MSc]. UNIVERSITY OF CALIFORNIA SAN DIEGO; 2018.
65. Zoccola D, Ganot P, Bertucci A, Caminiti-Segonds N, Techer N, Voolstra CR, et al. Bicarbonate transporters in corals point towards a key step in the evolution of cnidarian calcification. Scientific Reports. 4 juin 2015;5(1):9983.
66. Pedersen SF, Counillon L. The SLC9A-C Mammalian Na+/H+ Exchanger Family: Molecules, Mechanisms, and Physiology. Physiol Rev. 1 oct 2019;99(4):2015-113.
67. Tambutté É, Allemand D, Mueller E, Jaubert J. A compartmental approach to the mechanism of calcification in hermatypic corals. Journal of Experimental Biology. 1 mai 1996;199(5):1029-41.
68. Zoccola D, Tambutté E, Kulhanek E, Puverel S, Scimeca JC, Allemand D, et al. Molecular cloning and localization of a PMCA P-type calcium ATPase from the coral Stylophora pistillata. Biochimica et Biophysica Acta (BBA) - Biomembranes. 27 mai 2004;1663(1):117-26.
69. Barron ME, Thies AB, Espinoza JA, Barott KL, Hamdoun A, Tresguerres M. A vesicular Na+/Ca2+ exchanger in coral calcifying cells. PLOS ONE. 31 oct 2018;13(10):e0205367.
70. Palty R, Ohana E, Hershfinkel M, Volokita M, Elgazar V, Beharier O, et al. Lithium-Calcium Exchange Is Mediated by a Distinct Potassium-independent Sodium-Calcium Exchanger. Journal of Biological Chemistry. 2004;279(24):25234-40.
71. Poet M, Vigier N, Bouret Y, Jarretou G, Bendahhou S, Montanes M, et al. Biological fractionation of lithium isotopes by cellular Na+/H+ exchangers unravels fundamental transport mechanisms [Internet]. bioRxiv; 2022 [cité 14 nov 2022]. p. 2022.10.06.510772. Disponible sur: https://www.biorxiv.org/content/10.1101/2022.10.06.510772v1

INDEX OF FIGURES

Figure I-1 | Photographies du lagon de Nouvelle-Calédonie (photo de gauche ; © M. Dosdane) et de sa barrière récifale (photo de droite ; © P.-A. Pantz) 19
Figure I-2 | Photographie de la pente externe d'un récif barrière sur la côte ouest de la Grande Terre en Nouvelle-Calédonie (© F. Benzoni). 20
Figure I-3 | Diagramme de prédominance des espèces de carbone inorganique dissous en fonction du pH (© J.A. Wojtowicz, 2001). 21
Figure I-4 | Histologie d'un polype de corail (A) et du cœnosarque (B). D'après Vidal-Dupiol et al. (2009). 22
Figure I-5 | Schéma de fonctionnement de la "pompe à protons" (modifié d'après Eagle R., comm. pers.) 24
Figure I-6 | Photographies de Symbiodiniaceae (à gauche ; © T.C. LaJeunesse) et d'un polype de corail en symbiose avec des Symbiodiniaceae (à droite ; © C. Shinzato) 25
Figure I-7 | Classification phylogénétique révisée des genres de Symbiodiniaceae. D'après LaJeunesse et al. (2018). 26
Figure I-8 | Photographies de pontes de corail (photos du haut) : le corail relâche ses œufs roses composés de gamètes mâles et femelles (© C. Alessi). Photographies d'une larve planula et de deux premiers calices fixés sur un substrat naturel (en bas à gauche), et d'un individu juvénile (en bas à droite) (© D. Petersen). 29
Figure I-9 | Photographies de Corallinales dans le lagon de Bouraké (© R. Rodolfo-Metalpa). 30
Figure I-10 | Hydrolyse et dissociation du CO_2 dans l'océan (© UC Davis Biological Sciences, 2018). 31
Figure I-11 | Evolution temporelle du blanchissement corallien (© GBR Marine Park Authority) 33
Figure I-12 | Épisode de blanchissement des coraux sur la GBR en 2022, en pourcentage de la surface des récifs touchés (© GBR Marine Park Authority) 34
Figure I-13 | Photographies de différents environnements coralliens extrêmes et marginaux. (a,b) Sites hydrothermaux en Papouasie-Nouvelle-Guinée (© R. Rodolfo-Metalpa et J.M. Boré), (c) système de mangrove de la GBR (© E. Camp), (d) système de Bouraké en Nouvelle-Calédonie (© E. Camp), (e) herbier marin des îles Caïmans (© E. Camp), (f) récif turbide de Salvador au Brésil (© E. Camp), (g) récif macrotidal de Kimberley (© V. Schoepf). D'après Camp et al. (2018). 38

Figure I-14 | Diagramme de spéciation des formes de bore dans l'eau de mer en fonction du pH (à gauche) ; $\delta^{11}B$ des formes de bore inorganique dissous en fonction du pH de l'eau de mer (à droite). Modifié d'après Guillermic et al. (2020). 41
Figure II-1. | The semi-enclosed lagoon of Bouraké, New Caledonia (aerial photo taken at 130m height; © R. Rodolfo-Metalpa). 50
Figure II-2 | Illustration of the three coral species studied in this thesis (© F. Maggioni). 51
Figure II-3 | Coral individuals placed in beakers for light and dark incubations (© C. Tanvet). 52
Figure II-4 | Simplified schematic representation of the Kiel-IV Carbonate device coupled to a mass spectrometer MAT-253 IRMS (Thermo Fisher Scientific) (redrawn from F. Dewilde). .60
Figure II-5 | Illustrations of boron purification process. Loading of the 60 µL dissolved sample on the beaker cap (A). Microdistillation at 95°C for 15 hours in the digestion block (B). Cooling of the beakers at the end of the microdistillation with the distillate drop (containing the purified boron) on the conical side of the beaker (C). Caps containing the tiny drop of microdistillation residues (collected for final yield assessment later on) (D) (© C. Tanvet). 61
Figure II-6 | Simplified schematic representation of the MC-ICP-MS Neptune (Thermo Fisher Scientific) functioning (redrawn from J. Milot) 63
Figure III-1 | Map showing the location of the study sites in New Caledonia **(A)** and the position of the stations where the 2-year experiment took place **(B-D)**. Station B3 was located in the semi-enclosed lagoon of Bouraké **(B)**, while two other stations were located either near Bouraké (St R2) **(C)** or in Maa's Bay (St M1) **(D)**. 73
Figure III-2 | Seawater pH_T **(A–C)** and dissolved oxygen (DO) **(D–F)** variations (black lines) recorded during 48 hours at Bouraké (St B3) and stations R2 and M1. Data were collected at the end of March 2019 at St R2 for pH **(B)** and DO **(E)** and at St B3 for pH **(A)**. DO was measured at St B3 at the beginning of April 2019 **(D)**. At St M1, data were collected at the end of January 2019 **(C, F)**. Tidal variations (grey lines) are on the right y-axis. 77
Figure III-3 | Change in crustose coralline algae (CCA) **(A–C)** and Turf percent cover **(D–F)** on top sides of the tiles between the beginning (two months after the time of deployment, T_2) and the end (after ca two years of deployment, $T_{24/26}$) of collector deployment at study stations B3, R2 and M1 (number of tiles n = 15, 20 and 19, respectively). Data are median values ± 25th and 75th percentiles (box), minimum and maximum values (whiskers), and outliers (dots). Stars represent statistical significance (see **Table III-2**). 79
Figure III-4 | Number of coral recruits (per tile) found on the different sides of the tiles immersed during ca. two years at Bouraké (B3) and stations R2 and M1. Data are means ± SD (number of tiles n = 15, 20, and 19, for B3, R2, and M1, respectively). Data from the lateral sides were pooled. Stars represent statistical significance (see **Appendix Table VIII-3**). 81

Figure III-5 | Photos of the tiles (randomly selected) deployed at Bouraké B3 (left), station R2 (middle), and station M1 (right). Pictures of the top sides were taken after two months of deployment (T2) **(A–C)**, and after 24 **(D, E)** and 26 months of deployment **(F)**. Pictures of bottom sides of tiles after 24 months **(G, H)** and ca. 26 months of deployment **(I)**. 83
Figure IV-1 | Seawater pH_T variations recorded with a SeaFet during a 48-h cycle in four experimental pH conditions (Control, pH_{NBS} 8.11; Future, pH_{NBS} 7.76; Extreme, pH_{NBS} 7.54; and Variable, pH_{NBS} 7.56-8.07). See Table IV-1 and Appendix Table VIII-7 for all data. 104
Figure IV-2 | Reaction norm of the growth rates of corals from Bouraké (blue) and reference (grey) site maintained during 100 days at four pH conditions (Control, pH_{NBS} 8.11; Future, pH_{NBS} 7.76; Extreme, pH_{NBS} 7.54; and Variable, pH_{NBS} 7.56-8.07). The arrow indicates the direction of the change from the condition of origin, assuming that corals from Bouraké might originate from seawater at either pH 7.7 (Future pH) or 7.4 (Extreme pH), to the experimental pH condition. Data represented as dots are means of the three replicate tanks ± SE (overlapping SEs are in red) (n = 13-16, depending on species and pH condition; see Appendix Table VIII-11 for all post hoc comparisons). 106
Figure IV-3 | Relative electron transport rate (rETR) measured during RLC curves of corals after 100 days of incubation at four pH conditions (Control, pH_{NBS} 8.11; Future, pH_{NBS} 7.76; Extreme, pH_{NBS} 7.54; and Variable, pH_{NBS} 7.56-8.07). Bouraké corals are in blue, while reference corals are in grey. Data are mean ± SE; n=12-16, depending on species and pH condition; see Appendix Table VIII-11 for all post hoc comparisons). 108
Figure IV-4 | Gross photosynthesis (P_g) and respiration (R_{dark}) rates of corals from Bouraké (in blue) and the reference (in grey) site at four pH conditions (Control, pH_{NBS} 8.11; Future, pH_{NBS} 7.76; Extreme, pH_{NBS} 7.54; and Variable, pH_{NBS} 7.56-8.07). Data are median ± 25th and 75th percentiles (n = 7); see Appendix Table VIII-11 for all post hoc comparisons). 110
Figure IV-5 | Symbiodiniaceae density and total protein content of corals from Bouraké (in blue) and the reference (in grey) site after 100 days of incubation at four pH conditions (Control, pH_{NBS} 8.11; Future, pH_{NBS} 7.76; Extreme, pH_{NBS} 7.54; and Variable, pH_{NBS} 7.56-8.07). Data are median ± 25th and 75th percentiles (n = 6-8, depending on species and pH condition). No data are available for the protein content of Porites sp. from Bouraké incubated at the Extreme pH condition. Asterisks indicate statistical significance at $p < 0.05$; see Appendix Table VIII-11 for all post hoc comparisons. 111
Figure IV-6 | Predicted major ITS2 type profiles of corals from Bouraké and the reference site after 100 days of incubation at four pH conditions (Control, pH_{NBS} 8.11; Future, pH_{NBS} 7.76; Extreme, pH_{NBS} 7.54; and Variable, pH_{NBS} 7.56-8.07). Within each cell of this 3-by-4 matrix, samples are plotted as stacked bar charts with a single column representing a sample from a

specific origin: Bouraké (left) and reference (right). The number of individuals per condition varies from 2 to 6 depending on the number of samples available. 113
Figure V-1 | Net calcification (**A-C**), $\delta^{13}C$ and $\delta^{11}B$ (**D-F**), and B/Ca ratio (**G-I**) of Acropora tenuis, Montipora digitata and Porites sp. measured at the experimental stable pH_{sw} conditions (Extreme, pH_{NBS} 7.54; Future, pH_{NBS} 7.76; Control, pH_{NBS} 8.11). Blue circles and grey triangles correspond to Bouraké and Reference colonies, respectively. Largest symbols represent averaged values, while the smallest symbols represent data for each individual colony. Dashed lines represent linear model regressions fitted using linear model function in RStudio with 95% confidence interval represented by the envelopes. (n=7-17 per pH conditions, depending on parameters, site of origin and species). The black dots for Bouraké and the red squares for the reference site represent the respective geochemical parameters measured on samples collected in situ and not incubated in aquaria (n=3-22, depending on parameters, site of origin and species). $\delta^{11}B$ and B/Ca of the in situ samples were only measured for M. digitata (n=5 for Reference and n=10 for Bouraké). Please, note that the scales for net calcification are different between species and that for clarity we do not present the Variable pH_{sw} condition (see Appendix Figure VIII-14 and Figure VIII-15).....135
Figure V-2 | pH_{ECM} (**A-C**), $[CO_3^{2-}]_{ECM}$ (**D-F**), and DIC_{ECM} (**G-I**) of Acropora tenuis, Montipora digitata and Porites sp. calculated on boron proxies at the experimental stable pH_{sw} conditions (Extreme, pH_{NBS} 7.54; Future, pH_{NBS} 7.76; Control, pH_{NBS} 8.11). Blue circles and grey triangles correspond to Bouraké and Reference colonies, respectively. Largest symbols represent averaged values, while the smallest symbols represent data for each individual colony. Dashed lines represent linear model regressions fitted using linear model function in RStudio with 95% confidence interval represented by the envelopes. (n=6-11 per pH conditions, depending on parameters, site of origin and species). Continuous green lines represent DIC_{sw} or $[CO_3^{2-}]_{sw}$. Calcifying fluid parameters were also calculated for M. digitata individuals sampled in situ and represented by black dots for Bouraké (n=10) and red squares for Reference (n=5). ECM: Extracellular Calcifying Medium; SW: Seawater. Please, note that for clarity we do not present the Variable pH_{sw} condition (see Appendix Figure VIII-14 and Figure VIII-15).....137
Figure VI-1 | Temporal evolution of $\delta^{11}B$ (black) and $\delta^{13}C$ (blue) signatures in Porites sp. cores collected at Puen (left) and Bouraké (right), over 31 and 27 years, respectively. The estimated seawater pH corresponding to the $\delta^{11}B$ signatures is plotted on the second y-axis (right side of the graphs). The range of variation in seawater pH_T values measured in situ using SeaFet over several time intervals between February 2016 and April 2019 at Bouraké, and for two weeks in March 2019 at Puen (Maggioni et al., 2021), is represented by the green bars. To highlight the significance of trends, we applied linear models (dashed line with 95% confidence interval in grey). Historical, Severe (**S**; ± 0.5-1.5°C) or Moderate (**M**; ± 1.6-2.6°C) El Niño (**EN**; red)

and La Niña (**LN**; blue) events are identified by the Oceanic Niño Index (ONI) from the 3-month running mean of ERSST.v5 SST anomalies in the Niño 3.4 region (Huang et al., 2017). ENSO events are represented by arrows and their periods of occurrence are indicated in parentheses. 158

Figure VI-2 | Temporal evolution of $\delta^{18}O$ (purple) and Li/Mg (black) signatures in Porites sp. cores collected at Puen (left) and Bouraké (right), over 31 and 27 years, respectively. The estimated sea surface temperature (SST) corresponding to $\delta^{18}O$ and Li/Mg signatures is plotted on the second y-axis (right side of the graphs). Temperature recalculated from $\delta^{18}O$ signatures, and corrected with in-situ measured sea surface salinity (SSS), is represented by the orange curves. The range of SST values measured in-situ using SeaFet over a continuous period from January 2019 to April 2020 for Bouraké and Puen (Maggioni et al., 2021), is represented by the green bars. To highlight the significance of trends, we applied linear models (dashed line with 95% confidence interval in grey). Historical, Severe (**S**; ± 0.5-1.5°C) or Moderate (**M**; ± 1.6-2.6°C) El Niño (**EN**; red) and La Niña (**LN**; blue) events are identified by the Oceanic Niño Index (ONI) from the 3-month running mean of ERSST.v5 SST anomalies in the Niño 3.4 region (Huang et al., 2017). ENSO events are represented by arrows and their periods of occurrence are indicated in parentheses.....160

Figure VIII-1 | An example of the seawater pH_T coupled with the tidal variations, measured during 11 days at the end of March 2019 at St B3 and St R2 (A and B), and 11 days in January 2019 at St M1 (C). 184

Figure VIII-2 | An example of the seawater dissolved oxygen concentrations, coupled with the tidal variations, measured during 11 days at the beginning of April 2019 at St B3 (A), at the end of March 2019 at St R2 (B), and at the end of January 2019 at St M1 (C). 185

Figure VIII-3 | CCA (A) and Turf percent cover (B) measured on the bottom sides of the tiles after ca. two years of tile immersion at stations B3, R2, and M1 (number of tiles n = 15, 20, and 19, respectively). Data are median values ± 25th and 75th percentiles (box), minimum and maximum values (whiskers), and outliers (dots). Stars represent statistical significance (see Appendix Table VIII-3).....186

Figure VIII-4 | Mean relative abundances (%) of the coral families which settled on the tiles (all sides pooled) during the two years of tile immersion in Bouraké (B3) and stations R2 and M1. 186

Figure VIII-5 | Map of the study sites (B and R1) in New Caledonia where corals were collected. Photo (B) is an aerial pic of the Bouraké lagoon (taken at 130 m height). 191

Figure VIII-6 | Schematic representation of the experimental set up with four pH conditions (Control, pH_{NBS} 8.11; Future, pH_{NBS} 7.76; Extreme, pH_{NBS} 7.54; and Variable, pH_{NBS} 7.56-8.07), each replicated in three experimental tanks, and 6 tank sumps that alimented the experimental

tanks. In each experimental tank, 30 coral fragments were positioned, half from Bouraké and half from the reference site. The 'Variable' condition was supplied by one or more sumps simultaneously according to a time table mimicking pH variation in Bouraké (see Appendix Table VIII-6). Sump temperature was maintained at ca. ~26°C. 192
Figure VIII-7 | Example of the light intensity received by the corals during the 100-day incubation, and measured in two tanks having a different position below the LED lights (see Appendices Tables VIII-5 and VIII-6 for setting).....192
Figure VIII-8 | Photosynthetic efficiency (F_v/F_m) of corals from Bouraké (in blue) and reference (in grey) sites measured after 100 days of incubation at four pH conditions (Control, pH_{NBS} 8.11; Future, pH_{NBS} 7.76; Extreme, pH_{NBS} 7.54; and Variable, pH_{NBS} 7.56-8.07). Data are median ± 25th and 75th percentiles (n=12-16, depending on species and pH condition ; see Appendix Table VIII-11 for all post hoc comparisons).....193
Figure VIII-9 | Gross photosynthesis to respiration ratio (P_g:R) of corals from Bouraké (in blue) and the reference site (in grey) incubated at four pH conditions (Control, pH_{NBS} 8.11; Future, pH_{NBS} 7.76; Extreme, pH_{NBS} 7.54; and Variable, pH_{NBS} 7.56-8.07). Data are median ± 25th and 75th percentiles (n = 7; see Appendix Table VIII-11 for all post hoc comparisons). 193
Figure VIII-10 | Total chlorophyll ($a + c_2$) content of corals from Bouraké (in blue) and reference (in grey) sites after 100 days of incubation at four pH conditions (Control, pH_{NBS} 8.11; Future, pH_{NBS} 7.76; Extreme, pH_{NBS} 7.54; and Variable, pH_{NBS} 7.56-8.07). Data are median ± 25th and 75th percentiles (n = 7; see Appendix Table VIII-11 for all post hoc comparisons). 194
Figure VIII-11 | Relative abundance (%) of ITS2 sequence of corals from Bouraké and the reference site after 100 days of incubation at four pH conditions (Control, pH_{NBS} 8.11; Future, pH_{NBS} 7.76; Extreme, pH_{NBS} 7.54; and Variable, pH_{NBS} 7.56-8.07). Within each cell of this 3-by-4 matrix, samples are plotted as stacked bar charts with a single column representing a sample from a specific origin: Bouraké (left) and reference (right). Only the 30 most abundant ITS2 sequences have been assigned colors. Low-abundance sequences are in grey. Sequences with designated names (e.g., B1, C15, or C1) refer to sequences previously characterized in the literature or that have been run through the SymPortal analytical framework. Less common sequences and those that have not been used to characterize ITS2-type profiles are designated using a unique database ID and their associated clade/genera (e.g., X2409936_C; the latter letter refers to Cladocopium genera (Clade C)). 195
Figure VIII-12 | Control gels of the PCR. Negative controls are represented with a T. First, we ran random PCR samples on gels (A); after noticing some unsuccessful PCR, we checked all PCR samples from the same session on gels (B & C). The unsuccessful PCR were run again during a new session with adjustments of the hybridation time, and were checked again on gels (D). The remaining unsuccessful PCR (n=10), and those that did not pass the AGRF

quality control were removed from the study (n=4), leading to a total of 112 samples for ITS2 sequencing. 196
Figure VIII-13 | $\delta^{13}C_{Reference}$ - $\delta^{13}C_{Bouraké}$ (**A-C**), Gross photosynthesis (P_g) (**D-F**), dark respiration (R_{dark}) (**G-I**), and P_g:R_{dark} ratios (**J-L**) of Acropora tenuis, Montipora digitata and Porites sp. measured at the experimental pH_{sw} conditions. Black dots represent the difference between $\delta^{13}C_{Reference}$ and $\delta^{13}C_{Bouraké}$. Blue circles and grey triangles correspond to Bouraké and Reference colonies, respectively. Largest symbols represent averaged values, while the smallest symbols represent data for each individual colony. Dashed lines represent linear model regressions fitted using linear model function in RStudio with 95% confidence intervals represented by the envelopes. (n=7 per pH conditions, parameters, site of origin and species). The black symbols (dots for Bouraké and triangle for Reference) represent data for the Variable pH condition (incubated for photosynthesis and respiration rates measurements at both Extreme (7.53) and Control (8.11) pH) and are not included in the regressions. Stars represent statistical significance (Appendix Table VIII-14). Please, note that data in panels **D-L** comes from the study of chapter 4. 206
Figure VIII-14 | Comparisons according to colony origin (Bouraké and Reference) for the Variable pH condition. Net calcification (**A-C**), $\delta^{13}C$ (**D-F**), pH_{ECM} (**G-I**), and DIC_{ECM} (**J-L**) of Acropora tenuis, Montipora digitata and Porites sp. (n=7-16 depending on parameters, site of origin and species). Data are median values ± 25^{th} and 75^{th} percentiles (box), minimum and maximum values (whiskers), mean values (black dots) and outliers (red dots). Stars represent statistical significance at $p < 0.05$ (*) and $p < 0.01$ (**); see Appendix Table VIII-15. 207
Figure VIII-15 | Comparisons according to colony origin (Bouraké and Reference) for the Variable pH condition. $\delta^{11}B$ (**A-C**), B/Ca (**D-F**), $[CO_3^{2-}]_{ECM}$ (**G-I**) of Acropora tenuis, Montipora digitata and Porites sp. (n=7-13 depending on parameters, site of origin and species). Data are median values ± 25^{th} and 75^{th} percentiles (box), minimum and maximum values (whiskers), mean values (black dots) and outliers (red dots). Stars represent statistical significance at $p < 0.05$ (*) and $p < 0.01$ (**); see Appendix Table VIII-15. 208
Figure VIII-16 | (A) Location of coral core sampling sites, Bouraké (B2) and Puen (R1), in New-Caledonia. **(B)** Aerial photo of Bouraké lagoon (taken at 130 m altitude) with the coral core sampling site (B2). 216
Figure VIII-17 | Drilling and cutting of the two Porites sp. cores from Bouraké and Puen (core length: ~35 cm; core diameter: ~7 cm). 217
Figure VIII-18 | Positive X-radiographs of the two coral cores (Bouraké B2 and Puen R1) in New Caledonia. The model-age follows the density bands of the skeleton (red lines). 217

INDEX OF TABLES

Table II-1 | PCR program for DNA amplification cycle. 57
Table III-1 | Main environmental parameters measured at Bouraké (B3) and the stations M1 and R2. Study site B3 R2. Mean (SD), minimum (min) and maximum (max) values of temperature, pHT (total scale), and dissolved oxygen (DO). Values were calculated from data collected during August 2017, June 2018 and January 2019 at station M1, and during 3-year long-term monitoring at B3 and R2 considering both diel and seasonal fluctuations, and compiling several thousands of measurements (Camp et al., 2017; Maggioni et al., 2021). The temperature at station M1 was only occasionally recorded during the 2-year study period, therefore not presented. 76
Table III-2 | Statistical data on CCA, turf and empty cover on the top sides of tiles. **(A and B)** Non-parametric Wilcoxon tests between the beginning (T_0) and after two-month incubation (T_2); and between the T_2 and 2-year ($T_{24/26}$) at the three stations. **C)** Non-parametric Kruskal-Wallis test, followed by the Dunn's multiple comparisons, between stations for CCA, Turf and Empty measured at the beginning (T_2) and the end ($T_{24/26}$). Significant values are in bold ($p<0.05$). 80
Table IV-1 | Seawater parameters measured during the 100-day experiment, and carbonate chemistry calculated for each pH condition (the 3 replicated tanks were pooled). Seawater carbonate chemistry was calculated using mean values for A_T (2187, 2204, 2202, and 2202 µmol kg^{-1} for Control, pH_{NBS} 8.11; Future, pH_{NBS} 7.76; Extreme, pH_{NBS} 7.54; and Variable, pH_{NBS} 7.56-8.07, respectively), and mean salinity value of 35.61 PSU. 105
Table IV-2 | Two-way ANOVAs (type III) summary with Satterthwaite's method of linear mixed effect model (LMER) on the effects of colony origin (O), pH conditions and their interactions on the physiological responses of three coral species after 100 days of incubation. Non-parametric two-way Aligned Rank Transformed (ART) ANOVAs (Type III) followed by a Bonferroni p-levels adjusted post hoc test was used for F_v/F_m. Significant values are in bold ($p < 0.05$). All statistical analyses with the post hoc and random effects are in the Appendix Table VIII-11. 107
Table IV-3 | Three-factorial PERMANOVA analysis testing the effects of colony origin (O), pH conditions, coral species and their interactions on the Symbiodiniaceae ITS2 type profiles. Significant values are in bold ($p < 0.05$). 112
Table V-1 | Probability values from two-way ANOVAs testing the effects of colony origins (Bouraké and Reference sites), pH conditions (Extreme, pH_{NBS} 7.54; Future, pH_{NBS} 7.76;

Control, pH_{NBS} 8.11), and their interaction for the three coral species. Significant values are in bold ($p < 0.05$). All statistical analyses, including the post-hoc comparisons, are in the Appendix Table VIII-12. 136

Table V-2 | Results of a Welch T-test testing the differences between the two pH conditions Future, pH_{NBS} 7.76 and Variable pH_{NBS} 7.56 - 8.07 on the ECM carbonate chemistry (pH_{ECM}, $[CO_3]^{2-}_{ECM}$ and DIC_{ECM}) for each coral species. Significant values are in bold ($p < 0.05$). 138

Table VI-1 | Probability values from one-way ANOVAs testing the effects of time on each geochemical parameter over the study period for each site (Puen and Bouraké). Significant values are in bold ($p < 0.05$). 161

Table VIII-1 | List of coral species identified in the Bouraké lagoon (B3) and at sites R2 and M1. 187

Table VIII-2 | Summary of cover percentages of each category (CCA, Turf and suspension feeders) per site (B3, R2 and M1) for top (**A**) and bottom side (**B**). Data are mean ± SE (n=15, 20 and 19 for B3, R2 and M1, respectively). 189

Table VIII-3 | Statistical data for each category of organisms settled on tile bottom sides after two years of tile deployment (TF). Non-parametric Kruskal-Wallis tests, followed by Dunn's multiple comparisons, were run between stations for each category of organisms 190

Table VIII-4 | Non-parametric Kruskal-Wallis test between the three stations on Shannon Index Diversity (i.e., H= 4.17, 4.02, and 3.97 for stations B3, R2 and M1, respectively. 190

Table VIII-5 | Time table used by the IKS logger (Timer function) in the Variable condition to mimic the natural pH variation measured at Bouraké. For each time step, IKS activated the pump that supplied seawater from the sump to the experimental tanks at the desired value. 197

Table VIII-6 | Percentage of irradiance intensity for each of the LED light spectra during a diel cycle (from 6 am to 5 pm). 197

Table VIII-7 | Seawater carbonate chemistry daily measurements during the 100 days of incubation at four pH conditions (Control, pH_{NBS} 8.11; Future, pH_{NBS} 7.76; Extreme, pH_{NBS} 7.54; and Variable, pH_{NBS} 7.56-8.07), and for each replicate tank (A, B and C). Seawater carbonate chemistry was calculated using mean values for A_T (2187, 2204, 2202, and 2202 µmol kg^{-1} for Control, Future, Extreme, and Variable, respectively) and the mean salinity value of 35.61. 198

Table VIII-8 | Seawater daily measurements during 100 days in the 6 tank sumps (i.e., pH_T 7.4, 7.6, 7.7, 7.8, 7.9 and 8.1) that alimented the experimental tanks. 199

Table VIII-9 | Aligned Rank Transformed (ART) ANOVAs (Type III) summary with Kenward-Roger method of linear mixed effects model (LMER) on the effects of temperature, pH and

nutrients between pH conditions (Control, pH_{NBS} 8.11; Future, pH_{NBS} 7.76; Extreme, pH_{NBS} 7.54; and Variable, pH_{NBS} 7.56-8.07). Significant values are in bold ($p < 0.05$) 199

Table VIII-10 | Seawater nutrient contents measured two times a month during the 100 days of incubation at four pH conditions (Control, pH_{NBS} 8.11; Future, pH_{NBS} 7.76; Extreme, pH_{NBS} 7.54; and Variable, pH_{NBS} 7.56-8.07) , and for each replicated tank (A, B and C). 200

Table VIII-11 | Two-way ANOVAs (type III) summary with Satterthwaite's method of linear mixed effect model (LMER) on the effects of colony origin (Bouraké and reference), pH conditions (Control, pH_{NBS} 8.11; Future, pH_{NBS} 7.76; Extreme, pH_{NBS} 7.54; and Variable, pH_{NBS} 7.56-8.07), and their interactions for each coral species and for each physiological measurement. When a significant effect was found on pH (4 levels: Control, Future, Extreme and Variable), we used a post-hoc Tukey HSD. Non-parametric two-way Aligned Rank Transformed (ART) ANOVA (Type III) with Kenward-Roger method followed by a Bonferroni p-levels adjusted post hoc was used for F_v/F_m. For simplicity, Control = 8.1; Future = 7.8; Extreme = 7.5; Variable = Var; R = reference; B = Bouraké. Significant values are in bold ($p < 0.05$). 201

Table VIII-12 | Results of Two-way ANOVAs testing the effects of colony origins (Bouraké and Reference sites), pH treatments (Extreme, pH_{NBS} 7.54; Future, pH_{NBS} 7.76; Control, pH_{NBS} 8.11), and their interactions for the three coral species. Significant values are in bold ($p < 0.05$). Post hoc comparisons were performed on significant interactions (Tukey HSD) between pH and origin.....208

Table VIII-13 | $\delta^{11}B$ of the seawater measured in-situ at Bouraké and Reference (A) and during the aquaria experiment in each tank condition (B). Mean pH values measured are presented as mean ± SD for B. $\delta^{13}C$ of the two CO_2 gas bottles used during the aquaria experiments (C) with each replicate equivalent to n=3-5 sampling made through the length of the experiment. 211

Table VIII-14 | Results of a Wilcoxon testing the effect of pH on $\delta^{13}C_{Reference}$ - $\delta^{13}C_{Bouraké}$ (A). Results of Two-way ANOVAs testing the effects of colony origin (Bouraké and Reference); pH treatments (Extreme, pH_{NBS} 7.54; Future, pH_{NBS} 7.76; Control, pH_{NBS} 8.11), and their interactions for the three coral species (B). Significant values are in bold ($p < 0.05$). Post hoc comparisons were performed on significant interactions (Tukey HSD) between pH and origin. 211

Table VIII-15 | Probability values from non-parametric Wilcoxon tests testing the effects of colony origins (Bouraké and Reference) on geochemical data obtained in the Variable pH treatment for the three coral species. Significant values are in bold ($p < 0.05$).....213

Table VIII-16 | Measured values of net calcification, $\delta^{13}C$, $\delta^{11}B$ and elemental ratios (B/Ca) within the skeletons of A. tenuis, M. digitata and Porites sp. and corresponding reconstructed parameters of the extracellular calcifying medium (pH_{ECM} (total scale) and DIC_{ECM}). 213

LEXICON

ACC	Amorphous Calcium Carbonate
ATP	Adenosine Triphosphate
$CaCO_3$	Calcium carbonate
CCA	Crustose Coralline Algae
CO_2	Carbone dioxide (Carbonic gas)
CO_3^{2-}	Carbonate ion
DIC	Dissolved Inorganic Carbon
DIVs	Defining Intragenomic [ITS2 sequence] Variants
DNA	Deoxyribose Nucleic Acid
DO	Dissolved Oxygen
ECM	Extracellular Calcifying Medium
rETR	Relative Electron Transport Rate
F_v/F_m	Photosynthetic efficiency
H_2O	Water (also called MQ water for purified Milli-Q® water)
H_2O_2	Hydrogen peroxide
H_3PO_4	Orthophosphoric acid
HCl	Hydrochloric acid
HCO_3^-	Bicarbonate ion
HF	Hydrofluoric acid
HNO_3	Nitric acid
IPCC	Intergovernmental Panel on Climate Change (GIEC)
ITS2	Internal Transcribed Spacer 2
N_2	Dinitrogen (Nitrogen gas)
NADP	Nicotinamide Adenine Dinucleotide Phosphate
NaOH	Sodium hydroxide
NH_4OH	Ammonium hydroxide
NO_2^-	Nitrite
NO_3^-	Nitrate
NO_x	Pooled nitrate and nitrite
O_2	Dioxygen (Oxygen gas)
OA	Ocean Acidification
OD	Ocean Deoxygenation
OW	Ocean Warming

PAM	Pulse Amplitude Modulation
PAR	Photosynthetic Active Radiation
***p*CO_2**	Carbon dioxide partial pressure
PCR	Polymerase Chain Reaction
P_g	Gross Photosynthesis
P_g:R	Photosynthesis to Respiration ratio
pH	Hydrogen potential (pH_T for total scale ; pH_{NBS} for NBS scale)
P_n	Net Photosynthesis
PO_4^{3-}	Phosphates (orthophosphate ion)
PSII	Photosystem II
RLC	Rapid Light Curve
RCP	Representative Concentration Pathway (IPCC scenarios)
R_{dark}	Respiration rates in the dark
SEM	Scanning Electron Microscopy
$Si(OH)_4$	Silicates (orthosilicic acid)
ΦPSII	Effective quantum yield of PSII
Ω_{arag}	Aragonite saturation state

BIBLIOGRAPHY

Adjeroud, M., Penin, L., and Carroll, A. (2007). Spatio-temporal heterogeneity in coral recruitment around Moorea, French Polynesia: Implications for population maintenance. *J. Exp. Mar. Bio. Ecol.* 341, 204–218. doi:10.1016/j.jembe.2006.10.048.

Affek, H. P., and Yakir, D. (2014). *The Stable Isotopic Composition of Atmospheric CO2*. 2nd ed. Elsevier Ltd. doi:10.1016/B978-0-08-095975-7.00407-1.

Agostini, S., Harvey, B. P., Wada, S., Kon, K., Milazzo, M., Inaba, K., et al. (2018). Ocean acidification drives community shifts towards simplified non-calcified habitats in a subtropical−temperate transition zone. *Sci. Rep.* 8, 5–10. doi:10.1038/s41598-018-29251-7.

Agostini, S., Houlbrèque, F., Biscéré, T., Harvey, B. P., Heitzman, J. M., Takimoto, R., et al. (2021). Greater Mitochondrial Energy Production Provides Resistance to Ocean Acidification in “Winning” Hermatypic Corals. *Front. Mar. Sci.* 7, 1–11. doi:10.3389/fmars.2020.600836.

Aichelman, H. E., Bove, C. B., Castillo, K. D., Boulton, J. M., Knowlton, A. C., Nieves, O. C., et al. (2021). Exposure duration modulates the response of Caribbean corals to global change stressors. *Limnol. Oceanogr.* 66, 3100–3115. doi:10.1002/lno.11863.

Ainsworth, T. D., and Brown, B. E. (2021). Coral bleaching. *Curr. Biol.* 31, R5–R6. doi:10.1016/j.cub.2020.10.048.

Ainsworth, T. D., Heron, S. F., Ortiz, J. C., Mumby, P. J., Grech, A., Ogawa, D., et al. (2016). Climate change disables coral bleaching protection on the Great Barrier Reef. *Science (80-.).* 352, 338–342. doi:10.1126/science.aac7125.

Al-Horani, F. A., Al-Moghrabi, S. M., and De Beer, D. (2003). The mechanism of calcification and its relation to photosynthesis and respiration in the scleractinian coral *Galaxea fascicularis*. *Mar. Biol.* 142, 419–426. doi:10.1007/s00227-002-0981-8.

Albright, R., and Langdon, C. (2011). Ocean acidification impacts multiple early life history processes of the Caribbean coral Porites astreoides. *Glob. Chang. Biol.* 17, 2478–2487. doi:10.1111/j.1365-2486.2011.02404.x.

Albright, R., Mason, B., Miller, M., and Langdon, C. (2010). Ocean acidification compromises recruitment success of the threatened Caribbean coral Acropora palmata. *Proc. Natl. Acad. Sci. U. S. A.* 107, 20400–20404. doi:10.1073/pnas.1007273107.

Alderdice, R., Pernice, M., Cárdenas, A., Hughes, D. J., Harrison, P. L., Boulotte, N., et al. (2021). Hypoxia as a physiological cue and pathological stress for coral larvae. *Mol. Ecol.* 31, 1–17. doi:10.1111/mec.16259.

Alibert, C., and McCulloch, M. T. (1997). Strontium/calcium ratios in modern porites corals from the Great Barrier Reef as a proxy for sea surface temperature: Calibration of the thermometer and monitoring of ENSO. *Paleoceanography* 12, 345–363. doi:10.1029/97PA00318.

Allemand, D., Ferrier-Pagès, C., Furla, P., Houlbrèque, F., Puverel, S., Reynaud, S., et al. (2004). Biomineralisation in reef-building corals: From molecular mechanisms to environmental control. *Comptes Rendus - Palevol* 3, 453–467. doi:10.1016/j.crpv.2004.07.011.

Allen-Waller, L., and Barott, K. L. (2023). Symbiotic dinoflagellates divert energy away from mutualism during coral bleaching recovery. *Symbiosis*. doi:10.1007/s13199-023-00901-3.

Allison, N., Cohen, I., Finch, A. A., Erez, J., and Tudhope, A. W. (2014). Corals concentrate dissolved inorganic carbon to facilitate calcification. *Nat. Commun.* 5, 1–6. doi:10.1038/ncomms6741.

Altieri, A. H., Harrison, S. B., Seemann, J., Collin, R., Diaz, R. J., and Knowlton, N. (2017). Tropical dead zones and mass mortalities on coral reefs. *Proc. Natl. Acad. Sci. U. S. A.* 114, 3660–3665. doi:10.1073/pnas.1621517114.

Altieri, A. H., Johnson, M. D., Swaminathan, S. D., Nelson, H. R., and Gedan, K. B. (2021). Resilience of Tropical Ecosystems to Ocean Deoxygenation. *Trends Ecol. Evol.* 36, 227–238. doi:10.1016/j.tree.2020.11.003.

Anthony, K. R. N. (2006). Enhanced energy status of corals on coastal, high-turbidity reefs. *Mar. Ecol. Prog. Ser.* 319, 111–116. doi:10.3354/meps319111.

Anthony, K. R. N., Hoogenboom, M. O., Maynard, J. A., Grottoli, A. G., and Middlebrook, R. (2009). Energetics approach to predicting mortality risk from environmental stress: A case study of coral bleaching. *Funct. Ecol.* 23, 539–550. doi:10.1111/j.1365-2435.2008.01531.x.

Anthony, K. R. N., Kline, D. I., Diaz-Pulido, G., Dove, S., and Hoegh-Guldberg, O. (2008). Ocean acidification causes bleaching and productivity loss in coral reef builders. *Proc. Natl. Acad. Sci. U. S. A.* 105, 17442–17446. doi:10.1073/pnas.0804478105.

Arai, T., Kato, M., Heyward, A., Ikeda, Y., Iizuka, T., and Maruyama, T. (1993). Lipid composition of positively buoyant eggs of reef building corals. *Coral Reefs* 12, 71–75. doi:10.1007/BF00302104.

Arif, C., Daniels, C., Bayer, T., Banguera-Hinestroza, E., Barbrook, A., Howe, C. J., et al. (2014). Assessing Symbiodinium diversity in scleractinian corals via next-generation sequencing-based genotyping of the ITS2 rDNA region. *Mol. Ecol.* 23, 4418–4433. doi:10.1111/mec.12869.

Babcock, R. C., and Heyward, A. J. (1986). Larval development of certain gamete-spawning scleractinian corals. *Coral Reefs*. doi:10.1007/BF00298178.

Baird, A. H., Kospartov, M. C., and Purcell, S. (2010). Reproductive synchrony in acropora assemblages on reefs of new caledonia. *Pacific Sci.* 64, 405–412. doi:10.2984/64.3.405.

Baker, A. C. (2003). Flexibility and Specificity in Coral-Algal Symbiosis: Diversity, Ecology, and Biogeography of *Symbiodinium*. *Annu. Rev. Ecol. Evol. Syst.* 34, 661–689. doi:10.1146/annurev.ecolsys.34.011802.132417.

Barkley, H. C., Cohen, A. L., Golbuu, Y., Starczak, V. R., DeCarlo, T. M., and Shamberger, K. E. F. (2015). Changes in coral reef communities across a natural gradient in seawater pH. *Sci. Adv.* 1, 1–8. doi:10.1126/sciadv.1500328.

Barott, K. L., Venn, A. A., Perez, S. O., Tambutté, S., Tresguerres, M., and Somero, G. N. (2015). Coral host cells acidify symbiotic algal microenvironment to promote photosynthesis. *Proc. Natl. Acad. Sci. U.S.A.* 112, 607–612. doi:10.1073/pnas.1413483112.

Barott, K. L., Williams, G. J., Vermeij, M. J. A., Harris, J., Smith, J. E., Rohwer, F. L., et al. (2012). Natural history of coral-algae competition across a gradient of human activity in the Line Islands. *Mar. Ecol. Prog. Ser.* 460, 1–12. doi:10.3354/meps09874.

Barreto, M. M., Ziegler, M., Venn, A., Tambutté, E., Zoccola, D., Tambutté, S., et al. (2021). Effects of Ocean Acidification on Resident and Active Microbial Communities of Stylophora pistillata. *Front. Microbiol.* 12, 1–13. doi:10.3389/fmicb.2021.707674.

Barshis, D. J., Stillman, J. H., Gates, R. D., Toonen, R. J., Smith, L. W., and Birkeland, C. (2010). Protein expression and genetic structure of the coral *Porites lobata* in an environmentally extreme Samoan back reef: Does host genotype limit phenotypic plasticity? *Mol. Ecol.* 19, 1705–1720. doi:10.1111/j.1365-294X.2010.04574.x.

Bates, D., Mächler, M., Bolker, B. M., and Walker, S. C. (2015). Fitting linear mixed-effects models using lme4. *J. Stat. Softw.* 67. doi:10.18637/jss.v067.i01.

Bates, N. R., Astor, Y. M., Church, M. J., Currie, K., Dore, J. E., González-Dávila, M., et al. (2014). A time-series view of changing surface ocean chemistry due to ocean uptake of anthropogenic CO2 and ocean acidification. *Oceanography* 27, 126–141. doi:10.5670/oceanog.2014.16.

Baums, I. B., Devlin-Durante, M. K., and Lajeunesse, T. C. (2014). New insights into the dynamics between reef corals and their associated dinoflagellate endosymbionts from population genetic studies. *Mol. Ecol.* 23, 4203–4215. doi:10.1111/mec.12788.

Bay, R. A., and Palumbi, S. R. (2016). Transcriptome predictors of coral survival and growth in a highly variable environment. *Ecol. Evol.* 7, 4794–4803. doi:10.1002/ece3.2685.

Beck, J. W., Edwards, R. L., Ito, E., Taylor, F. W., Recy, J., Rougerie, F., et al. (1992). Sea-

Surface Temperature From Coral Skeletal Strontium Calcium Ratios. *Science (80-.).* 257, 0–3. doi:10.1126/science.257.5070.644.

Beck, M. W., Losada, I. J., Menéndez, P., Reguero, B. G., Díaz-Simal, P., and Fernández, F. (2018). The global flood protection savings provided by coral reefs. *Nat. Commun.* 9. doi:10.1038/s41467-018-04568-z.

Bell, T., Manullang, C., Kumagai, N. H., Sakai, K., Suzuki, A., and Iguchi, A. (2022). Calcification responses of subtropical corals to ocean acidification: a case study from Sesoko Island, Okinawa, Japan. *Galaxea, J. Coral Reef Stud.* 24, 51–61. doi:10.3755/galaxea.g2020_s2o.

Berkelmans, R., and Van Oppen, M. J. H. (2006). The role of zooxanthellae in the thermal tolerance of corals: A “nugget of hope” for coral reefs in an era of climate change. *Proc. R. Soc. B Biol. Sci.* 273, 2305–2312. doi:10.1098/rspb.2006.3567.

Bessell-Browne, P., Negri, A. P., Fisher, R., Clode, P. L., and Jones, R. (2017). Impacts of light limitation on corals and crustose coralline algae. *Sci. Rep.* 7, 1–12. doi:10.1038/s41598-017-11783-z.

Bijma, J., Pörtner, H. O., Yesson, C., and Rogers, A. D. (2013). Climate change and the oceans - What does the future hold? *Mar. Pollut. Bull.* 74, 495–505. doi:10.1016/j.marpolbul.2013.07.022.

Biscéré, T., Zampighi, M., Lorrain, A., Jurriaans, S., Foggo, A., Houlbrèque, F., et al. (2019). High pCO2 promotes coral primary production. *Biol. Lett.* doi:10.1098/rsbl.2018.0777.

Blank, R. J., and Trench, R. K. (1985). Speciation and symbiotic dinoflagellates. *Science.* 229, 656–658. doi:10.1126/science.229.4714.656.

Boron, W. F. (2004). Regulation of intracellular pH. *Am. J. Physiol. - Adv. Physiol. Educ.* 28, 160–179. doi:10.1152/advan.00045.2004.

Bove, C. B., Davies, S. W., Ries, J. B., Umbanhowar, J., Thomasson, B. C., Farquhar, E. B., et al. (2022). Global change differentially modulates Caribbean coral physiology. *PLoS One* 17, 1–21. doi:10.1371/journal.pone.0273897.

Bove, C. B., Umbanhowar, J., and Castillo, K. D. (2020). Meta-Analysis Reveals Reduced Coral Calcification Under Projected Ocean Warming but Not Under Acidification Across the Caribbean Sea. *Front. Mar. Sci.* 7, 1–11. doi:10.3389/fmars.2020.00127.

Boyd, P. W., Cornwall, C. E., Davison, A., Doney, S. C., Fourquez, M., Hurd, C. L., et al. (2016). Biological responses to environmental heterogeneity under future ocean conditions. *Glob. Chang. Biol.* 22, 2633–2650. doi:10.1111/gcb.13287.

Bradassi, F., Cumani, F., Bressan, G., and Dupont, S. (2013). Early reproductive stages in the crustose coralline alga Phymatolithon lenormandii are strongly affected by mild ocean acidification. *Mar. Biol.* 160. doi:10.1007/s00227-013-2260-2.

Bramanti, L., and Edmunds, P. J. (2016). Density-associated recruitment mediates coral population dynamics on a coral reef. *Coral Reefs* 35, 543–553. doi:10.1007/s00338-016-1413-4.

Breitburg, D., Levin, L. A., Oschlies, A., Grégoire, M., Chavez, F. P., Conley, D. J., et al. (2018). Declining oxygen in the global ocean and coastal waters. *Science.* 359, doi:10.1126/science.aam7240.

Briand, M. J., Bonnet, X., Goiran, C., Guillou, G., and Letourneur, Y. (2015). Major sources of organic matter in a complex coral reef lagoon: Identification from isotopic signatures (δ13C and δ15N). *PLoS One* 10, 1–21. doi:10.1371/journal.pone.0131555.

Brown, B. E., Le Tissier, M. D. A., and Bythell, J. C. (1995). Mechanisms of bleaching deduced from histological studies of reef corals sampled during a natural bleaching event. *Mar. Biol.* 122, 655–663. doi:10.1007/BF00350687.

Brown, K. T., Mello-Athayde, M. A., Sampayo, E. M., Chai, A., Dove, S., and Barott, K. L. (2022). Environmental memory gained from exposure to extreme *p*CO2 variability promotes coral cellular acid-base homeostasis. *Proc. R. Soc. B Biol. Sci.* 289, 20220941. doi:10.1098/rspb.2022.0941.

Cahyarini, S. Y. (2006). Paired $\delta^{18}O$ and Sr/Ca records of Porites corals from Tahiti (French Polynesia) and Timor (Indonesia). *Thesis*.

Cai, W. J., Ma, Y., Hopkinson, B. M., Grottoli, A. G., Warner, M. E., Ding, Q., et al. (2016). Microelectrode characterization of coral daytime interior pH and carbonate chemistry. *Nat. Commun.* 7, 1–8. doi:10.1038/ncomms11144.

Caldeira, K., and Wickett, M. E. (2003). Anthropogenic carbon and ocean pH. *Nature* 425, 365. doi:10.1038/425365a.

Camacho, C., Coulouris, G., Avagyan, V., Ma, N., Papadopoulos, J., Bealer, K., et al. (2009). BLAST+: Architecture and applications. *BMC Bioinformatics* 10, 1–9. doi:10.1186/1471-2105-10-421.

Cameron, L. P., Reymond, C. E., Bijma, J., Büscher, J. V, Beer, D. De, Guillermic, M., et al. (2022). Impacts of Warming and Acidification on Coral Calcification Linked to Photosymbiont Loss and Deregulation of Calcifying Fluid pH. *J. Mar. Sci. Eng.* 10, 1–23.

Camp, E. F., Edmondson, J., Doheny, A., Rumney, J., Grima, A. J., Huete, A., et al. (2019). Mangrove lagoons of the Great Barrier Reef support coral populations persisting under extreme environmental conditions. *Mar. Ecol. Prog. Ser.* doi:10.3354/meps13073.

Camp, E. F., Nitschke, M. R., Rodolfo-Metalpa, R., Houlbreque, F., Gardner, S. G., Smith, D. J., et al. (2017). Reef-building corals thrive within hot-acidified and deoxygenated waters. *Sci. Rep.* 7, 1–9. doi:10.1038/s41598-017-02383-y.

Camp, E. F., Schoepf, V., Mumby, P. J., Hardtke, L. A., Rodolfo-Metalpa, R., Smith, D. J., et

al. (2018). The future of coral reefs subject to rapid climate change: Lessons from natural extreme environments. *Front. Mar. Sci.* doi:10.3389/fmars.2018.00004.

Camp, E. F., Smith, D. J., Evenhuis, C., Enochs, I., Manzello, D., Woodcock, S., et al. (2016a). Acclimatization to high-variance habitats does not enhance physiological tolerance of two key Caribbean corals to future temperature and pH. *Proc. R. Soc. B Biol. Sci.* 283. doi:10.1098/rspb.2016.0442.

Camp, E. F., Suggett, D. J., Gendron, G., Jompa, J., Manfrino, C., and Smith, D. J. (2016b). Mangrove and seagrass beds provide different biogeochemical services for corals threatened by climate change. *Front. Mar. Sci.* 3, 1–16. doi:10.3389/fmars.2016.00052.

Camp, E. F., Suggett, D. J., Pogoreutz, C., Nitschke, M. R., Houlbreque, F., Hume, B. C. C., et al. (2020). Corals exhibit distinct patterns of microbial reorganisation to thrive in an extreme inshore environment. *Coral Reefs* 39, 701–716. doi:10.1007/s00338-019-01889-3.

Cantin, N. E., Van Oppen, M. J. H., Willis, B. L., Mieog, J. C., and Negri, A. P. (2009). Juvenile corals can acquire more carbon from high-performance algal symbionts. *Coral Reefs* 28, 405–414. doi:10.1007/s00338-009-0478-8.

Cao, L., Zhang, H., Zheng, M., and Wang, S. (2014). Response of ocean acidification to a gradual increase and decrease of atmospheric CO2. *Environ. Res. Lett.* 9. doi:10.1088/1748-9326/9/2/024012.

Capasso, L., Ganot, P., Planas-Bielsa, V., Tambutté, S., and Zoccola, D. (2021). Intracellular pH regulation: characterization and functional investigation of H+ transporters in Stylophora pistillata. *BMC Mol. Cell Biol.* 22, 1–19. doi:10.1186/s12860-021-00353-x.

Carbonne, C., Teixido, N., Moore, B., Mirasole, A., Guttierez, T., Gattuso, J.-P., et al. (2021). Two temperate corals are tolerant to low pH regardless of previous exposure to natural CO 2 vents. *Limnol. Oceanogr.*, 1–16. doi:10.1002/lno.11942.

Carter, B. R., Feely, R. A., Wanninkhof, R., Kouketsu, S., Sonnerup, R. E., Pardo, P. C., et al. (2019). Pacific Anthropogenic Carbon Between 1991 and 2017. *Global Biogeochem. Cycles*, 597–617. doi:10.1029/2018GB006154.

Casey, J. R., Grinstein, S., and Orlowski, J. (2010). Sensors and regulators of intracellular pH. *Nat. Rev. Mol. Cell Biol.* 11, 50–61. doi:10.1038/nrm2820.

Castillo, K. D., Ries, J. B., Bruno, J. F., and Westfield, I. T. (2014). The reef-building coral *Siderastrea siderea* exhibits parabolic responses to ocean acidification and warming. *Proc. R. Soc. B Biol. Sci.* 281. doi:10.1098/rspb.2014.1856.

Chan, P., Halfar, J., Adey, W. H., Lebednik, P. A., Steneck, R., Norley, C. J. D., et al. (2019). Recent density decline in wild-collected subarctic crustose coralline algae reveals climate change signature. *Geology* 48, 2017–2020. doi:doi.org/10.1130/G46804.1.

Chen, X., D'Olivo, J. P., Wei, G., and McCulloch, M. (2019). Anthropogenic ocean warming and acidification recorded by Sr/Ca, Li/Mg, δ11B and B/Ca in Porites coral from the Kimberley region of northwestern Australia. *Palaeogeogr. Palaeoclimatol. Palaeoecol.* 528, 50–59. doi:10.1016/j.palaeo.2019.04.033.

Chen, X., Deng, W., Kang, H., Zeng, T., Zhang, L., Zhao, J. xin, et al. (2021). A Replication Study on Coral δ11B and B/Ca and Their Variation in Modern and Fossil Porites: Implications for Coral Calcifying Fluid Chemistry and Seawater pH Changes Over the Last Millennium. *Paleoceanogr. Paleoclimatology* 36. doi:10.1029/2021PA004319.

Cinner, J. (2014). Coral reef livelihoods. *Curr. Opin. Environ. Sustain.* 7, 65–71. doi:10.1016/j.cosust.2013.11.025.

Cobb, K. M., Charles, C. D., Cheng, H., and Edwards, R. L. (2003). El Niño/Southern Oscillation and tropical Pacific climate during the last millennium. *Nature* 424, 271–276. doi:10.1038/nature01779.

Cohen, A. L., and Holcomb, M. (2009). Why corals care about ocean acidification uncovering the mechanism. *Oceanography* 22, 118–127. doi:10.5670/oceanog.2009.102.

Cohen, A. L., McCorkle, D. C., De Putron, S., Gaetani, G. A., and Rose, K. A. (2009). Morphological and compositional changes in the skeletons of new coral recruits reared in acidified seawater: Insights into the biomineralization response to ocean acidification. *Geochemistry, Geophys. Geosystems* 10, 1–12. doi:10.1029/2009GC002411.

Comeau, S., Cornwall, C. E., DeCarlo, T. M., Doo, S. S., Carpenter, R. C., and McCulloch, M. T. (2019a). Resistance to ocean acidification in coral reef taxa is not gained by acclimatization. *Nat. Clim. Chang.* 9, 477–483. doi:10.1038/s41558-019-0486-9.

Comeau, S., Cornwall, C. E., and McCulloch, M. T. (2017). Decoupling between the response of coral calcifying fluid pH and calcification to ocean acidification. *Sci. Rep.* 7, 1–10. doi:10.1038/s41598-017-08003-z.

Comeau, S., Cornwall, C. E., Pupier, C. A., DeCarlo, T. M., Alessi, C., Trehern, R., et al. (2019b). Flow-driven micro-scale pH variability affects the physiology of corals and coralline algae under ocean acidification. *Sci. Rep.* 9, 1–12. doi:10.1038/s41598-019-49044-w.

Comeau, S., Cornwall, C. E., Shlesinger, T., Hoogenboom, M., Mana, R., McCulloch, M. T., et al. (2022). pH variability at volcanic CO 2 seeps regulates coral calcifying fluid chemistry. *Glob. Chang. Biol.*, 1–13. doi:10.1111/gcb.16093.

Comeau, S., Edmunds, P. J., Spindel, N. B., and Carpenter, R. C. (2013). The responses of eight coral reef calcifiers to increasing partial pressure of CO2 do not exhibit a tipping point. *Limnol. Oceanogr.* 58, 388–398. doi:10.4319/lo.2013.58.1.0388.

Conroy, J. L., Thompson, D. M., Cobb, K. M., Noone, D., Rea, S., and Legrande, A. N. (2017).

Spatiotemporal variability in the δ18O-salinity relationship of seawater across the tropical Pacific Ocean. *Paleoceanography* 32, 484–497. doi:10.1002/2016PA003073.

Cornwall, C. E., Comeau, S., DeCarlo, T. M., Moore, B., D'Alexis, Q., and McCulloch, M. T. (2018). Resistance of corals and coralline algae to ocean acidification: Physiological control of calcification under natural pH variability. *Proc. R. Soc. B Biol. Sci.* 285, 1168–1176. doi:10.1098/rspb.2018.1168.

Cornwall, C. E., Comeau, S., Donner, S. D., Perry, C. T., Dunne, J. P., Hooidonk, R. Van, et al. (2023). Coral adaptive capacity insufficient to halt global transition of coral reefs into net erosion under climate change. *Glob. Chang. Biol.*, 1–9. doi:10.1111/gcb.16647.

Cornwall, C. E., Comeau, S., Kornder, N. A., Perry, C. T., van Hooidonk, R., DeCarlo, T. M., et al. (2021a). Global declines in coral reef calcium carbonate production under ocean acidification and warming. *Proc. Natl. Acad. Sci. U. S. A.* 118, 1–10. doi:10.1073/pnas.2015265118.

Cornwall, C. E., Diaz-Pulido, G., and Comeau, S. (2019). Impacts of ocean warming on coralline algae: Knowledge gaps and key recommendations for future research. *Front. Mar. Sci.* 6, 1–10. doi:10.3389/fmars.2019.00186.

Cornwall, C. E., Harvey, B. P., Comeau, S., Cornwall, D. L., Hall-, J. M., Peña, V., et al. (2021b). Understanding coralline algal responses to ocean acidification : analysis and synthesis. *Glob. Chang. Biol.*, 1–13. doi:10.1111/gcb.15899.

Corrège, T. (2006). Sea surface temperature and salinity reconstruction from coral geochemical tracers. *Palaeogeogr. Palaeoclimatol. Palaeoecol.* 232, 408–428. doi:10.1016/j.palaeo.2005.10.014.

Costanza, R., de Groot, R., Sutton, P., van der Ploeg, S., Anderson, S. J., Kubiszewski, I., et al. (2014). Changes in the global value of ecosystem services. *Glob. Environ. Chang.* 26, 152–158. doi:10.1016/j.gloenvcha.2014.04.002.

Cunning, R., Gates, R. D., and Edmunds, P. J. (2017). Using high-throughput sequencing of ITS2 to describe Symbiodinium metacommunities in St. John, US Virgin Islands. *PeerJ* 2017, 1–23. doi:10.7717/peerj.3472.

Cunning, R., Gillette, P., Capo, T., Galvez, K., and Baker, A. C. (2015). Growth tradeoffs associated with thermotolerant symbionts in the coral *Pocillopora damicornis* are lost in warmer oceans. *Coral Reefs* 34, 155–160. doi:10.1007/s00338-014-1216-4.

Cuny-Guirriec, K. (2020). Le rapport élémentaire Li/Mg dans les coraux scléractiniaires : un nouveau et puissant traceur des paléo-températures de l'océan ? *Thèse*. Available at: https://www.researchgate.net/publication/344805391_Le_rapport_elementaire_LiMg_dans_les_coraux_scleractiniaires_un_nouveau_et_puissant_traceur_des_paleo-temperatures_de_l'ocean.

Cuny-Guirriec, K., Douville, E., Reynaud, S., Allemand, D., Bordier, L., Canesi, M., et al. (2019). Coral Li/Mg thermometry: Caveats and constraints. *Chem. Geol.* 523, 162–178. doi:10.1016/j.chemgeo.2019.03.038.

D'Olivo, J. P., Ellwood, G., DeCarlo, T. M., and McCulloch, M. T. (2019). Deconvolving the long-term impacts of ocean acidification and warming on coral biomineralisation. *Earth Planet. Sci. Lett.* 526, 115785. doi:10.1016/j.epsl.2019.115785.

D'Olivo, J. P., McCulloch, M. T., Eggins, S. M., and Trotter, J. (2015). Coral records of reef-water pH across the central Great Barrier Reef, Australia: Assessing the influence of river runoff on inshore reefs. *Biogeosciences* 12, 1223–1236. doi:10.5194/bg-12-1223-2015.

D'Olivo, J. P., Sinclair, D. J., Rankenburg, K., and McCulloch, M. T. (2018). A universal multi-trace element calibration for reconstructing sea surface temperatures from long-lived Porites corals: Removing 'vital-effects.' *Geochim. Cosmochim. Acta* 239, 109–135. doi:10.1016/j.gca.2018.07.035.

Darwin, C. (1842). The Structure and Distribution of Coral Reefs. Being the first part of the geology of the voyage of the Beagle, under the Command of Capt. Fitzroy, R.N. during the years 1832 to 1836. *London Smith, Elder Co.*

Davies, P. S. (1989). Short-term growth measurements of corals using an accurate buoyant weighing technique. *Mar. Biol.* 101, 389–395. doi:10.1007/BF00428135.

De'Ath, G., Fabricius, K. E., Sweatman, H., and Puotinen, M. (2012). The 27-year decline of coral cover on the Great Barrier Reef and its causes. *Proc. Natl. Acad. Sci. U. S. A.* 109, 17995–17999. doi:10.1073/pnas.1208909109.

De Lacaze-Duthiers, H. (1873). Développement des coralliaires. Arctiniaires à Polypiers. *Arch. Zool. Exp. Gen.* 2, 269–348.

Decarlo, T. M., Comeau, S., Cornwall, C. E., and McCulloch, M. T. (2018a). Coral resistance to ocean acidification linked to increased calcium at the site of calcification. *Proc. R. Soc. B Biol. Sci.* 285. doi:10.1098/rspb.2018.0564.

Decarlo, T. M., Holcomb, M., and McCulloch, M. T. (2018b). Reviews and syntheses: Revisiting the boron systematics of aragonite and their application to coral calcification. *Biogeosciences* 15, 2819–2834. doi:10.5194/bg-15-2819-2018.

Delcroix, T., and Hénin, C. (1991). Seasonal and interannual variations of sea surface carbon dioxide in the subtropical Indian Ocean. *J. Geophys. Res. Ocean.* 96, 22135–22150. doi:https://doi.org/10.1029/91JC02124.

Diaz-Pulido, G., Anthony, K. R. N., Kline, D. I., Dove, S., and Hoegh-Guldberg, O. (2012). Interactions between ocean acidification and warming on the mortality and dissolution of coralline algae. *J. Phycol.* 48, 32–39. doi:10.1111/j.1529-8817.2011.01084.x.

Dickson, A. G. (1990). Thermodynamics of the Dissociation of Boric Acid in Potassium Chloride

Solutions from 273.15 to 318.15 K. *J. Chem. Eng. Data* 35, 253–257. doi:10.1021/je00061a009.

Dissard, D., Jan Reichart, G., Menkes, C., Mangeas, M., Frickenhaus, S., and Bijma, J. (2021). Mg/Ca, Sr/Ca and stable isotopes from the planktonic foraminifera T. sacculifer: Testing a multi-proxy approach for inferring paleotemperature and paleosalinity. *Biogeosciences* 18, 423–439. doi:10.5194/bg-18-423-2021.

Doney, S. C., Fabry, V. J., Feely, R. A., and Kleypas, J. A. (2009). Ocean acidification: The other CO2 problem. *Ann. Rev. Mar. Sci.* 1, 169–192. doi:10.1146/annurev.marine.010908.163834.

Doropoulos, C., and Diaz-Pulido, G. (2013). High CO2 reduces the settlement of a spawning coral on three common species of crustose coralline algae. *Mar. Ecol. Prog. Ser.* 475, 93–99. doi:10.3354/meps10096.

Doropoulos, C., Roff, G., Visser, M. S., and Mumby, P. J. (2017). Sensitivity of coral recruitment to subtle shifts in early community succession. *Ecology* 98, 304–314. doi:10.1002/ecy.1663.

Doropoulos, C., Ward, S., Diaz-Pulido, G., Hoegh-Guldberg, O., and Mumby, P. J. (2012). Ocean acidification reduces coral recruitment by disrupting intimate larval-algal settlement interactions. *Ecol. Lett.* 15, 338–346. doi:10.1111/j.1461-0248.2012.01743.x.

Douglas, A. E. (1998). Host benefit and the evolution of specialization in symbiosis. *Heredity (Edinb).* 81, 599–603. doi:10.1038/sj.hdy.6884550.

Drenkard, E. J., Cohen, A. L., McCorkle, D. C., de Putron, S. J., Starczak, V. R., and Zicht, A. E. (2013). Calcification by juvenile corals under heterotrophy and elevated CO2. *Coral Reefs* 32, 727–735. doi:10.1007/s00338-013-1021-5.

Dufault, A. M., Cumbo, V. R., Fan, T. Y., and Edmunds, P. J. (2012). Effects of diurnally oscillating pCO2 on the calcification and survival of coral recruits. *Proc. R. Soc. B Biol. Sci.* 279, 2951–2958. doi:10.1098/rspb.2011.2545.

Eagle, R. A., Guillermic, M., Corte, I. De, Caraveo, B. A., Bove, C. B., Cameron, L. P., et al. (2022). Physicochemical control of Caribbean coral calcification linked to host and symbiont responses to varying p CO 2 and tempera- ture. *J. Mar. Sci. Eng.* 10, 1–26.

Edmunds, P. J. (2011). Zooplanktivory ameliorates the effects of ocean acidification on the reef coral Porites spp. *Limnol. Oceanogr.* 56, 2402–2410. doi:10.4319/lo.2011.56.6.2402.

Edmunds, P. J. (2021). Recruitment hotspots and bottlenecks mediate the distribution of corals on a Caribbean reef. *Biol. Lett.* 17, 149–155. doi:10.1098/rsbl.2021.0149.

Edmunds, P. J., and Wall, C. B. (2014). Evidence that high pCO2 affects protein metabolism in tropical reef corals. *Biol. Bull.* 227, 68–77. doi:10.1086/BBLv227n1p68.

Elmer, F., Bell, J. J., and Gardner, J. P. A. (2018). Coral larvae change their settlement

preference for crustose coralline algae dependent on availability of bare space. *Coral Reefs* 37, 397–407. doi:10.1007/s00338-018-1665-2.

Enochs, I. C., Formel, N., Manzello, D., Morris, J., Mayfield, A. B., Boyd, A., et al. (2020). Coral persistence despite extreme periodic pH fluctuations at a volcanically acidified Caribbean reef. *Coral Reefs* 39, 523–528. doi:10.1007/s00338-020-01927-5.

Enochs, I. C., Manzello, D. P., Donham, E. M., Kolodziej, G., Okano, R., Johnston, L., et al. (2015). Shift from coral to macroalgae dominance on a volcanically acidified reef. *Nat. Clim. Chang.* 5, 1083–1088. doi:10.1038/nclimate2758.

Enríquez, S., and Borowitzka, M. A. (2010). "The use of the fluorescence signal in studies of seagrasses and macroalgae," in *Chlorophyll a Fluorescence in Aquatic Sciences: Methods and Applications*, ed. D. J. Suggett, 187–208. doi:10.1007/978-90-481-9268-7.

Epstein, H. E., Torda, G., Munday, P. L., and van Oppen, M. J. H. (2019a). Parental and early life stage environments drive establishment of bacterial and dinoflagellate communities in a common coral. *ISME J.* 13, 1635–1638. doi:10.1038/s41396-019-0358-3.

Epstein, H. E., Torda, G., and van Oppen, M. J. H. (2019b). Relative stability of the *Pocillopora acuta* microbiome throughout a thermal stress event. *Coral Reefs* 38, 373–386. doi:10.1007/s00338-019-01783-y.

Epstein, S., and Mayeda, T. (1953). Variation of O18 content of waters from natural sources. *Geochim. Cosmochim. Acta* 4, 213–224. doi:10.1016/0016-7037(53)90051-9.

Eren, A. M., Morrison, H. G., Lescault, P. J., Reveillaud, J., Vineis, J. H., and Sogin, M. L. (2015). Minimum entropy decomposition: Unsupervised oligotyping for sensitive partitioning of high-throughput marker gene sequences. *ISME J.* 9, 968–979. doi:10.1038/ismej.2014.195.

Fabina, N. S., Putnam, H. M., Franklin, E. C., Stat, M., and Gates, R. D. (2013). Symbiotic specificity, association patterns, and function determine community responses to global changes: Defining critical research areas for coral-symbiodinium symbioses. *Glob. Chang. Biol.* 19, 3306–3316. doi:10.1111/gcb.12320.

Fabricius, K. E., Kluibenschedl, A., Harrington, L., Noonan, S., and De'Ath, G. (2015). In situ changes of tropical crustose coralline algae along carbon dioxide gradients. *Sci. Rep.* 5, 1–7. doi:10.1038/srep09537.

Fabricius, K. E., Langdon, C., Uthicke, S., Humphrey, C., Noonan, S., De'ath, G., et al. (2011). Losers and winners in coral reefs acclimatized to elevated carbon dioxide concentrations. *Nat. Clim. Chang.* 1, 165–169. doi:10.1038/nclimate1122.

Fabricius, K. E., Noonan, S. H. C., Abrego, D., Harrington, L., and De'Ath, G. (2017). Low recruitment due to altered settlement substrata as primary constraint for coral communities under ocean acidification. *Proc. R. Soc. B Biol. Sci.* 284, 1536–1545.

doi:10.1098/rspb.2017.1536.

Fabricius, K. E., and Wolanski, E. (2000). Rapid Smothering of Coral Reef Organisms by Muddy. *Estuar. Coast. Shelf Sci.* 50, 115–120. Available at: http://www.idealibrary.comon.

Fantazzini, P., Mengoli, S., Pasquini, L., Bortolotti, V., Brizi, L., Mariani, M., et al. (2015). Gains and losses of coral skeletal porosity changes with ocean acidification acclimation. *Nat. Commun.* 6, 77–85. doi:10.1038/ncomms8785.

Ferrario, F., Beck, M. W., Storlazzi, C. D., Micheli, F., Shepard, C. C., and Airoldi, L. (2014). The effectiveness of coral reefs for coastal hazard risk reduction and adaptation. *Nat. Commun.* 5, 1–9. doi:10.1038/ncomms4794.

Figueiredo, M. A., Kain, J. M., and Norton, T. A. (1996). Biotic interactions in the colonization of crustose coralline algae by epiphytes. *J. Exp. Mar. Bio. Ecol.* 199, 303–318. doi:10.1016/0022-0981(96)00018-4.

Fisher, P. L., Malme, M. K., and Dove, S. (2012). The effect of temperature stress on coral-Symbiodinium associations containing distinct symbiont types. *Coral Reefs* 31, 473–485. doi:10.1007/s00338-011-0853-0.

Fisher, R., O'Leary, R. A., Low-Choy, S., Mengersen, K., Knowlton, N., Brainard, R. E., et al. (2015). Species richness on coral reefs and the pursuit of convergent global estimates. *Curr. Biol.* 25, 500–505. doi:10.1016/j.cub.2014.12.022.

Fitt, W. K., Gates, R. D., Hoegh-Guldberg, O., Bythell, J. C., Jatkar, A., Grottoli, A. G., et al. (2009). Response of two species of Indo-Pacific corals, *Porites cylindrica* and *Stylophora pistillata*, to short-term thermal stress: The host does matter in determining the tolerance of corals to bleaching. *J. Exp. Mar. Bio. Ecol.* 373, 102–110. doi:10.1016/j.jembe.2009.03.011.

Fitt, W. K., McFarland, F. K., Warner, M. E., and Chilcoat, G. C. (2000). Seasonal patterns of tissue biomass and densities of symbiotic dinoflagellates in reef corals and relation to coral bleaching. *Limnol. Oceanogr.* 45, 677–685. doi:10.4319/lo.2000.45.3.0677.

Foster, T., Falter, J. L., McCulloch, M. T., and Clode, P. L. (2016). Climate Science: Ocean acidification causes structural deformities in juvenile coral skeletons. *Sci. Adv.* 2, 1–8. doi:10.1126/sciadv.1501130.

Fowell, S. E., Foster, G. L., Ries, J. B., Castillo, K. D., de la Vega, E., Tyrrell, T., et al. (2018). Historical Trends in pH and Carbonate Biogeochemistry on the Belize Mesoamerican Barrier Reef System. *Geophys. Res. Lett.* 45, 3228–3237. doi:10.1002/2017GL076496.

Fridovich, I. (1998). Oxygen toxicity: A radical explanation. *J. Exp. Biol.* 201, 1203–1209. doi:10.1242/jeb.201.8.1203.

Füger, A., Konrad, F., Leis, A., Dietzel, M., Mavromatis, V., Füger, A., et al. (2019). Effect of growth rate and pH on lithium incorporation in calcite To cite this version : HAL Id : hal-

03363233 ScienceDirect Effect of growth rate and pH on lithium incorporation in calcite. *Geochim. Cosmochim. Acta*, 14–24. doi:10.1016/j.gca.2018.12.040.

Furla, P., Bénazet-Tambutté, S., Jaubert, J., and Allemand, D. (1998). Functional polarity of the tentacle of the sea anemone Anemonia viridis: Role in inorganic carbon acquisition. *Am. J. Physiol. - Regul. Integr. Comp. Physiol.* 274, 303–310. doi:10.1152/ajpregu.1998.274.2.r303.

Furla, P., Galgani, I., Durand, I., and Allemand, D. (2000). Sources and mechanisms of inorganic carbon transport for coral calcification and photosynthesis. *J. Exp. Biol.* 203, 3445–3457. doi:10.1242/jeb.203.22.3445.

Gaillardet, J., Lemarchand, D., Göpel, C., and Manhès, G. (2001). Evaporation and sublimation of boric acid: Application for boron purification from organic rich solutions. *Geostand. Newsl.* 25, 67–75. doi:10.1111/j.1751-908X.2001.tb00788.x.

Galli, G., and Solidoro, C. (2018). ATP supply may contribute to light-enhanced calcification in corals more than abiotic mechanisms. *Front. Mar. Sci.* 5. doi:10.3389/fmars.2018.00068.

Ganot, P., Zoccola, D., Tambutté, E., Voolstra, C. R., Aranda, M., Allemand, D., et al. (2015). Structural Molecular Components of Septate Junctions in Cnidarians Point to the Origin of Epithelial Junctions in Eukaryotes. *Mol. Biol. Evol.* 32, 44–62. doi:10.1093/molbev/msu265.

Gattuso, J. P., Allemand, D., and Frankignoulle, M. (1999). Photosynthesis and calcification at cellular, organismal and community levels in coral reefs: A review on interactions and control by carbonate chemistry. *Am. Zool.* 39, 160–183. doi:10.1093/icb/39.1.160.

Gattuso, J. P., Frankignoulle, M., Bourge, I., Romaine, S., and Buddemeier, R. W. (1998). Effect of calcium carbonate saturation of seawater on coral calcification. *Glob. Planet. Change* 18, 37–46. doi:10.1016/S0921-8181(98)00035-6.

Gattuso, J. P., Magnan, A., Billé, R., Cheung, W. W. L., Howes, E. L., Joos, F., et al. (2015). Contrasting futures for ocean and society from different anthropogenic CO2 emissions scenarios. *Science (80-.).* 349. doi:10.1126/science.aac4722.

Ge, R., Liang, J., Yu, K., Chen, B., Yu, X., Deng, C., et al. (2021). Regulation of the Coral-Associated Bacteria and Symbiodiniaceae in *Acropora valida* Under Ocean Acidification. *Front. Microbiol.* 12. doi:10.3389/fmicb.2021.767174.

Georgiou, L., Falter, J., Trotter, J., Kline, D. I., Holcomb, M., Dove, S. G., et al. (2015). PH homeostasis during coral calcification in a free ocean CO2 enrichment (FOCE) experiment, Heron Island reef flat, Great Barrier Reef. *Proc. Natl. Acad. Sci. U. S. A.* 112, 13219–13224. doi:10.1073/pnas.1505586112.

Gibbin, E. M., and Davy, S. K. (2014). The photo-physiological response of a model cnidarian-dinoflagellate symbiosis to CO2-induced acidification at the cellular level. *J. Exp. Mar.*

Bio. Ecol. 457, 1–7. doi:10.1016/j.jembe.2014.03.015.

Gibbin, E. M., Putnam, H. M., Davy, S. K., and Gates, R. D. (2014). Intracellular pH and its response to CO2-driven seawater acidification in symbiotic versus non-symbiotic coral cells. *J. Exp. Biol.* 217, 1963–1969. doi:10.1242/jeb.099549.

Giorgia, P., Erik, C., Teresa, T., Amico, F. D., Fiorella, P., and Arianna, M. (2022). Metagenomic shifts in mucus , tissue and skeleton of the coral *Balanophyllia europaea* living along a natural CO 2 gradient. *ISME J.*, 1–12. doi:10.1038/s43705-022-00152-1.

Glassom, D., Zakai, D., and Chadwick-Furman, N. E. (2004). Coral recruitment: A spatio-temporal analysis along the coastline of Eilat, northern Red Sea. *Mar. Biol.* 144, 641–651. doi:10.1007/s00227-003-1243-0.

Gleason, M. G. (1996). Coral recruitment in Moorea, French Polynesia: The importance of patch type and temporal variation. *J. Exp. Mar. Bio. Ecol.* 207, 79–101. doi:10.1016/S0022-0981(96)02647-0.

Goffredo, S., Prada, F., Caroselli, E., Capaccioni, B., Zaccanti, F., Pasquini, L., et al. (2014). Biomineralization control related to population density under ocean acidification. *Nat. Clim. Chang.* 4, 593–597. doi:10.1038/nclimate2241.

Goldberg, W. M. (2018). *Coral Food, Feeding, Nutrition, and Secretion: A Review*. Springer, Cham doi:10.1007/978-3-319-92486-1_18.

Golden, C. D., Allison, E. H., Dey, M. M., Halpern, B. S., McCauley Douglas J., Smith Matthew, et al. (2016). Fall in Fish Catch Threatens Human Health. *Nature* 534, 317–320. Available at: http://environment.harvard.edu/sites/default/files/golden_et_al._2016._nature._fall_in_fish_catch_threatens_human_health-with_si.pdf.

Gómez-Lemos, L. A., Doropoulos, C., Bayraktarov, E., and Diaz-Pulido, G. (2018). Coralline algal metabolites induce settlement and mediate the inductive effect of epiphytic microbes on coral larvae. *Sci. Rep.* 8, 1–11. doi:10.1038/s41598-018-35206-9.

Gouriou, Y., and Delcroix, T. (2002). Seasonal and ENSO variations of sea surface salinity and temperature in the South Pacific convergence Zone during 1976-2000. *J. Geophys. Res. Ocean.* 107. doi:10.1029/2001jc000830.

Grafeld, S., Oleson, K. L. L., Teneva, L., and Kittinger, J. N. (2017). Follow that fish : Uncovering the hidden blue economy in coral reef fisheries. *PLoS One* 12, 1–25.

Graham, N. A. J., and Nash, K. L. (2013). The importance of structural complexity in coral reef ecosystems. *Coral Reefs* 32, 315–326. doi:10.1007/s00338-012-0984-y.

Grottoli, A. G. (2002). Effect of light and brine shrimp on skeletal δ13C in the Hawaiian coral *Porites compressa*: A tank experiment. *Geochim. Cosmochim. Acta* 66, 1955–1967. doi:10.1016/S0016-7037(01)00901-2.

Grottoli, A. G., Rodrigues, L. J., and Juarez, C. (2004). Lipids and stable carbon isotopes in two species of Hawaiian corals, Porites compressa and Montipora verrucosa, following a bleaching event. *Mar. Biol.* 145, 621–631. doi:10.1007/s00227-004-1337-3.

Grottoli, A. G., Rodrigues, L. J., Matthews, K. A., Palardy, J. E., and Gibb, O. T. (2005). Pre-treatment effects on coral skeletal θ13C and θ18O. *Chem. Geol.* 221, 225–242. doi:10.1016/j.chemgeo.2005.05.004.

Grottoli, A. G., Tchernov, D., and Winters, G. (2017). Physiological and biogeochemical responses of super-corals to thermal stress from the northern gulf of Aqaba, Red Sea. *Front. Mar. Sci.* 4, 1–12. doi:10.3389/fmars.2017.00215.

Grottoli, A. G., Wilkins, M. J., Johnston, M. D., Levas, S., Schoepf, V., Dalcin, M. P., et al. (2018). Coral physiology and microbiome dynamics under combined warming and ocean acidification. *PLoS One* 13, e0191156.

Guillermic, M., Cameron, L., De Corte, I., Misra, S., Bijma, J., De Beer, D., et al. (2021). Thermal stress reduces pocilloporid coral resilience to ocean acidification by impairing control over calcifying fluid chemistry. *Sci. Adv.*

Guillermic, M., Misra, S., Eagle, R., Villa, A., Chang, F., and Tripati, A. (2020). Seawater pH reconstruction using boron isotopes in multiple planktonic foraminifera species with different depth habitats and their potential to constrain pH and pCO_2 gradients. *Biogeosciences Discuss.*, 1–38. doi:10.5194/bg-2019-266.

Gutjahr, M., Bordier, L., Douville, E., Farmer, J., Foster, G. L., Hathorne, E. C., et al. (2021). Sub-Permil Interlaboratory Consistency for Solution-Based Boron Isotope Analyses on Marine Carbonates. *Geostand. Geoanalytical Res.* 45, 59–75. doi:10.1111/ggr.12364.

Haas, A. F., Smith, J. E., Thompson, M., and Deheyn, D. D. (2014). Effects of reduced dissolved oxygen concentrations on physiology and fluorescence of hermatypic corals and benthic algae. *PeerJ* 2014, 1–19. doi:10.7717/peerj.235.

Hall-Spencer, J. M., Rodolfo-Metalpa, R., Martin, S., Ransome, E., Fine, M., Turner, S. M., et al. (2008). Volcanic carbon dioxide vents show ecosystem effects of ocean acidification. *Nature* 454, 96–99. doi:10.1038/nature07051.

Halliwell, B., and Gutteridge, J. (1999). Free Radicals in Biology and Medicine. *Oxford Univ. Press. Oxford*.

Harrington, L., Fabricius, K., De'Ath, G., and Negri, A. (2004). Recognition and selection of settlement substrata determine post-settlement survival in corals. *Ecology* 85, 3428–3437. doi:10.1890/04-0298.

Harrison, P. L. (2011). Sexual Reproduction of Scleractinian Corals. *Coral Reefs An Ecosyst. Transit.*, 59–85. doi:10.1007/978-94-007-0114-4.

Harrison, P., and Wallace, C. (1990). Reproduction, dispersal and recruitment of scleractinian

corals. *Coral Reefs* 25, 133–207.

Haydon, T. D., Matthews, J. L., Seymour, J. R., Raina, J., Seymour, J. E., Chartrand, K., et al. (2023). Metabolomic signatures of corals thriving across extreme reef habitats reveal strategies of heat stress tolerance. *Proc. R. Soc. B Biol. Sci.* 290, 1–12. doi:doi.org/10.1098/rspb.2022.1877.

Haydon, T. D., Seymour, J. R., Raina, J. B., Edmondson, J., Siboni, N., Matthews, J. L., et al. (2021). Rapid Shifts in Bacterial Communities and Homogeneity of Symbiodiniaceae in Colonies of *Pocillopora acuta* Transplanted Between Reef and Mangrove Environments. *Front. Microbiol.* 12. doi:10.3389/fmicb.2021.756091.

Hemming, N. G., and Hanson, G. N. (1992). Boron isotopic composition and concentration in modern marine carbonates. *Geochim. Cosmochim. Acta* 56, 537–543. doi:10.1016/0016-7037(92)90151-8.

Heyward, A. J., and Negri, A. P. (1999). Natural inducers for coral larval metamorphosis. *Coral Reefs* 18, 273–279. doi:10.1007/s003380050193.

Hoadley, K. D., Lewis, A. M., Wham, D. C., Pettay, D. T., Grasso, C., Smith, R., et al. (2019). Host–symbiont combinations dictate the photo-physiological response of reef-building corals to thermal stress. *Sci. Rep.* 9, 1–15. doi:10.1038/s41598-019-46412-4.

Hoadley, K. D., Pettay, D. T., Dodge, D., and Warner, M. E. (2016). Contrasting physiological plasticity in response to environmental stress within different cnidarians and their respective symbionts. *Coral Reefs* 35, 529–542. doi:10.1007/s00338-016-1404-5.

Hoadley, K. D., Pettay, D. T., Lewis, A., Wham, D., Grasso, C., Smith, R., et al. (2021). Different functional traits among closely related algal symbionts dictate stress endurance for vital Indo-Pacific reef-building corals. *Glob. Chang. Biol.* 27, 5295–5309. doi:10.1111/gcb.15799.

Hoegh-Guldberg, O. (1999). Climate change, coral bleaching and the future of the world's coral reefs. *Mar. Freshw. Res.* 50, 839–866. doi:10.1071/MF99078.

Hoegh-Guldberg, O., and Jones, R. J. (1999). Photoinhibition and photoprotection in symbiotic dinoflagellates from reef-building corals. *Mar. Ecol. Prog. Ser.* 183, 73–86. doi:10.3354/meps183073.

Hoegh-Guldberg, O., Poloczanska, E. S., Skirving, W., and Dove, S. (2017). Coral reef ecosystems under climate change and ocean acidification. *Front. Mar. Sci.* 4. doi:10.3389/fmars.2017.00158.

Hoeksema, B. ., and Cairns, S. (2022). Worlds List of Scleractinia. Available at: https://www.marinespecies.org/scleractinia.

Hohn, S., and Merico, A. (2015). Quantifying the relative importance of transcellular and paracellular ion transports to coral polyp calcification. *Front. Earth Sci.* 2, 1–11.

doi:10.3389/feart.2014.00037.

Holcomb, M., DeCarlo, T. M., Gaetani, G. A., and McCulloch, M. (2016). Factors affecting B/Ca ratios in synthetic aragonite. *Chem. Geol.* 437, 67–76. doi:10.1016/j.chemgeo.2016.05.007.

Holcomb, M., Venn, A. A., Tambutté, E., Tambutté, S., Allemand, D., Trotter, J., et al. (2014). Coral calcifying fluid pH dictates response to ocean acidification. *Sci. Rep.* 4, 1–4. doi:10.1038/srep05207.

Holland, K., Branson, O., Haynes, L. L., Hönisch, B., Allen, K. A., Russell, A. D., et al. (2020). Constraining multiple controls on planktic foraminifera Mg/Ca. *Geochim. Cosmochim. Acta*. doi:10.1016/j.gca.2020.01.015.

Hoogenboom, M., Beraud, E., and Ferrier-Pagès, C. (2010). Relationship between symbiont density and photosynthetic carbon acquisition in the temperate coral *Cladocora caespitosa*. *Coral Reefs* 29, 21–29. doi:10.1007/s00338-009-0558-9.

Horton, T., Kroh, A., Ahyong, S., and Bailly, N. (2022). World Register of Marine Species (WoRMS). *WoRMS Editor. Board*. doi:https://doi.org/10.14284/170.

Houlbrèque, F., and Ferrier-Pagès, C. (2009). Heterotrophy in tropical scleractinian corals. *Biol. Rev.* 84, 1–17. doi:10.1111/j.1469-185X.2008.00058.x.

Houlbrèque, F., Reynaud, S., Godinot, C., Oberhänsli, F., Rodolfo-Metalpa, R., and Ferrier-Pagés, C. (2015). Ocean acidification reduces feeding rates in the scleractinian coral *Stylophora pistillata*. *Limnol. Oceanogr.* 60, 89–99. doi:10.1002/lno.10003.

Howells, E. J., Abrego, D., Meyer, E., Kirk, N. L., and Burt, J. A. (2016). Host adaptation and unexpected symbiont partners enable reef-building corals to tolerate extreme temperatures. *Glob. Chang. Biol.* 22, 2702–2714. doi:10.1111/gcb.13250.

Howells, E. J., Bauman, A. G., Vaughan, G. O., Hume, B. C. C., Voolstra, C. R., and Burt, J. A. (2020). Corals in the hottest reefs in the world exhibit symbiont fidelity not flexibility. *Mol. Ecol.* 29, 899–911. doi:10.1111/mec.15372.

Howells, E. J., Beltran, V. H., Larsen, N. W., Bay, L. K., Willis, B. L., and Van Oppen, M. J. H. (2012). Coral thermal tolerance shaped by local adaptation of photosymbionts. *Nat. Clim. Chang.* 2, 116–120. doi:10.1038/nclimate1330.

Howes, E. L., Joos, F., Eakin, C. M., and Gattuso, J. P. (2015). An updated synthesis of the observed and projected impacts of climate change on the chemical, physical and biological processes in the oceans. *Front. Mar. Sci.* 2, 1–27. doi:10.3389/fmars.2015.00036.

Huang, B., Thorne, P. W., Banzon, V. F., Boyer, T., Chepurin, G., Lawrimore, J. H., et al. (2017). Extended reconstructed Sea surface temperature, Version 5 (ERSSTv5): Upgrades, validations, and intercomparisons. *J. Clim.* 30, 8179–8205. doi:10.1175/JCLI-

D-16-0836.1.

Huffmyer, A. S., Johnson, C. J., Epps, A. M., Lemus, J. D., and Gates, R. D. (2021). Feeding and thermal conditioning enhance coral temperature tolerance in juvenile Pocillopora acuta. *R. Soc. Open Sci.* 8, 1–13. doi:10.1098/rsos.210644.

Hughes, D. J., Alderdice, R., Cooney, C., Kühl, M., Pernice, M., Voolstra, C. R., et al. (2020). Coral reef survival under accelerating ocean deoxygenation. *Nat. Clim. Chang.* 10, 296–307. doi:10.1038/s41558-020-0737-9.

Hughes, T. P., Anderson, K. D., Connolly, S. R., Heron, S. F., Kerry, J. T., Lough, J. M., et al. (2018a). Spatial and temporal patterns of mass bleaching of corals in the Anthropocene. *Science (80-.).* 359, 80–83. doi:10.1126/science.aan8048.

Hughes, T. P., Barnes, M. L., Bellwood, D. R., Cinner, J. E., Cumming, G. S., Jackson, J. B. C., et al. (2017). Coral reefs in the Anthropocene. *Nature* 546, 82–90. doi:10.1038/nature22901.

Hughes, T. P., Kerry, J. T., Baird, A. H., Connolly, S. R., Dietzel, A., Eakin, C. M., et al. (2018b). Global warming transforms coral reef assemblages. *Nature* 556, 492–496. doi:10.1038/s41586-018-0041-2.

Hume, B. C. C., Smith, E. G., Ziegler, M., Warrington, H. J. M., Burt, J. A., LaJeunesse, T. C., et al. (2019). SymPortal: A novel analytical framework and platform for coral algal symbiont next-generation sequencing ITS2 profiling. *Mol. Ecol. Resour.* 19, 1063–1080. doi:10.1111/1755-0998.13004.

Hume, B. C. C., Voolstra, C. R., Arif, C., D'Angelo, C., Burt, J. A., Eyal, G., et al. (2016). Ancestral genetic diversity associated with the rapid spread of stress-tolerant coral symbionts in response to holocene climate change. *Proc. Natl. Acad. Sci. U. S. A.* 113, 4416–4421. doi:10.1073/pnas.1601910113.

IPCC Report, I. (2021). Climate change 2021: The physical science basis summary for policymakers. Contribution of Working Group I to the Sixth Assessment Report of the Intergovernmental Panel on Climate Change. *United Nations Environ. Program. UNEP* AR6.

IPCC Report, I. (2022). Climate change 2022: Impacts, Adaptation and Vulnerability. Summary for policymakers. Contribution of Working Group II to the Sixth Assessment Report of the Intergovernmental Panel on Climate Change. *United Nations Environ. Program. UNEP* AR6, xxiii–xxxiii.

IPCC Report, I. (2023). Synthesis Report of the IPCC Sixth Assessment Report (AR6). *United Nations Environ. Program. UNEP* AR6.

Jacquemont, J., Houlbrèque, F., Tanvet, C., and Metalpa, R. R. (2022). Long - term exposure to an extreme environment induces species - specific responses in corals ' photosynthesis

and respiration rates. *Mar. Biol.*, 1–15. doi:10.1007/s00227-022-04063-6.

Jeffrey, S. W., and Humphrey, G. F. (1975). New spectrophotometric equations for determining chlorophylls a, b, c1 and c2 in higher plants, algae and natural phytoplankton. *Biochem. und Physiol. der Pflanz.* 167, 191–194. doi:10.1016/s0015-3796(17)30778-3.

Jiang, L., Guo, M. L., Zhang, F., Zhang, Y. Y., Zhou, G. W., Lei, X. M., et al. (2020). Impacts of elevated temperature and pCO2 on the brooded larvae of Pocillopora damicornis from Luhuitou Reef, China: evidence for local acclimatization. *Coral Reefs* 39, 331–344. doi:10.1007/s00338-020-01894-x.

Jiang, L., Sun, Y. F., Zhang, Y. Y., Zhou, G. W., Li, X. B., McCook, L. J., et al. (2017). Impact of diurnal temperature fluctuations on larval settlement and growth of the reef coral Pocillopora damicornis. *Biogeosciences* 14, 5741–5752. doi:10.5194/bg-14-5741-2017.

Johnson, M. D., Bravo, L. M. R., O'Connor, S. E., Varley, N. F., and Altieri, A. H. (2019). pH variability exacerbates effects of ocean acidification on a caribbean crustose coralline alga. *Front. Mar. Sci.* 6. doi:10.3389/fmars.2019.00150.

Johnson, M. D., Comeau, S., Lantz, C. A., and Smith, J. E. (2017). Complex and interactive effects of ocean acidification and temperature on epilithic and endolithic coral-reef turf algal assemblages. *Coral Reefs* 36, 1059–1070. doi:10.1007/s00338-017-1597-2.

Jokiel, P. L. (2011). The reef coral two compartment proton flux model: A new approach relating tissue-level physiological processes to gross corallum morphology. *J. Exp. Mar. Bio. Ecol.* 409, 1–12. doi:10.1016/j.jembe.2011.10.008.

Jokiel, P. L. (2013). Coral reef calcification: Carbonate, bicarbonate and proton flux under conditions of increasing ocean acidification. *Proc. R. Soc. B Biol. Sci.* 280, 1–4. doi:10.1098/rspb.2013.0031.

Jokiel, P. L., Rodgers, K. S., Kuffner, I. B., Andersson, A. J., Cox, E. F., and Mackenzie, F. T. (2008). Ocean acidification and calcifying reef organisms: A mesocosm investigation. *Coral Reefs* 27, 473–483. doi:10.1007/s00338-008-0380-9.

Jones, A., and Berkelmans, R. (2010). Potential costs of acclimatization to a warmer climate: Growth of a reef coral with heat tolerant vs. sensitive symbiont types. *PLoS One* 5. doi:10.1371/journal.pone.0010437.

Jones, A. M., Berkelmans, R., Van Oppen, M. J. H., Mieog, J. C., and Sinclair, W. (2008). A community change in the algal endosymbionts of a scleractinian coral following a natural bleaching event: Field evidence of acclimatization. *Proc. R. Soc. B Biol. Sci.* 275, 1359–1365. doi:10.1098/rspb.2008.0069.

Jones, R., Ricardo, G. F., and Negri, A. P. (2015). Effects of sediments on the reproductive cycle of corals. *Mar. Pollut. Bull.* 100, 13–33. doi:10.1016/j.marpolbul.2015.08.021.

Jorissen, H., Galand, P. E., Bonnard, I., Meiling, S., Raviglione, D., Meistertzheim, A. L., et al.

(2021). Coral larval settlement preferences linked to crustose coralline algae with distinct chemical and microbial signatures. *Sci. Rep.* 11, 1–11. doi:10.1038/s41598-021-94096-6.

Jorissen, H., and Nugues, M. M. (2021). Coral larvae avoid substratum exploration and settlement in low-oxygen environments. *Coral Reefs* 40, 31–39. doi:10.1007/s00338-020-02013-6.

Jorissen, H., Nugues, M. M., and Steneck, R. S. (2020). Contrasting effects of crustose coralline algae from exposed and subcryptic habitats on coral recruits. 39, 1767–1778. doi:10.1007/s00338-020-02002-9.

Jury, C. P., and Toonen, R. J. (2019). Adaptive responses and local stressor mitigation drive coral resilience in warmer, more acidic oceans. *Proc. R. Soc. B Biol. Sci.* 286. doi:10.1098/rspb.2019.0614.

K.Barott, S.Perez, L.Linsmayer, and M.Tresguerres (2015). Differential localization of ion transporters suggests distinct cellular mechanisms for calcification and photosynthesis between two coral species. *Gen. Comp. Endocrinol.* 146, 235–246. doi:10.1016/j.tree.2011.11.016.

Kamenos, N. A., Perna, G., Gambi, M. C., Micheli, F., and Kroeker, K. J. (2016). Coralline algae in a naturally acidified ecosystem persist by maintaining control of skeletal mineralogy and size. *Proc. R. Soc. B Biol. Sci.* 283, 1–8. doi:10.1098/rspb.2016.1159.

Kapsenberg, L., and Cyronak, T. (2019). Ocean acidification refugia in variable environments. *Glob. Chang. Biol.* 25, 3201–3214. doi:10.1111/gcb.14730.

Kapsenberg, L., Kelley, A. L., Shaw, E. C., Martz, T. R., and Hofmann, G. E. (2015). Near-shore Antarctic pH variability has implications for the design of ocean acidification experiments. *Sci. Rep.* 5, 1–10. doi:10.1038/srep09638.

Keeling, C. D., Piper, S. C., Bacastow, R. B., Wahlen, M., Whorf, T. P., Heimann, M., et al. (2001). UC San Diego SIO Reference Title Exchanges of Atmospheric CO2 and 13CO2 with the Terrestrial Biosphere and Oceans from 1978 to 2000. I. Global Aspects Publication Date Exchanges of Atmospheric CO 2 and 13 CO 2 with the Terrestrial Biosphere and Oceans fro.

Kenkel, C. D., and Matz, M. V. (2017). Gene expression plasticity as a mechanism of coral adaptation to a variable environment. *Nat. Ecol. Evol.* 1, 1–6. doi:10.1038/s41559-016-0014.

Klepac, C. N., and Barshis, D. J. (2020). Reduced thermal tolerance of massive coral species in a highly variable environment: Reduced heat tolerance of massive corals. *Proc. R. Soc. B Biol. Sci.* 287, 19–21. doi:10.1098/rspb.2020.1379rspb20201379.

Kleypas, J. A., Buddemeier, R. W., Archer, D., Gattuso, J. P., Langdon, C., and Opdyke, B. N.

(1999a). Geochemical consequences of increased atmospheric carbon dioxide on coral reefs. *Science (80-.).* 284, 118–120. doi:10.1126/science.284.5411.118.

Kleypas, J. A., McManu, J. W., and Mene, L. A. B. (1999b). Environmental limits to coral reef development: Where do we draw the line? *Am. Zool.* 39, 146–159. doi:10.1093/icb/39.1.146.

Kleypas, J. A., and Yates, K. K. (2009). Coral reefs and ocean acidification. *Oceanography* 22, 108–117. doi:10.5670/oceanog.2009.101.

Klochko, K., Kaufman, A. J., Yao, W., Byrne, R. H., and Tossell, J. A. (2006). Experimental measurement of boron isotope fractionation in seawater. *Earth Planet. Sci. Lett.* 248, 276–285. doi:10.1016/j.epsl.2006.05.034.

Komornicki, J. (1988). Etude de l ' ichtyofaune de la mangrove de Bouraké (Nouvelle Calédonie) Etude de l ' ichtyofaune de la mangrove de Bouraké (Nouvelle Calédonie). *Mem. stage*, 1–20.

Krief, S., Hendy, E. J., Fine, M., Yam, R., Meibom, A., Foster, G. L., et al. (2010). Physiological and isotopic responses of scleractinian corals to ocean acidification. *Geochim. Cosmochim. Acta* 74, 4988–5001. doi:10.1016/j.gca.2010.05.023.

Kroeker, K. J., Kordas, R. L., Crim, R. N., and Singh, G. G. (2010). Meta-analysis reveals negative yet variable effects of ocean acidification on marine organisms. *Ecol. Lett.* 13, 1419–1434. doi:10.1111/j.1461-0248.2010.01518.x.

Kroeker, K. J., Micheli, F., and Gambi, M. C. (2013). Ocean acidification causes ecosystem shifts via altered competitive interactions. *Nat. Clim. Chang.* 3, 156–159. doi:10.1038/nclimate1680.

Kuffner, I. B., Andersson, A. J., Jokiel, P. L., Rodgers, K. S., and MacKenzie, F. T. (2008). Decreased abundance of crustose coralline algae due to ocean acidification. *Nat. Geosci.* 1, 114–117. doi:10.1038/ngeo100.

Kurihara, H., Watanabe, A., Tsugi, A., Mimura, I., Hongo, C., Kawai, T., et al. (2021). Potential local adaptation of corals at acidified and warmed Nikko Bay, Palau. *Sci. Rep.* 11, 1–10. doi:10.1038/s41598-021-90614-8.

LaJeunesse, T. C., Loh, W. K. W., Van Woesik, R., Hoegh-Guldberg, O., Schmidt, G. W., and Fitt, W. K. (2003). Low symbiont diversity in southern Great Barrier Reef corals, relative to those of the Caribbean. *Limnol. Oceanogr.* 48, 2046–2054. doi:10.4319/lo.2003.48.5.2046.

LaJeunesse, T. C., Parkinson, J. E., Gabrielson, P. W., Jeong, H. J., Reimer, J. D., Voolstra, C. R., et al. (2018). Systematic Revision of Symbiodiniaceae Highlights the Antiquity and Diversity of Coral Endosymbionts. *Curr. Biol.* 28, 2570-2580.e6. doi:10.1016/j.cub.2018.07.008.

Lajeunesse, T. C., Wham, D. C., Pettay, D. T., Parkinson, J. E., Keshavmurthy, S., and Chen, C. A. (2014). Ecologically differentiated stress-tolerant endosymbionts in the dinoflagellate genus Symbiodinium (Dinophyceae) Clade D are different species. *Phycologia* 53, 305–319. doi:10.2216/13-186.1.

Langdon, C., Takahashi, T., Sweeney, C., Chipman, D., and Atkinson, J. (2000). rate of an experimental coral reef responds to manipulations in the concentrations of both Ca CO •. *Global Biogeochem. Cycles* 14, 639–654.

Lauvset, S. K., Gruber, N., Landschützer, P., Olsen, A., and Tjiputra, J. (2015). Trends and drivers in global surface ocean pH over the past 3 decades. *Biogeosciences* 12, 1285–1298. doi:10.5194/bg-12-1285-2015.

Lee, K., Kim, T. W., Byrne, R. H., Millero, F. J., Feely, R. A., and Liu, Y. M. (2010). The universal ratio of boron to chlorinity for the North Pacific and North Atlantic oceans. *Geochim. Cosmochim. Acta* 74, 1801–1811. doi:10.1016/j.gca.2009.12.027.

Lemarchand, D., Gaillardet, J., Lewin, and Allégre, C. J. (2000). The influence of rivers on marine boron isotopes and implications for reconstructing past ocean pH. *Nature* 408, 951–954. doi:10.1038/35050058.

Leopold, A., Marchand, C., Deborde, J., Chaduteau, C., and Allenbach, M. (2013). Influence of mangrove zonation on CO2 fluxes at the sediment – air interface (New Caledonia). *Geoderma*, 62–70. doi:10.1016/j.geoderma.2013.03.008.

Lesser, M. P., Stat, M., and Gates, R. D. (2013). The endosymbiotic dinoflagellates (Symbiodinium sp.) of corals are parasites and mutualists. *Coral Reefs* 32, 603–611. doi:10.1007/s00338-013-1051-z.

Leung, J. Y. S., Zhang, S., and Connell, S. D. (2022). Is Ocean Acidification Really a Threat to Marine Calcifiers ? A Systematic Review and Meta-Analysis of 980 + Studies Spanning Two Decades. *Small J.* 1, 1–32. doi:10.1002/smll.202107407.

Little, A. F., Van Oppen, M. J. H., and Willis, B. L. (2004). Flexibility in algal endosymbioses shapes growth in reef corals. *Science (80-.).* 304, 1492–1494. doi:10.1126/science.1095733.

Liu, Y., Peng, Z., Zhou, R., Song, S., Liu, W., You, C. F., et al. (2014). Acceleration of modern acidification in the South China Sea driven by anthropogenic CO2. *Sci. Rep.* 4, 1–5. doi:10.1038/srep05148.

Liu, Y. W., Sutton, J. N., Ries, J. B., and Eagle, R. A. (2020). Regulation of calcification site pH is a polyphyletic but not always governing response to ocean acidification. *Sci. Adv.* 6. doi:10.1126/sciadv.aax1314.

Lueker, T. J., Dickson, A. G., and Keeling, C. D. (2000). Ocean pCO_2 calculated from DIC, TA, and the Mehrbach equations for K1 and K2: Validation using laboratory measurements of

CO_2 in gas and seawater at equilibrium. *Mar. Chem.* 70, 105–119.

Maggioni, F., Pujo-Pay, M., Aucan, J., Cerrano, C., Calcinai, B., Payri, C., et al. (2021). The Bouraké semi-enclosed lagoon (New Caledonia) - A natural laboratory to study the life-long adaptation of a coral reef ecosystem to climate change-like conditions. *Biogeosciences* 18, 5117–5140. doi:10.5194/bg-18-5117-2021.

Mantua, N. J., and Hare, S. R. (2001). Costs of secondary parasitism in the facultative hyperparasitoid Pachycrepoideus dubius: Does host size matter? *J. Oceanogr.* 58, 35–44. doi:10.1023/A:1015820616384.

Marsh, J. A. (1967). Primary productivity of reef-building calcareous red algae. *Angew. Chemie Int. Ed. 6(11), 951–952.* 51, 5–24.

Martin, S., Charnoz, A., and Gattuso, J. P. (2013). Photosynthesis, respiration and calcification in the Mediterranean crustose coralline alga Lithophyllum cabiochae (Corallinales, Rhodophyta). *Eur. J. Phycol.* 48, 163–172. doi:10.1080/09670262.2013.786790.

Martin, S., and Gattuso, J. P. (2009). Response of Mediterranean coralline algae to ocean acidification and elevated temperature. *Glob. Chang. Biol.* 15, 2089–2100. doi:10.1111/j.1365-2486.2009.01874.x.

Martin, S., Rodolfo-Metalpa, R., Ransome, E., Rowley, S., Buia, M. C., Gattuso, J. P., et al. (2008). Effects of naturally acidified seawater on seagrass calcareous epibionts. *Biol. Lett.* 4, 689–692. doi:10.1098/rsbl.2008.0412.

Mass, T., Giuffre, A. J., Sun, C. Y., Stifler, C. A., Frazier, M. J., Neder, M., et al. (2017). Amorphous calcium carbonate particles form coral skeletons. *Proc. Natl. Acad. Sci. U. S. A.* 114, 8. doi:10.1073/pnas.1707890114.

Mavromatis, V., Montouillout, V., Noireaux, J., Gaillardet, J., and Schott, J. (2015). Characterization of boron incorporation and speciation in calcite and aragonite from co-precipitation experiments under controlled pH, temperature and precipitation rate. *Geochim. Cosmochim. Acta* 150, 299–313. doi:10.1016/j.gca.2014.10.024.

McClanahan, T. R., Darling, E. S., Maina, J. M., Muthiga, N. A., 'agata, S. D., Jupiter, S. D., et al. (2019). Temperature patterns and mechanisms influencing coral bleaching during the 2016 El Niño. *Nat. Clim. Chang.* 9, 845–851. doi:10.1038/s41558-019-0576-8.

McConnaughey, T. (1989). 13C and 18O isotopic disequilibrium in biological carbonates: I. Patterns. *Geochim. Cosmochim. Acta* 53, 151–162. doi:10.1016/0016-7037(89)90282-2.

Mccoy, S. J., and Kamenos, N. A. (2015). Coralline algae (Rhodophyta) in a changing world: Integrating ecological, physiological, and geochemical responses to global change. *J. Phycol.* 51, 6–24. doi:10.1111/jpy.12262.

McCulloch, M., Falter, J., Trotter, J., and Montagna, P. (2012a). Coral resilience to ocean acidification and global warming through pH up-regulation. *Nat. Clim. Chang.* 2, 623–627.

doi:10.1038/nclimate1473.

McCulloch, M. T., D'Olivo, J. P., Falter, J., Georgiou, L., Holcomb, M., Montagna, P., et al. (2017a). *Boron isotopic systematics in scleractinian corals and the role of pH up-regulation*. doi:10.1007/978-3-662-44185-5_811.

McCulloch, M. T., D'Olivo, J. P., Falter, J., Holcomb, M., and Trotter, J. A. (2017b). Coral calcification in a changing World and the interactive dynamics of pH and DIC upregulation. *Nat. Commun.* 8, 1–8. doi:10.1038/ncomms15686.

McCulloch, M., Trotter, J., Montagna, P., Falter, J., Dunbar, R., Freiwald, A., et al. (2012b). Resilience of cold-water scleractinian corals to ocean acidification: Boron isotopic systematics of pH and saturation state up-regulation. *Geochim. Cosmochim. Acta* 87, 21–34. doi:10.1016/j.gca.2012.03.027.

McIlroy, S. E., Wong, J. C. Y., and Baker, D. M. (2020). Competitive traits of coral symbionts may alter the structure and function of the microbiome. *ISME J.* 14, 2424–2432. doi:10.1038/s41396-020-0697-0.

McNicholl, C., and Koch, M. S. (2021). Irradiance, photosynthesis and elevated pCO2 effects on net calcification in tropical reef macroalgae. *J. Exp. Mar. Bio. Ecol.* 535, 151489. doi:10.1016/j.jembe.2020.151489.

Meunier, V., Geissler, L., Bonnet, S., Rädecker, N., Perna, G., Grosso, O., et al. (2021). Microbes support enhanced nitrogen requirements of coral holobionts in a high CO 2 environment . *Mol. Ecol.*, 1–12. doi:10.1111/mec.16163.

Mieog, J. C., Van Oppen, M. J. H., Berkelmans, R., Stam, W. T., and Olsen, J. L. (2009). Quantification of algal endosymbionts (Symbiodinium) in coral tissue using real-time PCR. *Mol. Ecol. Resour.* 9, 74–82. doi:10.1111/j.1755-0998.2008.02222.x.

Misra, S., Owen, R., Kerr, J., Greaves, M., and Elderfield, H. (2014). Determination of δ11B by HR-ICP-MS from mass limited samples: Application to natural carbonates and water samples. *Geochim. Cosmochim. Acta* 140, 531–552. doi:10.1016/j.gca.2014.05.047.

Montagna, P., McCulloch, M., Douville, E., López Correa, M., Trotter, J., Rodolfo-Metalpa, R., et al. (2014). Li/Mg systematics in scleractinian corals: Calibration of the thermometer. *Geochim. Cosmochim. Acta* 132, 288–310. doi:10.1016/j.gca.2014.02.005.

Morgans, C. A., Hung, J. Y., Bourne, D. G., and Quigley, K. M. (2020). Symbiodiniaceae probiotics for use in bleaching recovery. *Restor. Ecol.* 28, 282–288. doi:10.1111/rec.13069.

Morse, D. E., Hooker, N., Morse, A. N. C., and Jensen, R. A. (1988). Control of larval metamorphosis and recruitment in sympatric agariciid corals. *J. Exp. Mar. Bio. Ecol.* 116, 193–217. doi:10.1016/0022-0981(88)90027-5.

Mumby, P. J., Wolff, N. H., Bozec, Y. M., Chollett, I., and Halloran, P. (2014). Operationalizing

the resilience of coral reefs in an era of climate change. *Conserv. Lett.* 7, 176–187. doi:10.1111/conl.12047.

Munday, P. L., Warner, R. R., Monro, K., Pandolfi, J. M., and Marshall, D. J. (2013). Predicting evolutionary responses to climate change in the sea. *Ecol. Lett.* 16, 1488–1500. doi:10.1111/ele.12185.

Muscatine, L., and Porter, J. W. (1977). Reef Corals: Mutualistic Symbioses Adapted to Nutrient-Poor Environments. Bioscience. *Bioscience* 27, 454–460. doi:doi:10.2307/1297526.

Naumann, M. S., Niggl, W., Laforsch, C., Glaser, C., and Wild, C. (2009). Coral surface area quantification-evaluation of established techniques by comparison with computer tomography. *Coral Reefs* 28, 109–117. doi:10.1007/s00338-008-0459-3.

Nelson, H. R., and Altieri, A. H. (2019). Oxygen: the universal currency on coral reefs. *Coral Reefs* 38, 177–198. doi:10.1007/s00338-019-01765-0.

Nelson, W. A. (2009). Calcified macroalgae critical to coastal ecosystems and vulnerable to change: A review. *Mar. Freshw. Res.* 60, 787–801. doi:10.1071/MF08335.

Newton, J. A., Feely, R. A., Jewett, E. B., Williamson, P., and Mathis, J. (2014). Global Ocean Acidification Observing Network: requirements and governance Plan. *Glob. Ocean Acidif. Obs. Netw.*, 5–28. Available at: www.iaea.org/ocean-acidification.

Ng, T. Y., and Ang, P. (2016). Low symbiont diversity as a potential adaptive strategy in a marginal non-reefal environment: a case study of corals in Hong Kong. *Coral Reefs* 35, 941–957. doi:10.1007/s00338-016-1458-4.

Nitschke, M. R., Gardner, S. G., Goyen, S., Fujise, L., Camp, E. F., Ralph, P. J., et al. (2018). Utility of photochemical traits as diagnostics of thermal tolerance amongst great barrier reef corals. *Front. Mar. Sci.* 5, 1–18. doi:10.3389/fmars.2018.00045.

Nock, R., and Nielsen, F. (2004). Statistical region merging. *IEEE Trans. Pattern Anal. Mach. Intell.* 26, 1452–1458. doi:10.1109/TPAMI.2004.110.

Noireaux, J., Mavromatis, V., Gaillardet, J., Schott, J., Montouillout, V., Louvat, P., et al. (2015). Crystallographic control on the boron isotope paleo-pH proxy. *Earth Planet. Sci. Lett.* 430, 398–407. doi:10.1016/j.epsl.2015.07.063.

O'Connor, M. I., Bruno, J. F., Gaines, S. D., Halpern, B. S., Lester, S. E., Kinlan, B. P., et al. (2007). Temperature control of larval dispersal and the implications for marine ecology, evolution, and conservation. *Proc. Natl. Acad. Sci. U. S. A.* 104, 1266–1271. doi:10.1073/pnas.0603422104.

O'Leary, J. K., Potts, D. C., Braga, J. C., and McClanahan, T. R. (2012). Indirect consequences of fishing: Reduction of coralline algae suppresses juvenile coral abundance. *Coral Reefs* 31, 547–559. doi:10.1007/s00338-012-0872-5.

O'Leary, J. K., Potts, D., Schoenrock, K. M., and McClahanan, T. R. (2013). Fish and sea urchin grazing opens settlement space equally but urchins reduce survival of coral recruits. *Mar. Ecol. Prog. Ser.* 493, 165–177. doi:10.3354/meps10510.

Ohno, Y., Iguchi, A., Shinzato, C., Inoue, M., Suzuki, A., Sakai, K., et al. (2017). An aposymbiotic primary coral polyp counteracts acidification by active pH regulation. *Sci. Rep.* 7. doi:10.1038/srep40324.

Oliver, T. A., and Palumbi, S. R. (2011a). Do fluctuating temperature environments elevate coral thermal tolerance? *Coral Reefs* 30, 429–440. doi:10.1007/s00338-011-0721-y.

Oliver, T. A., and Palumbi, S. R. (2011b). Many corals host thermally resistant symbionts in high-temperature habitat. *Coral Reefs* 30, 241–250. doi:10.1007/s00338-010-0696-0.

Oprandi, A., Montefalcone, M., Morri, C., Benelli, F., and Bianchi, C. N. (2019). Water circulation, and not ocean acidification, affects coral recruitment and survival at shallow hydrothermal vents. *Estuar. Coast. Shelf Sci.* 217, 158–164. doi:10.1016/j.ecss.2018.11.017.

Orr, J. C., Fabry, V. J., Aumont, O., Bopp, L., Doney, S. C., Feely, R. A., et al. (2005). Anthropogenic ocean acidification over the twenty-first century and its impact on calcifying organisms. *Nature* 437, 681–686. doi:10.1038/nature04095.

Padilla-Gamiño, J. L., Gaitán-Espitia, J. D., Kelly, M. W., and Hofmann, G. E. (2016). Physiological plasticity and local adaptation to elevated pCO2 in calcareous algae: an ontogenetic and geographic approach. *Evol. Appl.* 9, 1043–1053. doi:10.1111/eva.12411.

Page, H. N., Hewett, C., Tompkins, H., and Hall, E. R. (2021). Ocean acidification and direct interactions affect coral, macroalga, and sponge growth in the florida keys. *J. Mar. Sci. Eng.* 9, 739. doi:10.3390/jmse9070739.

Page, H. N., Mccoy, S. J., Bahr, K. D., Cyronak, T., Jewett, E. B., Johnson, M. D., et al. (2022). Responses of benthic calcifying algae to ocean acidification differ between laboratory and field settings. *ICES J. Mar. Sci.* 79, 1–11.

Palumbi, S. R., Barshis, D. J., Traylor-Knowles, N., and Bay, R. A. (2014). Mechanisms of reef coral resistance to future climate change. *Science (80-.).* 344, 895–898. doi:10.1126/science.1251336.

Paracer, S., and Ahmadjian, V. (2000). *Symbiosis: An Introduction to Biological Associations*. 2nd ed. , ed. N. Y. Oxford Univ Press.

Penin, L., Michonneau, F., Carroll, A., and Adjeroud, M. (2011). Effects of predators and grazers exclusion on early post-settlement coral mortality. *Hydrobiologia* 663, 259–264. doi:10.1007/s10750-010-0569-0.

Perez, F. F., and Fraga, F. (1987). Association constant of fluoride and hydrogen ions in seawater. *Mar. Chem.* 21, 161–168. doi:10.1016/0304-4203(87)90036-3.

Pichler, T., Biscéré, T., Kinch, J., Zampighi, M., Houlbrèque, F., and Rodolfo-Metalpa, R. (2019). Suitability of the shallow water hydrothermal system at Ambitle Island (Papua New Guinea) to study the effect of high pCO2 on coral reefs. *Mar. Pollut. Bull.* doi:10.1016/j.marpolbul.2018.11.003.

Pochon, X., Pawlowski, J., Zaninetti, L., and Rowan, R. (2001). High genetic diversity and relative specificity among Symbiodinium-like endosymbiotic dinoflagellates in soritid foraminiferans. *Mar. Biol.* 139, 1069–1078. doi:10.1007/s002270100674.

Porzio, L., Garrard, S. L., and Buia, M. C. (2013). The effect of ocean acidification on early algal colonization stages at natural CO2 vents. *Mar. Biol.* 160, 2247–2259. doi:10.1007/s00227-013-2251-3.

Price, N. (2010). Habitat selection, facilitation, and biotic settlement cues affect distribution and performance of coral recruits in French Polynesia. *Oecologia* 163, 747–758. doi:10.1007/s00442-010-1578-4.

Putnam, H. M. (2021). Avenues of reef-building coral acclimatization in response to rapid environmental change. *J. Exp. Biol.* 224. doi:10.1242/jeb.239319.

Putnam, H. M., Barott, K. L., Ainsworth, T. D., and Gates, R. D. (2017). The Vulnerability and Resilience of Reef-Building Corals. *Curr. Biol.* 27, R528–R540. doi:10.1016/j.cub.2017.04.047.

Putnam, H. M., Davidson, J. M., and Gates, R. D. (2016). Ocean acidification influences host DNA methylation and phenotypic plasticity in environmentally susceptible corals. *Evol. Appl.* 9, 1165–1178. doi:10.1111/eva.12408.

Putnam, H. M., Stat, M., Pochon, X., and Gates, R. D. (2012). Endosymbiotic flexibility associates with environmental sensitivity in scleractinian corals. *Proc. R. Soc. B Biol. Sci.* 279, 4352–4361. doi:10.1098/rspb.2012.1454.

Quigley, K. M., Willis, B. L., and Bay, L. K. (2017). Heritability of the Symbiodinium community in vertically-and horizontally-transmitting broadcast spawning corals. *Sci. Rep.* 7, 1–14. doi:10.1038/s41598-017-08179-4.

Quigley, K. M., Willis, B. L., and Kenkel, C. D. (2019). Transgenerational inheritance of shuffled symbiont communities in the coral *Montipora digitata*. *Sci. Rep.* 9, 1–11. doi:10.1038/s41598-019-50045-y.

Quinn, M., Taylor, W., Crowley, J., and Link, M. (1996). Evaluation of sampling resolution in coral stable isotope records A case study using records from New Caledonia and Tarawa. 11, 529–542.

Quinn, T. M., Crowley, T. J., Taylor, F. W., Henin, C., Joannot, P., and Join, Y. (1998). A multicentury stable isotope record from a New Caledonia coral: Interannual and decadal sea surface temperature variability in the southwest Pacific since 1657 A.D.

Paleoceanography 13, 412–426. doi:10.1029/98PA00401.

Ragazzola, F., Foster, L. C., Form, A. U., Büscher, J., Hansteen, T. H., and Fietzke, J. (2013). Phenotypic plasticity of coralline algae in a High CO2 world. *Ecol. Evol.* 3, 3436–3446. doi:10.1002/ece3.723.

Ralph, P. J., and Gademann, R. (2005). Rapid light curves: A powerful tool to assess photosynthetic activity. *Aquat. Bot.* 82, 222–237. doi:10.1016/j.aquabot.2005.02.006.

Ralph, P. J., Gademann, R., Larkum, A. W. D., and Schreiber, U. (1999). Ln Situ Underwater Measurements of Photosynthetic Activity of Coral Zooxanthellae and Other. *Mar Ecol Prog Ser* 180, 139–147.

Ramos, R. D., Goodkin, N. F., Siringan, F. P., and Hughen, K. A. (2019). Coral Records of Temperature and Salinity in the Tropical Western Pacific Reveal Influence of the Pacific Decadal Oscillation Since the Late Nineteenth Century. *Paleoceanogr. Paleoclimatology* 34, 1344–1358. doi:10.1029/2019PA003684.

Rathbone, M., Brown, K. T., and Dove, S. (2021). Tolerance to a highly variable environment does not infer resilience to future ocean warming and acidification in a branching coral. *Limnol. Oceanogr.* 2100, 1–13. doi:10.1002/lno.11991.

Ricardo, G. F., Jones, R. J., Nordborg, M., and Negri, A. P. (2017). Settlement patterns of the coral Acropora millepora on sediment-laden surfaces. *Sci. Total Environ.* 609, 277–288. doi:10.1016/j.scitotenv.2017.07.153.

Ries, J. B. (2011). A physicochemical framework for interpreting the biological calcification response to CO2-induced ocean acidification. *Geochim. Cosmochim. Acta*. doi:10.1016/j.gca.2011.04.025.

Ries, J. B., Cohen, A. L., and McCorkle, D. C. (2009). Marine calcifiers exhibit mixed responses to CO2-induced ocean acidification. *Geology* 37, 1131–1134. doi:10.1130/G30210A.1.

Rivest, E. B., Comeau, S., and Cornwall, C. E. (2017). The Role of Natural Variability in Shaping the Response of Coral Reef Organisms to Climate Change. *Curr. Clim. Chang. Reports* 3, 271–281. doi:10.1007/s40641-017-0082-x.

Rodolfo-Metalpa, R., Houlbrèque, F., Tambutté, É., Boisson, F., Baggini, C., Patti, F. P., et al. (2011). Coral and mollusc resistance to ocean acidification adversely affected by warming. *Nat. Clim. Chang.* 1, 308–312. doi:10.1038/nclimate1200.

Rodolfo-Metalpa, R., Martin, S., Ferrier-Pagès, C., and Gattuso, J. -P (2010). Response of the temperate coral Cladocora caespitosa to mid- and long-term exposure to pCO2 and temperature levels projected for the year 2100AD. *Biogeosciences*, 289–300. Available at: http://www.biogeosciences.net/7/289/2010/bg-7-289-2010.html.

Rodolfo-Metalpa, R., Montagna, P., Aliani, S., Borghini, M., Canese, S., Hall-Spencer, J. M., et al. (2015). Calcification is not the Achilles' heel of cold-water corals in an acidifying

ocean. *Glob. Chang. Biol.* 21, 2238–2248. doi:10.1111/gcb.12867.

Rodrigues, L. J., and Grottoli, A. G. (2007). Energy reserves and metabolism as indicators of coral recovery from bleaching. *Limnol. Oceanogr.* 52, 1874–1882. doi:10.4319/lo.2007.52.5.1874.

Rollion-Bard, C., and Blamart, D. (2015). Possible controls on Li, Na, and Mg incorporation into aragonite coral skeletons. *Chem. Geol.* 396, 98–111. doi:10.1016/j.chemgeo.2014.12.011.

Rollion-Bard, C., Chaussidon, M., and France-Lanord, C. (2011). Biological control of internal pH in scleractinian corals: Implications on paleo-pH and paleo-temperature reconstructions. *Comptes Rendus - Geosci.* 343, 397–405. doi:10.1016/j.crte.2011.05.003.

Rollion-Bard, C., Milner Garcia, S., Burckel, P., Angiolini, L., Jurikova, H., Tomašových, A., et al. (2019). Assessing the biomineralization processes in the shell layers of modern brachiopods from oxygen isotopic composition and elemental ratios: Implications for their use as paleoenvironmental proxies. *Chem. Geol.* 524, 49–66. doi:10.1016/j.chemgeo.2019.05.031.

Ros, M., Suggett, D. J., Edmondson, J., Haydon, T., Hughes, D. J., Kim, M., et al. (2021). Symbiont shuffling across environmental gradients aligns with changes in carbon uptake and translocation in the reef-building coral *Pocillopora acuta*. *Coral Reefs* 40, 595–607. doi:10.1007/s00338-021-02066-1.

Sampaio, E., Santos, C., Rosa, I. C., Ferreira, V., Pörtner, H. O., Duarte, C. M., et al. (2021). Impacts of hypoxic events surpass those of future ocean warming and acidification. *Nat. Ecol. Evol.* 5, 311–321. doi:10.1038/s41559-020-01370-3.

Sampayo, E. M., Ridgway, T., Bongaerts, P., and Hoegh-Guldberg, O. (2008). Bleaching susceptibility and mortality of corals are determined by fine-scale differences in symbiont type. *Proc. Natl. Acad. Sci. U. S. A.* 105, 10444–10449. doi:10.1073/pnas.0708049105.

Schloss, P. D., Westcott, S. L., Ryabin, T., Hall, J. R., Hartmann, M., Hollister, E. B., et al. (2009). Introducing mothur: Open-source, platform-independent, community-supported software for describing and comparing microbial communities. *Appl. Environ. Microbiol.* 75, 7537–7541. doi:10.1128/AEM.01541-09.

Schmidt, C. A., Stifler, C. A., Luffey, E. L., Fordyce, B. I., Ahmed, A., Barreiro Pujol, G., et al. (2022). Faster Crystallization during Coral Skeleton Formation Correlates with Resilience to Ocean Acidification. *J. Am. Chem. Soc.* 144, 1332–1341. doi:10.1021/jacs.1c11434.

Schmidt, M. W., Spero, H. J., and Lea, D. W. (2004). Links between salinity variation in the Caribbean and North Atlantic thermohaline circulation. *Lett. to Nat.* 428, 1302–1315. doi:doi.org/10.1038/nature02346.

Schoepf, V., Baumann, J. H., Barshis, D. J., Browne, N. K., Camp, E. F., Comeau, S., et al. (2023). Preprint_Corals at the edge of environmental limits: A new conceptual framework to re-define marginal and extreme coral communities. *SSRN*, 1–67. doi:http://dx.doi.org/10.2139/ssrn.4343592.

Schoepf, V., Grottoli, A. G., Warner, M. E., Cai, W. J., Melman, T. F., Hoadley, K. D., et al. (2013). Coral Energy Reserves and Calcification in a High-CO2 World at Two Temperatures. *PLoS One* 8. doi:10.1371/journal.pone.0075049.

Schoepf, V., Jung, M. U., McCulloch, M. T., White, N. E., Stat, M., and Thomas, L. (2020). Thermally Variable, Macrotidal Reef Habitats Promote Rapid Recovery From Mass Coral Bleaching. *Front. Mar. Sci.* 7, 1–12. doi:10.3389/fmars.2020.00245.

Schoepf, V., Jury, C. P., Toonen, R. J., and McCulloch, M. T. (2017). Coral calcification mechanisms facilitate adaptive responses to ocean acidification. *Proc. R. Soc. B Biol. Sci.* doi:10.1098/rspb.2017.2117.

Schoepf, V., Stat, M., Falter, J. L., and McCulloch, M. T. (2015). Limits to the thermal tolerance of corals adapted to a highly fluctuating, naturally extreme temperature environment. *Sci. Rep.* 5, 1–14. doi:10.1038/srep17639.

Schreiber, U., Schliwa, U., and Bilger, W. (1986). Continuous recording of photochemical and non-photochemical chlorophyll fluorescence quenching with a new type of modulation fluorometer. *Photosynth. Res.* 10, 51–62. doi:10.1007/BF00024185.

Sevilgen, D. S., Venn, A. A., Hu, M. Y., Tambutté, E., De Beer, D., Planas-Bielsa, V., et al. (2019). Full in vivo characterization of carbonate chemistry at the site of calcification in corals. *Sci. Adv.* 5, 1–10. doi:10.1126/sciadv.aau7447.

Shamberger, K. E. F., Lentz, S. J., and Cohen, A. L. (2018). Low and variable ecosystem calcification in a coral reef lagoon under natural acidification. *Limnol. Oceanogr.* 63, 714–730. doi:10.1002/lno.10662.

Silverstein, R. N., Correa, A. M. S., and Baker, A. C. (2012). Specificity is rarely absolute in coral–algal symbiosis: Implications for coral response to climate change. *Proc. R. Soc. B Biol. Sci.* 279, 2609–2618. doi:10.1098/rspb.2012.0055.

Silverstein, R. N., Cunning, R., and Baker, A. C. (2017). Tenacious D: Symbiodinium in clade D remain in reef corals at both high and low temperature extremes despite impairment. *J. Exp. Biol.* 220, 1192–1196. doi:10.1242/jeb.148239.

Simkiss, K., and Wilbur, K. M. (1989). *Biomineralization Cell Biology and Mineral Deposition*. Academic P.

Smith, E. G., Gurskaya, A., Hume, B. C. C., Voolstra, C. R., Todd, P. A., Bauman, A. G., et al. (2020). Low Symbiodiniaceae diversity in a turbid marginal reef environment. *Coral Reefs* 39, 545–553. doi:10.1007/s00338-020-01956-0.

Smith, E. G., Vaughan, G. O., Ketchum, R. N., McParland, D., and Burt, J. A. (2017). Symbiont community stability through severe coral bleaching in a thermally extreme lagoon. *Sci. Rep.* 7, 1–9. doi:10.1038/s41598-017-01569-8.

Spalding, M., Burke, L., Wood, S. A., Ashpole, J., Hutchison, J., and zu Ermgassen, P. (2017). Mapping the global value and distribution of coral reef tourism. *Mar. Policy* 82, 104–113. doi:10.1016/j.marpol.2017.05.014.

Stat, M., and Gates, R. D. (2011). Clade D Symbiodinium in Scleractinian Corals: A “Nugget” of Hope, a Selfish Opportunist, an Ominous Sign, or All of the Above? . *J. Mar. Biol.* 2011, 1–9. doi:10.1155/2011/730715.

Stat, M., Loh, W. K. W., Hoegh-Guldberg, O., and Carter, D. A. (2008a). Symbiont acquisition strategy drives host-symbiont associations in the southern Great Barrier Reef. *Coral Reefs* 27, 763–772. doi:10.1007/s00338-008-0412-5.

Stat, M., Morris, E., and Gates, R. D. (2008b). Functional diversity in coral-dinoflagellate symbiosis. *Proc. Natl. Acad. Sci. U. S. A.* 105, 9256–9261. doi:10.1073/pnas.0801328105.

Stat, M., Pochon, X., Cowie, R. O. M., and Gates, R. D. (2009). Specificity in communities of symbiodinium in corals from Johnston Atoll. *Mar. Ecol. Prog. Ser.* 386, 83–96. doi:10.3354/meps08080.

Stat, M., Pochon, X., Franklin, E. C., Bruno, J. F., Casey, K. S., Selig, E. R., et al. (2013). The distribution of the thermally tolerant symbiont lineage (Symbiodinium clade D) in corals from Hawaii: Correlations with host and the history of ocean thermal stress. *Ecol. Evol.* 3, 1317–1329. doi:10.1002/ece3.556.

Steen, R. G., and Muscatine, L. (1987). Low Temperature Evokes Rapid Exocytosis of Symbiotic Algae By a Sea Anemone. *Biol. Bull.* 172, 246–263. doi:10.2307/1541797.

Stevenson, S., McGregor, H. V., Phipps, S. J., and Fox-Kemper, B. (2013). Quantifying errors in coral-based ENSO estimates: Toward improved forward modeling of δ18O. *Paleoceanography* 28, 633–649. doi:10.1002/palo.20059.

Stevenson, S., Powell, B. S., Merrifield, M. A., Cobb, K. M., Nusbaumer, J., and Noone, D. (2015). Characterizing seawater oxygen isotopic variability in a regional ocean modeling framework: Implications for coral proxy records. *Paleoceanography* 30, 1573–1593. doi:10.1002/2015PA002824.

Stimson, J., and Kinzie, R. A. (1991). Temporal pattern and rate of release of zooxanthellae from the reef coral *Pocillopora damicornis* (Linnaeus). *J. Exp. Mar. Bio. Ecol.* 153, 63–74. Available at: http://www2.hawaii.edu/~kinzie/documents/CV & pubs/stimson001.pdf.

Suggett, D. J., Warner, M. E., and Leggat, W. (2017). Symbiotic Dinoflagellate Functional Diversity Mediates Coral Survival under Ecological Crisis. *Trends Ecol. Evol.* 32, 735–

745. doi:10.1016/j.tree.2017.07.013.

Sutton, A. J., Feely, R. A., Sabine, C. L., McPhaden, M. J., Takahashi, T., Chavez, F. P., et al. (2014). Natural variability and anthropogenic change in equatorial Pacific surface ocean pCO2 and pH. *Global Biogeochem. Cycles* 28, 131–145. doi:doi:10.1002/2013GB004679.

Sutton, A. J., Wanninkhof, R., Sabine, C. L., Feely, R. A., Cronin, M. F., and Weller, R. A. (2017). Variability and trends in surface seawater pCO2 and CO2 flux in the Pacific Ocean. *Geophys. Res. Lett.* 44, 5627–5636. doi:10.1002/2017GL073814.

Sutton, J. N., Liu, Y. W., Ries, J. B., Guillermic, M., Ponzevera, E., and Eagle, R. A. (2018). δ11B as monitor of calcification site pH in divergent marine calcifying organisms. *Biogeosciences* 15, 1447–1467. doi:10.5194/bg-15-1447-2018.

Swart, P. K., Greer, L., Rosenheim, B. E., Moses, C. S., Waite, A. J., Winter, A., et al. (2010). The 13 C Suess effect in scleractinian corals mirror changes in the anthropogenic CO 2 inventory of the surface oceans . *Geophys. Res. Lett.* 37, n/a-n/a. doi:10.1029/2009gl041397.

Swart, P. K., Leder, J. J., Szmant, A. M., and Dodge, R. E. (1996). The origin of variations in the isotopic record of scleractinian corals: II. Carbon. *Geochim. Cosmochim. Acta* 60, 2871–2885. doi:10.1016/0016-7037(96)00119-6.

Swierts, T., and Vermeij, M. J. A. (2016). Competitive interactions between corals and turf algae depend on coral colony form. *PeerJ* 2016, 1–18. doi:10.7717/peerj.1984.

Takahashi, T., Sutherland, S. C., Chipman, D. W., Goddard, J. G., and Ho, C. (2014). Climatological distributions of pH, pCO2, total CO2, alkalinity, and CaCO3 saturation in the global surface ocean, and temporal changes at selected locations. *Mar. Chem.* 164, 95–125. doi:10.1016/j.marchem.2014.06.004.

Tambutté, E., Venn, A. A., Holcomb, M., Segonds, N., Techer, N., Zoccola, D., et al. (2015). Morphological plasticity of the coral skeleton under CO2-driven seawater acidification. *Nat. Commun.* 6. doi:10.1038/ncomms8368.

Tambutté, S., Holcomb, M., Ferrier-Pagès, C., Reynaud, S., Tambutté, É., Zoccola, D., et al. (2011). Coral biomineralization: From the gene to the environment. *J. Exp. Mar. Bio. Ecol.* 408, 58–78. doi:10.1016/j.jembe.2011.07.026.

Tanvet, C., Benzoni, F., Peignon, C., Thouzeau, G., and Rodolfo-metalpa, R. (2022). High Coral Recruitment Despite Coralline Algal Loss Under Extreme Environmental Conditions. *Front. Mar. Sci.* 9, 1–15. doi:10.3389/fmars.2022.837877.

Tarique, M., and Rahaman, W. (2022). Recent ocean acidi B cation trends from boron isotope (d 11 B) records of coral : Role of oceanographic processes and anthropogenic CO 2 forcing. *J. Earth Syst. Sci.* 165, 1–21. doi:10.1007/s12040-022-01907-z.

Tarique, M., Rahaman, W., Fousiya, A. A., Lathika, N., Thamban, M., Achyuthan, H., et al. (2021). Surface pH Record (1990–2013) of the Arabian Sea From Boron Isotopes of Lakshadweep Corals—Trend, Variability, and Control. *J. Geophys. Res. Biogeosciences* 126, 1–28. doi:10.1029/2020JG006122.

Tebben, J., Motti, C. A., Siboni, N., Tapiolas, D. M., Negri, A. P., Schupp, P. J., et al. (2015). Chemical mediation of coral larval settlement by crustose coralline algae. *Sci. Rep.* 5, 1–11. doi:10.1038/srep10803.

Teixidó, N., Caroselli, E., Alliouane, S., Ceccarelli, C., Comeau, S., Gattuso, J. P., et al. (2020). Ocean acidification causes variable trait-shifts in a coral species. *Glob. Chang. Biol.* 26, 6813–6830. doi:10.1111/gcb.15372.

Thollot, P. (1992). Importance des mangroves pour la faune ichtyologique des récifs coralliens de Nouvelle-Calédonie. *Cybium* 16, 331–344. Available at: http://cat.inist.fr/?aModele=afficheN&cpsidt=4560914.

Thollot, P., Kulbicki, M., and Harmelin-Vivien, M. (1999). Reseaux trophiques et fonctionnement trophodynamique de l'ichtyofaune des mangroves de Nouvelle-Caledonie. *Comptes Rendus l'Academie des Sci. - Ser. III* 322, 607–619. doi:10.1016/S0764-4469(00)88531-5.

Thompson, D. (2022). Environmental records from coral skeletons: A decade of novel insights and innovation. *Wiley Interdiscip. Rev. Clim. Chang.* 13, 1–40. doi:10.1002/wcc.745.

Thompson, D. M., Ault, T. R., Evans, M. N., Cole, J. E., and Emile-Geay, J. (2011). Comparison of observed and simulated tropical climate trends using a forward model of coral δ18O. *Geophys. Res. Lett.* 38, 1–6. doi:10.1029/2011GL048224.

Thompson, D., McCulloch, M., Cole, J. E., Reed, E. V., D'Olivo, J. P., Dyez, K., et al. (2022). Marginal Reefs Under Stress: Physiological Limits Render Galápagos Corals Susceptible to Ocean Acidification and Thermal Stress. *AGU Adv.* 3, 1–21. doi:10.1029/2021av000509.

Thornhill, D. J., Xiang, Y., Fitt, W. K., and Santos, S. R. (2009). Reef endemism, host specificity and temporal stability in populations of symbiotic dinoflagellates from two ecologically dominant Caribbean corals. *PLoS One* 4. doi:10.1371/journal.pone.0006262.

Torda, G., Donelson, J. M., Aranda, M., Barshis, D. J., Bay, L., Berumen, M. L., et al. (2017). Rapid adaptive responses to climate change in corals. *Nat. Clim. Chang.* 7, 627–636. doi:10.1038/nclimate3374.

Towle, E. K., Enochs, I. C., and Langdon, C. (2015). Threatened Caribbean coral is able to mitigate the adverse effects of ocean acidification on calcification by increasing feeding rate. *PLoS One* 10, 1–17. doi:10.1371/journal.pone.0123394.

Trygonis, V., and Sini, M. (2012). PhotoQuad: A dedicated seabed image processing software,

and a comparative error analysis of four photoquadrat methods. *J. Exp. Mar. Bio. Ecol.* 424–425, 99–108. doi:10.1016/j.jembe.2012.04.018.

Underwood, A. J., and Jernakoff, P. (1984). The effects of tidal height, wave-exposure, seasonality and rock-pools on grazing and the distribution of intertidal macroalgae in New South Wales. *J. Exp. Mar. Bio. Ecol.* 75, 71–96. doi:10.1016/0022-0981(84)90024-8.

Vargas, C. A., Lagos, N. A., Lardies, M. A., Duarte, C., Manríquez, P. H., Aguilera, V. M., et al. (2017). Species-specific responses to ocean acidification should account for local adaptation and adaptive plasticity. *Nat. Ecol. Evol.* 1. doi:10.1038/s41559-017-0084.

Venn, A. A., Bernardet, C., Chabenat, A., Tambutté, É., and Tambutté, S. (2020). Paracellular transport to the coral calcifying medium: Effects of environmental parameters. *J. Exp. Biol.* 223. doi:10.1242/jeb.227074.

Venn, A. A., Tambutté, E., Caminiti-Segonds, N., Techer, N., Allemand, D., and Tambutté, S. (2019). Effects of light and darkness on pH regulation in three coral species exposed to seawater acidification. *Sci. Rep.* 9, 1–12. doi:10.1038/s41598-018-38168-0.

Venn, A. A., Tambutte, E., Comeau, S., and Tambutté, S. (2022). Proton gradients across the coral calcifying cell layer : Effects of light, ocean acidification and carbonate chemistry. *Front. Mar. Sci.* 9, 1–15. doi:10.3389/fmars.2022.973908.

Venn, A. A., Tambutté, E., Holcomb, M., Laurent, J., Allemand, D., and Tambutté, S. (2013). Impact of seawater acidification on pH at the tissue-skeleton interface and calcification in reef corals. *Proc. Natl. Acad. Sci. U. S. A.* 110, 1634–1639. doi:10.1073/pnas.1216153110.

Venn, A. A., Tambutté, E., Lotto, S., Zoccola, D., Allemand, D., and Tambutté, S. (2009). Imaging intracellular pH in a reef coral and symbiotic anemone. *Proc. Natl. Acad. Sci. U. S. A.* 106, 16574–16579. doi:10.1073/pnas.0902894106.

Venn, A., Tambutté, E., Holcomb, M., Allemand, D., and Tambutté, S. (2011). Live tissue imaging shows reef corals elevate pH under their calcifying tissue relative to seawater. *PLoS One* 6, 1–9. doi:10.1371/journal.pone.0020013.

Victor, S. (2008). Stability of reef framework and post settlement mortality as the structuring factor for recovery of Malakal Bay Reef, Palau, Micronesia: 25 years after a severe COTS outbreak. *Estuar. Coast. Shelf Sci.* 77, 175–180. doi:10.1016/j.ecss.2007.09.009.

Vidal-Dupiol, J., Adjeroud, M., Roger, E., Foure, L., Duval, D., Mone, Y., et al. (2009). Coral bleaching under thermal stress: Putative involvement of host/symbiont recognition mechanisms. *BMC Physiol.* 9, 1–16. doi:10.1186/1472-6793-9-14.

Vogel, N., Cantin, N. E., Strahl, J., Kaniewska, P., Bay, L., Wild, C., et al. (2016). Interactive effects of ocean acidification and warming on coral reef associated epilithic algal communities under past, present-day and future ocean conditions. *Coral Reefs* 35, 715–

728. doi:10.1007/s00338-015-1392-x.

Von Euw, S., Zhang, Q., Manichev, V., Murali, N., Gross, J., Feldman, L. C., et al. (2017). Biological control of aragonite formation in stony corals. *Science (80-.).* 356, 933–938. doi:10.1126/science.aam6371.

Voolstra, C. R., and Ziegler, M. (2020). Adapting with Microbial Help: Microbiome Flexibility Facilitates Rapid Responses to Environmental Change. *BioEssays* 42, 1–9. doi:10.1002/bies.202000004.

Wall, C. B., Fan, T. Y., and Edmunds, P. J. (2014). Ocean acidification has no effect on thermal bleaching in the coral *Seriatopora caliendrum*. *Coral Reefs* 33, 119–130. doi:10.1007/s00338-013-1085-2.

Wall, C. B., Kaluhiokalani, M., Popp, B. N., Donahue, M. J., and Gates, R. D. (2020). Divergent symbiont communities determine the physiology and nutrition of a reef coral across a light-availability gradient. *ISME J.* 14, 945–958. doi:10.1038/s41396-019-0570-1.

Wall, C. B., Mason, R. A. B., Ellis, W. R., Cunning, R., and Gates, R. D. (2017). Elevated pCO2 affects tissue biomass composition, but not calcification, in a reef coral under two light regimes. *R. Soc. Open Sci.* 4, 1–13. doi:10.1098/rsos.170683.

Wall, C. B., Ricci, C. A., Wen, A. D., Ledbetter, B. E., Delania, E., Mydlarz, L. D., et al. (2021). Shifting Baselines: Physiological legacies contribute to the response of reef coral to frequent heat waves. *Funct. Ecol.*, 1366–78.

Wall, M., Fietzke, J., Crook, E. D., and Paytan, A. (2019a). Using B isotopes and B/Ca in corals from low saturation springs to constrain calcification mechanisms. *Nat. Commun.* 10, 1–9. doi:10.1038/s41467-019-11519-9.

Wall, M., Prada, F., Fietzke, J., Caroselli, E., Dubinsky, Z., Brizi, L., et al. (2019b). Linking Internal Carbonate Chemistry Regulation and Calcification in Corals Growing at a Mediterranean CO2 Vent. *Front. Mar. Sci.* 6, 1–12. doi:10.3389/fmars.2019.00699.

Wang, B. S., You, C. F., Huang, K. F., Wu, S. F., Aggarwal, S. K., Chung, C. H., et al. (2010). Direct separation of boron from Na- and Ca-rich matrices by sublimation for stable isotope measurement by MC-ICP-MS. *Talanta* 82, 1378–1384. doi:10.1016/j.talanta.2010.07.010.

Wanninkhof, R., Pickers, P. A., Omar, A. M., Sutton, A., Murata, A., Olsen, A., et al. (2019). A surface ocean CO2 reference network, SOCONET and associated marine boundary layer CO2 measurements. *Front. Mar. Sci.* 6. doi:10.3389/fmars.2019.00400.

Webster, N. S., Uthicke, S., Botté, E. S., Flores, F., and Negri, A. P. (2013). Ocean acidification reduces induction of coral settlement by crustose coralline algae. *Glob. Chang. Biol.* 19, 303–315. doi:10.1111/gcb.12008.

Wei, G., McCulloch, M. T., Mortimer, G., Deng, W., and Xie, L. (2009). Evidence for ocean

acidification in the Great Barrier Reef of Australia. *Geochim. Cosmochim. Acta* 73, 2332–2346. doi:10.1016/j.gca.2009.02.009.

Weis, V. M. (2008). Cellular mechanisms of Cnidarian bleaching: Stress causes the collapse of symbiosis. *J. Exp. Biol.* 211, 3059–3066. doi:10.1242/jeb.009597.

Wierzbowski, H. (2007). Effects of pre-treatments and organic matter on oxygen and carbon isotope analyses of skeletal and inorganic calcium carbonate. *Int. J. Mass Spectrom.* 268, 16–29. doi:10.1016/j.ijms.2007.08.002.

Williams, B., Chan, P. T. W., Westfield, I. T., Rasher, D. B., and Ries, J. (2021). Ocean Acidification Reduces Skeletal Density of Hardground-Forming High-Latitude Crustose Coralline Algae. *Geophys. Res. Lett.* 48, 1–10. doi:10.1029/2020GL091499.

Wilson, J., and Harrison, P. (2005). Post-settlement mortality and growth of newly settled reef corals in a subtropical environment. *Coral Reefs* 24, 418–421. doi:10.1007/s00338-005-0033-1.

Wooldridge, S. A. (2009). A new conceptual model for the warm-water breakdown of the coralalgae endosymbiosis. *Mar. Freshw. Res.* 60, 483–496. doi:10.1071/MF08251.

Wooldridge, S. A. (2013). Breakdown of the coral-algae symbiosis: Towards formalising a linkage between warm-water bleaching thresholds and the growth rate of the intracellular zooxanthellae. *Biogeosciences* 10, 1647–1658. doi:10.5194/bg-10-1647-2013.

Wu, H. C., Dissard, D., Douville, E., Blamart, D., Bordier, L., Tribollet, A., et al. (2018). Surface ocean pH variations since 1689 CE and recent ocean acidification in the tropical South Pacific. *Nat. Commun.* 9. doi:10.1038/s41467-018-04922-1.

Wu, H. C., Moreau, M., Linsley, B. K., Schrag, D. P., and Corrège, T. (2014). Investigation of sea surface temperature changes from replicated coral Sr/Ca variations in the eastern equatorial Pacific (Clipperton Atoll) since 1874. *Palaeogeogr. Palaeoclimatol. Palaeoecol.* 412, 208–222. doi:10.1016/j.palaeo.2014.07.039.

Zeebe, R. E., and Wolf-Gladrow, D. (2001). *CO2 in seawater: Equilibrium, Kinetics, Isotopes*. Elsevier. , ed. D. Halpern Elsevier Oceanographic Series.

Zhou, G., Tong, H., Cai, L., and Huang, H. (2021). Transgenerational Effects on the Coral Pocillopora damicornis Microbiome Under Ocean Acidification. *Microb. Ecol.* 82, 572–580. doi:10.1007/s00248-021-01690-2.

Ziegler, M., Anton, A., Klein, S. G., Rädecker, N., Geraldi, N. R., Schmidt-Roach, S., et al. (2021). Integrating environmental variability to broaden the research on coral responses to future ocean conditions. *Glob. Chang. Biol.* 27, 5532–5546. doi:10.1111/gcb.15840.

Ziegler, M., Arif, C., Burt, J. A., Dobretsov, S., Roder, C., LaJeunesse, T. C., et al. (2017). Biogeography and molecular diversity of coral symbionts in the genus Symbiodinium around the Arabian Peninsula. *J. Biogeogr.* 44, 674–686. doi:10.1111/jbi.12913.

Ziegler, M., Roder, C., Bchel, C., and Voolstra, C. R. (2015). Niche acclimatization in Red Sea corals is dependent on flexibility of host-symbiont association. *Mar. Ecol. Prog. Ser.* 533, 163–176. doi:10.3354/meps11365.

Titre : Acclimatation des récifs coralliens aux changements climatiques : Écophysiologie et signatures géochimiques dans un contexte d'acidification des océans.

Mots clés : Coraux, Acclimatation, Climat, Physiologie, Proxies géochimiques

Résumé : Dans un contexte de changements climatiques rapides et sévères, les récifs coralliens sont menacés de disparition. L'élévation des teneurs en CO_2 d'origine anthropique génère une acidification des océans qui peut avoir des effets dévastateurs sur les organismes marins à squelette carbonaté, tels que les coraux. Les coraux ont la capacité de s'acclimater via différents mécanismes, notamment écophysiologiques. Cette thèse explore les capacités d'acclimatation des récifs coralliens au changement climatique et plus particulièrement à l'acidification des océans. Des études récentes ont permis de découvrir un site naturel en Nouvelle-Calédonie (mangroves de Bouraké) hébergeant des récifs coralliens diversifés malgré des conditions extrêmes et fluctuantes de pH/Température/Oxygène dissous de l'eau de mer. En couplant des approches écophysiologiques, métagénomiques et géochimiques, les objectifs de cette thèse sont d'identifier les mécanismes adaptatifs mis en jeu par les coraux de Bouraké en réponse à ces conditions en les comparant à des coraux d'un site de référence adjacent. Les premiers résultats de cette thèse ont montré un fort recrutement corallien à Bouraké. De plus, les coraux de Bouraké exposés à différents niveaux de pCO_2 ont présenté une calcification accrue par rapport aux coraux du site de référence. Nous avons montré des associations symbiotiques propres aux coraux de Bouraké, ainsi que l'influence des communautés symbiotiques sur la régulation de la calcification des coraux. Enfin, nous avons confirmé par une étude paléoenvironnementale que les coraux de Bouraké sont acclimatés à des conditions extrêmes de pH depuis au moins les 3 dernières décennies. Cette thèse souligne le potentiel adaptatif de certains coraux aux changements climatiques rapides en cours.

Title: Acclimatization of coral reefs to climate change: Ecophysiology and geochemical signatures in an ocean acidification context.

Keywords: Corals, Acclimatization, Climate, Physiology, Geochemical proxies

Abstract: In a context of rapid and severe climate change, coral reefs are threatened with extinction. The increase in anthropogenic CO_2 levels leads to ocean acidification, which can have devastating effects on marine organisms with carbonate skeletons, such as corals. Corals have the ability to acclimate through various mechanisms, including ecophysiological. This thesis explores the acclimatization capacities of coral reefs to climate change, particularly to ocean acidification. Recent studies have revealed a natural site in New Caledonia (Bouraké mangroves) hosting diverse coral reefs despite extreme and fluctuating pH/Temperature/Dissolved oxygen seawater conditions. By coupling ecophysiological, metagenomic and geochemical approaches, the objectives of this thesis are to identify the mechanisms set up by Bouraké corals in response to these conditions, by comparing them to corals from an adjacent reference site. The first results of this thesis showed a strong coral recruitment at Bouraké. In addition, corals from Bouraké exposed to different levels of pCO_2 showed increased calcification compared to corals from the reference site. We have shown symbiotic associations specific to Bouraké corals, as well as the influence of symbiotic communties on the regulation of coral calcification. Finally, we confirmed by a paleoenvironmental study that Bouraké corals have been acclimatized to extreme pH conditions for at least the last three decades. This thesis highlights the adaptive potential of some corals to the rapid climate change underway.